National Library
of Canada

Acquisitions and
Bibliographic Services Branch

395 Wellington Street
Ottawa, Ontario
K1A 0N4

Bibliothèque nationale
du Canada

Direction des acquisitions et
des services bibliographiques

395, rue Wellington
Ottawa (Ontario)
K1A 0N4

Your file Votre référence

Our file Notre référence

NOTICE

The quality of this microform is heavily dependent upon the quality of the original thesis submitted for microfilming. Every effort has been made to ensure the highest quality of reproduction possible.

If pages are missing, contact the university which granted the degree.

Some pages may have indistinct print especially if the original pages were typed with a poor typewriter ribbon or if the university sent us an inferior photocopy.

Reproduction in full or in part of this microform is governed by the Canadian Copyright Act, R.S.C. 1970, c. C-30, and subsequent amendments.

AVIS

La qualité de cette microforme dépend grandement de la qualité de la thèse soumise au microfilmage. Nous avons tout fait pour assurer une qualité supérieure de reproduction.

S'il manque des pages, veuillez communiquer avec l'université qui a conféré le grade.

La qualité d'impression de certaines pages peut laisser à désirer, surtout si les pages originales ont été dactylographiées à l'aide d'un ruban usé ou si l'université nous a fait parvenir une photocopie de qualité inférieure.

La reproduction, même partielle, de cette microforme est soumise à la Loi canadienne sur le droit d'auteur, SRC 1970, c. C-30, et ses amendements subséquents.

Canada

UNIVERSITY OF ALBERTA

Contiguous Hyperhybrid Grids in Steam Injection Simulation

by

George Paul Demetre

©

A THESIS
SUBMITTED TO THE FACULTY OF GRADUATE STUDIES AND RESEARCH
IN PARTIAL FULFILLMENT OF THE REQUIREMENTS FOR THE DEGREE OF
DOCTOR OF PHILOSOPHY
IN
PETROLEUM ENGINEERING

DEPARTMENT OF MINING, METALLURGICAL
AND PETROLEUM ENGINEERING

EDMONTON, ALBERTA
SPRING, 1993

National Library
of Canada

Acquisitions and
Bibliographic Services Branch

395 Wellington Street
Ottawa, Ontario
K1A 0N4

Bibliothèque nationale
du Canada

Direction des acquisitions et
des services bibliographiques

395, rue Wellington
Ottawa (Ontario)
K1A 0N4

Your file Votre référence

Our file Notre référence

The author has granted an irrevocable non-exclusive licence allowing the National Library of Canada to reproduce, loan, distribute or sell copies of his/her thesis by any means and in any form or format, making this thesis available to interested persons.

L'auteur a accordé une licence irrévocable et non exclusive permettant à la Bibliothèque nationale du Canada de reproduire, prêter, distribuer ou vendre des copies de sa thèse de quelque manière et sous quelque forme que ce soit pour mettre des exemplaires de cette thèse à la disposition des personnes intéressées.

The author retains ownership of the copyright in his/her thesis. Neither the thesis nor substantial extracts from it may be printed or otherwise reproduced without his/her permission.

L'auteur conserve la propriété du droit d'auteur qui protège sa thèse. Ni la thèse ni des extraits substantiels de celle-ci ne doivent être imprimés ou autrement reproduits sans son autorisation.

ISBN 0-315-82045-4

Canada

SPE International

Society of Petroleum Engineers

MAIL ADDRESS: P.O. BOX 833836, RICHARDSON, TX 75083-3836, U.S.A. • **FACSIMILE:** 214/952-9435 **TELEX:** 163245 SPEUT
STREET ADDRESS: 222 PALISADES CREEK DRIVE, RICHARDSON, TEXAS 75080, U.S.A. • **TELEPHONE:** 214/952-9393

February 17, 1993

Mr. George P. Demetre
P.O. Box 822, Station M
Calgary, Alberta
CANADA T2P 2J6

RE: Use of material copyrighted to SPE

Dear Mr. Demetre:

Thank you for your recent request to use material copyrighted to the Society of Petroleum Engineers. This is to grant one-time permission for you to use the material identified in your letter of February 5, 1993, for the purpose specified, provided that you include full and proper notice of SPE copyright ownership and acknowledgment of the source. Please see enclosed information.

The Society's copyright position encourages the broadest possible distribution of technical material to which it holds copyright, as is consistent with our copyright agreements with authors. Thank you for your cooperation in this matter, which is essential to protect the rights of the many authors who make technical material generally available through the Society.

Sincerely,

Carol J Paschetag

Carol Paschetag
Librarian

Enclosure

USE OF MATERIAL COPYRIGHTED TO SOCIETY OF PETROLEUM ENGINEERS

SPE Copyright Notice

Proper notice of SPE copyright ownership is required on (1) any copy or substantial portion of an SPE paper or other SPE publication and (2) any figure, table, or other portion of any publication to which SPE holds copyright.

Proper notice of SPE copyright ownership consists of the word "Copyright" or the copyright symbol, the year of first publication by SPE, and the words "Society of Petroleum Engineers" or "SPE." This acknowledgment must appear legibly on each copy of the work or portion thereof.

In addition, SPE requests that each acknowledgment include either (1) the date of publication and the book or journal in which published or (2) the name, location and dates of the meeting where first presented.

UNIVERSITY OF ALBERTA

RELEASE FORM

NAME OF AUTHOR George Paul Demetre

TITLE OF THESIS Contiguous Hyperhybrid Grids in Steam Injection Simulation

DEGREE FOR WHICH THESIS WAS PRESENTED Doctor of Philosophy
Petroleum Engineering

YEAR THIS DEGREE GRANTED Spring, 1993

Permission is hereby granted to the University of Alberta Library to reproduce single copies of this thesis and to lend or sell such copies for private, scholarly or scientific research purposes only.

The author reserves all other publication and other rights in association with the copyright in the thesis, and except as hereinbefore provided neither the thesis nor any substantial portion thereof may be printed or otherwise reproduced in any material form whatever without the author's prior written permission.

George Demetre.

P.O. Box 822, Station M
Calgary, Alberta
Canada T2P 2J6

April 14, 93

© 1993 George P. Demetre
All Rights Reserved

"Though this be madness, yet there is method in 't."

—From Shakespeare "Hamlet"

"You know my methods. Use them."

—Sir Arthur Conan Doyle

UNIVERSITY OF ALBERTA
FACULTY OF GRADUATE STUDIES AND RESEARCH

The undersigned certify that they have read, and recommend to the Faculty of Graduate Studies and Research for acceptance, a thesis entitled Contiguous Hyperhybrid Grids in Steam Injection Simulation submitted by George Paul Demetre in partial fulfillment of the requirements for the degree of Doctor of Philosophy in Petroleum Engineering.

Supervisor: Dr. S.M. Farouq Ali

AkAmbastha
Dr. A.K. Ambastha

Ramon Bentsen
Dr. R.G. Bentsen

WS Tortike
Dr. W.S. Tortike

John Whiting
Dr. J.M. Whiting

M. N. Oguztoreli
Dr. M.N. Oguztoreli

R G Moore
Dr. R.G. Moore

March 26, 93

To my wife Colleen
and to the memory of my good friends
Emma and Tigger

ABSTRACT

Effective fieldwide cyclic steam stimulation simulation is still in the future, when the next generation computers become available. It is recognized in the industry that only a limited number of wells can be included in a thermal simulation. Even at present, a fieldwide cyclic steam stimulation simulation requires a tremendous amount of computer storage and computation time. Yet, such a simulation customarily employs a rectilinear grid that is inadequate for simulating radial flow—an essential flow feature of cyclic steam stimulation—near the wells. In recognition of the fact that the next generation computers are nearby, the objective of this work is to develop a tool that will assist the simulation engineers in their field studies. The existence of the next generation of computers will not eliminate the need to have radial geometry around the wells.

A steam injection reservoir simulator was developed with the objective of improving the resolution of the information concerning the flow around a well and between wells. To accomplish this objective, it was necessary to develop the contiguous hyperhybrid grid refinement method.

With better well region representation, it has been shown that hyperhybrid grid refinement is useful in studying well operating changes and well interactions, particularly when the regions are made contiguous. Local well effects, interwell interference, multiwell cyclic steaming and conversion to steamflood were examined using hyperhybrid grid refinement.

It is recommended that contiguous hyperhybrid grid refinement be used for analyzing problems where the local well region behaviour is important in the context of a field simulation. Furthermore, it is recommended that this refinement technique be used to study interwell interactions where near-well effects are important and the communication path between the wells requires better representation.

PREFACE

The underlying philosophy used in the preparation of this manuscript is to provide a learning tool to those beginning their study of reservoir simulation. The result is a longer, more detailed, manuscript. The detail provided, particularly in the development of the model along with the numerous references to the literature, achieves this goal.

Little detail is provided for the construction of the computer model as this is left to others more skilled.

ACKNOWLEDGEMENTS

A special thank-you to Dr. S.M. Farouq Ali for his encouragement and support throughout the research. The guidance of Dr. J.M. Whiting and the supervisory committee is hereby acknowledged.

I would like to thank the management of Husky Oil Operations Ltd., and in particular Dr. J.M. Campbell, for the financial support, time and computing resources. In addition, the encouragement of my contemporaries at Husky and the graduate students of this department is greatly appreciated. I would also like to thank Dr. T.B. Tan for his help and insight.

TABLE OF CONTENTS

Chapter Page

1.0 INTRODUCTION 1
  1.1 Raison d'être of the Research 1
  1.2 Model Description 2
2.0 LITERATURE REVIEW 5
  2.1 Methods of Representing Well Regions in Simulators 5
    2.1.1 Analytical Well Models 6
    2.1.2 Grid Refinement Techniques 16
    2.1.3 Hybrid Grid Techniques 22
  2.2 Simulators 27
    2.2.1 Black Oil Simulators 27
    2.2.2 Cyclic Steam Stimulation Simulators 29
  2.3 Coning 30
  2.4 Special Topics 31
    2.4.1 Non-Newtonian Fluids 32
    2.4.2 Mild Thermal Cracking/Visbreaking 36
3.0 STATEMENT OF THE PROBLEM 38
  3.1 Statement of the Problem 38
4.0 MODEL DEVELOPMENT 39
  4.1 Mathematical Model 39
    4.1.1 Summary of Equations and Unknowns 39
    4.1.2 Functional Relationships 41
    4.1.3 Summary of Assumptions 41
    4.1.4 Well Model 42

4.1.5 Boundary and Initial Conditions 44

4.2 Grid Construction 45

4.2.1 Fundamental Grid Construction 45

4.2.2 Areal and Vertical Cartesian Grid Construction 46

4.2.3 Radial and Vertical Cylindrical Grid Construction 48

4.2.4 Treatment of Irregularly Shaped Grid Blocks 49

4.3 Numerical Model 52

4.3.1 Combined Continuity/Momentum Balance Equations 53

4.3.2 Total Energy Balance Equation 54

4.3.3 Cylindrical Form of Equations 55

4.4 Fluid and Rock Property Models 56

4.4.1 Three-Phase Relative Permeabilities 56

4.4.2 Porosity 62

4.4.3 Capillary Pressure 62

4.4.4 Equilibrium Constants 63

4.4.5 Density 65

4.4.6 Viscosity 68

4.4.7 Enthalpy and Internal Energy 71

4.4.8 Overburden and Underburden Heat Loss 74

4.4.9 Rock Thermal Properties 75

4.5 Solution Method 76

4.5.1 Newton's Method 76

4.5.2 Derivatives of the *F* Equations at Node *i*, *j*, *k*........................ 88

4.5.3 Derivatives of the *G* Equation at Node *i*, *j*, *k*........................ 96

4.5.4 Derivatives of the *X* Equations at All Nodes........................ 103

4.5.5 Derivatives of the *S* Equation at All Nodes........................ 104

4.5.6 Derivatives of the *W* Equation at All Nodes........................ 105

4.6 Computer Model 106
4.7 Miscellaneous Items 114
  4.7.1 Automatic Time Step Selection 114
  4.7.2 Model Initialization 114
  4.7.3 Wellbore Pressure Gradient 115
  4.7.4 End of Time Step Checks 116
  4.7.5 Treatment of Visbreaking 117
5.0 MODEL VALIDATION AND APPLICATION RESULTS 118
5.1 Preliminary Testing 118
5.2 Simple Model Testing 118
  5.2.1 Single Grid Block Testing 118
  5.2.2 Linear Horizontal Testing 124
  5.2.3 Linear Vertical Testing 124
5.3 Two-Dimensional Rectilinear Model Testing 124
5.4 Cylindrical/Cylindrical Equivalent Series Testing 130
5.5 Contiguous Regions Testing 153
5.6 Local Well Effects 167
  5.6.1 Base Runs 171
  5.6.2 Non-Newtonian Oil Viscosity Runs 171
  5.6.3 Visbreaking Run 173
  5.6.4 Two-Layer Run 174
5.7 Interwell Interference 206
  5.7.1 Interference Illustration and Grid Type Comparison 206
  5.7.2 Pressure Interference 218
5.8 Multiwell Cyclic Steaming 224
  5.8.1 Two-Well Runs 224

5.8.2 Four-Well Runs 239

5.9 Cyclic to Continuous Steaming 244

CONCLUSIONS 267

REFERENCES 269

APPENDIX I Development of Mathematical and Numerical Models 283

I.1 Mathematical Model 283

I.1.1 Equations of Continuity for a Multicomponent Mixture 283

I.1.2 Momentum Equation 287

I.1.3 Combined Continuity/Momentum Balance Equations 287

I.1.4 Total Energy Balance Equation 290

I.2 Numerical Model 294

I.2.1 Treatment of Transmissibilities 294

I.2.2 Combined Continuity/Momentum Balance Equations 298

I.2.3 Total Energy Balance Equation 302

I.2.4 Cylindrical Form of Equations 305

I.3 Fundamental Grid Construction 309

APPENDIX II Derivatives of Equations at Nodes other than i, j, k 312

II.1 Derivatives of the F Equations at Nodes i+1, j, k and i-1, j, k and other nodes 312

II.2 Derivatives of the G Equation at Nodes i+1, j, k and i-1, j, k and other nodes 316

APPENDIX III Derivatives of Well Equation 321

III.1 Shut-in Well 321

III.2 Constant Total Volume Injection Well 322

III.3 Constant Pressure Production/Injection Well 324

III.4 Constant Liquid Rate Production Well 324

III.5 Constant Oil Rate Production Well 324

APPENDIX IV Extracts From a Typical Set of Input and Output Files 325

IV.1 Data Input File 325

IV.2 Abbreviated Plot Files 327

IV.3 Abbreviated Run File 328

IV.4 Abbreviated Log File 337

COLOPHON 339

LIST OF TABLES

Table Page

4.4.4.1 Saturation pressure correlation constants 64

4.4.5.1 Steam density correlation constants 66

4.4.6.1 Steam viscosity correlation constants 70

4.4.7.1 Steam enthalpy correlation constants 71

4.6.0.1 Definition of flag array `IHYBRID` 109

4.6.0.2 Summary of CPU time for the major runs 113

5.0.0.1 Summary of runs 119

5.1.0.1 General fluid properties 120

5.1.0.2 General rock properties 121

5.6.0.1 Non-Newtonian oil parameters 169

5.8.1.1 Multiwell cyclic steaming Runs 1–8 results summary 228–9

5.8.1.2 Multiwell cyclic steaming Runs 1–4 and 10 end of injection and production phase results 230

5.8.1.3 Multiwell cyclic steaming Runs 1–8 ranking 236

5.8.1.4 Multiwell cyclic steaming Runs 9 and 10 results summary 237

5.8.2.1 Multiwell cyclic steaming Run 12 results summary 241

5.8.2.2 Multiwell cyclic steaming Run 13 results summary 241

5.9.0.1 Cyclic to continuous steaming Runs 1–5 operating conditions 246

5.9.0.2 Cyclic to continuous steaming Runs 1–5 results summary 246

LIST OF FIGURES

Figure		Page
1.2.0.1	Illustration of hybrid and hyperhybrid grid refinement	3
2.1.1.1	Block 0 containing a well and its four neighbouring blocks	7
2.1.2.1	Refined mesh	18
2.1.2.2	Locally refined mesh	18
2.1.2.3	Effects of rules of refinement	19
2.1.2.4	Configurations for analogs	19
2.1.3.1	Relation of radial model to three-dimensional model—plan view	25
4.2.2.1	Typical areal grid construction	47
4.2.2.2	Typical vertical grid construction	47
4.2.3.1	Typical radial grid construction	49
4.2.4.1	Irregularly shaped block ($\Delta\alpha = \pi/2$)	50
4.2.4.2	Hyperhybrid grid spanning several fundamental grid blocks	52
4.5.1.1	Typical grid and Jacobian matrix for a rectilinear system	79
4.5.1.2	Jacobian matrix for a rectilinear system	80
4.5.1.3	Typical grid and Jacobian matrix for a cylindrical system	81
4.5.1.4	Jacobian matrix for a cylindrical system	82
4.5.1.5	Typical grid and Jacobian matrix for a rectilinear system with a single hybrid grid	83
4.5.1.6	Jacobian matrix for a rectilinear system with a single hybrid grid	84
4.5.1.7	Typical grid and Jacobian matrix for a rectilinear system with contiguous hybrid/hyperhybrid grids	85
4.5.1.8	Jacobian matrix for a rectilinear system with contiguous hybrid/hyperhybrid grids	86
4.5.1.9	Grid and Jacobian matrix for a three-dimensional problem with 6 hybrid/hyperhybrid regions	87
4.6.0.1	Simplified flow diagram of computational procedure	108

4.6.0.2 Intragrid block property population logic 110
4.6.0.3 Intergrid block property population logic 112
5.1.0.1 Oil viscosity as a function of temperature 121
5.1.0.2 Water and oil relative permeability 122
5.1.0.3 Gas and oil relative permeability 122
5.1.0.4 Three-phase oil relative permeability 123
5.3.0.1 Run XY data summary 125
5.3.0.2 Run XY Liquid and gas production rates 126
5.3.0.3 Run XY Cumulative liquid and gas production 127
5.3.0.4 Run XY Production well grid block pressure 127
5.3.0.5 Run XY Production well bottom hole pressure 128
5.3.0.6 Run XY Injection well grid block pressure 128
5.3.0.7 Run XY Injection well bottom hole pressure 129
5.3.0.8 Run XY Injection well grid block temperature 129
5.4.0.1 Cylindrical/cylindrical equivalent runs data summary 133–4
5.4.0.2 Run R-1c Jacobian matrix 135
5.4.0.3 Run C-1c Jacobian matrix 135
5.4.0.4 Run H-1c Jacobian matrix 136
5.4.0.5 Run Z-1c Jacobian matrix 137
5.4.0.6 Run R-1c Steam injection rate 138
5.4.0.7 Run R-1c Liquid production rates 138
5.4.0.8 Run R-1c Cumulative injection and production 139
5.4.0.9 Run R-1c Well grid block pressure 139
5.4.0.10 Run R-1c Well grid block temperature 140
5.4.0.11 Run R-1c Well pressure history 140
5.4.0.12 Run R-1c2 Steam injection rate 141
5.4.0.13 Run R-1c2 Liquid production rates 141

5.4.0.14 Run R-1c2 Cumulative injection and production 142
5.4.0.15 Run R-1c2 Well grid block pressure 142
5.4.0.16 Run R-1c2 Well grid block temperature 143
5.4.0.17 Run R-1c2 Well pressure history 143
5.4.0.18 Run C-1c Steam injection rate 144
5.4.0.19 Run C-1c Liquid production rates 144
5.4.0.20 Run C-1c Cumulative injection and production 145
5.4.0.21 Run C-1c Well grid block pressure 145
5.4.0.22 Run C-1c Well grid block temperature 146
5.4.0.23 Run C-1c Well pressure history 146
5.4.0.24 Run H-1c Steam injection rate 147
5.4.0.25 Run H-1c Liquid production rates 147
5.4.0.26 Run H-1c Cumulative injection and production 148
5.4.0.27 Run H-1c Well grid block pressure 148
5.4.0.28 Run H-1c Well grid block temperature 149
5.4.0.29 Run H-1c Well pressure history 149
5.4.0.30 Run Z-1c Steam injection rate 150
5.4.0.31 Run Z-1c Liquid production rates 150
5.4.0.32 Run Z-1c Cumulative injection and production 151
5.4.0.33 Run Z-1c Well grid block pressure 151
5.4.0.34 Run Z-1c Well grid block temperature 152
5.4.0.35 Run Z-1c Well pressure history 152
5.5.0.1 Runs H-2 and Z-2 data summary 153–4
5.5.0.2 Run H-2 Jacobian matrix 155
5.5.0.3 Run Z-2 Jacobian matrix 156
5.5.0.4 Run H-2 Steam injection rate 158
5.5.0.5 Run H-2 Cumulative steam injection 159

5.5.0.6 Run H-2 Liquid production rates 159

5.5.0.7 Run H-2 Cumulative liquid production 160

5.5.0.8 Run H-2 Well grid block pressure 160

5.5.0.9 Run H-2 Well pressure history 161

5.5.0.10 Run H-2 Well grid block temperature 161

5.5.0.11 Run H-2 Grid block pressure profiles between wells 162

5.5.0.12 Run H-2 Grid block temperatures profile between wells 162

5.5.0.13 Run Z-2 Steam injection rate 163

5.5.0.14 Run Z-2 Cumulative steam injection 163

5.5.0.15 Run Z-2 Liquid production rates 164

5.5.0.16 Run Z-2 Cumulative liquid production 164

5.5.0.17 Run Z-2 Well grid block pressure 165

5.5.0.18 Run Z-2 Well pressure history 165

5.5.0.19 Run Z-2 Grid block pressure profiles between wells 166

5.5.0.20 Run Z-2 Grid block temperature profiles between wells 166

5.6.0.1 Runs R-3, H-3 and Z-3 data summary 167–8

5.6.0.2 Oil viscosity as a function of shear rate 169

5.6.0.3 Oil viscosity as a function of frontal velocity 170

5.6.0.4 Visbreaking fraction as a function of time for several temperatures 170

5.6.1.1 Run R-3 Steam injection rate 175

5.6.1.2 Run R-3 Liquid production rates 175

5.6.1.3 Run R-3 Cumulative injection and production 176

5.6.1.4 Run R-3 Well grid block pressure 176

5.6.1.5 Run R-3 Well pressure history 177

5.6.1.6 Run R-3 Well grid block temperature 177

5.6.1.7 Run R-3 Grid block pressure profiles at selected times 178

5.6.1.8 Run R-3 Grid block temperature profiles at selected times 178

5.6.1.9 Run H-3 Steam injection rate 179
5.6.1.10 Run H-3 Liquid production rates 179
5.6.1.11 Run H-3 Cumulative injection and production 180
5.6.1.12 Run H-3 Well grid block pressure 180
5.6.1.13 Run H-3 Well pressure history 181
5.6.1.14 Run H-3 Well grid block temperature 181
5.6.1.15 Run H-3 Grid block pressure profiles at selected times 182
5.6.1.16 Run H-3 Grid block temperature profiles at selected times 182
5.6.1.17 Run Z-3 Steam injection rate 183
5.6.1.18 Run Z-3 Liquid production rates 183
5.6.1.19 Run Z-3 Cumulative injection and production 184
5.6.1.20 Run Z-3 Well grid block pressure 184
5.6.1.21 Run Z-3 Well pressure history 185
5.6.1.22 Run Z-3 Well grid block temperature 185
5.6.1.23 Run Z-3 Grid block pressure profiles at selected times 186
5.6.1.24 Run Z-3 Grid block temperature profiles at selected times 186
5.6.2.1 Run R-3b Steam injection rate 187
5.6.2.2 Run R-3b Liquid production rates 187
5.6.2.3 Run R-3b Cumulative injection and production 188
5.6.2.4 Run R-3b Well grid block pressure 188
5.6.2.5 Run R-3b Well pressure history 189
5.6.2.6 Run R-3b Well grid block temperature 189
5.6.2.7 Run R-3b Grid block pressure profiles at selected times 190
5.6.2.8 Run R-3b Grid block temperature profiles at selected times 190
5.6.2.9 Run H-3b Steam injection rate 191
5.6.2.10 Run H-3b Liquid production rates 191
5.6.2.11 Run H-3b Cumulative injection and production 192

5.6.2.12 Run H-3b Well grid block pressure 192

5.6.2.13 Run H-3b Well pressure history 193

5.6.2.14 Run H-3b Well grid block temperature 193

5.6.2.15 Run H-3b Grid block pressure profiles at selected times 194

5.6.2.16 Run H-3b Grid block temperature profiles at selected times 194

5.6.2.17 Runs H-3 and H-3b Well grid block oil saturation 195

5.6.2.18 Run Z-3b Steam injection rate 195

5.6.2.19 Run Z-3b Liquid production rates 196

5.6.2.20 Run Z-3b Cumulative injection and production 196

5.6.2.21 Run Z-3b Well grid block pressure 197

5.6.2.22 Run Z-3b Well pressure history 197

5.6.2.23 Run Z-3b Well grid block temperature 198

5.6.2.24 Run Z-3b Grid block pressure profiles at selected times 198

5.6.2.25 Run Z-3b Grid block temperature profiles at selected times 199

5.6.3.1 Run Z-3c Steam injection rate 199

5.6.3.2 Run Z-3c Liquid production rates 200

5.6.3.3 Run Z-3c Cumulative injection and production 200

5.6.3.4 Run Z-3c Well grid block pressure 201

5.6.3.5 Run Z-3c Well pressure history 201

5.6.3.6 Run Z-3c Well grid block temperature 202

5.6.3.7 Run Z-3c Grid block pressure profiles at selected times 202

5.6.3.8 Run Z-3c Grid block temperature profiles at selected times 203

5.6.4.1 Run Z-3e Steam injection rate 203

5.6.4.2 Run Z-3e Liquid production rates 204

5.6.4.3 Run Z-3e Cumulative injection and production 204

5.6.4.4 Run Z-3e Well grid block temperature 205

5.6.4.5 Run Z-3e Well grid block oil saturation 205

5.7.1.1 Runs R-5 and Z-5 data summary 207–8
5.7.1.2 Run R-5 Steam injection rate 209
5.7.1.3 Run R-5 Cumulative steam injection 209
5.7.1.4 Run R-5 Liquid production rates 210
5.7.1.5 Run R-5 Cumulative liquid production 210
5.7.1.6 Run R-5 Well grid block pressure 211
5.7.1.7 Run R-5 Well pressure history 211
5.7.1.8 Run R-5 Well grid block temperature 212
5.7.1.9 Run R-5 Grid block pressure profiles at selected times 212
5.7.1.10 Run R-5 Grid block temperature profiles at selected times 213
5.7.1.11 Run Z-5 Steam injection rate 213
5.7.1.12 Run Z-5 Cumulative steam injection 214
5.7.1.13 Run Z-5 Liquid production rates 214
5.7.1.14 Run Z-5 Cumulative liquid production 215
5.7.1.15 Run Z-5 Well grid block pressure 215
5.7.1.16 Run Z-5 Well pressure history 216
5.7.1.17 Run Z-5 Well grid block temperature 216
5.7.1.18 Run Z-5 Grid block pressure profiles at selected times 217
5.7.1.19 Run Z-5 Grid block temperature profiles at selected times 217
5.7.2.1 Interference runs data summary 219–20
5.7.2.2 Interference comparison 221
5.7.2.3 Grid block pressure profiles 222
5.7.2.4 Grid block pressure profiles about injection well 222
5.7.2.5 Grid block pressure profiles about observation point 223
5.7.2.6 Interference comparison 223
5.8.1.1 Multiwell cyclic steaming Runs 1–8 data summary 226–7
5.8.1.2 Multiwell cyclic steaming Runs 1–4 steam-oil ratio 231

5.8.1.3 Multiwell cyclic steaming Runs 1–4 water-oil ratio 231
5.8.1.4 Multiwell cyclic steaming Runs 1–4 average daily oil rate 231
5.8.1.5 Multiwell cyclic steaming Runs 1 and 5 steam-oil ratio 232
5.8.1.6 Multiwell cyclic steaming Runs 1 and 5 water-oil ratio 232
5.8.1.7 Multiwell cyclic steaming Runs 1 and 5 average daily oil rate 232
5.8.1.8 Multiwell cyclic steaming Runs 2 and 6 steam-oil ratio 233
5.8.1.9 Multiwell cyclic steaming Runs 2 and 6 water-oil ratio 233
5.8.1.10 Multiwell cyclic steaming Runs 2 and 6 average daily oil rate 233
5.8.1.11 Multiwell cyclic steaming Runs 3 and 7 steam-oil ratio 234
5.8.1.12 Multiwell cyclic steaming Runs 3 and 7 water-oil ratio 234
5.8.1.13 Multiwell cyclic steaming Runs 3 and 7 average daily oil rate 234
5.8.1.14 Multiwell cyclic steaming Runs 4 and 8 steam-oil ratio 235
5.8.1.15 Multiwell cyclic steaming Runs 4 and 8 water-oil ratio 235
5.8.1.16 Multiwell cyclic steaming Runs 4 and 8 average daily oil rate 235
5.8.1.17 Multiwell cyclic steaming Runs 2, 9 and 10 steam-oil ratio 238
5.8.1.18 Multiwell cyclic steaming Runs 2, 9 and 10 water-oil ratio 238
5.8.1.19 Multiwell cyclic steaming Runs 2, 9 and 10 average daily oil rate 238
5.8.2.2 Multiwell cyclic steaming Runs 12 and 13 data summary 239–40
5.8.2.2 Multiwell cyclic steaming Run 12 steam-oil ratio 242
5.8.2.3 Multiwell cyclic steaming Run 12 water-oil ratio 242
5.8.2.4 Multiwell cyclic steaming Run 12 average daily oil rate 242
5.8.2.5 Multiwell cyclic steaming Run 13 steam-oil ratio 243
5.8.2.6 Multiwell cyclic steaming Run 13 water-oil ratio 243
5.8.2.7 Multiwell cyclic steaming Run 13 average daily oil rate 243
5.9.0.1 Cyclic to continuous steaming Run 1 Steam injection rate 247
5.9.0.2 Cyclic to continuous steaming Run 1 Liquid production rates 247
5.9.0.3 Cyclic to continuous steaming Run 1 Well grid block pressure 248

5.9.0.4 Cyclic to continuous steaming Run 1 Well grid block temperature 248

5.9.0.5 Cyclic to continuous steaming Run 1 Well pressure history 249

5.9.0.6 Cyclic to continuous steaming Run 1 Grid block pressure profiles at selected times 249

5.9.0.7 Cyclic to continuous steaming Run 1 Grid block temperature profiles at selected times 250

5.9.0.8 Cyclic to continuous steaming Run 1 Grid block oil saturation profiles at selected times 250

5.9.0.9 Cyclic to continuous steaming Run 2 Steam injection rate 251

5.9.0.10 Cyclic to continuous steaming Run 2 Liquid production rates 251

5.9.0.11 Cyclic to continuous steaming Run 2 Well grid block pressure 252

5.9.0.12 Cyclic to continuous steaming Run 2 Well grid block temperature 252

5.9.0.13 Cyclic to continuous steaming Run 2 Well pressure history 253

5.9.0.14 Cyclic to continuous steaming Run 2 Grid block pressure profiles at selected times 253

5.9.0.15 Cyclic to continuous steaming Run 2 Grid block temperature profiles at selected times 254

5.9.0.16 Cyclic to continuous steaming Run 2 Grid block oil saturation profiles at selected times 254

5.9.0.17 Cyclic to continuous steaming Run 3 Steam injection rate 255

5.9.0.18 Cyclic to continuous steaming Run 3 Liquid production rates 255

5.9.0.19 Cyclic to continuous steaming Run 3 Well grid block pressure 256

5.9.0.20 Cyclic to continuous steaming Run 3 Well grid block temperature 256

5.9.0.21 Cyclic to continuous steaming Run 3 Well pressure history 257

5.9.0.22 Cyclic to continuous steaming Run 3 Grid block pressure profiles at selected times 257

5.9.0.23 Cyclic to continuous steaming Run 3 Grid block temperature profiles at selected times 258

5.9.0.24 Cyclic to continuous steaming Run 3 Grid block oil saturation profiles at selected times 258

5.9.0.25 Cyclic to continuous steaming Run 4 Steam injection rate 259

5.9.0.26 Cyclic to continuous steaming Run 4 Liquid production rates 259

5.9.0.27 Cyclic to continuous steaming Run 4 Well grid block pressure 260

5.9.0.28 Cyclic to continuous steaming Run 4 Well grid block temperature 260

5.9.0.29 Cyclic to continuous steaming Run 4 Well pressure history 261

5.9.0.30 Cyclic to continuous steaming Run 4 Grid block pressure profiles at selected times 261

5.9.0.31 Cyclic to continuous steaming Run 4 Grid block temperature profiles at selected times 262

5.9.0.32 Cyclic to continuous steaming Run 4 Grid block oil saturation profiles at selected times 262

5.9.0.33 Cyclic to continuous steaming Run 5 Steam injection rate 263

5.9.0.34 Cyclic to continuous steaming Run 5 Liquid production rates 263

5.9.0.35 Cyclic to continuous steaming Run 5 Well grid block pressure 264

5.9.0.36 Cyclic to continuous steaming Run 5 Well grid block temperature 264

5.9.0.37 Cyclic to continuous steaming Run 5 Well pressure history 265

5.9.0.38 Cyclic to continuous steaming Run 5 Grid block pressure profiles at selected times 265

5.9.0.39 Cyclic to continuous steaming Run 5 Grid block temperature profiles at selected times 266

5.9.0.40 Cyclic to continuous steaming Run 5 Grid block oil saturation profiles at selected times 266

I.1.1.1 Control volume representation of reservoir 284

I.1.3.1 Phase distribution of a multicomponent system 289

I.3.0.1 Block-centred grid 311

I.3.0.2 Point-distributed grid 311

NOMENCLATURE

a	Constant in rheological model (t) [s]
a_j	Distance from well to its j^{th} image (L) [m]
A	Area (L^2) [m^2]
A	Correlation parameter in the Andrade equation ($mL^{-1}t^{-1}$) [Pa·s]
A_{ij}	Area of irregularly shaped block i, j (L^2) [m^2]
b	Constant in rheological model (t^{-1}) [s^{-1}]
B	Constant in rheological model ($t^{(y-1)/y}$) [$s^{(y-1)/y}$]
B	Formation volume factor (volume at reservoir conditions divided by volume at standard conditions)
B	Correlation parameter in the Andrade equation (Θ) [K]
c_f	Rock compressibility ($m^{-1}Lt^2$) [Pa^{-1}]
c_t	Total compressibility ($m^{-1}Lt^2$) [Pa^{-1}]
c_w	Water compressibility ($m^{-1}Lt^2$) [Pa^{-1}]
C	Correlation parameter in the Antoine equation (Θ) [K]
C_A	Concentration of component A
C_{iA}	Initial concentration of component A
C_p	Heat capacity at constant pressure ($L^2t^{-2}\Theta^{-1}$) [J kg^{-1} K^{-1}]
C_{pr}	Constant in rock heat capacity model ($m^{-2}L^2t^{-2}\Theta^{-1}$) [J m^{-3} rock K^{-1}]
C_{prt}	Constant in rock heat capacity model (Θ^{-1}) [K^{-1}]
D_{ip}	Diffusion coefficient of component i in phase p (L^2t^{-1}) [m^2 s^{-1}]
E_a	Activation energy (L^2t^{-2}) [J $kmol^{-1}$]
E_c	Energy stored in the over/underburden (mL^2t^{-2}) [J]
E_t	Total energy (mL^2t^{-2}) [J $kmol^{-1}$]
f	Fraction of well associated with the well block
$f(k)$	Rheological model correlation constant as a function of pore size distribution and tortuosity in a porous medium

f_g	Geometrical factor
f_h	Layer thickness factor
f_1, f_2	Correlation parameters in the general viscosity correlation
F_i	Empirical drainage radius factor
F_{wo}	Maximum water/oil ratio
g	Gravitational vector ($L\ t^{-2}$) [$m\ s^{-2}$]
G_{ij}	Binary interaction parameter
h	Thickness (L) [m]
$h(v')$	Rheological model fitting function
h_{jk}	Pressure drop from the bottom hole to layer *j* in well *k* ($mL^{-1}t^{-2}$) [Pa]
H_p	Enthalpy of phase *p* (mL^2t^{-2}) [$J\ kmol^{-1}$]
J	Productivity index ($m^{-1}L^4t$) [$m^3\ s^{-1}\ Pa^{-1}$]
J'	Constant portion of productivity index
J_{ijk}	Layer productivity/injectivity of phase *i* of layer *j* of well *k* ($m^{-1}L^4t$) [$m^3\ s^{-1}\ Pa^{-1}$]
J_{ip}	Rate of diffusion of component *i* in phase *p* (L^2t^{-1}) [$m^2\ s^{-1}$]
k	Absolute permeability (L^2) [m^2]
k	Effective isotropic permeability (L^2) [m^2]
k'	Reaction rate constant (t^{-1}) [s^{-1}]
k_r	Relative permeability
k_r	Reference permeability (L^2) [m^2]
k_{roiw}	Relative permeability to oil at connate water saturation
k_{rog}	Relative permeability to oil in a gas-oil system with connate water
k_{row}	Relative permeability to oil in an oil-water system
k_{rwro}	Relative permeability to water at residual oil saturation
k_x	Permeability in the *x* direction (L^2) [m^2]
k_y	Permeability in the *y* direction (L^2) [m^2]
k_z	Permeability in the *z* direction (L^2) [m^2]

K	Consistency constant in rheological model ($mL^{-1}t^{n-1}$) [$kg\ m^{-1}s^{n-1}$]
K_{vip}	Equilibrium ratio of component i in phase p
l	Characteristic length in rheological model (L) [m]
$l(v')$	Rheological model fitting function
L_i	Apparent length of the irregularly shaped block (L) [m]
m	Non-Newtonian fluid parameter
M_i	Molecular weight of component i [$kg\ kmol^{-1}$]
M_f	Volumetric heat capacity of the reservoir matrix ($m^{-2}L^{2}t^{-2}\Theta^{-1}$) [$J\ m^{-3}$ rock K^{-1}]
n	Time level
n	Power law fluid exponent
n_i	Mass flux vector ($mL^{-2}t^{-1}$) [$kmol\ s^{-1}\ m^{-2}$]
n_{ix}	Rectangular x component of the mass flux vector ($mL^{-2}t^{-1}$) [$kmol\ s^{-1}\ m^{-2}$]
n_g	Exponent on gas saturation for k_{rg}
n_{og}	Exponent on oil saturation for k_{rog}
n_{ow}	Exponent on oil saturation for k_{row}
n_w	Exponent on water saturation for k_{rw}
N_c	Number of components
N_p	Dimensionless ratio of transient production rate from pressure transients to steady flow production rate
N_p	Number of phases
N_{sp}	Dimensionless ratio of transient production rate from saturation changes to steady flow production rate
p	Pressure ($mL^{-1}t^{-2}$) [Pa]
p	Rheological model fitting fitting parameter
p_c	Critical pressure ($mL^{-1}t^{-2}$) [Pa]
p_e	Pressure at drainage radius r_e ($mL^{-1}t^{-2}$) [Pa]
p_{gb}	Pressure of oil in the grid block ($mL^{-1}t^{-2}$) [Pa]
p_i	Pressure at node i ($mL^{-1}t^{-2}$) [Pa]

p_{vp}	Vapour pressure (mL^{-1}t^{-2}) [Pa]
p_{wf}	Flowing bottom hole pressure (mL^{-1}t^{-2}) [Pa]
p_{wfs}	Specified injection/production flowing pressure (mL^{-1}t^{-2}) [Pa]
p_{wfk}	Bottom hole flowing pressure of well k (mL^{-1}t^{-2}) [Pa]
p_{ojk}	Oil phase pressure in the grid block containing layer j of well k (mL^{-1}t^{-2}) [Pa]
p_p	Pressure of phase p (mL^{-1}t^{-2}) [Pa]
p°	Reference pressure (mL^{-1}t^{-2}) [Pa]
P_{cgo}	Capillary pressure in an gas/oil system (mL^{-1}t^{-2}) [Pa]
P_{cow}	Capillary pressure in an oil/water system (mL^{-1}t^{-2}) [Pa]
q	Production rate (L^{3}t^{-1}) [m^3 s^{-1}]
q	Energy source/sink (mL^{2}t^{-3}) [J s^{-1}]
$\tilde{q}$	Production rate per unit reservoir volume [kmol s^{-1} m^{-3}]
$\tilde{q}$	Energy source/sink per unit reservoir volume [J s^{-1} m^{-3}]
q_{flux}	Heat flux at the reservoir over/underburden interface (mt^{-3}) [J s^{-1} m^{-2}]
q_{gf}	Free gas production rate (L^{3}t^{-1}) [m^3 s^{-1}]
q_{gk}	Specified total gas rate (L^{3}t^{-1}) [m^3 s^{-1}]
q_H	Production rate of enthalpy from grid block associated with fluid production (mL^{2}t^{-3}) [J s^{-1}]
q^*_h	Energy production (mL^{2}t^{-3}) [J s^{-1}]
q_i	Production rate of component i from grid block (L^{3}t^{-1}) [kmol s^{-1}]
q_{ijk}	Rate of production of phase i from layer j of well k (L^{3}t^{-1}) [m^3 s^{-1}]
q_{loss}	Heat loss to over/underburden (mL^{2}t^{-3}) [J s^{-1}]
q_{ok}	Specified total oil rate (L^{3}t^{-1}) [m^3 s^{-1}]
q_{Lk}	Specified total liquid rate (L^{3}t^{-1}) [m^3 s^{-1}]
q_{Tk}	Specified total injection rate (L^{3}t^{-1}) [m^3 s^{-1}]
r	Radial distance (L) [m]
r_b	Radius of a circle whose area is $\Delta x\ \Delta y$ (L) [m]

r_e	Radius of drainage or external boundary (L) [m]
r_i	Rate of production of component i (L^3t^{-1}) [kmol s^{-1}]
$r_{i,j}$	Distance from Grid point i to Well j (L) [m]
$r_{i,j}$	Radius of a circle whose area is $\Delta x\ \Delta y$ (L) [m]
$r_{i+1/2}$	Radius evaluated at $i+1/2$ (L) [m]
r_{kf}	Reaction rate between component and matrix (t^{-1}) [s^{-1}]
r^L	Logarithmic mean radius
r_o	Equivalent radius of well block (L) [m]
r_o	Radius at which the steady-state pressure for the actual well is equal to the numerically calculated pressure for the well block (L) [m]
$r_o{}^A$	Equivalent radius of well block based on the assumption that the well block pressure equals the areal average pressure (L) [m]
r_w	Radius of wellbore (L) [m]
R	Universal gas constant [8.314×10^3 J $kmol^{-1}$ K^{-1}]
R_s	Solution gas oil ratio [m^3 m^{-3}]
s	Skin effect term
s	Constant in rheological model
S	Saturation
S_{gb}	Saturation of oil in the grid block
S_p	Saturation of phase p
S_{orw}	Residual oil saturation
S_{wc}	Connate water saturation
S_L	Liquid saturation
t	Time (t) [s]
t_{sc}	Time scale for pressure or saturation change in near wellbore flow (t) [s]
T	Fluid flow transmissibility (m^{-1} L^4 t) [m^3 Pa^{-1} s^{-1}]
T_i	Transmissibility coefficient for flow from block i to the well block (m^{-1} L^4 t) [m^3 Pa^{-1} s^{-1}]

T_R	Radiation transmissibility
T_x	Transmissibility in the x direction (m^{-1} L^4 t) [m^3 Pa^{-1} s^{-1}]
T_y	Transmissibility in the y direction (m^{-1} L^4 t) [m^3 Pa^{-1} s^{-1}]
T_z	Transmissibility in the z direction (m^{-1} L^4 t) [m^3 Pa^{-1} s^{-1}]
$T_{Xi+1/2}$	x direction transmissibility for flow between grid blocks i and i+1(m^{-1} L^4 t) [m^3 Pa^{-1} s^{-1}]
u	Dependent variable
$u_{e,x}$	Total energy flux in the x direction (mt^{-3}) [J s^{-1} m^{-2}]
u_T	Convective energy flux (mt^{-3}) [J s^{-1} m^{-2}]
$u_{\lambda x}$	Rate of heat transfer by conduction in the positive x direction per unit cross sectional area normal to the x direction (mt^{-3}) [J s^{-1} m^{-2}]
v'	Shear rate (t^{-1}) [s^{-1}]
v_i	Velocity vector (L t^{-1}) [m s^{-1}]
v_x	Velocity (L t^{-1}) [m s^{-1}]
V	Volume (L^3) [m^3]
V_b	Bulk volume (L^3) [m^3]
w	Arrhenius constant (t^{-1}) [s^{-1}]
x	Space coordinate for areal model (L) [m]
x	Compositional parameter
x_{ip}	Mole fraction of component i in phase p
X_i	Mole fraction of component i in the component's master phase
y	Space coordinate for areal model (L) [m]
y	Rheological model correlation parameter (L^{-1}) [s^{-1}/ft day^{-1}]
z	Space coordinate for areal model, depth, positive downwards (L) [m]

Greek

α	Aspect ratio, $\Delta y/\Delta x$
α_j	Angle [radians]

γ	Euler's constant 0.5772157…
γ	Specific gravity
γ_p	Specific weight of phase p
γ_{wf}	Volumetric average wellbore gradient ($mL^{-2}t^{-2}$)[$Pa{\cdot}m^{-1}$]
Δx	Grid spacing in x direction (L) [m]
Δy	Grid spacing in y direction (L) [m]
Δz	Grid spacing in z direction (L) [m]
η	Non-Newtonian fluid parameter
θ	Temperature (Θ) [K]
θ_c	Critical temperature (Θ) [K]
θ_i	Original reservoir temperature (Θ) [K]
θ_j	Angular coordinate of block j
θ_r	Reduced temperature
θ_r	Reference temperature (Θ) [K]
κ	Thermal diffusivity ($L^2\ t^{-1}$) [$m^2\ s^{-1}$]
λ	Mobility ($m^{-1}Lt$) [$Pa^{-1}{\cdot}s^{-1}$]
λ_c	Thermal conductivity ($mLt^{-3}\Theta^{-1}$) [$J\ s^{-1}\ m^{-1}\ K^{-1}$]
μ	Viscosity ($mL^{-1}t^{-1}$) [$Pa{\cdot}s$]
μ_L	Viscosity of a liquid ($mL^{-1}t^{-1}$) [$Pa{\cdot}s$]
μ_{mix}	Viscosity of a mixture ($mL^{-1}t^{-1}$) [$Pa{\cdot}s$]
μ_{oD}	Viscosity of a dead oil ($mL^{-1}t^{-1}$) [$Pa{\cdot}s$]
μ_p	Viscosity of phase p ($mL^{-1}t^{-1}$) [$Pa{\cdot}s$]
μ_{SL}	Viscosity of the saturated liquid at P_{vp} ($mL^{-1}t^{-1}$) [$Pa{\cdot}s$]
ρ	Density (mL^{-3}) [$kmol\ m^{-3}$] or [$kg\ m^{-3}$]
ρ_f	Density of matrix (mL^{-3}) [$kg\ m^{-3}$]
ρ_p	Density of phase p (mL^{-3}) [$kg\ m^{-3}$]
Θ_c	Heat conduction transmissibility

Θ_R	Radiation transmissibility
τ_o	Yield stress ($mL^{-1}t^{-2}$) [Pa]
τ_{yx}	Shear force per unit area ($mL^{-3}t^{2}$) [Pa m^2]
ϕ	Porosity
ϕ^r	Porosity at the reference pressure
Φ_g	Gas potential ($p_g - \rho_g g z$) ($mL^{-1}t^{-2}$) [Pa]
Φ_o	Oil potential ($p_o - \rho_o g z$) ($mL^{-1}t^{-2}$) [Pa]
Φ_w	Water potential ($p_w - \rho_w g z$) ($mL^{-1}t^{-2}$) [Pa]
ω	Acentric factor
ω	Weighting factor

Subscripts

dg	Dissolved gas
f	Rock, matrix material
fg	Free gas
g	Gas
i	Component index
i	Grid point i
i	Initial condition
j	Grid point j
k	Grid point k
o	Oil
p	Phase index
RC	Reservoir conditions
s	Solution
STC	Stock tank conditions or standard conditions
w	Water

Operators

δu	$u_{n+1} - u_n$ (time)
Δu	$u_1 - u_2$ (space)
$\nabla \bullet \boldsymbol{u}$	Divergence of vector $\boldsymbol{u}$
∇u	Gradient of scalar u

1.0 INTRODUCTION

1.1 Raison d'être of the Research

At the present time, there are steam injection simulators that may be satisfactory if there are no sharp fronts for steamflood simulation. When it comes to cyclic steaming, simulators are suited best for single well modelling, but multiwell modelling is possible only with difficulties arising from the necessary adjustments of relative permeabilities, hysteresis, formation compressibility and grid size. Some adjustments may also be required for single wells; however, a radial grid system is better suited for representing a well.

Effective fieldwide cyclic steam stimulation simulation is still in the future when the next generation computers[1] become available. It is recognized in the industry that computational hardware/software allow for the inclusion of a limited number of wells in a thermal simulator[2]. Even at present, a fieldwide cyclic steam stimulation simulation requires a tremendous amount of computer storage and computation time. Yet, such a simulation customarily employs a rectilinear grid that is inadequate for simulating radial flow—an essential flow feature of cyclic steam stimulation—near the wells. In recognition of the fact that the next generation computers are nearby, the objective of this work is to develop a tool that will provide an effective fieldwide simulation. The existence of the next generation computers will not eliminate the need to have radial geometry around the wells.

The objective of this research is to develop a comprehensive cyclic steam stimulation simulator using present day modelling techniques. Stated simply:

> It is desired to develop a single well cyclic steam stimulation simulator that can be embedded into a fieldwide thermal simulator to improve the accuracy of flow calculations around the well. By embedding several wells into the thermal simulator, a fieldwide simulation of a steam project is possible.

---

[1] As an aside, a comment on the further development of hardware and software is appropriate here: "computing will grow more powerful, sophisticated and flexible by an order of magnitude in the next decade" and "the technology will become an intellectual utility, widely available, ultimately as ubiquitous as the telephone" (Peled (1987)).

[2] Recent work by Boberg *et al.* (1990, 1992) illustrates this point well—their study contained 4,500 rectangular grid blocks and up to only eight wells.

The areal model fails to provide an adequate simulation of reservoir conditions near the wellbore, hence the requirement for a well region model to be embedded into it.

In his textbook, Calhoun (1976) summarized the significance and the rôle of a well within the reservoir with the following statement. "The importance of the well itself cannot be overlooked. It is the means of access to the reservoir, the medium through which all measurements on the reservoir and its fluids are possible, and is the means of operational control on the reservoir. The number of wells in a reservoir, the position of these wells, and the manner in which they are completed and operated have a significant bearing upon the control of the individual reservoir." This is more relevant in cyclic steaming where complex heat transport is involved in addition to mass transport.

Furthermore, Peaceman (1977) pointed out that numerical reservoir simulation has gained wide acceptance as a result of an increase in computing speed and capacity, improvements in the numerical algorithms for solving the partial differential equations and the generality built into the simulators. These generalities have allowed for the studying of complex and realistic problems.

This intent of this research is to add to the tools available to the simulation engineer.

1.2 Model Description

This is the first model to use hyperhybrid grids in thermal simulation and the first to make available to the general public the use of hybrid grids in thermal simulation. A *hybrid* grid is defined as a cylindrical grid system embedded into a single fundamental rectilinear grid block and a *hyperhybrid*[1] grid is defined as a cylindrical grid system embedded into several contiguous fundamental rectilinear grid blocks. These grids are illustrated in Figure 1.2.0.1. Regions 1, 3 and 5 are hybrid while Regions 2, 4 and 6 are hyperhybrid grids. In addition, this is the first model, black oil or thermal, to offer hybrid and hyperhybrid grid regions that can be contiguous.

---

[1] This is the first introduction of the term *hyperhybrid* grid to the literature. The word "hyper" stems from the Greek "υπερ" meaning "more than".

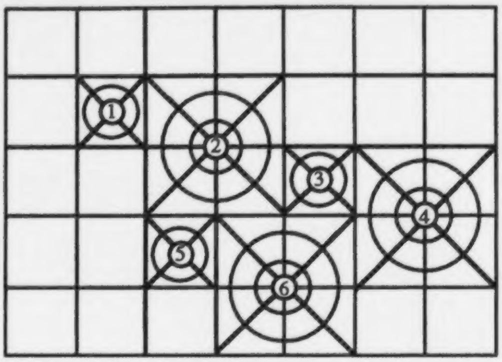

Hybrid Regions are 1, 3 and 5
Hyperhybrid regions are 2, 4 and 6

Figure 1.2.0.1 Illustration of hybrid and hyperhybrid grid refinement.

This model is a three-dimensional numerical reservoir simulator developed to study the usefulness of hybrid/hyperhybrid grids. The model is capable of simulating three-dimensional flow in both rectilinear and cylindrical coordinate systems along with the hybrid/hyperhybrid refinement options. Options are available to define the locations of the radial boundaries and node location. In addition, the well index in cylindrical coordinates can be calculated based on a user selected radius[1].

The model is capable of simulating hot waterflooding, cyclic steam stimulation and steam drive. In-situ combustion capabilities have not been included.

Mass and energy balance equations, along with constraint equations, are solved simultaneously. These equations are written in an implicit finite difference formulation. Some properties, such as gravity head, are calculated explicitly. The primary variables that are calculated implicitly are phase pressure, temperature, phase saturation, composition and bottom hole pressure. Muskat's extension of Darcy's law describes the multiphase flow of fluids and includes the effects of gravity, capillary and viscous forces. Heat is transported in the reservoir by convection and conduction and by vertical conduction in the over/underburden.

---

[1] Most models calculate the well index on the basis of the first grid block radius in a cylindrical coordinate system.

Phase partitioning of the components is through (equilibrium) K-values. The rock and fluid properties that depend on one or more primary variables are represented by simple equations and not tabular input. All components of the oleic phase can have their viscosity also as a function of an average grid block velocity so that non-Newtonian behaviour can be studied. In addition, the heavy oil component can be converted to a light oil component to represent visbreaking—this is done through the sink/source term. Section 4.1.2 summarizes the functional dependence of various parameters. An uncommon feature in reservoir simulation models is that all partial derivatives are obtained *analytically* with the exception of the gas supercompressibility factor.

Several basic injection and production controls are available: shut-in well, constant total volume injection well, constant flowing bottom hole pressure, specified oil rate and specified liquid rate. Others can be added easily.

The `FORTRAN NAMELIST` statement controls all data input. While there is some error checking of the data, it is very rudimentary. All input data are in metric units.

The model has the feature of automatic time step selection. There is a high degree of control of detailed output—it is possible to output all parameters and their derivatives for each Newton iteration. Several output files are created as input to a spreadsheet program used for plotting the results. The user has control of outer iteration convergence tolerances and time step selection parameters.

Initialization of the model can be done either manually or automatically. Heat loss is calculated using an analytical model. At the end of each time step, incremental and cumulative material and energy balances as well as residuals are calculated.

The system of equations is solved using Gaussian elimination for dense matrices for the smaller problems and the *Yale Sparse Matrix Package* for larger problems.

2.0 LITERATURE REVIEW

This section reviews the literature beginning with the methods of treatment for wells in a rectilinear grid using an analytical model, grid refinement and hybrid grids. The literature review also discusses briefly black oil and cyclic steam stimulation simulators. Following this, there are two sections dealing with coning and well modelling. A section comprising the topics of non-Newtonian flow and mild thermal cracking, or visbreaking, completes the literature review.

2.1 Methods of Representing Well Regions in Simulators

A reservoir simulation results in the determination of a pressure at a grid point that is the average pressure of the block surrounding the grid point. A well located in this grid block cannot use the calculated pressure of the grid block, particularly if the grid block is large. This problem is more of a concern for areal simulations where the grid block sizes can be quite large, and not so much of a concern for radial, single well problems.

Several techniques have been developed in the literature which attempt to solve the above problem. The solutions of note are: analytical well models, pseudofunctions, refined grids, locally refined grids, decoupled well coning models, hybrid grid (coupled well coning models), multigrid methods and dynamic orthogonal grid generation.

The areas of analytical well models, grid refinement and decoupled and coupled well coning models are discussed in this section. Additional details on these and the remaining areas can be found in the literature. Suggested sources are Aziz and Settari (1979), Behie and Forsyth (1981, 1982, 1983), Chappelear and Hirasaki (1976), Collins and Mourits (1991), Emanuel and Cook (1974), Heinemann and Brand (1989), Heinemann *et al.* (1991), Palagi and Aziz (1991), Sonier and Chaumet (1974), Starley (1988), Thomas (1983) and Woods and Khurana (1977). The area of dynamic orthogonal grid generation is one of active research.

2.1.1 Analytical Well Models

Schwabe and Brand (1967) showed that for multiphase flow in two dimensions, the relationships below can be used to "link the reservoir capacity in the vicinity of each well with the physical characteristics of the well and its production mechanism". The development begins with Equation 2.1.1.1, for the sake of simplicity. The radial form of Darcy's law including a skin factor, s , is

$$q = \frac{2\pi kh}{\mu} \frac{p_e - p_{wf}}{\ln(r_e/r_w) + s} , \tag{2.1.1.1}$$

where r_e is taken equal to Δx (grid block spacing), and p_e is obtained from

$$p_e = p_o + F_i \sum_{i=1}^{4} (p_i - p_o) . \tag{2.1.1.2}$$

Using the notation[1] of Peaceman (1978), F_i is an empirical drainage radius factor determining the influence of the pressures p_i in the horizontal plane and p_o is the simulator well block pressure. The summation is taken over the four blocks adjacent to the block containing the well, as is illustrated in Figure 2.1.1.1.

Equation 2.1.1.2 from Schwabe and Brand (1967) is an estimate of the pressure at the drainage radius for detailed calculations when many blocks are available. Hence, p_e is calculated from the pressures in blocks adjoining the block with the well. Schwabe and Brand (1967) did not define F_i, but Peaceman (1978) suggests that they imply it to be zero. Crichlow (1977) suggests that F_i lies between 0.5 and 0.7. Essentially, as F_i approaches zero, p_e approaches p_o. Hence, Equation 2.1.1.1 simplifies to

$$q = \frac{2\pi kh}{\mu} \frac{p_o - p_{wf}}{\ln(\Delta x/r_w)} , \tag{2.1.1.3}$$

---

[1] The original equation from Schwabe and Brand (1967) was

$$p_e = p_o + F_i \left[\frac{\sum_{j=1}^{4} (h\lambda)_j (p_j - p_o)}{\sum_{j=1}^{4} (h\lambda)_j} \right]_i .$$

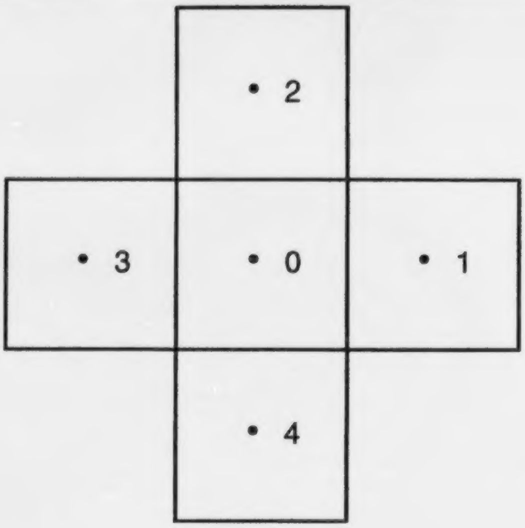

Figure 2.1.1.1

Block 0 containing a well and its four neighbouring blocks,
©SPE after Peaceman (1978).

in the absence of a skin effect.

By the use of large grid sizes, the fundamental flow equations are not represented correctly due to the use of difference equations to replace the differential equations. Difference equations represent discrete points whereas differential equations represent a continuum. The grid network represents a set of interconnected material balances with flow terms as a function of pressures and saturations (temperature and compositions should be included for completeness). Based on this realization, van Poollen *et al.* (1968) described a method of handling wellbores in models where grid sizes are many times the wellbore diameter.

van Poollen *et al.* (1968) calculated the average flowing pressure, or dynamic pressure in a circle with an area equivalent to that of a node (grid block). The pressure distribution is given by

$$p = p_{wf} + \frac{q\mu}{2\pi kh}\ln\left(r/r_w\right) \ . \tag{2.1.1.4}$$

This is the areal averaged pressure in the portion of the reservoir represented by the block. Integration over a circle with an area equal to that of the block with dimensions Δx by Δy yields

$$\overline{p} = p_{wf} + \frac{q\mu}{2\pi kh}\left[\ln(r_b/r_w) - \frac{1}{2}\right] , \tag{2.1.1.5}$$

where

$$\pi r_b^2 = \Delta x \, \Delta y \ . \tag{2.1.1.6}$$

If the grid blocks are square; that is, if $\Delta x = \Delta y$, then

$$r_b = \frac{\Delta x}{\sqrt{\pi}} \ . \tag{2.1.1.7}$$

van Poollen *et al.* (1968) made the basic assumption that the well block pressure is the same as the areal average pressure. Thus, Equation 2.1.1.5 can be written as

$$q = \frac{2\pi kh}{\mu} \frac{p_o - p_{wf}}{\ln\left(\dfrac{\Delta x}{r_w\sqrt{\pi}}\right) - \dfrac{1}{2}} \ . \tag{2.1.1.8}$$

A productivity index[1], *PI*, can be defined such that

$$q = \frac{PI\left(p_o - p_{wf}\right)}{\mu} , \tag{2.1.1.9}$$

where

$$PI = \frac{2\pi kh}{\ln\left(\dfrac{\sqrt{\Delta x \, \Delta y/\pi}}{r_w}\right) - \dfrac{1}{2}} \ . \tag{2.1.1.10}$$

This is similar to the productivity index defined by Coats *et al.* (1974) in the development of a three-dimensional steamflood simulator. For the sake of comparison, the skin effect term has been omitted from the denominator. These results were generalized by Odeh and Al Hussainy (1969) to relate field to model pressures for various shapes of drainage area, well location and grid configurations.

---

[1] The definition of productivity index usually includes the viscosity term.

In a brief paper, van Poollen *et al.* (1970) pointed out that in a reservoir model, a pressure for a grid block is calculated rather than for the well. On the other hand, the pressure for the well is usually measured in the field. Hence, it is usually necessary to modify either the field or grid block pressure for consistency. In general, it is easier to modify the field measurement than to correct the calculated model pressure.

The work of van Poollen *et al.* (1968) was the most significant on the treatment of wells until Peaceman (1978) showed that the well block pressure is equal to the actual flowing pressure at a radius of 0.2 times the grid spacing in a square configuration, and that it is not an average pressure for the block. Peaceman (1978) stated that this is the proper interpretation of the well block pressure. The calculation of the flowing bottom hole pressure can then be made using the equation for steady-state radial flow.

Defining r_o as the radius at which the steady-state flowing pressure for the actual well is equal to the numerically calculated pressure for the well block, gives

$$q = \frac{2\pi kh}{\mu} \frac{p_o - p_{wf}}{\ln(r_o/r_w)} \ . \tag{2.1.1.11}$$

Peaceman (1978) examined the solution of Laplace's equation near a single well by solving for the steady-state pressure distribution in a repeated five-spot pattern. A semi-log plot of the numerical solution for the various blocks versus a function of radius yielded a straight line with an intercept of

$$r_o = 0.2\,\Delta x \ . \tag{2.1.1.12}$$

A comparison of the Peaceman (1978) Equation 2.1.1.11 with Equation 2.1.1.8 of van Poollen (1968) shows that

$$\ln\left(\frac{\Delta x}{r_w\sqrt{\pi}}\right) - \frac{1}{2} = \ln\frac{r_o^A}{r_w} \ . \tag{2.1.1.13}$$

Equation 2.1.1.13 can be written as

$$r_o^A = \frac{\Delta x}{\sqrt{\pi}}\exp(-1/2) = 0.342\,\Delta x \ . \tag{2.1.1.14}$$

The result of Equation 2.1.1.14 is based on the assumption that the well block pressure is equal to the areal averaged pressure, which leads to the conclusion that the well block pressure is equal to the flowing pressure at 0.342 Δx, in contradiction of the result of Equation 2.1.1.12. By using an approximate calculation of the equivalent radius for an interior well in a uniform square, Peaceman (1978) showed that

$$\frac{r_o}{\Delta x} = \exp(-\pi/2) = 0.208 \ . \qquad (2.1.1.15)$$

Furthermore, Peaceman (1978), using an exact solution based on the work of Muskat (1937), showed that

$$0.194 < \frac{r_o}{\Delta x} < 0.198 \ , \qquad (2.1.1.16)$$

hence substantiating his result of Equation 2.1.1.12.

Au *et al.* (1980) stated Equation 2.1.1.1 as

$$q = \frac{2\pi khff_h}{\mu} \frac{p_o - p_{wf}}{\ln\left(f_g r_e / r_w\right) + s} \ , \qquad (2.1.1.17)$$

where $f_h \cdot h$ is the layer completion length and

$$r_e = \sqrt{\frac{\Delta x \, \Delta y}{\pi f}} \ . \qquad (2.1.1.18)$$

The geometrical factor f_g, first introduced by Peaceman (1978), accounts for the fact that p_o is not necessarily equal to the pressure at the effective radius. Note that Peaceman (1978) only considered a well at the centre of a square grid. The well factor fraction f, introduced in Equation 2.1.1.18, reduces the sensitivity of f_g to the geometrical location of the well within the grid block. The Au *et al.* (1980) definition of the geometrical factor differs from that of Peaceman (1978) by $(\pi f)^{0.5}$. Hence, Au *et al.* (1980) showed that the geometrical factor defined by Equation 2.1.1.15, that is $f_g = 0.208$, can be written as

$$f_g = \sqrt{\pi} e^{-\pi/2} = 0.37 \ . \qquad (2.1.1.19)$$

In general, Au *et al.* (1980) found that for various geometries, f_g is approximately 0.5.

Kuniansky and Hillestad (1980) obtained analytical solutions based on potential flow theory that can be applied to finite difference formulations that are based on five or nine points. The configurations considered were for one or two wells located in a rectangular area and for *n* wells located in an infinite area.

Peaceman (1982, 1983) extended his previous work from square grid blocks to rectangular grid blocks; that is, for the case where $\Delta x \neq \Delta y$. The same approach used to obtain Equation 2.1.1.15 for a non-square grid yields

$$\frac{r_o}{\Delta x} = \exp\left[\frac{\ln\alpha - \pi\alpha}{1+\alpha^2}\right], \qquad (2.1.1.20)$$

where α is the aspect ratio $\Delta y/\Delta x$. The effect of the aspect ratio was shown by Peaceman (1982, 1983) to be important. For an aspect ratio outside the range of 0.5 to 2, Equation 2.1.1.20 was shown to be invalid. The assumption made was that the pressures calculated for the blocks adjacent to the well block satisfy the radial flow equation.

Numerical solutions for single phase flow show that the effective well block radius is given by

$$r_o = 0.14\left(\Delta x^2 + \Delta y^2\right)^{0.5} \qquad (2.1.1.21)$$

for a uniform rectangular grid. Peaceman (1982, 1983) showed that the exact value of the constant in Equation 2.1.1.21 is $e^{-\gamma}/4$, where γ is Euler's constant.

In addition to the above, Peaceman (1982, 1983) showed that the equivalent well block radius for an anisotropic medium (where $k_x \neq k_y$) is given by

$$r_o = 0.28\frac{\left[\left(k_y/k_x\right)^{0.5}\Delta x^2 + \left(k_x/k_y\right)^{0.5}\Delta y^2\right]^{0.5}}{\left(k_y/k_x\right)^{0.25} + \left(k_x/k_y\right)^{0.25}}. \qquad (2.1.1.22)$$

Abou-Kassem and Aziz (1985) recognized that some important aspects of the computation of the flowing well bottom hole pressure from the pressure of the block containing the well are not treated adequately in the literature. They presented an analytical method for computing well block factors for a well located anywhere in a square or rectangular block, provided that the aspect ratio does not exceed that defined by Peaceman (1982, 1983). Abou-Kassem and Aziz (1985) divided the difficulties which can arise in reservoir simulators into two categories:

1. the block size is usually large compared to the diameter of the wellbore, and hence the pressure of the block computed by the simulator is not a good approximation for the well pressure, and
2. the complex interaction (coupling) between the reservoir and the wellbore in both injection and production wells can cause problems.

The equations provided by Abou-Kassem and Aziz (1985) can be used for either block-centred or point-distributed grids in five- and nine-point two-dimensional finite difference formulations. The equivalent well block radius is given by

$$r_o = \left\{ \exp(-2\pi f) \prod_i \left[r_{i,1}^{T_i} \prod_j \left(\frac{r_{i,j}}{a_j} \right)^{T_i} \right] \right\}^b , \tag{2.1.1.23}$$

where

$$b = 1 / \sum_i T_i \ . \tag{2.1.1.24}$$

The summation and the product over *i* are over all existing surrounding grid points, and the product over *j* is over all existing well images.

Equation 2.1.1.23 has been incorporated into a black oil model by Chang *et al.* (1989) to calculate the productivity index of a horizontal or slanted well. Their results were checked against the analytical treatment of transient wellbore pressure and found to agree within 4%. They claim that this was the first mathematical model to be validated for slanted well simulation.

Williamson and Chappelear (1981), in their two part paper, presented the theoretical background of well models. They also included the calculations of sandface pressure and saturation boundary conditions, going on to show how the well can be replaced, albeit approximately, by a source/sink function.

The diversity of the practical situations which require special consideration was illustrated by Williamson and Chappelear (1981). For incompressible single-phase flow, the cases of a single well anywhere in a grid block, several wells in a grid block, permeability contrast in adjacent grid blocks, and skin factor were discussed. As well, the more realistic cases of compressible single-phase, incompressible multiphase flow and a brief discussion of compressible multiphase flow were examined.

One of the effects of fluid compressibility is that the flow is not steady (the equation of mass conservation has a time derivative). There are two types of transient effects: the first being a step change in boundary pressure and the second is due to continuous change in bottom hole pressure. Williamson and Chappelear (1981), using perturbation analysis of near-well flow, defined the following dimensionless number which measures the ratio of transient to steady contributions to the well flow rate:

$$N_p = \frac{\phi \mu c_t \Delta x^2}{k t_{sc}} , \tag{2.1.1.25}$$

where

$$t_{sc} = \left| \frac{p_i - p_{wf}}{dp/dt} \right| = \left| \frac{p_i - p_{wf}}{d\left(p_i - p_{wf}\right)/dt} \right| . \tag{2.1.1.26}$$

By combining Equations 2.1.1.25 and 2.1.1.26, and writing as

$$N_p = \left| \frac{\phi \, \Delta x^2 h c_t \left(dp_{wf}/dt\right)}{\left(k/\mu\right) h \Delta x \left(p_i - p_{wf}\right)/\Delta x} \right| , \tag{2.1.1.27}$$

allows for an easier physical interpretation. In Equation 2.1.1.27, the numerator is a measure of the rate of change of fluid stored in the grid block and the denominator is a measure of the steady flow into the grid block. For $N_p << 1$, the flow is dominated by a steady contribution. Williamson and Chappelear (1981) suggest monitoring the value of N_p during a simulation.

For multiphase flow, the common practice is to introduce the concept of relative permeability. Thus, the flow equation can be written easily by substituting kk_{rp} for k. Equation 2.1.1.17 can be written as

$$q = \frac{2\pi k k_{rp} h f f_h}{\mu_p} \frac{p_o - p_{wf}}{\ln\left(f_g r_e / r_w\right) + s} \ . \tag{2.1.1.28}$$

Again, Williamson and Chappelear (1981), using perturbation analysis, defined a dimensionless quantity that is a measure of the ratio of the rate at which each phase is stored in the well block to the rate at which each phase flows into the well block. The quantity, N_{sp}, is given by

$$N_{sp} = \frac{\phi \Delta x^2}{\left(k k_{rp} / \mu_p\right)\left(p_i - p_{wf}\right)} \frac{dS_p}{dt} \ . \tag{2.1.1.29}$$

When N_{sp} is small, the flow may be considered to be steady.

Siu and Nghiem (1982) presented a model for the case of non-radial flow around a well resulting in an elliptical flow equation for vertical fractures.

Odeh (1983, 1985) determined an interpretation of field pressure data with respect to the simulator. It was concluded that, if the pressure drop component caused by skin is to be equal to the field determined value, it should be multiplied by the factor

$$\frac{\sum_{i}^{h} \Delta z_i k_i}{\overline{kh}} \ ,$$

where h is the length of the producing interval. In addition, Odeh (1983, 1985) presented an equation to determine the shut-in time necessary for the shut-in pressure of an actual well to be equal to the well block pressure of a simulator. Independently of Odeh (1983, 1985), Litlehamar and Larsen (1986) developed an equation for the buildup time at which the wellbore pressure matches the average kh of the simulator well block pressure of a two layer reservoir.

In a third paper, Peaceman (1987, 1990) presented methods of calculating the equivalent well block radius for several additional well geometries, the most notable being

1. two wells in adjacent or neighbouring well blocks,
2. a single well on or near the edge of the computing grid, and
3. a single well at or near the corner of the computing grid.

In addition, Peaceman (1987, 1990) stated that the analytical approach to calculating an equivalent well block radius assumes that the pressures calculated for the blocks adjacent to the well block are correct. The assumption is valid only for $\Delta y = \Delta x$, but for an aspect ratio $\Delta y/\Delta x$ equal to 1/2 or 2, it yields incorrect results unless the well is near the centre of the block. The highlights from the papers presented by Peaceman (1978, 1982, 1983, 1987, 1990) have been summarized by Peaceman (1988).

Carey and Chow (1987) derived the results of Peaceman (1978) by use of the concepts of the Mean Value Theorem and the Poisson Integral formulation to represent the solution of the well. The results obtained were more general in nature because it did not use any specific information related to the order of the difference scheme used to compute the grid point pressures.

Lee (1987, 1989) provided an analysis of the productivity of inclined wells for inclusion into a finite difference reservoir simulator. The paper presented the special cases of

1. an infinitely long horizontal well between two impermeable plane boundaries (a two-dimensional problem),
2. a well of finite length in an unbounded domain, and
3. an inclined well between two impermeable plane boundaries.

With these three cases, Lee (1987, 1989) examined the effects of reservoir boundaries, well location, formation thickness, inclination angle and anisotropic behaviour on well productivity.

Lee (1987, 1989) found that for two-dimensional flow problems, the Peaceman (1982, 1983) method was a good approximation provided an impermeable boundary was not too close to the well. For the case of three-dimensional flow, Peaceman's (1982, 1983) method may be erroneous. Reasonable results can be obtained for a horizontal or vertical well that are completed in several grid blocks. In addition, Lee (1987, 1989) showed that there is no accurate analytical formula to estimate the productivity of a well with an arbitrary inclination angle. Hence, a numerical method must be employed to estimate the productivity.

Further work in this area has been presented by Shiralkar (1988, 1989) for calculating the flowing well pressures in simulators using nine-point differencing. A rigourous, closed form expression for an isolated well, valid for nine-point differencing, is

$$r_o = 0.140365\left[\left(T_x + T_y\right)\frac{\Delta x\,\Delta y}{kh}\right]^{0.5} \qquad (2.1.1.30)$$

in a homogeneous and isotropic porous medium, while in an anisotropic porous medium the equivalent expression is

$$r_o = \frac{0.28073\left[\left(T_x + T_y\right)\frac{\Delta x\,\Delta y}{kh}\right]^{0.5}}{\left(k_x/k_y\right)^{0.25} + \left(k_y/k_x\right)^{0.25}} , \qquad (2.1.1.31)$$

where k is the effective isotropic permeability defined by

$$k = \sqrt{k_x k_y} \; . \qquad (2.1.1.32)$$

Results were presented for the cases of arbitrary location of a well in the well block and a well in an edge or corner block. Unlike the work of Peaceman (1982, 1983), Shiralkar (1988, 1989) concluded that the expression was valid for any grid aspect ratio.

The body of literature continues to grow quickly in the area of the representation of horizontal wells in numerical simulation. This topic is excluded from this review.

2.1.2 Grid Refinement Techniques

Irregular grids are used to increase the definition in regions where better control is required. This type of grid can have non-uniform spacing in both the x and y directions (Settari and Aziz (1972, 1974a)). Examples of where grid refinement can be used are near-wellbore effects and fractures in very large fields. In addition, numerical dispersion can be reduced through the use of finer grids in specific areas of the reservoir.

When grid refinement techniques were first used, the finely spaced mesh lines were extended throughout the simulator resulting in refinement in areas of the simulator which were not of interest. This caused an increase in computer time, storage and cost. There is also a change in the results of the simulation by the creation of preferential flow paths. Von

Rosenberg (1982) introduced to reservoir simulation, and tested, a method of localized grid refinement for use with finite difference techniques based on Taylor series expansions for constant coefficient problems. The conventional and locally refined grid systems are shown in Figures 2.1.2.1 and 2.1.2.2.

The local grid refinement technique introduces several configurations for use with finite difference analogs. Von Rosenberg (1982) used the following two rules to restrict the number of configurations to a manageable quantity:

1. if any two elements adjoining a third are refined, then the third element must be refined, and
2. if a smaller element adjacent to a larger one is refined, then the larger element must also be refined.

These rules were introduced originally for the refinement of finite elements by Bank and Sherman (1979). Examples of the implications of these rules are shown in Figure 2.1.2.3. The number of configurations imposed by these rules is only four. This is easy enough to manage. These configurations are shown in Figure 2.1.2.4.

For the *cross* configuration, the finite difference analogs for the first and second derivative of a dependent variable u are given by

$$\frac{\partial u}{\partial x} = \frac{u_2 - u_1}{2\Delta x} - \frac{\partial^3 u}{\partial x^3}\frac{(\Delta x)^2}{6} - \ldots \qquad (2.1.2.1)$$

and

$$\frac{\partial^2 u}{\partial x^2} = \frac{u_2 - 2u_o + u_1}{(\Delta x)^2} - \frac{\partial^4 u}{\partial x^4}\frac{(\Delta x)^2}{12} - \ldots \qquad (2.1.2.2)$$

for the x direction. Because all four distances are of equal length, the derivatives for the y direction are similar to Equations 2.1.2.1 and 2.1.2.2.

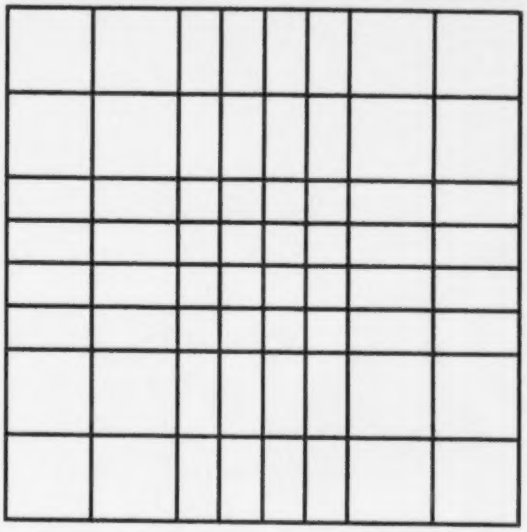

Figure 2.1.2.1 Refined mesh, ©SPE after von Rosenberg (1982).

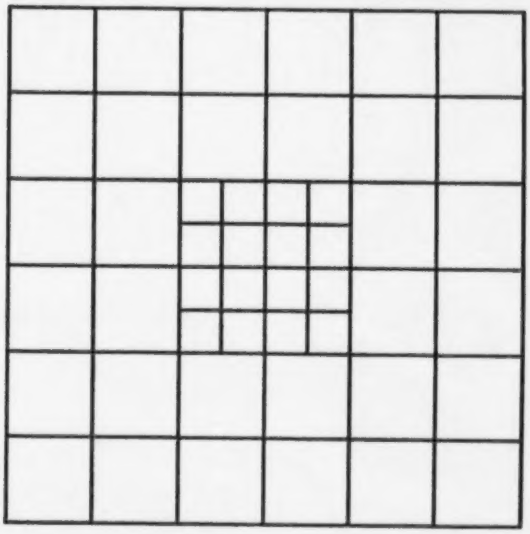

Figure 2.1.2.2 Locally refined mesh, ©SPE after von Rosenberg (1982).

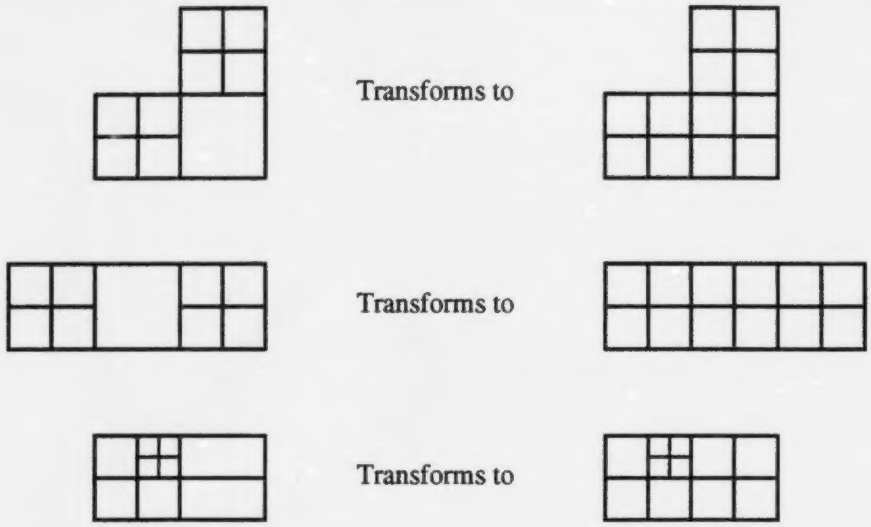
Transforms to
Transforms to
Transforms to

Figure 2.1.2.3 Effects of rules of refinement, ©SPE from von Rosenberg (1982).

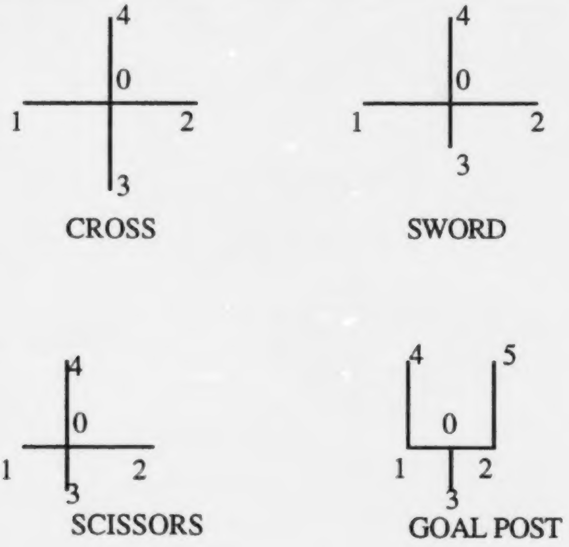
4
0
1
2
3
CROSS
4
0
1
2
3
SWORD
4
0
1
2
3
SCISSORS
4
5
0
1
2
3
GOAL POST

Figure 2.1.2.4 Configurations for analogs, ©SPE from von Rosenberg (1982).

For the *sword* configuration, the x direction distances are equal and hence the derivatives are given by Equations 2.1.2.1 and 2.1.2.2 above. For the y direction, one length is twice the other which yields the following for the first and second derivative analogs:

$$\frac{\partial u}{\partial y} = \frac{u_4 + 3u_o - 4u_3}{6\Delta y} - \frac{\partial^3 u}{\partial y^3}\frac{(\Delta y)^2}{3} + \cdots \qquad (2.1.2.3)$$

and

$$\frac{\partial^2 u}{\partial y^2} = \frac{u_4 - 3u_o + 2u_3}{3(\Delta y)^2} - \frac{\partial^3 u}{\partial y^3}\frac{\Delta y}{3} + \cdots \; . \qquad (2.1.2.4)$$

For the *scissors* configuration, one length is twice the other for both the x and y directions. The resulting equations are similar to Equations 2.1.2.3 and 2.1.2.4.

For the *goal post* configuration, the x direction derivatives are given by Equations 2.1.2.1 and 2.1.2.2; however, the y direction derivatives are given by

$$\frac{\partial u}{\partial y} = \frac{u_4 + u_5 + 8u_o - u_1 - u_2 - 8u_3}{12\Delta y} - \frac{\partial^3 u}{\partial x^2 \partial y}\frac{(\Delta x)^2}{6} - \frac{\partial^3 u}{\partial y^3}\frac{(\Delta y)^2}{3} + \cdots \qquad (2.1.2.5)$$

and

$$\frac{\partial^2 u}{\partial y^2} = \frac{u_4 + u_5 + 4u_3 - u_1 - u_2 - 4u_0}{6(\Delta y)^2} - \frac{\partial^3 u}{\partial x^2 \partial y}\frac{(\Delta x)^2}{3\Delta y} - \frac{\partial^3 u}{\partial y^3}\frac{\Delta y}{3} + \cdots \; . \qquad (2.1.2.6)$$

Note that this configuration is a new one that arises from local grid refinement. The other configurations are also present in conventional grid refinement techniques.

Von Rosenberg (1982) tested the effectiveness of local grid refinement by obtaining the finite difference solutions to the problem of a repeated five-spot pattern in a homogeneous reservoir with unit mobility. This analytical solution is from Muskat (1937). Von Rosenberg (1982) found that the type of refinement to be used for a particular reservoir problem will be a compromise between the cost of extra grid blocks and the accuracy desired.

Quandalle and Besset (1983) summarized the advantages of local grid refinement over both conventional simulators and simulators with traditional grid refinement. The design of grids for problems, such as faulted reservoirs, is complicated for conventional models. The result is usually a large number of inactive blocks. This can be complicated further if a multiple layer model is used. Traditional grid refinement simulators cause refinements in areas of the model where none is necessary. With local grid refinement, all inactive blocks can be withdrawn, thus leading to a grid system for which the number of grid blocks can be considered a minimum.

Quandalle and Besset (1983) obtained results using a black oil simulator (implicit in pressure, implicit in saturation) with a refined grid and compared them to those obtained with both coarse and fine grids. They concluded that the use of local grid refinement gives results comparable to a fine grid model. However, the running time of the refined model was much less than the fine grid model.

Heinemann *et al.* (1983) described an application of dynamic local grid refinement in a multiple application reservoir simulator. They concluded that the integration of local grid refinement into their model showed no significant differences in the numerical results in comparison to a conventional grid system. However, dynamic grid refinement enabled more accurate descriptions of the pressure and saturation relationships changing with time and space without increasing the number of grid blocks.

Forsyth and Sammon (1984, 1984a, 1985, 1986) and Forsyth (1984) continued to pursue the interest in local grid refinement initiated by Quandalle and Besset (1983) and Heinemann *et al.* (1983). It was shown that near-wellbore effects can be simulated more accurately without increasing the work. By using a method of variable implicitness with local grid refinement, large regions away from wells were handled easily with explicit methods while implicit methods were used near wellbores.

In a composite grid (composed of a conventional grid with local grid refinements), Quandalle and Besset (1985) found that the approximation of material exchange between two blocks by the classical two-point finite difference technique may be less accurate than that in a conventional grid system. This grid effect can be induced by computing flows between neighbouring blocks belonging to different sub-gridding levels. They eliminated this effect with a more sophisticated numerical scheme involving more than two points for the flow calculations. Two schemes were developed: nine-point and simplified five-point. Each scheme was incorporated into a black oil simulator using a sequential solution method. The simulator was designed for three-dimensional, three-phase flow for use in a large reservoir involving a composite grid system and "several thousands" of blocks.

There are two general types of local grid refinement techniques: fixed (or static) and dynamic. Wasserman (1987) developed a static local grid refinement technique for implementation into a three-dimensional, three-phase reservoir simulator to increase simulator accuracy without a significant increase in computing cost. The fixed technique is useful for problems with fractures, pinchouts and faults. Fixed methods are also used to treat flow around a wellbore.

Han *et al.* (1987) developed further a dynamic grid refinement technique which is useful in tracking the movement of a displacement front. Han *et al.* (1987) pointed out that the application proposed by Heinemann *et al.* (1983) is very restrictive and results in increased storage requirements and difficulty of use. The approach of Han *et al.* (1987) removes these restrictions and hence the storage requirements are decreased and the technique is easier to use.

The body of literature dealing with various aspects of grid refinement is growing rapidly; for example, Behie *et al.* (1984), Ewing (1988), Brand *et al.* (1989), Heinemann and Brand (1989), Biterge and Ertekin (1989, 1992) and Forsyth (1989, 1990). Furthermore, the body of literature dealing with local grid refinement extends into many areas of science and engineering; for example, Ciment and Sweet (1973), Markatos *et al.* (1986) and Fletcher (1988). It is beyond the scope of this work to present a comprehensive review of grid refinement.

2.1.3 Hybrid Grid Techniques

There are only a few published papers that discuss the use of hybrid grids. Hybrid grids consist of combining a radial/cylindrical grid to represent the well with a rectangular grid to represent the remainder of the reservoir. This was proposed first by Akbar *et al.* (1974) and Mrosovsky and Ridings (1974). More recently, another treatment of the subject has been made by Pedrosa (1984) and Pedrosa and Aziz (1985, 1986). Hybrid grid techniques may be thought of as extensions of the local grid refinement concept. Hybrid grids are used because of the shortcoming of inadequate description of the reservoir conditions by local grid refinement around a wellbore; that is, local grid refinement cannot take advantage of the radial (or nearly radial) flow nature around a wellbore.

Akbar *et al.* (1974) extended the ideas from the simulation of gas and water coning at individual wells described by MacDonald and Coats (1970) and Letkeman and Ridings (1970) by combining the radial simulation of individual wells with the conventional rectangular grid system of multiwell simulators. The mathematical model developed by Akbar *et al.* (1974) embeds a radial coordinate well simulator into a two-dimensional, three-phase rectangular simulation model. The areal model was a simple conventional simulator that accounts for variable grid spacing, effects of relative permeability, reservoir heterogeneity, anisotropy and structural dip. The radial model was a one-dimensional, three-phase model. The equation that formed the basis of the radial model was

$$\left(B_o - B_g R_s\right)\frac{\partial}{\partial r}\left[\frac{kk_{ro}r}{B_o\mu_o}\frac{\partial \Phi_o}{\partial r}\right] + B_g\frac{\partial}{\partial r}\left[\frac{kk_{ro}rR_s}{B_o\mu_o}\frac{\partial \Phi_o}{\partial r}\right] + B_g\frac{\partial}{\partial r}\left[\frac{kk_{rg}r}{B_g\mu_g}\frac{\partial \Phi_g}{\partial r}\right] + B_w\frac{\partial}{\partial r}\left[\frac{kk_{rw}r}{B_w\mu_w}\frac{\partial \Phi_w}{\partial r}\right]$$

$$= \frac{q_oB_o + q_{fg}B_g + q_wB_w}{2\pi \Delta rh} + r\phi\left[c_r + S_wc_w - \frac{S_o}{B_o}\frac{dB_o}{dP} - \frac{S_g}{B_g}\frac{dB_g}{dP} + \frac{S_oB_g}{B_o}\frac{dR_s}{dP}\right]\frac{\partial p}{\partial t}\ , \qquad (2.1.3.1)$$

where the symbols are defined in the Nomenclature.

Because the radial system is embedded into a rectangular grid system, Akbar *et al.* (1974) established the following criteria for equivalence of the two systems.

1. The pore volume of both systems must be equal; hence, the radius of the well model is given by a form of Equation 2.1.1.6:

   $$r_{i,j} = \sqrt{\Delta x_i\, \Delta y_j / \pi}\ , \qquad (2.1.3.2)$$

   where $r_{i,j}$ is the radius of a circle whose area is $\Delta x\, \Delta y$. Although only the case where $\Delta x_i = \Delta y_j$ was investigated by Akbar *et al.* (1974), their method should be applicable for the range of aspect ratio suggested by Peaceman (1982, 1983).
2. The volumetrically weighted average pressure within the radial model should equal the weighted average pressure in the areal model.
3. The summation of the fluxes into the four vertical faces of the well grid block is taken as the influx into the radial system.

Akbar *et al.* (1974) found that there was only a small increase in the computer time required for the hybrid model.

Mrosovsky and Ridings (1974) extended the work of Akbar *et al.* (1974) with the use of a two-dimensional cylindrical model embedded into a three-dimensional, rectangular grid reservoir model as illustrated in Figure 2.1.3.1. The well model was solved more frequently; that is, with smaller time step increments, than the areal reservoir model. The results obtained confirmed the need for this technique.

Both Akbar *et al.* (1974) and Mrosovsky and Ridings (1974) did not take into account the flows across the boundaries of the mixed geometry. Pedrosa (1984) and Pedrosa and Aziz (1985, 1986) presented a treatment of the irregularly shaped blocks which arise in hybrid grid systems.

Pedrosa (1984) and Pedrosa and Aziz (1985, 1986) applied a technique where an arbitrarily fine curvilinear orthogonal grid is used for the well region and a conventional rectangular grid is used for the remainder of the reservoir. Their model was designed as an abbreviated black oil model capable of handling only two phases. The well model is allowed to span many blocks of the rectangular grid but contiguous regions were not incorporated. By using an integral approach[1] to derive the flow equations and decoupling the various regions so that different levels of implicitness in the treatment of the transmissibilities can be used, it was possible to obtain satisfactory results for a black oil problem.

Because the reservoir model is now comprised of two different geometries, irregularly shaped blocks are created at the border between the two regions. The irregularly shaped blocks are bounded in the direction of flow by curvilinear and rectilinear surfaces. The flow through the curvilinear surface is either radial (cylindrical) or elliptical, depending on the reservoir properties being either isotropic or anisotropic, respectively. The external radius of the apparent radial block is given by

---

[1] The reader is referred to Aziz and Settari (1979) for a discussion of the Taylor series, integral and variational approaches available for the discretization of any given operator.

$$r_{i+\frac{1}{2}} = \sqrt{\frac{2A_{ij}}{\Delta\theta_j} + r_{i-\frac{1}{2}}^2}\ , \tag{2.1.3.3}$$

where A_{ij} is the area of the irregularly shaped block. The apparent length of the irregularly shaped block is given by

$$L_i = \frac{A_{ij}}{\Delta x_i}\ . \tag{2.1.3.4}$$

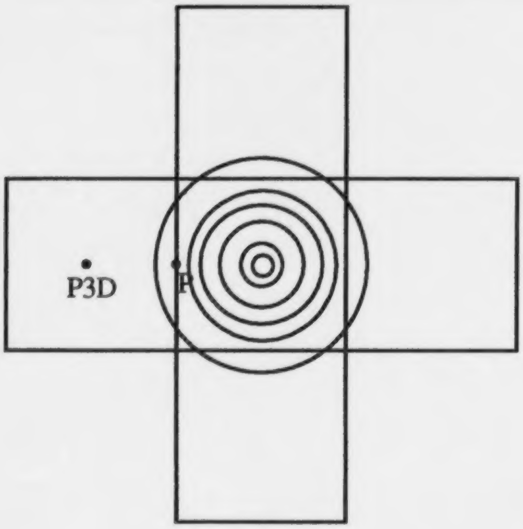

Figure 2.1.3.1

Relation of radial model to three-dimensional model—plan view, ©SPE after Mrosovsky and Ridings (1974).

Ewing and Lazarov (1988) and Ewing *et al.* (1989) have shown that hybrid grids can be incorporated as coning models in a full field scale application without destroying the efficiency of the original simulator. The numerical model used was a three-phase, fully implicit black oil simulator in which a cylindrical grid was incorporated into a global rectangular grid, using the geometry proposed by Pedrosa and Aziz (1985, 1986).

Ewing *et al.* (1989) have shown that the main difficulties of the Pedrosa and Aziz (1985, 1986) approximation lies at the irregular surfaces where a match is made in

Cartesian and cylindrical coordinate systems. The approximation approach used by Pedrosa and Aziz (1985, 1986) is based on the assumption that the potential is constant over a finite volume element. The matching approach described above leads to a symmetric system of equations with the approximation being $O\ (\Delta x^{0.5})$. Improvement can be made in the angular direction to $O\ (\Delta x^{1.5})$, but the symmetry of the system of equations is lost.

The above technique has been implemented, tested and released in a commercially available black oil simulator (Collins (1989)). This model allows for variable thickness/variable depth refinement and vertical subdivision of the Cartesian grid using the cylindrical grid. However, this model lacks both the hyperhybrid grid feature and regions cannot be contiguous. This model has confirmed that a hybrid grid has potential to be an efficient method to model more accurately large field scale problems.

Local and hybrid grid refinement are desirable and effective for fixed problems and have some promise for dynamic refinement. There is a need for better accuracy at the intersection of grids of different sizes (Ewing *et al.* (1989)).

Gottardi and Vignati (1990) presented the results of a simulation of a hypothetical three-dimensional, three-phase hybrid grid model. The approach was to use a fully implicit method (simultaneous solution method, SS) for the well region and a semi-implicit (implicit pressure explicit saturation, IMPES) method for the reservoir region. The well model equations were strongly coupled to the reservoir equations. The solution method consisted of two steps: solution of the flow equations for the entire reservoir using IMPES and a conventional rectangular grid, and solution of the well region equations by using SS with an orthogonal cylindrical/elliptical grid system. By using the pressures and saturations of the block surrounding the well block determined in the first step as boundary conditions, the second step was implemented. Finally, the well flow rates computed by the well model were then used as source/sink terms in the reservoir model. The advantages, compared to a conventional rectangular grid system, were summarized as possessing the potential to describe better the processes occurring around a well and the potential for saving computational work.

Hiebert *et al.* (1991) presented results of a study of a comparison of several methods for discretizing the near-wellbore region, among these being hybrid grids.

Although they presented results using a thermal simulator, this study was initiated prior to theirs. The hybrid grid used by Hiebert *et al.* (1991) was limited as was the Collins (1989) model; that is, no hyperhybrid refinement and regions which cannot be contiguous.

Hiebert *et al.* (1991) concluded that hybrid grids can model more accurately a thermal process with *fewer* grid blocks than can conventional rectilinear grids. As it was concluded by others for black oil models, Hiebert *et al.* (1991) concluded that hybrid grids model better near the wellbore. The near-wellbore region was found to be less important in the steamdrive process.

Hybrid grids are finding application in the simulation of horizontal wells. This literature review excludes these works; however, Collins *et al.* (1991) is a recent example.

2.2 Simulators

For the purpose of this report, only general comments on black oil and cyclic steam stimulation simulators are made. The subjects are treated well in the literature; for example, the text by Aziz and Settari (1979) considers the black oil model almost exclusively.

2.2.1 Black Oil Simulators

The basic equations in a black oil simulator describe the flow of oil, water and gas through a porous medium where the wetting fluid is usually the water, oil has an intermediate wettability and the gas is the non-wetting phase. It is assumed that the oil and water are immiscible, there is no mass exchange between these two phases and there is no phase change. Furthermore, gas is assumed to be soluble in the oil. Details may be found either in Aziz and Settari (1979), in Peaceman (1977) or in Mattax and Dalton (1990a).

The pressure-volume-temperature behaviour of the three phases is given by the following equations:

$$B_o = \frac{\left[V_o + V_{dg}\right]_{RC}}{\left[V_o\right]_{STC}} = f(p_o) \ , \qquad (2.2.1.1)$$

$$B_w = \frac{[V_w]_{RC}}{[V_w]_{STC}} = f(p_w) \ , \qquad (2.2.1.2)$$

and

$$B_g = \frac{[V_g]_{RC}}{[V_g]_{STC}} = f(p_g) \ , \qquad (2.2.1.3)$$

where V represents the volume of the various phases at stock tank conditions (STC) or reservoir conditions (RC). Note that these formation volume factors are functions of pressure.

The mass exchange between the oil and gas phases is given by

$$R_s = \left[\frac{V_{dg}}{V_o}\right]_{STC} = f(p_o) \ , \qquad (2.2.1.4)$$

which is the solution gas-oil ratio. This ratio gives the amount of gas dissolved in the oil as a function of the oil phase pressure. The phase densities are given by the following relationships:

$$\rho_o = \frac{1}{B_o}\left(\rho_{oSTC} + R_s\rho_{gSTC}\right) \ , \qquad (2.2.1.5)$$

$$\rho_w = \frac{1}{B_w}\left(\rho_{wSTC}\right) \ , \qquad (2.2.1.6)$$

and

$$\rho_g = \frac{1}{B_g}\left(\rho_{gSTC}\right) \ . \qquad (2.2.1.7)$$

The equations for the oil, water and gas phases are given by:

$$\nabla \bullet \left[\frac{1}{B_o}\frac{kk_{ro}}{\mu_o}(\nabla p_o + \rho_o \mathbf{g})\right] = \frac{\partial}{\partial t}\left[\frac{1}{B_o}\phi S_o\right] + q_o \ , \qquad (2.2.1.8)$$

$$\nabla \bullet \left[\frac{1}{B_w}\frac{kk_{rw}}{\mu_w}(\nabla p_w + \rho_w \mathbf{g})\right] = \frac{\partial}{\partial t}\left[\frac{1}{B_w}\phi S_w\right] + q_w \ , \qquad (2.2.1.9)$$

and

$$\nabla \bullet \left[\frac{R_s}{B_o} \frac{kk_{ro}}{\mu_o} (\nabla p_o + \rho_o \mathrm{g}) \right] + \nabla \bullet \left[\frac{1}{B_g} \frac{kk_{rg}}{\mu_g} (\nabla p_g + \rho_g \mathrm{g}) \right]$$
$$= \frac{\partial}{\partial t} \left[\frac{R_s}{B_o} \phi S_o + \frac{1}{B_g} \phi S_g \right] + q_{fg} + R_s q_o \ , \tag{2.2.1.10}$$

respectively. Note that

$$\rho \mathrm{g} = -\gamma \nabla z \ , \tag{2.2.1.11}$$

if the coordinate in the vertical downward direction is positive.

2.2.2 Cyclic Steam Stimulation Simulators

The equations describing steam stimulation and steamflooding have been discussed extensively in the literature. A good source of reference is the work by Coats *et al.* (1974), Coats (1976, 1978, 1980) or Kasraie (1987). The mathematical model consists of a set of mass and energy balance equations along with constraint equations for the fluid saturations of the phases and the mole fractions of the components. Note that the mass balance equations and the fluid saturation equation are extensions of those for a black oil system. For a system consisting of N_c components and N_p phases, the total number of equations is given by:

- N_c components mass balance equations,
- 1 energy balance equation,
- N_p mole fraction constraint equations, and
- 1 fluid saturation constraint equation,

for a total of $N_c + N_p + 2$.

Using the notation of the above cited references, the component mass balances for $i = 1, 2, ..., N_c$ are given by

$$\frac{V}{\Delta t} \delta \left[\phi \sum_{p=1}^{N_p} \rho_p S_p x_{ip} \right] = \sum_{p=1}^{N_p} \Delta \left[T \rho_p x_{ip} \frac{k_{rp}}{\mu_p} \left(\Delta p_p + \Delta P_{cp} - \gamma_p \Delta z \right) \right] - q_i \ , \tag{2.2.2.1}$$

the energy balance is given by

$$\frac{V}{\Delta t}\delta\left[\phi\sum_{p=1}^{N_p}\rho_p S_p U_p+(1-\phi)M_f(\theta-\theta_r)\right]$$

$$=\sum_{p=1}^{N_p}\Delta\left[T\rho_p H_p\frac{k_{rp}}{\mu_p}\left(\Delta p_p+\Delta P_{cp}-\gamma_p\Delta z\right)\right]+\Delta(T_c\,\Delta\theta)+\Delta\left(T_R\,\Delta\theta^4\right)-q_H-q_{loss}\ , \quad (2.2.2.2)$$

the saturation constraint is given by

$$\sum_{p=1}^{N_p}\delta S_p=0\ , \quad (2.2.2.3)$$

and the mole fraction constraints are given by

$$\sum_{i=1}^{N_c}\delta x_{ip}=1 \quad (2.2.2.4)$$

for $p = 1, 2, \ldots, N_p$. The difference notations are given by the following expressions:

$$\delta X = X_{n+1}-X_n \quad (time)\ , \quad (2.2.2.5)$$

$$\Delta X = X_1 - X_2 \quad (space)\ , \quad (2.2.2.6)$$

$$\Delta(T\,\Delta X)=\Delta_X(T_X\,\Delta_X X)+\Delta_Y(T_Y\,\Delta_Y X)+\Delta_Z(T_Z\,\Delta_Z X)\ , \quad (2.2.2.7)$$

and

$$\Delta_X(T_X\,\Delta_X X)=T_{Xi+\frac{1}{2}}(X_{i+1}-X_i)-T_{Xi-\frac{1}{2}}(X_i-X_{i-1})\ , \quad (2.2.2.8)$$

where $T_{Xi+1/2}$ is the x-direction transmissibility for flow between grid blocks i and i+1 and n is the time step level. The reader should consult the references cited above for further details of steamflood simulation.

2.3 Coning

Because this work involves radial flow about a well, it is appropriate that a brief review of coning be included. Only the bellwethers are presented, although there is a fair amount of literature available. Coning in this context refers to near-well flow behaviour.

Coning simulations typically suffer from severe saturation instabilities around the well. This usually results in rather small time steps being required to ensure stability;

however, larger time steps can be taken if the problem is formulated implicitly. Weinstein *et al.* (1986) presented the results of a difficult coning problem by eleven different simulators.

Blair and Weinaug (1969) used an implicit formulation of the flow equations and showed that a significant increase in time step size was permissible while still maintaining stability. This was confirmed by Spivak and Coats (1970) with the use of implicit production terms in the difference equations. Letkeman and Ridings (1970) extrapolated implicitly the production rates and mobilities to increase the stability of the problem.

MacDonald and Coats (1970) investigated three numerical methods for coning simulation. The first method used an implicit pressure-explicit saturation (IMPES) formulation with implicit flow terms, The second method used the IMPES formulation, but treated the interblock transmissibilities implicitly. The final method was a fully implicit formulation. It was concluded that the implicit transmissibilities allowed for a larger time step, while a fully implicit formulation could use the largest time step. Each of the cases studied have advantages over the others depending on the magnitude of capillary forces, grid spacing, time step size desired, stability and computing time/ efficiency.

Nolan and Berry (1972) approximated the relative permeabilities using a semi-implicit approximation. They also presented a method of allocating production in a multiple grid block case. Nolan and Berry (1972) concluded that the semi-implicit approximation is highly stable and converges quickly. Sonier *et al.* (1973) included the outlet effect and compatibility condition at the well[1] but the pressure drop due to friction in the wellbore was not included. The outlet effect and compatibility condition were incorporated into a model, using a sequential solution method, by Ko *et al.* (1980).

2.4 Special Topics

This section covers briefly the topics of non-Newtonian fluids and mild thermal cracking effects. Sufficient conceptual background is provided here for the development of simple mathematical representations.

---

[1] Settari and Aziz (1974) recommend that these effects be included. The outlet effect requires that the capillary pressure approach zero at the sand face. The compatibility condition requires that the vertical pressure gradient in the well be the same as the pressure gradient at the reservoir/wellbore boundary.

2.4.1 Non-Newtonian Fluids

Newton's law of viscosity states that the shear force per unit area is proportional to the negative of the local velocity gradient:

$$\tau_{yx} = -\mu \frac{dv_x}{dy} \ . \tag{2.4.1.1}$$

Fluids which obey this law are termed Newtonian fluids. Equation 2.4.1.1 can be generalized in the following form:

$$\tau_{yx} = -\eta \frac{dv_x}{dy} \ , \tag{2.4.1.2}$$

where η can be expressed as either a function of dv_x/dy or τ_{yx}. Pseudoplastic behaviour is characterized by η decreasing with increasing rate of shear, and dilatant behaviour is characterized by η increasing with increasing rate of shear. Equation 2.4.1.2 reduces to Newton's law when η is equal to μ.

The rheological behaviour of fluids can be modelled in several ways, the most familiar being the Bingham and Ostwald-de Waele models[1] given by:

$$\tau_{yx} = -\mu_o \frac{dv_x}{dy} \pm \tau_o \qquad \text{if } |\tau_{yx}| > \tau_o \tag{2.4.1.3}$$

and

$$\frac{dv_x}{dy} = 0 \qquad \text{if } |\tau_{yx}| < \tau_o \ , \tag{2.4.1.4}$$

for the Bingham model, and

$$\tau_{yx} = -m \left| \frac{dv_x}{dy} \right|^{n-1} \frac{dv_x}{dy} \tag{2.4.1.5}$$

for the Ostwald-de Waele model, more commonly known as the Power Law model. For the case where m is equal to μ and n is equal to unity, Equation 2.4.1.5 reduces to

---

[1] The reader is referred to Bird, Stewart and Lightfoot (1960) and Savin (1969) for a more complete discussion of non–Newtonian fluids and to Reid, Prausnitz and Sherwood (1977) or Reid, Prausnitz and Poling (1987) for a discussion of Newtonian fluids. Pascal (1990) discusses the question of the rheological effects of non–Newtonian fluids on non–isothermal flow through porous media.

Newton's law of viscosity given by Equation 2.4.1.1. These two models have parameters which may be functions of temperature, pressure, composition and shear. Some fluids show a change in viscosity with time; those that have a decrease in η with time are termed thixotropic and those that increase with time are rheopectic.

The viscosity of a liquid is a function of temperature, pressure and composition if the oil is Newtonian. For a non-Newtonian liquid, the shear rate adds another dependency. Poon and Kisman (1991) observed that the non-Newtonian behaviour depends on factors such as temperature, low/high shear rate, sand content and emulsion type.

The viscosity of a liquid decreases with increasing temperature and this dependence can be represented by relationships such as the Andrade[1] equation:

$$\mu_L = Ae^{B/\theta} \, , \tag{2.4.1.6}$$

or the more general equation

$$\mu_L f_1 = A\exp\left(\frac{Bf_2}{\theta}\right) , \tag{2.4.1.7}$$

where f_1 and f_2 are correlation functions. Other modifications are available in the literature, but the most commonly used is the Andrade equation for showing the effect of temperature on liquid viscosity except at low temperatures where the Antoine equation performs better:

$$\mu_L = A\exp\left(\frac{B}{\theta + C}\right) . \tag{2.4.1.8}$$

Reid *et al.* (1987) suggested a correlation for estimating the effects of increasing pressure on the liquid viscosity. Beggs and Robinson (1975) introduced a set of expressions for determining the viscosity of dead oil and live oil. Using a modified version of the Arrhenius equation, Shu (1984) presented a correlation for a binary mixture of a heavy crude oil with a lighter petroleum solvent. The prediction of viscosity of binary mixtures can be found with this correlation where the only required information is the density and viscosity of the components.

---

[1] Reid, Prausnitz and Poling (1987) provides a good summary of the viscosity of liquids.

The apparent viscosity of a non-Newtonian fluid can be represented by

$$\mu = F(v') \, , \tag{2.4.1.9}$$

where F is some function of shear rate v'. For example, the following represents the viscosity for a Power Law fluid:

$$\mu_o = \mu_{o\,Newtonian} v' \, . \tag{2.4.1.10}$$

By definition, the length of a vector, or modulus, is given by

$$|a| = \sqrt{a_1^2 + a_2^2 + a_3^2} \, . \tag{2.4.1.11}$$

The average velocity of a fluid in a grid block can be calculated from (Kasraie and Farouq Ali (1989)):

$$\frac{\bar{q}_o}{A} = \left\{ \left[\left(\frac{\bar{q}_o}{A} \right)_{i+1,j,k} + \left(\frac{\bar{q}_o}{A} \right)_{i-1,j,k} \right]^2 + \left[\left(\frac{\bar{q}_o}{A} \right)_{i,j+1,k} + \left(\frac{\bar{q}_o}{A} \right)_{i,j-1,k} \right]^2 \right.$$
$$\left. + \left[\left(\frac{\bar{q}_o}{A} \right)_{i,j,k+1} + \left(\frac{\bar{q}_o}{A} \right)_{i,j,k-1} \right]^2 \right\}^{0.5} \, , \tag{2.4.1.12}$$

from which the average velocity can now be calculated using

$$\bar{v} = \frac{\bar{q}_o}{A\phi} \, . \tag{2.4.1.13}$$

The model presented by Gogarty (1967) was incorporated into this model. Following the development of Gogarty (1967), the characteristic length, as defined by McKinley *et al.* (1966), in a porous medium can be expressed as

$$l = f(k)\sqrt{\frac{k}{\phi}} \, , \tag{2.4.1.14}$$

where $f(k)$ is affected by the pore size distribution and tortuosity of the porous medium, which in turn are functions of permeability. Combining Equations 2.4.1.13 and 2.4.1.14 gives

$$\overline{v}' = \frac{\overline{v}}{l} = \frac{\dfrac{\overline{q}_o}{A\phi}}{f(k)\sqrt{\dfrac{k}{\phi}}} \ , \tag{2.4.1.15}$$

which can be generalized as

$$\overline{v}' = \left[\frac{B\overline{v}}{f(k)\sqrt{\dfrac{k}{\phi}}} \right]^y \ , \tag{2.4.1.16}$$

where B and y are experimentally determined constants. Other variations of Equation 2.4.1.16 are given in Odeh and Yang (1979). Gogarty (1967) determined experimentally that the functional form of $f(k)$ was

$$f(k) = m \log \frac{k}{k_r} + p \ , \tag{2.4.1.17}$$

where m and p are constants, k is the specific permeability and k_r is the reference permeability. Equation 2.4.1.17 shows that $f(k)$ is a linear function of the logarithm of the permeability. Gogarty (1967) concluded that this function accounts, only partially, for the type of shear field existing between a non-Newtonian fluid and the porous medium. Equation 2.4.1.9 was written as

$$\mu_o = F(v') = \frac{\mu_{o\ Newtonian}}{l(v') + \dfrac{\mu_{o\ Newtonian}}{K \cdot (v')^n} h(v')} \ , \tag{2.4.1.18}$$

where the functions $l(v')$ and $h(v')$ are given by

$$l(v') = \frac{1}{1 + (av')^s} \tag{2.4.1.19}$$

and

$$h(v') = \frac{1}{1 + \left(b/v' \right)^s} \ , \tag{2.4.1.20}$$

respectively.

There are other correlations available in the literature. Chew and Connally (1959) presented a correlation to predict the viscosity of gas saturated crudes at reservoir conditions. Lohrenz *et al.* (1964) developed a procedure to calculate the viscosity of gases and liquids as a function of their composition. Little and Kennedy (1968) developed an equation that accounted for pressure, temperature and composition. Houpeurt and Thelliez (1974) also developed a procedure for determining viscosity of liquids from their compositions. Recently, Egbogah and Ng (1990) presented an improved form of the Beggs and Robinson (1975) correlation, Closmann and Seba (1990) correlated viscosity with molecular weight and Abdul-Majeed *et al.* (1990) presented a correlation for estimating the viscosity of undersaturated crudes as a function of pressure, bubble point pressure, bubble point viscosity, solution gas-oil ratio at the bubble point and API gravity. Mehrotra (1991) presented an approach to model the viscosity of a diluent-bitumen mixture, as a function of temperature and composition, based on a two-parameter viscosity-temperature correlation and an additive viscosity mixing rule.

2.4.2 Mild Thermal Cracking/Visbreaking

A permanent reduction in oil viscosity can often accompany steam recovery processes, where the oil has been exposed to mild thermal cracking conditions (Henderson and Weber (1965), Venkatesan and Shu (1986)). Shu and Hartman (1986) have found that numerous heavy oils experience significant visbreaking, or mild thermal cracking, at temperatures in the range of 260–370 °C. Mild thermal cracking is characterized by some decomposition, minimum coke formation and retention of products in the liquid phase.

Mild thermal cracking can be represented by

$$A \xrightarrow{k'} B \,, \tag{2.4.2.1}$$

which is a first-order reaction. The conversion of heavy oil is a representation of the extent of mild thermal cracking and is given by

$$\frac{dC_A}{dt} = -k' C_A \tag{2.4.2.2}$$

in differential form, or

$$C_A = C_{iA} \exp\left[-\int_0^t k' dt \right] . \tag{2.4.2.3}$$

The reaction rate constant, *k'*, is given by the Arrhenius equation:

$$k' = w \exp(-E/R\theta) . \tag{2.4.2.4}$$

Shu and Hartman (1986) reported an Arrhenius constant, *w*, of 2.952 x 10^{11} day^{-1} and activation energy, *E*, of 31,800 cal/g mol for a Cold Lake crude. Substitution of Equation 2.4.2.4 into Equation 2.4.2.3 yields

$$\frac{C_{iA} - C_A}{C_{iA}} = 1 - \exp\left[-w \int_0^t \exp(-E/R\theta) dt \right] . \tag{2.4.2.5}$$

Shu and Hartman (1986) pointed out that the crude oil experiences various degrees of cooling and heating during a mild thermal recovery process with the result that the temperature history of the oil is a complex function of time. This leads to the impossible task of evaluating the integral in Equation 2.4.2.5. Shu and Hartman (1986) concluded that the mechanisms that affect oil recovery are the lowering of the oil phase viscosity and the creation of a transition zone with a more favourable mobility ratio for the displacement process.

Recent work by Samadi and Hill (1987) and Mazza and Cormack (1988, 1988a) present laboratory data for Saskatchewan heavy oil and Athabasca bitumen, respectively. Monin and Audlbert (1988) studied the alteration of four crudes with different geochemical compositions in the presence of water and a mineral matrix representation of the reservoir porous medium. They observed the formation of significant amounts of insoluble organic material. Fassihi *et al.* (1990) present the results of a study on an immature heavy oil and two biodegraded crudes. It was observed that permanent reductions in viscosity and density begin at temperatures above 260 °C, then became more pronounced at temperatures above 343 °C.

Kasraie and Farouq Ali (1989) represented the mild thermal cracking process by a viscosity reduction in a steam simulator. It was concluded that mild thermal cracking would not be significant in steamfloods of short duration, but it might play a role in longer term projects. They recommended including mild thermal cracking effects in a steam simulator.

3.0 STATEMENT OF THE PROBLEM

The intent of this research is to provide the engineer with a useful tool for understanding and enhancing cyclic steaming performance, especially when interference between wells is occurring. With today's computers, a fieldwide steam injection simulation which contains a large number of wells is not practical due to the large number of grid blocks. The intent of this research is to provide an approach that will make a fieldwide steam injection simulation to be more feasible.

3.1 Statement of the Problem

It was stated in the Introduction that the objective of this research is to develop a single well cyclic steam stimulation simulator that can be embedded into a fieldwide steam injection simulator. The design of the following is required.

- A numerical reservoir simulator with steam injection capabilities will be written. The development will be from first principles. This model is to have the features described in the Introduction.
- A new "hyperhybrid grid" region approach, as defined in the Introduction and illustrated in Figure 1.2.0.1 (page 3), to represent the flow around a thermal well in the reservoir more accurately will be developed. Moreover, the option of contiguous hyperhybrid regions to represent the flow between wells will be included in the design of the simulator.

In order to demonstrate the application potential of contiguous hyperhybrid grid refinement, the following applications will be made.

- Local well effects will be studied in the context of cyclic steam stimulation using hyperhybrid grid refinement.
- The interwell interference problem of multiple cyclic steam stimulations using contiguous hyperhybrid grid refinement will be studied using both pressure interference analysis and multiwell cyclic steaming.
- Using contiguous hyperhybrid grid refinement, the conversion from cyclic steaming to continuous steaming operations will be studied.

Hyperhybrid grids will allow one to study well regions of different sizes and contiguous hyperhybrid regions will allow one to design a grid better suited to problems with interwell interference.

4.0 MODEL DEVELOPMENT

In the creation of a reservoir simulator, there are three distinct models that are developed—mathematical, numerical and computer models. In the mathematical model, the physics of the system is expressed in appropriate mathematical equations, usually partial differential equations. The partial differential equations are, in general, nonlinear. The mathematical description is usually completed with a set of constraint equations, initial conditions and boundary conditions. Generally, these equations are too complex to be solved analytically.

This leads to the numerical model. This model puts the equations in a form that allows the use of a computer to solve a large system of simultaneous linear algebraic equations. In this model, this is accomplished by a Taylor series expansion of the derivatives. Other methods were mentioned in Chapter 2.

The computer model is a set of instruction code, typically and historically FORTRAN in reservoir simulation, used to solve the system of simultaneous linear algebraic equations developed.

4.1 Mathematical Model

In the development of the mathematical model, there are, in general, three balance equations of interest: the mass (or mole) balance of a component, the momentum balance of a phase and the total energy balance of a phase. Appendix I provides the mathematical development of each of these balance equations. In this section is a summary of the assumptions used in the development.

4.1.1 Summary of Equations and Unknowns

The combined continuity/momentum balance equations are given by

$$\nabla \cdot \sum_{p=w,o,g} \frac{K_{vip} X_i \rho_p k k_{rp}}{\mu_p} \left(\nabla p_p - \rho_p g \nabla D \right) = \frac{\partial}{\partial t} \left[\phi \sum_{p=o,w,g} K_{vip} X_i \rho_p S_p \right] + \tilde{q}_i \; , \qquad (4.1.1.1)$$

and the energy balance equation is given by

$$\nabla \bullet \sum_{p=w,o,g} \frac{H_p \rho_p k k_{rp}}{\mu_p} \left(\nabla p_p - \rho_p g \nabla D \right) + \nabla \bullet \left(\lambda_c \nabla \theta \right) = \frac{\partial}{\partial t} \left[(1-\phi) M_f \Delta \theta + \phi \sum_{p=o,w,g} S_p \rho_p E_p \right] + \tilde{q} \ . \qquad (4.1.1.2)$$

Auxiliary equations consist of the saturation constraint,

$$\sum_{p=w,o,g} S_p = 1 \ , \qquad (4.1.1.3)$$

and the mole fraction constraints

$$\sum_{i=1}^{N_c} x_{ip} = \sum_{i=1}^{N_c} K_{vip} X_i = 1 \qquad p = w,o,g \ . \qquad (4.1.1.4)$$

In addition, the capillary pressure equations are, for a water-wet porous medium,

$$P_{cow} = p_o - p_w \qquad (4.1.1.5)$$

and

$$P_{cgo} = p_g - p_o \ . \qquad (4.1.1.6)$$

The auxiliary equations complete the set of equations for a total of N_c combined continuity/momentum balance equations, 1 energy balance equation, (N_p-1) capillary pressure equations, 1 saturation constraint and N_p mole fraction constraints for a total of (N_c+2N_p+1) equations. The unknowns for this problem are p_o, p_w, p_g, S_o, S_w, S_g, θ and X_i for a total of (N_c+2N_p+1) unknowns.

By combining the continuity/momentum balance equations and capillary pressure equations, the number of equations reduces to N_c combined continuity/momentum balance equations, 1 energy balance equation, 1 saturation constraint,and N_p mole fraction constraints for a total of (N_c+N_p+2) equations. The unknowns for this problem are p_o, S_w, S_o, S_g, θ and X_i for a total of (N_c+N_p+2) unknowns.

Aziz and Wong (1988) provide an exhaustive list of equations and variables for a multipurpose reservoir simulation model.

4.1.2 Functional Relationships

The functional relationships for the variables are

$$\rho = \rho(p, \theta, X) \ , \tag{4.1.2.1}$$

$$\mu = \mu(p, \theta, X) \ , \tag{4.1.2.2}$$

$$k_{rw} = k_{rw}(S_w, \theta) \ , \tag{4.1.2.3}$$

$$k_{ro} = k_{ro}(S_w, S_g, \theta) \ , \tag{4.1.2.4}$$

$$k_{rg} = k_{rg}(S_g, \theta) \ , \tag{4.1.2.5}$$

$$P_{cow} = P_{cow}(S_w, \theta, X) \ , \tag{4.1.2.6}$$

$$P_{cgo} = P_{cgo}(S_g, \theta, X) \ , \tag{4.1.2.7}$$

$$\phi = \phi(p) \ , \tag{4.1.2.8}$$

$$E = E(p, \theta, X) \ , \tag{4.1.2.9}$$

$$H = H(p, \theta, X) \ , \tag{4.1.2.10}$$

$$C_p = C_p(\theta) \ , \tag{4.1.2.11}$$

$$L_v = L_v(\theta) \ , \tag{4.1.2.12}$$

$$\lambda_c = \text{constant} \ , \tag{4.1.2.13}$$

and

$$K_{vip} = K_{vip}(p, \theta) \ . \tag{4.1.2.14}$$

4.1.3 Summary of Assumptions

In the development of the mathematical model above, the assumptions that have been made are summarized below. The assumptions that are made for the continuity equations are:

- the control volume is representative of the porous medium,
- component *i* does not react with the matrix material,
- Δx, Δy and Δz are invariant with time,
- phase equilibrium is attained instantaneously,
- diffusion/dispersion effects are negligible,
- no chemical reactions occur, and
- there is no rock dissolution.

The assumptions that must be made for Darcy's law to be valid are:

- the entire pore space of the reservoir material is filled with the fluid flowing (modified for multiphase flow by introducing the concept of relative permeability),
- $\vec{v}_p$ is not an actual, but an apparent, velocity equivalent to $\vec{q}/A$,
- the fluid is homogeneous,
- there are no chemical reactions occurring between the porous medium and the fluid,
- the permeability is independent of fluid, temperature, pressure and location,
- the flow is laminar and viscous,
- there are no electrokinetic effects[1],
- there are no Klinkenberg effects, and
- the fluid is Newtonian.

The assumptions that are made for the total energy balance are:

- the kinetic energy and mechanical work done by the thermal expansion of the reservoir on its surroundings are neglected,
- at every point in the reservoir, a condition of thermodynamic equilibrium exists,
- radiation energy transfer, and other forms of energy such as nuclear and electromagnetic are neglected, and
- the kinetic energy change is neglected.

4.1.4 Well Model

The statement presented in the Introduction by Calhoun (1976) can be extended to a reservoir simulator. Crichlow (1977) stated "The well in the simulator is equally important, since it is the location at which the disturbances are initiated in the system. The way in which the reservoir system responds to the perturbations represents its behaviour, and this accurate representation is the primary goal in making a study. The ways in which wells are handled in the simulator have a significant impact on the calculated response of the simulator".

---

[1] Streaming potential—production of a potential difference when a liquid is forced through a porous membrane or capillary, this can be measured and is commonly called zeta potential.

In general, the rate of production of a phase from a layer can be defined as

$$q_{ijk} = J_{ijk}\left(p_{ojk} - p_{wfk} - h_{jk}\right) . \tag{4.1.4.1}$$

Rubin and Buchanan (1985) presented the following well flow conditions, which are variations of Equation 4.1.4.1. These equations can be thought of as conditions. Note that the head term lags by one time step.

Shut-in well:

$$\sum_{j} \sum_{i=o,w,g} J_{ijk}^{n+1}\left(p_{ojk}^{n+1} - p_{wfk}^{n+1} - h_{jk}^{n}\right) = 0 . \tag{4.1.4.2}$$

Constant total volume injection well:

$$q_{Tk} - \sum_{j} \sum_{i=o,w,g} J_{ijk}^{n+1}\left(p_{ojk}^{n+1} - p_{wfk}^{n+1} - h_{jk}^{n}\right) = 0 . \tag{4.1.4.3}$$

Constant pressure injection/production well:

$$p_{wfs} - p_{wfk}^{n+1} = 0 . \tag{4.1.4.4}$$

Constant oil rate production well:

$$q_{ok} - \sum_{j} J_{ojk}^{n+1}\left(p_{ojk}^{n+1} - p_{wfk}^{n+1} - h_{jk}^{n}\right) = 0 . \tag{4.1.4.5}$$

Constant gas rate production well:

$$q_{gk} - \sum_{j} J_{gjk}^{n+1}\left(p_{ojk}^{n+1} - p_{wfk}^{n+1} - h_{jk}^{n}\right) = 0 . \tag{4.1.4.6}$$

Constant liquid rate production well:

$$q_{Lk} - \sum_{j} \left(J_{wjk}^{n+1} + J_{ojk}^{n+1}\right)\left(p_{ojk}^{n+1} - p_{wfk}^{n+1} - h_{jk}^{n}\right) = 0 . \tag{4.1.4.7}$$

In addition to these conditions, well constraints can be written also.

Maximum water/oil ratio:

$$\sum_j \left(J_{wjk}^{n+1} - F_{wok} J_{ojk}^{n+1}\right)\left(p_{ojk}^{n+1} - p_{wfk}^{n+1} - h_{jk}^{n}\right) = 0 \ . \qquad (4.1.4.8)$$

Maximum water rate:

$$\sum_j J_{wjk}^{n+1}\left(p_{ojk}^{n+1} - p_{wfk}^{n+1} - h_{jk}^{n}\right) - q_{wk} = 0 \ . \qquad (4.1.4.9)$$

Other constraints that can be represented include maximum gas/oil ratio, maximum water/gas ratio, maximum bottom hole pressure, minimum bottom hole pressure, minimum oil rate, minimum gas rate and maximum well temperature.

For greater stability, the well equations are solved simultaneously with the reservoir equations. In addition, the well equations are treated implicitly.

Finally, the energy production is determined from

$$q_h^{*} = q_o \sum_i x_{io} E_{io} + q_w \sum_i x_{iw} E_{iw} + q_g \sum_i x_{ig} E_{ig} \ . \qquad (4.1.4.10)$$

A simplified flash calculation was used to convert the reservoir rates to surface rates. Based on the assumptions that the water component exists only in the aqueous phase, oil components exist only in the oleic phase and gas components exist only in the gaseous phase *at surface conditions*, it was easy to convert the subsurface rate of component *i* production.

4.1.5 Boundary and Initial Conditions

The mathematical description is incomplete without a set of initial and boundary conditions. The initial conditions in the reservoir must first be known. For this model, the initial oleic phase pressure, saturations, temperature and master phase compositions must be known. These conditions can be expressed, for a Cartesian coordinate system, mathematically as

$$p_o(x, y, z, 0) = p_{oi} \ , \qquad (4.1.5.1)$$

$$S_w(x,y,z,0)=S_{wi}\ , \tag{4.1.5.2}$$

$$S_o(x,y,z,0)=S_{oi}\ , \tag{4.1.5.3}$$

$$S_g(x,y,z,0)=S_{gi}\ , \tag{4.1.5.4}$$

$$\theta(x,y,z,0)=\theta_i\ , \tag{4.1.5.5}$$

and

$$X_i(x,y,z,0)=X_{ii}\ . \tag{4.1.5.6}$$

Similar expressions can be written for cylindrical coordinates in r, α, and z.

The outer boundary conditions are assumed here to be closed to the flow of fluids but open to the flow of energy. The inner boundary conditions at the wells were discussed in the previous section. On the outer boundary in the x direction for example:

$$\frac{\partial \Phi_o}{\partial x}=0 \tag{4.1.5.7}$$

and for temperature flow in the z direction,

$$\frac{\partial \theta}{\partial z}\neq 0\ . \tag{4.1.5.8}$$

Similar expressions in Cartesian coordinates can be written for the no-flow of mass across the boundary and also in cylindrical coordinates. Initialization of the model is discussed further in Section 4.7.2.

4.2 Grid Construction

This section discusses the methods of construction of rectilinear and cylindrical grids in general. Of particular note is the use of point-distributed and block-centred grids. The treatment of the irregularly shaped blocks which arise at the junction between the two grid types is also discussed here.

4.2.1 Fundamental Grid Construction

There are two methods available for a fundamental grid construction: point-distributed grids and block-centred grids. Details as to the procedure for constructing these grids may be found in Aziz and Settari (1979), Peaceman (1977) or Heinemann and Brand (1988). For an irregular grid spacing, as is the most common case in reservoir simulation, Settari and Aziz (1972, 1974a) have shown that the point-distributed grid is the correct approach. The principle behind this is that the differential equations are approximated at the grid points and not the block boundaries. Aziz and Settari (1979) showed that the point-distributed approximation is consistent, and hence any stable approximation of the right hand side of the residual equation will be convergent. This was not the case for a block-centred grid; that is, there is no guarantee of convergence, although for well behaved problems this is not a concern. Heinemann and Brand (1988) and Nacul and Aziz (1991) provide a concise review of grid construction techniques.

Aziz and Settari (1979) recommend the use of the point-distributed grid. Note that the only difference is the location and treatment of the boundary conditions. The point-distributed grid offers advantages in the ease of the treatment of the boundary conditions. On the other hand, the block-centred grid offers advantages in setting up the grid for a layered problem.

Appendix I.3 summarizes the equations for determining the node and boundary locations for both a rectilinear grid and a cylindrical grid.

4.2.2 Areal and Vertical Cartesian Grid Construction

In the construction of the grid for this model, it was determined that the block-centred grid would provide flexibility within the following restrictions:

- location of well block, and
- square well block for hyperhybrid grid refinement.

The areal grid is illustrated in Figure 4.2.2.1.

For a vertical cross section, with layers, the grid construction is similar, and requires a block-centred construction. This is illustrated in Figure 4.2.2.2.

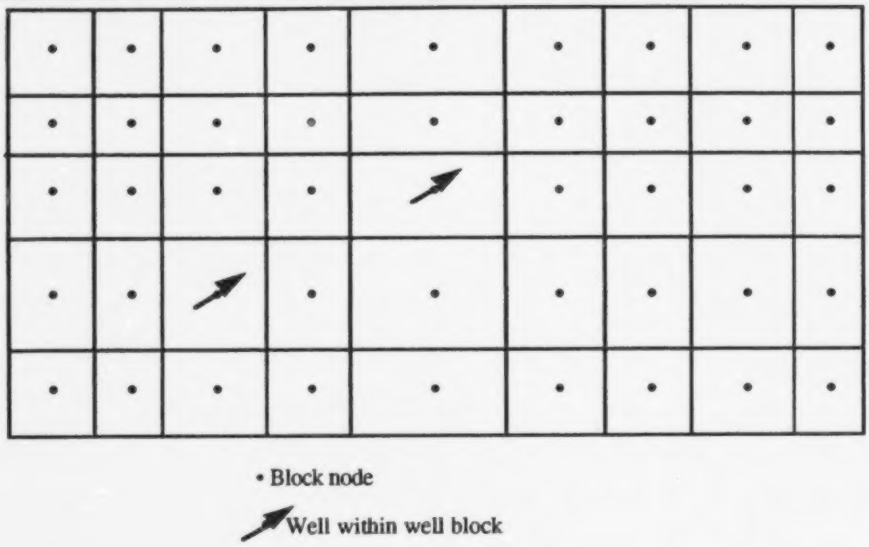
• Block node
Well within well block

Figure 4.2.2.1

Typical areal grid construction.

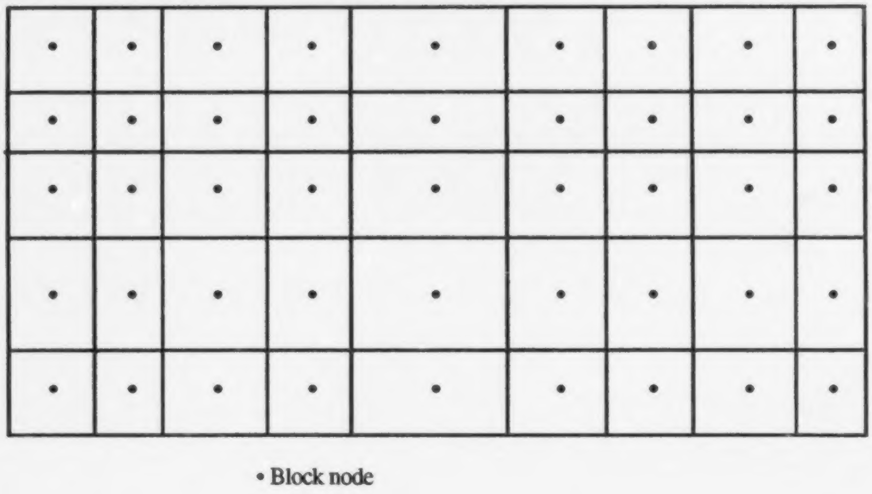

Figure 4.2.2.2

Typical vertical grid construction.

4.2.3 Radial and Vertical Cylindrical Grid Construction

In the construction of the grid for this model, it was determined that the block-centred grid for the vertical cross section as in the previous section would be used.

A typical radial grid is illustrated in Figure 4.2.3.1. Note that the innermost grid block is not subdivided so that the well is in one block. Some simulators do subdivide the inner grid block.

There are several methods for obtaining the radial grid block centres and boundaries in the literature. Some of the most common grid block centre options are:

- the logarithmic mean where the block centre is calculated as the logarithmic mean value of the boundary radii

$$r = \frac{r_2 - r_1}{\ln\left(\frac{r_2}{r_1}\right)} , \qquad (4.2.3.1)$$

- the volumetric mean where the block centre is calculated as a volumetric centroid of adjacent boundary radii

$$r = \sqrt{\frac{\left(r_1^2 + r_2^2\right)}{2}} , \qquad (4.2.3.2)$$

and

- the mid point where the block centre is located at the mid point of the block boundaries

$$r = r_1 + \frac{r_2 - r_1}{2} . \qquad (4.2.3.3)$$

The geometric mean may also be used. Other more complex methods are available such as solving a nonlinear equation ((Pedrosa 1984)) or solving a system of equations (Heinemann and Brand (1988)). This model has the three options of logarithmic mean, volumetric mean and mid point. Other methods can be incorporated into the code easily.

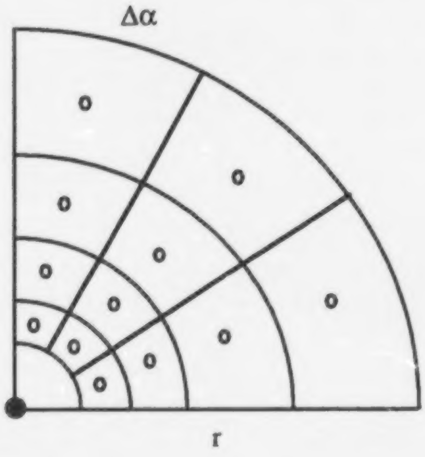

Figure 4.2.3.1 Typical radial grid construction.

This model has the following options for determining the block boundaries:

- specification of radial increments, and
- specification of well radius, first radius, number of rings and logarithmic calculation of spacing.

This model limits the choices to the following: if the block boundaries are specified, then the nodes are calculated using any of the three options; if the second choice is used, then the nodes are located logarithmically only.

4.2.4 Treatment of Irregularly Shaped Grid Blocks

Irregularly shaped blocks arise at the junction between the areal grid and the embedded radial/cylindrical grid. The irregularly shaped blocks are bounded in the direction of flow by curvilinear and rectilinear surfaces. The flow through the curvilinear surface is either radial (cylindrical) or elliptical, depending on the reservoir properties being either isotropic or anisotropic, respectively. The treatment of these blocks is discussed briefly in Pedrosa (1984), Pedrosa and Aziz (1985, 1986). Presented below is a more detailed summary of a radial grid system.

Consider the case where the well region is divided into several radial, vertical and four angular[1] ($\Delta\alpha = \pi/2$) pieces as illustrated in Figure 4.2.4.1.

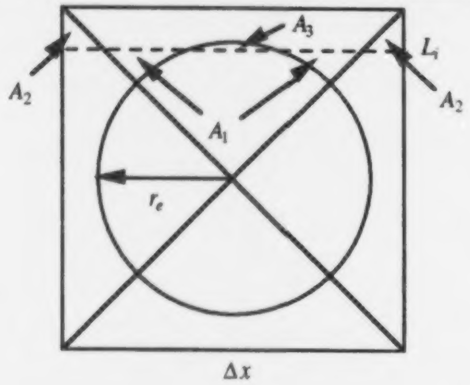

Figure 4.2.4.1 Irregularly shaped block ($\Delta\alpha = \pi/2$).

The area of the irregularly shaped block, A_{ij}, is given by

$$A_{ij} = \Delta x^2 - \pi r_e^2 \ . \tag{4.2.4.1}$$

Transforming the irregularly shaped block on one side, that is one quarter of the area, to a rectangle of equivalent area of dimensions,

$$L_i \Delta x = \frac{A_{ij}}{4} \ , \tag{4.2.4.2}$$

gives

$$L_i = \frac{A_{ij}}{4}\frac{1}{\Delta x} = \frac{\Delta x^2 - \pi r_e^2}{4\,\Delta x} \ . \tag{4.2.4.3}$$

In effect and by design, this results in a balance of the areas such that

$$2A_1 = 2A_2 + A_3 \ . \tag{4.2.4.4}$$

---

[1] Dividing this grid block into more than four angular pieces requires a treatment of the transmissibilities similar to that in conventional local grid refinement for flow across the rectilinear surfaces.

The above is for the case where $r_e > \Delta x - L_i$. For the case where $r_e < \Delta x - L_i$, A_3 is equal to zero. Equation 4.2.4.3 can be used to calculate the length of the fictitious block when transmissibilities are required for flow from the Cartesian grid into the cylindrical grid.

For the case when transmissibilities are required for flow from the cylindrical grid into the Cartesian grid, the irregularly shaped block is transformed into a cylindrical block. The volume of this block is

$$V_{i,j,k} = A_{i,j,k}\Delta z_k = A_{ij}\Delta z_k \ . \tag{4.2.4.5}$$

The volume of an annulus is given by

$$V = \frac{\Delta\alpha}{2} h\left(r_2^2 - r_1^2\right) . \tag{4.2.4.6}$$

Combining these two equations

$$A_{ij}\Delta z_k = \frac{\Delta\alpha_j}{2}\Delta z_k\left(r^2_{i+\frac{1}{2}} - r^2_{i-\frac{1}{2}}\right) , \tag{4.2.4.7}$$

and solving for the outer radius results in

$$r_{i+\frac{1}{2}} = \sqrt{\frac{2A_{ij}}{\Delta\alpha_j} + r^2_{i-\frac{1}{2}}} \ . \tag{4.2.4.8}$$

This radius can be used to calculate the radial and angular transmissibility while the vertical transmissibility is calculated in the usual manner.

Similar expressions can be derived for other angular divisions such as eight, twelve and sixteen pieces. These are the expressions required for hyperhybrid grid refinement. Consider the examples in Figure 4.2.4.2 which is a hyperhybrid grid replacing several (9 and 16) fundamental grid blocks.

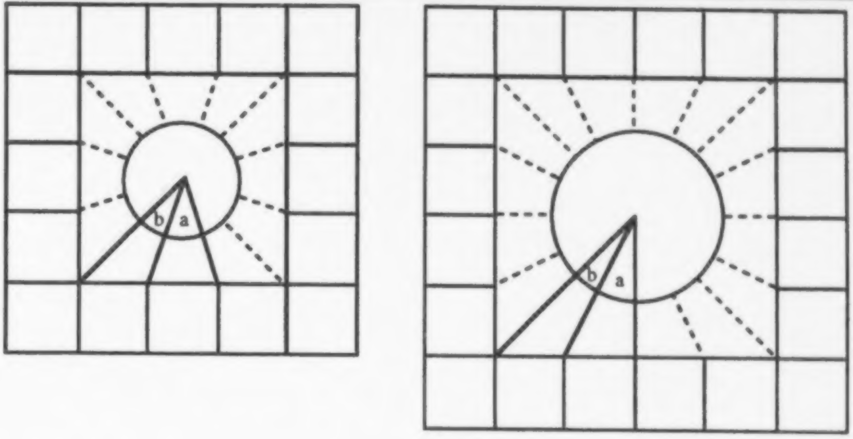

Figure 4.2.4.2

Hyperhybrid grid spanning several fundamental grid blocks.

In these two cases, the angles *a* and *b* are not equal. As a result, the area of the irregular grid block under the angle *a* is less than that under angle *b*. For the nine fundamental grid block case,

$$\angle a = 2\tan^{-1}\frac{1}{3} = 36.87^\circ \text{ and } \angle b = 45^\circ - \frac{\angle a}{2} = 26.57^\circ \ ,$$

while for the sixteen fundamental grid block case

$$\angle a = \tan^{-1}\frac{1}{2} = 26.57^\circ \text{ and } \angle b = 45^\circ - \angle a = 18.43^\circ \ .$$

Note that this is true only if the hyperhybrid grid block is a square. The consequence of these angles being unequal is that the size of the irregular grid blocks is unequal. This in turn affects the distance between the irregular grid block and the fundamental grid block, which is as it should be.

4.3 Numerical Model

The numerical treatment of the mathematical equations in Section 4.1 is a finite difference approximation. Any approximation method attempts to replace the original partial differential equation problem by another problem that is *easier* to solve and whose solution is close to the solution of the original partial differential equation. Appendix I details the treatment of the transmissibility terms and the finite difference approximations to Equations 4.1.1.1 and 4.1.1.2.

4.3.1 Combined Continuity/Momentum Balance Equations

Equation 4.1.1.1 can be written in the following form

$$\underset{i,j,k}{F_i^{n+1}} = \sum_{p}\left[\sum_{m} \underset{l}{T_p^{n+1}}\left[\left(\underset{m}{p_p^{n+1}} - \underset{i,j,k}{p_p^{n+1}}\right) - \underset{l}{\rho_p^{n+1}} g\left(z_m - z_{i,j,k}\right)\right]\right.$$
$$\left. - \frac{\underset{i,j,k}{V_b}}{\Delta t}\left(\left[\phi K_{vip} X_i \rho_p S_p\right]_{i,j,k}^{n+1} - \left[\phi K_{vip} X_i \rho_p S_p\right]_{i,j,k}^{n}\right) - \underset{i,j,k}{V_b}\ \underset{i,j,k}{\bar{q}_{ip}^{n+1}}\right], \qquad (4.3.1.1)$$

where *p* represents the aqueous, oleic and gaseous phase, *m* represents the grid blocks adjacent to block *i, j, k* (*i*+1, *j, k*; *i*-1, *j, k*; *i, j*+1, *k*; *i, j*-1, *k*; *i, j, k*+1; *i, j, k*-1) and *l* represents the interface between block *i, j, k* and the six adjacent blocks (*i*+1/2, *j, k*; *i*-1/2, *j, k*; *i, j*+1/2, *k*; *i, j*-1/2, *k*; *i, j, k*+1/2; *i, j, k*-1/2).

The source/sink term is given by

$$\underset{i,j,k}{V_b}\ \underset{i,j,k}{\tilde{q}_{ip}^{n+1}} = \underset{i,j,k}{q_{ip}^{n+1}} \ . \qquad (4.3.1.2)$$

Specifically, the production term is

$$\underset{i,j,k}{q_{ip}^{n+1}} = J'_{i,j,k}\left[\frac{k_{rp}}{\mu_p}\rho_p K_{vip} X_i\right]_{i,j,k}^{n+1}\left[p_o - p_{wf}\right]_{i,j,k}^{n+1}, \qquad (4.3.1.3)$$

where *J'* is the invariant portion of the productivity index of grid block *i, j, k* given by

$$J'_{i,j,k} = \frac{2\pi k h f_h f}{\ln\left(f_g \dfrac{r_e}{r_w}\right) + s} \qquad (4.3.1.4)$$

and

$$r_e = \sqrt{\frac{(\Delta x)^2 + (\Delta y)^2}{\pi f}} \;. \tag{4.3.1.5}$$

For the injection term, the phase mobility is replaced by a total mobility. If only the injected phase mobility is used, it may not be possible to inject that phase into the grid block if the phase mobility is zero. This does not agree with reality, hence

$$\underset{i,j,k}{q_{ip}^{n+1}} = J'_{i,j,k}\left[\sum_p \frac{k_{rp}}{\mu_p}\right]_{i,j,k}^{n+1} \underset{i,j,k}{\left[\rho_p K_{vip} X_i\right]_{wb}^{n+1}} \left[p_o - p_{wf}\right]_{i,j,k}^{n+1} \;. \tag{4.3.1.6}$$

Note the the term $\rho_p K_{vip} X_i$ is evaluated at the wellbore conditions. For the case of water component injection as gaseous and aqueous phases,

$$K_{v11} X_1 = 1 - x \tag{4.3.1.7}$$

and

$$K_{v13} X_1 = x \tag{4.3.1.8}$$

where x is the injection quality.

4.3.2 Total Energy Balance Equation

The finite difference form of Equation 4.1.1.2 can be written in the following form:

$$\begin{aligned} G_{i,j,k}^{n+1} = \sum_{p=o,w,g}\Bigg[\sum_m \underset{l}{T_p^{*}}{}^{n+1}\left[\left(\underset{m}{p_p^{n+1}} - \underset{i,j,k}{p_p^{n+1}}\right) - \underset{l}{\rho_p^{n+1}}\, g\left(z_m - z_{i,j,k}\right)\right] - \frac{\underset{i,j,k}{V_b}}{\Delta t}\left(\left[\phi E_p \rho_p S_p\right]_{i,j,k}^{n+1} - \left[\phi E_p \rho_p S_p\right]_{i,j,k}^{n}\right)\Bigg] \\ + \sum_m \underset{l}{T_c^{n+1}}\left[\theta_m^{n+1} - \theta_{i,j,k}^{n+1}\right] - \frac{\underset{i,j,k}{V_b}}{\Delta t}\left(\left[(1-\phi)\rho_f H_f\right]_{i,j,k}^{n+1} - \left[(1-\phi)\rho_f H_f\right]_{i,j,k}^{n}\right) - \underset{i,j,k}{V_b}\, \tilde{q}_{i,j,k} \;. \end{aligned} \tag{4.3.2.1}$$

The quantity $\tilde{q}$ in Equation 4.3.2.1 is made of the components of heat loss to the overburden/underburden and heat produced/injected along with the fluids.

The source/sink term is given by

$$\underset{i,j,k}{V_b}\ \tilde{q}_{i,j,k}^{n+1} = q_{i,j,k}^{n+1} = \underset{i,j,k}{q_{loss}^{n+1}} + \sum_{p} \underset{i,j,k}{q_p^{n+1}}\ \underset{i,j,k}{E_p^{n+1}}\ , \tag{4.3.2.2}$$

where q_{loss} is the heat loss to the overburden and underburden. This term exists only for the top and bottom layers. Note that the enthalpy is evaluated at wellbore conditions.

4.3.3 Cylindrical Form of Equations

Beginning with the combined continuity/momentum balance equation, and the total energy balance equation, it is a straightforward matter to derive the finite difference equations similar to Equations 4.3.1.1 and 4.3.2.1. However, it is much simpler to write the finite difference equations in cylindrical form directly by noting that the only differences lie in the geometric portion of the definitions of transmissibilities and block bulk volume. The treatment and definition of the transmissibilities is in Appendix I. Thus, in finite difference form,

$$\begin{aligned} \underset{i,j,k}{F_i^{n+1}} = \sum_{p} \Bigg[& \sum_{m} \underset{l}{T_p^{n+1}} \left[\left(\underset{m}{p_p^{n+1}} - \underset{i,j,k}{p_p^{n+1}} \right) - \underset{l}{\rho_p^{n+1}} g\left(z_m - z_{i,j,k} \right) \right] \\ & - \frac{\underset{i,j,k}{V_b}}{\Delta t} \left(\left[\phi K_{vip} X_i \rho_p S_p \right]_{i,j,k}^{n+1} - \left[\phi K_{vip} X_i \rho_p S_p \right]_{i,j,k}^{n} \right) - \underset{i,j,k}{V_b}\ \underset{i,j,k}{\tilde{q}_{ip}^{n+1}} \Bigg] \end{aligned} \tag{4.3.3.1}$$

and

$$\begin{aligned} G_{i,j,k}^{n+1} = & \sum_{p=o,w,g} \left[\sum_{m} \underset{l}{T_p^{*\,n+1}} \left[\left(\underset{m}{p_p^{n+1}} - \underset{i,j,k}{p_p^{n+1}} \right) - \underset{l}{\rho_p^{n+1}} g\left(z_m - z_{i,j,k} \right) \right] - \frac{\underset{i,j,k}{V_b}}{\Delta t} \left(\left[\phi E_p \rho_p S_p \right]_{i,j,k}^{n+1} - \left[\phi E_p \rho_p S_p \right]_{i,j,k}^{n} \right) \right] \\ & + \sum_{m} \underset{l}{T_c^{n+1}} \left[\theta_m^{n+1} - \theta_{i,j,k}^{n+1} \right] - \frac{\underset{i,j,k}{V_b}}{\Delta t} \left(\left[(1-\phi) \rho_f H_f \right]_{i,j,k}^{n+1} - \left[(1-\phi) \rho_f H_f \right]_{i,j,k}^{n} \right) - \underset{i,j,k}{V_b}\ \tilde{q}_{i,j,k}\ . \end{aligned} \tag{4.3.3.2}$$

4.4 Fluid and Rock Property Models

This section discusses the various mathematical models used to represent the fluid and rock properties.

4.4.1 Three-Phase Relative Permeabilities

It was stated in Section 4.1.6 that the functional dependence of the relative permeability is

$$k_{rw} = k_{rw}\left(S_w, \theta\right) \ , \tag{4.4.1.1}$$

$$k_{ro} = k_{ro}\left(S_w, S_g, \theta\right) \ , \tag{4.4.1.2}$$

and

$$k_{rg} = k_{rg}\left(S_g, \theta\right) \ . \tag{4.4.1.3}$$

The relationship expressing the function given by Equation 4.4.1.2 can be given in a number of ways, the most common being the Stone models (Stone 1970, 1973). Aziz and Settari (1979) proposed the following modified form of the models. First, define

$$k_{ro}\left(S_{wc}\right) = k_{rog}\left(S_L = 1\right) = k_{roiw} \ , \tag{4.4.1.4}$$

where

$$S_L = 1 - S_g = S_o + S_{wc} \tag{4.4.1.5}$$

for an oil-gas system. For Model I, the relative permeability to oil in a three-phase system is given by

$$k_{ro} = k_{roiw} S_o^* \beta_w \beta_g \ , \tag{4.4.1.6}$$

where

$$\beta_w = \frac{k_{row}\left(S_w\right)/k_{roiw}}{1 - S_w^*} \ , \tag{4.4.1.7}$$

$$\beta_g = \frac{k_{rog}(S_L)/k_{roiw}}{1-S_g^*} \ , \tag{4.4.1.8}$$

$$S_o^* = \frac{S_o - S_{orw}}{1 - S_{wc} - S_{orw}} \qquad S_o \geq S_{orw} \ , \tag{4.4.1.9}$$

$$S_w^* = \frac{S_w - S_{wc}}{1 - S_{wc} - S_{orw}} \qquad S_w \geq S_{wc} \ , \tag{4.4.1.10}$$

and

$$S_g^* = \frac{S_g}{1 - S_{wc} - S_{orw}} \ . \tag{4.4.1.11}$$

For Model II, the relative permeability to oil in a three-phase system is given by

$$k_{ro} = k_{roiw}\left[\left(k_{row}/k_{roiw} + k_{rw}\right)\left(k_{rog}/k_{roiw} + k_{rg}\right) - \left(k_{rw} + k_{rg}\right)\right] . \tag{4.4.1.12}$$

Other models are available in the literature, but are not discussed here[1].

The relationships given by Equations 4.4.1.1 and 4.4.1.3 can be expressed as (Coats (1980), Aziz *et al.* (1987))

$$k_{rw}(S_w, \theta) = k_{rwro}(\theta)\left[\frac{S_w - S_{wc}(\theta)}{1 - S_{orw}(\theta) - S_{wc}(\theta)}\right]^{n_w} , \tag{4.4.1.13}$$

$$k_{row}(S_w, \theta) = k_{roiw}(\theta)\left[\frac{1 - S_{orw}(\theta) - S_w}{1 - S_{orw}(\theta) - S_{wc}(\theta)}\right]^{n_{ow}} , \tag{4.4.1.14}$$

$$k_{rog}(S_g, \theta) = k_{roiw}(\theta)\left[\frac{1 - S_{wc}(\theta) - S_{org}(\theta) - S_g}{1 - S_{wc}(\theta) - S_{org}(\theta)}\right]^{n_{og}} , \tag{4.4.1.15}$$

and

$$k_{rg}(S_g, \theta) = k_{rgro}(\theta)\left[\frac{S_g - S_{gc}(\theta)}{1 - S_{wc}(\theta) - S_{org}(\theta) - S_{gc}(\theta)}\right]^{n_g} . \tag{4.4.1.16}$$

---

[1] The reader is referred to Aziz and Settari (1979), Baker (1988), Naar and Wygal (1961), Naar and Henderson (1961) and Naar, Wygal and Henderson (1962). Honarpour *et al.* (1986) present a comprehensive review of the subject of relative permeability. Further improvements to the models of Stone can be found in Kokal and Maini (1990).

The critical saturations and end point relative permeabilities are adjusted for temperature by using a linear relationship. For example,

$$S_{wc}(\theta) = a + b\theta \ , \tag{4.4.1.17}$$

or

$$S_{wc}(\theta) = S_{wc}(\theta_1) - \frac{S_{wc}(\theta_2) - S_{wc}(\theta_1)}{\theta_2 - \theta_1}\theta_1 + \frac{S_{wc}(\theta_2) - S_{wc}(\theta_1)}{\theta_2 - \theta_1}\theta \ , \tag{4.4.1.18}$$

where

$$a = S_{wc}(\theta_1) - \frac{S_{wc}(\theta_2) - S_{wc}(\theta_1)}{\theta_2 - \theta_1}\theta_1 \tag{4.4.1.19}$$

and

$$b = \frac{S_{wc}(\theta_2) - S_{wc}(\theta_1)}{\theta_2 - \theta_1} \ . \tag{4.4.1.20}$$

Equation 4.4.1.18 can be written more compactly as

$$S_{wc}(\theta) = S_{wc}(\theta_1) + \frac{S_{wc}(\theta_2) - S_{wc}(\theta_1)}{\theta_2 - \theta_1}(\theta - \theta_1) \ . \tag{4.4.1.21}$$

Similar expressions can be written for $S_{orw}(\theta)$, $S_{gc}(\theta)$ and $S_{org}(\theta)$:

$$S_{orw}(\theta) = S_{orw}(\theta_1) + \frac{S_{orw}(\theta_2) - S_{orw}(\theta_1)}{\theta_2 - \theta_1}(\theta - \theta_1) \ , \tag{4.4.1.22}$$

$$S_{gc}(\theta) = S_{gc}(\theta_1) + \frac{S_{gc}(\theta_2) - S_{gc}(\theta_1)}{\theta_2 - \theta_1}(\theta - \theta_1) \ , \tag{4.4.1.23}$$

and

$$S_{org}(\theta) = S_{org}(\theta_1) + \frac{S_{org}(\theta_2) - S_{org}(\theta_1)}{\theta_2 - \theta_1}(\theta - \theta_1) \ . \tag{4.4.1.24}$$

The end point permeabilities are adjusted for temperature using the following relationships:

$$k_{rwro}(\theta)=k_{rwro}(\theta_1)\left[1+\frac{k_{rwro}(\theta_2)-k_{rwro}(\theta_1)}{\theta_2-\theta_1}(\theta-\theta_1)\right], \tag{4.4.1.25}$$

$$k_{roiw}(\theta)=k_{roiw}(\theta_1)\left[1+\frac{k_{roiw}(\theta_2)-k_{roiw}(\theta_1)}{\theta_2-\theta_1}(\theta-\theta_1)\right], \tag{4.4.1.26}$$

and

$$k_{rgro}(\theta)=k_{rgro}(\theta_1)\left[1+\frac{k_{rgro}(\theta_2)-k_{rgro}(\theta_1)}{\theta_2-\theta_1}(\theta-\theta_1)\right]. \tag{4.4.1.27}$$

Beginning with Equation 4.4.1.13 for the relative permeability to water as a function of saturation only, adjusting the critical saturations for temperature using Equation 4.4.1.21 and 4.4.1.22 and adjusting the end point permeabilities for temperature using Equations 4.4.1.25 yields the relative permeability to water as a function of saturation and temperature:

$$k_{rw}(S_w,\theta)=k_{rw}(S_w(\theta))k_{rwro}(\theta)\ . \tag{4.4.1.28}$$

A similar procedure is used for the other relative permeabilities:

$$k_{row}(S_w,\theta)=k_{row}(S_w(\theta))k_{roiw}(\theta)\ , \tag{4.4.1.29}$$

$$k_{rog}(S_g,\theta)=k_{rog}(S_g(\theta))k_{roiw}(\theta)\ , \tag{4.4.1.30}$$

and

$$k_{rg}(S_g,\theta)=k_{rg}(S_g(\theta))k_{rgro}(\theta)\ . \tag{4.4.1.31}$$

Once the relative permeabilities have been adjusted, one of the Stone models can be used to calculate the relative permeability to oil in a three-phase system.

Equation 4.4.1.1 states that k_{rw} is a function of S_w and θ; hence, the partial derivatives of Equation 4.4.1.13 are

$$\frac{\partial k_{rw}}{\partial S_w}=k_{rwro}n_w\left[\frac{S_w-S_{wc}}{1-S_{orw}-S_{wc}}\right]^{n_w-1}\left[\frac{1}{1-S_{orw}-S_{wc}}\right] \tag{4.4.1.32}$$

and

$$\frac{\partial k_{rw}}{\partial \theta}=k_{rwro}n_w\left[\frac{S_w-S_{wc}}{1-S_{orw}-S_{wc}}\right]^{n_w-1}\left[\frac{\left(1-S_{orw}-S_{wc}\right)\left(-\frac{\partial S_{wc}}{\partial \theta}\right)-\left(S_w-S_{wc}\right)\left(-\frac{\partial S_{orw}}{\partial \theta}-\frac{\partial S_{wc}}{\partial \theta}\right)}{\left(1-S_{orw}-S_{wc}\right)^2}\right]$$

$$+\frac{\partial k_{rwro}}{\partial \theta}\left[\frac{S_w-S_{wc}}{1-S_{orw}-S_{wc}}\right]^{n_w}, \tag{4.4.1.33}$$

where

$$\frac{\partial k_{rwro}}{\partial \theta}=k_{rwro}\left(\theta_1\right)\left[\frac{k_{rwro}\left(\theta_2\right)-k_{rwro}\left(\theta_1\right)}{\theta_2-\theta_1}\right], \tag{4.4.1.34}$$

$$\frac{\partial S_{wc}}{\partial \theta}=\frac{S_{wc}\left(\theta_2\right)-S_{wc}\left(\theta_1\right)}{\theta_2-\theta_1}, \tag{4.4.1.35}$$

and

$$\frac{\partial S_{orw}}{\partial \theta}=\frac{S_{orw}\left(\theta_2\right)-S_{orw}\left(\theta_1\right)}{\theta_2-\theta_1}. \tag{4.4.1.36}$$

Equation 4.4.1.3 states that k_{rg} is a function of S_g and θ; hence, the partial derivatives of Equation 4.4.1.16 are

$$\frac{\partial k_{rg}}{\partial S_g}=k_{rgro}n_g\left[\frac{S_g-S_{gc}}{1-S_{wc}-S_{org}-S_{gc}}\right]^{n_g-1}\left[\frac{1}{1-S_{wc}-S_{org}-S_{gc}}\right] \tag{4.4.1.37}$$

and

$$\frac{\partial k_{rg}}{\partial \theta}=k_{rgro}n_g\left[\frac{S_g-S_{gc}}{1-S_{wc}-S_{org}-S_{gc}}\right]^{n_g-1}$$

$$\left[\frac{\left(1-S_{wc}-S_{org}-S_{gc}\right)\left(-\frac{\partial S_{gc}}{\partial \theta}\right)-\left(S_g-S_{gc}\right)\left(-\frac{\partial S_{wc}}{\partial \theta}-\frac{\partial S_{org}}{\partial \theta}-\frac{\partial S_{gc}}{\partial \theta}\right)}{\left(1-S_{wc}-S_{org}-S_{gc}\right)^2}\right]$$

$$+\frac{\partial k_{rgro}}{\partial \theta}\left[\frac{S_g-S_{gc}}{1-S_{wc}-S_{org}-S_{gc}}\right]^{n_g}, \tag{4.4.1.38}$$

where

$$\frac{\partial k_{rgro}}{\partial \theta} = k_{rgro}(\theta_1)\left[\frac{k_{rgro}(\theta_2) - k_{rgro}(\theta_1)}{\theta_2 - \theta_1}\right], \tag{4.4.1.39}$$

$$\frac{\partial S_{gc}}{\partial \theta} = \frac{S_{gc}(\theta_2) - S_{gc}(\theta_1)}{\theta_2 - \theta_1}, \tag{4.4.1.40}$$

and

$$\frac{\partial S_{org}}{\partial \theta} = \frac{S_{org}(\theta_2) - S_{org}(\theta_1)}{\theta_2 - \theta_1}. \tag{4.4.1.41}$$

Equation 4.4.1.2 states that k_{ro} is a function of S_w, S_g and θ; hence, the partial derivatives of Equation 4.4.1.12 are

$$\frac{\partial k_{ro}}{\partial S_w} = k_{roiw}\left[\left(\frac{1}{k_{roiw}}\frac{\partial k_{row}}{\partial S_w} + \frac{\partial k_{rw}}{\partial S_w}\right)\left(\frac{k_{rog}}{k_{roiw}} + k_{rg}\right) - \frac{\partial k_{rw}}{\partial S_w}\right], \tag{4.4.1.42}$$

$$\frac{\partial k_{ro}}{\partial S_g} = k_{roiw}\left[\left(\frac{k_{row}}{k_{roiw}} + k_{rw}\right)\left(\frac{1}{k_{roiw}}\frac{\partial k_{rog}}{\partial S_g} + \frac{\partial k_{rg}}{\partial S_g}\right) - \frac{\partial k_{rg}}{\partial S_g}\right], \tag{4.4.1.43}$$

and

$$\begin{aligned}\frac{\partial k_{ro}}{\partial \theta} = {} & \frac{\partial k_{roiw}}{\partial \theta}\left[\left(\frac{k_{row}}{k_{roiw}} + k_{rw}\right)\left(\frac{k_{rog}}{k_{roiw}} + k_{rg}\right) - \left(k_{rw} + k_{rg}\right)\right] \\ & + k_{roiw}\left[\left(\frac{k_{roiw}\dfrac{\partial k_{row}}{\partial \theta} - k_{row}\dfrac{\partial k_{roiw}}{\partial \theta}}{k_{roiw}^2} + \frac{\partial k_{rw}}{\partial \theta}\right)\left(\frac{k_{rog}}{k_{roiw}} + k_{rg}\right)\right. \\ & \left. + \left(\frac{k_{row}}{k_{roiw}} + k_{rw}\right)\left(\frac{k_{roiw}\dfrac{\partial k_{rog}}{\partial \theta} - k_{rog}\dfrac{\partial k_{roiw}}{\partial \theta}}{k_{roiw}^2} + \frac{\partial k_{rg}}{\partial \theta}\right) - \left(\frac{\partial k_{rw}}{\partial \theta} + \frac{\partial k_{rg}}{\partial \theta}\right)\right],\end{aligned} \tag{4.4.1.44}$$

where

$$\frac{\partial k_{row}}{\partial S_w} = k_{roiw} n_{ow}\left[\frac{1 - S_{orw} - S_w}{1 - S_{orw} - S_{wc}}\right]^{n_{ow}-1}\left[-\frac{1}{1 - S_{orw} - S_{wc}}\right], \tag{4.4.1.45}$$

$$\frac{\partial k_{rog}}{\partial S_g} = k_{roiw} n_{og}\left[\frac{1 - S_{wc} - S_{org} - S_g}{1 - S_{org} - S_{wc}}\right]^{n_{og}-1}\left[-\frac{1}{1 - S_{org} - S_{wc}}\right], \tag{4.4.1.46}$$

$$\frac{\partial k_{roiw}}{\partial \theta} = k_{roiw}(\theta_1)\left[\frac{k_{roiw}(\theta_2) - k_{roiw}(\theta_1)}{\theta_2 - \theta_1}\right], \tag{4.4.1.47}$$

$$\frac{\partial k_{row}}{\partial \theta} = k_{roiw} n_{ow} \left[\frac{1 - S_{orw} - S_w}{1 - S_{orw} - S_{wc}} \right]^{n_{ow} - 1} \left[\frac{(1 - S_{orw} - S_{wc})\left(-\frac{\partial S_{orw}}{\partial \theta} \right) - (1 - S_{orw} - S_w)\left(-\frac{\partial S_{orw}}{\partial \theta} - \frac{\partial S_{wc}}{\partial \theta} \right)}{(1 - S_{orw} - S_{wc})^2} \right] + \frac{\partial k_{roiw}}{\partial \theta} \left[\frac{1 - S_{orw} - S_w}{1 - S_{orw} - S_{wc}} \right]^{n_{ow}} , \tag{4.4.1.48}$$

and

$$\frac{\partial k_{rog}}{\partial \theta} = k_{roiw} n_{og} \left[\frac{1 - S_{wc} - S_{org} - S_g}{1 - S_{wc} - S_{org}} \right]^{n_{og} - 1} \left[\frac{(1 - S_{wc} - S_{org})\left(-\frac{\partial S_{wc}}{\partial \theta} - \frac{\partial S_{org}}{\partial \theta} \right) - (1 - S_{wc} - S_{org} - S_g)\left(-\frac{\partial S_{wc}}{\partial \theta} - \frac{\partial S_{org}}{\partial \theta} \right)}{(1 - S_{wc} - S_{org})^2} \right] + \frac{\partial k_{roiw}}{\partial \theta} \left[\frac{1 - S_{wc} - S_{org} - S_g}{1 - S_{wc} - S_{org}} \right]^{n_{og}} . \tag{4.4.1.49}$$

4.4.2 Porosity

The porosity of the rock is dependent on pressure due to the rock compressibility. If the rock compressibility is considered to be constant, then the porosity is given by

$$\phi = \phi^* \left[1 + c_f \left(p - p^* \right) \right] . \tag{4.4.2.1}$$

The porosity can be a function of temperature also, but this is not considered here. The partial derivative of Equation 4.4.2.1 is

$$\frac{\partial \phi}{\partial p} = \phi^* c_f . \tag{4.4.2.2}$$

4.4.3 Capillary Pressure

Capillary pressure is a function of saturation, temperature, composition and hysteresis. For this model, composition and hysteresis were not taken into account. Tan (1990) demonstrates the representation of capillary pressure in reservoir simulators. Using the equations of Coats (1980):

$$P_{cow} = \left[A + B(1 - S_w) + C(1 - S_w)^3\right]\left[1 - D(\theta - \theta_{ref})\right] \tag{4.4.3.1}$$

and

$$P_{cgo} = \left[A' + B'S_g + C'S_g^3\right]\left[1 - D'(\theta - \theta_{ref})\right] . \tag{4.4.3.2}$$

Note that these equations are simply polynomial curve fits, with a modification for temperature effects, to capillary pressure data. The required derivatives are

$$\frac{\partial P_{cow}}{\partial S_w} = \left[-B - 3C(1 - S_w)^2\right]\left[1 - D(\theta - \theta_{ref})\right] , \tag{4.4.3.3}$$

$$\frac{\partial P_{cow}}{\partial \theta} = \left[A + B(1 - S_w) + C(1 - S_w)^3\right]\left[-D\right] , \tag{4.4.3.4}$$

$$\frac{\partial P_{cgo}}{\partial S_g} = \left[B' + 3C'S_g^2\right]\left[1 - D'(\theta - \theta_{ref})\right] , \tag{4.4.3.5}$$

and

$$\frac{\partial P_{cgo}}{\partial \theta} = \left[A' + B'S_g + C'S_g^3\right]\left[-D'\right] . \tag{4.4.3.6}$$

4.4.4 Equilibrium Constants

The equilibrium constants are a function of pressure and temperature. Coats (1980), based on the work of Crookston *et al.* (1979) used the following relationship:

$$K_{vip} = \left[K_{v1,ip} + \frac{K_{v2,ip}}{p} + K_{v3,ip}\,p\right]\exp\left[-\frac{K_{v4,ip}}{\theta - K_{v5,ip}}\right] . \tag{4.4.4.1}$$

The partial derivatives are

$$\frac{\partial K_{vip}}{\partial p} = \left[-\frac{K_{v2,ip}}{p^2} + K_{v3,ip}\right]\exp\left[-\frac{K_{v4,ip}}{\theta - K_{v5,ip}}\right] \tag{4.4.4.2}$$

and

$$\frac{\partial K_{vip}}{\partial \theta} = \left[K_{v1,ip} + \frac{K_{v2,ip}}{p} + K_{v3,ip}\,p\right]\exp\left[-\frac{K_{v4,ip}}{\theta - K_{v5,ip}}\right]\left[\frac{K_{v4,ip}}{\left(\theta - K_{v5,ip}\right)^2}\right] . \tag{4.4.4.3}$$

Recall that the equilibrium constant for a component in its master phase is unity while if a component is insoluble in a particular phase the equilibrium constant is zero.

For water in the vapour phase, Raoult's law[1] is used:

$$K_{vip} = \frac{p_{sat}}{p} \; , \tag{4.4.4.4}$$

where the saturation pressure is calculated from (Tortike and Farouq Ali (1989))[2]

$$p_{sat} = \left[A + B\theta + C\theta^2 + D\theta^3 + E\theta^4 + F\theta^5\right]^2 \tag{4.4.4.5}$$

and the temperature derivative is

$$\frac{\partial p_{sat}}{\partial \theta} = 2\left[A + B\theta + C\theta^2 + D\theta^3 + E\theta^4 + F\theta^5\right]\left[B + 2C\theta + 3D\theta^2 + 4E\theta^3 + 5F\theta^4\right] \; . \tag{4.4.4.6}$$

The constants for the above equations are given in Table 4.4.4.1.

	p_{sat} (kPa)
A	$-1.75776\text{x}10^{2}$
B	2.29272
C	$-1.13953\text{x}10^{-2}$
D	$2.62780\text{x}10^{-5}$
E	$-2.73726\text{x}10^{-8}$
F	$1.13816\text{x}10^{-11}$

Table 4.4.4.1

Saturation pressure correlation constants.

---

[1] Raoult's law is a simple and useful equation that results from the combination of the ideal gas and ideal solution models of phase behaviour. An implicit assumption is that the formation of an ideal solution results in no change in molecular energies or volumes. Note also ideal solution behaviour is best approximated by solutions with similar molecules with respect to size and chemical nature.

[2] Many steam properties functional correlations have been published in the literature, for example Farouq Ali (1970), Ejiogu and Fiori (1987) and Al-Khafaji *et al.* (1989). Tortike and Farouq Ali (1989) are used because of the polynomial representation and ease of obtaining analytical derivatives.

4.4.5 Density

Density is a function of pressure, temperature and composition. The oleic phase density is obtained from Amagat's law of partial volumes:

$$v_p = \sum_{i=1}^{N_c} K_{vip} X_i v_{ip} \tag{4.4.5.1}$$

and the partial volumes are given by

$$v_{ip} = v_{ip}^{\circ}\left[1+\beta_i(\theta-\theta_r)\right]\left[1-c_i(p-p_r)\right] \ , \tag{4.4.5.2}$$

where β_i and c_i are the component thermal expansion coefficient and compressibility, respectively. Noting that the molar density is the inverse of the specific molar volume, Equation 4.4.5.1 can be written as

$$\rho_p = \frac{1}{\sum_{i=1}^{N_c} K_{vip} X_i \frac{1}{\rho_{ip}}} \ . \tag{4.4.5.3}$$

The partial derivative with respect to pressure is

$$\frac{\partial \rho_p}{\partial p} = -\frac{1}{\left(\sum_{i=1}^{N_c} K_{vip} X_i \frac{1}{\rho_{ip}}\right)^2} \sum_{i=1}^{N_c}\left(K_{vip} X_i \frac{\partial v_{ip}}{\partial p} + X_i v_{ip} \frac{\partial K_{vip}}{\partial p}\right) , \tag{4.4.5.4}$$

where

$$\frac{\partial v_{ip}}{\partial p} = v_{ip}^{\circ}\left[1+\beta_i(\theta-\theta_r)\right]\left[-c_i\right] \ . \tag{4.4.5.5}$$

The partial derivative with respect to temperature is

$$\frac{\partial \rho_p}{\partial \theta} = -\frac{1}{\left(\sum_{i=1}^{N_c} K_{vip} X_i \frac{1}{\rho_{ip}}\right)^2} \sum_{i=1}^{N_c}\left(K_{vip} X_i \frac{\partial v_{ip}}{\partial \theta} + X_i v_{ip} \frac{\partial K_{vip}}{\partial \theta}\right) , \tag{4.4.5.6}$$

where

$$\frac{\partial v_{ip}}{\partial \theta} = v_{ip}^{\circ}[\beta_i][1 - c_i(p - p_r)] \ . \qquad (4.4.5.7)$$

The partial derivative with respect to composition is

$$\frac{\partial \rho_p}{\partial X_m} = -\frac{1}{\left(\sum_{i=1}^{N_c} K_{vip} X_i \frac{1}{\rho_{ip}}\right)^2} K_{vmp} v_{mp} \ . \qquad (4.4.5.8)$$

The aqueous phase density is calculated using similar expressions as Equations 4.4.5.1 to 4.4.5.8 with the addition of steam condensate density being obtained from the correlation of Tortike and Farouq Ali (1989):

$$\rho_{ww} = A + B\theta + C\theta^2 + D\theta^3 + E\theta^4 + F\theta^5 \ . \qquad (4.4.5.9)$$

The constants are given in Table 4.4.5.1.

	$\rho_{ww}\,(kg/m^3)$	$\rho_{wg}\,(kg/m^3)$
A	$3.78631\text{x}10^{3}$	$-9.37072\text{x}10^{1}$
B	$-3.72487\text{x}10^{1}$	$8.33941\text{x}10^{-1}$
C	$1.96246\text{x}10^{-1}$	$-3.20809\text{x}10^{-3}$
D	$-5.04708\text{x}10^{-4}$	$6.57652\text{x}10^{-6}$
E	$6.29368\text{x}10^{-7}$	$-6.93747\text{x}10^{-9}$
F	$-3.08480\text{x}10^{-10}$	$2.97203\text{x}10^{-12}$

Table 4.4.5.1

Steam density correlation constants.

The density of the gaseous phase containing the hydrocarbon components is obtained from the gas law:

$$\rho_{HC} = \frac{pM}{zR\theta} \ , \qquad (4.4.5.10)$$

where the gas supercompressibility factor is obtained as given by Dranchuk and Abou-Kassem (1975). The density of the water component in the gaseous phase is obtained from Tortike and Farouq Ali (1989):

$$\ln\rho_{wg} = A + B\theta + C\theta^2 + D\theta^3 + E\theta^4 + F\theta^5 \ . \tag{4.4.5.11}$$

Amyx, Bass and Whiting (1960) suggest four methods of calculating the specific volume (or density) of a gaseous phase. These are treatment as a perfect gas, treatment as a real gas using additive volumes and compressibility factors of individual components, treatment as a real gas using additive volumes and densities, and treatment as a real gas using pseudo-reduced properties. These treatments are discussed fully in the above cited reference. Using the third treatment, then by Amagat's law of partial volumes,

$$v_g = \sum_{i=2}^{N_c} x_{ig} v_{ig} + x_{wg} v_{wg} \ . \tag{4.4.5.12}$$

Hence, the gaseous phase density is

$$\rho_g = \frac{1}{\displaystyle\sum_{i=2}^{N_c} \frac{K_{vig} X_i z_i R\theta}{pM_i} + \frac{K_{vwg} X_w}{\rho_{wg}}} \ . \tag{4.4.5.13}$$

The partial derivative of the gas density with respect to pressure is given by

$$\frac{\partial\rho_g}{\partial p} = -\rho_g^2 \sum_{i=1}^{N_c} \frac{1}{\rho_{ig}^2}\left(\rho_{ig}\frac{\partial K_{vig}}{\partial p}X_i - K_{vig}X_i\frac{\partial\rho_{ig}}{\partial p}\right) , \tag{4.4.5.14}$$

where

$$\begin{aligned} &\frac{\partial\rho_{wg}}{\partial p} = 0 && i = 1 \\ &\frac{\partial\rho_{ig}}{\partial p} = \frac{M_i}{R\theta}\frac{1}{z_i^2}\left(z_i - p\frac{\partial z_i}{\partial p}\right) && i = 2,\cdots,N_c \end{aligned} \ . \tag{4.4.5.15}$$

The partial derivative of the gas density with respect to temperature is given by

$$\frac{\partial\rho_g}{\partial\theta} = -\rho_g^2 \sum_{i=1}^{N_c} \frac{1}{\rho_{ig}^2}\left(\rho_{ig}\frac{\partial K_{vig}}{\partial\theta}X_i - K_{vig}X_i\frac{\partial\rho_{ig}}{\partial\theta}\right) , \tag{4.4.5.16}$$

where

$$\begin{aligned} \frac{\partial \rho_{wg}}{\partial \theta} &= \rho_{wg}\left(B + 2C\theta + 3D\theta^2 + 4E\theta^3 + 5F\theta^4\right) && i = 1 \\ \frac{\partial \rho_{ig}}{\partial \theta} &= -\frac{pM_i}{R}\frac{1}{z_i^2\theta^2}\left(z_i + \frac{\partial z_i}{\partial \theta}\theta\right) && i = 2,\cdots,N_c \end{aligned} \quad . \tag{4.4.5.17}$$

The partial derivative of the gas density with respect to composition is given by

$$\frac{\partial \rho_g}{\partial X_m} = -\rho_g^2 \sum_{i=1}^{N_c} \frac{1}{\rho_{ig}^2}\left(\rho_{ig} K_{vig} \frac{\partial X_i}{\partial X_m} - K_{vig} X_i \frac{\partial \rho_{ig}}{\partial X_m}\right) , \tag{4.4.5.18}$$

where

$$\begin{aligned} \frac{\partial \rho_{wg}}{\partial X_m} &= 0 && i = 1 \\ \frac{\partial \rho_{ig}}{\partial X_m} &= \frac{p}{z_i R\theta} && i = 2,\cdots,N_c, i = m \ , \\ \frac{\partial \rho_{ig}}{\partial X_m} &= 0 && i = 2,\cdots,N_c, i \neq m \end{aligned} \tag{4.4.5.19}$$

and

$$\frac{\partial X_i}{\partial X_m} = \begin{cases} 0 & i \neq m \\ 1 & i = m \end{cases} . \tag{4.4.5.20}$$

4.4.6 Viscosity

Viscosity is a function of pressure, temperature and composition. The viscosity can also be a function of velocity for non-Newtonian fluids (see Chapter 2). The oleic phase viscosity is obtained from

$$\mu_o = \prod_{i=1}^{N_c} \mu_{io}{}^{K_{vio} X_i} \ , \tag{4.4.6.1}$$

where the component viscosity is given by

$$\mu_{io} = A_i e^{(B_i/\theta)} \ . \tag{4.4.6.2}$$

The component viscosity is modified for non-Newtonian effects as discussed in Chapter 2. The partial derivatives are

$$\frac{\partial \mu_o}{\partial p} = \prod_{i=1}^{N_c} \mu_{io}{}^{K_{vio} X_i} \sum_{i=1}^{N_c} X_i \frac{\partial K_{vio}}{\partial p} \ln \mu_{io} \ , \qquad (4.4.6.3)$$

$$\frac{\partial \mu_o}{\partial \theta} = \prod_{i=1}^{N_c} \mu_{io}{}^{K_{vio} X_i} \sum_{i=1}^{N_c} \left[\frac{K_{vio} X_i}{\mu_{io}} \frac{\partial \mu_{io}}{\partial \theta} + X_i \frac{\partial K_{vio}}{\partial \theta} \ln \mu_{io} \right] , \qquad (4.4.6.4)$$

and

$$\frac{\partial \mu_o}{\partial X_m} = K_{vmo} \ln \mu_{mo} \prod_{i=1}^{N_c} \mu_{io}{}^{K_{vio} X_i} \ . \qquad (4.4.6.5)$$

The velocity effect on the viscosity is evaluated at the old time level. Evaluation implicitly leads to complex derivatives which is unnecessary. This approach is adequate provided the dependence on velocity is not strong.

The viscosity of the aqueous phase is taken from Tortike and Farouq Ali (1989):

$$\mu_{ww} = A + \frac{B}{\theta} + \frac{C}{\theta^2} + \frac{D}{\theta^3} + \frac{E}{\theta^4} + \frac{F}{\theta^5} \qquad (4.4.6.6)$$

and the derivative with respect to temperature is

$$\frac{\partial \mu_{ww}}{\partial \theta} = -\frac{B}{\theta^2} - 2\frac{C}{\theta^3} - 3\frac{D}{\theta^4} - 4\frac{E}{\theta^5} - 5\frac{F}{\theta^6} \ . \qquad (4.4.6.7)$$

The constants are given in Table 4.4.6.1.

The gaseous phase viscosity (Coats (1980)) is given by

$$\mu_g = \sum_{i=1}^{N_c} K_{vig} X_i \mu_{ig} \ , \qquad (4.4.6.8)$$

where the component viscosity is given by

$$\mu_{ig} = a_i \theta^{b_i} \qquad (4.4.6.9)$$

and the steam condensate viscosity is given by Tortike and Farouq Ali (1989) as

	$\mu_{ww}\,(Pa\cdot s)$	$\mu_{wg}\,(Pa\cdot s)$
A	$-1.23274\text{x}10^{-2}$	$-5.46807\text{x}10^{-4}$
B	$2.71038\text{x}10^{1}$	$6.8949\text{x}10^{-6}$
C	$-2.35275\text{x}10^{4}$	$-3.39999\text{x}10^{-8}$
D	$1.01425\text{x}10^{7}$	$8.29842\text{x}10^{-11}$
E	$-2.17342\text{x}10^{9}$	$-9.97060\text{x}10^{-14}$
F	$1.86935\text{x}10^{11}$	$4.71914\text{x}10^{-17}$

Table 4.4.6.1 Steam viscosity correlation constants.

$$\mu_{wg} = A + B\theta + C\theta^2 + D\theta^3 + E\theta^4 + F\theta^5 \ . \tag{4.4.6.10}$$

The partial derivatives are

$$\frac{\partial \mu_g}{\partial p} = \sum_{i=1}^{N_c} \frac{\partial K_{vig}}{\partial p} X_i \mu_{ig} \ , \tag{4.4.6.11}$$

$$\frac{\partial \mu_g}{\partial \theta} = \sum_{i=1}^{N_c} \left[\frac{\partial K_{vig}}{\partial \theta} X_i \mu_{ig} + K_{vig} X_i \frac{\partial \mu_{ig}}{\partial \theta} \right] , \tag{4.4.6.12}$$

and

$$\frac{\partial \mu_g}{\partial X_m} = K_{vmg} \mu_{mg} \ , \tag{4.4.6.13}$$

where

$$\frac{\partial \mu_{ig}}{\partial \theta} = \frac{b_i \mu_{ig}}{\theta} \tag{4.4.6.14}$$

for hydrocarbon components, and

$$\frac{\partial \mu_{ig}}{\partial \theta} = B + 2C\theta + 3D\theta^2 + 4E\theta^3 + 5F\theta^4 \tag{4.4.6.15}$$

for the water component.

4.4.7 Enthalpy and Internal Energy

The component enthalpy of water in the aqueous phase is given by (Tortike and Farouq Ali (1989)) the following polynomial:

$$H_{ww} = A + B\theta + C\theta^2 + D\theta^3 + E\theta^4 + F\theta^5 + G\theta^6 \ , \qquad (4.4.7.1)$$

and the component enthalpy of water in the gaseous phase is given by (Tortike and Farouq Ali (1989)) the following polynomial:

$$H_{wg} = A + B\theta + C\theta^2 + D\theta^3 + E\theta^4 + F\theta^5 + G\theta^6 \ , \qquad (4.4.7.2)$$

where the constants in the above two equations are given in the table below.

The component enthalpy of hydrocarbons in the oleic phase is given by

$$H_{io} = \int_{\theta_r}^{\theta} C_{p_{io}} d\theta \ , \qquad (4.4.7.3)$$

where the liquid heat capacity can be expressed as the following polynomial:

$$C_{p_{io}} = A + B\theta + C\theta^2 + D\theta^3 \ , \qquad (4.4.7.4)$$

and *A*, *B*, *C* and *D* are input constants.

	$H_{ww}\ (kJ/kg)$	$H_{wg}\ (kJ/kg)$
A	$2.36652 \text{x} 10^{4}$	$-2.20269 \text{x} 10^{4}$
B	$-3.66232 \text{x} 10^{2}$	$3.65317 \text{x} 10^{2}$
C	2.26952	-2.25837
D	$-7.30365 \text{x} 10^{-4}$	$7.37420 \text{x} 10^{-3}$
E	$1.30241 \text{x} 10^{-5}$	$-1.33437 \text{x} 10^{-5}$
F	$-1.22103 \text{x} 10^{-8}$	$1.26913 \text{x} 10^{-8}$
G	$4.70878 \text{x} 10^{-12}$	$-4.96880 \text{x} 10^{-12}$

Table 4.4.7.1

Steam enthalpy correlation constants.

A typical value of liquid heat capacity of crude oil is approximately 2090 J/kg K (0.5 BTU/lb°F) and of gaseous methane is approximately 1050 J/kg K (0.25 BTU/lb°F). For the case of vaporizing crude oils, the component enthalpy of heavy and light oil in the gaseous phase is given by similar expressions:

$$H_{ig} = \int_{\theta_r}^{\theta} C_{p_{ig}} d\theta \ , \tag{4.4.7.5}$$

where the gaseous heat capacity can be expressed as the following polynomial:

$$C_{p_{ig}} = A + B\theta + C\theta^2 + D\theta^3 \ , \tag{4.4.7.6}$$

and *A*, *B*, *C* and *D* are input constants.

The phase enthalpy is given by

$$H_p = \sum_{i=1}^{N_c} K_{vip} X_i H_{ip} \ , \tag{4.4.7.7}$$

where it is assumed that ideal mixing takes place and the component enthalpy is independent of pressure and composition.

For the liquid phases, aqueous and oleic, the internal energy can be approximated by

$$E_p = H_p \ , \tag{4.4.7.8}$$

whereas the internal energy for the gaseous phase is obtained from

$$E_p = H_p - \frac{p}{\rho_p} \ . \tag{4.4.7.9}$$

The partial derivatives of the phase enthalpy with respect to pressure, temperature and composition are

$$\frac{\partial H_p}{\partial p_o} = \sum_{i=1}^{N_c} \frac{\partial K_{vip}}{\partial p_o} X_i H_{ip} \ , \tag{4.4.7.10}$$

$$\frac{\partial H_p}{\partial \theta} = \sum_{i=1}^{N_c} \frac{\partial K_{vip}}{\partial \theta} X_i H_{ip} + K_{vip} X_i \frac{\partial H_{ip}}{\partial \theta} \ , \tag{4.4.7.11}$$

and

$$\frac{\partial H_p}{\partial X_j} = K_{vjp} H_{jp} \ , \tag{4.4.7.12}$$

where

$$\frac{\partial H_{ip}}{\partial \theta} = C_{p_{ip}} \ . \tag{4.4.7.13}$$

The partial derivatives of the phase internal energy with respect to pressure, temperature and composition are

$$\frac{\partial E_p}{\partial p_o} = \begin{cases} \dfrac{\partial H_p}{\partial p_o} & p = w,o \\ \dfrac{\partial H_p}{\partial p_o} - \dfrac{\rho_g - \left(P_{cgo} + p_o\right)\dfrac{\partial \rho_g}{\partial p_o}}{\rho_g^2} & p = g \end{cases} \ , \tag{4.4.7.14}$$

$$\frac{\partial E_p}{\partial \theta} = \begin{cases} \dfrac{\partial H_p}{\partial \theta} & p = w,o \\ \dfrac{\partial H_p}{\partial \theta} - \dfrac{\rho_g \dfrac{\partial P_{cgo}}{\partial \theta} - \left(P_{cgo} + p_o\right)\dfrac{\partial \rho_g}{\partial \theta}}{\rho_g^2} & p = g \end{cases} \ , \tag{4.4.7.15}$$

and

$$\frac{\partial E_p}{\partial X_j} = \begin{cases} \dfrac{\partial H_p}{\partial X_j} & p = w,o \\ \dfrac{\partial H_p}{\partial X_j} - \dfrac{\rho_g \dfrac{\partial P_{cgo}}{\partial X_j} - \left(P_{cgo} + p_o\right)\dfrac{\partial \rho_g}{\partial X_j}}{\rho_g^2} & p = g \end{cases} \ . \tag{4.4.7.16}$$

4.4.8 Overburden and Underburden Heat Loss

Vinsome and Westerveld (1980) presented a simple method for calculating the heat losses to the overburden and underburden. They suggest using the fitting function

$$\theta(z,t) = \left(\theta + pz + qz^2\right)e^{-z/d} \tag{4.4.8.1}$$

for the temperature profile into the over/underburden where θ is the temperature at the reservoir over/underburden interface, p and q are fitting parameters and d is the diffusion length given by

$$d = \frac{\sqrt{\kappa t}}{2} \ , \tag{4.4.8.2}$$

where κ is the thermal diffusivity. Vinsome and Westerveld (1980) showed that the fitting parameters are given by

$$p = \frac{\dfrac{\kappa \Delta t \theta^{n+1}}{d^{n+1}} + \theta^n d^n + p^n\left(d^n\right)^2 + 2q^n\left(d^n\right)^3 - \dfrac{\left(d^{n+1}\right)^3\left(\theta^{n+1} - \theta^n\right)}{\kappa \Delta t}}{3\left(d^{n+1}\right)^2 + \kappa \Delta t} \tag{4.4.8.3}$$

and

$$q = \frac{2p^{n+1}d^{n+1} - \theta^{n+1} + \left(d^{n+1}\right)^2 \dfrac{\left(\theta^{n+1} - \theta^n\right)}{\kappa \Delta t}}{2\left(d^{n+1}\right)^2} \ . \tag{4.4.8.4}$$

The heat flux at the interface, q_{flux}, is given by Fourier's law and using Equation 4.4.8.1 gives

$$q_{flux}^{n+1} = -\lambda \frac{d\theta}{dz}\bigg|_{z=0}^{n+1} = \lambda\left(\frac{\theta^{n+1}}{d^{n+1}} - p^{n+1}\right) , \tag{4.4.8.5}$$

hence, the heat loss is given by

$$q_{loss}^{n+1} = q_{flux}^{n+1} A \ . \tag{4.4.8.6}$$

The energy stored in the over/underburden, E_c, is given by

$$E_c^{n+1} = \frac{\lambda}{\kappa}\int_0^{\infty} \theta dz = \frac{\lambda}{\kappa} d^{n+1}\left[\theta^{n+1} + p^{n+1}d^{n+1} + 2q^{n+1}\left(d^{n+1}\right)^2\right] . \qquad (4.4.8.7)$$

The derivative of q_{loss} with respect to temperature is given by

$$\frac{dq_{loss}^{n+1}}{d\theta^{n+1}} = \lambda A\left(\frac{1}{d^{n+1}} - \frac{dp^{n+1}}{d\theta^{n+1}}\right) , \qquad (4.4.8.8)$$

where

$$\frac{\partial p^{n+1}}{\partial \theta^{n+1}} = \frac{1}{3\left(d^{n+1}\right)^2 + \kappa\Delta t}\left[\frac{\kappa\Delta t}{d^{n+1}} - \frac{\left(d^{n+1}\right)^3}{\kappa\Delta t}\right] . \qquad (4.4.8.9)$$

4.4.9 Rock Thermal Properties

The term $\rho_f H_f$ in Equation 4.3.3.5 can be written as

$$\rho_f H_f = M_f(\theta - \theta_r) , \qquad (4.4.9.1)$$

where the rock heat capacity is defined as (Coats (1980))

$$M_f = C_{pr}\left[1 + C_{prt}(\theta - \theta_r)\right] \qquad (4.4.9.2)$$

and C_{pr} and C_{prt} are constants. The partial derivative required is

$$\frac{\partial \rho_f H_f}{\partial \Theta} = C_{pr}C_{prt}(\theta - \theta_r) + M_f \ . \qquad (4.4.9.3)$$

4.5 Solution Method

4.5.1 Newton's Method

Equation 4.3.1.1 can be written in residual form as

$$\underset{i,j,k}{F_i^{n+1}} = 0 \qquad i = 1, N_c \ \text{Combined continuity / momentum balance equations}. \qquad (4.5.1.1)$$

Similarly, Equations 4.3.2.1, 4.1.1.4, 4.1.1.3 and 4.1.4.1 can be written in residual form as

$$G_{i,j,k}^{n+1} = 0 \qquad \text{Energy balance equation}\ , \qquad (4.5.1.2)$$

$$\underset{i,j,k}{X_p^{n+1}} = 0 \qquad p = w,\ o,\ g \qquad \text{Mole fraction constraint equations}\ , \qquad (4.5.1.3)$$

$$S_{i,j,k}^{n+1} = 0 \qquad \text{Saturation constraint equation}\ , \qquad (4.5.1.4)$$

and

$$W_{i,j,k}^{n+1} = 0 \qquad \text{Well equation}\ . \qquad (4.5.1.5)$$

For a fully implicit formulation, the system of equations consists of a set of equations that describe the flow of mass and energy through the reservoir and a set of equations which describe flow through a well. These equation are, in general, nonlinear. The system of nonlinear equations can be solved by Newton's method. Following the development of Aziz and Settari (1979), Newton's method can be written as

$$\mathbf{u}^{(m)} - \mathbf{u}^{(m-1)} = -\left[\mathbf{J}^{(m-1)}\right]^{-1} \mathbf{f}^{(m-1)} \qquad m = 1, 2, \ldots\ , \qquad (4.5.1.6)$$

where **J** is the Jacobian matrix of the vector function **f**

$$\mathbf{J}^{(m)} = \left(\frac{\partial f_i}{\partial u_j}\right)^{(m)}\ . \qquad (4.5.1.7)$$

Rewriting Equation 4.5.1.6 as

$$\mathbf{J}^{(m-1)} \boldsymbol{\delta}^{(m)} = -\mathbf{f}^{(m-1)}\ , \qquad (4.5.1.8)$$

where

$$\mathbf{u}^{(m)} = \mathbf{u}^{(m-1)} + \boldsymbol{\delta}^{(m)} \qquad m = 1,2,... \qquad (4.5.1.9)$$

and noting that

$$\mathbf{u}^{(0)} = \mathbf{u}^{n} \qquad (4.5.1.10)$$

allows for a convenient formulation. The process is iterative and, if convergent, continues until $\boldsymbol{\delta}$ and $\mathbf{f}$ approach $\mathbf{0}$ (or some tolerance).

For a problem with N number of unknowns and N_b number of grid blocks, the Jacobian matrix $\mathbf{J}$ is of a size $(N \bullet N_b) \bullet (N \bullet N_b)$, $\boldsymbol{\delta}$ is the vector on unknowns of size $(N \bullet N_b)$ and the residual vector is of size $(N \bullet N_b)$.

The derivatives required to assemble the Jacobian matrix may be determined either numerically[1] or analytically. In this work, all of the derivatives have been determined analytically except for the gas supercompressibility factor derivatives[2]. Although numerical derivatives are generally simpler to obtain and require less computing and programming effort, analytical derivatives are exact and rigourous. Note that most of the analytical derivatives in this work were also calculated numerically to verify them.

For simple problems, the structure of the Jacobian matrix is banded. Factors that contribute to a more complex Jacobian matrix are the combination of explicit/implicit time discretization methods, inclusion of wells (implicit wells), complexities associated with naturally fractured reservoirs and a variable number of primary unknowns[3] per grid block (Nghiem and Rozon (1988)). In addition to the above, hybrid and hyperhybrid grids introduce a further decay in structure.

Figure 4.5.1.1 illustrates the grid and Jacobian matrix for a two-dimensional rectilinear system with several wells and Figure 4.5.1.2 illustrates the Jacobian matrix in more detail. Figures 4.5.1.3 and 4.5.1.4 illustrate the same information for a two-dimensional cylindrical system.

---

[1] For a complete discussion on the subject of numerical derivatives and their pitfalls, the reader is referred to Press *et al.* (1992).

[2] The analytical derivatives are complex and tedious to obtain. For application in the model, they are unnecessary.

[3] A variable number of primary unknowns is associated generally with compositional and thermal simulators.

Figures 4.5.1.5 and 4.5.1.6 are for a simple rectilinear system with a single hybrid grid. Note the new cross-terms for the coupling of the rectilinear reservoir and cylindrical well regions. Figures 4.5.1.7 and 4.5.1.8 are for a simple rectilinear system with hybrid and hyperhybrid contiguous regions. Finally, Figure 4.5.1.9 shows the grid and Jacobian for a problem with six regions. Again, note the cross-terms for coupling the rectilinear reservoir and cylindrical well regions. In addition, note the new cross-terms coupling the contiguous hybrid/hyperhybrid regions.

In the figures below, the partial derivatives for the rectilinear and cylindrical systems have the following significance:

$\frac{\partial R_{rf}}{\partial P_{rf}}$	derivatives of the rectilinear flow equations with respect to the rectilinear flow variables,
$\frac{\partial R_{rf}}{\partial P_{rw}}$	derivatives of the rectilinear flow equations with respect to the rectilinear well variables,
$\frac{\partial R_{rw}}{\partial P_{rf}}$	derivatives of the rectilinear well equations with respect to the rectilinear flow variables,
$\frac{\partial R_{rw}}{\partial P_{rw}}$	derivatives of the rectilinear well equations with respect to the rectilinear well variables,
$\frac{\partial R_{cf}}{\partial P_{cf}}$	derivatives of the cylindrical flow equations with respect to the cylindrical flow variables,
$\frac{\partial R_{cf}}{\partial P_{cw}}$	derivatives of the cylindrical flow equations with respect to the cylindrical well variables,
$\frac{\partial R_{cw}}{\partial P_{cf}}$	derivatives of the cylindrical well equations with respect to the cylindrical flow variables,
$\frac{\partial R_{cw}}{\partial P_{cw}}$	derivatives of the cylindrical well equations with respect to the cylindrical well variables,
$\frac{\partial R_{rf}}{\partial P_{cf}}$	derivatives of the rectilinear flow equations with respect to the cylindrical flow variables,
$\frac{\partial R_{cf}}{\partial P_{rf}}$	derivatives of the cylindrical flow equations with respect to the rectilinear flow variables, while for the hybrid and hyperhybrid regions
$\frac{\partial R_{rf}}{\partial P_{c_i f}}$	derivatives of the rectilinear flow equations with respect the hybrid region *i* flow variables,

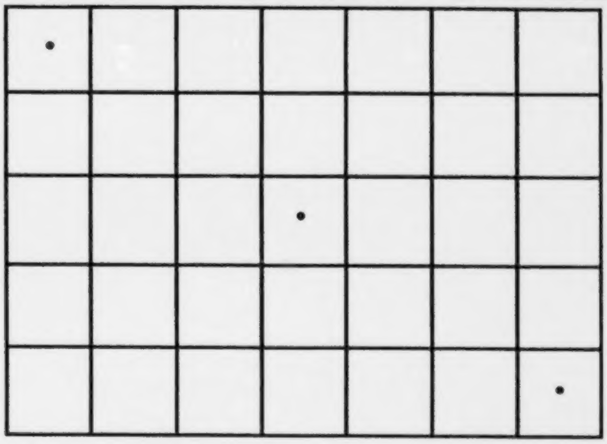

$$\left|\begin{array}{c:c} \dfrac{\partial R_{rf}}{\partial P_{rf}} & \dfrac{\partial R_{rf}}{\partial P_{rw}} \\ \hdashline \dfrac{\partial R_{rw}}{\partial P_{rf}} & \dfrac{\partial R_{rw}}{\partial P_{rw}} \end{array}\right|$$

Figure 4.5.1.1

Typical grid and Jacobian matrix for a rectilinear system.

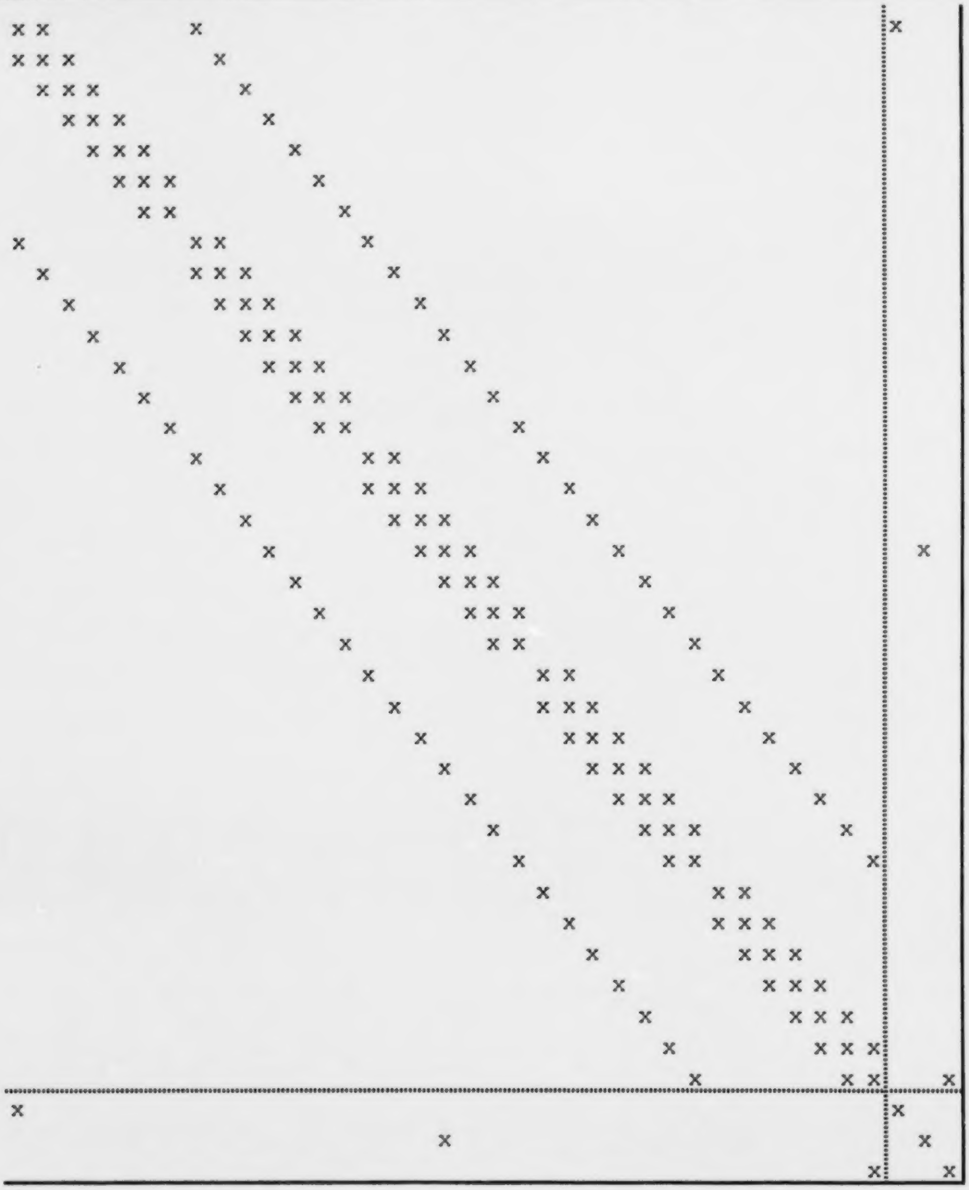

Figure 4.5.1.2

Jacobian matrix for a rectilinear system.

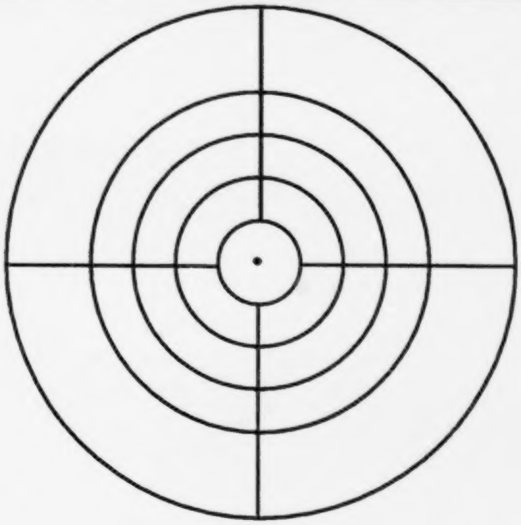

$$\left|\begin{array}{c:c} \dfrac{\partial R_{cf}}{\partial P_{cf}} & \dfrac{\partial R_{cf}}{\partial P_{cw}} \\ \hdashline \dfrac{\partial R_{cw}}{\partial P_{cf}} & \dfrac{\partial R_{cw}}{\partial P_{cw}} \end{array}\right|$$

Figure 4.5.1.3

Typical grid and Jacobian matrix for a cylindrical system.

$$
\begin{array}{ccccccccccccccccc|c}
x & x & x & x & x & & & & & & & & & & & & & x \\
x & x & x & & x & x & & & & & & & & & & & & \\
x & x & x & x & & & x & & & & & & & & & & & \\
x & & x & x & x & & & x & & & & & & & & & & \\
x & x & & x & x & & & & x & & & & & & & & & \\
 & x & & & & x & x & & x & x & & & & & & & & \\
 & & x & & & x & x & x & & & x & & & & & & & \\
 & & & x & & & x & x & x & & & x & & & & & & \\
 & & & & x & x & & x & x & & & & x & & & & & \\
 & & & & & x & & & & x & x & & x & x & & & & \\
 & & & & & & x & & & x & x & x & & & x & & & \\
 & & & & & & & x & & & x & x & x & & & x & & \\
 & & & & & & & & x & x & & x & x & & & & x & \\
 & & & & & & & & & x & & & & x & x & & x & \\
 & & & & & & & & & & x & & & x & x & x & & \\
 & & & & & & & & & & & x & & & x & x & x & \\
 & & & & & & & & & & & & x & x & & x & x & \\
\hline
x & & & & & & & & & & & & & & & & & x
\end{array}
$$

Figure 4.5.1.4

Jacobian matrix for a cylindrical system.

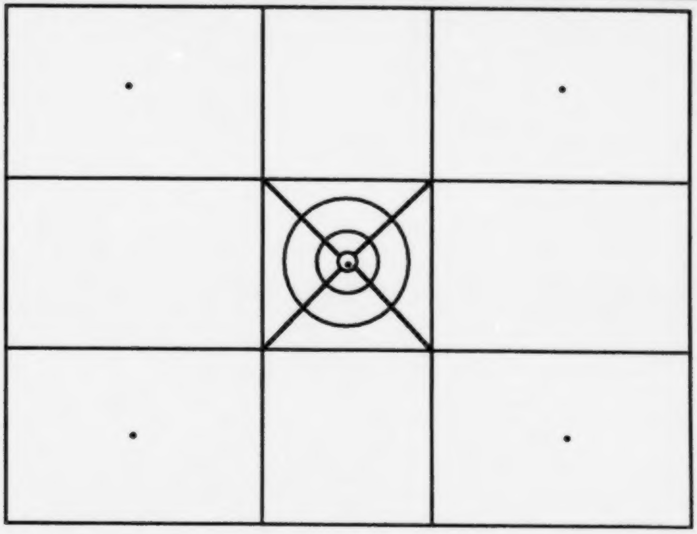

$$\left|\begin{array}{cc|cc}
\frac{\partial R_{rf}}{\partial P_{rf}} & \frac{\partial R_{rf}}{\partial P_{rw}} & \frac{\partial R_{rf}}{\partial P_{cf}} & \\
\frac{\partial R_{rw}}{\partial P_{rf}} & \frac{\partial R_{rw}}{\partial P_{rw}} & & \\
\hline
\frac{\partial R_{cf}}{\partial P_{rf}} & & \frac{\partial R_{cf}}{\partial P_{cf}} & \frac{\partial R_{cf}}{\partial P_{cw}} \\
 & & \frac{\partial R_{cw}}{\partial P_{cf}} & \frac{\partial R_{cw}}{\partial P_{cw}}
\end{array}\right|$$

Figure 4.5.1.5

Typical grid and Jacobian matrix for a rectilinear system with a single hybrid grid.

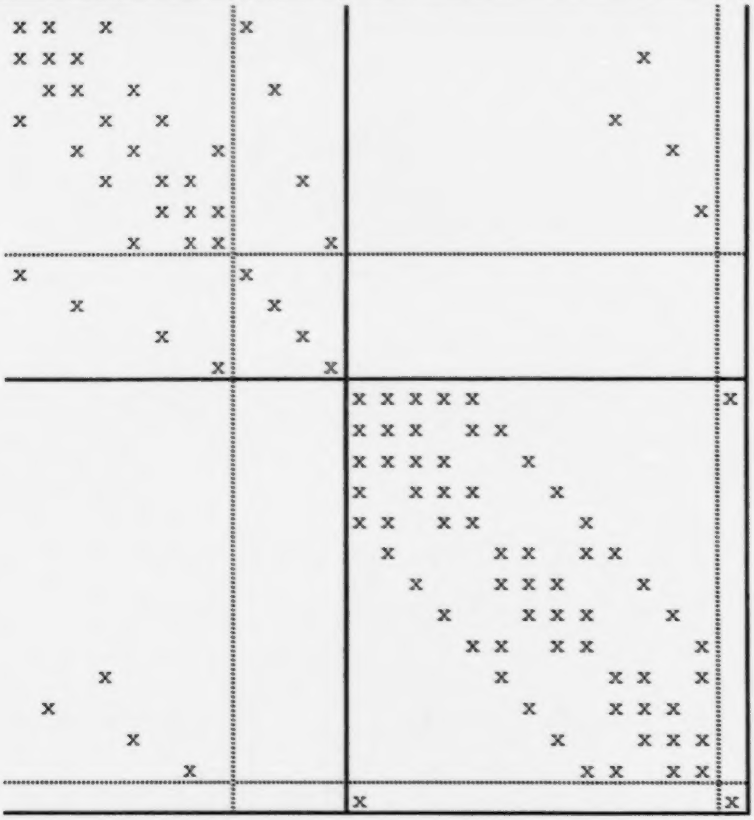

Figure 4.5.1.6

Jacobian matrix for a rectilinear system with a single hybrid grid.

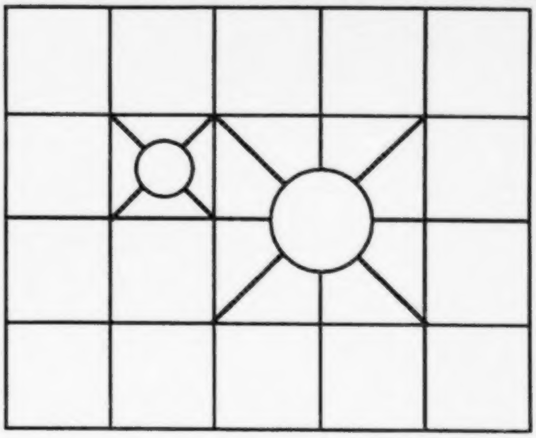

$$\left|\begin{array}{cc|cc|cc}
\dfrac{\partial R_{rf}}{\partial P_{rf}} & \dfrac{\partial R_{rf}}{\partial P_{rw}} & \dfrac{\partial R_{rf}}{\partial P_{c_1 f}} & & \dfrac{\partial R_{rf}}{\partial P_{c_2 f}} & \\
\hline
\dfrac{\partial R_{rw}}{\partial P_{rf}} & \dfrac{\partial R_{rw}}{\partial P_{rw}} & & & & \\
\hline
\dfrac{\partial R_{c_1 f}}{\partial P_{rf}} & & \dfrac{\partial R_{c_1 f}}{\partial P_{c_1 f}} & \dfrac{\partial R_{c_1 f}}{\partial P_{c_1 w}} & \dfrac{\partial R_{c_1 f}}{\partial P_{c_2 f}} & \\
\hline
 & & \dfrac{\partial R_{c_1 w}}{\partial P_{c_1 f}} & \dfrac{\partial R_{c_1 w}}{\partial P_{c_1 w}} & & \\
\hline
\dfrac{\partial R_{c_2 f}}{\partial P_{rf}} & & \dfrac{\partial R_{c_2 f}}{\partial P_{c_1 f}} & & \dfrac{\partial R_{c_2 f}}{\partial P_{c_2 f}} & \dfrac{\partial R_{c_2 f}}{\partial P_{c_2 w}} \\
\hline
 & & & & \dfrac{\partial R_{c_2 w}}{\partial P_{c_2 f}} & \dfrac{\partial R_{c_2 w}}{\partial P_{c_2 w}}
\end{array}\right|$$

Figure 4.5.1.7

Typical grid and Jacobian matrix for a rectilinear system with contiguous hybrid/hyperhybrid grids.

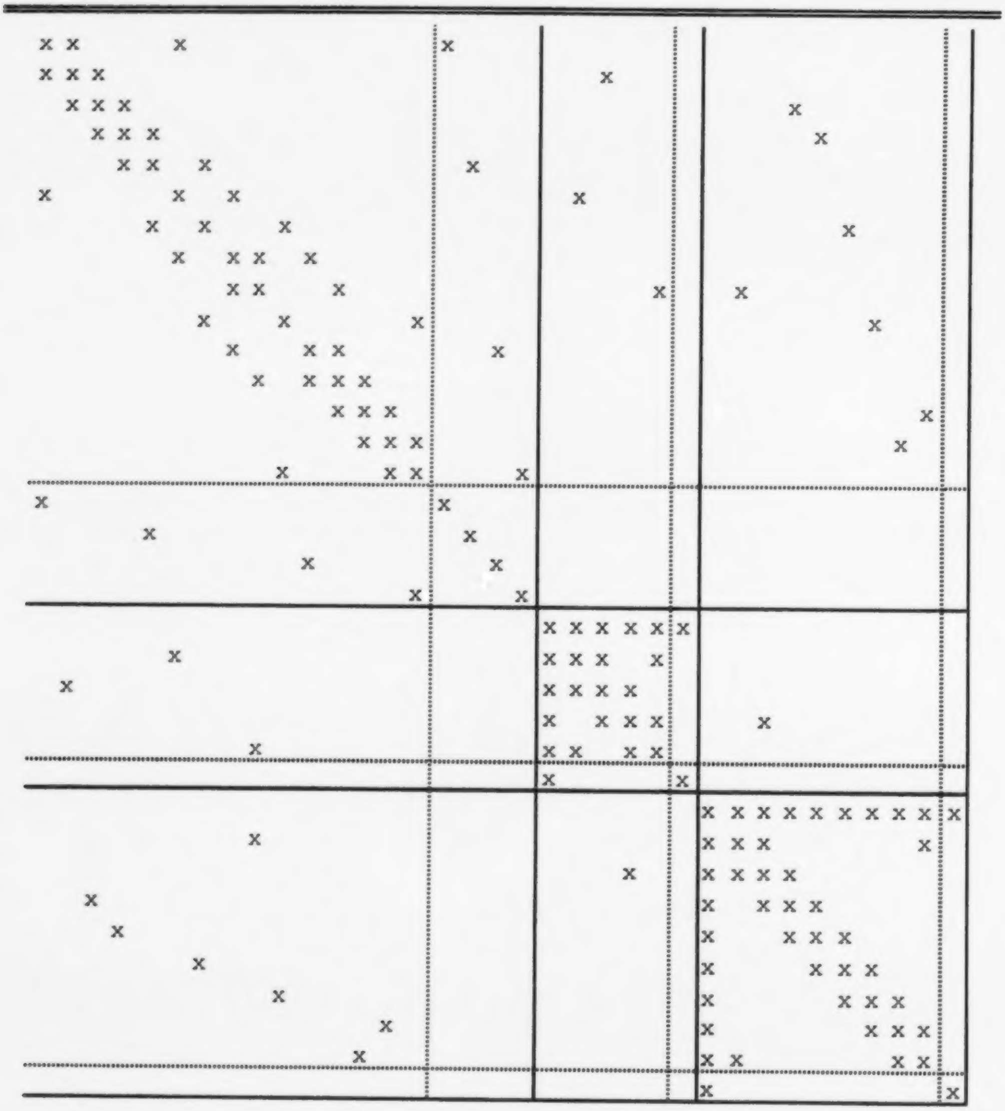

Figure 4.5.1.8

Jacobian matrix for a rectilinear system with contiguous hybrid/hyperhybrid grids.

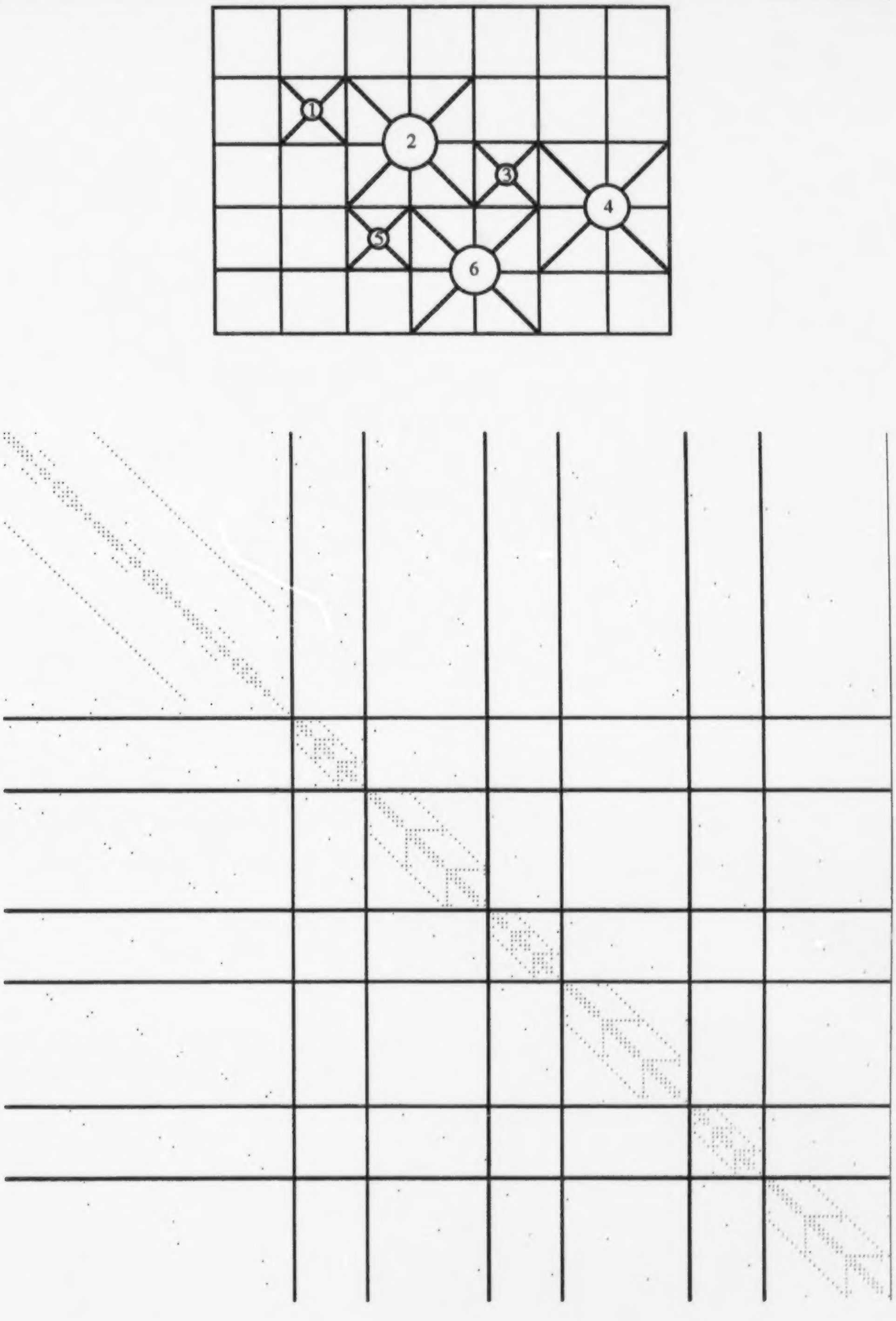

Figure 4.5.1.9 Grid and Jacobian matrix for a three-dimensional problem with 6 hybrid/hyperhybrid regions.

$\frac{\partial R_{c_i f}}{\partial P_{rf}}$ derivatives of the hybrid region *i* flow equations with respect to the rectilinear flow variables, and

$\frac{\partial R_{c_i f}}{\partial P_{c_j f}}$ derivatives of the hybrid region *i* flow equations with respect to the hybrid region *j* flow variables.

4.5.2 Derivatives of the *F* Equations at Node *i, j, k*

The partial derivatives required for the *F* equation are given below. For the pressure derivative at node *i, j, k*,

$$\frac{\partial \underset{i,j,k}{F_i^{n+1}}}{\partial \underset{i,j,k}{p_o^{n+1}}} = \sum_{p=1}^{N_p}\left[\sum_m\left(\frac{\partial \underset{l}{T_p^{n+1}}}{\partial \underset{i,j,k}{p_o^{n+1}}}\left[\left(\underset{m}{p_p^{n+1}} - \underset{i,j,k}{p_p^{n+1}}\right) - \underset{l}{\rho_p^{n+1}} g\left(z_m - z_{i,j,k}\right)\right]\right.\right.$$

$$\left.\left. + \underset{l}{T_p^{n+1}}\left(\left[-\frac{\partial p_p}{\partial p_o}\right]_{i,j,k}^{n+1} - \frac{\partial \underset{l}{\rho_p^{n+1}}}{\partial \underset{i,j,k}{p_o^{n+1}}} g\left(z_m - z_{i,j,k}\right)\right)\right)\right.$$

$$\left. - \frac{\underset{i,j,k}{V_b}}{\Delta t}\left[X_i S_p\left(K_{vip}\phi \frac{\partial \rho_p}{\partial p_o} + K_{vip}\rho_p \frac{\partial \phi}{\partial p_o} + \phi\rho_p \frac{\partial K_{vip}}{\partial p_o}\right)\right]_{i,j,k}^{n+1} - \left[\frac{\partial q_{ip}}{\partial p_o}\right]_{i,j,k}^{n+1}\right], \qquad (4.5.2.1)$$

where

$$m = i+1,j,k;\; i-1,j,k;\; i,j+1,k;\; i,j-1,k;\; i,j,k+1;\; i,j,k-1\ . \qquad (4.5.2.2)$$

Note that

$$l = i+\frac{1}{2},j,k;\; i-\frac{1}{2},j,k;\; i,j+\frac{1}{2},k;\; i,j-\frac{1}{2},k;\; i,j,k+\frac{1}{2};\; i,j,k-\frac{1}{2} \qquad (4.5.2.3)$$

and

$$\underset{l}{\rho_p} = \frac{1}{2}\left(\underset{m}{\rho_p} + \underset{i,j,k}{\rho_p}\right) \qquad (4.5.2.4)$$

is an example of the average density between grid blocks. The partial derivatives in Equation 4.5.2.1 are given by

$$\frac{\partial p_p}{\partial p_o} = \begin{cases} \dfrac{\partial}{\partial p_o}\left(p_o - P_{cow}\right) = 1 & p = w \\ 1 & p = o \;, \\ \dfrac{\partial}{\partial p_o}\left(p_o + P_{cgo}\right) = 1 & p = g \end{cases} \tag{4.5.2.5}$$

$$\frac{\partial T^{n+1}_{\substack{px \\ i+\frac{1}{2},j,k}}}{\partial p^{n+1}_{\substack{o \\ i,j,k}}} = \left[\frac{A_x k_x}{\Delta x}\right]_{i+\frac{1}{2},j,k} \omega_{\substack{px \\ i,j,k}} \left[\frac{X_i k_{rp}}{\mu_p}\left(K_{vip}\frac{\partial \rho_p}{\partial p_o} + \rho_p \frac{\partial K_{vip}}{\partial p_o} - \frac{K_{vip}\rho_p}{\mu_p}\frac{\partial \mu_p}{\partial p_o}\right)\right]^{n+1}_{i,j,k} \;, \tag{4.5.2.6}$$

and

$$\frac{\partial T^{n+1}_{\substack{px \\ i-\frac{1}{2},j,k}}}{\partial p^{n+1}_{\substack{o \\ i,j,k}}} = \left[\frac{A_x k_x}{\Delta x}\right]_{i-\frac{1}{2},j,k} \overset{*}{\omega}_{\substack{px \\ i,j,k}} \left[\frac{X_i k_{rp}}{\mu_p}\left(K_{vip}\frac{\partial \rho_p}{\partial p_o} + \rho_p \frac{\partial K_{vip}}{\partial p_o} - \frac{K_{vip}\rho_p}{\mu_p}\frac{\partial \mu_p}{\partial p_o}\right)\right]^{n+1}_{i,j,k} \;, \tag{4.5.2.7}$$

where similar expressions exist for the other directions. For a source/sink,

$$\begin{aligned} \frac{\partial q^{n+1}_{\substack{ip \\ i,j,k}}}{\partial p^{n+1}_{\substack{o \\ i,j,k}}} &= J'_{i,j,k}\left[\frac{X_i k_{rp}}{\mu_p}\left(K_{vip}\frac{\partial \rho_p}{\partial p_o} + \rho_p \frac{\partial K_{vip}}{\partial p_o} - \frac{K_{vip}\rho_p}{\mu_p}\frac{\partial \mu_p}{\partial p_o}\right)\right]^{n+1}_{i,j,k}\left[p_o - p_{wf}\right]^{n+1}_{i,j,k} \\ &+ J'_{i,j,k}\left[\frac{k_{rp}\rho_p}{\mu_p}K_{vip}X_i\right]^{n+1}_{i,j,k} \text{ (sink),} \end{aligned} \tag{4.5.2.8a}$$

and

$$\begin{aligned} \frac{\partial q^{n+1}_{\substack{ip \\ i,j,k}}}{\partial p^{n+1}_{\substack{o \\ i,j,k}}} &= \left[\rho_p K_{vip} X_i\right]^{n+1}_{\substack{wb \\ i,j,k}} J'_{i,j,k}\left[\sum_{p=1}^{N_p}\frac{k_{rp}}{\mu_p}\left(-\frac{1}{\mu_p}\right)\frac{\partial \mu_p}{\partial p_o}\right]^{n+1}_{i,j,k}\left[p_o - p_{wf}\right]^{n+1}_{i,j,k} \\ &+ \left[\rho_p K_{vip} X_i\right]^{n+1}_{\substack{wb \\ i,j,k}} J'_{i,j,k}\left[\sum_{p=1}^{N_p}\frac{k_{rp}}{\mu_p}\right]^{n+1}_{i,j,k} \text{ (source).} \end{aligned} \tag{4.5.2.8b}$$

For the aqueous saturation derivative at node *i*, *j*, *k*,

$$\frac{\partial F^{n+1}_{\substack{i \\ i,j,k}}}{\partial S^{n+1}_{\substack{w \\ i,j,k}}} = \sum_{p=1}^{N_p}\left[\sum_{m}\left(\frac{\partial T^{n+1}_{\substack{p \\ l}}}{\partial S^{n+1}_{\substack{w \\ i,j,k}}}\left[\left(p^{n+1}_{\substack{p \\ m}} - p^{n+1}_{\substack{p \\ i,j,k}}\right) - \rho^{n+1}_{\substack{p \\ l}} g\left(z_m - z_{i,j,k}\right)\right] + T^{n+1}_{\substack{p \\ l}}\left[-\frac{\partial p_p}{\partial S_w}\right]^{n+1}_{i,j,k}\right)\right.$$

$$-\frac{\underset{i,j,k}{V_b}}{\Delta t}\left[\frac{\partial}{\partial S_w}\left(\phi K_{vip}X_i\rho_p S_p\right)\right]_{i,j,k}^{n+1}-\left[\frac{\partial q_{ip}}{\partial S_w}\right]_{i,j,k}^{n+1}\Bigg] . \tag{4.5.2.9}$$

The partial derivatives in Equation 4.5.2.9 are given by

$$\frac{\partial p_p}{\partial S_w}=\begin{cases}\dfrac{\partial}{\partial S_w}\left(p_o-P_{cow}\right)=-\dfrac{\partial P_{cow}}{\partial S_w} & p=w\\ 0 & p=o\ ,\\ 0 & p=g\end{cases} \tag{4.5.2.10}$$

$$\frac{\partial}{\partial S_w}\left(\phi K_{vip}X_i\rho_p S_p\right)=\begin{cases}\phi K_{viw}X_i\rho_w & p=w\\ 0 & p=o\ ,\\ 0 & p=g\end{cases} \tag{4.5.2.11}$$

$$\frac{\partial \underset{i+\frac{1}{2},j,k}{T_{px}^{n+1}}}{\partial \underset{i,j,k}{S_w^{n+1}}}=\left[\frac{A_x k_x}{\Delta x}\right]_{i+\frac{1}{2},j,k}\underset{i,j,k}{\omega_{px}}\left[\frac{K_{vip}X_i\rho_p}{\mu_p}\frac{\partial k_{rp}}{\partial S_w}\right]_{i,j,k}^{n+1} , \tag{4.5.2.12}$$

and

$$\frac{\partial \underset{i-\frac{1}{2},j,k}{T_{px}^{n+1}}}{\partial \underset{i,j,k}{S_w^{n+1}}}=\left[\frac{A_x k_x}{\Delta x}\right]_{i-\frac{1}{2},j,k}\underset{i,j,k}{\omega_{px}^{*}}\left[\frac{K_{vip}X_i\rho_p}{\mu_p}\frac{\partial k_{rp}}{\partial S_w}\right]_{i,j,k}^{n+1} , \tag{4.5.2.13}$$

where similar expressions exist for the other directions. For a source/sink,

$$\frac{\partial \underset{i,j,k}{q_{ip}^{n+1}}}{\partial \underset{i,j,k}{S_w^{n+1}}}=J'_{i,j,k}\left[\frac{K_{vip}X_i\rho_p}{\mu_p}\frac{\partial k_{rp}}{\partial S_w}\right]_{i,j,k}^{n+1}\left[p_o-p_{wf}\right]_{i,j,k}^{n+1}\ \text{(sink)}, \tag{4.5.2.14a}$$

and

$$\frac{\partial \underset{i,j,k}{q_{ip}^{n+1}}}{\partial \underset{i,j,k}{S_w^{n+1}}}=\left[\rho_p K_{vip}X_i\right]_{\underset{i,j,k}{wb}}^{n+1}J'_{i,j,k}\left[\sum_{p=1}^{N_p}\frac{1}{\mu_p}\frac{\partial k_{rp}}{\partial S_w}\right]_{i,j,k}^{n+1}\left[p_o-p_{wf}\right]_{i,j,k}^{n+1}\ \text{(source)}. \tag{4.5.2.14b}$$

For the oleic saturation derivative at node *i*, *j*, *k*,

$$\frac{\partial F_{i\,i,j,k}^{n+1}}{\partial S_{o\,i,j,k}^{n+1}} = \sum_{p=1}^{N_p}\left[\sum_m\left(\frac{\partial T_{p\,l}^{n+1}}{\partial S_{o\,i,j,k}^{n+1}}\left[\left(p_{p\,m}^{n+1} - p_{p\,i,j,k}^{n+1}\right) - \rho_{p\,l}^{n+1} g\left(z_m - z_{i,j,k}\right)\right] + T_{p\,l}^{n+1}\left[-\frac{\partial p_p}{\partial S_o}\right]_{i,j,k}^{n+1}\right)\right.$$

$$\left. - \frac{V_{b\,i,j,k}}{\Delta t}\left[\frac{\partial}{\partial S_o}\left(\phi K_{vip} X_i \rho_p S_p\right)\right]_{i,j,k}^{n+1} - \left[\frac{\partial q_{ip}}{\partial S_o}\right]_{i,j,k}^{n+1}\right]. \qquad (4.5.2.15)$$

The partial derivatives in Equation 4.5.2.15 are given by

$$\frac{\partial p_p}{\partial S_o} = \begin{cases} 0 & p = w \\ 0 & p = o \\ 0 & p = g \end{cases}, \qquad (4.5.2.16)$$

$$\frac{\partial}{\partial S_o}\left(\phi K_{vip} X_i \rho_p S_p\right) = \begin{cases} 0 & p = w \\ \phi K_{vio} X_i \rho_o & p = o \\ 0 & p = g \end{cases}, \qquad (4.5.2.17)$$

$$\frac{\partial T_{px\,i+\frac{1}{2},j,k}^{n+1}}{\partial S_{o\,i,j,k}^{n+1}} = \left[\frac{A_x k_x}{\Delta x}\right]_{i+\frac{1}{2},j,k} \omega_{px\,i,j,k} \left[\frac{K_{vip} X_i \rho_p}{\mu_p}\frac{\partial k_{rp}}{\partial S_o}\right]_{i,j,k}^{n+1}, \qquad (4.5.2.18)$$

and

$$\frac{\partial T_{px\,i-\frac{1}{2},j,k}^{n+1}}{\partial S_{o\,i,j,k}^{n+1}} = \left[\frac{A_x k_x}{\Delta x}\right]_{i-\frac{1}{2},j,k} \omega_{px\,i,j,k}^{*} \left[\frac{K_{vip} X_i \rho_p}{\mu_p}\frac{\partial k_{rp}}{\partial S_o}\right]_{i,j,k}^{n+1}, \qquad (4.5.2.19)$$

where similar expressions exist for the other directions. For a source/sink

$$\frac{\partial q_{ip\,i,j,k}^{n+1}}{\partial S_{o\,i,j,k}^{n+1}} = J'_{i,j,k}\left[\frac{K_{vip} X_i \rho_p}{\mu_p}\frac{\partial k_{rp}}{\partial S_o}\right]_{i,j,k}^{n+1}\left[p_o - p_{wf}\right]_{i,j,k}^{n+1} \text{ (sink)}, \qquad (4.5.2.20a)$$

and

$$\frac{\partial \underset{i,j,k}{q_{ip}^{n+1}}}{\partial \underset{i,j,k}{S_o^{n+1}}} = \left[\rho_p K_{vip} X_i\right]^{n+1}_{\substack{wb \\ i,j,k}} J'_{i,j,k} \left[\sum_{p=1}^{N_p} \frac{1}{\mu_p} \frac{\partial k_{rp}}{\partial S_o}\right]^{n+1}_{i,j,k} \left[p_o - p_{wf}\right]^{n+1}_{i,j,k} \text{ (source).} \qquad (4.5.2.20b)$$

For the gaseous saturation derivative at node *i*, *j*, *k*,

$$\frac{\partial \underset{i,j,k}{F_i^{n+1}}}{\partial \underset{i,j,k}{S_g^{n+1}}} = \sum_{p=1}^{N_p} \left[\sum_m \left(\frac{\partial \underset{l}{T_p^{n+1}}}{\partial \underset{i,j,k}{S_g^{n+1}}} \left[\left(\underset{m}{p_p^{n+1}} - \underset{i,j,k}{p_p^{n+1}} \right) - \underset{l}{\rho_p^{n+1}} g\left(z_m - z_{i,j,k}\right) \right] + \underset{l}{T_p^{n+1}} \left[-\frac{\partial p_p}{\partial S_g} \right]^{n+1}_{i,j,k} \right) \right.$$

$$\left. - \frac{\underset{i,j,k}{V_b}}{\Delta t} \left[\frac{\partial}{\partial S_g} \left(\phi K_{vip} X_i \rho_p S_p \right) \right]^{n+1}_{i,j,k} - \left[\frac{\partial q_{ip}}{\partial S_g} \right]^{n+1}_{i,j,k} \right]. \qquad (4.5.2.21)$$

The partial derivatives in Equation 4.5.2.21 are given by

$$\frac{\partial p_p}{\partial S_g} = \begin{cases} 0 & p = w \\ 0 & p = o \\ \dfrac{\partial}{\partial S_g}\left(p_o + P_{cgo}\right) = \dfrac{\partial P_{cgo}}{\partial S_g} & p = g \end{cases}, \qquad (4.5.2.22)$$

$$\frac{\partial}{\partial S_g}\left(\phi K_{vip} X_i \rho_p S_p\right) = \begin{cases} 0 & p = w \\ 0 & p = o \\ \phi K_{vig} X_i \rho_g & p = g \end{cases}, \qquad (4.5.2.23)$$

$$\frac{\partial \underset{i+\frac{1}{2},j,k}{T_{px}^{n+1}}}{\partial \underset{i,j,k}{S_g^{n+1}}} = \left[\frac{A_x k_x}{\Delta x}\right]_{i+\frac{1}{2},j,k} \underset{i,j,k}{\omega_{px}} \left[\frac{K_{vip} X_i \rho_p}{\mu_p} \frac{\partial k_{rp}}{\partial S_g}\right]^{n+1}_{i,j,k}, \qquad (4.5.2.24)$$

and

$$\frac{\partial \underset{i-\frac{1}{2},j,k}{T_{px}^{n+1}}}{\partial \underset{i,j,k}{S_g^{n+1}}} = \left[\frac{A_x k_x}{\Delta x}\right]_{i-\frac{1}{2},j,k} \underset{i,j,k}{\omega_{px}^{*}} \left[\frac{K_{vip} X_i \rho_p}{\mu_p} \frac{\partial k_{rp}}{\partial S_g}\right]^{n+1}_{i,j,k}, \qquad (4.5.2.25)$$

where similar expressions exist for the other directions. For a source/sink,

$$\frac{\partial \underset{i,j,k}{q_{ip}^{n+1}}}{\partial \underset{i,j,k}{S_g^{n+1}}} = J'_{i,j,k} \left[\frac{K_{vip} X_i \rho_p}{\mu_p} \frac{\partial k_{rp}}{\partial S_g}\right]^{n+1}_{i,j,k} \left[p_o - p_{wf}\right]^{n+1}_{i,j,k} \text{ (sink),} \qquad (4.5.2.26a)$$

and

$$\frac{\underset{i,j,k}{\partial q_{ip}^{n+1}}}{\underset{i,j,k}{\partial S_{g}^{n+1}}} = \left[\rho_p K_{vip} X_i\right]_{\substack{wb\\i,j,k}}^{n+1} J'_{i,j,k} \left[\sum_{p=1}^{N_p} \frac{1}{\mu_p} \frac{\partial k_{rp}}{\partial S_g}\right]_{i,j,k}^{n+1} \left[p_o - p_{wf}\right]_{i,j,k}^{n+1} \text{ (source).} \qquad (4.5.2.26b)$$

For the temperature derivative at node *i*, *j*, *k*,

$$\frac{\underset{i,j,k}{\partial F_i^{n+1}}}{\partial \theta_{i,j,k}^{n+1}} = \sum_{p=1}^{N_p} \left[\sum_m \left(\frac{\underset{l}{\partial T_p^{n+1}}}{\partial \theta_{i,j,k}^{n+1}} \left[\left(\underset{m}{p_p^{n+1}} - \underset{i,j,k}{p_p^{n+1}} \right) - \underset{l}{\rho_p^{n+1}} g\left(z_m - z_{i,j,k}\right) \right] \right. \right.$$

$$\left. + \underset{l}{T_p^{n+1}} \left(\left[-\frac{\partial p_p}{\partial \theta} \right]_{i,j,k}^{n+1} - \frac{\underset{l}{\partial \rho_p^{n+1}}}{\partial \theta_{i,j,k}^{n+1}} g\left(z_m - z_{i,j,k}\right) \right) \right)$$

$$\left. - \frac{\underset{i,j,k}{V_b}}{\Delta t} \left[\phi X_i S_p \left(K_{vip} \frac{\partial \rho_p}{\partial \theta} + \rho_p \frac{\partial K_{vip}}{\partial \theta} \right) \right]_{i,j,k}^{n+1} - \left[\frac{\partial q_{ip}}{\partial \theta} \right]_{i,j,k}^{n+1} \right] . \qquad (4.5.2.27)$$

The partial derivatives in Equation 4.5.2.27 are given by

$$\frac{\partial p_p}{\partial \theta} = \begin{cases} \dfrac{\partial}{\partial \theta}\left(p_o - P_{cow}\right) = -\dfrac{\partial P_{cow}}{\partial \theta} & p = w \\ 0 & p = o \;, \\ \dfrac{\partial}{\partial \theta}\left(p_o + P_{cgo}\right) = \dfrac{\partial P_{cgo}}{\partial \theta} & p = g \end{cases} \qquad (4.5.2.28)$$

$$\frac{\underset{i+\frac{1}{2},j,k}{\partial T_{px}^{n+1}}}{\partial \theta_{i,j,k}^{n+1}} = \left[\frac{A_x k_x}{\Delta x} \right]_{i+\frac{1}{2},j,k} \underset{i,j,k}{\omega_{px}}$$

$$\left[\frac{X_i}{\mu_p} \left(K_{vip} \rho_p \frac{\partial k_{rp}}{\partial \theta} + K_{vip} k_{rp} \frac{\partial \rho_p}{\partial \theta} + \rho_p k_{rp} \frac{\partial K_{vip}}{\partial \theta} - \frac{K_{vip} \rho_p k_{rp}}{\mu_p} \frac{\partial \mu_p}{\partial \theta} \right) \right]_{i,j,k}^{n+1} , \qquad (4.5.2.29)$$

and

$$\frac{\underset{i-\frac{1}{2},j,k}{\partial T_{px}^{n+1}}}{\partial \theta_{i,j,k}^{n+1}} = \left[\frac{A_x k_x}{\Delta x} \right]_{i-\frac{1}{2},j,k} \underset{i,j,k}{\overset{\bullet}{\omega}_{px}}$$

$$\left[\frac{X_i}{\mu_p}\left(K_{vip}\rho_p\frac{\partial k_{rp}}{\partial\theta}+K_{vip}k_{rp}\frac{\partial\rho_p}{\partial\theta}+\rho_p k_{rp}\frac{\partial K_{vip}}{\partial\theta}-\frac{K_{vip}\rho_p k_{rp}}{\mu_p}\frac{\partial\mu_p}{\partial\theta}\right)\right]_{i,j,k}^{n+1}, \qquad (4.5.2.30)$$

where similar expressions exist for the other directions. For a source/sink,

$$\frac{\partial \underset{i,j,k}{q_{ip}^{n+1}}}{\partial\theta_{i,j,k}^{n+1}}=J'_{i,j,k}\left[\frac{X_i}{\mu_p}\left(K_{vip}\rho_p\frac{\partial k_{rp}}{\partial\theta}+K_{vip}k_{rp}\frac{\partial\rho_p}{\partial\theta}+\rho_p k_{rp}\frac{\partial K_{vip}}{\partial\theta}-\frac{K_{vip}\rho_p k_{rp}}{\mu_p}\frac{\partial\mu_p}{\partial\theta}\right)\right]_{i,j,k}^{n+1}$$

$$\left[p_o-p_{wf}\right]_{i,j,k}^{n+1}\ \text{(sink)}, \qquad (4.5.2.31a)$$

and

$$\frac{\partial \underset{i,j,k}{q_{ip}^{n+1}}}{\partial\theta_{i,j,k}^{n+1}}=\left[\rho_p K_{vip}X_i\right]_{\substack{wb\\ i,j,k}}^{n+1}J'_{i,j,k}\left[\sum_{p=1}^{Np}\frac{1}{\mu_p}\left(\frac{\partial k_{rp}}{\partial\theta}-\frac{k_{rp}}{\mu_p}\frac{\partial\mu_p}{\partial\theta}\right)\right]_{i,j,k}^{n+1}\left[p_o-p_{wf}\right]_{i,j,k}^{n+1}\ \text{(source)}. \qquad (4.5.2.31b)$$

For each of the composition derivatives at node *i*, *j*, *k*,

$$\frac{\partial \underset{i,j,k}{F_i^{n+1}}}{\partial \underset{i,j,k}{X_j^{n+1}}}=\sum_{p=1}^{N_p}\left[\sum_m\left(\frac{\partial \underset{l}{T_p^{n+1}}}{\partial \underset{i,j,k}{X_j^{n+1}}}\left[\left(\underset{m}{p_p^{n+1}}-\underset{i,j,k}{p_p^{n+1}}\right)-\underset{l}{\rho_p^{n+1}}g\left(z_m-z_{i,j,k}\right)\right]\right.\right.$$

$$\left.\left.+\underset{l}{T_p^{n+1}}\left(\left[-\frac{\partial\rho_p}{\partial X_j}\right]_{i,j,k}^{n+1}-\frac{\partial \underset{l}{\rho_p^{n+1}}}{\partial \underset{i,j,k}{X_j^{n+1}}}g\left(z_m-z_{i,j,k}\right)\right)\right)\right.$$

$$\left.-\frac{\underset{i,j,k}{V_b}}{\Delta t}\left[\phi K_{vip}S_p\left(X_i\frac{\partial\rho_p}{\partial X_j}+\rho_p\frac{\partial X_i}{\partial X_j}\right)\right]_{i,j,k}^{n+1}-\left[\frac{\partial q_{ip}}{\partial X_j}\right]_{i,j,k}^{n+1}\right], \qquad (4.5.2.32)$$

The partial derivatives in Equation 4.5.2.32 are given by

$$\frac{\partial p_p}{\partial X_j}=\begin{cases}\dfrac{\partial}{\partial X_j}\left(p_o-P_{cow}\right)=-\dfrac{\partial P_{cow}}{\partial X_j} & p=w\\ 0 & p=o\\ \dfrac{\partial}{\partial X_j}\left(p_o+P_{cgo}\right)=\dfrac{\partial P_{cgo}}{\partial X_j} & p=g\end{cases}, \qquad (4.5.2.33)$$

$$\frac{\partial T^{n+1}_{\substack{px\\i+\frac{1}{2},j,k}}}{\partial X^{n+1}_{\substack{j\\i,j,k}}} = \left[\frac{A_x k_x}{\Delta x}\right]_{i+\frac{1}{2},j,k} \omega_{\substack{px\\i,j,k}} \left[\frac{K_{vip} k_{rp}}{\mu_p}\left(X_i \frac{\partial \rho_p}{\partial X_j} + \rho_p \frac{\partial X_i}{\partial X_j} - \frac{X_i \rho_p}{\mu_p}\frac{\partial \mu_p}{\partial X_j}\right)\right]^{n+1}_{i,j,k}, \quad (4.5.2.34)$$

$$\frac{\partial T^{n+1}_{\substack{px\\i-\frac{1}{2},j,k}}}{\partial X^{n+1}_{\substack{j\\i,j,k}}} = \left[\frac{A_x k_x}{\Delta x}\right]_{i-\frac{1}{2},j,k} \overset{*}{\omega}_{\substack{px\\i,j,k}} \left[\frac{K_{vip} k_{rp}}{\mu_p}\left(X_i \frac{\partial \rho_p}{\partial X_j} + \rho_p \frac{\partial X_i}{\partial X_j} - \frac{X_i \rho_p}{\mu_p}\frac{\partial \mu_p}{\partial X_j}\right)\right]^{n+1}_{i,j,k}, \quad (4.5.2.35)$$

and

$$\frac{\partial X_i}{\partial X_j} = \begin{cases} 1 & i = j \\ 0 & i \neq j \end{cases}, \quad (4.5.2.36)$$

where similar expressions exist for the other directions. For a source/sink,

$$\frac{\partial q^{n+1}_{\substack{ip\\i,j,k}}}{\partial X^{n+1}_{\substack{j\\i,j,k}}} = J'_{i,j,k}\left[\frac{K_{vip} k_{rp}}{\mu_p}\left(X_i \frac{\partial \rho_p}{\partial X_j} + \rho_p \frac{\partial X_i}{\partial X_j} - \frac{X_i \rho_p}{\mu_p}\frac{\partial \mu_p}{\partial X_j}\right)\right]^{n+1}_{i,j,k} \left[p_o - p_{wf}\right]^{n+1}_{i,j,k} \text{ (sink)}, \quad (4.5.2.37a)$$

and

$$\frac{\partial q^{n+1}_{\substack{ip\\i,j,k}}}{\partial X^{n+1}_{\substack{j\\i,j,k}}} = \left[\rho_p K_{vip} X_i\right]^{n+1}_{\substack{wb\\i,j,k}} J'_{i,j,k}\left[\sum_{p=1}^{N_p}\frac{k_{rp}}{\mu_p}\left(-\frac{1}{\mu_p}\frac{\partial \mu_p}{\partial X_j}\right)\right]^{n+1}_{i,j,k} \left[p_o - p_{wf}\right]^{n+1}_{i,j,k} \text{ (source)}. \quad (4.5.2.37b)$$

For the well pressure derivative at node *i*, *j*, *k*,

$$\frac{\partial F^{n+1}_{\substack{i\\i,j,k}}}{\partial p^{n+1}_{\substack{wf\\i,j}}} = \sum_{p=1}^{N_p} -\left[\frac{\partial q_{ip}}{\partial p_{wf}}\right]^{n+1}_{i,j,k}, \quad (4.5.2.38)$$

where for a source/sink,

$$\frac{\partial q^{n+1}_{\substack{ip\\i,j,k}}}{\partial p^{n+1}_{\substack{wf\\i,j}}} = -J'_{i,j,k}\left[\frac{k_{rp}\rho_p}{\mu_p} K_{vip} X_i\right]^{n+1}_{i,j,k} \text{ (sink)}, \quad (4.5.2.39a)$$

and

$$\begin{aligned}\frac{\underset{i,j,k}{\partial q_{ip}^{n+1}}}{\underset{i,j}{\partial p_{wf}^{n+1}}}=&\frac{\partial\left[\rho_p K_{vip} X_i\right]_{\substack{wb\\i,j,k}}^{n+1}}{\underset{i,j}{\partial p_{wf}^{n+1}}}J'_{i,j,k}\left[\sum_{p=1}^{N_p}\frac{k_{rp}}{\mu_p}\right]_{i,j,k}^{n+1}\left[p_o-p_{wf}\right]_{i,j,k}^{n+1}\\&-\left[\rho_p K_{vip} X_i\right]_{\substack{wb\\i,j,k}}^{n+1}J'_{i,j,k}\left[\sum_{p=1}^{N_p}\frac{k_{rp}}{\mu_p}\right]_{i,j,k}^{n+1}\quad\text{(source)},\end{aligned}\tag{4.5.2.39b}$$

and the derivatives with respect to the other nodes are zero.

The derivatives of *F* with respect to the variables at the other nodes are similar to those above except that they are less complicated. They are given in Appendix II.

4.5.3 Derivatives of the *G* Equation at Node *i*, *j*, *k*

The partial derivatives required for the *G* equation are given below. For the pressure derivative at node *i*, *j*, *k*,

$$\begin{aligned}\frac{\partial G_{i,j,k}^{n+1}}{\underset{i,j,k}{\partial p_o^{n+1}}}=\sum_{p=1}^{N_p}&\left[\sum_m\left(\frac{\partial \underset{l}{T_p^{*}}^{n+1}}{\underset{i,j,k}{\partial p_o^{n+1}}}\left[\left(\underset{m}{p_p^{n+1}}-\underset{i,j,k}{p_p^{n+1}}\right)-\underset{l}{\rho_p^{n+1}}g\left(z_m-z_{i,j,k}\right)\right]\right.\right.\\&\left.+\underset{l}{T_p^{*}}^{n+1}\left(\left[-\frac{\partial\rho_p}{\partial p_o}\right]_{i,j,k}^{n+1}-\frac{\partial\underset{l}{\rho_p^{n+1}}}{\underset{i,j,k}{\partial p_o^{n+1}}}g\left(z_m-z_{i,j,k}\right)\right)\right)\\&\left.-\frac{\underset{i,j,k}{V_b}}{\Delta t}\left[S_p\left(E_p\phi\frac{\partial\rho_p}{\partial p_o}+E_p\rho_p\frac{\partial\phi}{\partial p_o}+\phi\rho_p\frac{\partial E_p}{\partial p_o}\right)\right]_{i,j,k}^{n+1}\right]-\left[\frac{\partial q}{\partial p_o}\right]_{i,j,k}^{n+1}\\&-\frac{\underset{i,j,k}{V_b}}{\Delta t}\left[-M_f(\theta-\theta_r)\frac{\partial\phi}{\partial p_o}\right]_{i,j,k}^{n+1},\end{aligned}\tag{4.5.3.1}$$

where

$$m=i+1,j,k;\ i-1,j,k;\ i,j+1,k;\ i,j-1,k;\ i,j,k+1;\ i,j,k-1\tag{4.5.3.2}$$

and

$$l = i+\frac{1}{2},j,k;\ i-\frac{1}{2},j,k;\ i,j+\frac{1}{2},k;\ i,j-\frac{1}{2},k;\ i,j,k+\frac{1}{2};\ i,j,k-\frac{1}{2}\ . \tag{4.5.3.3}$$

The partial derivatives in Equation 4.5.3.1 are given by

$$\frac{\partial p_p}{\partial p_o} = \begin{cases} \dfrac{\partial}{\partial p_o}\left(p_o - P_{cow}\right) = 1 & p = w \\ 1 & p = o\ , \\ \dfrac{\partial}{\partial p_o}\left(p_o + P_{cgo}\right) = 1 & p = g \end{cases} \tag{4.5.3.4}$$

$$\frac{\partial \underset{i+\frac{1}{2},j,k}{\overset{n+1}{T^{*}_{px}}}}{\underset{i,j,k}{\partial p_o^{n+1}}} = \left[\frac{A_x k_x}{\Delta x}\right]_{i+\frac{1}{2},j,k} \underset{i,j,k}{\omega_{px}} \left[\frac{k_{rp}}{\mu_p}\left(H_p \frac{\partial \rho_p}{\partial p_o} + \rho_p \frac{\partial H_p}{\partial p_o} - \frac{H_p \rho_p}{\mu_p}\frac{\partial \mu_p}{\partial p_o}\right)\right]_{i,j,k}^{n+1}\ , \tag{4.5.3.5}$$

and

$$\frac{\partial \underset{i-\frac{1}{2},j,k}{T^{n+1}_{px}}}{\underset{i,j,k}{\partial p_o^{n+1}}} = \left[\frac{A_x k_x}{\Delta x}\right]_{i-\frac{1}{2},j,k} \underset{i,j,k}{\omega^{*}_{px}} \left[\frac{k_{rp}}{\mu_p}\left(H_p \frac{\partial \rho_p}{\partial p_o} + \rho_p \frac{\partial H_p}{\partial p_o} - \frac{H_p \rho_p}{\mu_p}\frac{\partial \mu_p}{\partial p_o}\right)\right]_{i,j,k}^{n+1}\ , \tag{4.5.3.6}$$

where similar expressions exist for the other directions, and

$$\frac{\partial q^{n+1}_{i,j,k}}{\underset{i,j,k}{\partial p_o^{n+1}}} = \sum_p \left[E_p \sum_i \frac{\partial q_{ip}}{\partial p_o}\right]_{i,j,k}^{n+1}\ . \tag{4.5.3.7}$$

For the aqueous saturation derivative at node *i*, *j*, *k*

$$\frac{\partial G^{n+1}_{i,j,k}}{\underset{i,j,k}{\partial S_w^{n+1}}} = \sum_{p=1}^{N_p}\left[\sum_m \left(\frac{\partial \underset{l}{\overset{n+1}{T^{*}_p}}}{\underset{i,j,k}{\partial S_w^{n+1}}}\left[\left(\underset{m}{p_p^{n+1}} - \underset{i,j,k}{p_p^{n+1}}\right) - \underset{l}{\rho_p^{n+1}} g\left(z_m - z_{i,j,k}\right)\right] + \underset{l}{\overset{n+1}{T^{*}_p}}\left[-\frac{\partial p_p}{\partial S_w}\right]_{i,j,k}^{n+1}\right)\right.$$

$$\left. - \frac{\underset{i,j,k}{V_b}}{\Delta t}\left[\frac{\partial}{\partial S_w}\left(\phi E_p \rho_p S_p\right)\right]_{i,j,k}^{n+1}\right] - \left[\frac{\partial q}{\partial S_w}\right]_{i,j,k}^{n+1}\ . \tag{4.5.3.8}$$

The partial derivatives in Equation 4.5.3.8 are given by

$$\frac{\partial p_p}{\partial S_w} = \begin{cases} \dfrac{\partial}{\partial S_w}\left(p_o - P_{cow}\right) = -\dfrac{\partial P_{cow}}{\partial S_w} & p = w \\ 0 & p = o \\ 0 & p = g \end{cases} , \tag{4.5.3.9}$$

$$\frac{\partial}{\partial S_w}\left(\phi E_p \rho_p S_p\right) = \begin{cases} \phi E_w \rho_w & p = w \\ 0 & p = o \\ 0 & p = g \end{cases} , \tag{4.5.3.10}$$

$$\frac{\partial \overset{n+1}{\underset{i+\frac{1}{2},j,k}{T^{*}_{px}}}}{\partial \underset{i,j,k}{S_w^{n+1}}} = \left[\frac{A_x k_x}{\Delta x}\right]_{i+\frac{1}{2},j,k} \underset{i,j,k}{\omega_{px}} \left[\frac{H_p \rho_p}{\mu_p} \frac{\partial k_{rp}}{\partial S_w}\right]^{n+1}_{i,j,k} , \tag{4.5.3.11}$$

and

$$\frac{\partial \overset{n+1}{\underset{i-\frac{1}{2},j,k}{T^{*}_{px}}}}{\partial \underset{i,j,k}{S_w^{n+1}}} = \left[\frac{A_x k_x}{\Delta x}\right]_{i-\frac{1}{2},j,k} \underset{i,j,k}{\overset{*}{\omega}_{px}} \left[\frac{H_p \rho_p}{\mu_p} \frac{\partial k_{rp}}{\partial S_w}\right]^{n+1}_{i,j,k} , \tag{4.5.3.12}$$

where similar expressions exist for the other directions, and

$$\frac{\partial q^{n+1}_{i,j,k}}{\partial \underset{i,j,k}{S_w^{n+1}}} = \sum_p \left[E_p \sum_i \frac{\partial q_{ip}}{\partial S_w}\right]^{n+1}_{i,j,k} . \tag{4.5.3.13}$$

For the oleic saturation derivative at node *i*, *j*, *k*,

$$\begin{aligned} \frac{\partial G^{n+1}_{i,j,k}}{\partial \underset{i,j,k}{S_o^{n+1}}} = \sum_{p=1}^{N_p} \Bigg[\sum_m \Bigg(& \frac{\partial \overset{n+1}{\underset{l}{T^{*}_p}}}{\partial \underset{i,j,k}{S_o^{n+1}}} \left[\left(\underset{m}{p_p^{n+1}} - \underset{i,j,k}{p_p^{n+1}}\right) - \underset{l}{\rho_p^{n+1}} g\left(z_m - z_{i,j,k}\right)\right] + \overset{n+1}{\underset{l}{T^{*}_p}} \left[-\frac{\partial p_p}{\partial S_o}\right]^{n+1}_{i,j,k} \Bigg) \\ & - \frac{\underset{i,j,k}{V_b}}{\Delta t} \left[\frac{\partial}{\partial S_o}\left(\phi E_p \rho_p S_p\right)\right]^{n+1}_{i,j,k} \Bigg] - \left[\frac{\partial q}{\partial S_o}\right]^{n+1}_{i,j,k} . \end{aligned} \tag{4.5.3.14}$$

The partial derivatives in Equation 4.5.3.14 are given by

$$\frac{\partial p_p}{\partial S_o} = \begin{cases} 0 & p = w \\ 0 & p = o \ , \\ 0 & p = g \end{cases} \qquad (4.5.3.15)$$

$$\frac{\partial}{\partial S_o}\left(\phi E_p \rho_p S_p\right) = \begin{cases} 0 & p = w \\ \phi E_o \rho_o & p = o \ , \\ 0 & p = g \end{cases} \qquad (4.5.3.16)$$

$$\frac{\partial \overset{n+1}{\underset{i+\frac{1}{2},j,k}{T^{*}_{px}}}}{\underset{i,j,k}{\partial S_o^{n+1}}} = \left[\frac{A_x k_x}{\Delta x}\right]_{i+\frac{1}{2},j,k} \underset{i,j,k}{\omega_{px}} \left[\frac{H_p \rho_p}{\mu_p}\frac{\partial k_{rp}}{\partial S_o}\right]^{n+1}_{i,j,k} , \qquad (4.5.3.17)$$

and

$$\frac{\partial \overset{n+1}{\underset{i-\frac{1}{2},j,k}{T^{*}_{px}}}}{\underset{i,j,k}{\partial S_o^{n+1}}} = \left[\frac{A_x k_x}{\Delta x}\right]_{i-\frac{1}{2},j,k} \underset{i,j,k}{\omega^{*}_{px}} \left[\frac{H_p \rho_p}{\mu_p}\frac{\partial k_{rp}}{\partial S_o}\right]^{n+1}_{i,j,k} , \qquad (4.5.3.18)$$

where similar expressions exist for the other directions, and

$$\frac{\partial q^{n+1}_{i,j,k}}{\underset{i,j,k}{\partial S_o^{n+1}}} = \sum_{p}\left[E_p \sum_{i} \frac{\partial q_{ip}}{\partial S_o}\right]^{n+1}_{i,j,k} . \qquad (4.5.3.19)$$

For the gaseous saturation derivative at node *i*, *j*, *k*,

$$\frac{\partial G^{n+1}_{i,j,k}}{\underset{i,j,k}{\partial S_g^{n+1}}} = \sum_{p=1}^{N_p}\left[\sum_{m}\left(\frac{\partial \overset{n+1}{\underset{l}{T^{*}_{p}}}}{\underset{i,j,k}{\partial S_g^{n+1}}}\left[\left(\underset{m}{p_p^{n+1}} - \underset{i,j,k}{p_p^{n+1}}\right) - \underset{l}{\rho_p^{n+1}} g\left(z_m - z_{i,j,k}\right)\right] + \overset{n+1}{\underset{l}{T^{*}_{p}}}\left[-\frac{\partial p_p}{\partial S_g}\right]^{n+1}_{i,j,k}\right)\right.$$

$$\left. - \frac{\underset{i,j,k}{V_b}}{\Delta t}\left[\frac{\partial}{\partial S_g}\left(\phi E_p \rho_p S_p\right)\right]^{n+1}_{i,j,k}\right] - \left[\frac{\partial q}{\partial S_g}\right]^{n+1}_{i,j,k} . \qquad (4.5.3.20)$$

The partial derivatives in Equation 4.5.3.20 are given by

$$\frac{\partial p_p}{\partial S_g}=\begin{cases}0 & p=w\\ 0 & p=o\\ \dfrac{\partial}{\partial S_g}\left(p_o+P_{cgo}\right)=\dfrac{\partial P_{cgo}}{\partial S_g} & p=g\end{cases}, \tag{4.5.3.21}$$

$$\frac{\partial}{\partial S_g}\left(\phi E_p \rho_p S_p\right)=\begin{cases}0 & p=w\\ 0 & p=o\\ \phi E_g \rho_g & p=g\end{cases}, \tag{4.5.3.22}$$

$$\frac{\partial \overset{n+1}{T^{*}_{px}}_{i+\frac{1}{2},j,k}}{\partial \underset{i,j,k}{S_g^{n+1}}}=\left[\frac{A_x k_x}{\Delta x}\right]_{i+\frac{1}{2},j,k}\underset{i,j,k}{\omega_{px}}\left[\frac{H_p\rho_p}{\mu_p}\frac{\partial k_{rp}}{\partial S_g}\right]^{n+1}_{i,j,k}, \tag{4.5.3.23}$$

and

$$\frac{\partial \overset{n+1}{T^{*}_{px}}_{i-\frac{1}{2},j,k}}{\partial \underset{i,j,k}{S_g^{n+1}}}=\left[\frac{A_x k_x}{\Delta x}\right]_{i-\frac{1}{2},j,k}\underset{i,j,k}{\omega^{*}_{px}}\left[\frac{H_p\rho_p}{\mu_p}\frac{\partial k_{rp}}{\partial S_g}\right]^{n+1}_{i,j,k}, \tag{4.5.3.24}$$

where similar expressions exist for the other directions, and

$$\frac{\partial q^{n+1}_{i,j,k}}{\partial \underset{i,j,k}{S_g^{n+1}}}=\sum_p\left[E_p\sum_i\frac{\partial q_{ip}}{\partial S_g}\right]^{n+1}_{i,j,k}. \tag{4.5.3.25}$$

For the temperature derivative at node *i*, *j*, *k*,

$$\begin{aligned}\frac{\partial G^{n+1}_{i,j,k}}{\partial\theta^{n+1}_{i,j,k}}=\sum_{p=1}^{N_p}\Bigg[\sum_m\Bigg(&\frac{\partial \overset{n+1}{\underset{l}{T^{*}_p}}}{\partial\theta^{n+1}_{i,j,k}}\left[\left(\underset{m}{p_p^{n+1}}-\underset{i,j,k}{p_p^{n+1}}\right)-\underset{l}{\rho_p^{n+1}}g\left(z_m-z_{i,j,k}\right)\right]\\
&+\overset{n+1}{\underset{l}{T^{*}_p}}\left(\left[-\frac{\partial p_p}{\partial\theta}\right]^{n+1}_{i,j,k}-\frac{\partial \underset{l}{\rho_p^{n+1}}}{\partial\theta^{n+1}_{i,j,k}}g\left(z_m-z_{i,j,k}\right)\right)\Bigg)-\frac{\underset{i,j,k}{V_b}}{\Delta t}\left[\phi S_p\left(E_p\frac{\partial\rho_p}{\partial\theta}+\rho_p\frac{\partial E_p}{\partial\theta}\right)\right]^{n+1}_{i,j,k}\Bigg]\\
&-\sum_m\underset{l}{T_c^{n+1}}-\left[\frac{\partial q}{\partial\theta}\right]^{n+1}_{i,j,k}-\frac{\underset{i,j,k}{V_b}}{\Delta t}\left[(1-\phi)\frac{\partial M_f\Delta\theta}{\partial\theta}\right]^{n+1}_{i,j,k}.\end{aligned} \tag{4.5.3.26}$$

The partial derivatives in Equation 4.5.3.26 are given by

$$\frac{\partial p_p}{\partial \theta} = \begin{cases} \dfrac{\partial}{\partial \theta}\left(p_o - P_{cow}\right) = -\dfrac{\partial P_{cow}}{\partial \theta} & p = w \\ 0 & p = o \ , \\ \dfrac{\partial}{\partial \theta}\left(p_o + P_{cgo}\right) = \dfrac{\partial P_{cgo}}{\partial \theta} & p = g \end{cases} \tag{4.5.3.27}$$

$$\frac{\partial \underset{i+\frac{1}{2},j,k}{\overset{n+1}{T^*_{px}}}}{\partial \theta^{n+1}_{i,j,k}} = \left[\frac{A_x k_x}{\Delta x}\right]_{i+\frac{1}{2},j,k} \underset{i,j,k}{\omega_{px}} \left[\frac{1}{\mu_p}\left(H_p \rho_p \frac{\partial k_{rp}}{\partial \theta} + H_p k_{rp} \frac{\partial \rho_p}{\partial \theta} + \rho_p k_{rp} \frac{\partial H_p}{\partial \theta} - \frac{H_p \rho_p k_{rp}}{\mu_p} \frac{\partial \mu_p}{\partial \theta}\right)\right]^{n+1}_{i,j,k} , \tag{4.5.3.28}$$

and

$$\frac{\partial \underset{i-\frac{1}{2},j,k}{\overset{n+1}{T^*_{px}}}}{\partial \theta^{n+1}_{i,j,k}} = \left[\frac{A_x k_x}{\Delta x}\right]_{i-\frac{1}{2},j,k} \underset{i,j,k}{\omega^*_{px}} \left[\frac{1}{\mu_p}\left(H_p \rho_p \frac{\partial k_{rp}}{\partial \theta} + H_p k_{rp} \frac{\partial \rho_p}{\partial \theta} + \rho_p k_{rp} \frac{\partial H_p}{\partial \theta} - \frac{H_p \rho_p k_{rp}}{\mu_p} \frac{\partial \mu_p}{\partial \theta}\right)\right]^{n+1}_{i,j,k} , \tag{4.5.3.29}$$

where similar expressions exist for the other directions, and

$$\frac{\partial q^{n+1}_{i,j,k}}{\partial \theta^{n+1}_{i,j,k}} = \frac{\partial \underset{i,j,k}{q^{n+1}_{loss}}}{\partial \theta^{n+1}_{i,j,k}} + \sum_{p=1}^{N_p}\left[E_p \sum_{i=1}^{N_c} \frac{\partial q_{ip}}{\partial \theta}\right]^{n+1}_{i,j,k} . \tag{4.5.3.30}$$

For each of the composition derivatives at node *i*, *j*, *k*,

$$\frac{\partial G^{n+1}_{i,j,k}}{\partial \underset{i,j,k}{X^{n+1}_j}} = \sum_{p=1}^{N_p}\left[\sum_m \left(\frac{\partial \underset{l}{\overset{n+1}{T^*_p}}}{\partial \underset{i,j,k}{X^{n+1}_j}}\left[\left(\underset{m}{p^{n+1}_p} - \underset{i,j,k}{p^{n+1}_p}\right) - \underset{l}{\rho^{n+1}_p} g\left(z_m - z_{i,j,k}\right)\right]\right.\right.$$

$$+\overset{n+1}{\underset{l}{T^{*}_{p}}}\left(\left[-\frac{\partial p_p}{\partial X_j}\right]^{n+1}_{i,j,k}-\frac{\partial \underset{l}{\rho^{n+1}_{p}}}{\underset{i,j,k}{\partial X^{n+1}_{j}}}g\left(z_m-z_{i,j,k}\right)\right)\Bigg)$$

$$-\frac{\underset{i,j,k}{V_b}}{\Delta t}\left[\phi S_p\left(E_p\frac{\partial \rho_p}{\partial X_j}+\rho_p\frac{\partial E_p}{\partial X_j}\right)\right]^{n+1}_{i,j,k}\Bigg]-\left[\frac{\partial q}{\partial X_j}\right]^{n+1}_{i,j,k}. \tag{4.5.3.31}$$

The partial derivatives in Equation 4.5.3.31 are given by

$$\frac{\partial p_p}{\partial X_j}=\begin{cases}\frac{\partial}{\partial X_j}\left(p_o-P_{cow}\right)=-\frac{\partial P_{cow}}{\partial X_j} & p=w\\ 0 & p=o\ ,\\ \frac{\partial}{\partial X_j}\left(p_o+P_{cgo}\right)=\frac{\partial P_{cgo}}{\partial X_j} & p=g\end{cases} \tag{4.5.3.32}$$

$$\frac{\partial \overset{n+1}{\underset{i+\frac{1}{2},j,k}{T^{*}_{px}}}}{\underset{i,j,k}{\partial X^{n+1}_{j}}}=\left[\frac{A_x k_x}{\Delta x}\right]_{i+\frac{1}{2},j,k}\underset{i,j,k}{\omega_{px}}\left[\frac{k_{rp}}{\mu_p}\left(H_p\frac{\partial \rho_p}{\partial X_j}+\rho_p\frac{\partial H_p}{\partial X_j}-\frac{\rho_p H_p}{\mu_p}\frac{\partial \mu_p}{\partial X_j}\right)\right]^{n+1}_{i,j,k}, \tag{4.5.3.33}$$

and

$$\frac{\partial \overset{n+1}{\underset{i-\frac{1}{2},j,k}{T^{*}_{px}}}}{\underset{i,j,k}{\partial X^{n+1}_{j}}}=\left[\frac{A_x k_x}{\Delta x}\right]_{i-\frac{1}{2},j,k}\underset{i,j,k}{\omega^{*}_{px}}\left[\frac{k_{rp}}{\mu_p}\left(H_p\frac{\partial \rho_p}{\partial X_j}+\rho_p\frac{\partial H_p}{\partial X_j}-\frac{H_p\rho_p}{\mu_p}\frac{\partial \mu_p}{\partial X_j}\right)\right]^{n+1}_{i,j,k}, \tag{4.5.3.34}$$

where similar expressions exist for the other directions, and

$$\frac{\partial q^{n+1}_{i,j,k}}{\underset{i,j,k}{\partial X^{n+1}_{j}}}=\sum_{p=1}^{N_p}\left[E_p\sum_{i=1}^{N_c}\frac{\partial q_{ip}}{\partial X_j}\right]^{n+1}_{i,j,k}. \tag{4.5.3.35}$$

For the well pressure derivative at node *i*, *j*, *k*,

$$\frac{\partial G^{n+1}_{i,j,k}}{\underset{i,j}{\partial p^{n+1}_{wf}}}=-\left[\frac{\partial q}{\partial p_{wf}}\right]^{n+1}_{i,j,k}, \tag{4.5.3.36}$$

where

$$\frac{\partial q^{n+1}_{i,j,k}}{\partial p^{n+1}_{wf\,i,j}} = \sum_{p=1}^{N_p}\left[q_p \frac{\partial E_p}{\partial p_{wf}} + E_p \sum_{i=1}^{N_c} \frac{\partial q_{ip}}{\partial p_{wf}} \right]^{n+1}_{i,j,k} . \qquad (4.5.3.37)$$

The derivatives of *G* with respect to the variables at the other nodes are similar to those above except that they are less complicated. They are given in Appendix II.

4.5.4 Derivatives of the *X* Equations at All Nodes

The partial derivatives required for the *X* equation are given below. For the pressure derivative at node *i*, *j*, *k*,

$$\frac{\partial X^{n+1}_{p\,i,j,k}}{\partial p^{n+1}_{o\,i,j,k}} = \sum_{i=1}^{N_c}\left[\frac{\partial K_{vip}}{\partial p_o} X_i \right]^{n+1}_{i,j,k} \qquad p = w,o,g \ . \qquad (4.5.4.1)$$

For the aqueous, oleic and gaseous phase derivatives at node *i*, *j*, *k*,

$$\frac{\partial X^{n+1}_{p\,i,j,k}}{\partial S^{n+1}_{p\,i,j,k}} = 0 \qquad p = w,o,g \ . \qquad (4.5.4.2)$$

For the temperature derivative at node *i*, *j*, *k*,

$$\frac{\partial X^{n+1}_{p\,i,j,k}}{\partial \theta^{n+1}_{i,j,k}} = \sum_{i=1}^{N_c}\left[\frac{\partial K_{vip}}{\partial \theta} X_i \right]^{n+1}_{i,j,k} \qquad p = w,o,g \ . \qquad (4.5.4.3)$$

For the compositions derivatives at node *i*, *j*, *k*,

$$\frac{\partial X^{n+1}_{p\,i,j,k}}{\partial X^{n+1}_{j\,i,j,k}} = \left[K_{vjp} \right]^{n+1}_{i,j,k} \qquad p = w,o,g \ . \qquad (4.5.4.4)$$

For the well pressure derivative at node *i*, *j*, *k*,

$$\frac{\partial X_{p\,i,j,k}^{n+1}}{\partial p_{wf\,i,j}^{n+1}} = 0 \qquad p = w, o, g \ . \tag{4.5.4.5}$$

All derivatives at all other nodes are zero.

4.5.5 Derivatives of the *S* Equation at All Nodes

The partial derivatives required for the *S* equation are given below. For the pressure derivative at node *i*, *j*, *k*,

$$\frac{\partial S_{i,j,k}^{n+1}}{\partial p_{o\,i,j,k}^{n+1}} = 0 \ . \tag{4.5.5.1}$$

For the aqueous, oleic and gaseous phase derivatives at node *i*, *j*, *k*,

$$\frac{\partial S_{i,j,k}^{n+1}}{\partial S_{p\,i,j,k}^{n+1}} = 1 \qquad p = w, o, g \ . \tag{4.5.5.2}$$

For the temperature derivative at node *i*, *j*, *k*,

$$\frac{\partial S_{i,j,k}^{n+1}}{\partial \theta_{i,j,k}^{n+1}} = 0 \ . \tag{4.5.5.3}$$

For the compositions derivatives at node *i*, *j*, *k*,

$$\frac{\partial S_{i,j,k}^{n+1}}{\partial X_{j\,i,j,k}^{n+1}} = 0 \ . \tag{4.5.4.4}$$

For the well pressure derivative at node *i*, *j*, *k*,

$$\frac{\partial S_{i,j,k}^{n+1}}{\partial p_{wf\,i,j}^{n+1}} = 0 \ . \tag{4.5.5.5}$$

All derivatives at all other nodes are zero.

4.5.6 Derivatives of the *W* Equation at All Nodes

Consider the well constraint given by Equation 4.1.4.2 for a shut-in well,

$$\underset{i,j}{W_1^{n+1}} = -\sum_{k}\sum_{p=1}^{N_p}\sum_{i=1}^{N_c} J'_{i,j,k}\left[K_{vip}X_i\frac{k_{rp}}{\mu_p}\frac{\rho_p}{\rho_{p,STC}}\right]_{i,j,k}^{n+1}\left[p_o - p_{wf}\right]_{i,j,k}^{n+1} = 0 \ . \tag{4.5.6.1}$$

For the pressure derivative at node *i*, *j*, *k*,

$$\frac{\partial \underset{i,j}{W_1^{n+1}}}{\partial \underset{i,j,k}{p_o^{n+1}}} = -J'_{i,j,k}\sum_{p=1}^{N_p}\left[\frac{k_{rp}}{\mu_p}\frac{\rho_p}{\rho_{p,STC}}\sum_{i=1}^{N_c}\frac{\partial K_{vip}}{\partial p_o}X_i + \frac{k_{rp}}{\mu_p}\frac{1}{\rho_{p,STC}}\left(\frac{\partial \rho_p}{\partial p_o} - \frac{\rho_p}{\mu_p}\frac{\partial \mu_p}{\partial p_o}\right)\right]_{i,j,k}^{n+1}\left[p_o - p_{wf}\right]_{i,j,k}^{n+1}$$

$$+\left[\frac{k_{rp}}{\mu_p}\frac{\rho_p}{\rho_{p,STC}}\right]_{i,j,k}^{n+1} . \tag{4.5.6.2}$$

For the aqueous, oleic and gaseous phase saturation derivatives,

$$\frac{\partial \underset{i,j}{W_1^{n+1}}}{\partial \underset{i,j,k}{S_w^{n+1}}} = -J'_{i,j,k}\sum_{p=1}^{N_p}\left[\frac{1}{\mu_p}\frac{\rho_p}{\rho_{p,STC}}\frac{\partial k_{rp}}{\partial S_w}\right]_{i,j,k}^{n+1}\left[p_o - p_{wf}\right]_{i,j,k}^{n+1} , \tag{4.5.6.3}$$

$$\frac{\partial \underset{i,j}{W_1^{n+1}}}{\partial \underset{i,j,k}{S_o^{n+1}}} = -J'_{i,j,k}\sum_{p=1}^{N_p}\left[\frac{1}{\mu_p}\frac{\rho_p}{\rho_{p,STC}}\frac{\partial k_{rp}}{\partial S_o}\right]_{i,j,k}^{n+1}\left[p_o - p_{wf}\right]_{i,j,k}^{n+1} , \tag{4.5.6.4}$$

and

$$\frac{\partial \underset{i,j}{W_1^{n+1}}}{\partial \underset{i,j,k}{S_g^{n+1}}} = -J'_{i,j,k}\sum_{p=1}^{N_p}\left[\frac{1}{\mu_p}\frac{\rho_p}{\rho_{p,STC}}\frac{\partial k_{rp}}{\partial S_g}\right]_{i,j,k}^{n+1}\left[p_o - p_{wf}\right]_{i,j,k}^{n+1} , \tag{4.5.6.5}$$

respectively. For the temperature derivative at node *i*, *j*, *k*,

$$\frac{\partial \underset{i,j}{W_1^{n+1}}}{\partial \theta_{i,j,k}^{n+1}} = -J'_{i,j,k}\sum_{p=1}^{N_p}\left[\frac{k_{rp}}{\mu_p}\frac{\rho_p}{\rho_{p,STC}}\sum_{i=1}^{N_c}\frac{\partial K_{vip}}{\partial \theta}X_i + \frac{1}{\mu_p}\frac{\rho_p}{\rho_{p,STC}}\frac{\partial k_{rp}}{\partial \theta}\right.$$

$$\left.+\frac{k_{rp}}{\mu_p}\frac{1}{\rho_{p,STC}}\left(\frac{\partial \rho_p}{\partial \theta} - \frac{\rho_p}{\mu_p}\frac{\partial \mu_p}{\partial \theta}\right)\right]_{i,j,k}^{n+1}\left[p_o - p_{wf}\right]_{i,j,k}^{n+1} . \tag{4.5.6.6}$$

For each composition derivative at node *i*, *j*, *k*,

$$\frac{\partial W^{n+1}_{1_{i,j}}}{\partial X^{n+1}_{j_{i,j,k}}} = -J'_{i,j,k} \sum_{p=1}^{N_p} \left[\frac{k_{rp}}{\mu_p} \frac{\rho_p}{\rho_{p,STC}} \sum_{i=1}^{N_c} K_{vip} \frac{\partial X_i}{\partial X_j} + \frac{k_{rp}}{\mu_p} \frac{1}{\rho_{p,STC}} \left(\frac{\partial \rho_p}{\partial X_j} - \frac{\rho_p}{\mu_p} \frac{\partial \mu_p}{\partial X_j} \right) \right]^{n+1}_{i,j,k} \left[p_o - p_{wf} \right]^{n+1}_{i,j,k} . \quad (4.5.6.7)$$

For the well pressure derivative at node *i*, *j*,

$$\frac{\partial W^{n+1}_{1_{i,j}}}{\partial p_{wf_{i,j}}} = \sum_{k} J'_{i,j,k} \sum_{p=1}^{N_p} \left[\frac{k_{rp}}{\mu_p} \frac{\rho_p}{\rho_{p,STC}} \right]^{n+1}_{i,j,k} . \qquad (4.5.6.8)$$

At nodes *i*±1, *j*, *k* and *i*, *j*±1, *k*, all derivatives are zero. At nodes *i*, *j*, *k*±1, the pressure derivative is given by

$$\frac{\partial W^{n+1}_{1_{i,j}}}{\partial p^{n+1}_{o_{i,j,k\pm1}}} = -J'_{i,j,k\pm1} \sum_{p=1}^{N_p} \left[\frac{k_{rp}}{\mu_p} \frac{\rho_p}{\rho_{p,STC}} \sum_{i=1}^{N_c} \frac{\partial K_{vip}}{\partial p_o} X_i + \frac{k_{rp}}{\mu_p} \frac{1}{\rho_{p,STC}} \left(\frac{\partial \rho_p}{\partial p_o} - \frac{\rho_p}{\mu_p} \frac{\partial \mu_p}{\partial p_o} \right) \right]^{n+1}_{i,j,k\pm1} \left[p_o - p_{wf} \right]^{n+1}_{i,j,k\pm1}$$
$$+ \left[\frac{k_{rp}}{\mu_p} \frac{\rho_p}{\rho_{p,STC}} \right]^{n+1}_{i,j,k\pm1} . \qquad (4.5.6.9)$$

This equation is identical to Equation 4.5.6.2 except for the change in the subscript *i*, *j*, *k* to *i*, *j*, *k*±1; the same is true for Equations 4.5.6.3 to 4.5.6.7.

In Appendix III are equivalent expressions to the above for several other constraints as discussed in Section 4.1.9. These expressions have derivatives that also are very similar to those above.

4.6 Computer Model

The computer model was written in VAX FORTRAN on VMS operating systems. Extensive use was made of the VMS debugger feature available. The code was organized in a highly structured and modularized manner. The FORTRAN INCLUDE statement was used for code that was needed in most of the modules, such as array dimension declarations and common blocks.

A few modules were obtained from various sources. These modules, or collection of modules are:

- `TABLE` (Christoffersen and Whitson (1989)) for generating data in tabular form easily,
- `ZSTAR` (Dranchuk and Abou-Kassem (1975)) for calculating the gas supercompressibility factor, and
- (`YSMP`) Yale Sparse Matrix Package for solving a large system of equations.

All other modules were written specifically for the problem at hand. The program logic is best and most easily illustrated with the use of a flowchart as shown in Figure 4.6.0.1.

The use of analytical derivatives requires that either they be calculated once per iteration and stored or that they be calculated when required (which can be several times in an iteration). This is the classical trade off between memory and speed. The former was decided upon and as a result the memory requirements for this program can be quite large depending on the dimensions of various vectors of the program. Limits of the computer used limited the number of unknowns to about 2000.

A major factor affecting speed is coding inefficiencies. Many are known to exist in the current code and some are as yet undiscovered. It was beyond the scope of this study to optimize speed of execution.

Each fundamental grid block has a flag array `IHYBRID(I,J,8)` associated with it. Table 4.6.0.1 summarizes the definitions of the flag array. Elements 1 to 6 are key to calculating the intergrid block properties between reservoir/region and region/region grid blocks.

The technique used to allocate and change the grid block properties was different for intragrid block and intergrid block properties. Figure 4.6.0.2 illustrates the logic used to populate the grid blocks with porosity. This property is allocated in one sweep through the grid, which is the technique used for the intragrid block properties.

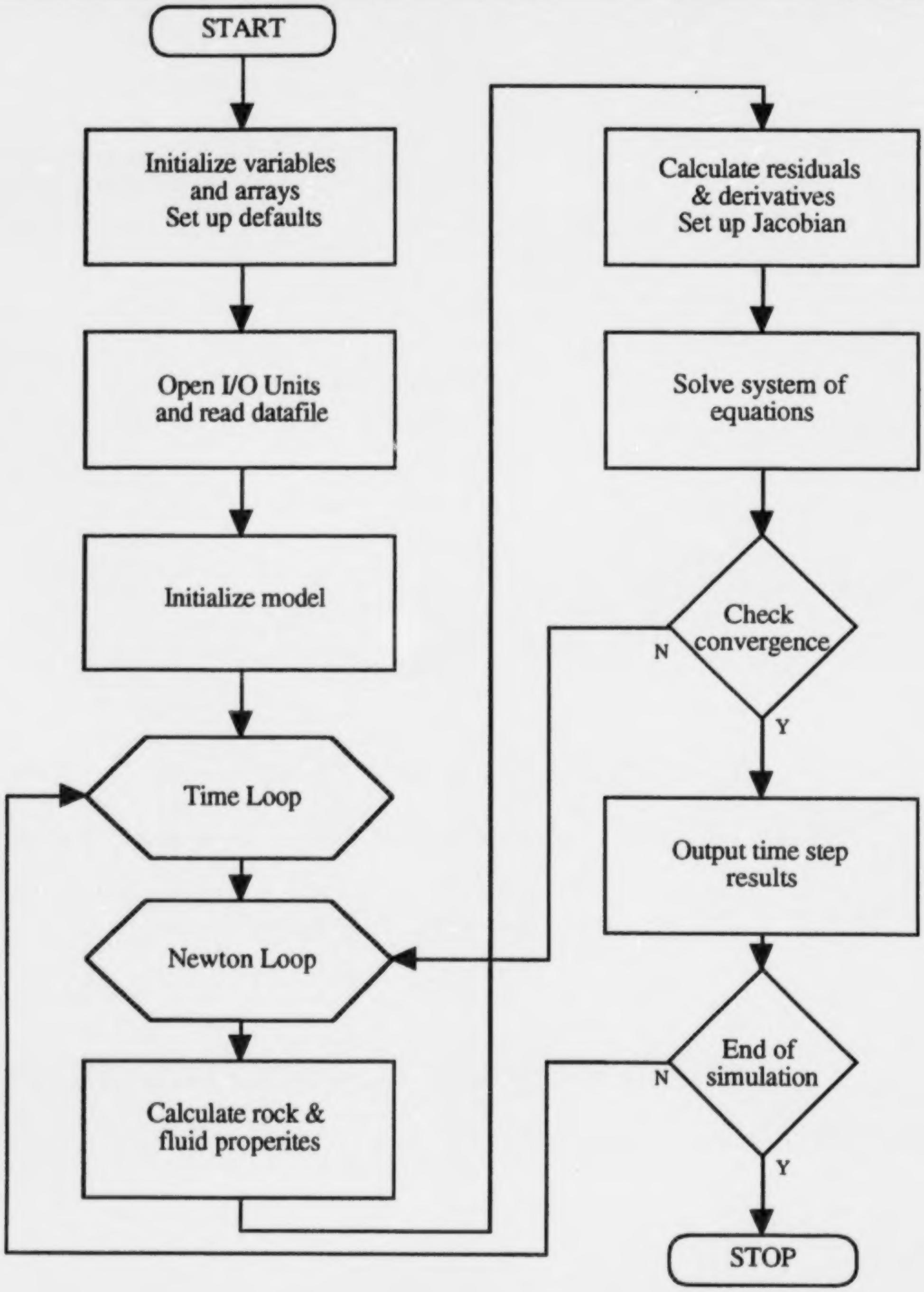
START
Initialize variables
and arrays
Set up defaults
Open I/O Units
and read datafile
Initialize model
Time Loop
Newton Loop
Calculate rock &
fluid properites
Calculate residuals
& derivatives
Set up Jacobian
Solve system of
equations
Check
convergence
N
Y
Output time step
results
End of
simulation
N
Y
STOP

Figure 4.6.0.1 Simplified flow diagram of computational procedure.

`IHYBRID`	Value	Definition
1	0	Fundamental grid block
	1	Hyperhybrid grid block
2	1,2,...	Side of square of hyperhybrid grid block
3	0	Non-reference grid block
	1	Reference (I,J) grid block
4	1,2,...	Hyperhybrid region number **
5	I	I reference grid block
6	J	J reference grid block
7	0	Use Δr for boundary calculation (default)
	1	Use logarithmic boundary calculation
8	0	Use midpoint to locate node (default)
	1	Use logarithmic mean to locate node
	2	Use volumetric centroid to locate node

** Regions are numbered by the user with the convention of smallest J, smallest I being the first region. Subsequent regions are numbered sequentially with increasing I, increasing J.

Table 4.6.0.1

Definition of flag array `IHYBRID`.

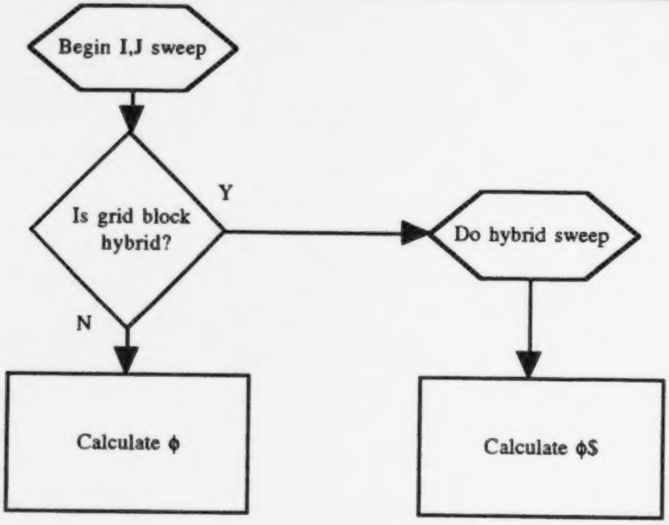
Begin I,J sweep
Is grid block hybrid?
Y
N
Do hybrid sweep
Calculate ϕ
Calculate ϕ$

Figure 4.6.0.2

Intragrid block property population logic.

For the intergrid block properties, such as potential, three passes (I,J sweep) are made through the grid. Figure 4.6.0.3 illustrates the logic. The first pass calculates the potential between active fundamental grid blocks, the second pass calculates the potential between reservoir/region and region/region grid blocks and the third pass calculates the potential within the cylinders of each region. This process can be changed to do the population in one sweep; however, the logic is simpler in structure and easier to debug. Note that the code was written in stages over a long period of time.

The Yale Sparse Matrix Package (YSMP) requires that the sparse matrix be stored using a scheme that is common to other solvers. A real valued array contains the non-zero row-wise entries of the Jacobian. Two integers vectors are used as pointers. The first indicates the column of the entry while the second denotes the starting location of each row.

Equipped with the YSMP scheme and the knowledge of the structure of the Jacobian, it is straightforward, albeit tedious, to write the FORTRAN module to prepare the three arrays needed. The final module written for this program was built and tested in stages, starting with a simple two-dimensional rectilinear problem and ending with a general three-dimensional hyperhybrid grid.

A comment is worthwhile here with respect to solving the large system of equations which result in a simulator. The initial model was tested using Gaussian elimination for dense matrices. This method can become very slow for even moderate problems and requires far too much storage, 85% of which are zeros. The memory requirements alone eliminate Gaussian elimination as a viable method to solve large systems. The larger problems were solved using YSMP for sparse matrices. This solver required about 15% of the storage and was up to thirty times faster on small problems (less than 100 unknowns).

The rate of convergence is sometimes slow, particularly when changes per time step are high. This effect was more pronounced for hyperhybrid grids than their rectilinear equivalents. A simple acceleration scheme was tested but there was little, if any, improvement; hence, it was removed from the code. A more efficient acceleration scheme should be incorporated.

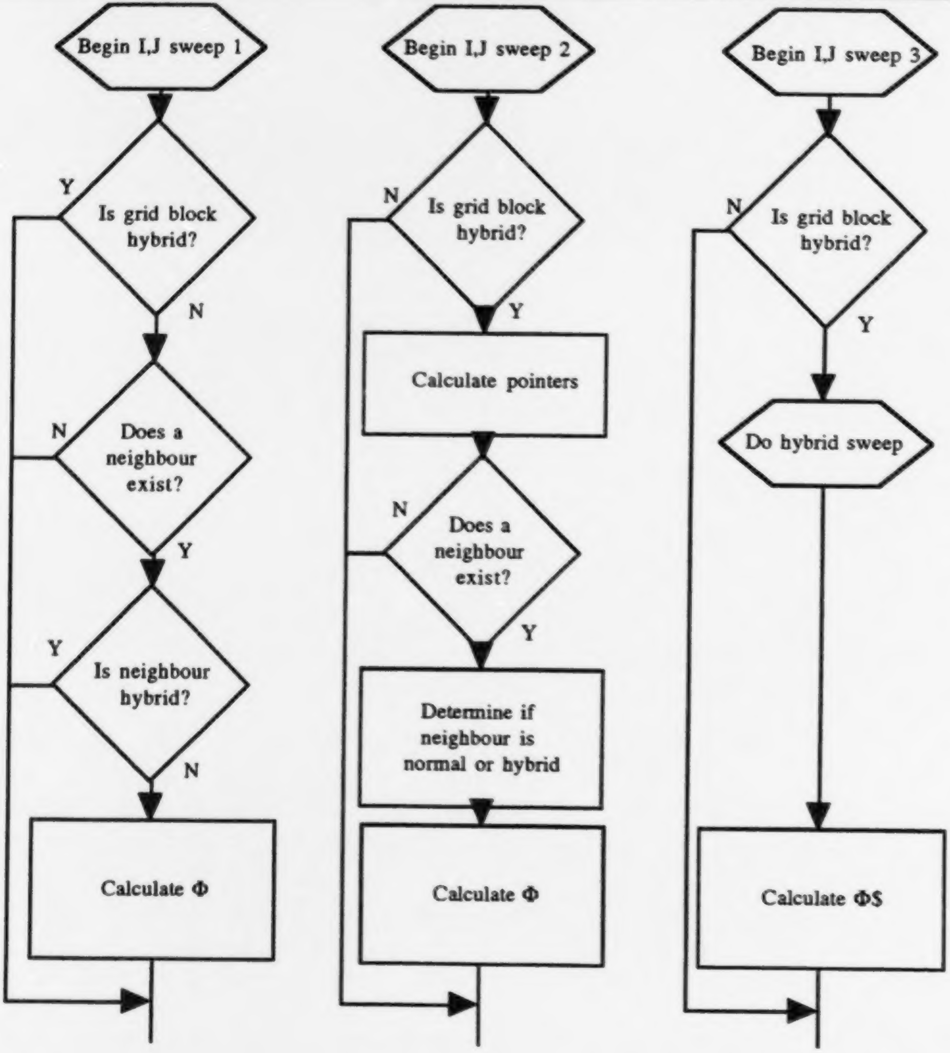
Begin I,J sweep 1
Is grid block hybrid?
Y
N
Does a neighbour exist?
N
Y
Is neighbour hybrid?
Y
N
Calculate Φ
Begin I,J sweep 2
Is grid block hybrid?
N
Y
Calculate pointers
Does a neighbour exist?
N
Y
Determine if neighbour is normal or hybrid
Calculate Φ
Begin I,J sweep 3
Is grid block hybrid?
N
Y
Do hybrid sweep
Calculate Φ$

Sweep 1 sweeps the grid and calculates the potential between fundamental grid blocks only. Sweep 2 sweeps the grid and calculates the potential between reservoir/region and region/region grid blocks only. Sweep 3 sweeps the grid and calculates the potential for all internal cylindrical grid blocks.

Figure 4.6.0.3

Intergrid block property population logic.

The computer model requires a single data input file and it creates several output files:

- detailed run file with the capability of printing all properties and their derivatives at each iteration (useful for debugging purposes only),
- general run file with input data echo and end of time step summary, and
- plot files as input to spreadsheet and plotting software.

A run time screen is also preserved as a log file. Extracts from a typical set of files are given in Appendix IV.

Finally, a comment with regards to run execution time is appropriate. Table 4.6.0.2 summarizes the CPU time for the major runs in this study. Although some of the runs used in excess of 25 CPU hours (with one run requiring 125 CPU hours), most runs required less than 25 CPU hours. This limited the number of runs that were made, particularly when the total wall clock time was typically five times the CPU time. Note that the FORTRAN code was not compiled with optimization. Also, the individual runs were not optimized with respect to maximum allowable time step.

SECTION			RUN NAME	CPU TIME (hrs:min)
5.8		Multiwell Cyclic Steaming		
	.1	Two-Well Runs	Cyclic Run 1	9:17
			Cyclic Run 2	10:58
			Cyclic Run 3	8:32
			Cyclic Run 4	9:34
			Cyclic Run 5	16:42
			Cyclic Run 6	15:34
			Cyclic Run 7	10:54
			Cyclic Run 8	12:03
			Cyclic Run 9	125:00
			Cyclic Run 10	49:55
	.2	Four-Well Runs	Cyclic Run 12	32:33
			Cyclic Run 13	33:04
5.9		Cyclic to Continuous Steaming	Flood Run 1	5:03
			Flood Run 2	6:01
			Flood Run 3	16:03
			Flood Run 4	16:17
			Flood Run 5	12:28

Table 4.6.0.2 Summary of CPU time for the major runs.

4.7 Miscellaneous Items

4.7.1 Automatic Time Step Control

A simulator is more efficient if the capability of automatic time step control is built in. In this model, a simple estimation procedure is used. Grabowski *et al.* (1979) estimated the time step by comparing the ***maximum*** changes of each primary variable over the previous time step against user defined limits, or input norms. The new time step is given by

$$\Delta t^{n+1} = \Delta t^{n} \min_{i} \frac{(1+\omega)\eta_i}{\delta_i + \omega\eta_i} , \tag{4.7.1.1}$$

where the subscript i runs over all primary variables, ω is a damping factor that the authors suggest is approximately unity, δ_i is the maximum change of the primary variable and η_i is the input norm.

4.7.2 Model Initialization

Prior to starting the simulation, it is necessary to know the initial state of the model. In this work, the options of both user input and self-initialization are available. Self-initialization is founded on the assumption that the same capillary pressure curves and critical saturations that apply to the production state also apply to the equilibrium state[1].

Static equilibrium occurs in the reservoir when all velocities of all phases are zero. To uniquely determine the pressure and saturation distributions, it is necessary to specify a reference oleic phase pressure, a reference saturation in the oleic-aqueous transition zone and a reference saturation in the gaseous-oleic transition zone.

In outline form, the initialization proceeds as follows. The oleic phase pressure and oleic phase density are used to calculate the oleic phase pressure distribution with the relationship

$$p_{k+1} = p_k + \rho g z \ . \tag{4.7.2.1}$$

---

[1] For a more detailed discussion, the reader is referred to Aziz and Settari (1979) and Mattax and Dalton (1990).

Next, the aqueous phase pressure distribution can be calculated with the capillary pressure defining equation arranged as

$$p_w = p_o - P_{cow} \ . \tag{4.7.2.2}$$

The gaseous phase pressure distribution is found from

$$p_g = p_o + P_{cgo} \ . \tag{4.7.2.3}$$

Finally, the aqueous and gaseous phase saturation, and as a consequence the oleic saturation, distributions are found from the capillary pressure functions in inverse; that is,

$$S_w = S_w\left(P_{cow}\right) \tag{4.7.2.4}$$

and

$$S_g = S_g\left(P_{cgo}\right) \ , \tag{4.7.2.5}$$

then

$$S_o = 1 - S_w - S_g \ . \tag{4.7.2.6}$$

4.7.3 Wellbore Pressure Gradient

The source term contains an additional unknown p_{wf} referenced at the top of the reservoir. The volumetric average wellbore gradient (Coats (1980)) is given by

$$\underset{i,j,k}{\gamma^n_{wf}} = \left[\frac{\sum\limits_p \frac{k_{rp}}{\mu_p} p\gamma_p}{\sum\limits_p \frac{k_{rp}}{\mu_p} p}\right]^n_{i,j,k} \tag{4.7.3.1}$$

for each layer. For the sake of simplicity, Equation 4.7.3.1 is evaluated at the old time step. The pressure gradient is calculated from

$$\underset{i,j,k}{p^{n+1}_{wf}} = \underset{i,j,k-1}{p^{n+1}_{wf}} + \left(\underset{i,j,k-1}{\gamma^n_{wf}} \alpha_{i,j,k-1} + \underset{i,j,k}{\gamma^n_{wf}} \alpha_{i,j,k}\right)\left(z_{i,j,k} - z_{i,j,k-1}\right) \qquad k = 2,3,\cdots \ , \tag{4.7.3.2}$$

where

$p_{wf_{i,j,1}}$ unknown bottom hole flowing pressure, and

$$\alpha_{i,j,k} = \frac{0.5\Delta z_{i,j,k}}{z_{i,j,k} - z_{i,j,k-1}} \qquad k = 2,3,\cdots \tag{4.7.3.3}$$

and

$$\alpha_{i,j,k-1} = 1 - \alpha_{i,j,k} \qquad k = 2,3,\cdots\ . \tag{4.7.3.4}$$

4.7.4 End of Time Step Checks

At the end of each time step, the following checks are made

- incremental and cumulative material balance check,
- incremental and cumulative energy balance check,
- saturation constraint check,
- mole fraction constraint check, and
- maximum absolute residuals check, noting grid blocks with largest residuals.

The incremental material balance is calculated from

$$Incremental\ \ Material\ \ Balance = \frac{\sum_{i,j,k} Mass\,accumulation}{\sum_{i,j,k} Net\ mass\,throughput} = 1 \tag{4.7.4.1}$$

and the cumulative material balance is calculated from

$$Cumulative\ \ Material\ \ Balance = \sum_{\Delta t} Incremental\ \ Material\ \ Balance\ . \tag{4.7.4.2}$$

Similarly, the incremental and cumulative energy balance is calculated from

$$Incremental\ \ Energy\ \ Balance = \frac{\sum_{i,j,k} Energy\,Accumulation}{\sum_{i,j,k} Net\ \ Energy\ \ Throughput} = 1 \tag{4.7.4.3}$$

and

$$Cumulative\ \ Energy\ \ Balance = \sum_{\Delta t} Incremental\ \ Energy\ \ Balance\ , \tag{4.7.4.4}$$

respectively.

4.7.5 Treatment of Visbreaking

Visbreaking is represented by the conversion of the heavy oil component into the light oil component. This is treated through the sink/source term in the mass and energy balance equations; that is, the heavy oil component is "produced" and the light oil component is "injected".

In order to calculate the fraction of heavy component that is converted, Equation 2.4.2.5, reproduced below,

$$f = 1 - \exp\left[-w \int_{t_1}^{t_2} \exp\left(-\frac{E}{R\theta} \right) dt \right] , \tag{4.7.5.1}$$

requires the evaluation of an integral over the time step. Furthermore, the temperature in the integrand is not necessarily a constant. This model can treat the temperature as a constant and as a linear function of time using

$$\theta(t) = \theta_1 + \frac{\theta_2 - \theta_1}{t_2 - t_1} t \ . \tag{4.7.5.2}$$

The integral is evaluated using Simpson's rule. It becomes obvious that an analytical derivative is extremely complex. To overcome this complexity, the sink/source terms are evaluated explicitly; hence

$$\underset{cracked}{q_{22}^{n+1}} = \frac{f^n K_{v22}^n X_2^n (OIP)^n}{\Delta t} \tag{4.7.5.5}$$

and

$$\underset{cracked}{q_{32}^{n+1}} = -\underset{cracked}{q_{22}^{n+1}} \ . \tag{4.7.5.6}$$

5.0 MODEL VALIDATION AND APPLICATION RESULTS

This section presents the validation procedure used and application results obtained along with a detailed discussion of the results. Table 5.0.0.1 summarizes the runs made in this study and includes the table and figure numbers of both the input data and the results.

5.1 Preliminary Testing

Before any testing of the complete model was done, several intermediate steps were taken. Firstly, all routines which calculate a fluid or rock property were tested individually using both a FORTRAN program and a spreadsheet. This was done in order to verify both the coding and the analytical derivatives.

The model was then built in a piecewise manner with appropriate testing to the model with new routines incorporated into it. Tables 5.1.0.1 and 5.1.0.2 show the general fluid properties and rock properties used, respectively. The oil viscosity as a function of temperature is illustrated also in Figure 5.1.0.1. Figures 5.1.0.2 to 5.1.0.4 illustrate the two- and three-phase relative permeabilities. Note that the relative permeability curve definitions were completed using a straight line, represented by a dashed line in the figures.

5.2 Simple Model Testing

Many simple tests were run on this model before attempting any two- or three-dimensional hybrid or hyperhybrid grid simulations. The results of these simple tests are not presented.

5.2.1 Single Grid Block Testing

The simplest test is to run the model in a single-phase, single grid block (zero-dimensional) mode. The objectives of such a test are to verify the general logic of the program, convergence of Newton's method, material and energy balance and size of the residuals. Note that this type of test excludes the interface terms in the balance equations. Following this simple test, the problem was increased in complexity by increasing the number of phases to three with the objectives being the same as above.

SECTION			RUN NAME	DATA		RESULTS	
				Tables	Figures	Tables	Figures
5.1		Preliminary Testing	—	5.1.0.1–.2	5.1.0.1–.4	—	—
5.2		Simple Model Testing	—	—	—	—	—
	.1	Single Grid Block Testing	—	—	—	—	—
	.2	Linear Horizontal Testing	—	—	—	—	—
	.3	Linear Vertical Testing	—	—	—	—	—
5.3		Two-Dimensional Rectilinear Model Testing	XY	—	5.3.0.1	—	5.3.0.2–.8
5.4		Cylindrical/Cylindrical Equivalent Series					
			R-1c	—	5.4.0.1	—	5.4.0.6–.11
			R-1c2	—	5.4.0.1	—	5.4.0.12–.17
			C-1c	—	5.4.0.1	—	5.4.0.18–.23
			H-1c	—	5.4.0.1	—	5.4.0.24–.29
			Z-1c	—	5.4.0.1	—	5.4.0.30–.35
5.5		Contiguous Regions Testing	H-2	—	5.5.0.1	—	5.5.0.4–.12
			Z-2	—	5.5.0.1	—	5.5.0.13–.20
5.6		Local Well Effects					
	.1	Base Runs	R-3	—	5.6.0.1	—	5.6.1.1–.8
			H-3	—	5.6.0.1	—	5.6.1.9–.16
			Z-3	—	5.6.0.1	—	5.6.1.17–.24
	.2	Non-Newtonian Oil Viscosity	R-3b	5.6.0.1	5.6.0.2–.3	—	5.6.2.1–.8
			H-3b	5.6.0.1	5.6.0.2–.3	—	5.6.2.9–.17
			Z-3b	5.6.0.1	5.6.0.2–.3	—	5.6.2.18–.25
	.3	Visbreaking	Z-3c	—	5.6.0.4	—	5.6.3.1–.8
	.4	Two-Layer Run	Z-3e	—	5.6.0.1	—	5.6.4.1–.5
5.7		Interwell Interference					
	.1	Interference Illustration and Grid Comparison	R-5	—	5.7.1.1	—	5.7.1.2–.10
			Z-5	—	5.7.1.1	—	5.7.1.11–.19
	.2	Pressure Interference	Interference Run 1	—	5.7.2.1	—	5.7.2.2–.5
			Interference Run 2	—	5.7.2.1	—	5.7.2.2–.5
			Interference Run 3	—	5.7.2.1	—	5.7.2.2–.5
			Interference Run 4	—	5.7.2.1	—	5.7.2.2–.5
			Interference Run 5	—	5.7.2.1	—	5.7.2.6
			Interference Run 6	—	5.7.2.1	—	5.7.2.6
5.8		Multiwell Cyclic Steaming					
	.1	Two-Well Runs	Cyclic Run 1	—	5.8.1.1	5.8.1.1–.2	5.8.1.2–.4
			Cyclic Run 2	—	5.8.1.1	5.8.1.1–.2	5.8.1.2–.4
			Cyclic Run 3	—	5.8.1.1	5.8.1.1–.2	5.8.1.2–.4
			Cyclic Run 4	—	5.8.1.1	5.8.1.1–.2	5.8.1.2–.4
			Cyclic Run 5	—	5.8.1.1	5.8.1.1	5.8.1.5–.7
			Cyclic Run 6	—	5.8.1.1	5.8.1.1	5.8.1.8–.10
			Cyclic Run 7	—	5.8.1.1	5.8.1.1	5.8.1.11–.13
			Cyclic Run 8	—	5.8.1.1	5.8.1.1	5.8.1.14–.16
			Cyclic Run 9	5.8.1.4	—	5.8.1.2, .4	5.8.1.17–.19
			Cyclic Run 10	5.8.1.4	—	5.8.1.2, .4	5.8.1.17–.19
	.2	Four-Well Runs	Cyclic Run 12	—	5.8.2.1	5.8.2.1	5.8.2.2–.4
			Cyclic Run 13	—	5.8.2.1	5.8.2.2	5.8.2.5–.7
5.9		Cyclic to Continuous Steaming	Flood Run 1	5.9.0.1	5.8.1.1	5.9.0.2	5.9.0.1–.8
			Flood Run 2	5.9.0.1	5.8.1.1	5.9.0.2	5.9.0.9–.16
			Flood Run 3	5.9.0.1	5.8.1.1	5.9.0.2	5.9.0.17–.24
			Flood Run 4	5.9.0.1	5.8.1.1	5.9.0.2	5.9.0.25–.32
			Flood Run 5	5.9.0.1	5.8.1.1	5.9.0.2	5.9.0.33–.40

Table 5.0.0.1 Summary of runs

OIL PROPERTIES

		Heavy Component	Light Component
Density (kg/m^3)		972.	800.
Compressibility (kPa^{-1})		7.30×10^{-7}	7.30×10^{-7}
Thermal expansion (K^{-1})		-1.9095×10^{-3}	-1.9095×10^{-3}
Molecular weight		600.	500.
Viscosity coefficients	A (Pa·s)	1.0×10^{-7}	1.0×10^{-7}
(see Equation 4.4.6.2)	B (K)	4900.	4500.
Critical Temperature (K)		617.4	540.2
Critical Pressure (kPa)		2099.0	2736.0
Partial Volume (m^3/kmole)		0.6173	0.6250
Heat capacity (J/kg K)		2090.	2090.
Arrhenius constant (sec^{-1})		3.417×10^5	
Activation energy (J/kmole)		8.648×10^7	

WATER PROPERTIES

Calculated internally as described in Section 4.4

GAS PROPERTIES

Molecular weight		16.043
Viscosity coefficients	A (Pa·s/K)	6.647×10^{-10}
(see Equation 4.4.6.9)	B	1.709
Critical Temperature (K)		190.55
Critical Pressure (kPa)		4604
Partial Volume (m^3/kmole)		24.658
Heat capacity (J/kg K)		1050

Table 5.1.0.1 General fluid properties.

ROCK PROPERTIES

Thermal conductivity (W/m K)	3.5
Heat capacity (kJ/m^3 K)	2347
Rock compressibility (kPa^{-1})	5.0 x 10^{-7}

Relative permeability data (see Equations 4.4.1.13 to 4.4.1.16)

S_{wir}	0.20	k_{roiw}	0.80
S_{orw}	0.15	k_{rwro}	0.10
S_{org}	0.10	k_{rgro}	0.20
S_{gc}	0.06		
n_w	1.2	n_{og}	2.0
n_{ow}	2.0	n_g	1.5

No temperature effects

No capillary pressure effects

Table 5.1.0.2 General rock properties.

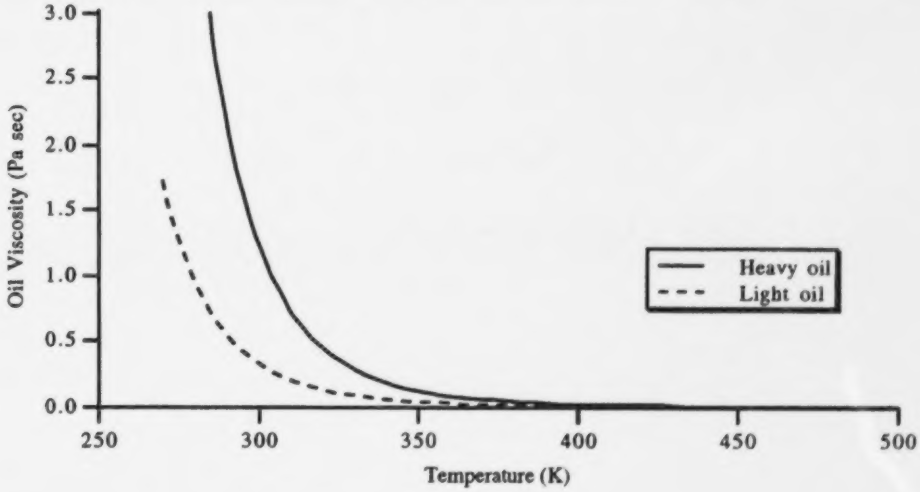

Figure 5.1.0.1

Oil viscosity as a function of temperature.

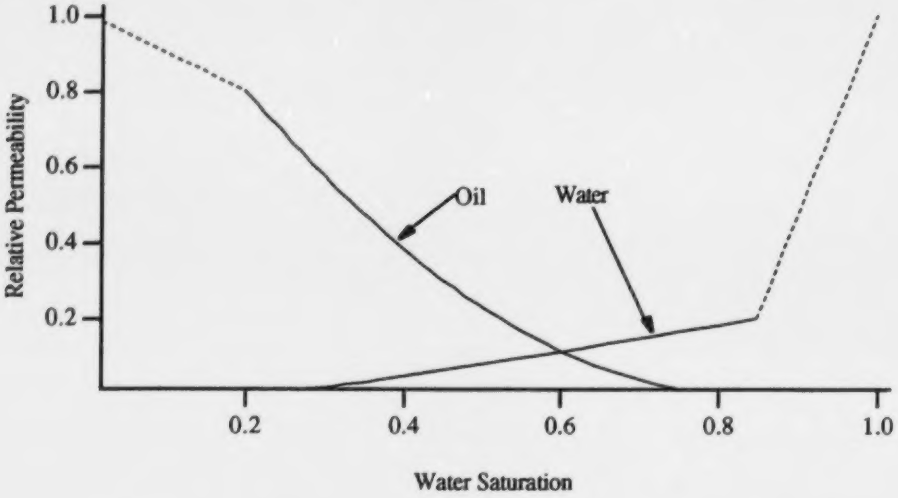

Figure 5.1.0.2

Water and oil relative permeability.

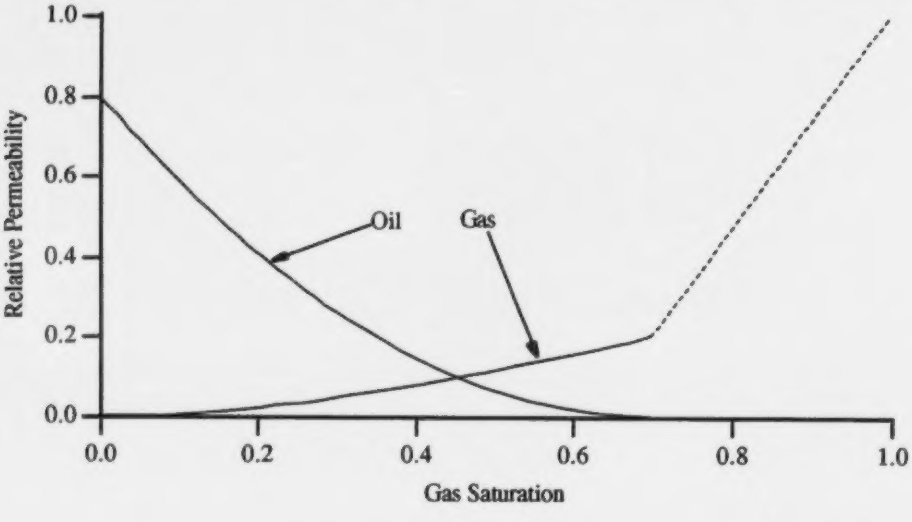

Figure 5.1.0.3

Gas and oil relative permeability.

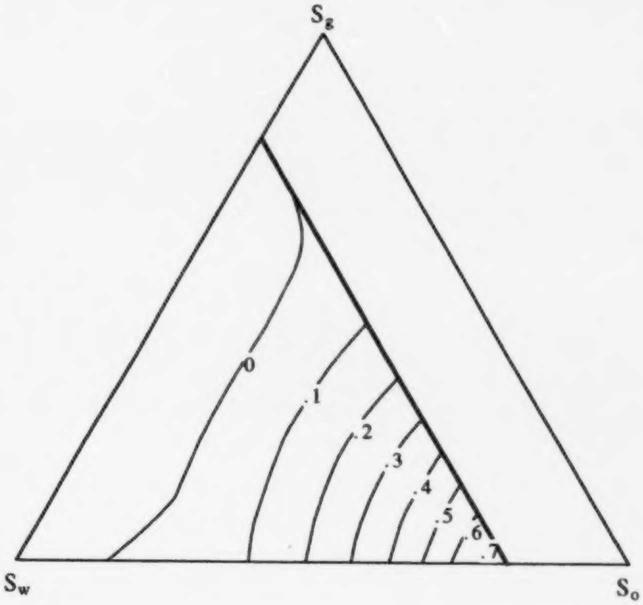

Figure 5.1.0.4

Three-phase oil relative permeability.

The result of these tests was that many logic and coding errors were detected fairly easily and corrected. The types of errors detected were many of the typical errors that are made in FORTRAN such as those associated with common blocks and typographical errors. Other errors detected were more fatal and difficult to detect such as faulty logic in obtaining the correct relative permeability when outside the normal operating limits and insidious errors such as the incorrect sign on the sink/source terms. These errors were found by keeping rock and fluid properties constant, then "turning on" the dependencies on primary variables in stages.

5.2.2 Linear Horizontal Testing

A simple one-dimensional five grid blocks problem was used with an injection well at the centre grid block and a production well at each end grid block. The objectives of this testing were to verify that the interblock flow terms were calculated properly and that the well controls were effective. Note that the design of the test required that the results should be symmetric about the injection well. The series of tests included one to three phases, injection of water and steam and three-phase production.

This testing was effective in finding a sign error in the calculation of the potential between two grid blocks and in detecting additional coding errors.

5.2.3 Linear Vertical Testing

Again, a simple linear five grid blocks problem was used with a single production well in the centre grid block. The objectives of this test were to verify the vertical initialization feature of the model and to verify the calculation of the head component in the well constraint equations. The results of these tests were compared with STARS[1] and there was excellent agreement. Note that STARS in its current form cannot handle hyperhybrid grids nor can it handle contiguous regions whether they be hybrid or hyperhybrid. The comparisons against that model are obtained with a degenerate version of the simulator developed in this work.

5.3 Two-Dimensional Rectilinear Model Testing

A 5 x 5 grid block model with an injection well at the centre and two production wells in opposite diagonal corners was used. The grid block information is shown in Figure 5.3.0.1. The model was tested with one to three phases present and initial saturation conditions that covered the complete range of possibilities.

---

[1] STARS (Steam and Additive Reservoir Simulator) is a product from the Computer Modelling Group.

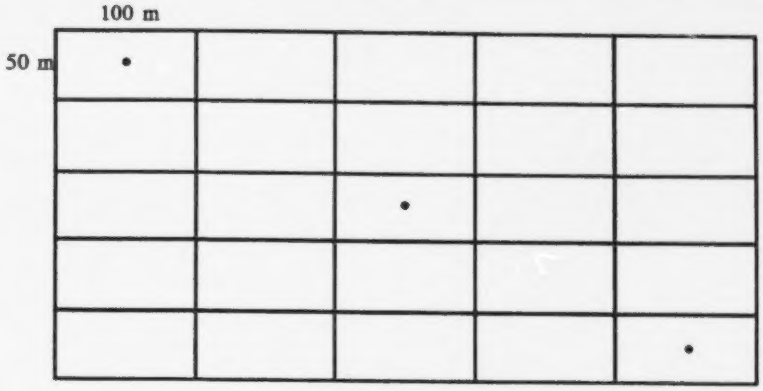

- Grid Dimensions
  All grid blocks are the same size
  Δx = 100 metres
  Δy = 50 metres
  Δz = 60 metres

- Rock Properties
  $k_x = k_y = 2000$ md
  $k_z = 1000$ md
  $\phi = 0.30$

- Initial Conditions
  $P = 500$ kPa
  $T = 51.7$ °C
  $S_w = 0.25$
  $S_o = 0.68$
  $S_g = 0.07$

- Operating Conditions

Time (days)	Well @ (1,1)		Well @ (3,3)		Well @ (5,5)	
0–400	BHP_{max} (kPa)	6900	BHP_{max} (kPa)	6900	BHP_{max} (kPa)	6900
	BHP_{min} (kPa)	100	BHP_{min} (kPa)	100	BHP_{min} (kPa)	100
	q_L (m^3/d)	5	q_T (m^3/d)	30	q_L (m^3/d)	5
			x	0.7		
			T_{inj} (°C)	250		

- Well Parameters

	Well @ (1,1)	Well @ (3,3)	Well @ (5,5)
Index	+1	-1	+1
Productivity	Internally calculated	Internally calculated	Internally calculated
J* multiplier	1.0	1.0	1.0
f_h	1.0	1.0	1.0
f	1.0	1.0	1.0
c_g	0.5	0.5	0.5
s	0.0	0.0	0.0
r_w (metres)	0.09	0.09	0.09

Figure 5.3.0.1

Run XY data summary.

This test was the first that attempted to check the "correctness" of the solutions obtained. A three-component, three-phase steam injection run was compared to STARS. These results are show in Figures 5.3.0.2 to 5.3.0.8. Figure 5.3.0.2 shows the liquid and gas production rates while Figure 5.3.0.3 illustrates the cumulative volumes. The production well grid block pressure and production well bottom hole pressure are shown in Figures 5.3.0.4 and 5.3.0.5, respectively. Similarly, the injection well grid block pressure and injection well bottom hole pressure are shown in Figures 5.3.0.6 and 5.3.0.7, respectively. Finally, the injection well grid block temperature is shown in Figure 5.3.0.8. A significant error that was detected early was one in the enthalpy calculation of steam. The corrected run agreed well[1] with the commercial simulator.

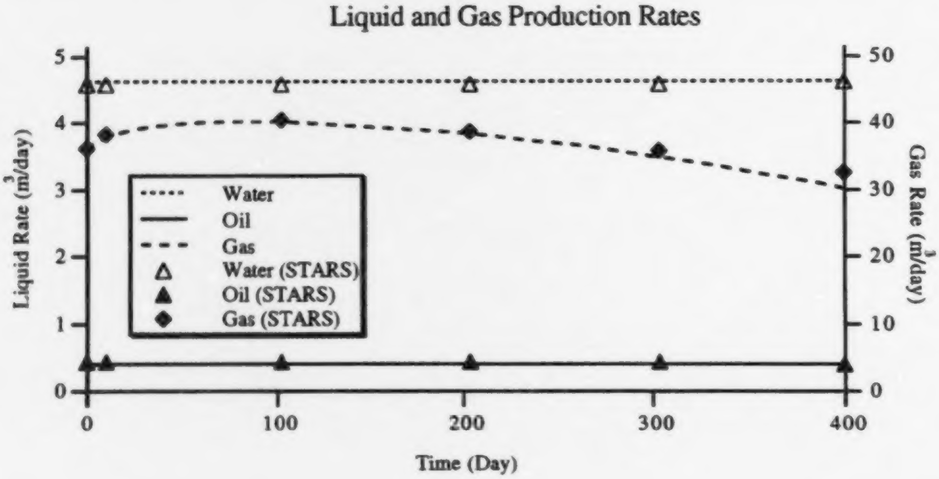

Figure 5.3.0.2 Run XY Liquid and gas production rates.

---

[1] For an example of the variation of agreement between simulators, the reader is referred to Aziz *et al.* (1987)

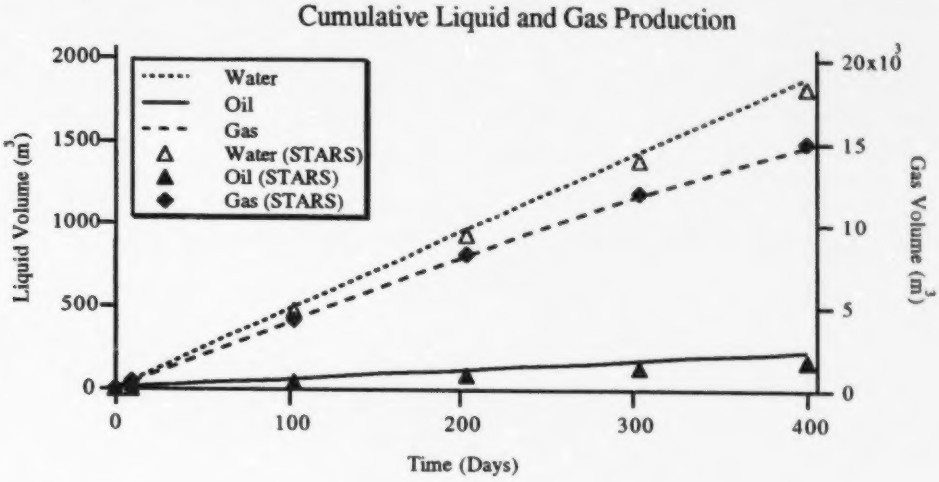

Figure 5.3.0.3 Run XY Cumulative liquid and gas production.

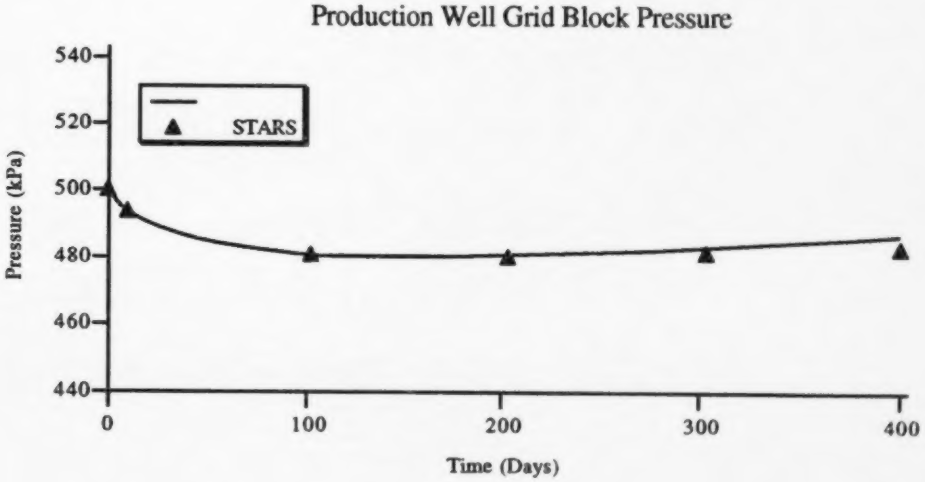

Figure 5.3.0.4 Run XY Production well grid block pressure.

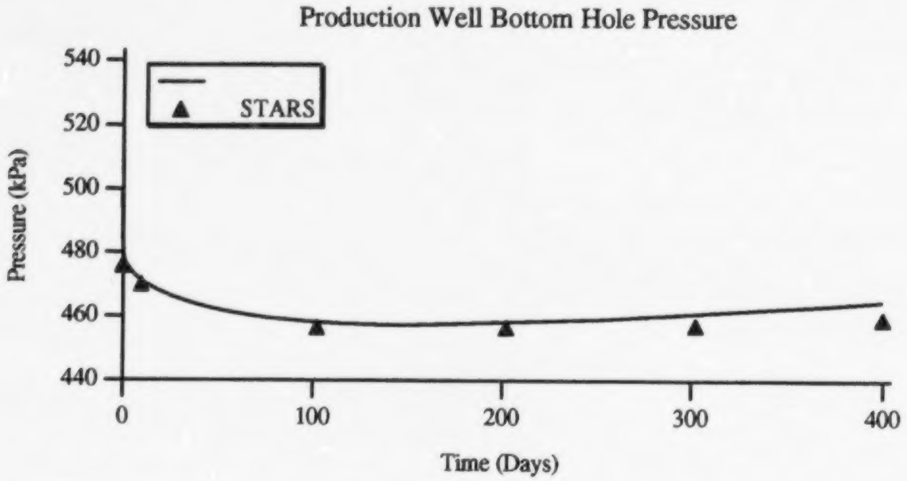

Figure 5.3.0.5 Run XY Production well bottom hole pressure.

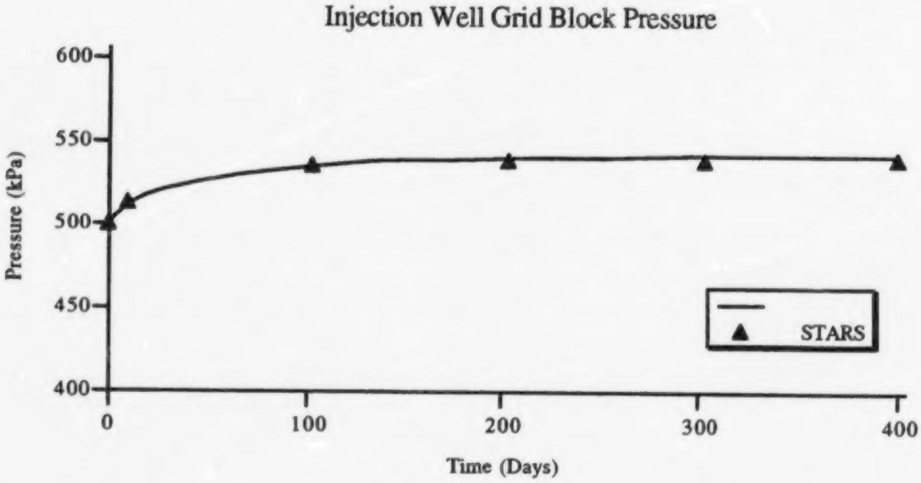

Figure 5.3.0.6 Run XY Injection well grid block pressure.

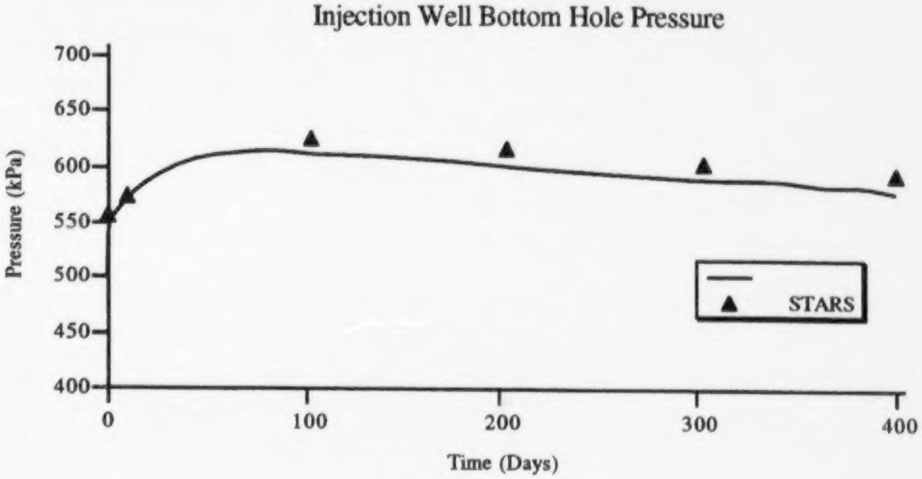

Figure 5.3.0.7 Run XY Injection well bottom hole pressure.

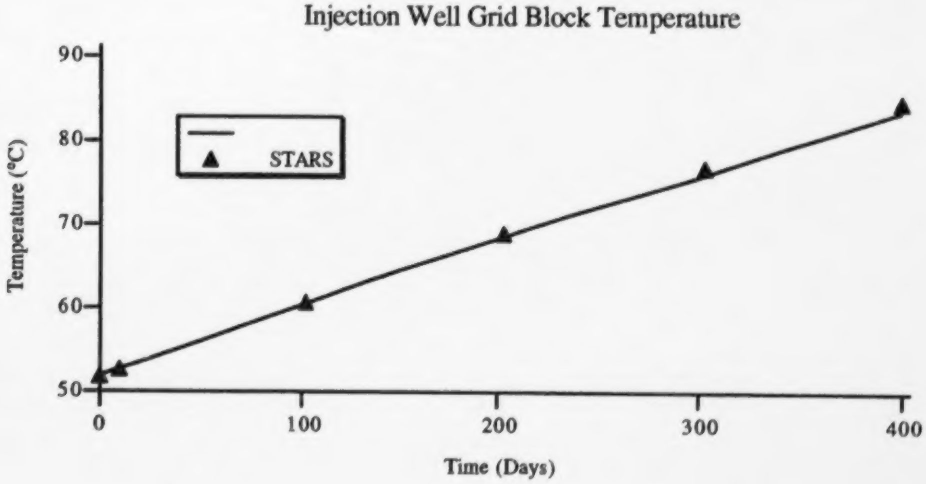

Figure 5.3.0.8 Run XY Injection well grid block temperature.

5.4 Cylindrical/Cylindrical Equivalent Series Testing

This series of runs had several objectives. The first was to demonstrate and to validate the model in both rectilinear and cylindrical coordinates. The model was compared to STARS for several runs (R-1c, C-1c and H-1c) as shown below. For all comparisons made, the results agreed and were excellent. The second objective was to illustrate and to compare various methods of modelling a single well. Finally, the last objective was to present results of a hyperhybrid grid and to compare these results to other grids.

The series was based on a cylindrical geometry and equal volumes. The volume of all problems was identical. Furthermore, the grid sizes whether rectilinear or cylindrical were matched. This is best illustrated by studying Figure 5.4.0.1 which summarizes the grids and run data.

Figures 5.4.0.2 to 5.4.0.5 illustrate the Jacobian for each problem; Runs R-1c, C-1c, H-1c and Z-1c, respectively. Note the increasing complexity of the Jacobian and accompanying loss of banded structure, especially when comparing Run R-1c and Z-1c. In addition, note that the price paid for better resolution about the well is more unknowns to be solved for.

For each run, the following Figures 5.4.0.6 to 5.4.0.35 show the steam injection rate, liquid production rate, cumulative injection and production, well grid block pressure, well grid block temperature and well pressure history.

Run R-1c was compared to STARS with good agreement in the results. Figure 5.4.0.6 shows the steam injection rate, Figure 5.4.0.7 shows the liquid production rates and Figure 5.4.0.8 shows the cumulative injected and produced volumes. The well grid block pressure, well grid block temperature and well pressure history are shown in Figures 5.4.0.9, 5.4.0.10 and 5.4.0.11, respectively. Run R-1c2 was not compared to STARS. The steam injection, liquid production rates and cumulative volume results for Run R-1c2 are shown in Figures 5.4.0.12, 5.4.0.13 and 5.4.0.14, respectively. The well grid block pressure, well grid block temperature and well pressure history are shown in Figures 5.4.0.15, 5.4.0.16 and 5.4.0.17, respectively.

The initial steam injection rate in Run R-1c, shown in Figure 5.4.0.6, was lower than the other runs due to the method used to calculate the well index for a rectilinear system. This was adjusted to match the well index calculated by the cylindrical mode and the results can be seen in the Run R-1c2 figures, particularly that of the steam injection rate shown in Figure 5.4.0.12. There are minor differences in the two runs in the production rates and, as a consequence, in the grid block pressures and bottom hole pressures. Although the volume of steam injected into Run R-1c2 was greater than Run R-1c, the increase in amount was not enough to affect the grid block temperature significantly.

For both Run R-1c and R-1c2, the character of the curves is very different from the cylindrical runs due to the geometry and grid block size. This result is not unexpected. For the second cycle injection, the curves became more similar in character because the injectivity had increased due to temperature and saturation changes.

Figures 5.4.0.18, 5.4.0.19 and 5.4.0.20 show the steam injection rate, liquid production rates and cumulative volumes, respectively, for Run C-1c. In addition, Figures 5.4.0.21, 5.4.0.22 and 5.4.0.23 show the well grid block pressure, well grid block temperature and well pressure history, respectively, for this run. Note on these figures the results of the comparison to the STARS simulator.

Firstly, a comparison of the injection rates of Run C-1c to Run R-1c (or R-1c2) shows that the injection rate was higher in Run C-1c and continued to increase due to the calculation of the well index. The continuing increase in the injection rate was due to a smaller grid block with increasing water saturation. Next, the production rates for Runs R-1c (or R-1c2) and C-1c shows that the cylindrical run had a higher initial water production rate because the water saturation of the inner block was higher then in the rectilinear runs. The subsequent production cycle shows the rates approaching each other because the injectivity/productivity has increased due to temperature and saturation changes.

The cumulative injection and production plots for these runs illustrate the effect of geometry on model prediction. Radial geometry is needed to represent the flow around a well versus a point sink/source representation. No attempt was made to match the rectilinear runs to the cylindrical ones, but normally the well index in Run R-1c would need to be set artificially high to give more realistic results. The well grid block pressure and temperature for Run R-1c was lower than for the cylindrical runs because of the consequences of the well index discussed above and the larger size of the grid block in Run R-1c.

Figures 5.4.0.24, 5.4.0.25 and 5.4.0.26 show the steam injection rate, liquid production rates and cumulative volumes, respectively, for Run H-1c. In addition, Figures 5.4.0.27, 5.4.0.28 and 5.4.0.29 show the well grid block pressure, well grid block temperature and well pressure history, respectively, for this run. Again, note on these figures the results of the comparison to the STARS simulator. Figures 5.4.0.30, 5.4.0.31 and 5.4.0.32 show the steam injection rate, liquid production rates and cumulative volumes, respectively, for Run Z-1c while Figures 5.4.0.33, 5.4.0.34 and 5.4.0.35 show the well grid block pressure, well grid block temperature and well pressure history, respectively, for Run Z-1c. Run Z-1c was not compared to the STARS simulator because that simulator does not have hyperhybrid capabilities.

Runs H-1c and Z-1c represent radial flow in the well grid block of Run R-1c. All results of these two runs were very similar in comparison to Run C-1c. Any variation can be attributed to the last ring in Run C-1c being represented as an irregular ring in Runs H-1c and Z-1c. As expected, Runs H-1c and Z-1c results are identical.

This model was demonstrated to represent flow in both rectilinear and cylindrical coordinates. A comparison of geometries of modelling a single well was made. Results were presented for a hyperhybrid grid with good agreement when compared to conventional grids.

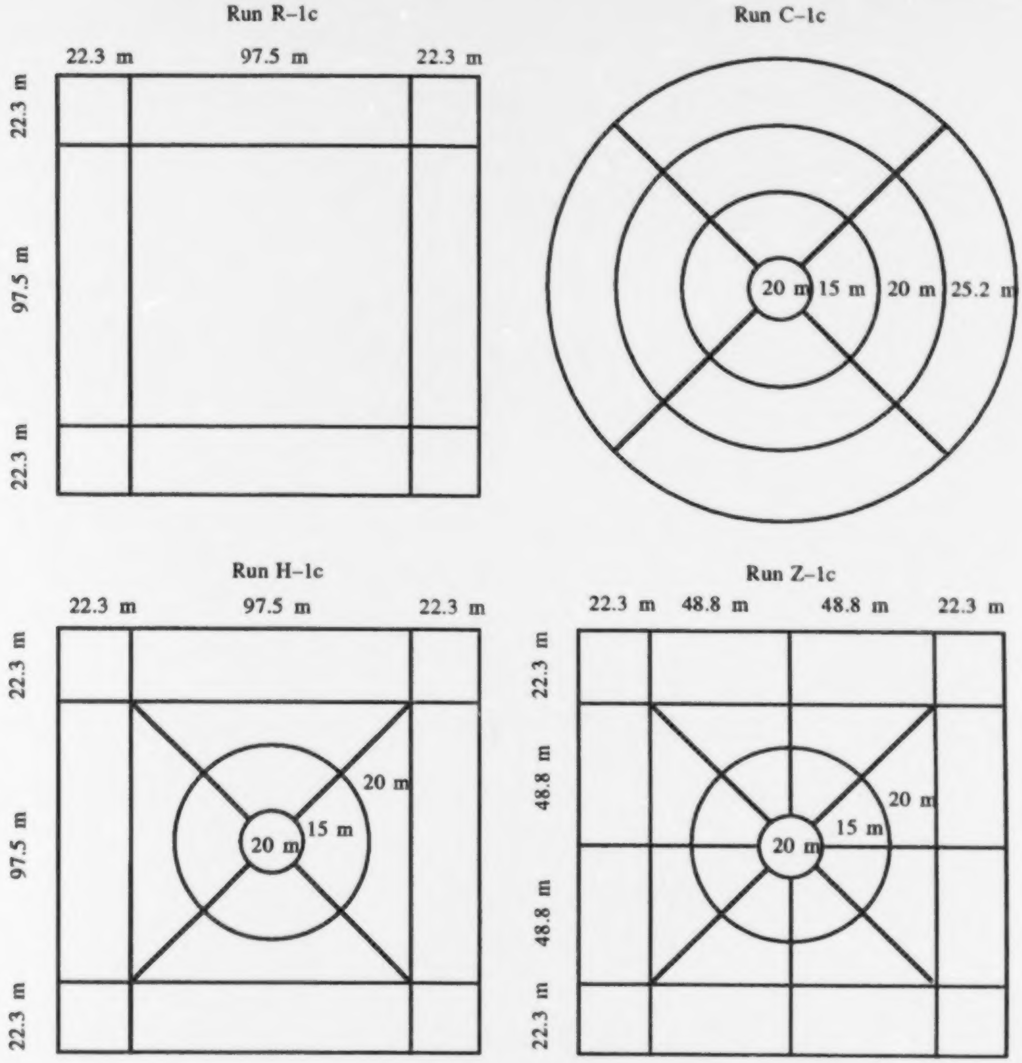
Run R-1c
22.3 m
97.5 m
22.3 m
22.3 m
97.5 m
22.3 m
Run C-1c
20 m
15 m
20 m
25.2 m
Run H-1c
22.3 m
97.5 m
22.3 m
22.3 m
97.5 m
22.3 m
20 m
15 m
20 m
Run Z-1c
22.3 m
48.8 m
48.8 m
22.3 m
22.3 m
48.8 m
48.8 m
22.3 m
20 m
15 m
20 m

- Grid Dimensions
  All grid blocks are as shown
  $\Delta z =$ 24.4 metres
- Rock Properties
  $k_x = k_y = 2000$ md
  $k_r = k_\theta = 2000$ md
  $k_z = 1000$ md
  $\phi = 0.30$
- Initial Conditions
  $P = 500$ kPa
  $T = 51.7$ °C
  $S_w = 0.20$
  $S_o = 0.80$
  $S_g = 0.00$

Figure 5.4.0.1 Cylindrical/cylindrical equivalent runs data summary.
(continued next page)

- Operating Conditions

Time (days)			Time (days)		
0–20	BHP_{max} (kPa)	6900	120–140	BHP_{max} (kPa)	6900
	BHP_{min} (kPa)	117		BHP_{min} (kPa)	117
	q_T (m^3/d)	159		q_T (m^3/d)	159
	x	0.7		x	0.7
	T_{inj} (°C)	232		T_{inj} (°C)	232
20–120	BHP_{max} (kPa)	6900	140–240	BHP_{max} (kPa)	6900
	BHP_{min} (kPa)	117		BHP_{min} (kPa)	117
	q_L (m^3/d)	20		q_L (m^3/d)	20

- Well Parameters

	Well
Index	+1/-1
Productivity	Internally calculated
J* multiplier	1.0
f_h	1.0
f	1.0
c_g	0.5
s	0.0
r_w (metres)	0.09

Figure 5.4.0.1 Cylindrical/cylindrical equivalent runs data summary.
(continued from previous page)

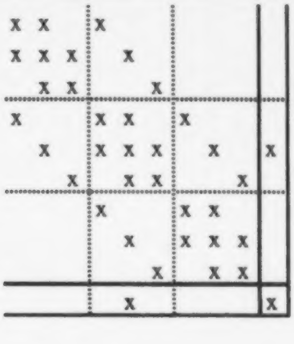

Figure 5.4.0.2 Run R-1c Jacobian matrix.

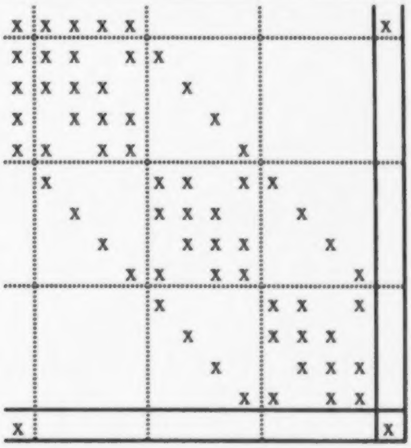

Figure 5.4.0.3 Run C-1c Jacobian matrix.

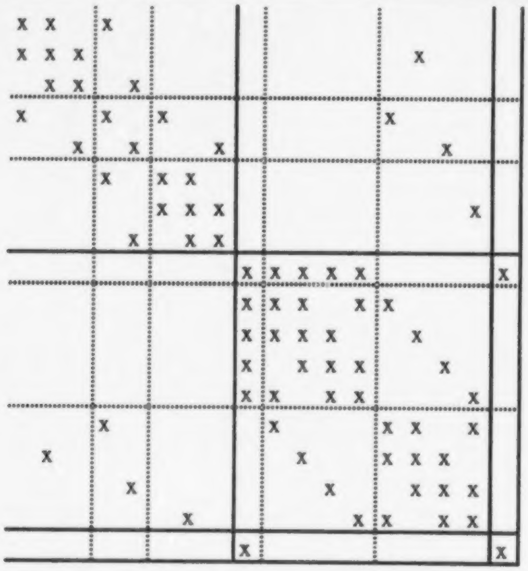

Figure 5.4.0.4 Run H-1c Jacobian matrix.

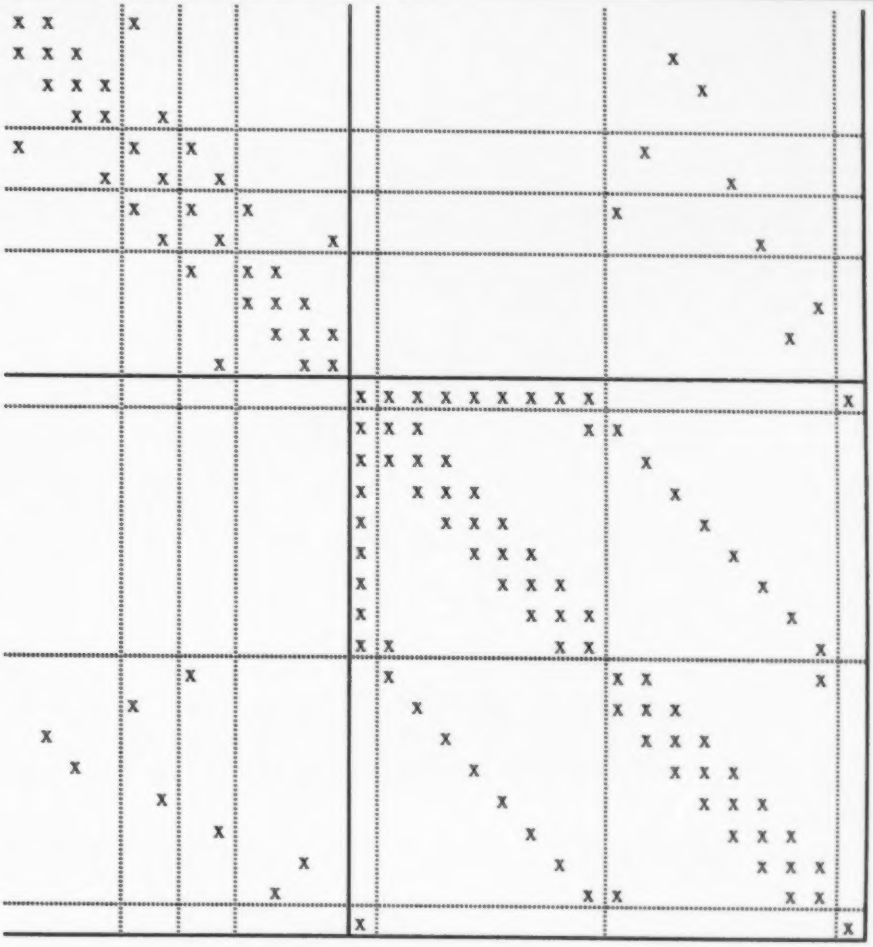

Figure 5.4.0.5 Run Z-1c Jacobian matrix.

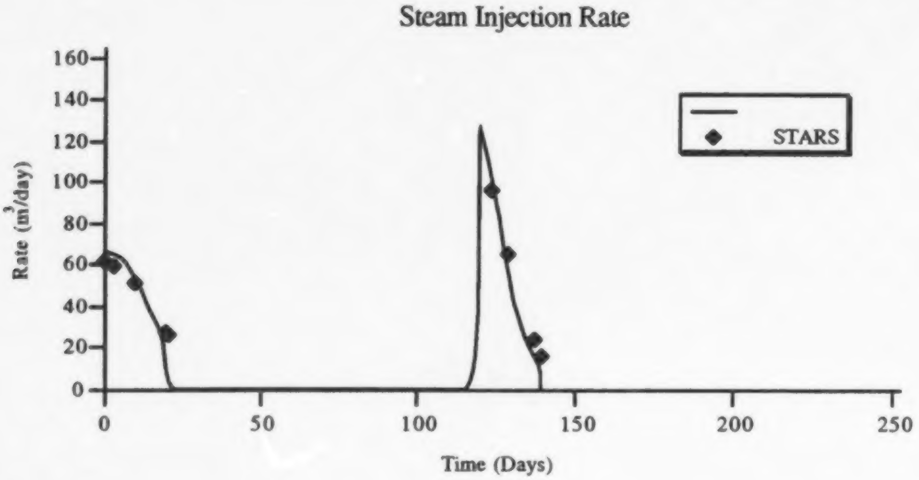

Figure 5.4.0.6 Run R-1c Steam injection rate.

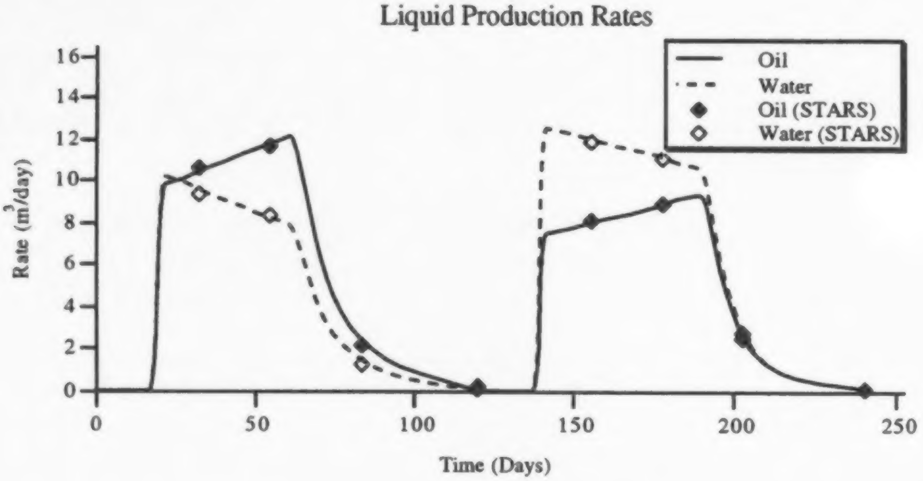

Figure 5.4.0.7 Run R-1c Liquid production rates.

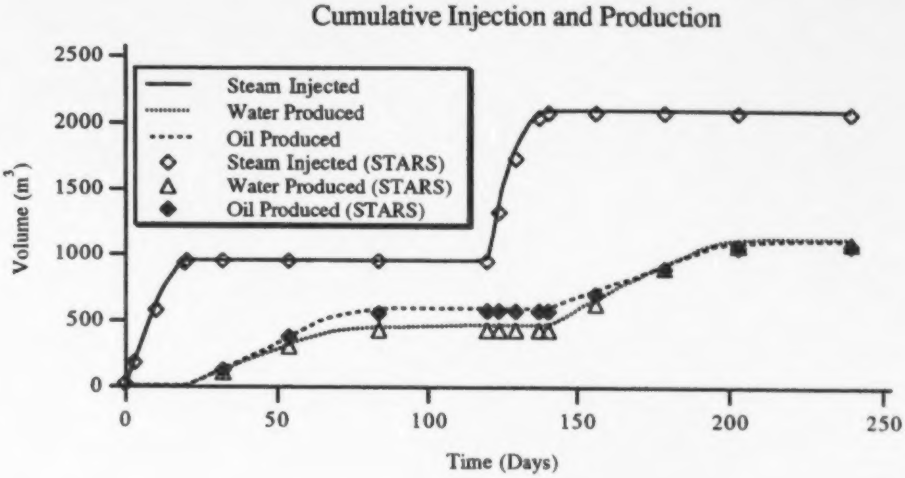

Figure 5.4.0.8 Run R-1c Cumulative injection and production.

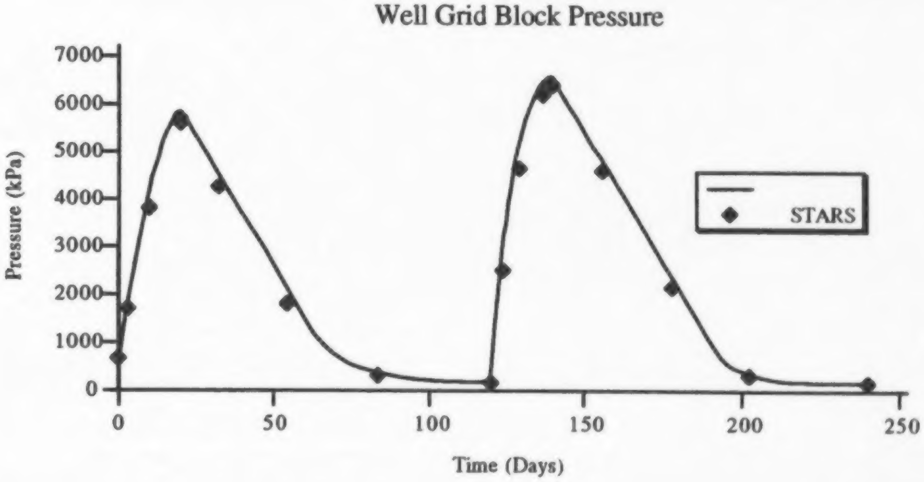

Figure 5.4.0.9 Run R-1c Well grid block pressure.

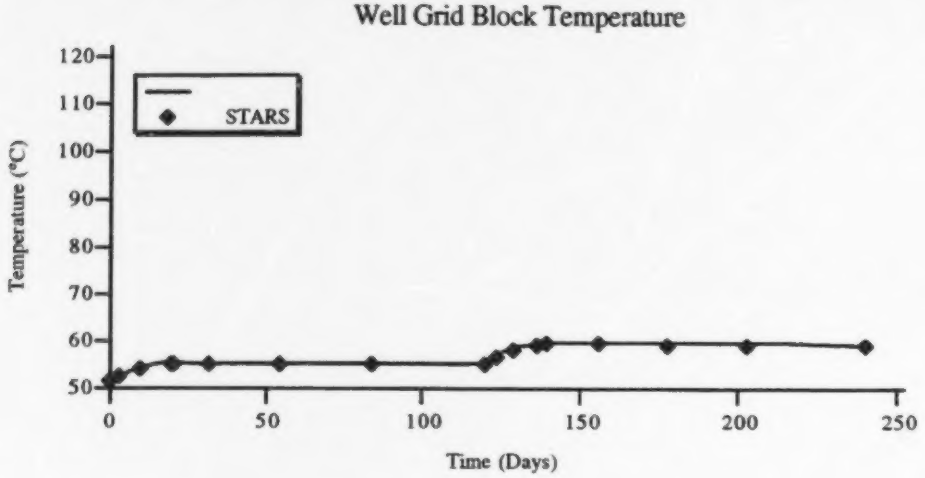

Figure 5.4.0.10 Run R-1c Well grid block temperature.

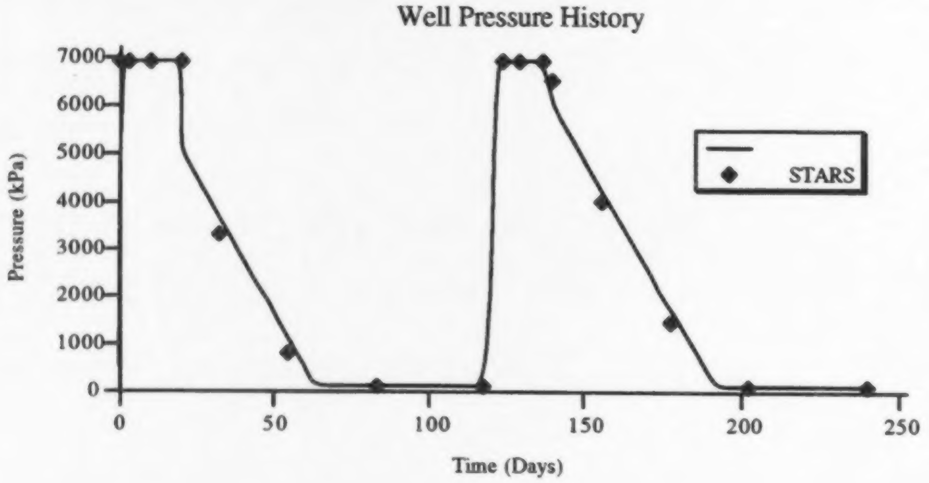

Figure 5.4.0.11 Run R-1c Well pressure history.

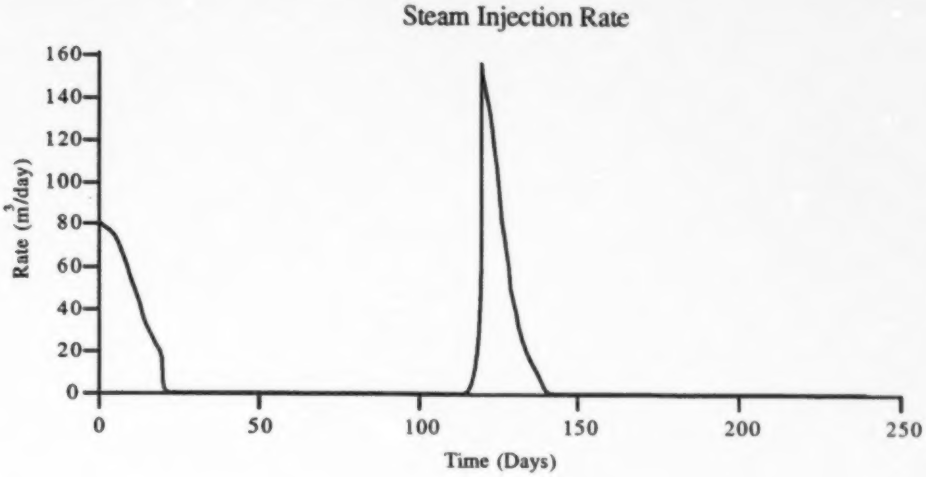

Figure 5.4.0.12 Run R-1c2 Steam injection rate.

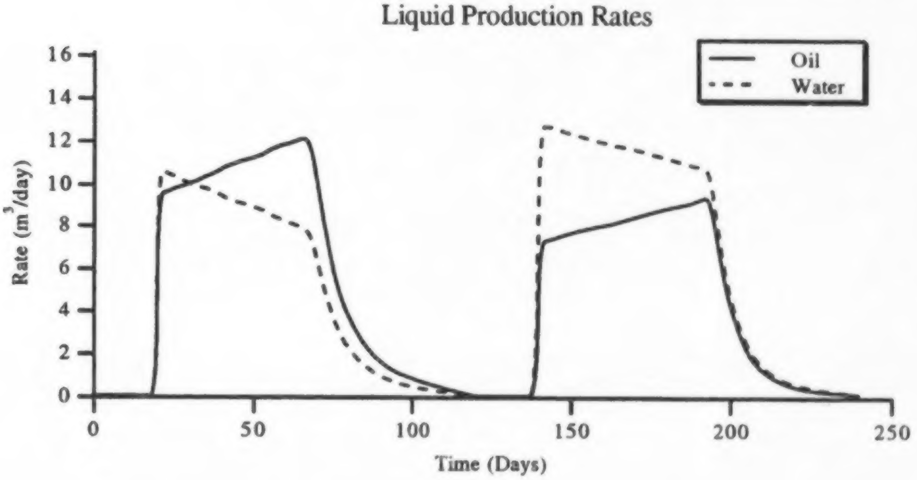

Figure 5.4.0.13 Run R-1c2 Liquid production rates.

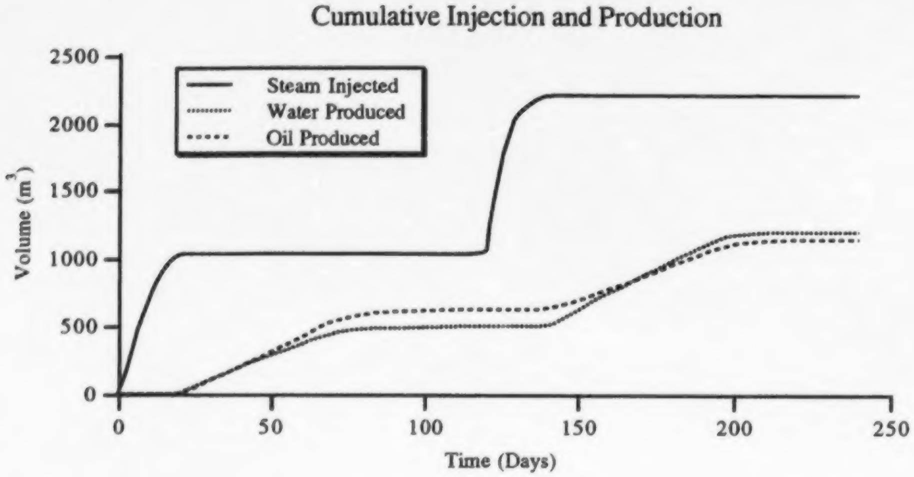

Figure 5.4.0.14 Run R-1c2 Cumulative injection and production.

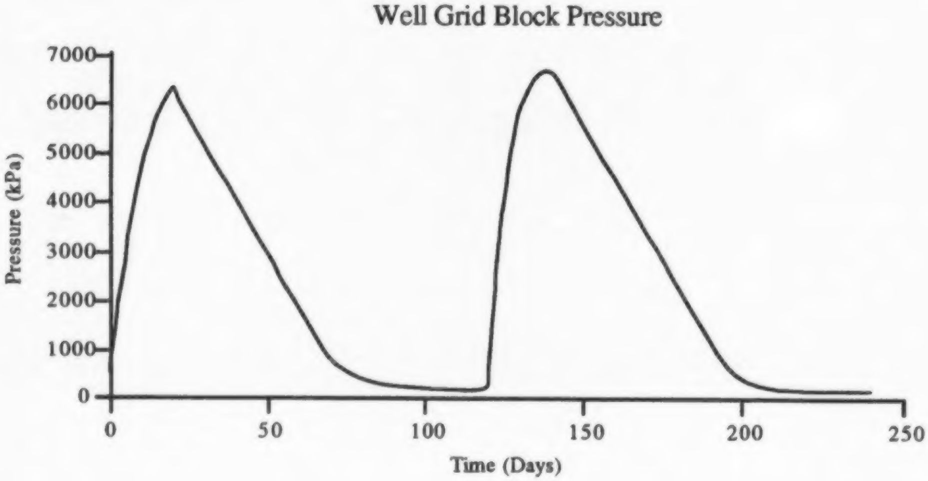

Figure 5.4.0.15 Run R-1c2 Well grid block pressure.

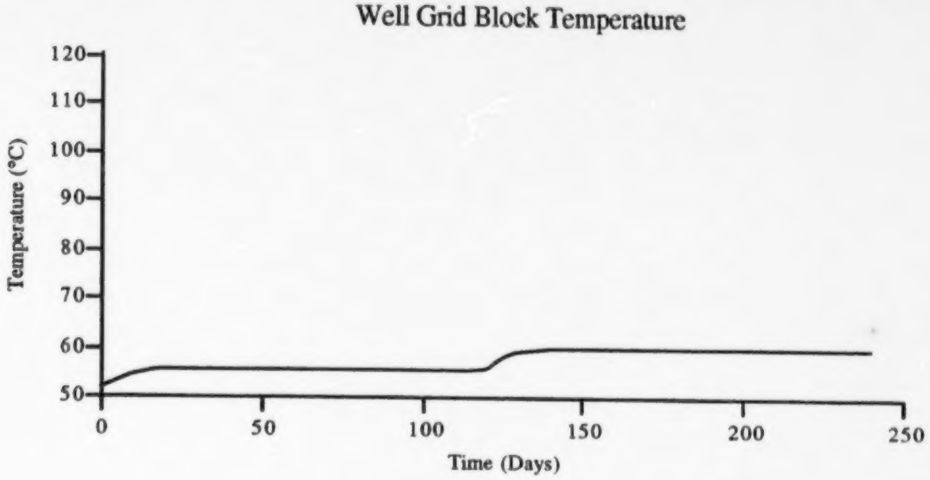

Figure 5.4.0.16 Run R-1c2 Well grid block temperature.

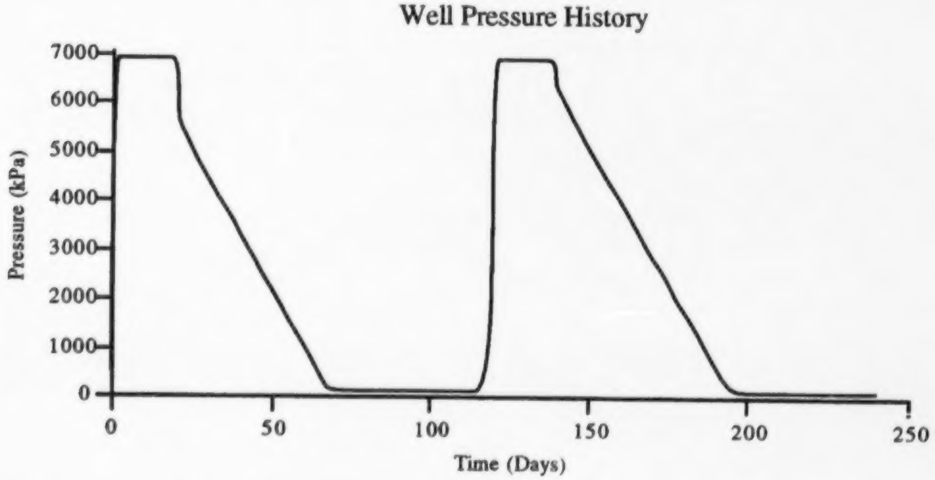

Figure 5.4.0.17 Run R-1c2 Well pressure history.

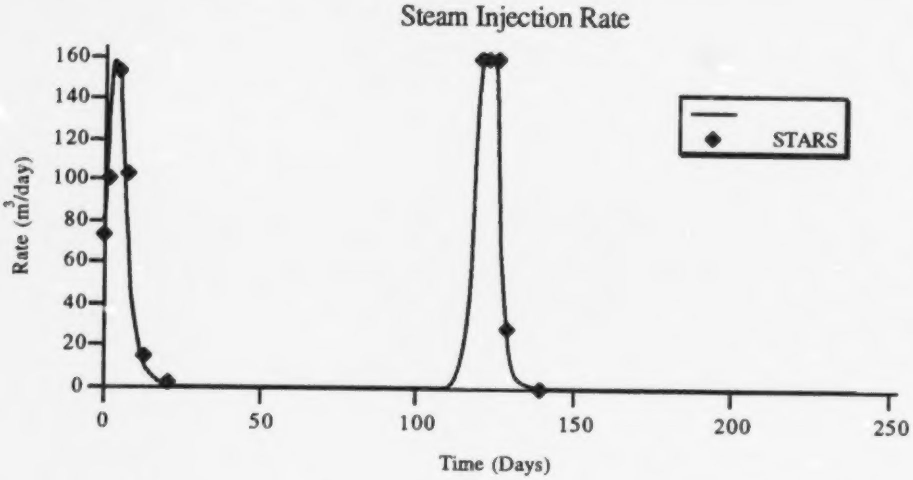

Figure 5.4.0.18 Run C-1c Steam injection rate.

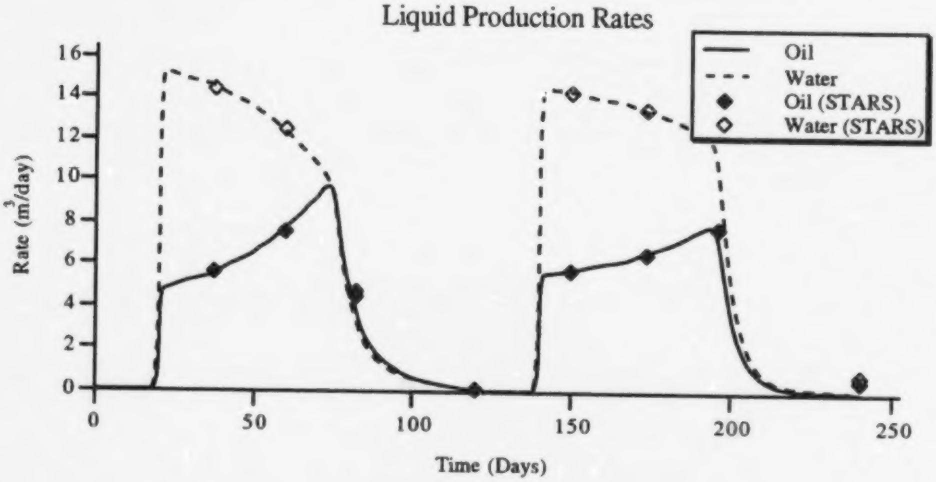

Figure 5.4.0.19 Run C-1c Liquid production rates.

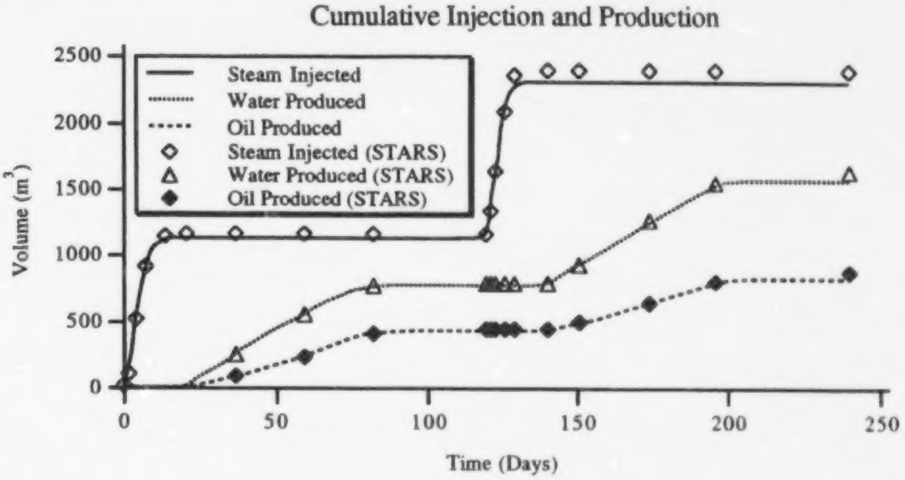

Figure 5.4.0.20 Run C-1c Cumulative injection and production.

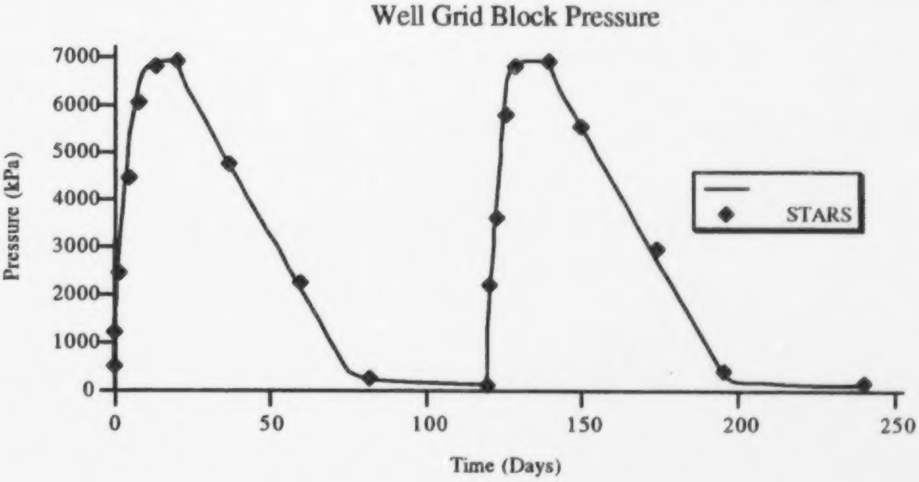

Figure 5.4.0.21 Run C-1c Well grid block pressure.

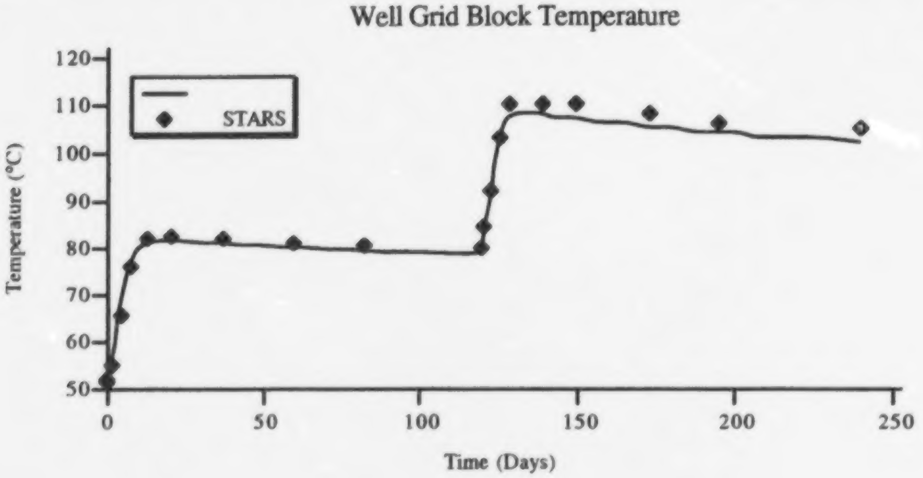

Figure 5.4.0.22 Run C-1c Well grid block temperature.

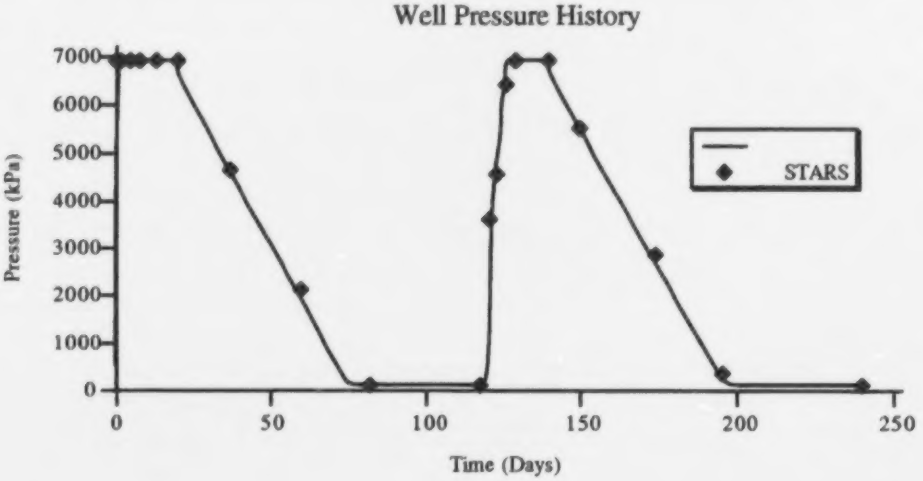

Figure 5.4.0.23 Run C-1c Well pressure history.

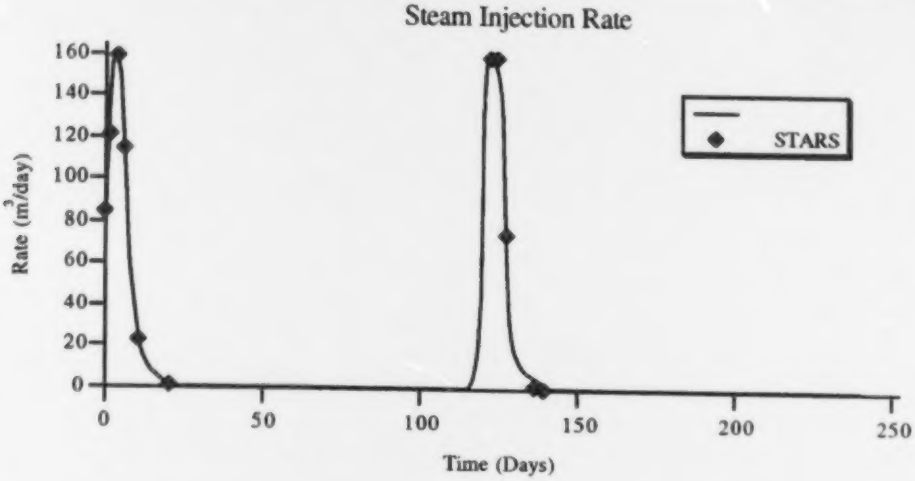

Figure 5.4.0.24 Run H-1c Steam injection rate.

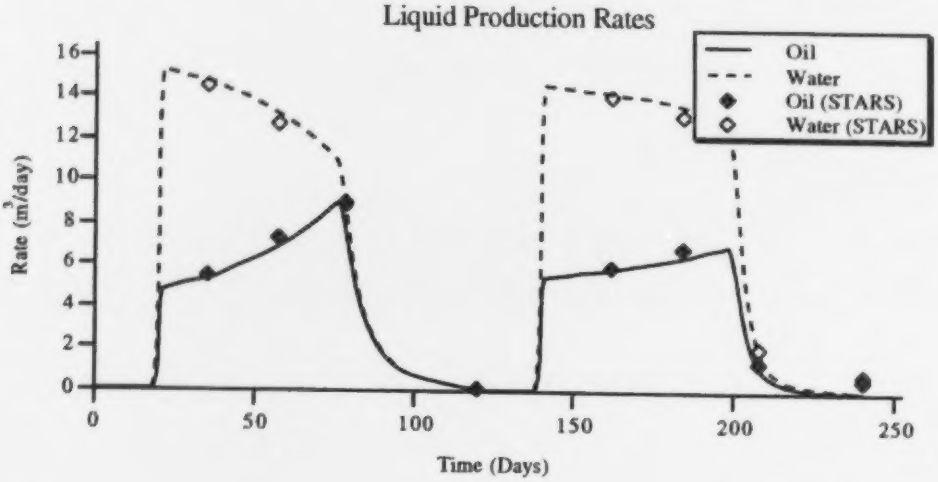

Figure 5.4.0.25 Run H-1c Liquid production rates.

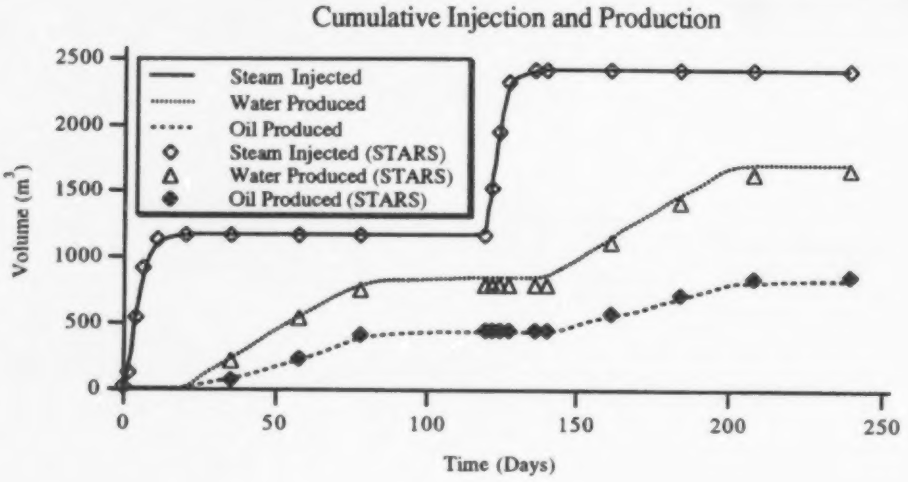

Figure 5.4.0.26 Run H-1c Cumulative injection and production.

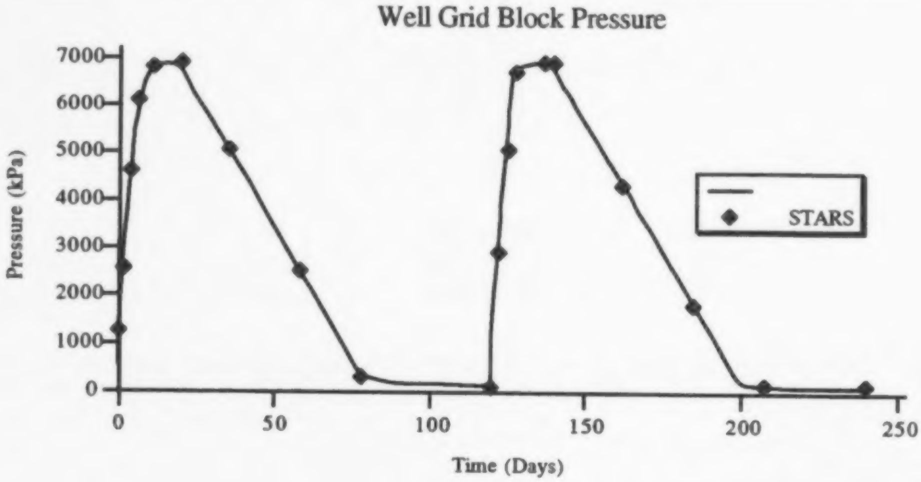

Figure 5.4.0.27 Run H-1c Well grid block pressure.

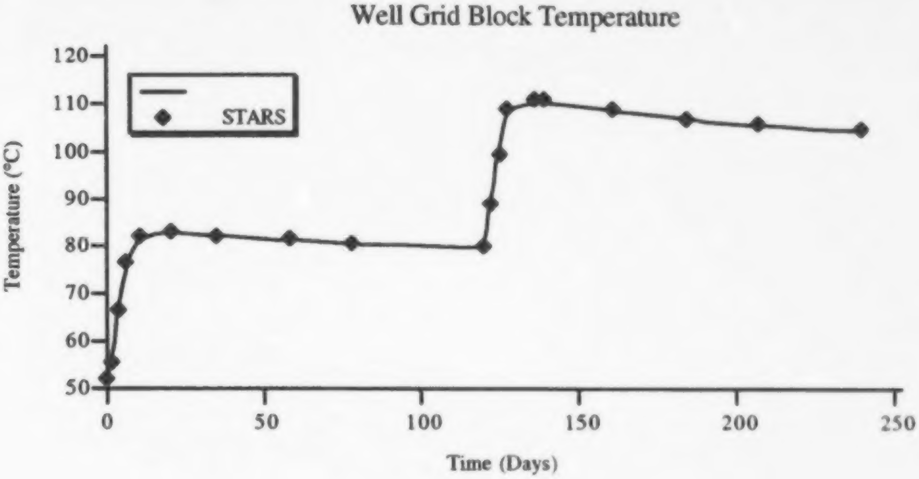

Figure 5.4.0.28 Run H-1c Well grid block temperature.

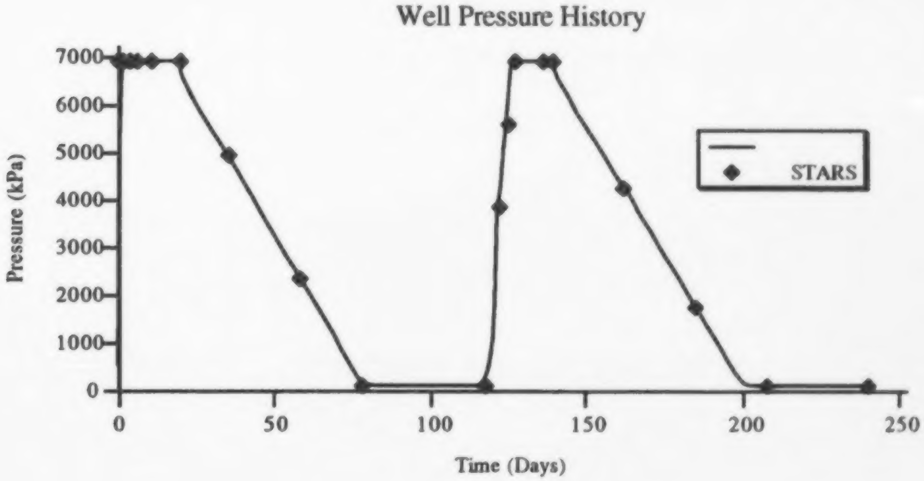

Figure 5.4.0.29 Run H-1c Well pressure history.

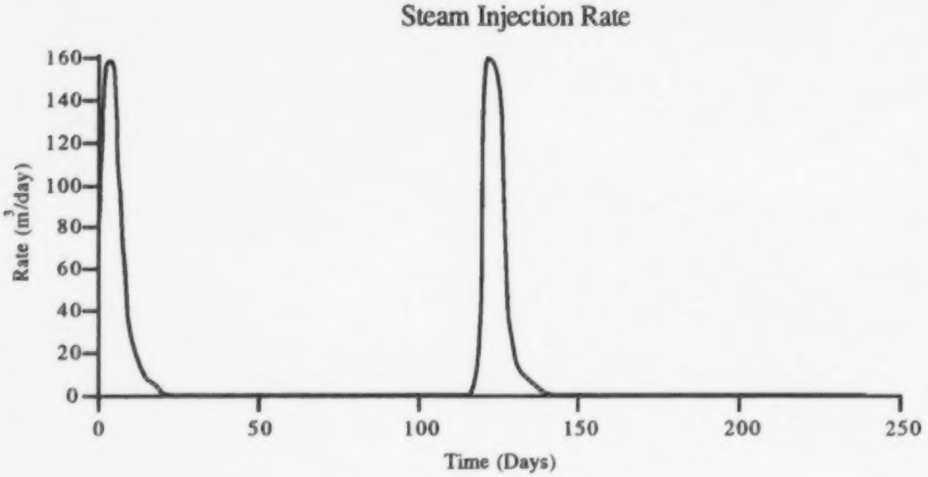

Figure 5.4.0.30 Run Z-1c Steam injection rate.

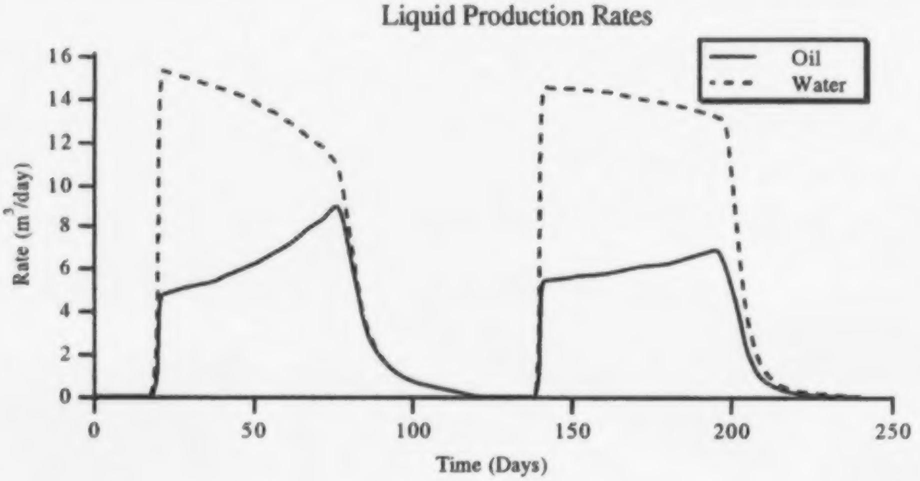

Figure 5.4.0.31 Run Z-1c Liquid production rates.

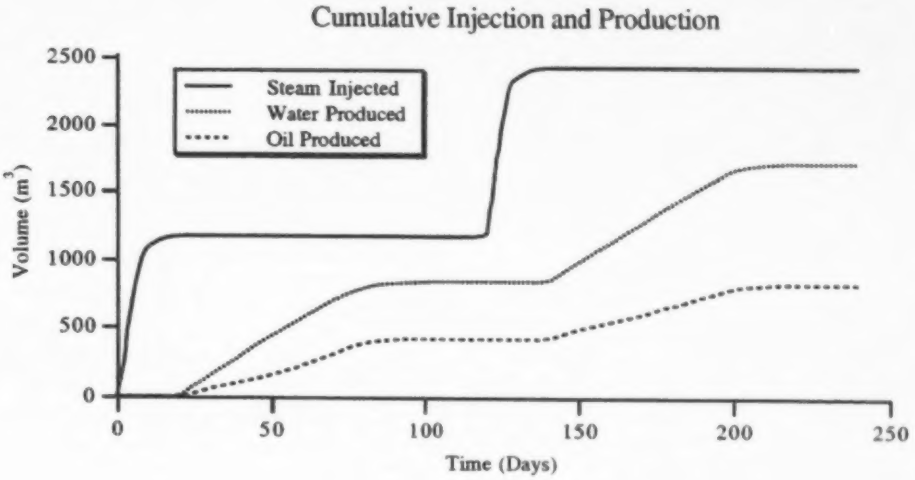

Figure 5.4.0.32 Run Z-1c Cumulative injection and production.

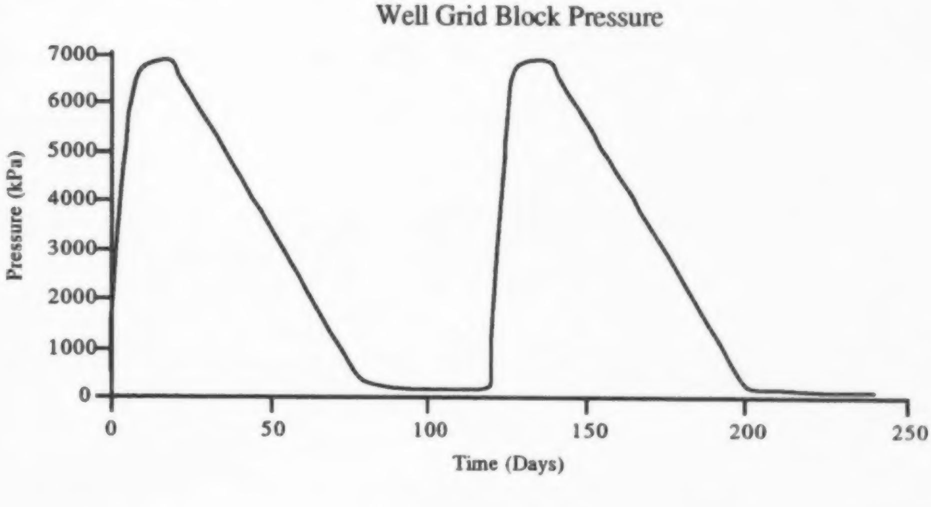

Figure 5.4.0.33 Run Z-1c Well grid block pressure.

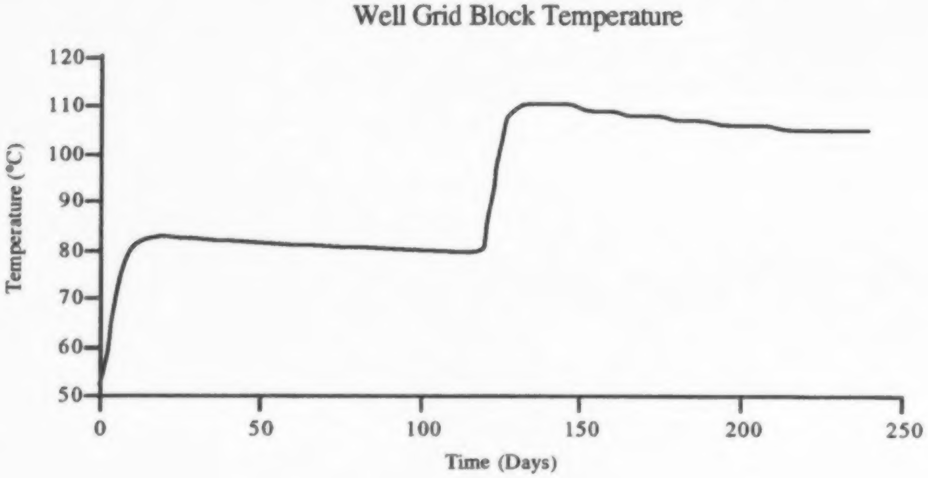

Figure 5.4.0.34 Run Z-1c Well grid block temperature.

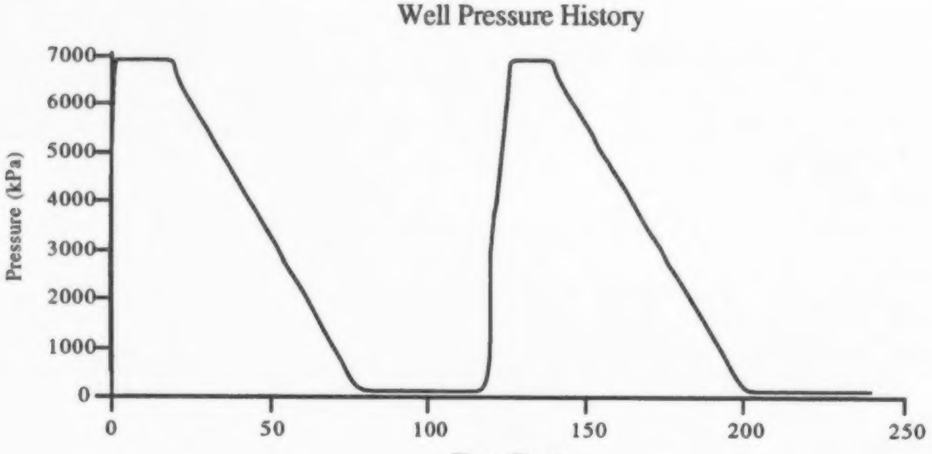

Figure 5.4.0.35 Run Z-1c Well pressure history.

5.5 Contiguous Regions Testing

Two small grid systems were used to test the code and demonstrate contiguous hybrid and hyperhybrid regions. Figure 5.5.0.1 illustrates the grids used and other details of Runs H-2 and Z-2. Figures 5.5.0.2 and 5.5.0.3 illustrate the Jacobians for these two problems. Note the cross terms between the reservoir/region 1, reservoir/region 2 and region 1/region 2.

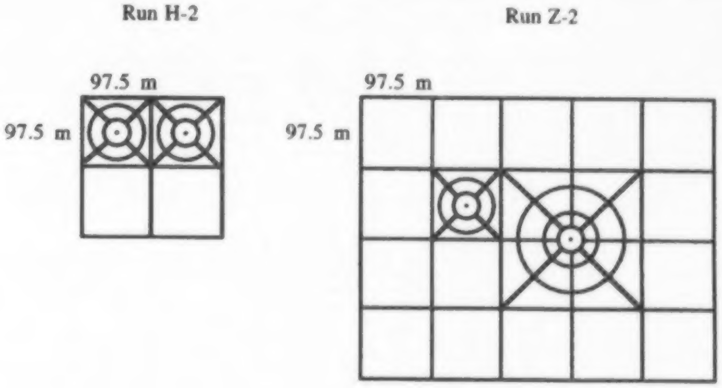

- Grid Dimensions
  All grid blocks are the same size
  $\Delta x =$ 97.5 metres
  $\Delta y =$ 97.5 metres
  $\Delta z =$ 24.4 metres
- Rock Properties
  $k_x = k_y = 2000$ md
  $k_r = k_\theta = 2000$ md
  $k_z = 1000$ md
  $\phi = 0.30$
- Initial Conditions
  $P = 500$ kPa
  $T = 51.7$ °C
  $S_w = 0.20$
  $S_o = 0.80$
  $S_g = 0.00$

	Run H-2		Run Z-2	
	Region 1	Region 2	Region 1	Region 2
Δr_1	20.0	20.0	20.0	20.0
Δr_2	15.0	15.0	15.0	25.0
Δr_3	20.0*	20.0*	20.0*	20.0
Δr_4	–	–	–	45.0*

Region 1 is on the left and Region 2 is on the right.

* calculated internally

Figure 5.5.0.1 Runs H-2 and Z-2 data summary (continued next page).

- Operating Conditions

Time (days)	Region 1		Region 2	
0–20	BHP_{max} (kPa)	6900	BHP_{max} (kPa)	6900
	BHP_{min} (kPa)	120	BHP_{min} (kPa)	120
	q_T (m^3/d)	159	q_T (m^3/d)	159
	x	0.7	x	0.7
	T_{inj} (°C)	232	T_{inj} (°C)	232
20–75	BHP_{max} (kPa)	6900	BHP_{max} (kPa)	6900
	BHP_{min} (kPa)	120	BHP_{min} (kPa)	120
	q_L (m^3/d)	20	q_L (m^3/d)	20
75–85	BHP_{max} (kPa)	6900	BHP_{max} (kPa)	6900
	BHP_{min} (kPa)	120	BHP_{min} (kPa)	120
	q_L (m^3/d)	20	q_T (m^3/d)	100
			x	0.7
			T_{inj} (°C)	232
85–240	BHP_{max} (kPa)	6900	BHP_{max} (kPa)	6900
	BHP_{min} (kPa)	120	BHP_{min} (kPa)	120
	q_L (m^3/d)	20	q_L (m^3/d)	10

- Well Parameters

	Region 1	Region 2
Index	+1/-1	+1/-1
Productivity	Internally calculated	Internally calculated
J* multiplier	1.0	1.0
f_h	1.0	1.0
f	1.0	1.0
c_g	0.5	0.5
s	0.0	0.0
r_w (metres)	0.09	0.09

Figure 5.5.0.1 Runs H-2 and Z-2 data summary (continued from previous page).

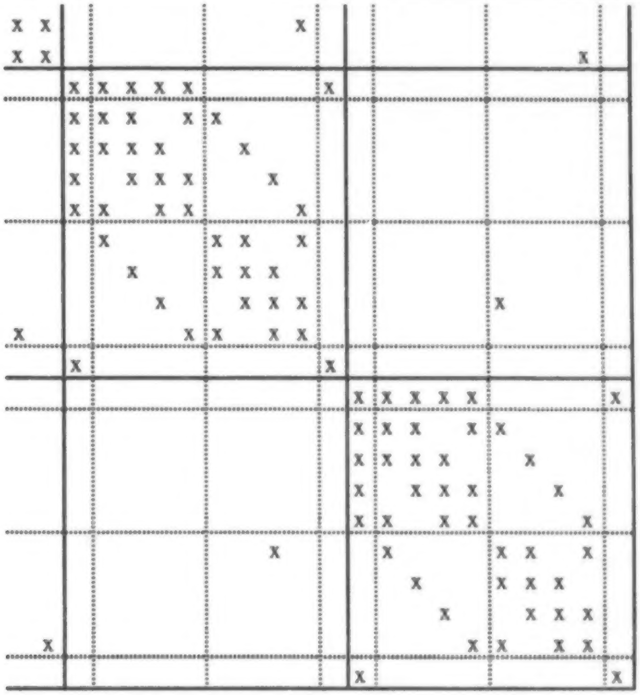

Figure 5.5.0.2 Run H-2 Jacobian matrix.

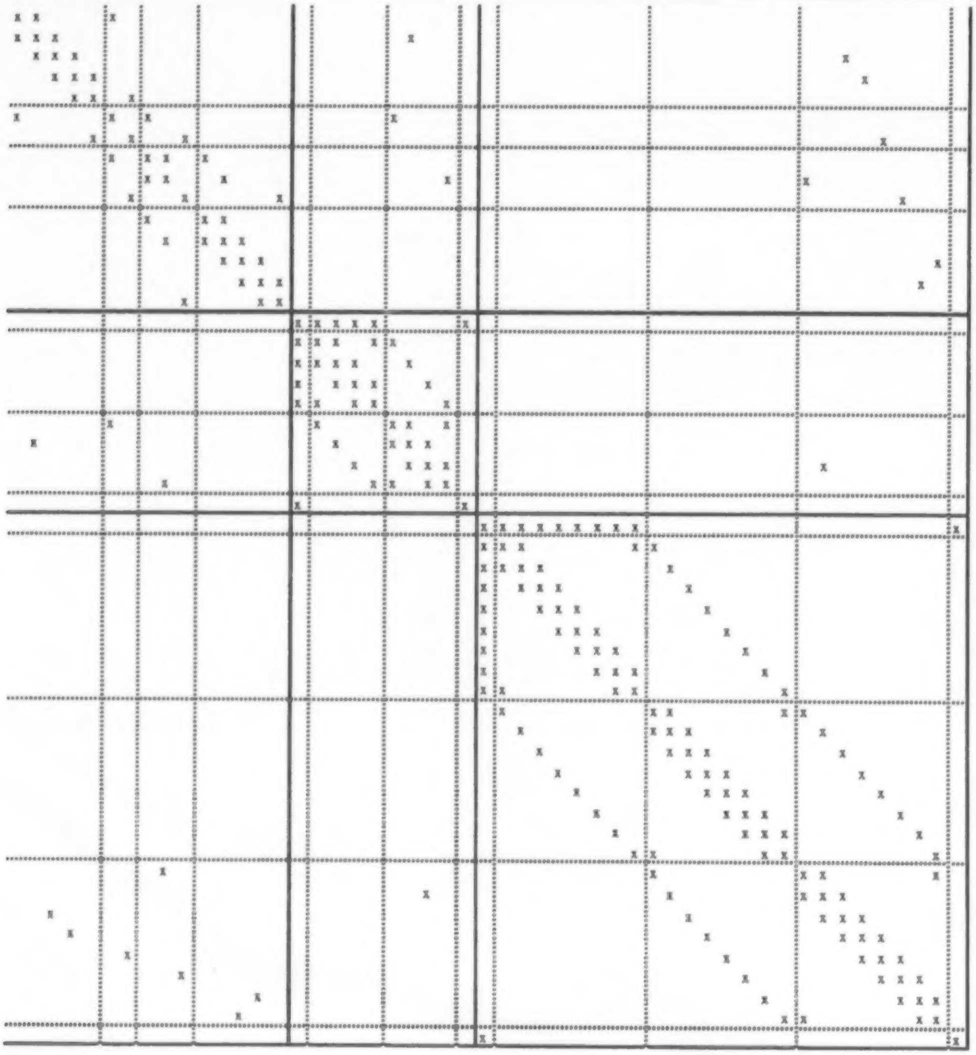

Figure 5.5.0.3 Run Z-2 Jacobian matrix.

Figures 5.5.0.4 and 5.5.0.13 show the steam injection rates while Figures 5.5.0.5 and 5.5.0.14 show the cumulative volumes of steam injected into each region for both runs. The major difference in the injection rates was that the rate in cycle 1 for Run H-2 did not reach the maximum due to the small size of the reservoir. The maximum bottom hole pressure was reached early as can be seen in Figure 5.5.0.9.

Figure 5.5.0.6 shows the liquid production rate for Run H-2. The liquid production rate behaviour was more interesting. For Run H-2, note that both the oil and water rates were boosted in Region 1 due to injection in Region 2 for the 75–85 day period. The effects of this injection were felt for up to day 120. Figure 5.5.0.7 shows the cumulative production for Run H-2.

Figures 5.5.0.8 and 5.5.0.9 show the well grid block pressure and well pressure history, respectively, for Run H-2. In addition to the production increase, both the grid block pressure and bottom hole pressure were affected in Region 1 by steam injection in Region 2.

Figure 5.5.0.10 illustrates the temperature change in the grid blocks containing the wells for Run H-2. Run H-2 did not show any interesting behaviour with respect to temperature.

Figures 5.5.0.11 and 5.5.0.12 show the pressure and temperature profiles at selected times between the wells for Run H-2. The hybrid grid provides six data points between the wells. Had a conventional rectilinear grid been used, only two data points would have been available. This illustrates that hybrid grids can be used to increase the resolution of detail about wells. Note that the temperature had not moved out of the well grid blocks significantly. Due to the size of the reservoir, a significant pressure gradient was created only during injection of the second cycle in region 2 while region 1 was on production.

Figures 5.5.0.15 and 5.5.0.16 show the production rates and cumulative production, respectively, for Run Z-2. The production rates for Run Z-2 were affected in a similar fashion as in Run H-2. Note that the injection effects were felt until day 220. This system was much larger than Run H-2.

Figures 5.5.0.17 and 5.5.0.18 show the well grid block pressure and well pressure history, respectively, for Run Z-2. The interwell behaviour of pressure in Run Z-2 was similar to Run H-2.

The pressure and temperature profiles at selected times are shown in Figures 5.5.0.19 and 5.5.0.20, respectively. The profiles are defined with seven data points with the use of hybrid and hyperhybrid grid refinement. Again as in Run H-2, note that the temperature had not moved out of the well grid blocks significantly and due to the size of the reservoir, a significant pressure gradient was created only during injection of the second cycle in region 2 while region 1 was on production. However, this gradient in Run Z-2 was less than that in Run H-2 because the distance between the wells was greater in Run Z-2.

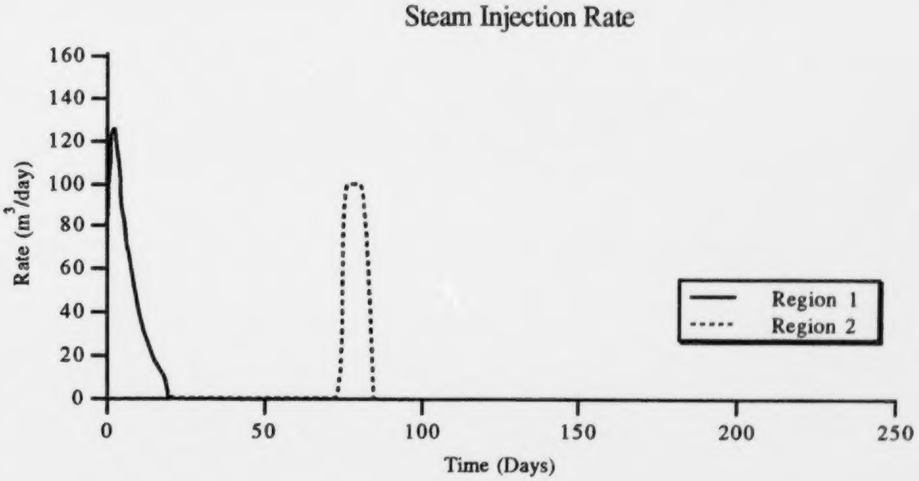

Figure 5.5.0.4 Run H-2 Steam injection rate.

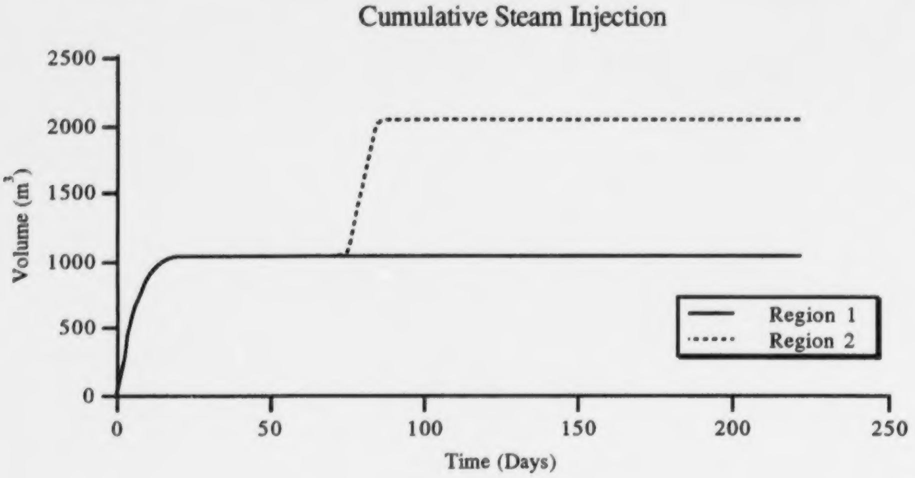

Figure 5.5.0.5 Run H-2 Cumulative steam injection.

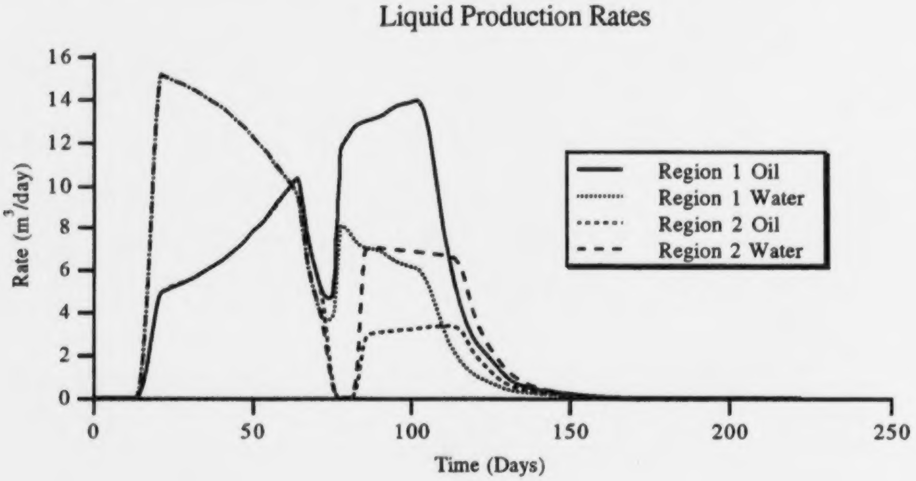

Figure 5.5.0.6 Run H-2 Liquid production rates.

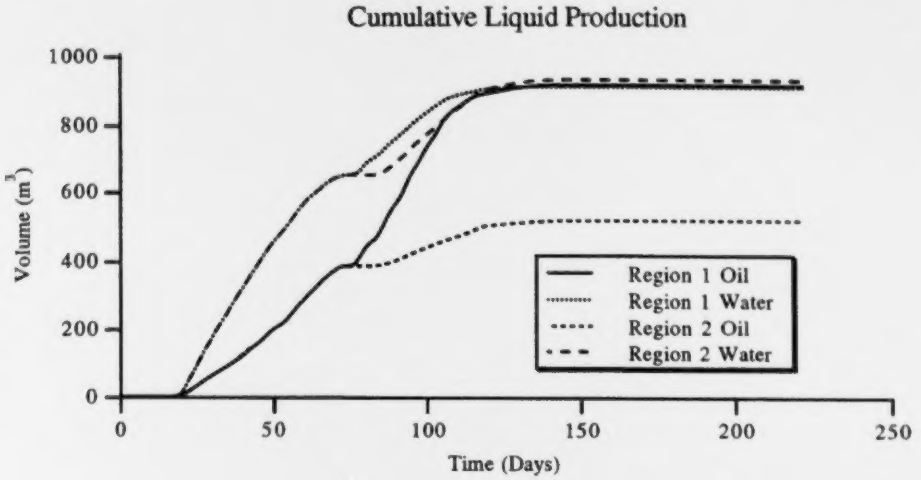

Figure 5.5.0.7 Run H-2 Cumulative liquid production.

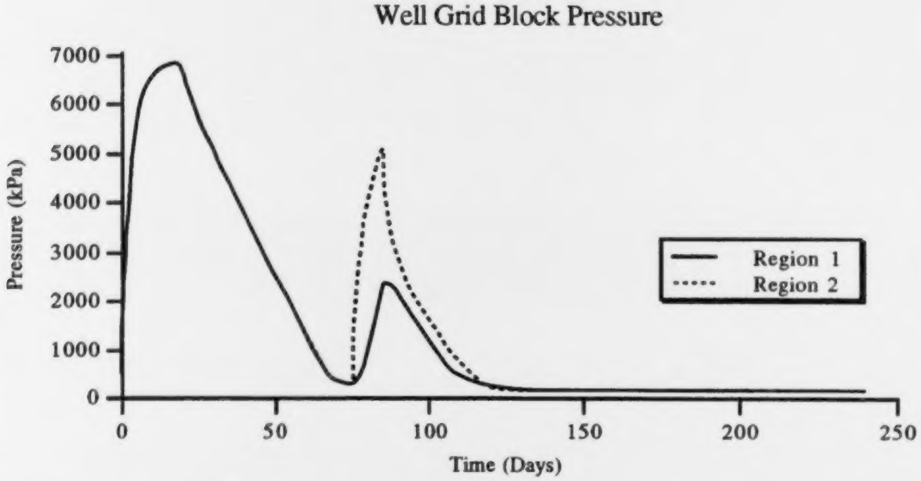

Figure 5.5.0.8 Run H-2 Well grid block pressure.

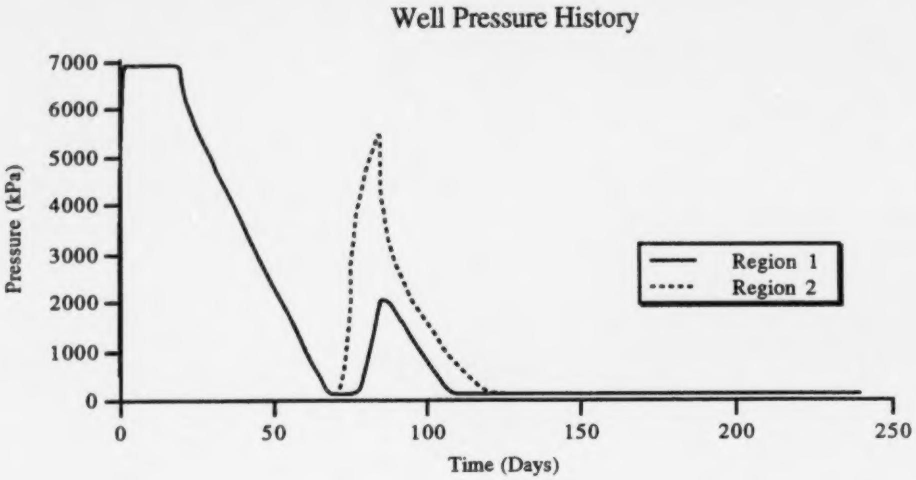

Figure 5.5.0.9 Run H-2 Well pressure history.

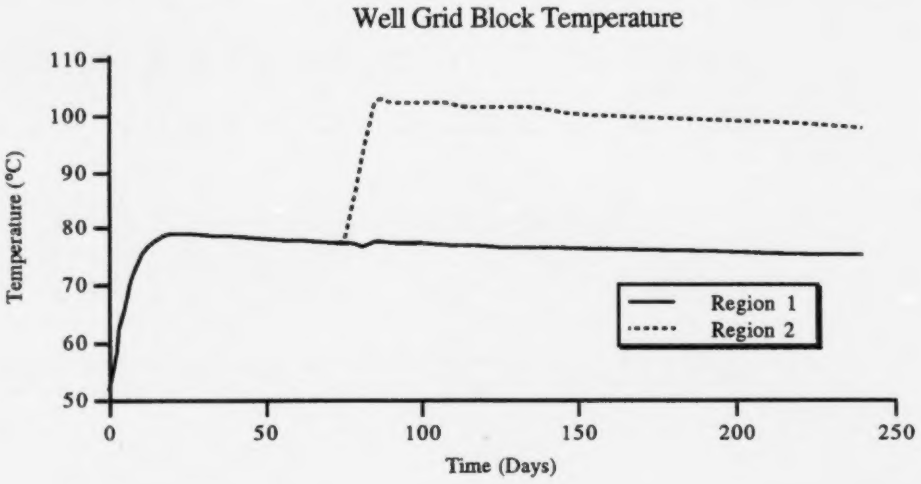

Figure 5.5.0.10 Run H-2 Well grid block temperature.

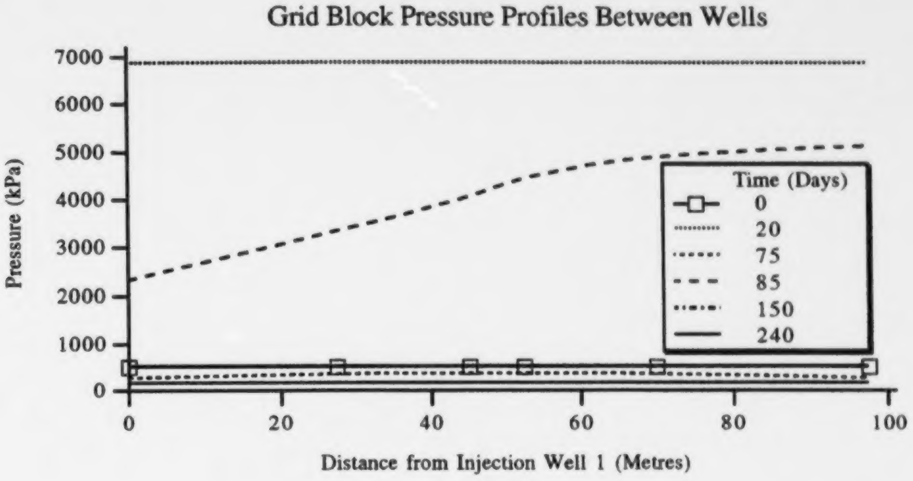

Figure 5.5.0.11 Run H-2 Grid block pressure profiles between wells.

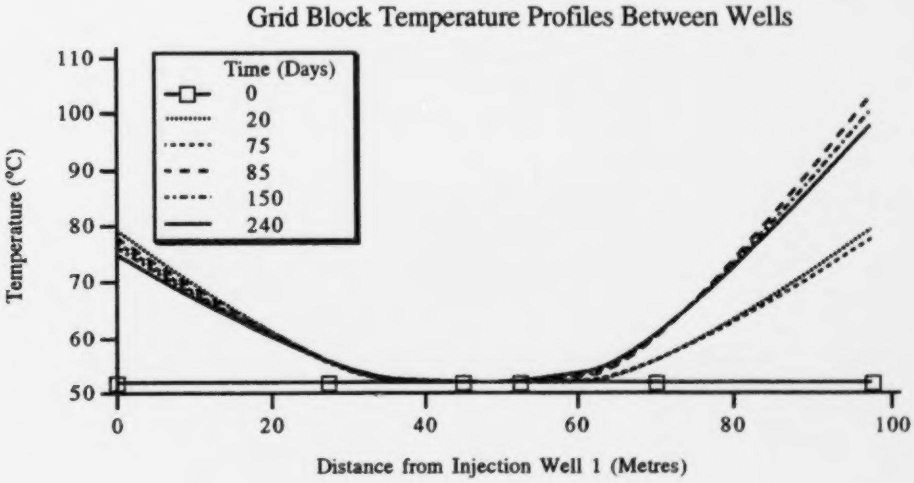

Figure 5.5.0.12 Run H-2 Grid block temperature profiles between wells.

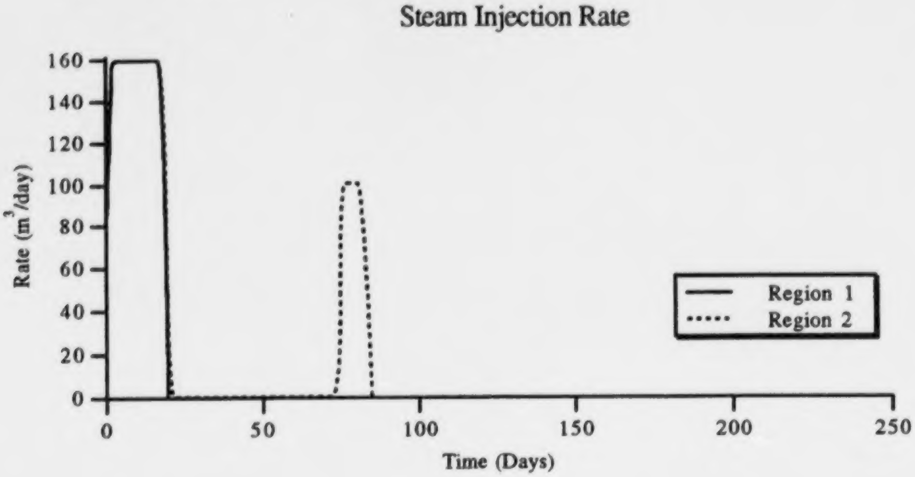

Figure 5.5.0.13 Run Z-2 Steam injection rate.

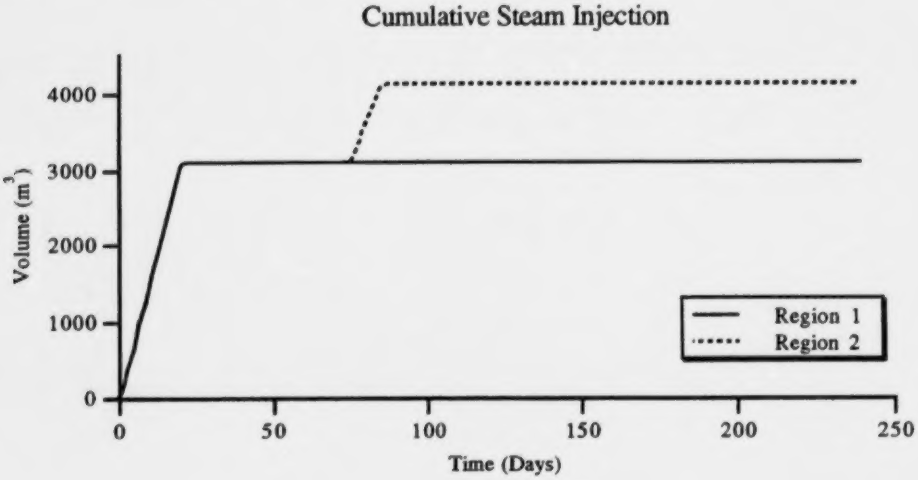

Figure 5.5.0.14 Run Z-2 Cumulative steam injection.

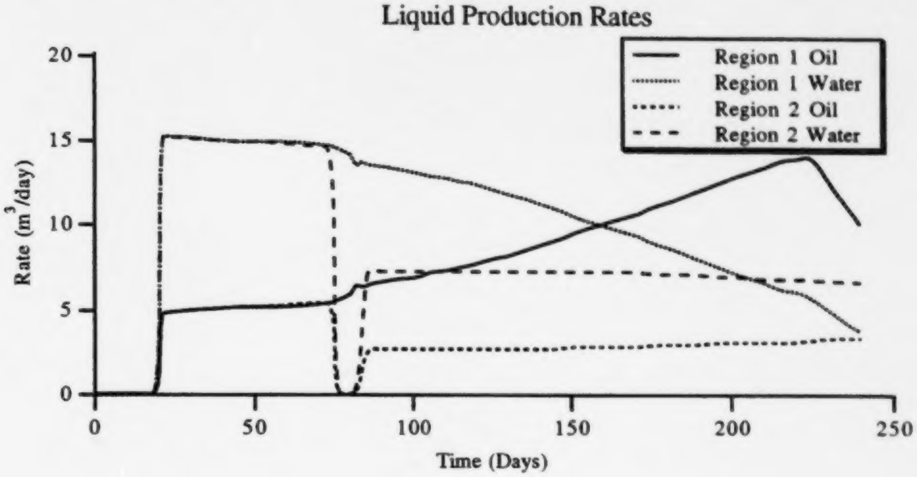

Figure 5.5.0.15 Run Z-2 Liquid production rates.

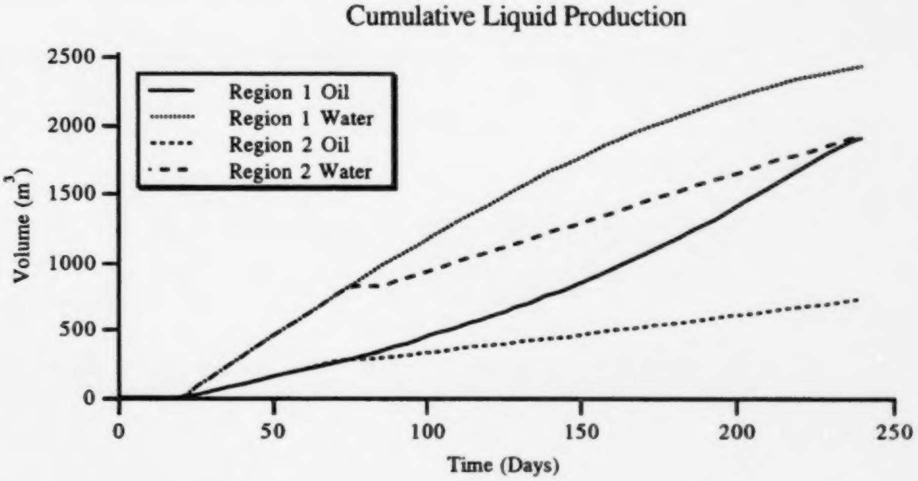

Figure 5.5.0.16 Run Z-2 Cumulative liquid production.

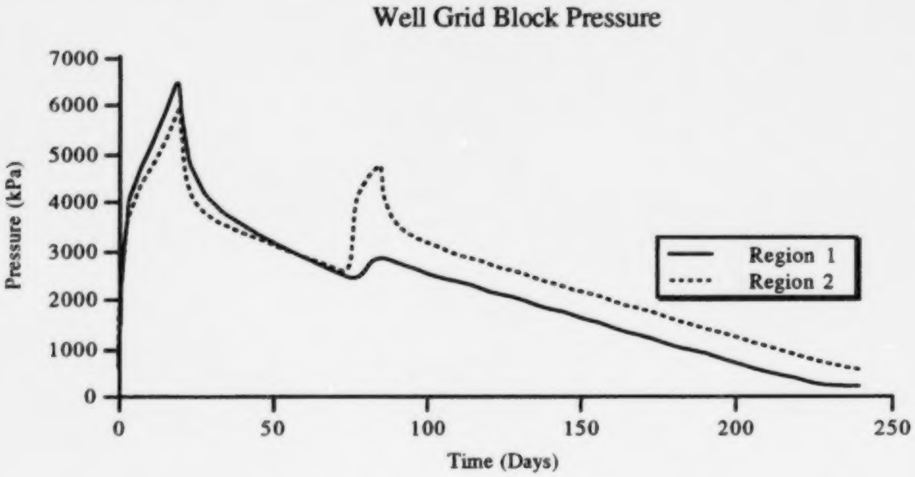

Figure 5.5.0.17 Run Z-2 Well grid block pressure.

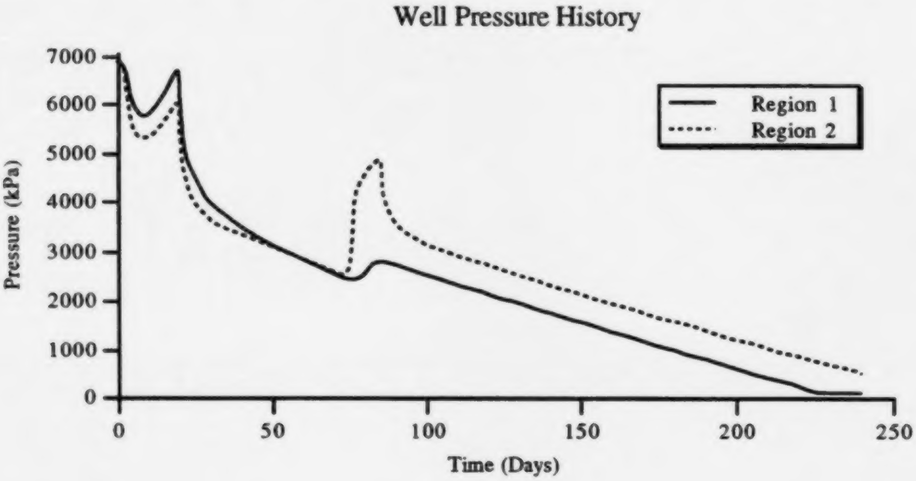

Figure 5.5.0.18 Run Z-2 Well pressure history.

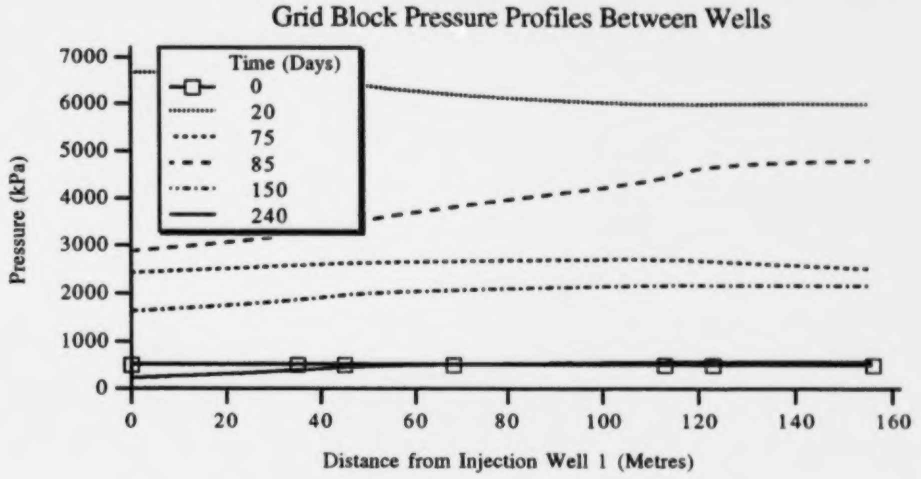

Figure 5.5.0.19 Run Z-2 Grid block pressure profiles between wells.

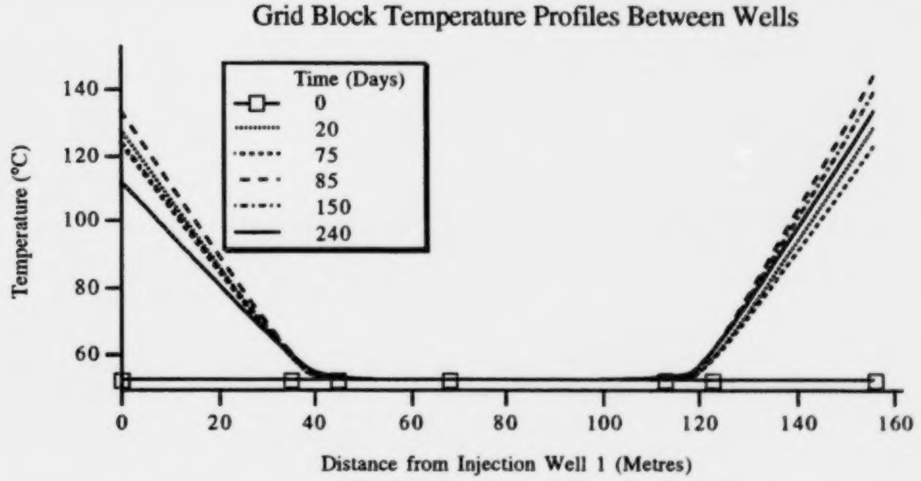

Figure 5.5.0.20 Run Z-2 Grid block temperature profiles between wells.

5.6 Local Well Effects

To illustrate the effects of grid design, several runs were made using rectilinear, hybrid and hyperhybrid grids to model a single well. In addition to a base case set of runs, a set of runs where the heavy oil component viscosity behaviour was non-Newtonian and a hyperhybrid grid run with visbreaking were made. Figure 5.6.0.1 illustrates the grids used and operating conditions for all runs in this section. Table 5.6.0.1 summarizes the parameters used to model non-Newtonian behaviour and Figures 5.6.0.2 and 5.6.0.3 illustrate the effect of shear rate and frontal velocity, respectively, on oil viscosity. Table 5.1.0.1 (page 120) summarizes the visbreaking parameters (Arrhenius constant and activation energy) used and the properties of the light oil component. Figure 5.1.0.1 (page 121) illustrates the viscosity of this light oil component as a function of temperature. Figure 5.6.0.4 illustrates the fraction of visbreaking as a function of time for various temperatures. Finally, a two-layer hyperhybrid run with bottom water was made—Run Z-3e.

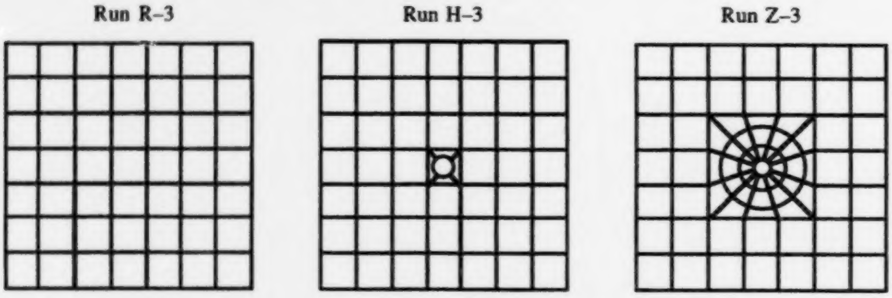

- Grid Dimensions
  All grid blocks are the same size
  Δx = 97.5 metres
  Δy = 97.5 metres
  Δz = 24.4 metres
- Rock Properties
  $k_x = k_y = 2000$ md
  $k_r = k_\theta = 2000$ md
  $k_z = 1000$ md
  $\phi = 0.30$
- Initial Conditions
  $P = 500$ kPa
  $T = 51.7$ °C
  $S_w = 0.20$
  $S_o = 0.80$
  $S_g = 0.00$

	Run H-3	Run Z-3
Δr_1	20.0	20.0
Δr_2	15.0	25.0
Δr_3	20.0*	20.0
Δr_4	–	45.0*

* calculated internally

Figure 5.6.0.1 Runs R-3, H-3 and Z-3 data summary (continued next page).

- Operating Conditions

Time (days)			Time (days)		
0–20	BHP_{max} (kPa)	6900	135–250	BHP_{max} (kPa)	6900
	BHP_{min} (kPa)	120		BHP_{min} (kPa)	120
	q_T (m^3/d)	100		q_L (m^3/d)	10
	x	0.7			
	T_{inj} (°C)	232	250–265	BHP_{max} (kPa)	6900
				BHP_{min} (kPa)	120
20–120	BHP_{max} (kPa)	6900		q_T (m^3/d)	80
	BHP_{min} (kPa)	120		x	0.7
	q_L (m^3/d)	20		T_{inj} (°C)	232
120–135	BHP_{max} (kPa)	6900	265–400	BHP_{max} (kPa)	6900
	BHP_{min} (kPa)	120		BHP_{min} (kPa)	120
	q_T (m^3/d)	80		q_L (m^3/d)	10
	x	0.7			
	T_{inj} (°C)	232			

- Well Parameters

	Region 1	Region 2
Index	+1/-1	+1/-1
Productivity	Internally calculated	Internally calculated
J* multiplier	1.0	1.0
f_h	1.0	1.0
f	1.0	1.0
c_g	0.5	0.5
s	0.0	0.0
r_w (metres)	0.09	0.09

Figure 5.6.0.1 Runs R-3, H-3 and Z-3 data summary.
(continued from previous page)

Parameter		Parameter	
k_r (md)	100.	K (kg $m^{-1}s^{n-1}$)	150.
y (s^{-1}/ft day^{-1})	0.609	n	-0.506
m	0.000425	a (s)	0.0219
p	0.00243	b(s^{-1})	5.
B ($s^{(y-1)/y}$)	1.0	s	2.

Table 5.6.0.1 Non-Newtonian oil parameters.

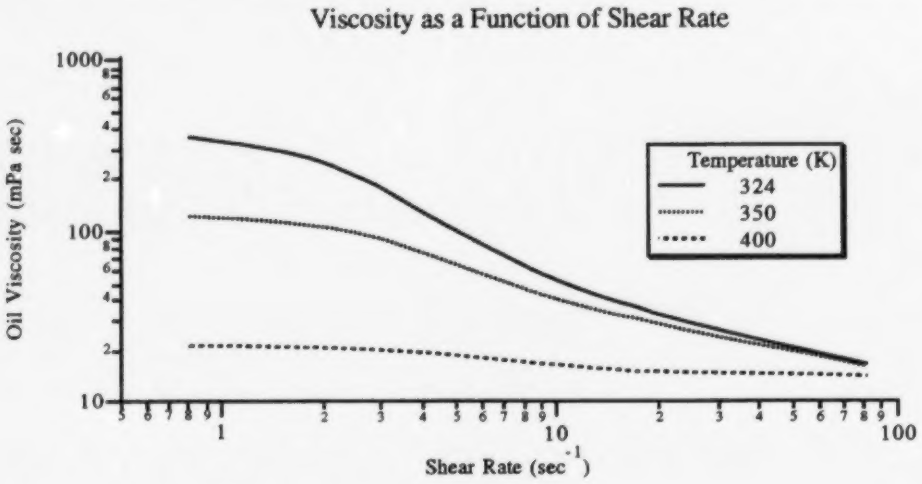
Viscosity as a Function of Shear Rate

Figure 5.6.0.2 Oil viscosity as a function of shear rate.

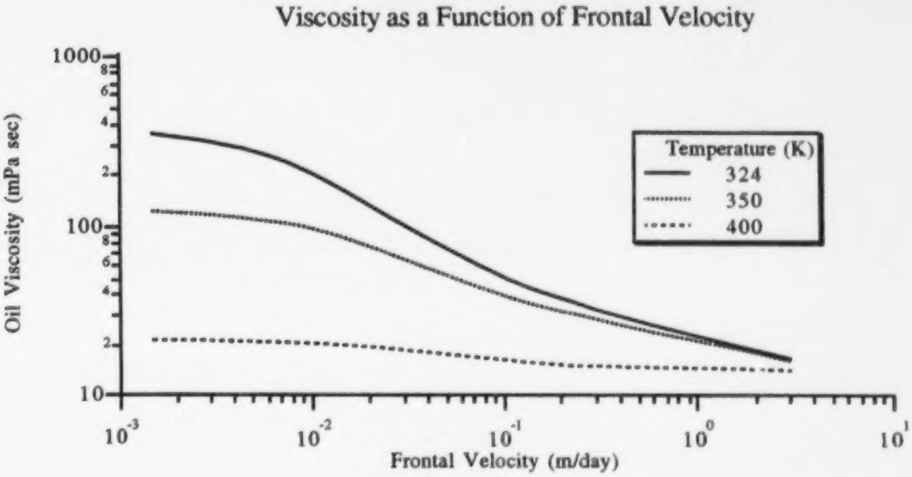

Figure 5.6.0.3 Oil viscosity as a function of frontal velocity.

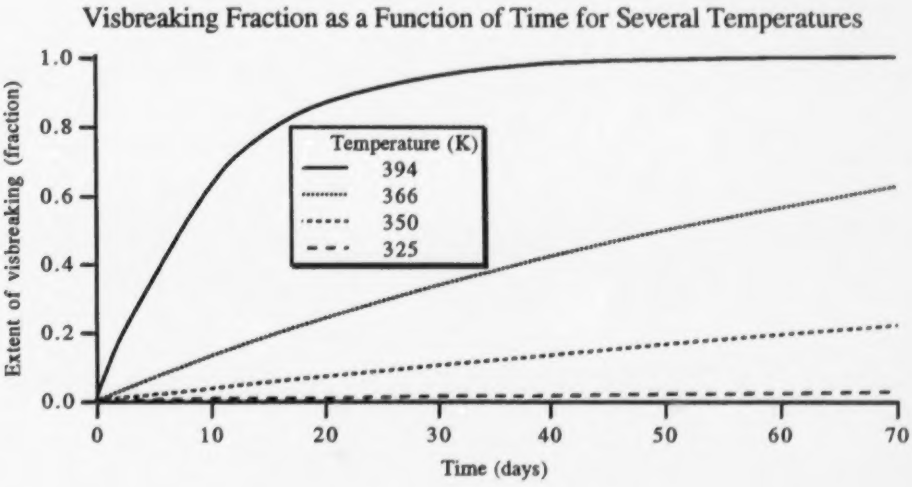

Figure 5.6.0.4 Visbreaking fraction as a function of time for several temperatures.

5.6.1 Base Runs

For Run R-3, the following figures summarize the results. Figures 5.6.1.1, 5.6.1.2 and 5.6.1.3 show the steam injection rate, production rates and cumulative volumes, respectively. The well grid block pressure, well grid block temperature and well pressure history are shown in Figures 5.6.1.4, 5.6.1.5 and 5.6.1.6, respectively. The grid block pressure and temperature profiles at selected times are shown in Figures 5.6.1.7 and 5.6.1.8, respectively.

For Run H-3, the following figures summarize the results. Figures 5.6.1.9, 5.6.1.10 and 5.6.1.11 show the steam injection rate, production rates and cumulative volumes, respectively. The well grid block pressure, well grid block temperature and well pressure history are shown in Figures 5.6.1.12, 5.6.1.13 and 5.6.1.14, respectively. The grid block pressure and temperature profiles at selected times are shown in Figures 5.6.1.15 and 5.6.1.16, respectively.

For Run Z-3, the following figures summarize the results. Figures 5.6.1.17, 5.6.1.18 and 5.6.1.19 show the steam injection rate, production rates and cumulative volumes, respectively. The well grid block pressure, well grid block temperature and well pressure history are shown in Figures 5.6.1.20, 5.6.1.21 and 5.6.1.22, respectively. The grid block pressure and temperature profiles at selected times are shown in Figures 5.6.1.23 and 5.6.1.24, respectively.

The base case Runs R-3, H-3 and Z-3 provide similar observations as discussed earlier in Section 5.4. Run R-3 had a lower injectivity/productivity in the first cycle but the injectivity/productivity approached the hybrid runs in later cycles due to temperature effects and saturation changes. A second observation is that the pressure and temperature profiles show better resolution as the level of hybrid refinement increases.

5.6.2 Non-Newtonian Oil Viscosity Runs

For Run R-3b, the following figures summarize the results. Figures 5.6.2.1, 5.6.2.2 and 5.6.2.3 show the steam injection rate, production rates and cumulative volumes, respectively. The well grid block pressure, well grid block temperature and well pressure history are shown in Figures 5.6.2.4, 5.6.2.5 and 5.6.2.6, respectively. The grid block pressure and temperature profiles at selected times are shown in Figures 5.6.2.7 and 5.6.2.8, respectively.

For Run H-3b, the following figures summarize the results. Figures 5.6.2.9, 5.6.2.10 and 5.6.2.11 show the steam injection rate, production rates and cumulative volumes, respectively. The well grid block pressure, well grid block temperature and well pressure history are shown in Figures 5.6.2.12, 5.6.2.13 and 5.6.2.14, respectively. The grid block pressure and temperature profiles at selected times are shown in Figures 5.6.2.15 and 5.6.2.16, respectively. Figure 5.6.2.17 shows the oil saturation changes with time for Runs H-2 and H-2b.

For Run Z-3b, the following figures summarize the results. Figures 5.6.2.18, 5.6.2.19 and 5.6.2.20 show the steam injection rate, production rates and cumulative volumes, respectively. The well grid block pressure, well grid block temperature and well pressure history are shown in Figures 5.6.2.21, 5.6.1.22 and 5.6.2.23, respectively. The grid block pressure and temperature profiles at selected times are shown in Figures 5.6.2.24 and 5.6.2.25, respectively.

Runs R-3b, H-3b and Z-3b include the non-Newtonian viscosity behaviour of the oil component. In comparing Run R-3b to the base Run R-3, it is observed that the steam injection rate was virtually unaffected. This is because initially velocities were low and later because the maximum rate was attained. Due to the size of the well grid block in both of these runs, the average pore velocity did not play a large role; hence, the production rates were very similar as illustrated in Figures 5.6.1.2 and 5.6.2.2. For the same reasons, the well grid block pressure and temperature remained unaffected for the most part, although the non-Newtonian run exhibited a slightly lower grid block pressure.

Comparing Runs H-3 and H-3b shows that the maximum injection rate was attained very quickly, with Run H-3b being only slightly more responsive. As a consequence, both runs received the same amount of steam resulting in the well grid block temperature behaviour being the same in both runs. Also note that the grid block temperature profiles were virtually identical. The production rates in these two runs were very similar with only a subtle difference. Run H-3 had a higher oil production rate early in the first cycle but Run

H-3b had the higher rate toward the end of the first cycle. Note that the water production rate was consistently higher in the non-Newtonian runs because of the higher oil mobility. Subsequent cycles show the water rate to be only marginally lower, and the oil production rate to be higher in the base case. This behaviour can be explained by noting the oil saturation changes in the well grid block. Due to velocity effects, the oil viscosity in Run H-3b was lower and hence the oil mobility was higher. As a consequence, more oil was flushed from the well grid block during the steam injection phase thus accounting for a higher water production rate in Run H-3. Figure 5.6.2.17 shows the oil saturation in the well grid block for both runs. Again, as a consequence of higher mobility, the well grid block pressure and well pressure history were significantly lower in the non-Newtonian run. This is demonstrated further in the pressure profiles. The maximum pressures attained were in the run without the non-Newtonian oil behaviour.

Similar comments can be made when comparing the hyperhybrid Runs Z-3 and Z-3b. In addition, the higher level of grid refinement gives better resolution around the well as illustrated in the pressure and temperature profiles.

5.6.3 Visbreaking Run

For Run Z-3c, the following figures summarize the results. Figures 5.6.3.1, 5.6.3.2 and 5.6.3.3 show the steam injection rate, production rates and cumulative volumes, respectively. The well grid block pressure, well grid block temperature and well pressure history are shown in Figures 5.6.3.4, 5.6.3.5 and 5.6.3.6, respectively. The grid block pressure and temperature profiles at selected times are shown in Figures 5.6.3.7 and 5.6.3.8, respectively.

Only a hyperhybrid run was made with the visbreaking option. Comparing Runs Z-3 and Z-3c, the injection behaviour was very similar because, early in the runs, temperature was not a factor and, later in the runs, the maximum rate was attained. The oil production rate was consistently higher in Run Z-3c due to a lower viscosity caused by visbreaking, especially in the first cycle. Subsequent cycles show the rates approached one another due to temperature-viscosity effects dominating temperature-visbreaking effects; that is, at higher temperatures, both oil component viscosities were very similar. The well grid block pressures showed an interesting effect—the terminal cycle pressure was higher in subsequent cycles. The pressure profiles in other grid blocks exhibited the same response. Both runs exhibited the same temperature profiles.

5.6.4 Two-Layer Run

In this run, the lower layer has a high water saturation to represent bottom water. The grid design is essentially the same as the other runs in this section with the following changes: the bottom water layer is 2 metres thick with a water saturation of 99% and the number of radial refinements has been reduced to three with the first radial refinement having a radius of 40 metres. This was done to increase the bulk volume of the thinner, bottom layer. The operating conditions are also similar with the exception of a 20 day primary production period prior to any steaming. The well is perforated only in the top layer.

Figure 5.6.4.1 illustrates the steam injection rate. The first cycle steam injection rate did not attain the maximum immediately due to the size of the well grid block. Also because the well was not perforated in the bottom water zone, there was resistance to injection. Figure 5.6.4.2 illustrates the production rates. During the primary production period, the oil rate was low but steady; however, the water rate began to increase. After the first steam injection, the oil rate resumed at approximately twice the primary rate and the water resumed at the rate at the end of the primary phase. However, the water rate increased extremely rapidly during this cycle due to an increased water saturation which provided a path for the water from the bottom layer to be produced. Subsequent cycles showed more even production as the well region increased in temperature and the oil mobility increased. The cumulative injection and production volumes are shown in Figure 5.6.4.3.

Figure 5.6.4.4 illustrates the temperature for each layer in the well grid block. The top layer showed a steady increase with each injection phase and some small decrease with production. The bottom layer showed an increase with each injection phase due to communication with the zone and continuing increase during the production phase. This increase was due to the oil in the upper layer being pushed into the bottom water layer. Figure 5.6.4.5 shows the oil saturation continuously increased throughout the run in the bottom layer to approximately 8.5%. Recall that the initial oil saturation in the bottom layer was 1%. The top layer behaved as expected—a decreasing oil saturation with production.

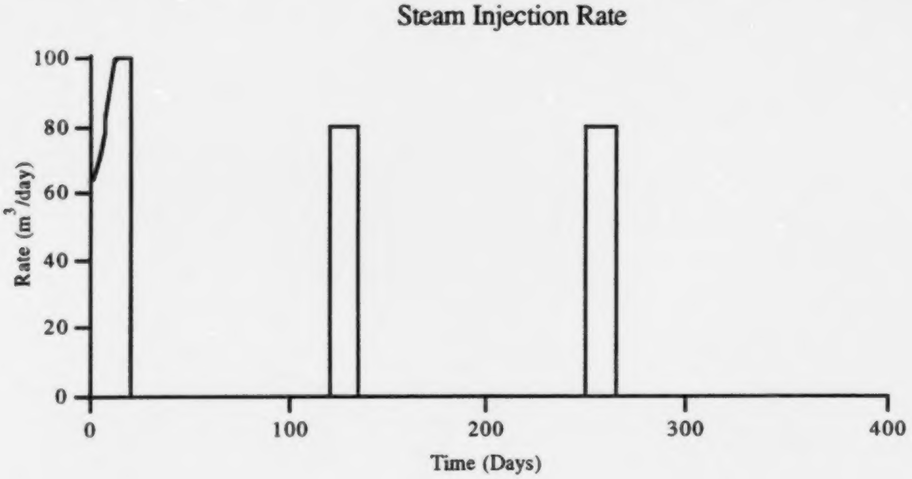

Figure 5.6.1.1 Run R-3 Steam injection rate.

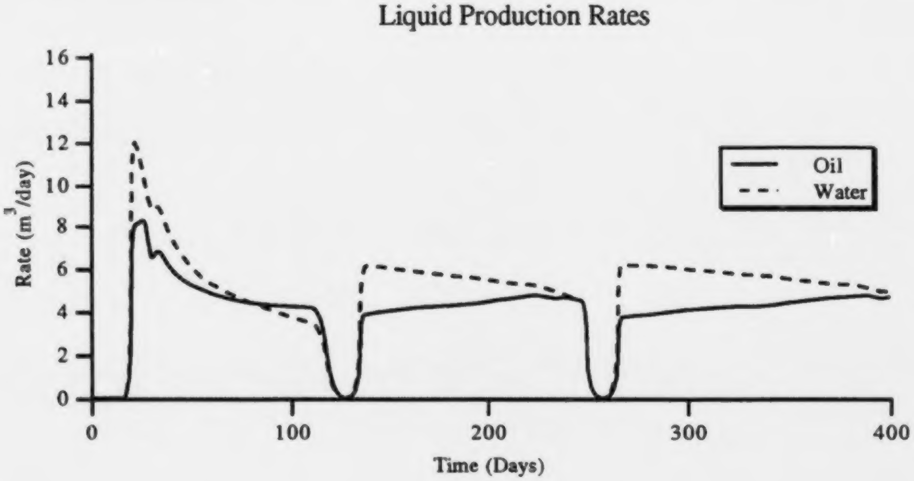

Figure 5.6.1.2 Run R-3 Liquid production rates.

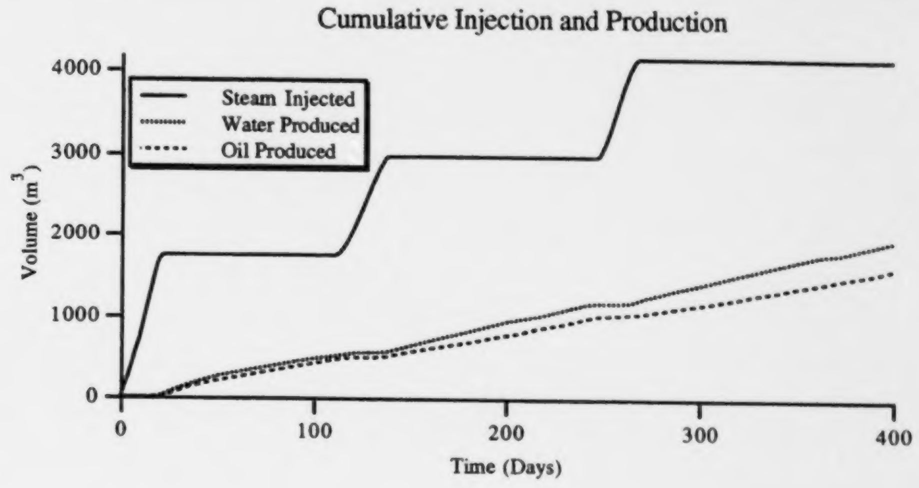

Figure 5.6.1.3 Run R-3 Cumulative injection and production.

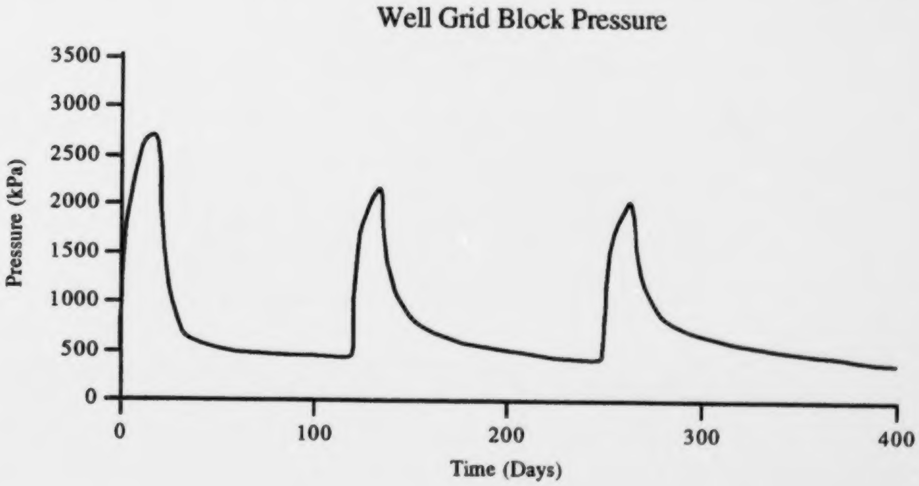

Figure 5.6.1.4 Run R-3 Well grid block pressure.

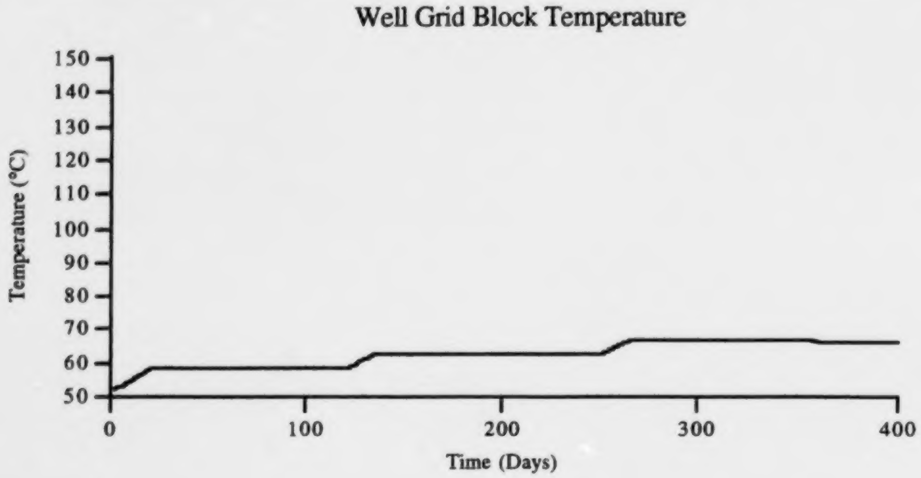

Figure 5.6.1.5 Run R-3 Well grid block temperature.

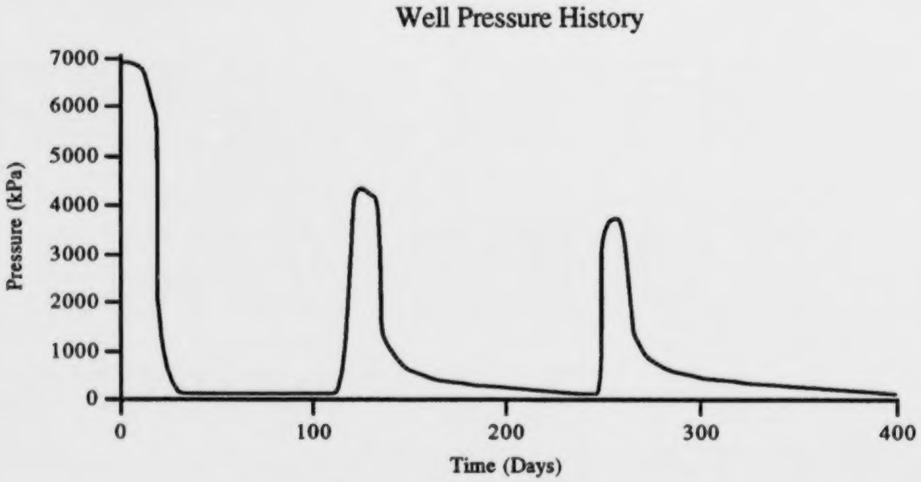

Figure 5.6.1.6 Run R-3 Well pressure history.

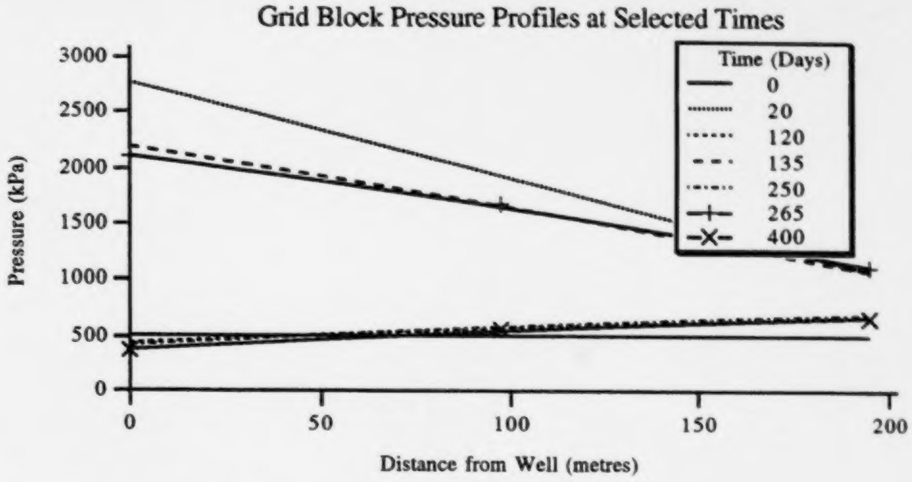

Figure 5.6.1.7 Run R-3 Grid block pressure profiles at selected times.

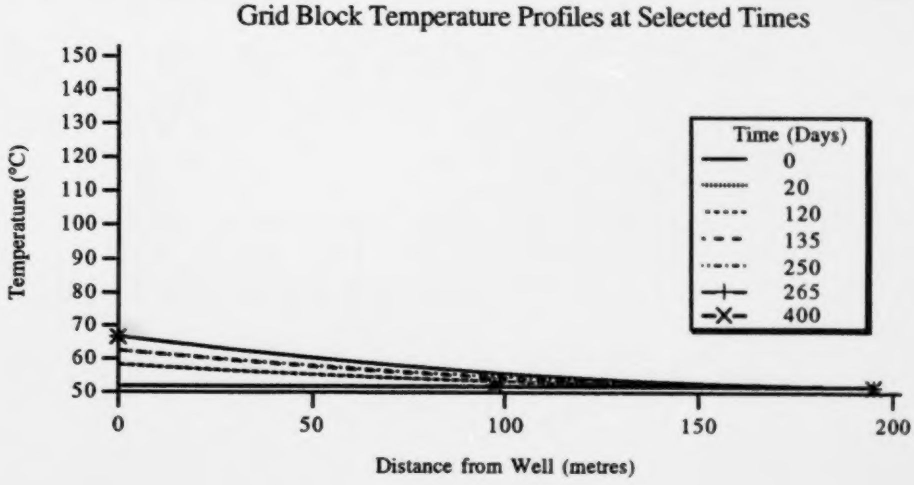

Figure 5.6.1.8 Run R-3 Grid block temperature profiles at selected times.

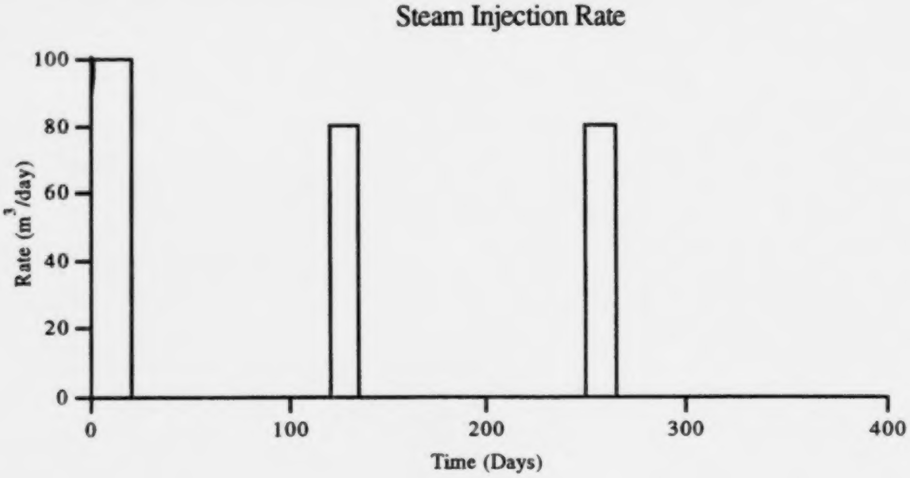

Figure 5.6.1.9 Run H-3 Steam injection rate.

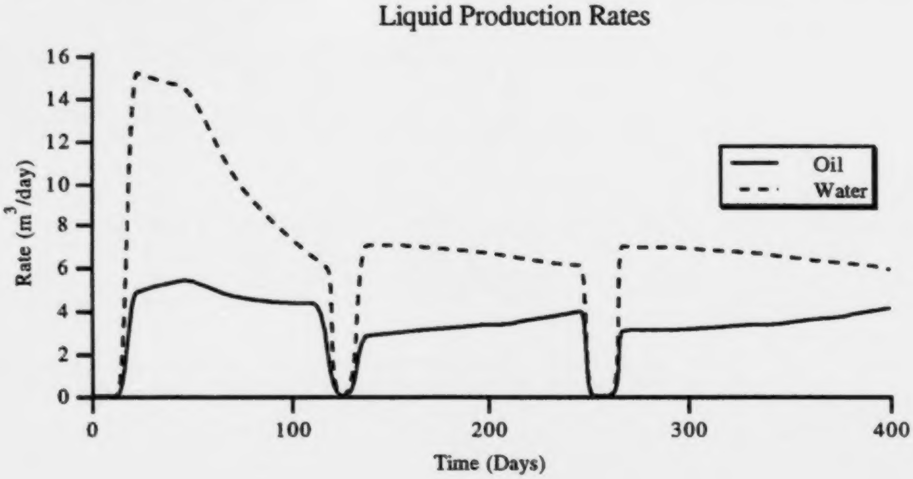

Figure 5.6.1.10 Run H-3 Liquid production rates.

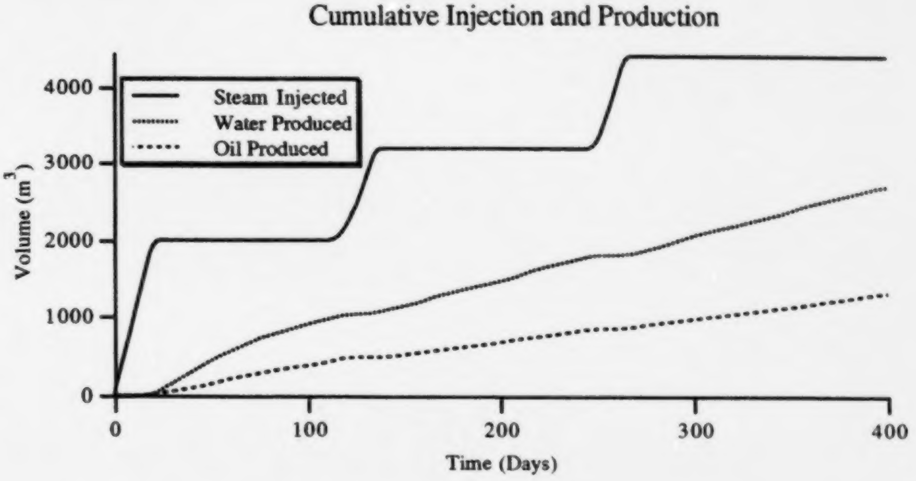

Figure 5.6.1.11 Run H-3 Cumulative injection and production.

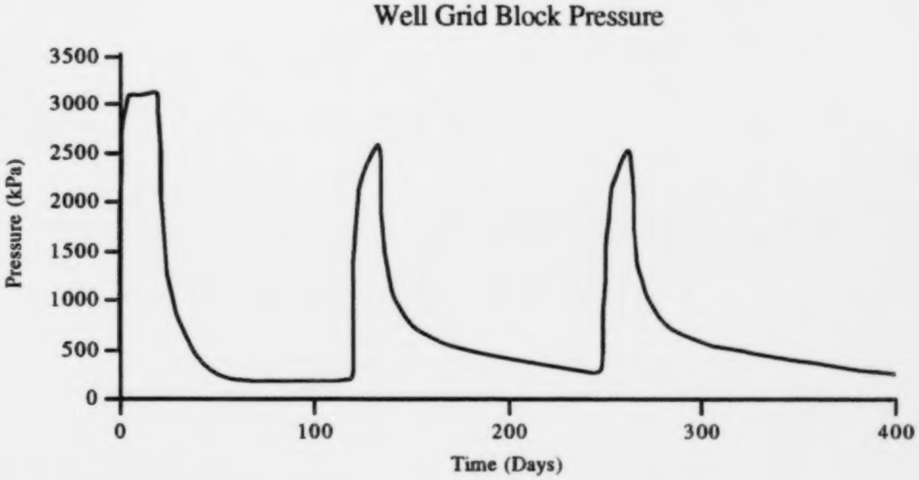

Figure 5.6.1.12 Run H-3 Well grid block pressure.

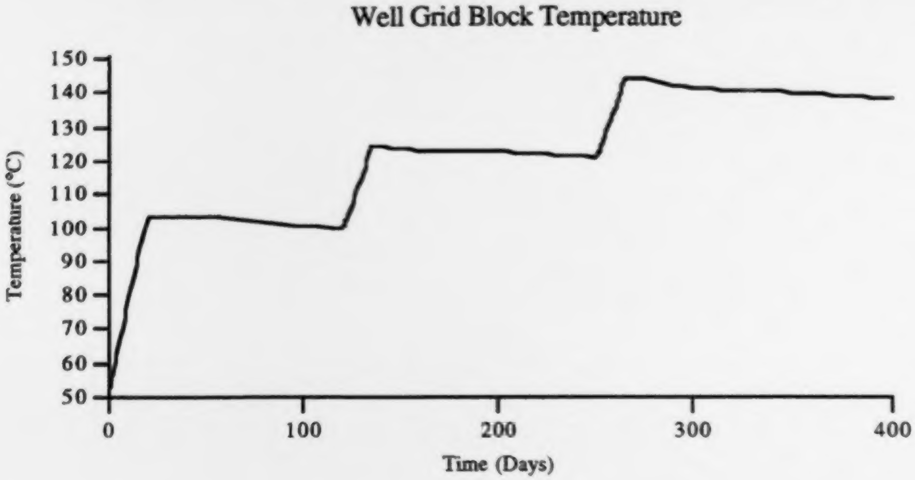

Figure 5.6.1.13 Run H-3 Well grid block temperature.

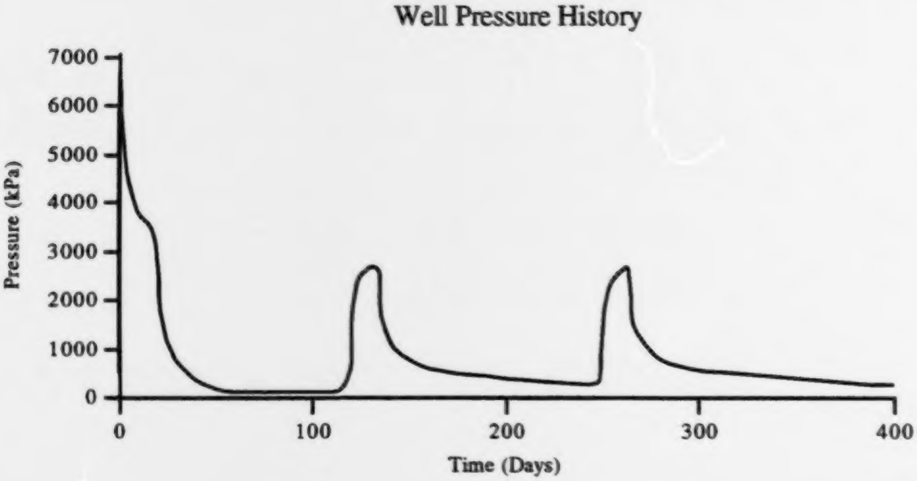

Figure 5.6.1.14 Run H-3 Well pressure history.

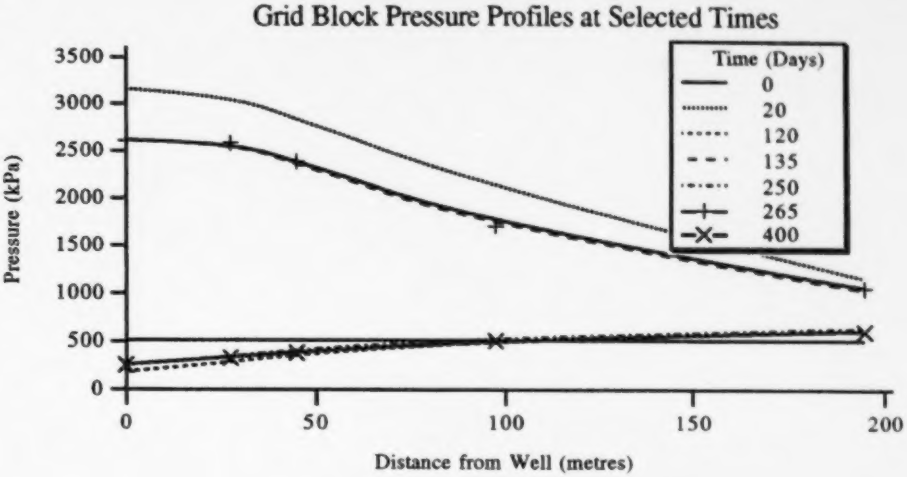

Figure 5.6.1.15 Run H-3 Grid block pressure profiles at selected times.

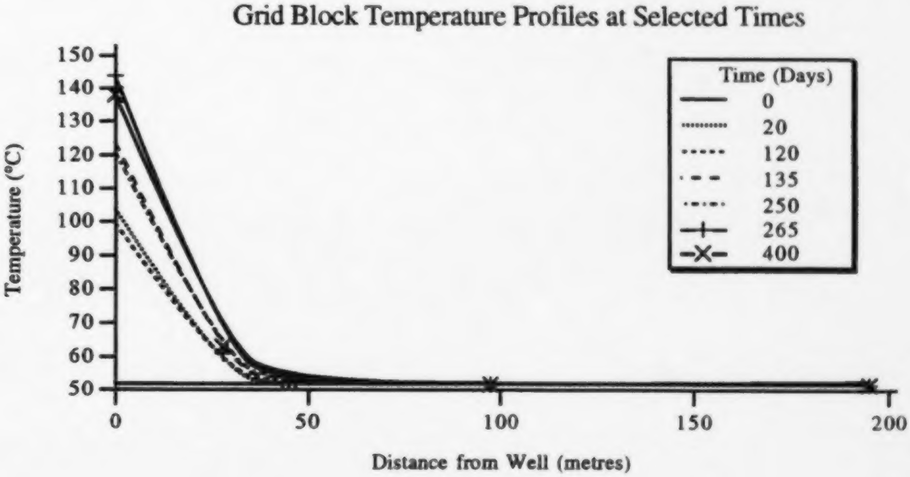

Figure 5.6.1.16 Run H-3 Grid block temperature profiles at selected times.

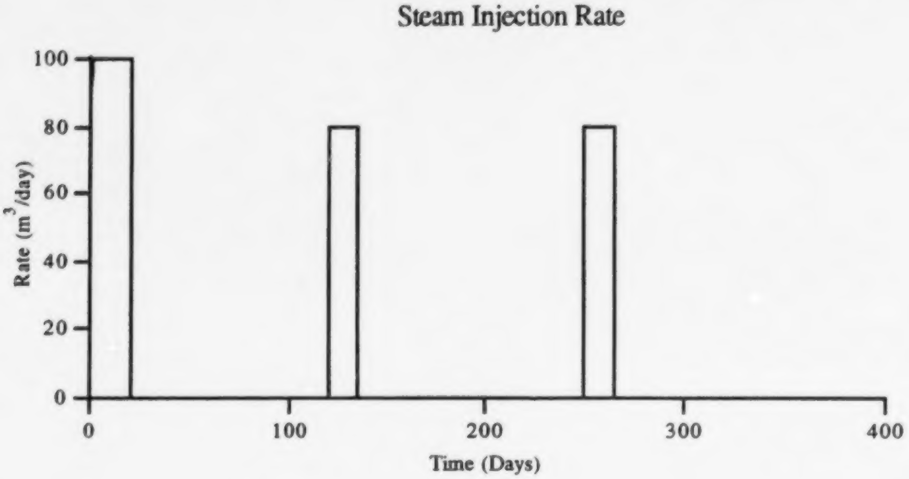

Figure 5.6.1.17 Run Z-3 Steam injection rate.

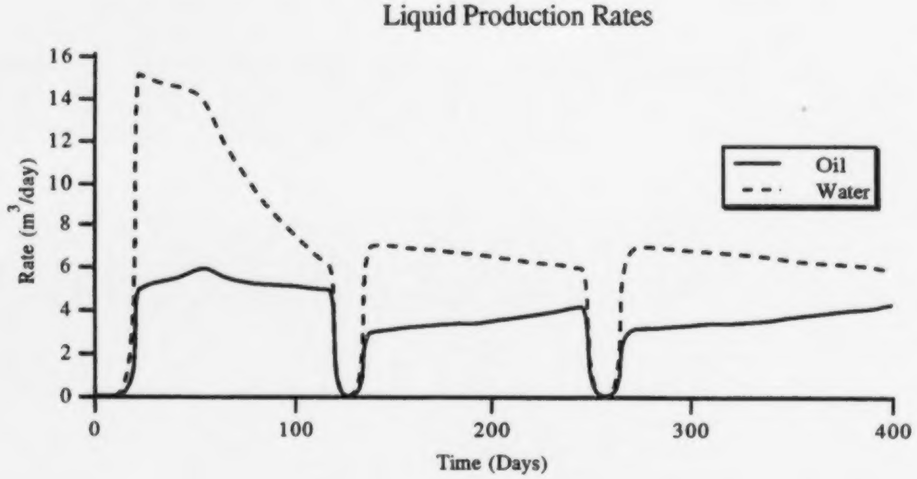

Figure 5.6.1.18 Run Z-3 Liquid production rates.

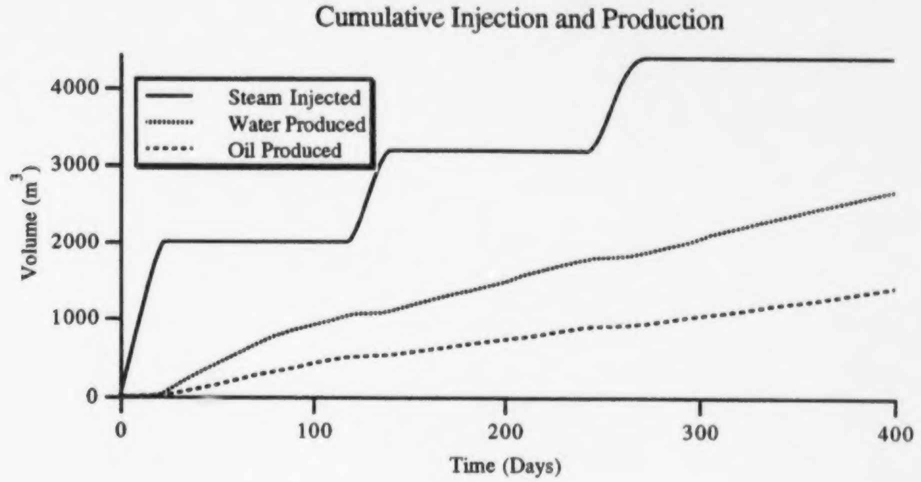

Figure 5.6.1.19 Run Z-3 Cumulative injection and production.

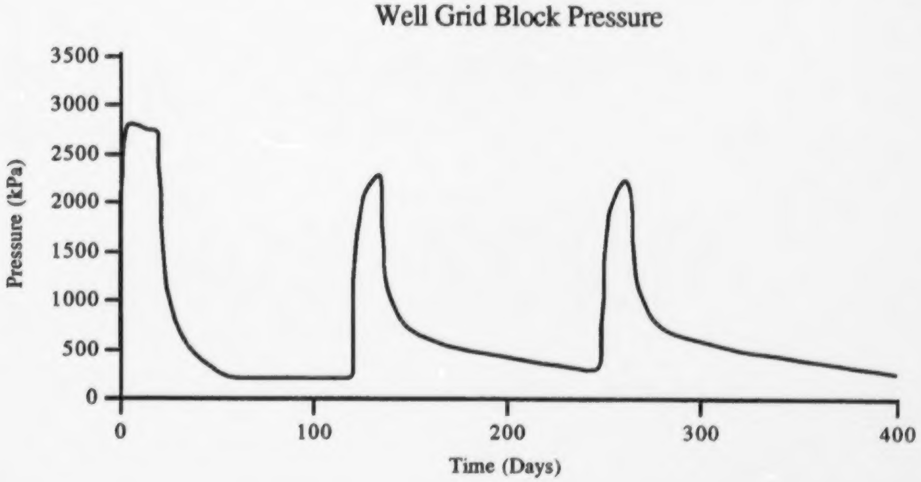

Figure 5.6.1.20 Run Z-3 Well grid block pressure.

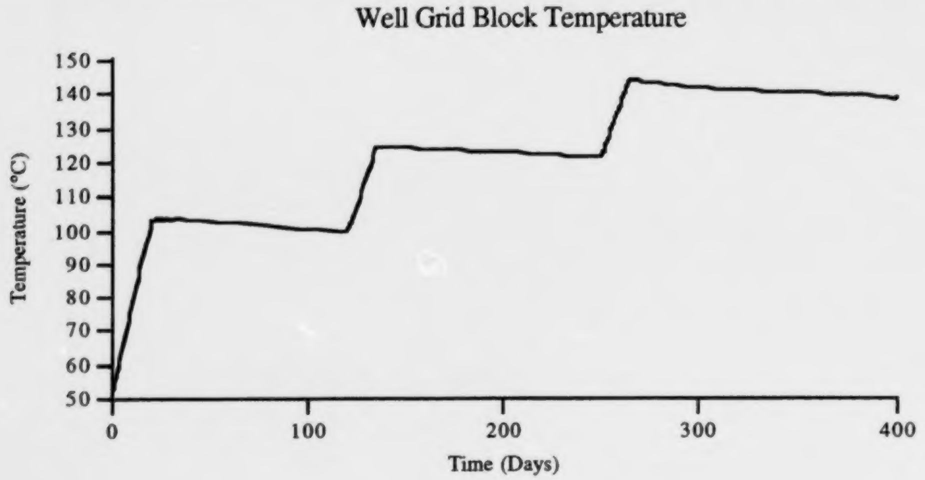

Figure 5.6.1.21 Run Z-3 Well grid block temperature.

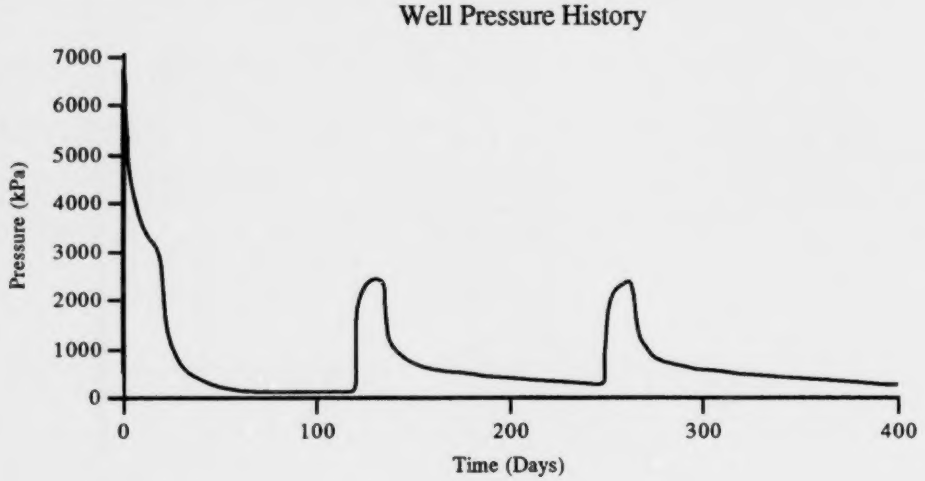

Figure 5.6.1.22 Run Z-3 Well pressure history.

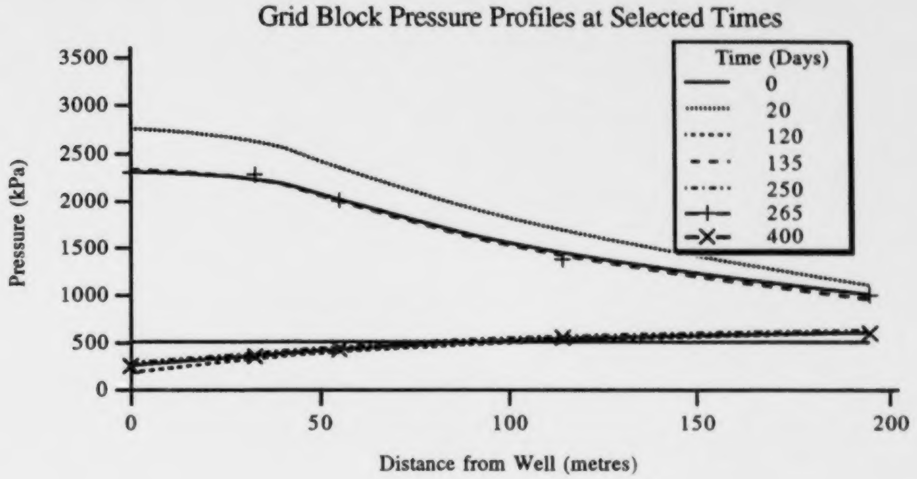

Figure 5.6.1.23 Run Z-3 Grid block pressure profiles at selected times.

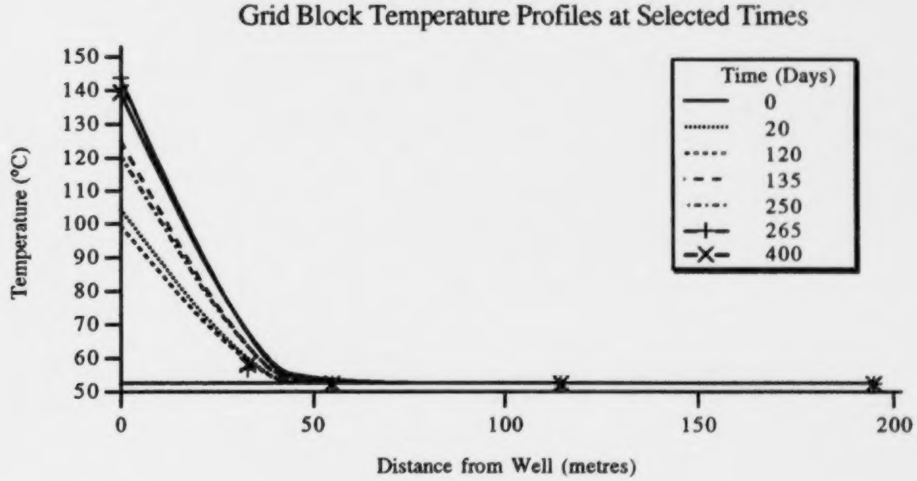

Figure 5.6.1.24 Run Z-3 Grid block temperature profiles at selected times.

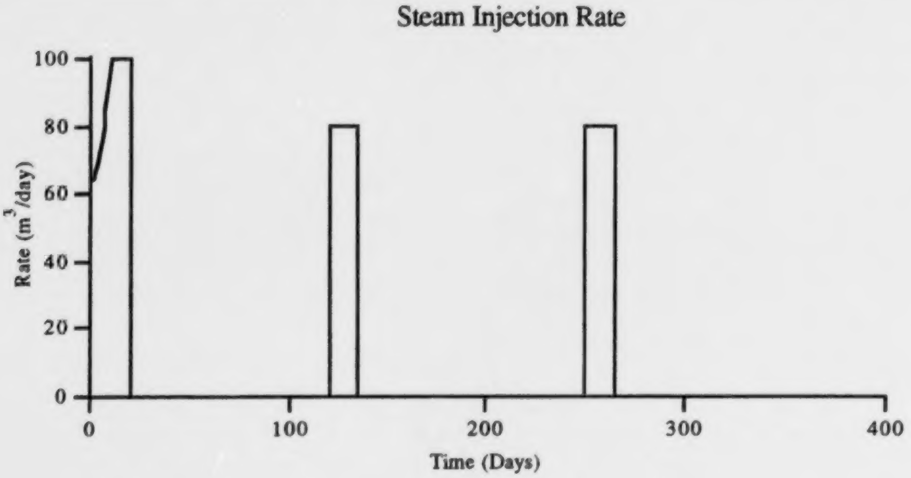

Figure 5.6.2.1 Run R-3b Steam injection rate.

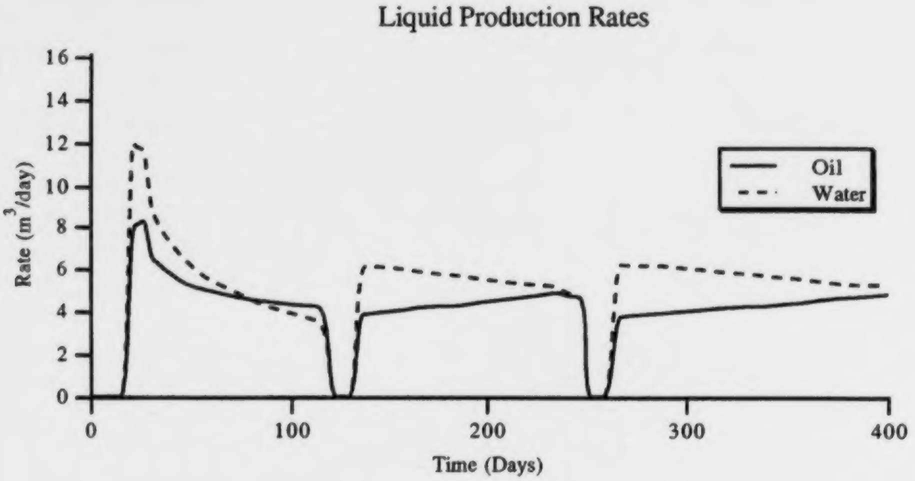

Figure 5.6.2.2 Run R-3b Liquid production rates.

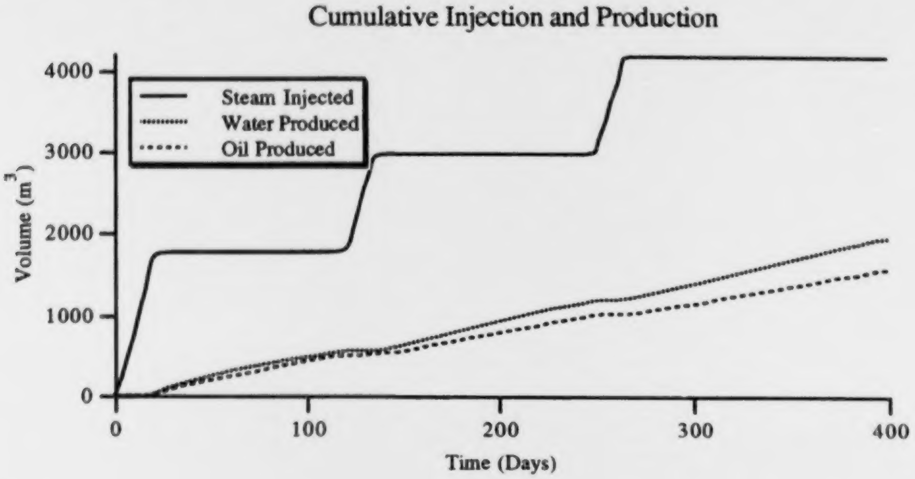

Figure 5.6.2.3 Run R-3b Cumulative injection and production.

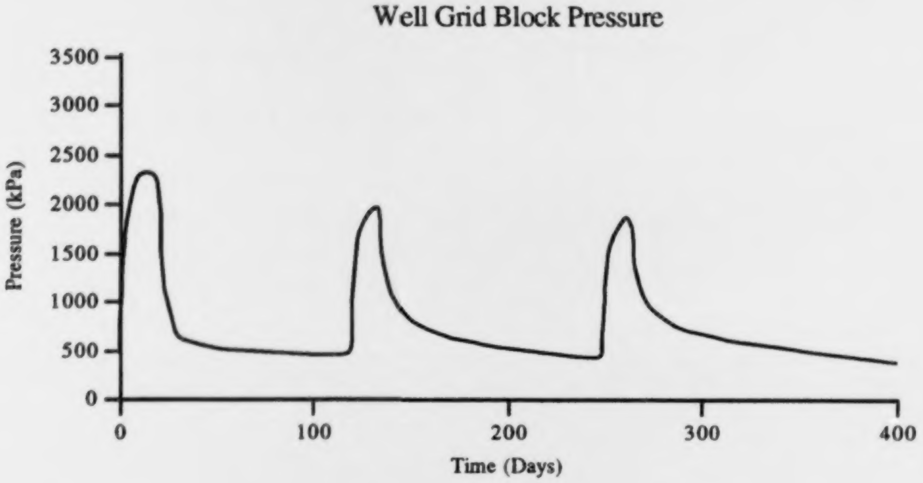

Figure 5.6.2.4 Run R-3b Well grid block pressure.

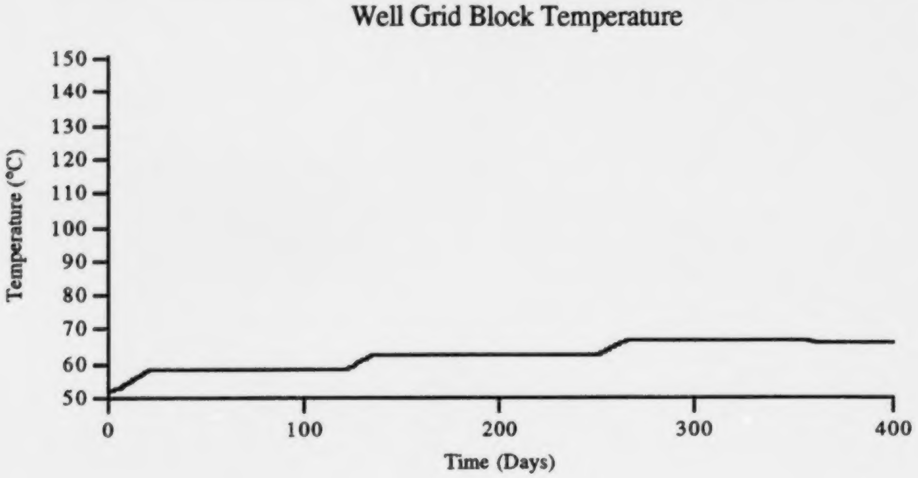

Figure 5.6.2.5 Run R-3b Well grid block temperature.

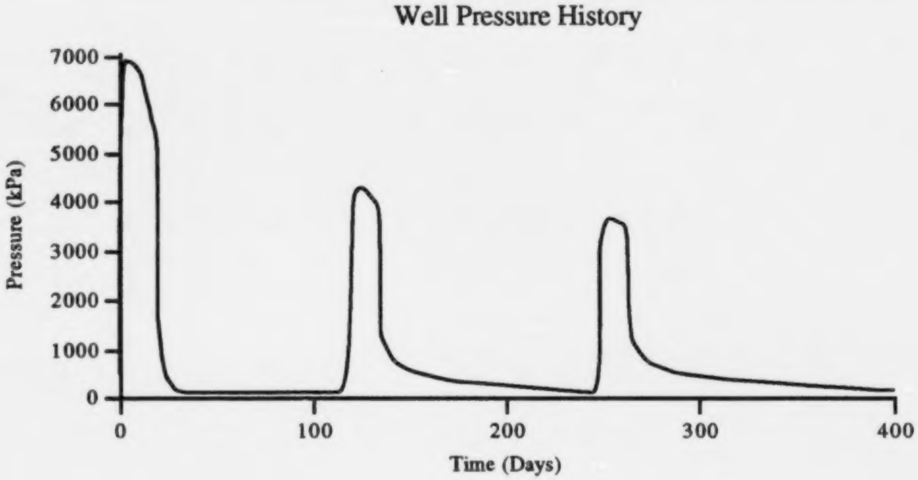

Figure 5.6.2.6 Run R-3b Well pressure history.

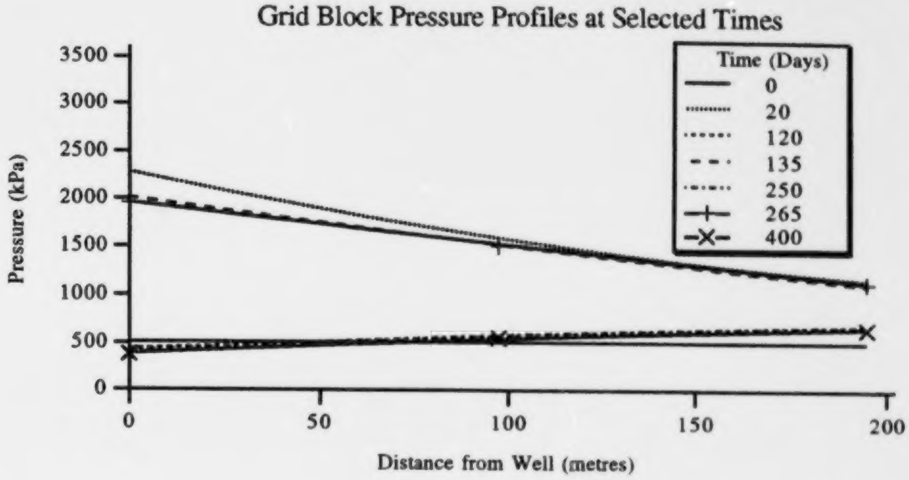

Figure 5.6.2.7 Run R-3b Grid block pressure profiles at selected times.

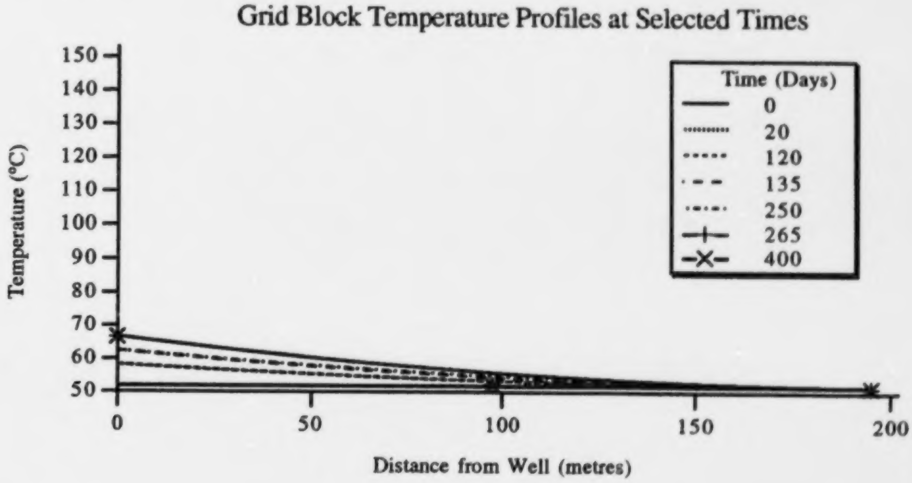

Figure 5.6.2.8 Run R-3b Grid block temperature profiles at selected times.

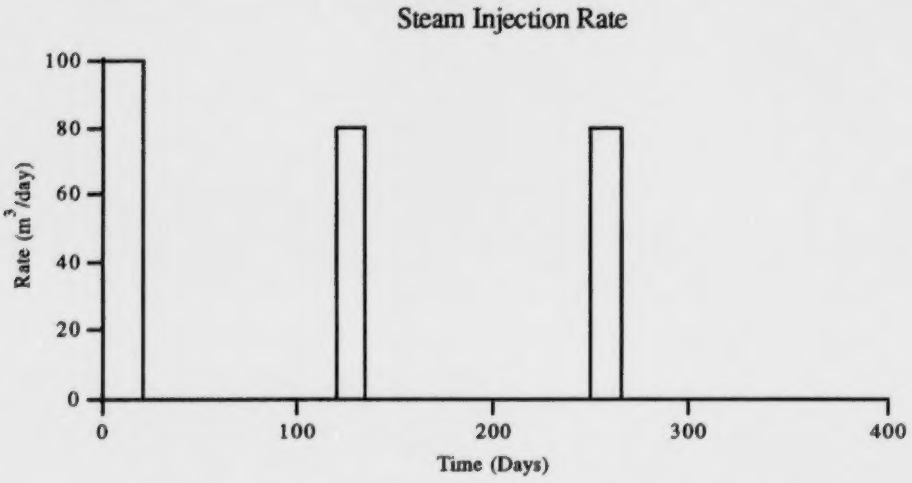

Figure 5.6.2.9 Run H-3b Steam injection rate.

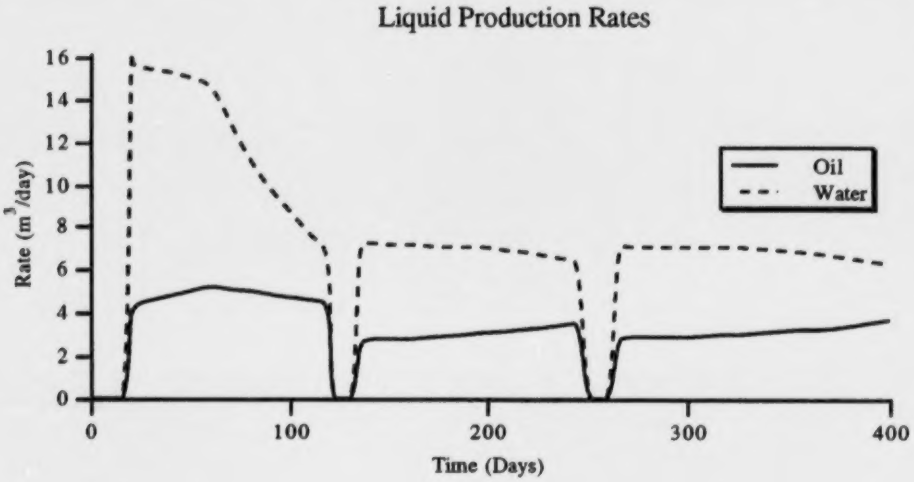

Figure 5.6.2.10 Run H-3b Liquid production rates.

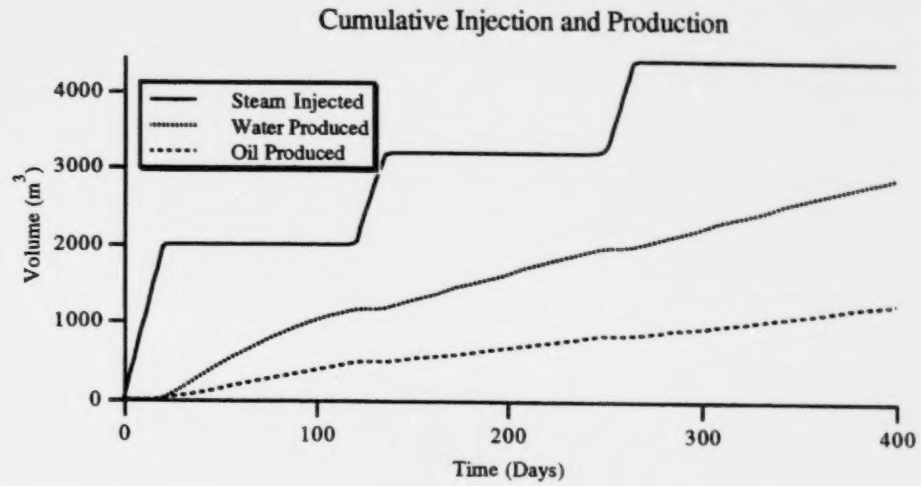

Figure 5.6.2.11 Run H-3b Cumulative injection and production.

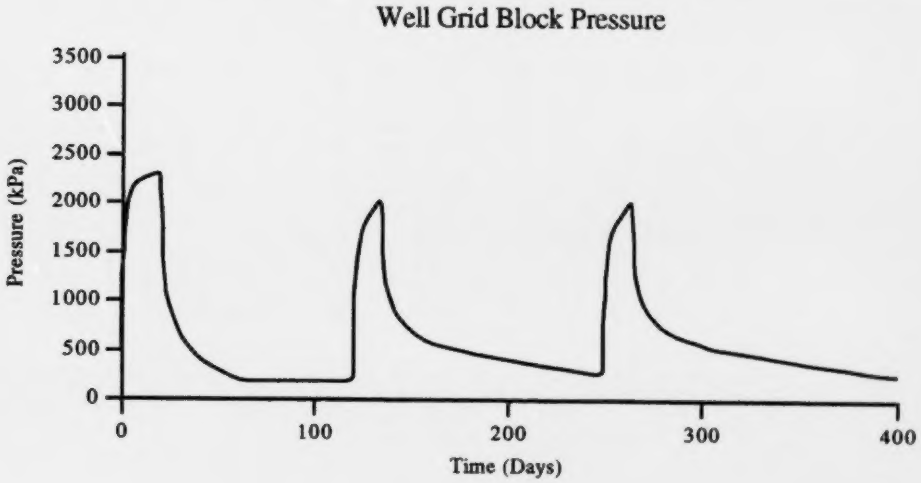

Figure 5.6.2.12 Run H-3b Well grid block pressure.

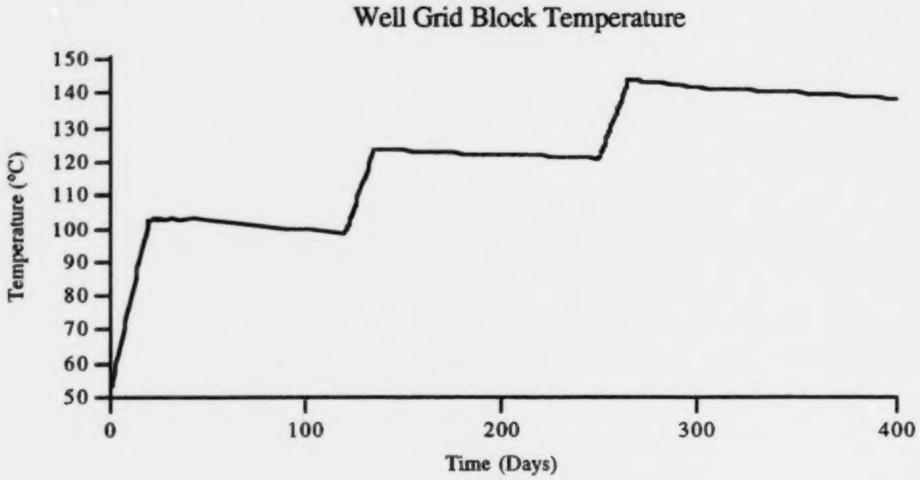

Figure 5.6.2.13 Run H-3b Well grid block temperature.

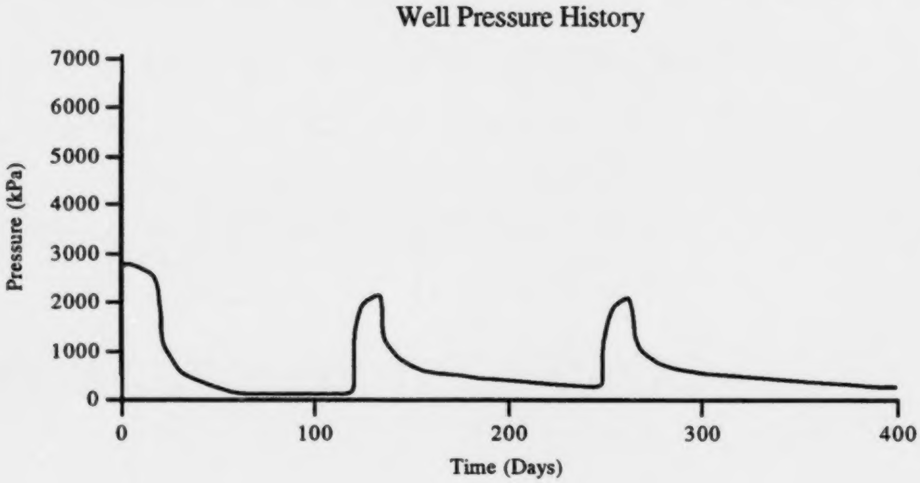

Figure 5.6.2.14 Run H-3b Well pressure history.

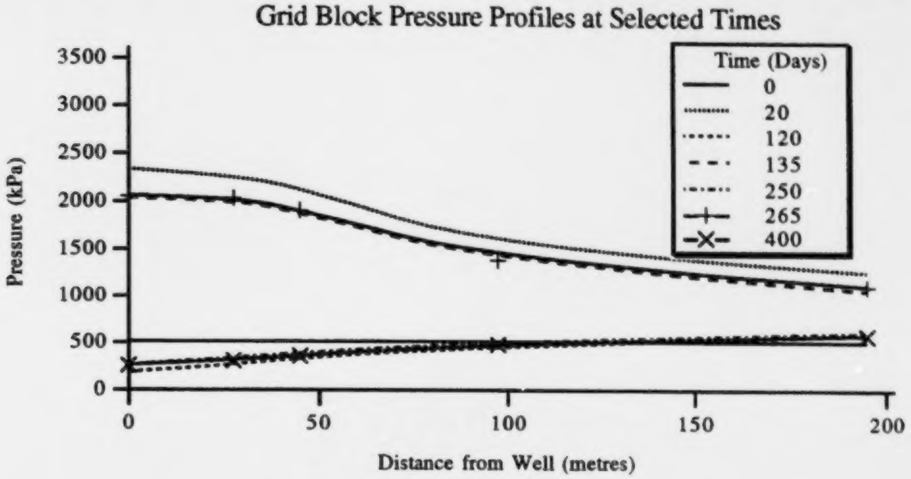

Figure 5.6.2.15 Run H-3b Grid block pressure profiles at selected times.

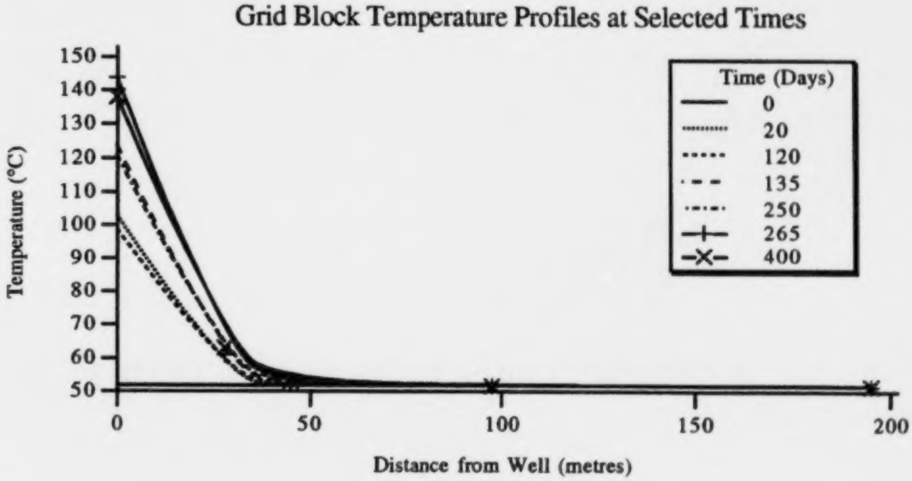

Figure 5.6.2.16 Run H-3b Grid block temperature profiles at selected times.

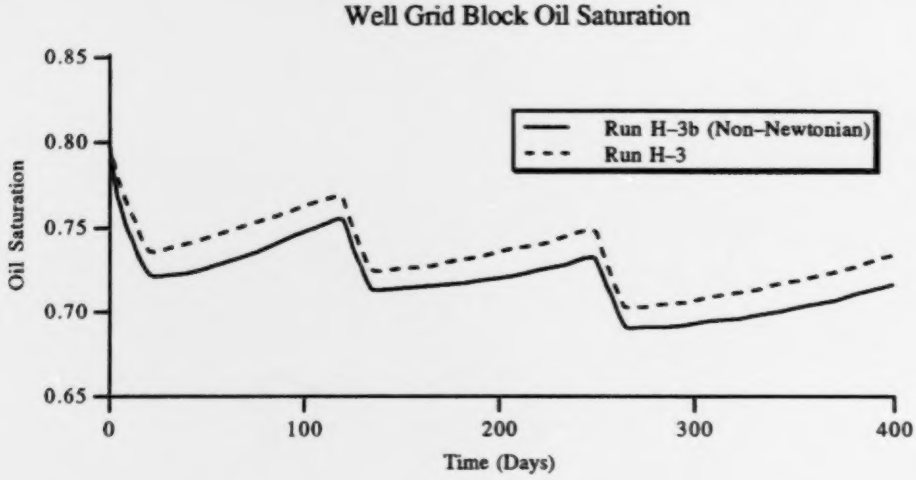

Figure 5.6.2.17 Runs H-3 and H-3b Well grid block oil saturation.

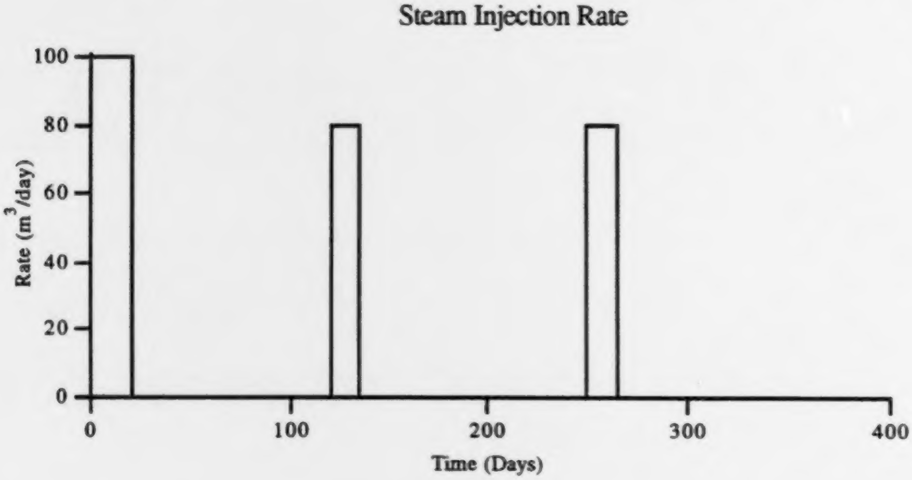

Figure 5.6.2.18 Run Z-3b Steam injection rate.

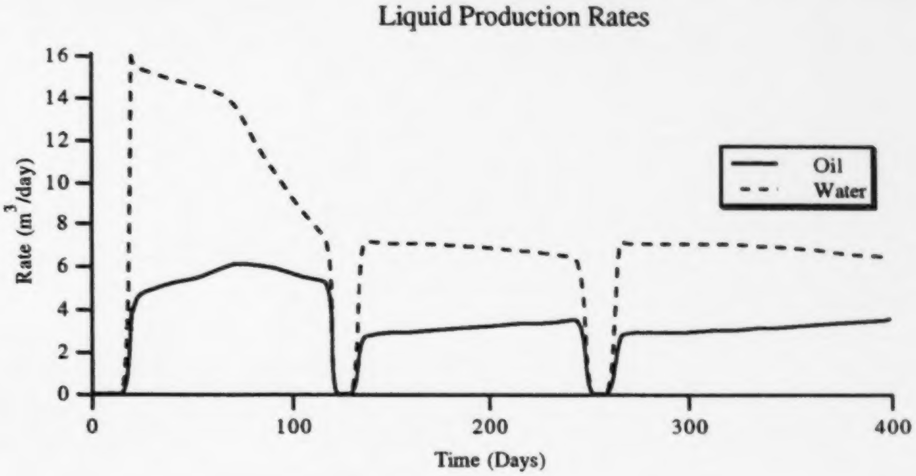

Figure 5.6.2.19 Run Z-3b Liquid production rates.

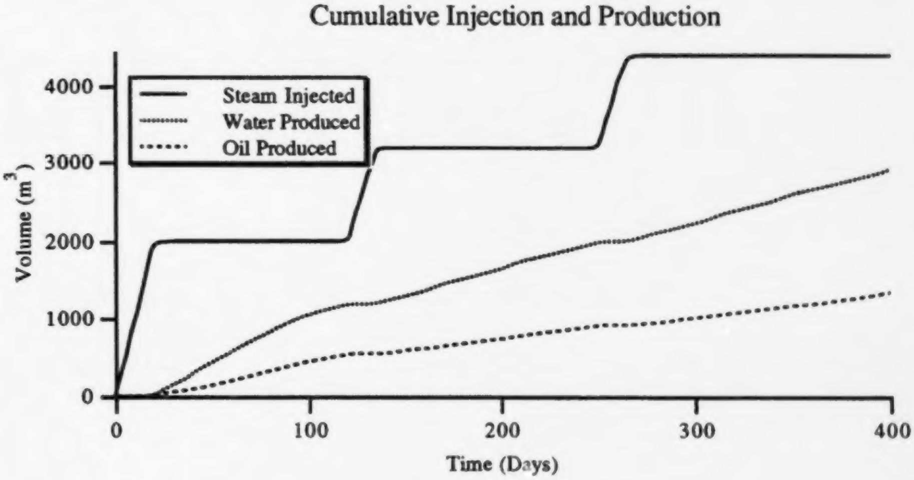

Figure 5.6.2.20 Run Z-3b Cumulative injection and production.

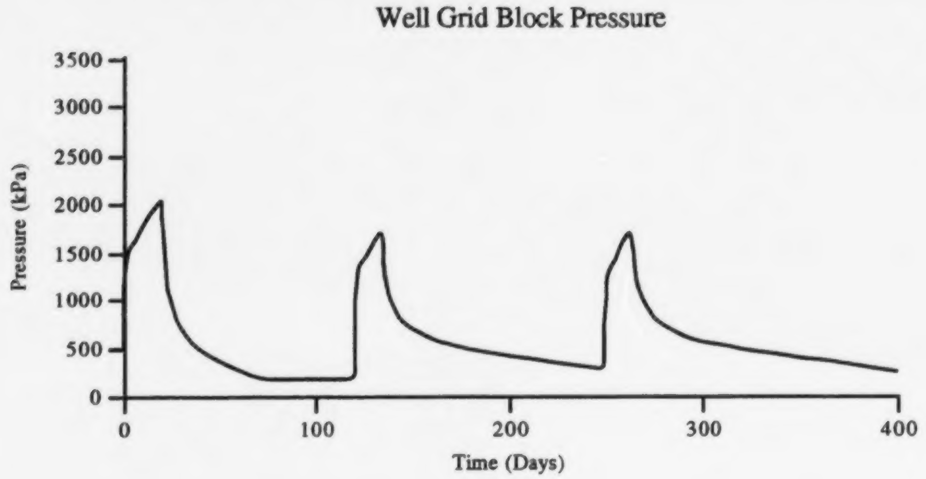

Figure 5.6.2.21 Run Z-3b Well grid block pressure.

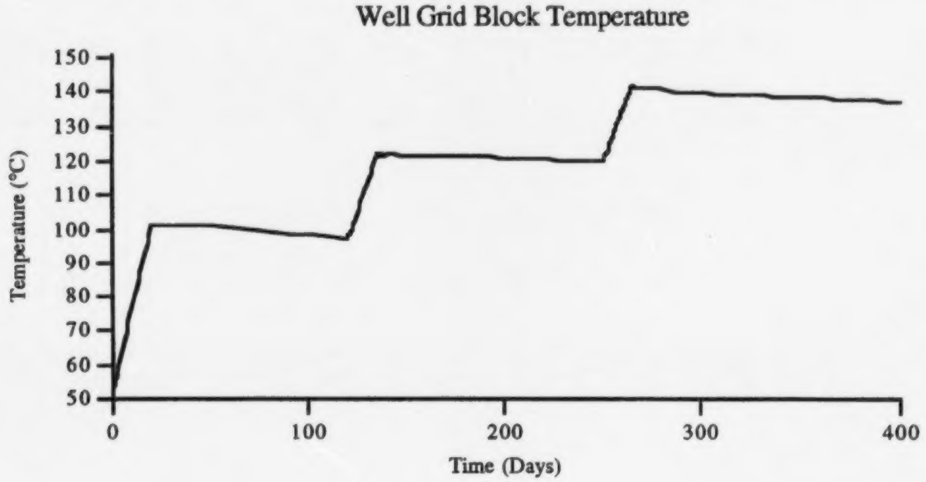

Figure 5.6.2.22 Run Z-3b Well grid block temperature.

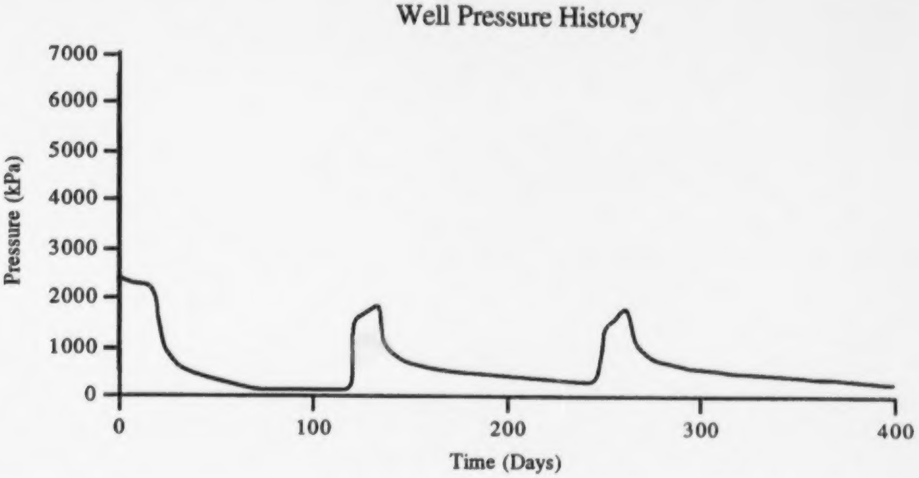

Figure 5.6.2.23 Run Z-3b Well pressure history.

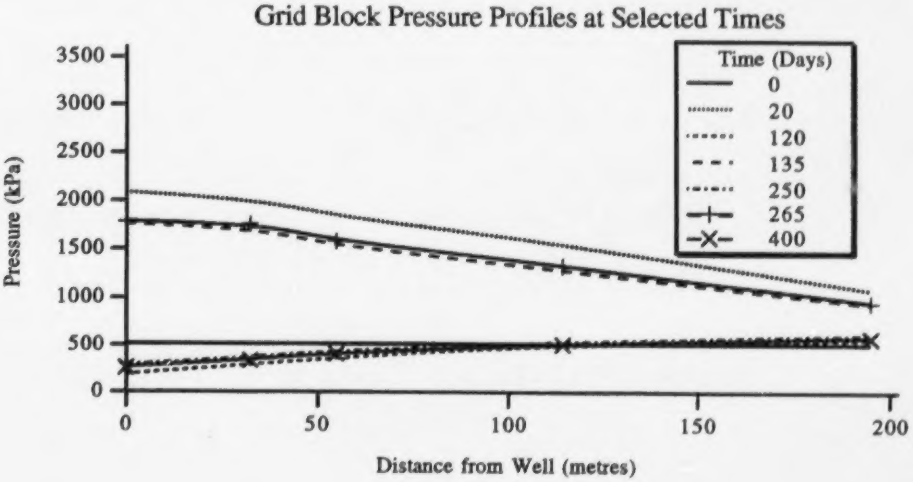

Figure 5.6.2.24 Run Z-3b Grid block pressure profiles at selected times.

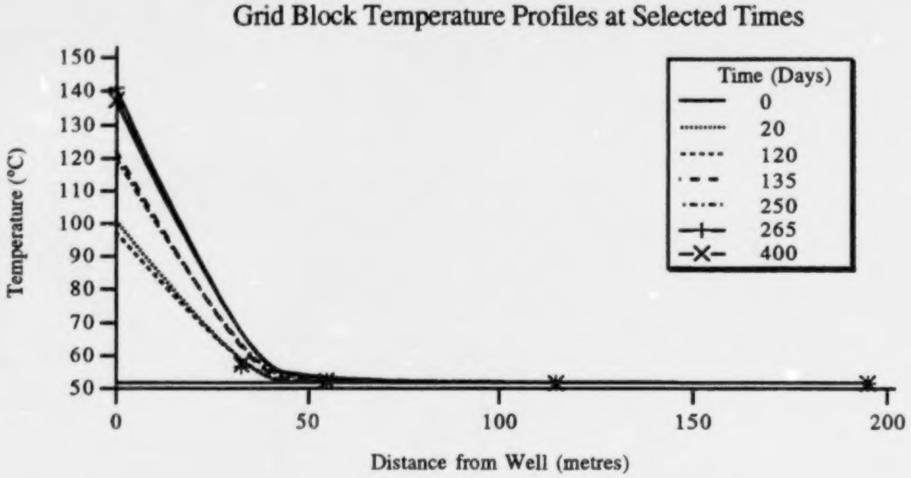

Figure 5.6.2.25 Run Z-3b Grid block temperature profiles at selected times.

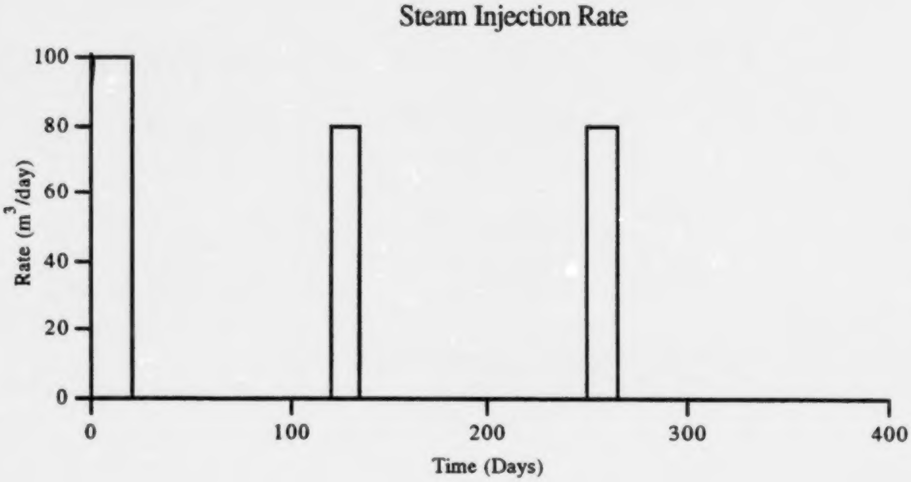

Figure 5.6.3.1 Run Z-3c Steam injection rate.

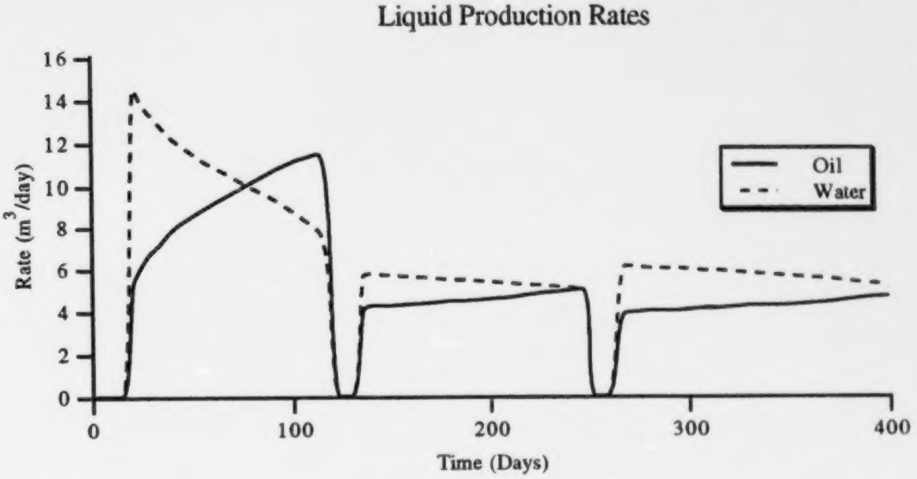

Figure 5.6.3.2 Run Z-3c Liquid production rates.

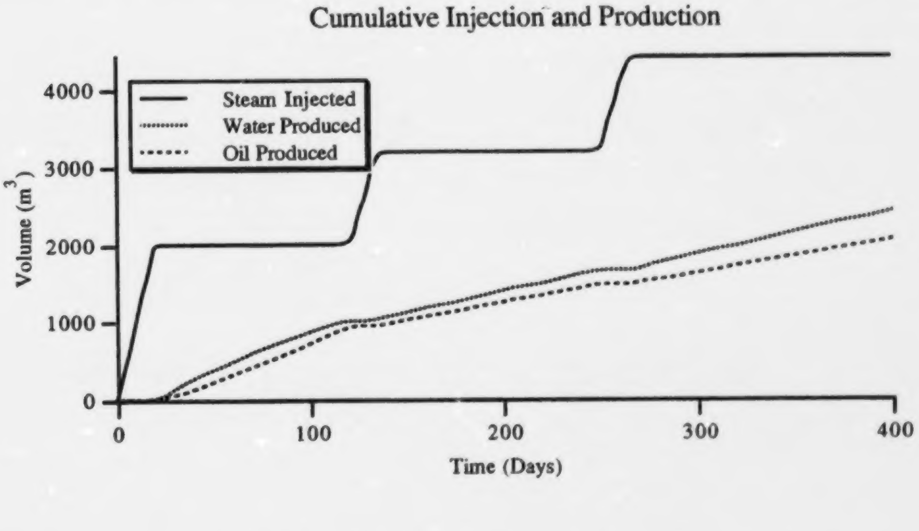

Figure 5.6.3.3 Run Z-3c Cumulative injection and production.

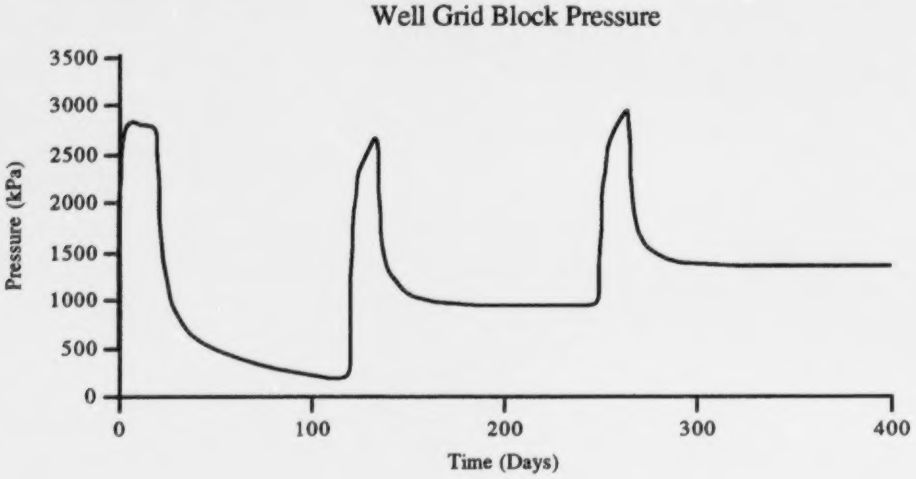

Figure 5.6.3.4 Run Z-3c Well grid block pressure.

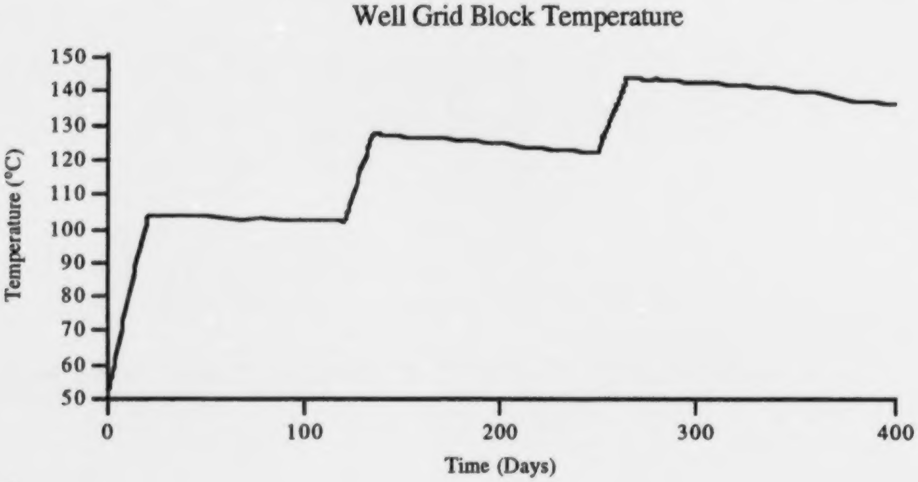

Figure 5.6.3.5 Run Z-3c Well grid block temperature.

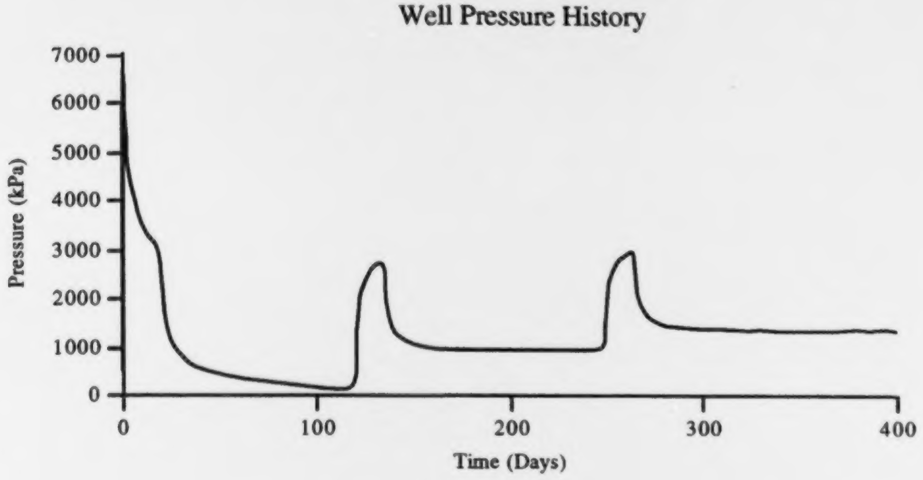

Figure 5.6.3.6 Run Z-3c Well pressure history.

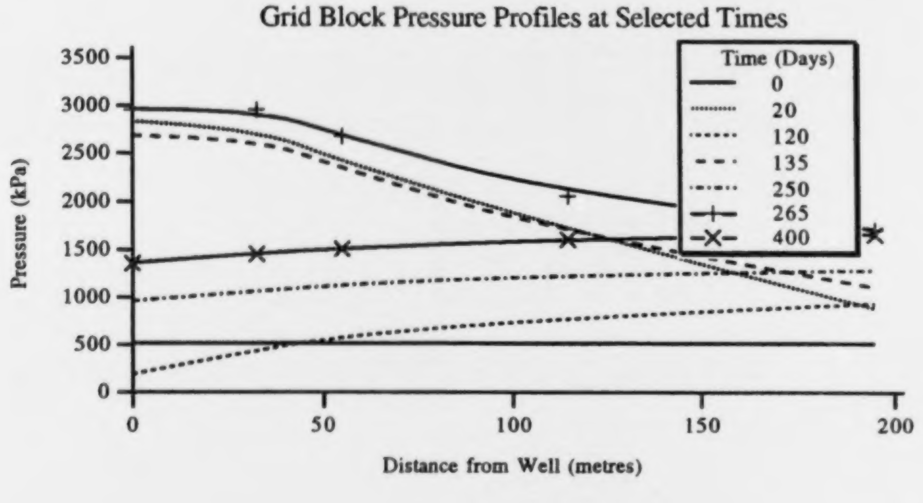

Figure 5.6.3.7 Run Z-3c Grid block pressure profiles at selected times.

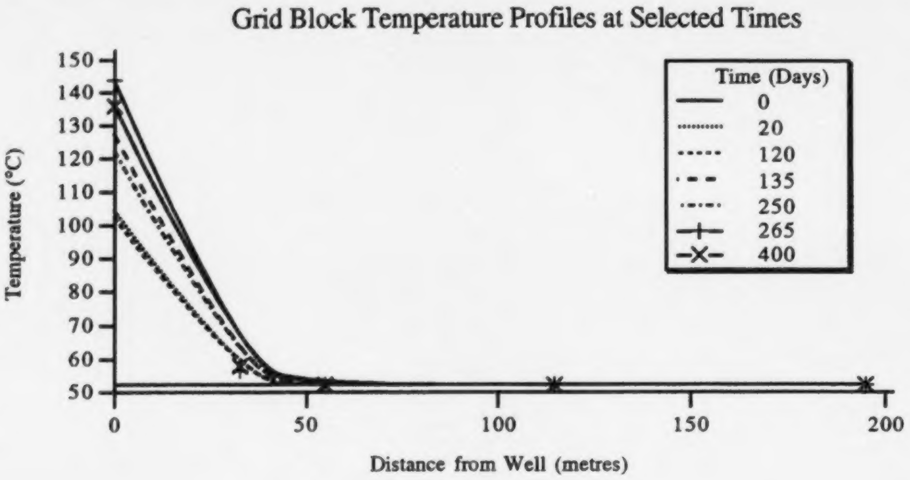

Figure 5.6.3.8 Run Z-3c Grid block temperature profiles at selected times.

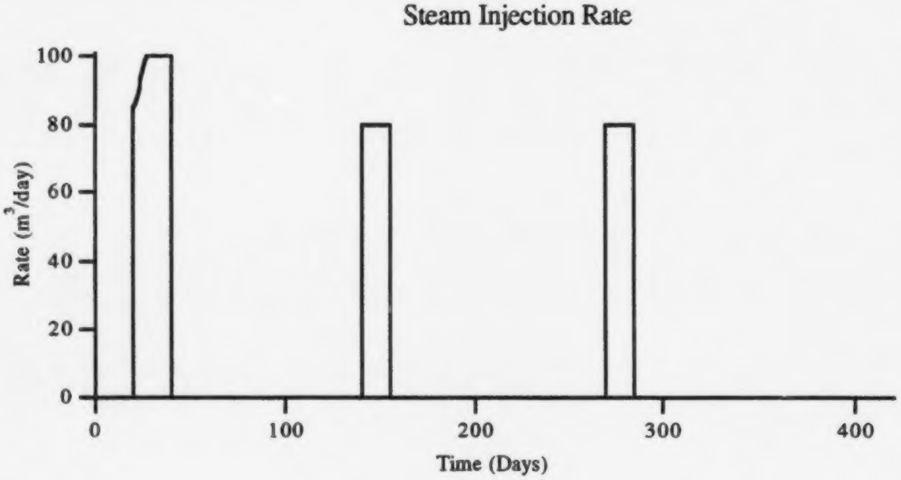

Figure 5.6.4.1 Run Z-3e Steam injection rate.

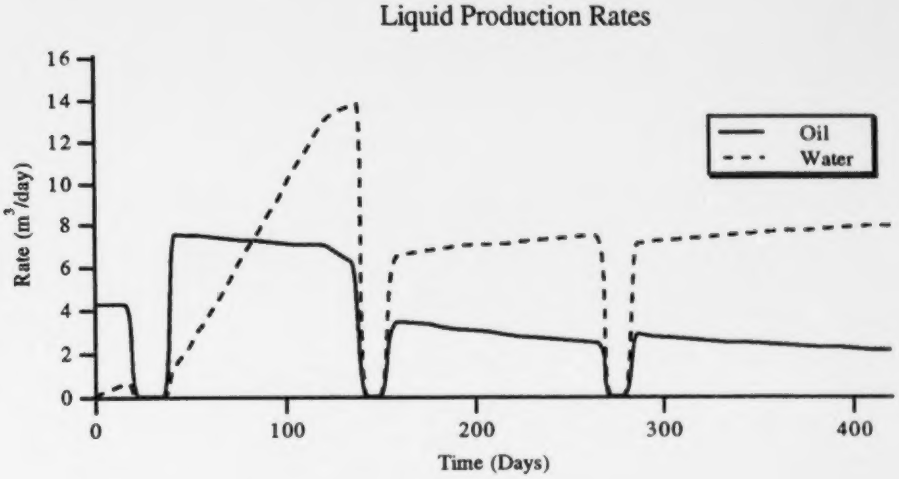

Figure 5.6.4.2 Run Z-3e Liquid production rates.

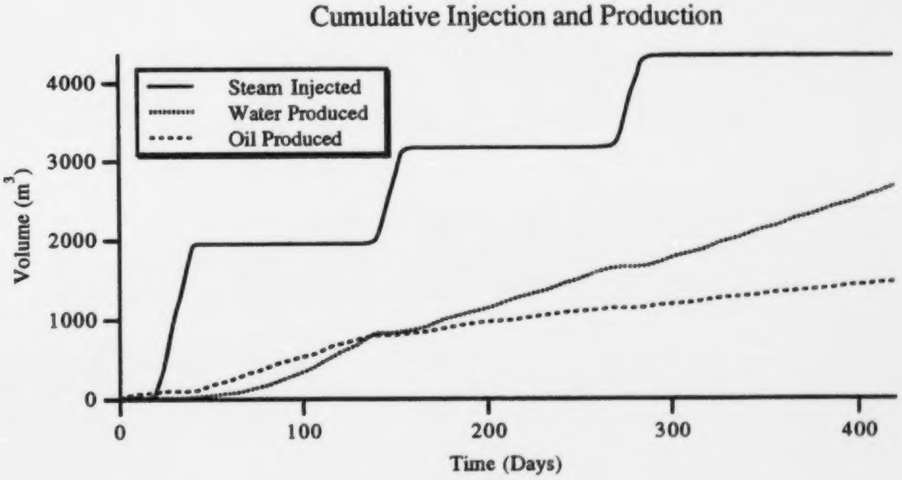

Figure 5.6.4.3 Run Z-3e Cumulative injection and production.

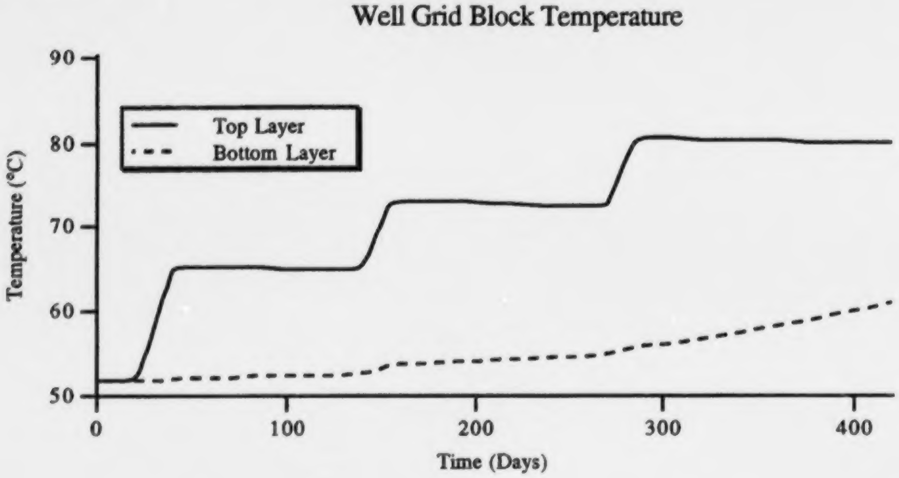

Figure 5.6.4.4 Run Z-3e Well grid block temperature.

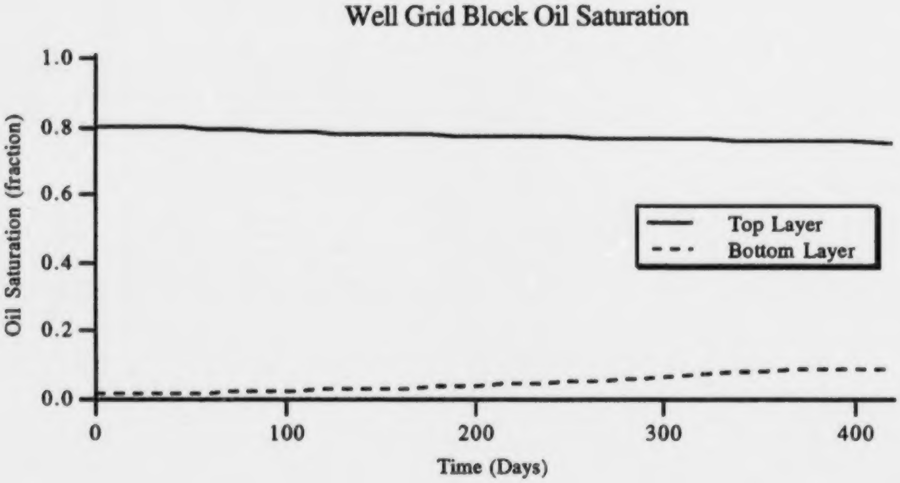

Figure 5.6.4.5 Run Z-3e Well grid block oil saturation.

5.7 Interwell Interference

Interwell interference has been described by Miller (1986) as "the normally smooth production response curves of some wells being disrupted by events at neighbouring wells". Both Miller (1986) and Vittoratos *et al.* (1988) give examples of interwell communication for very different reservoirs.

5.7.1 Interference Illustration and Grid Type Comparison

To illustrate interference and also to make a grid type comparison, Runs R-5 and Z-5 were made. Figure 5.7.1.1 summarizes the run data and Figures 5.7.1.2 to 5.7.1.19 present the results.

For Run R-5, Figures 5.7.1.2 and 5.7.1.3 illustrate the steam injection rate and cumulative injected volumes into both regions, respectively. Figures 5.7.1.4 and 5.7.1.5 illustrate the production rates and cumulative produced volumes from both regions, respectively. The well grid block pressure, well pressure history and well grid block temperature for each region are shown in Figures 5.7.1.6, 5.7.1.7 and 5.7.1.8, respectively. The grid block pressure and temperature profiles shown in Figures 5.7.1.9 and 5.7.1.10, respectively complete the set of figures for this run. For Run Z-5, a similar set of figures is provided. Figures 5.7.1.11 and 5.7.1.12 illustrate the steam injection rate and cumulative injected volumes into both regions, respectively. Figures 5.7.1.13 and 5.7.1.14 illustrate the production rates and cumulative produced volumes from both regions, respectively. The well grid block pressure, well pressure history and well grid block temperature for each region are shown in Figures 5.7.1.15, 5.7.1.16 and 5.7.1.17, respectively. The grid block pressure and temperature profiles are shown in Figures 5.7.1.18 and 5.7.1.19, respectively.

The production rate, Figures 5.7.1.4 and 5.7.1.13, at time 75–95 days in both runs at Well 1 was affected by injection at Well 2, although the level of resolution is better for the hyperhybrid run (Run Z-5). Note the change in the pressure gradient between the two wells shown in Figures 5.7.1.9 and 5.7.1.18. It changed from being almost flat at time 75 days to very steep at time 95 days. There was very little response in the temperature profile for Run R-5 in comparison to Run Z-5 due to the larger grid block size in the former.

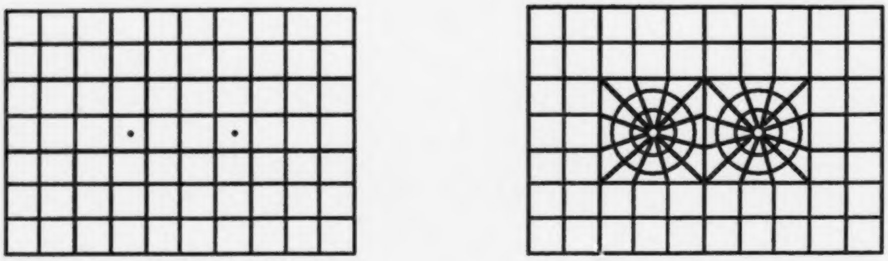
Run R-5

Run Z-5

- Grid Dimensions
  All grid blocks are the same size
  $\Delta x =$ 97.5 metres
  $\Delta y =$ 97.5 metres
  $\Delta z =$ 24.4 metres

- Rock Properties
  $k_x = k_y = 2000$ md
  $k_r = k_\theta = 2000$ md
  $k_z = 1000$ md
  $\phi = 0.30$

- Initial Conditions
  $P = 500$ kPa
  $T = 51.7$ °C
  $S_w = 0.20$
  $S_o = 0.80$
  $S_g = 0.00$

Run Z-5

	Region 1	Region 2
Δr_1	20.0	20.0
Δr_2	25.0	25.0
Δr_3	20.0	20.0
Δr_4	100.0*	100.0*

Region 1 is on the left and Region 2 is on the right.

* calculated internally

Figure 5.7.1.1 Runs R-5 and Z-5 data summary (continued next page).

- Operating Conditions

Time (days)	Well/Region 1		Well/Region 2	
0–20	BHP_{max} (kPa)	6900	BHP_{max} (kPa)	6900
	BHP_{min} (kPa)	120	BHP_{min} (kPa)	120
	q_T (m^3/d)	100	q_T (m^3/d)	100
	x	0.7	x	0.7
	T_{inj} (°C)	232	T_{inj} (°C)	232
20–75	BHP_{max} (kPa)	6900	BHP_{max} (kPa)	6900
	BHP_{min} (kPa)	120	BHP_{min} (kPa)	120
	q_L (m^3/d)	30	q_L (m^3/d)	30
75–95	BHP_{max} (kPa)	6900	BHP_{max} (kPa)	6900
	BHP_{min} (kPa)	120	BHP_{min} (kPa)	120
	q_L (m^3/d)	30	q_T (m^3/d)	100
			x	0.7
			T_{inj} (°C)	232
95–150	BHP_{max} (kPa)	6900	BHP_{max} (kPa)	6900
	BHP_{min} (kPa)	120	BHP_{min} (kPa)	120
	q_L (m^3/d)	30	q_L (m^3/d)	30

- Well Parameters

	Well/Region 1	Well/Region 2
Index	+1/-1	+1/-1
Productivity	Internally calculated	Internally calculated
J* multiplier	1.0	1.0
f_h	1.0	1.0
f	1.0	1.0
c_g	0.5	0.5
s	0.0	0.0
r_w (metres)	0.09	0.09

Figure 5.7.1.1 Runs R-5 and Z-5 data summary (continued from previous page).

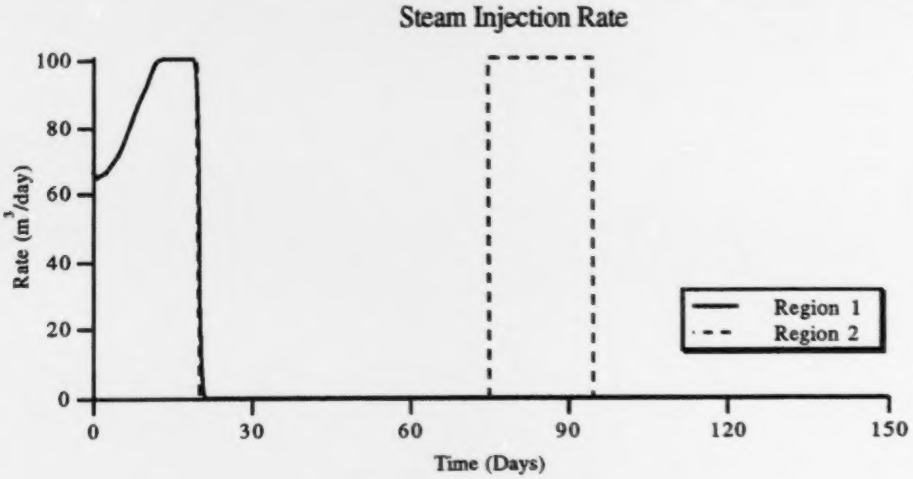

Figure 5.7.1.2 Run R-5 Steam injection rate.

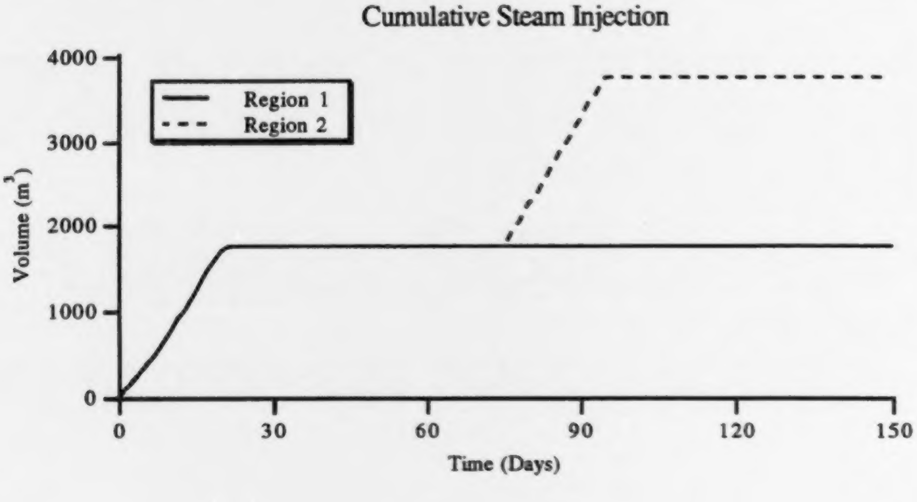

Figure 5.7.1.3 Run R-5 Cumulative steam injection.

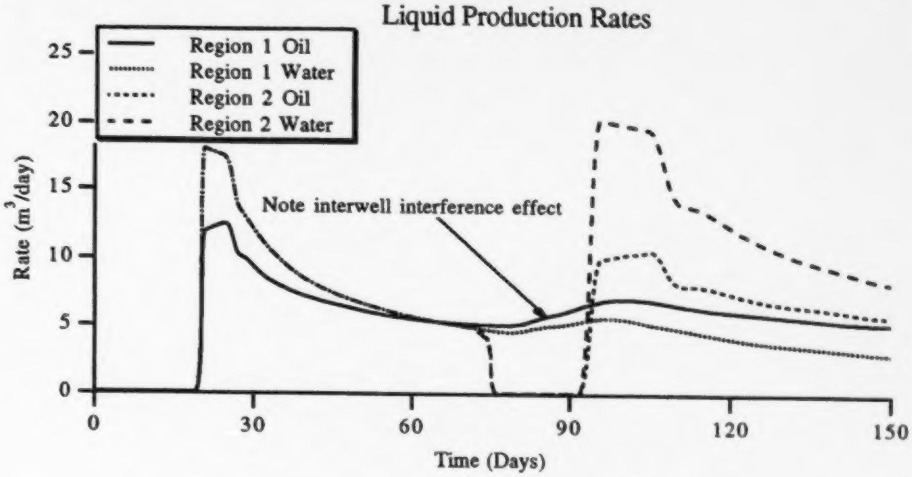

Figure 5.7.1.4 Run R-5 Liquid production rates.

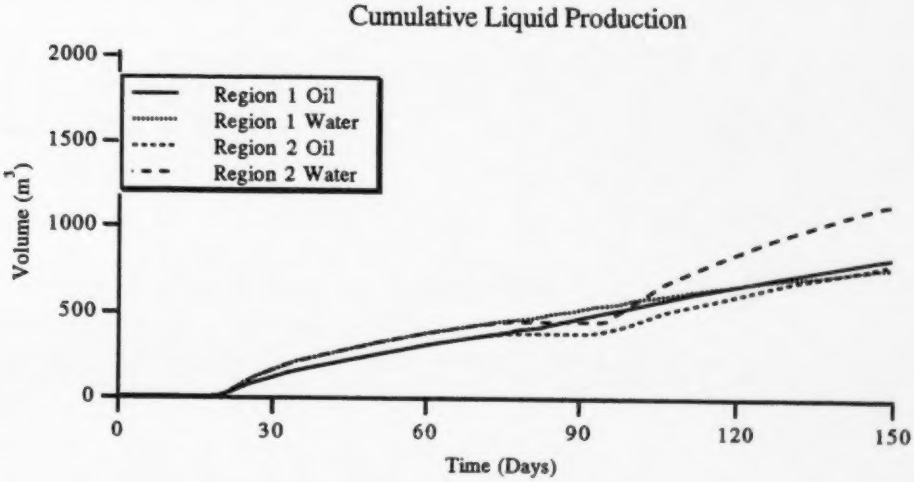

Figure 5.7.1.5 Run R-5 Cumulative liquid production.

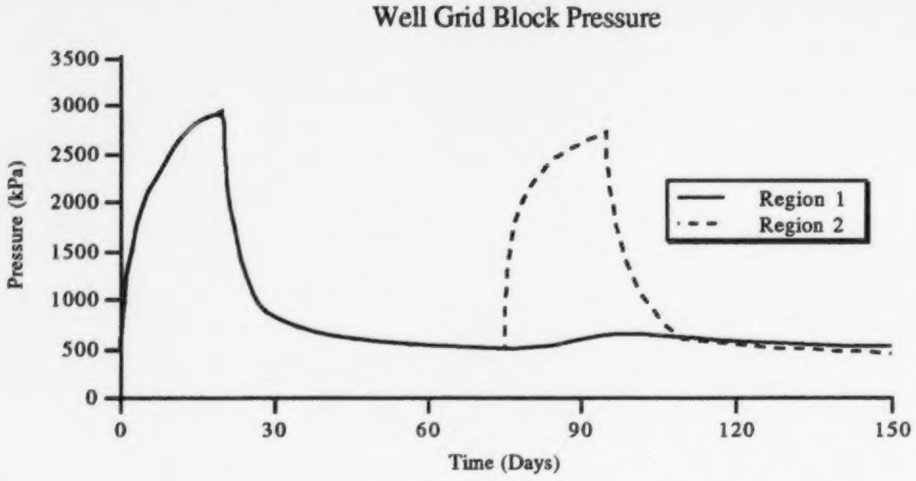

Figure 5.7.1.6 Run R-5 Well grid block pressure.

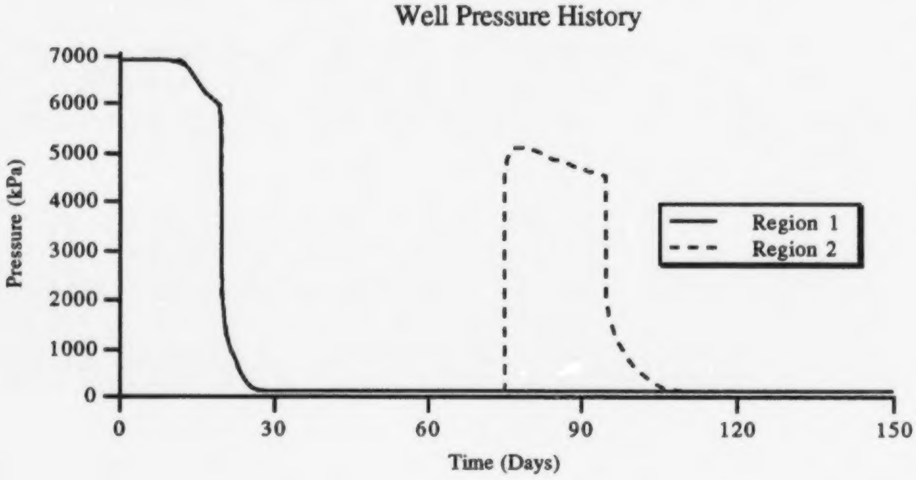

Figure 5.7.1.7 Run R-5 Well pressure history.

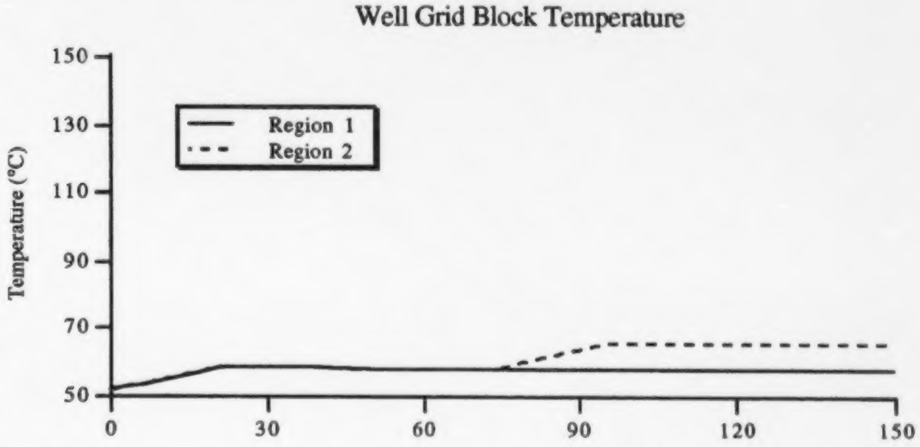

Figure 5.7.1.8 Run R-5 Well grid block temperature.

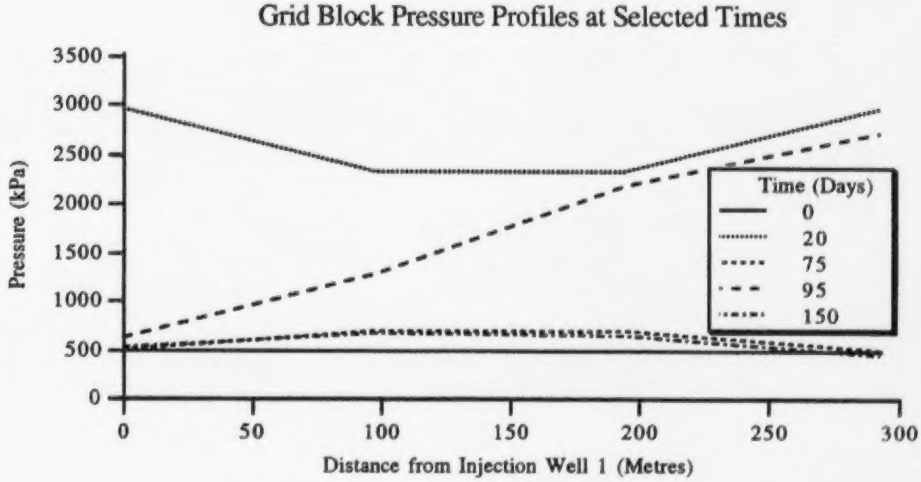

Figure 5.7.1.9 Run R-5 Grid block pressure profiles at selected times.

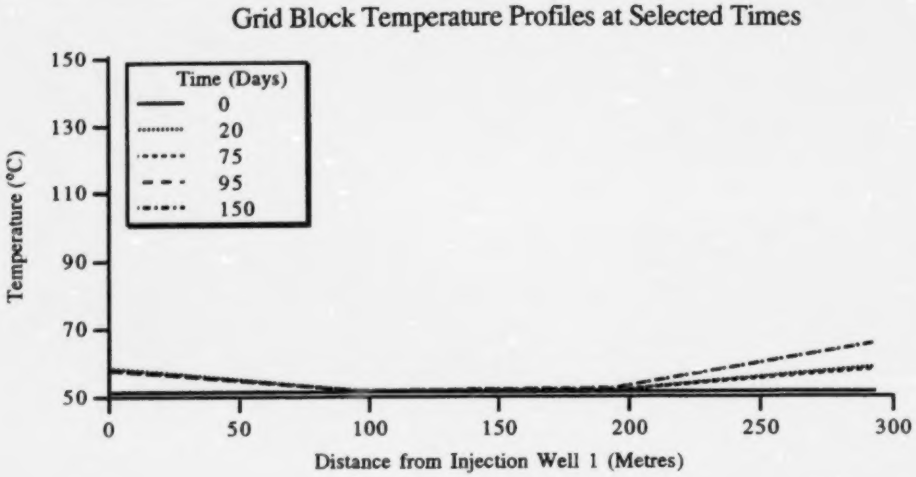

Figure 5.7.1.10 Run R-5 Grid block temperature profiles at selected times.

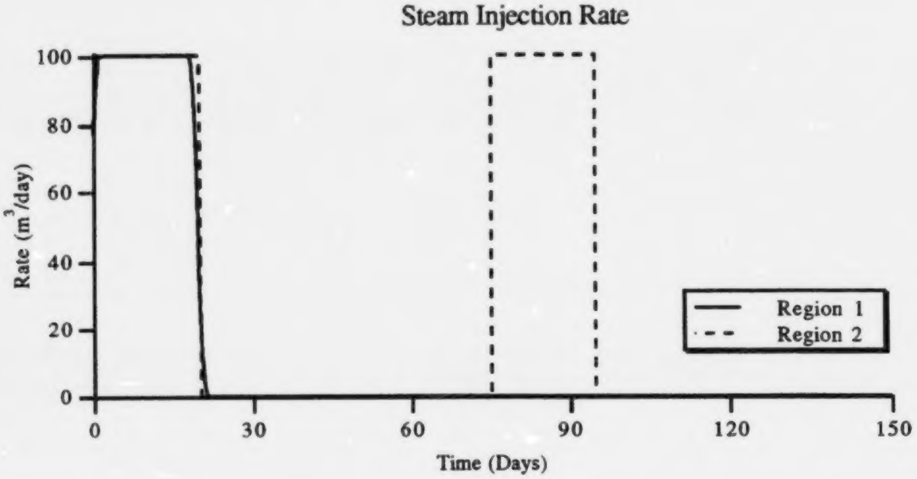

Figure 5.7.1.11 Run Z-5 Steam injection rate.

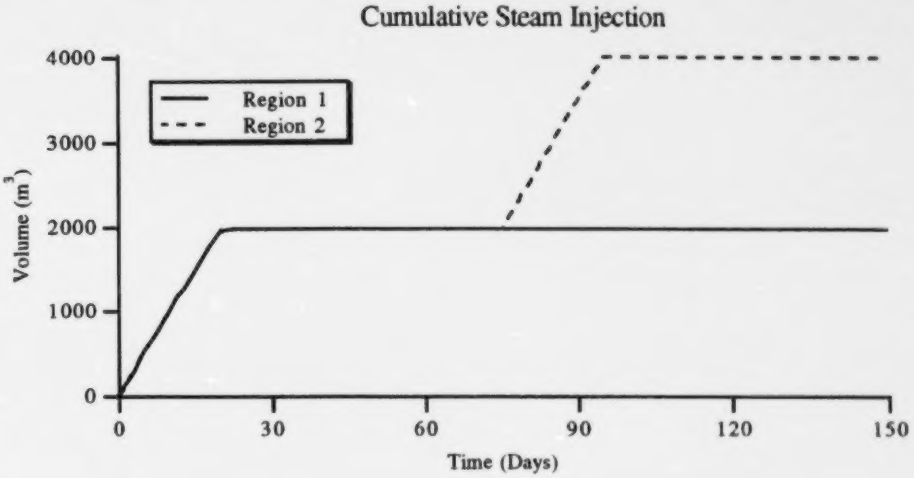

Figure 5.7.1.12 Run Z-5 Cumulative steam injection.

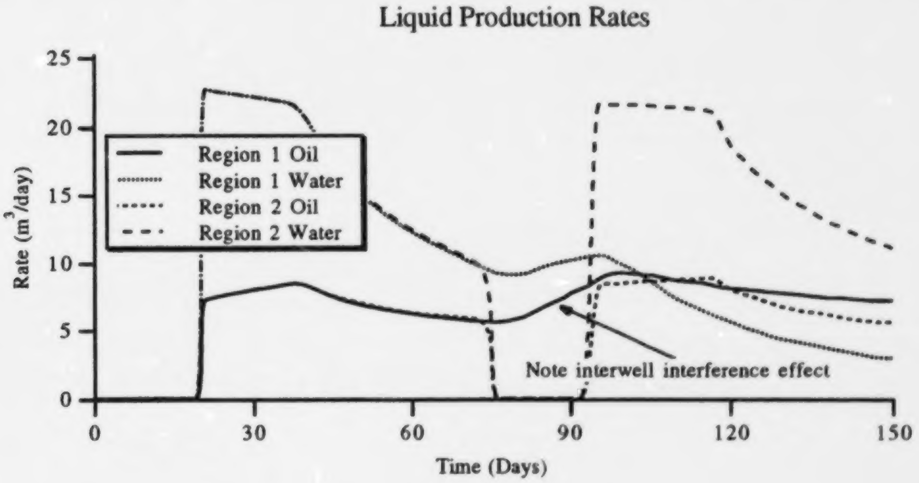

Figure 5.7.1.13 Run Z-5 Liquid production rates.

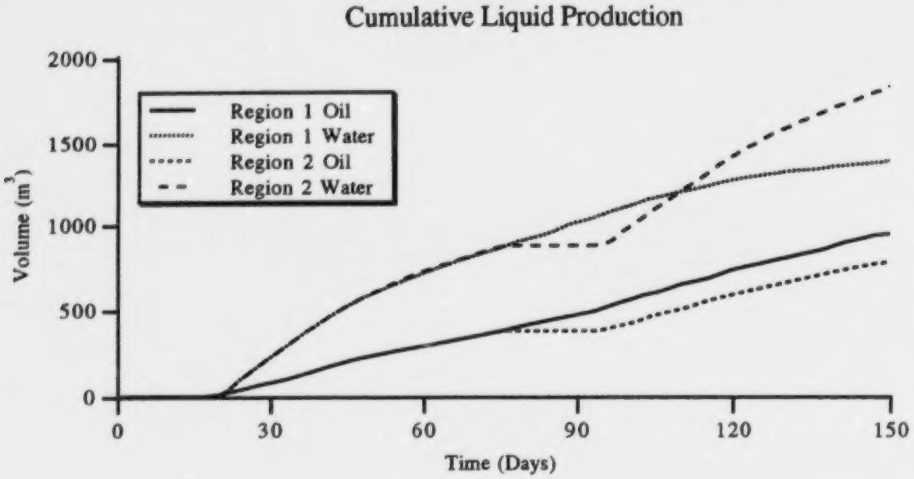

Figure 5.7.1.14 Run Z-5 Cumulative liquid production.

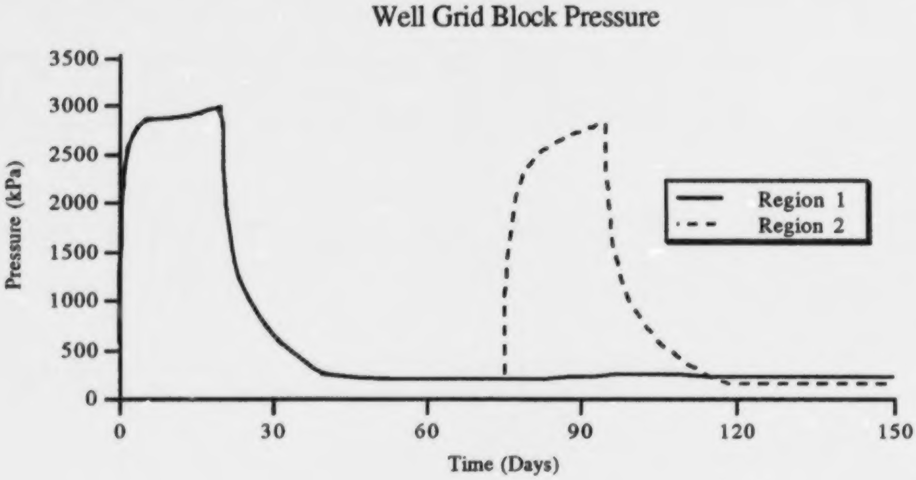

Figure 5.7.1.15 Run Z-5 Well grid block pressure.

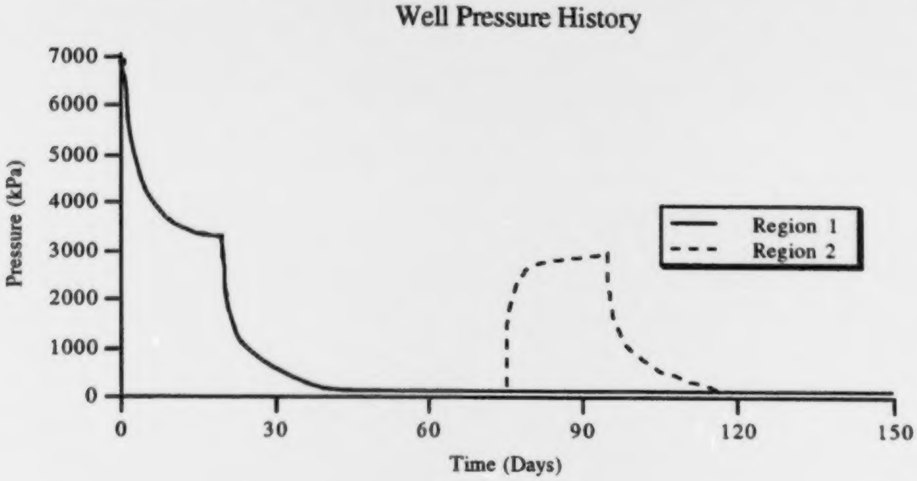

Figure 5.7.1.16 Run Z-5 Well pressure history.

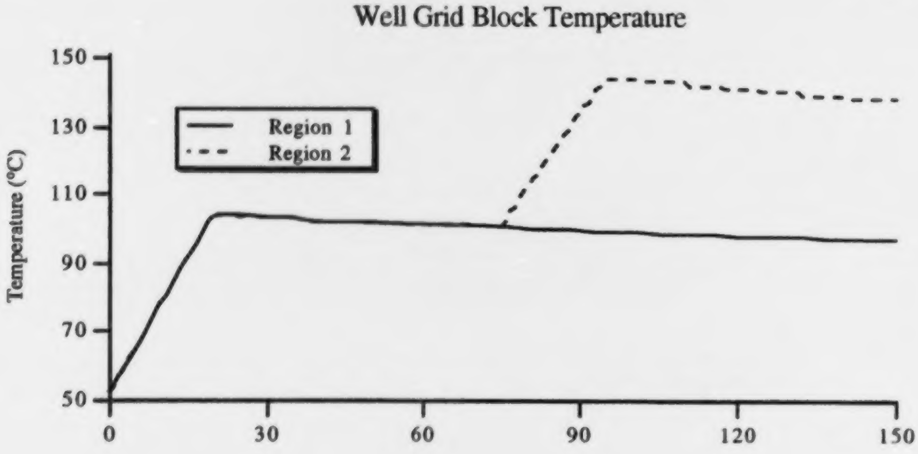

Figure 5.7.1.17 Run Z-5 Well grid block temperature.

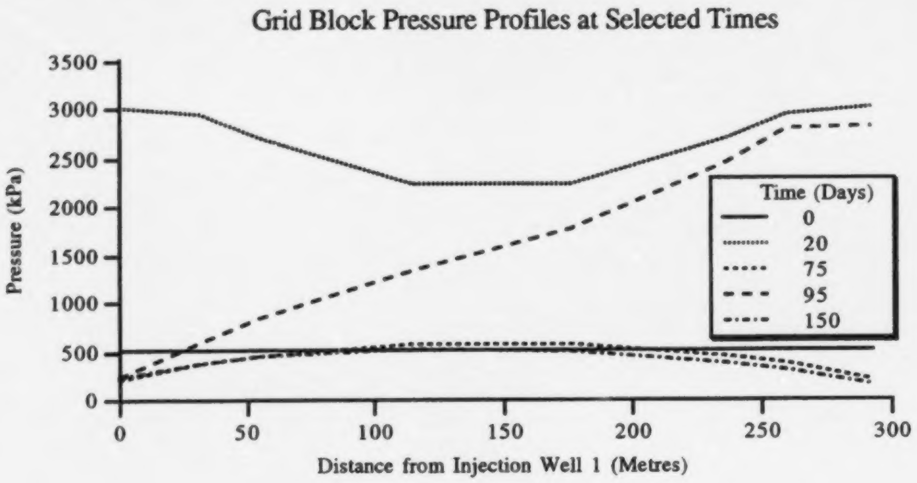

Figure 5.7.1.18 Run Z-5 Grid block pressure profiles at selected times.

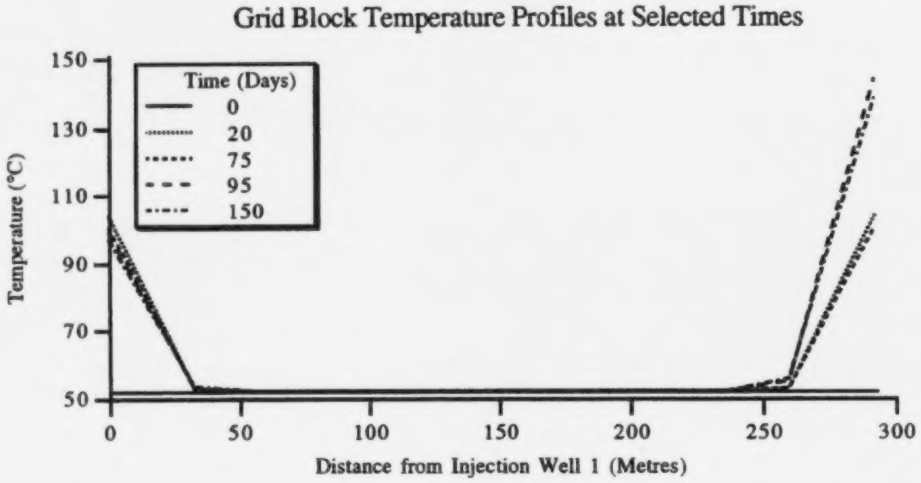

Figure 5.7.1.19 Run Z-5 Grid block temperature profiles at selected times.

5.7.2 Pressure Interference

The literature abounds with the analysis of pressure interference, beginning in the 1960's. A good starting point is Earlougher (1977). The author does not intend to review the literature here. The simplest interference test involves an injector/producer and an observation well.

Several simulation runs were made with the results being compared to theoretical solutions. The first set of runs is based on a rectangular reservoir with a width:length ratio of 2:1 and a second set based on a width:length ratio of 10:7. For the first set, Earlougher and Ramey (1973) provided solutions for the pressure change at the well and several selected points in the reservoir. They also illustrate the technique for building a solution to different problems in Earlougher *et al.* (1968).

Figure 5.7.2.1 illustrates the grids and data used. Note that there is only one active well in the problem. Run 1 is a simple problem with a well and observation point as shown and Run 2 involves some refinement about the observation point. Run 3 involves hyperhybrid refinement about the well and observation point whereas Run 4 has hyperhybrid refinement about the well and refinement similar to Run 2 about the observation point.

Figure 5.7.2.2 illustrates the pressure change at the observation point with time. Indicated on this figure are the exponential integral solution for an infinite reservoir and the Earlougher (1977) solution for a bounded reservoir. Run 1 fell somewhat below the Earlougher curve. Note that the pressure measured is some average grid block pressure and hence is artificially low. Run 2 shows closer agreement because the observation point is in a smaller grid block. Run 3 fell above the Earlougher curve.

As with Run 2, Run 4 approached the Earlougher solution. Figure 5.7.2.3 shows the pressure profiles from the well to the observation point. Figures 5.7.2.4 and 5.7.2.5 are enlargements about the well and observation point, respectively. Note the effects of the grid design on the profile.

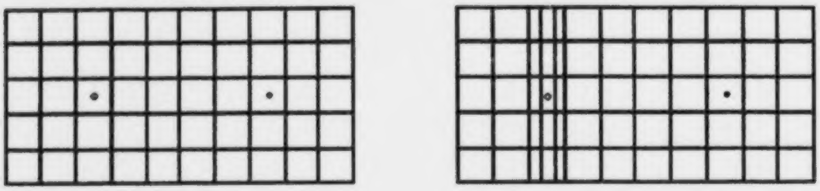

Interference Run 1

Interference Run 2

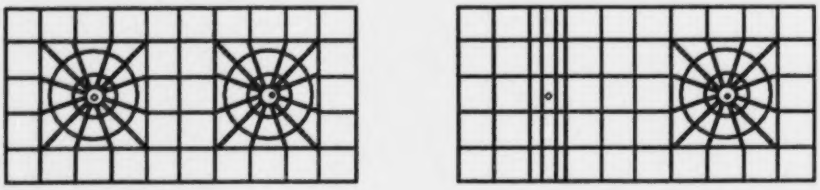

Interference Run 3

Interference Run 4

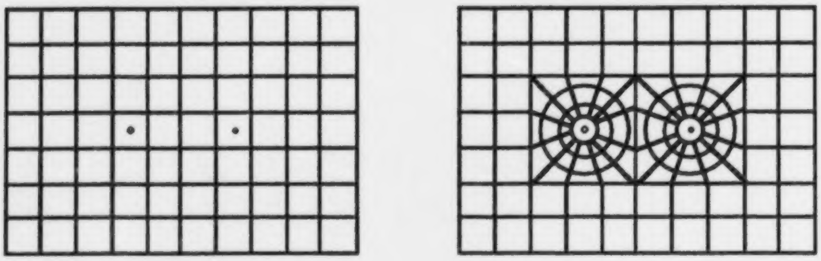

Interference Run 5

Interference Run 6

- Grid Dimensions
  All grid blocks are the same size
  $\Delta x =$ 97.5 metres
  $\Delta y =$ 97.5 metres
  $\Delta z =$ 24.4 metres
  except the refined area is
  43.75, 10.00, 43.75 metres

- Rock Properties
  $k_x = k_y = 2000$ md
  $k_r = k_\theta = 2000$ md
  $k_z = 1000$ md
  $\phi = 0.30$

- Initial Conditions
  $P = 500$ kPa
  $T = 51.7$ °C
  $S_w = 0.20$
  $S_o = 0.80$
  $S_g = 0.00$

Runs 3, 4, and 6

	Region 1	Region 2
Δr_1	20.0	20.0
Δr_2	25.0	25.0
Δr_3	20.0	20.0
Δr_4	45.0*	45.0*

Region 1 is on the left and Region 2 is on the right.

* calculated internally

Figure 5.7.2.1 Interference runs data summary (continued next page).

- Operating Conditions

Time (days)	Region 1	
0–25	BHP_{max} (kPa)	6900
	BHP_{min} (kPa)	120
	q_T (m^3/d)	100
	x	0.7
	T_{inj} (°C)	232

- Well Parameters

	Region 1	Region 2
Index	+1/-1	+1/-1
Productivity	Internally calculated	Internally calculated
J* multiplier	1.0	1.0
f_h	1.0	1.0
f	1.0	1.0
c_g	0.5	0.5
s	0.0	0.0
r_w (metres)	0.09	0.09

Figure 5.7.2.1 Interference runs data summary (continued from previous page).

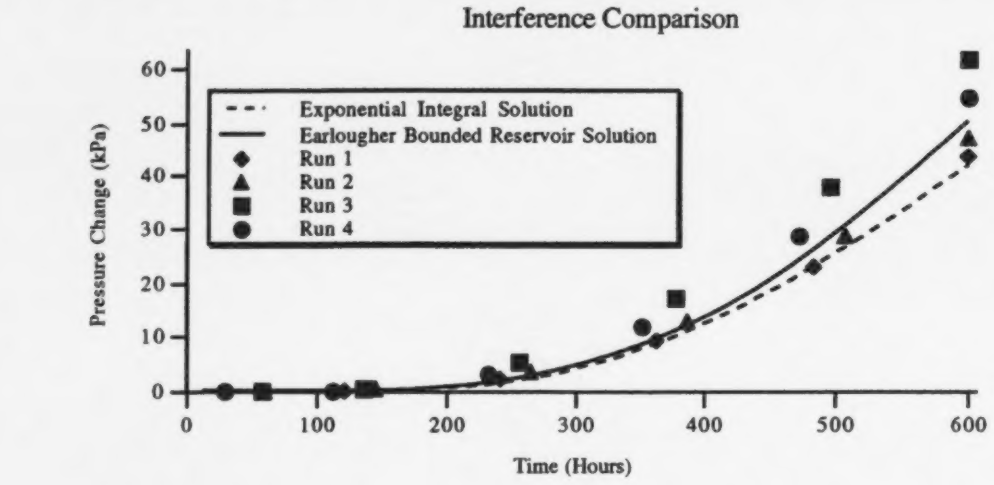

Figure 5.7.2.2 Interference comparison.

These results are a good example of grid design influencing the solution. This important conclusion can be made. If a well is not in operation for some extended period of time, or is not even drilled until later in the simulation, then the grid refinement should be removed or inserted when required. Hence, hyperhybrid and hybrid grid refinement should be a dynamic, not a static, process.

Using the width:length ratio of a 2:1 rectangle, with the active and observation wells positioned in such a manner as to be able to use the Earlougher solution, did not give a large pressure change at the observation well. To see a larger pressure change, the width:length ratio of a 10:7 rectangle was used. Earlougher (1977) did not provide the theoretical solution and one was not constructed here. Figure 5.7.2.6 shows the results for Runs 5 and 6 and also indicates the exponential integral solution. Note the larger difference of 50 kPa, showing the same trend as the width:length ratio of the 2:1 rectangle set of runs. It should be noted that in both of these runs, the boundary effects appeared towards the end of the run time.

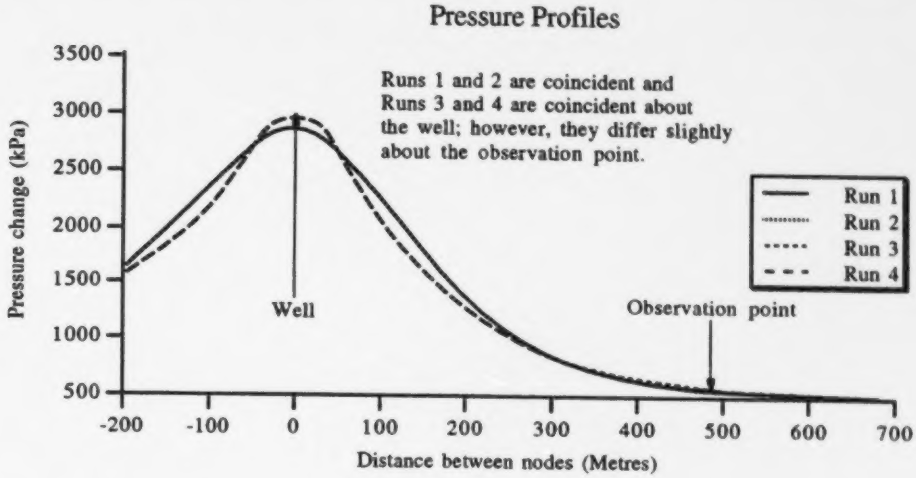

Figure 5.7.2.3 Pressure profiles.

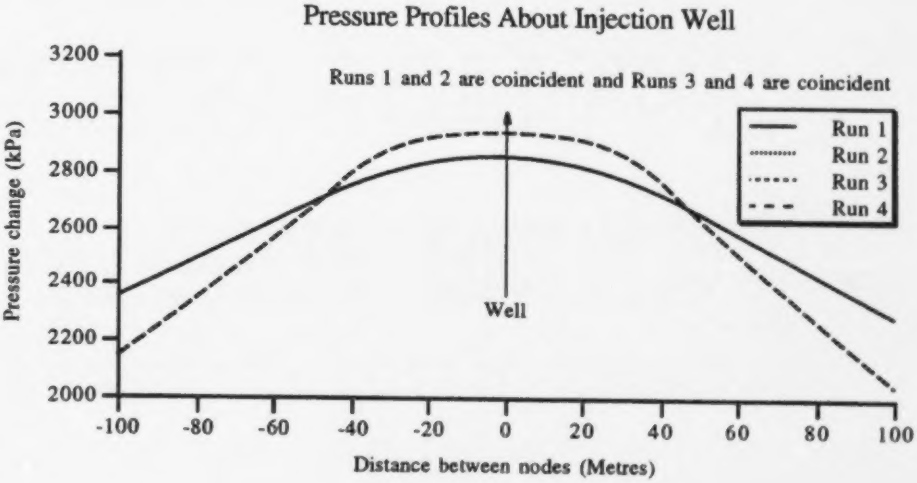

Figure 5.7.2.4 Pressure profiles about injection well.

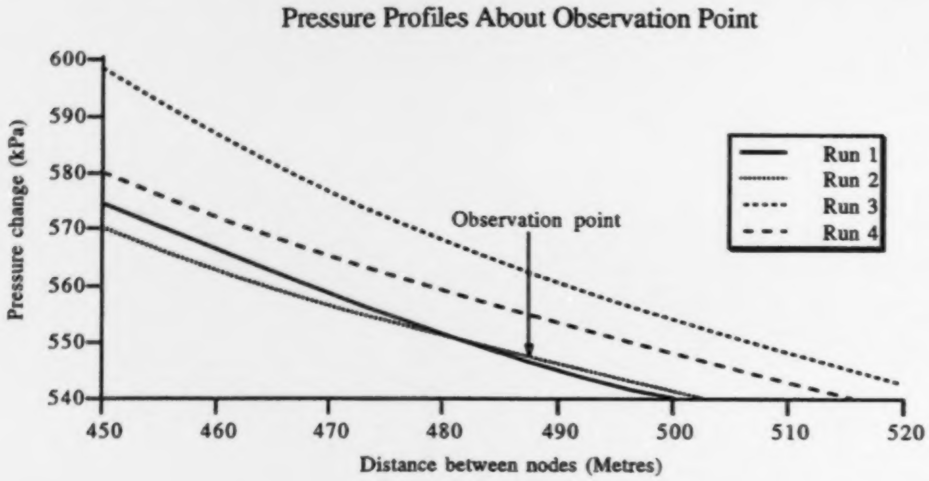

Figure 5.7.2.5 Pressure profiles about observation point.

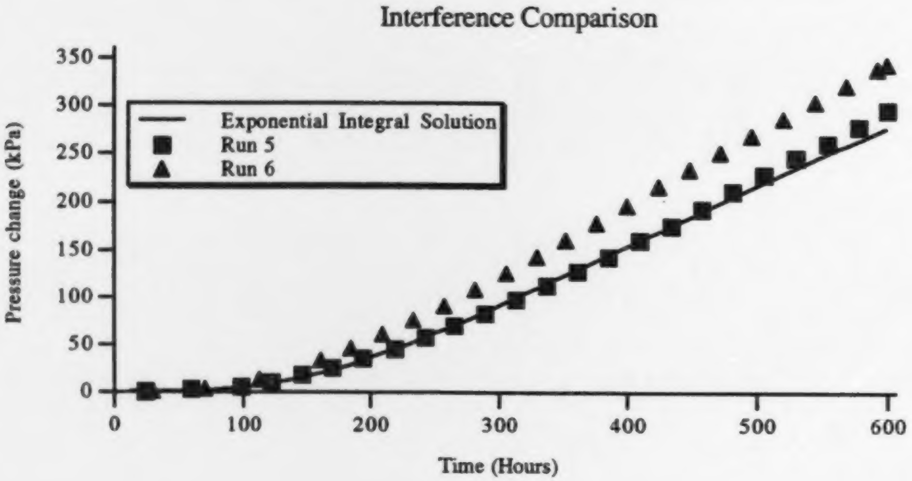

Figure 5.7.2.6 Interference comparison.

5.8 Multiwell Cyclic Steaming

The objective of this section is to show cyclic steaming operations well behaviour when wells interfere with each other. A series of runs with two wells, two dimensions and a series of runs with four wells, two dimensions were made.

5.8.1 Two-Well Runs

For the two-well, two-dimensional runs, the parameters varied were steam slug size[1], production period and mode of operation. Note that Hiebert *et al.* (1991) stated that less accurate results will be obtained using a rectilinear grid than on one based on a hybrid grid; however, they did not present the results of an optimization study. Figure 5.8.1.1 illustrates the grid used and the operating conditions for this set of runs.

Table 5.8.1.1 summarizes the results of Runs 1 to 8: steam injected, production, injection and production times, steam-oil ratio, water-oil ratio and average daily oil rate on a cycle and total run basis. Table 5.8.1.2 summarizes Runs 1–4 and 10 end of injection and production phase results.

Note that in Runs 5–8, Well 1 was on production prior to any steaming. This was accounted for in two ways. The first was to count production/injection as a cycle (5.1, 6.1, 7.1, 8.1) and the second, more realistic, way was to ignore the pre-injection production period and measure cycles from first injection (5a, 6a, 7a, 8a).

Figures 5.8.1.2 to 5.8.1.16 illustrate the cycle and total SOR (steam-oil ratio), WOR (water-oil ratio) and ADOR (average daily oil rate) for Runs 1–8. Table 5.8.1.3 ranks each run for minimum SOR, minimum WOR and maximum ADOR.

Run 2 had a larger slug size, and a longer production period. This resulted in the highest ADOR and it ranked second in SOR and WOR. Run 4 had the minimum SOR and WOR due to the long production period and small steam slug; however, the ADOR was among the lowest. The together and staggered runs performed similarly at the end of three cycles. Also, a comparison of the together and staggered companion runs showed that the first cycle SOR in the staggered mode was lower than in the together mode. They became very similar with increasing cycle number, although the staggered runs were marginally lower. There was little difference in the WOR when comparing the together and staggered runs. The ADOR was slightly higher in the together pair, especially in the first cycle.

---

[1] The injection period was kept constant, hence injection rate is the same parameter as steam slug size.

In general, the performance of the runs was similar. The temperature and oil saturation of the second ring of grid blocks did not change significantly in any of these runs; that is, the response was due mainly to the 'activity' in the well grid block. Performance variations were due to lower oil viscosity as a result of a hotter grid block and higher water relative permeability due to increased water saturation. At the end of each injection phase of the cycle, Run 1 was hotter than Run 3, resulting in more oil production. Similarly, Run 2 was hotter than Run 4 at the end of each injection phase. Run 1 and Run 2 had more steam injected than Runs 3 and 4 which resulted in the former runs producing more water. Note that Run 10 is an extension of Run 2. Run 10 showed a decreasing oil recovery as the well grid block was depleted of oil. At the end of cycle 5, the oil saturation had decreased to 0.7 from an initial value of 0.8. For Runs 1 to 4, as the cycle number increased, the cycle oil and water production increased. Again, most of the 'activity' was in the well grid block. At the end of each injection phase, the grid block was hotter than the previous cycle; hence, oil was more mobile. This trend reversed itself, as in Run 10, with additional cycles as the well grid block was depleted and the second ring grid blocks had not been heated enough to supply more oil.

These runs, consistent with observations in the field, showed that a larger steam slug size, and a longer production period (Run 2) were the better approach to operate the wells in early steaming. The mode of operation did not have any significant effect.

Runs 9 and 10 were carried out for five cycles. For Run 9, both wells were steamed initially for 20 days, Well 1 was produced for 70 days and Well 2 for 35 days. Subsequently, 20 day/70 day injection/production phases were used. The last cycle of Well 1 had a 35 day production period. For Run 10, the 20 day/70 day injection/production cycles were concurrent; that is, Run 2 with two additional cycles.

Table 5.8.1.4 summarizes the results of Runs 9 and 10 and Figures 5.8.1.17 to 5.8.1.19 illustrate the results compared to Run 2. It can be seen immediately the result of a short production period in Run 9 Well 1 Cycle 5 and Run 9 Well 2 Cycle 1 on the SOR whereas the other results were similar. The WOR increasing trend in the first three cycles remained unchanged in cycles 4 and 5, with the exception of the short production phase. Finally, the ADOR continued to decline slightly in the later cycles. Steaming both wells initially together before placing them in a staggered mode improved the performance.

Runs Cyclic 1 – 8

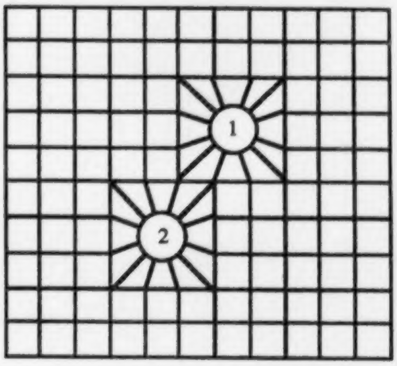

- Grid Dimensions
  - All grid blocks are the same size
  - Δx = 97.5 metres
  - Δy = 97.5 metres
  - Δz = 24.4 metres

- Rock Properties
  - $k_x = k_y$ = 2000 md
  - $k_r = k_\theta$ = 2000 md
  - k_z = 1000 md
  - ϕ = 0.30

- Initial Conditions
  - P = 500 kPa
  - T = 51.7 °C
  - S_w = 0.20
  - S_o = 0.80
  - S_g = 0.00

	Region 1	Region 2
Δr_1	25.0	25.0
Δr_2	140.0*	140.0*

* calculated internally

Figure 5.8.1.1 Multiwell cyclic steaming Runs 1–8 data summary.
(continued next page)

- Operating Conditions

Fixed parameters		Variable parameters	
No. of cycles	3	q_T (m^3/d)	50 & 100
BHP$_{max}$ (kPa)	6900	Production time (days)	35 & 70
BHP$_{min}$ (kPa)	120	Mode together and staggered	
q_L (m^3/d)	20		
x	0.7		
T_{inj} (°C)	250		

Run	q_T (m^3/d)	Production time (days)	Mode
1	100	35	Together
2	100	70	Together
3	50	35	Together
4	50	70	Together
5	100	35	Staggered
6	100	70	Staggered
7	50	35	Staggered
8	50	70	Staggered

- Well Parameters

	Region 1	Region 2
Index	+1/-1	+1/-1
Productivity	Internally calculated	Internally calculated
J* multiplier	1.0	1.0
f_h	1.0	1.0
f	1.0	1.0
c_g	0.5	0.5
s	0.0	0.0
r_w (metres)	0.09	0.09

Figure 5.8.1.1 Multiwell cyclic steaming Runs 1–8 data summary.
(continued from previous page)

Run	Cycle	Q_{inj} (m^3)	Q_w (m^3)	Q_o (m^3)	Time Inject (days)	Time Prod (days)	SOR	SOR cum	WOR	WOR cum	ADOR (m^3/d)
1	1	1974.3	356.5	188.7	20.0	35.0	10.5	10.5	1.9	1.9	5.4
	2	2000.0	456.8	243.1	20.0	35.0	8.2	9.2	1.9	1.9	6.9
	3	2000.0	459.6	240.4	20.0	35.0	8.3	8.9	1.9	1.9	6.9
	Sum	5974.3	1272.9	672.2	60.0	105.0	8.9		1.9		6.4
2	1	1974.3	542.6	429.2	20.0	70.0	4.6	4.6	1.3	1.3	6.1
	2	2000.0	792.6	577.0	20.0	70.0	3.5	3.9	1.4	1.3	8.2
	3	2000.0	830.4	569.6	20.0	70.0	3.5	3.8	1.5	1.4	8.1
	Sum	5974.3	2165.6	1575.8	60.0	210.0	3.8		1.4		7.5
3	1	1000.0	251.7	173.1	20.0	35.0	5.8	5.8	1.5	1.5	4.9
	2	1000.0	309.9	214.2	20.0	35.0	4.7	5.2	1.4	1.5	6.1
	3	1000.0	387.6	274.8	20.0	35.0	3.6	4.5	1.4	1.4	7.9
	Sum	3000.0	949.2	662.1	60.0	105.0	4.5		1.4		6.3
4	1	1000.0	345.4	331.0	20.0	70.0	3.0	3.0	1.0	1.0	4.7
	2	1000.0	430.6	417.7	20.0	70.0	2.4	2.7	1.0	1.0	6.0
	3	1000.0	512.0	486.6	20.0	70.0	2.1	2.4	1.1	1.0	7.0
	Sum	3000.0	1288.0	1235.3	60.0	210.0	2.4		1.0		5.9
5.1	1	1971.4	0.0	143.5	20.0	35.0	13.7	13.7	0.0	0.0	4.1
	2	2000.0	477.8	242.3	20.0	35.0	8.3	10.3	2.0	1.2	6.9
	3	2000.0	434.0	236.0	20.0	35.0	8.5	9.6	1.8	1.5	6.7
	Sum	5971.4	911.8	621.8	60.0	105.0	9.6		1.5		5.9
5.2	1	1974.3	379.5	198.7	20.0	35.0	9.9	9.9	1.9	1.9	5.7
	2	2000.0	464.9	235.1	20.0	35.0	8.5	9.2	2.0	1.9	6.7
	3	2000.0	466.2	233.7	20.0	35.0	8.6	9.0	2.0	2.0	6.7
	Sum	5974.3	1310.6	667.5	60.0	105.0	9.0		2.0		6.4
5a	1	1971.4	477.8	242.3	20.0	35.0	8.1	8.1	2.0	2.0	6.9
	2	2000.0	434.0	236.0	20.0	35.0	8.5	8.3	1.8	1.9	6.7
	Sum	3971.4	911.8	478.3	40.0	70.0	8.3		1.9		6.8

Table 5.8.1.1 Multiwell cyclic steam Runs 1–8 results summary.

(continued next page)

Run	Cycle	Q_{inj} (m^3)	Q_w (m^3)	Q_o (m^3)	Time Inject (days)	Time Prod (days)	SOR	SOR cum	WOR	WOR cum	ADOR (m^3/d)
6.1	1	1974.0	0.2	282.0	20.0	70.0	7.0	7.0	0.0	0.0	4.0
	2	1999.9	643.1	533.5	20.0	70.0	3.7	4.9	1.2	0.8	7.6
	3	1999.9	801.1	597.4	20.0	70.0	3.3	4.2	1.3	1.0	8.5
	Sum	5973.8	1444.4	1412.9	60.0	210.0	4.2		1.0		6.7
6.2	1	1974.3	516.5	385.7	20.0	70.0	5.1	5.1	1.3	1.3	5.5
	2	2000.0	785.0	570.3	20.0	70.0	3.5	4.2	1.4	1.4	8.1
	3	2000.0	831.8	568.1	20.0	70.0	3.5	3.9	1.5	1.4	8.1
	Sum	5974.3	2133.3	1524.1	60.0	210.0	3.9		1.4		7.3
6a	1	1974.0	643.1	533.5	20.0	70.0	3.7	3.7	1.2	1.2	7.6
	2	1999.9	801.1	597.4	20.0	70.0	3.3	3.5	1.3	1.3	8.5
	Sum	3973.9	1444.2	1130.9	40.0	140.0	3.5		1.3		8.1
7.1	1	1000.0	0.1	125.3	20.0	35.0	8.0	8.0	0.0	0.0	3.6
	2	1000.0	263.3	185.0	20.0	35.0	5.4	6.4	1.4	0.8	5.3
	3	999.9	354.3	247.6	20.0	35.0	4.0	5.4	1.4	1.1	7.1
	Sum	2999.9	617.7	557.9	60.0	105.0	5.4		1.1		5.3
7.2	1	1000.0	238.3	157.3	20.0	35.0	6.4	6.4	1.5	1.5	4.5
	2	1000.0	314.8	211.1	20.0	35.0	4.7	5.4	1.5	1.5	6.0
	3	999.9	388.7	270.9	20.0	35.0	3.7	4.7	1.4	1.5	7.7
	Sum	2999.9	941.8	639.3	60.0	105.0	4.7		1.5		6.1
7a	1	1000.0	263.3	185.0	20.0	35.0	5.4	5.4	1.4	1.4	5.3
	2	999.9	354.3	247.6	20.0	35.0	4.0	4.6	1.4	1.4	7.1
	Sum	1999.9	617.6	432.6	40.0	70.0	4.6		1.4		6.2
8.1	1	1000.0	0.1	240.8	20.0	70.0	4.2	4.2	0.0	0.0	3.4
	2	999.9	348.5	340.9	20.0	70.0	2.9	3.4	1.0	0.6	4.9
	3	1000.0	450.6	439.2	20.0	70.0	2.3	2.9	1.0	0.8	6.3
	Sum	2999.9	799.2	1020.9	60.0	210.0	2.9		0.8		4.9
8.2	1	1000.0	326.4	293.7	20.0	70.0	3.4	3.4	1.1	1.1	4.2
	2	1000.0	416.7	391.8	20.0	70.0	2.6	2.9	1.1	1.1	5.6
	3	999.9	501.3	468.3	20.0	70.0	2.1	2.6	1.1	1.1	6.7
	Sum	2999.9	1244.4	1153.8	60.0	210.0	2.6		1.1		5.5
8a	1	1000.0	348.5	340.9	20.0	70.0	2.9	2.9	1.0	1.0	4.9
	2	999.9	450.6	439.2	20.0	70.0	2.3	2.6	1.0	1.0	6.3
	Sum	1999.9	799.1	780.1	40.0	140.0	2.6		1.0		5.6

Table 5.8.1.1 Multiwell cyclic steam Runs 1–8 results summary.
(continued from previous page)

		Well Grid Block			Second Ring Grid Block Towards Neighbour Well		
Run	Time (Days)	Pressure (kPa)	Temp (°C)	Oil Saturation	Pressure (kPa)	Temp (°C)	Oil Saturation
1	20	1989.5	85.6	0.754	1713.3	51.7	0.798
	55	276.7	85.2	0.778	750.6	51.7	0.798
	75	2120.1	117.2	0.729	1994.7	51.8	0.796
	110	502.6	116.0	0.751	1030.4	51.8	0.796
	130	2353.5	145.2	0.700	2284.8	52.0	0.795
	165	849.9	143.0	0.718	1332.2	52.0	0.795
2	20	1989.5	85.6	0.754	1713.3	51.7	0.798
	90	261.3	85.5	0.787	592.7	51.7	0.798
	110	2020.8	116.3	0.733	1895.4	51.8	0.796
	180	193.6	114.1	0.768	678.2	51.9	0.797
	200	2081.5	142.7	0.710	2011.2	52.0	0.795
	270	291.8	139.0	0.742	810.6	52.0	0.796
3	20	1395.3	69.0	0.771	1127.7	51.7	0.799
	55	308.0	68.7	0.787	594.8	51.7	0.799
	75	1405.6	85.3	0.761	1248.6	51.7	0.798
	110	259.7	54.9	0.781	652.5	51.7	0.798
	130	1433.7	100.8	0.753	1330.6	51.8	0.797
	165	220.9	100.6	0.772	700.0	51.8	0.797
4	20	1395.3	69.0	0.771	1127.7	51.7	0.799
	90	298.4	68.5	0.793	511.0	51.7	0.799
	110	1342.6	85.1	0.764	1178.7	51.7	0.798
	180	243.2	84.2	0.788	517.0	51.7	0.798
	200	1311.1	100.2	0.757	1201.2	51.8	0.798
	270	200.9	98.8	0.782	508.1	51.8	0.798
10	20	1989.5	85.6	0.754	1713.3	51.7	0.798
	90	261.3	85.5	0.787	592.7	51.7	0.798
	110	2020.8	116.3	0.733	1895.4	51.8	0.796
	180	193.6	114.1	0.768	678.2	51.9	0.797
	200	2081.5	142.7	0.710	2011.2	52.0	0.795
	270	291.8	139.0	0.742	810.6	52.0	0.796
	290	2179.6	154.3	0.687	2128.0	52.2	0.794
	360	469.0	149.2	0.720	955.2	52.2	0.795
	380	2311.4	168.1	0.667	2271.2	52.4	0.794
	450	641.7	165.3	0.698	1102.1	52.4	0.794

Table 5.8.1.2

Multiwell cyclic steaming Runs 1–4 & 10 end of injection and production phase results.

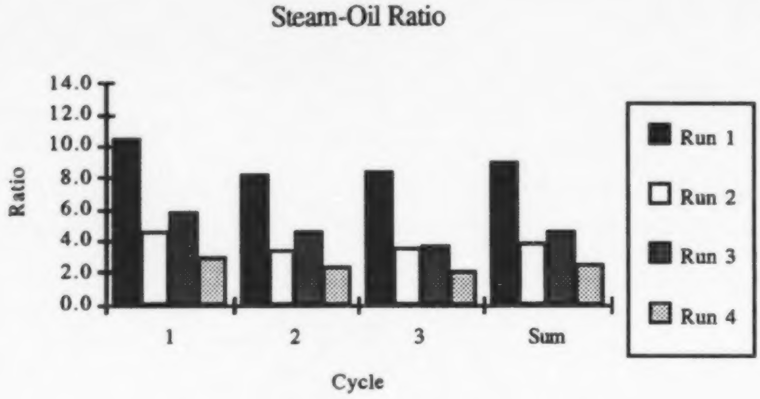

Figure 5.8.1.2 Multiwell cyclic steaming Runs 1–4 steam-oil ratio.

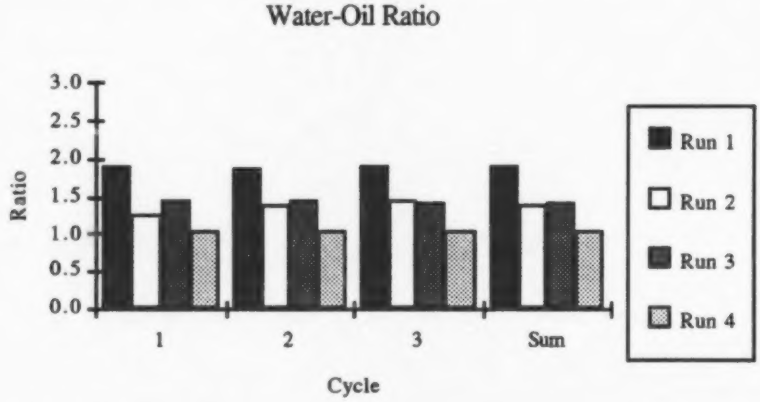

Figure 5.8.1.3 Multiwell cyclic steaming Runs 1–4 water-oil ratio.

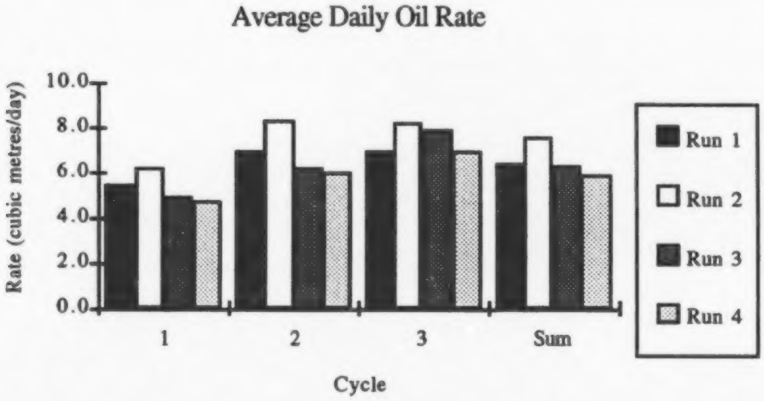

Figure 5.8.1.4 Multiwell cyclic steaming Runs 1–4 average daily oil rate.

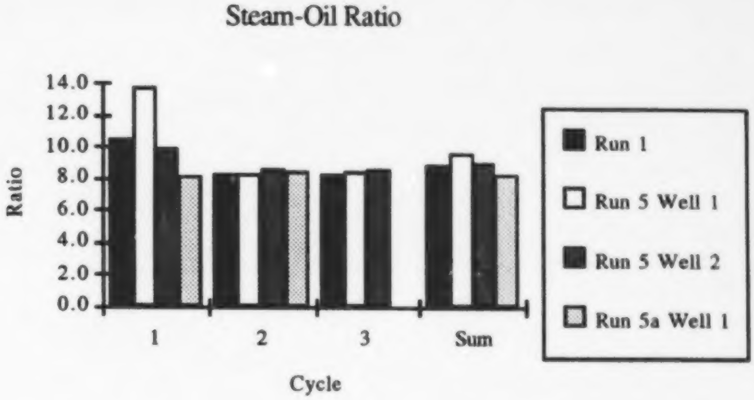

Figure 5.8.1.5 Multiwell cyclic steaming Runs 1 and 5 steam-oil ratio.

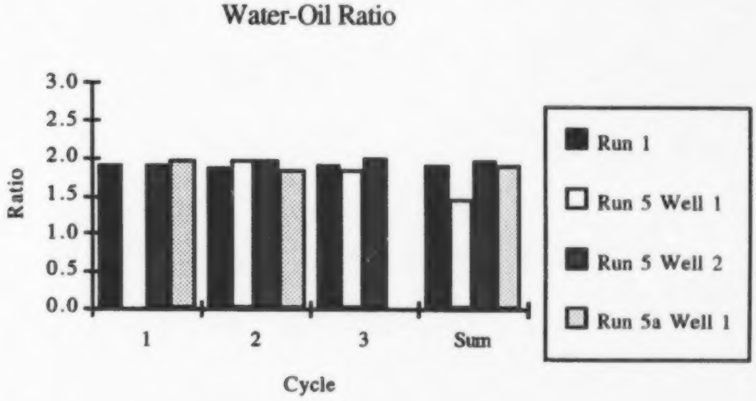

Figure 5.8.1.6 Multiwell cyclic steaming Runs 1 and 5 water-oil ratio.

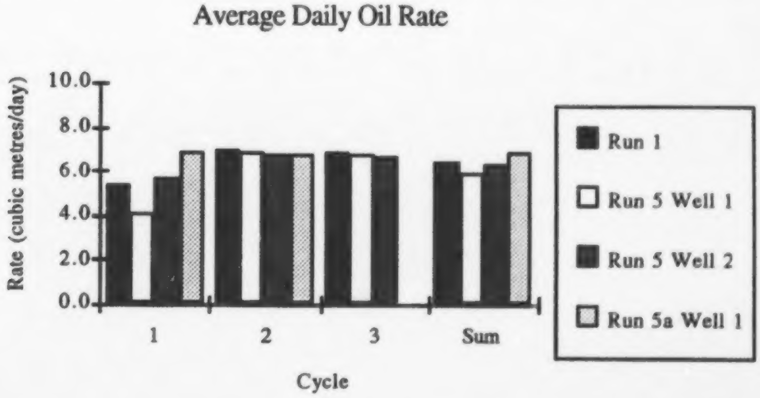

Figure 5.8.1.7 Multiwell cyclic steaming Runs 1 and 5 average daily oil rate.

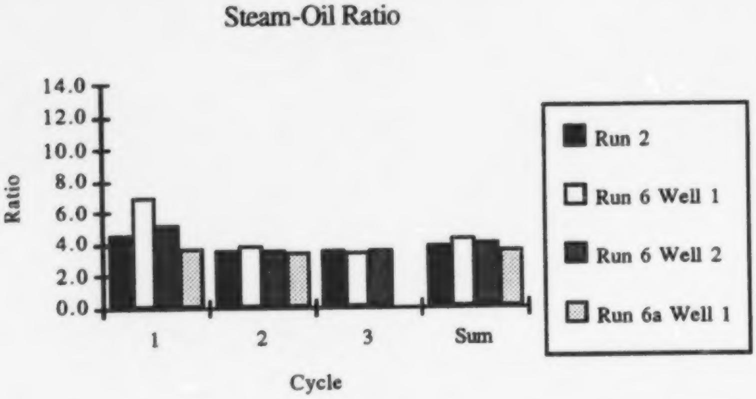

Figure 5.8.1.8 Multiwell cyclic steaming Runs 2 and 6 steam-oil ratio.

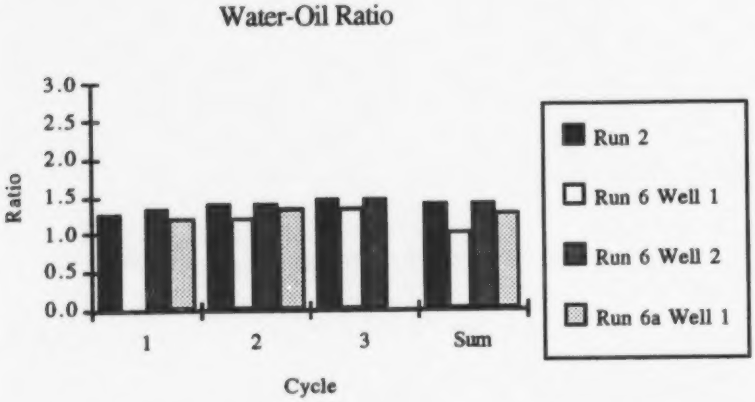

Figure 5.8.1.9 Multiwell cyclic steaming Runs 2 and 6 water-oil ratio.

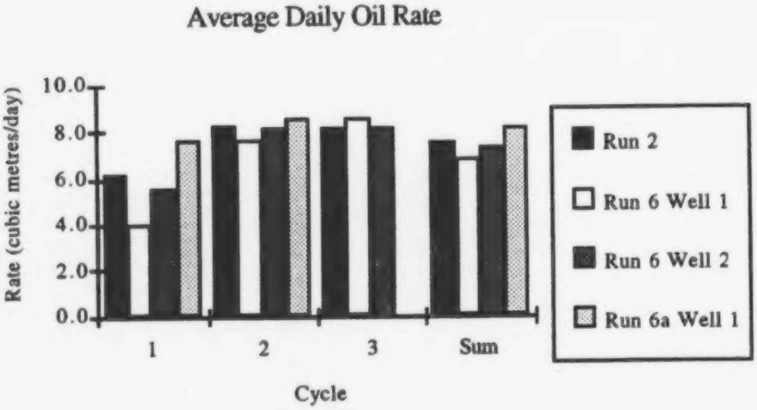

Figure 5.8.1.10 Multiwell cyclic steaming Runs 2 and 6 average daily oil rate.

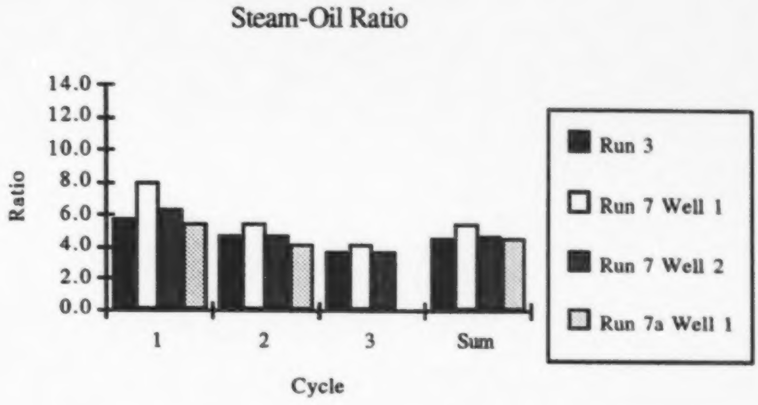

Figure 5.8.1.11 Multiwell cyclic steaming Runs 3 and 7 steam-oil ratio.

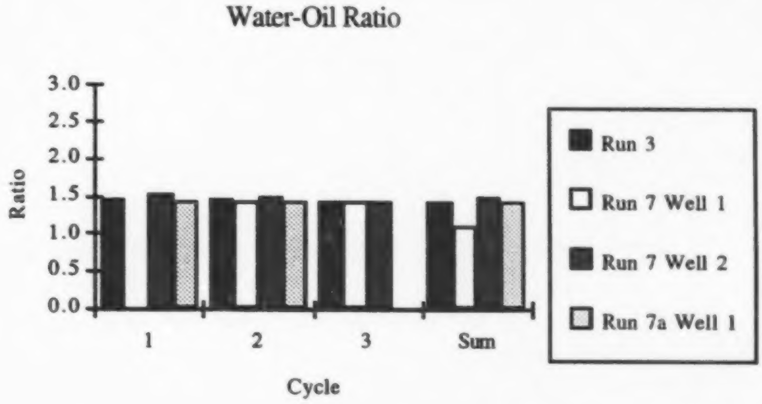

Figure 5.8.1.12 Multiwell cyclic steaming Runs 3 and 7 water-oil ratio.

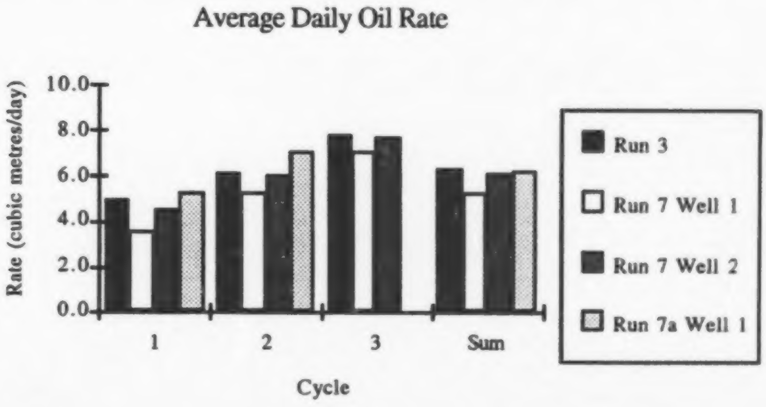

Figure 5.8.1.13 Multiwell cyclic steaming Runs 3 and 7 average daily oil rate.

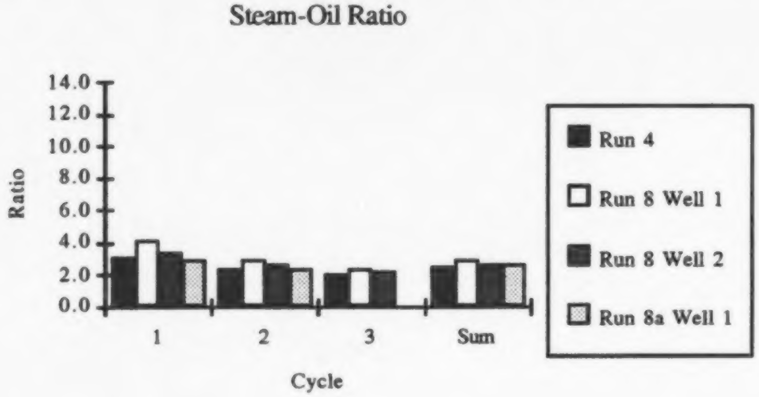

Figure 5.8.1.14 Multiwell cyclic steaming Runs 4 and 8 steam-oil ratio.

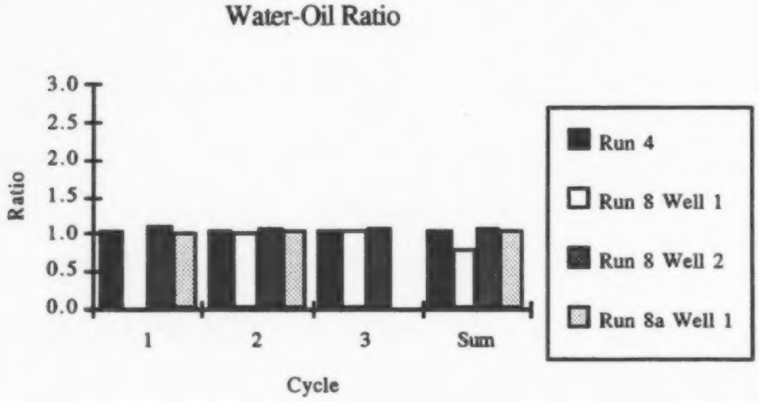

Figure 5.8.1.15 Multiwell cyclic steaming Runs 4 and 8 water-oil ratio.

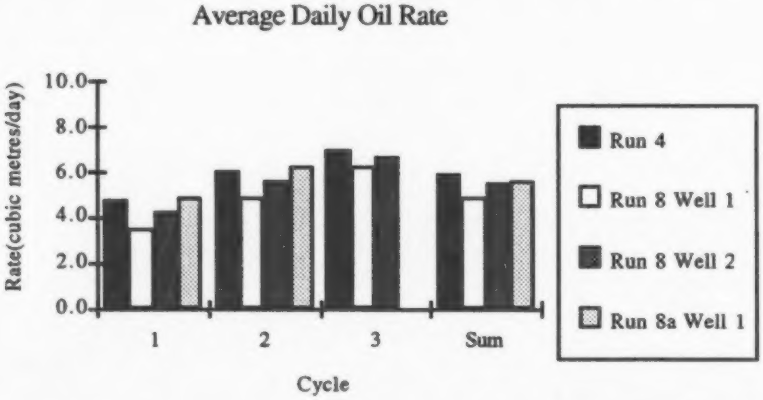

Figure 5.8.1.16 Multiwell cyclic steaming Runs 4 and 8 average daily oil rate.

Ranking by minimum SOR

Run	SOR	WOR	ADOR
4	2.4	1.0	5.9
8a	2.6	1.0	5.6
8.2	2.6	1.1	5.5
6a	3.5	1.3	8.1
2	3.8	1.4	7.5
6.2	3.9	1.4	7.3
3	4.5	1.4	6.3
7a	4.6	1.4	6.2
7.2	4.7	1.5	6.1
5a	8.3	1.9	6.8
5.2	9.0	2.0	6.4
1	9.1	1.9	6.2

Ranking by Minimum WOR

Run	SOR	WOR	ADOR
4	2.4	1.0	5.9
8a	2.6	1.0	5.6
8.2	2.6	1.1	5.5
6a	3.5	1.3	8.1
2	3.8	1.4	7.5
6.2	3.9	1.4	7.3
3	4.5	1.4	6.3
7a	4.6	1.4	6.2
7.2	4.7	1.5	6.1
5a	8.3	1.9	6.8
1	9.1	1.9	6.2
5.2	9.0	2.0	6.4

Ranking by Maximum ADOR

Run	SOR	WOR	ADOR
6a	3.5	1.3	8.1
2	3.8	1.4	7.5
6.2	3.9	1.4	7.3
5a	8.3	1.9	6.8
5.2	9.0	2.0	6.4
3	4.5	1.4	6.3
7a	4.6	1.4	6.2
1	9.1	1.9	6.2
7.2	4.7	1.5	6.1
4	2.4	1.0	5.9
8a	2.6	1.0	5.6
8.2	2.6	1.1	5.5

Table 5.8.1.3 Multiwell cyclic steaming Runs 1–8 ranking

Run/ Well	Cycle	Q_{inj} (m^3)	Q_w (m^3)	Q_o (m^3)	Time Inject (days)	Time Prod (days)	SOR	SOR cum	WOR	WOR cum	ADOR (m^3/d)
9/1	1	1974.3	584.4	513.1	20.0	70.0	3.8	3.8	1.1	1.1	7.3
	2	2000.0	800.6	598.9	20.0	70.0	3.3	3.6	1.3	1.2	8.6
	3	2000.0	825.2	575.2	20.0	70.0	3.5	3.5	1.4	1.3	8.2
	4	1999.8	844.9	547.3	20.0	69.0	3.7	3.6	1.5	1.4	7.9
	5	2101.5	449.4	193.4	21.0	35.0	10.9	4.1	2.3	1.4	5.5
	Sum	10075.6	3504.5	2427.9	101.0	314.0	4.1		1.4		7.7
9/2	1	1974.3	356.5	188.7	20.0	35.0	10.5	10.5	1.9	1.9	5.4
	2	2000.0	832.2	567.7	20.0	70.0	3.5	5.3	1.5	1.6	8.1
	3	2000.0	834.6	565.3	20.0	70.0	3.5	4.5	1.5	1.5	8.1
	4	2000.0	849.9	550.1	20.0	70.0	3.6	4.3	1.5	1.5	7.9
	5	1868.8	881.4	556.1	18.7	71.3	3.4	4.1	1.6	1.5	7.8
	Sum	9843.1	3754.6	2427.9	98.7	316.3	4.1		1.5		7.7
10	1	1974.3	538.1	432.3	20.0	70.0	4.6	4.6	1.2	1.2	6.2
	2	2000.0	791.8	577.8	20.0	70.0	3.5	3.9	1.4	1.3	8.3
	3	2000.0	831.1	568.9	20.0	70.0	3.5	3.8	1.5	1.4	8.1
	4	1999.5	893.8	506.3	20.0	70.0	3.9	3.8	1.8	1.5	7.2
	5	1999.9	909.1	495.2	20.0	70.0	4.0	3.9	1.8	1.5	7.1
	Sum	9973.7	3963.9	2580.5	100.0	350.0	3.9		1.5		7.4

Table 5.8.1.4 Multiwell cyclic steaming Runs 9 and 10 results summary.

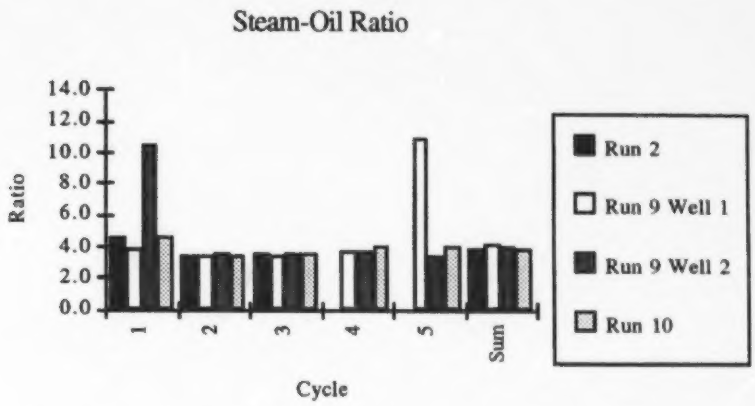

Figure 5.8.1.17 Multiwell cyclic steaming Runs 2, 9 and 10 steam-oil ratio.

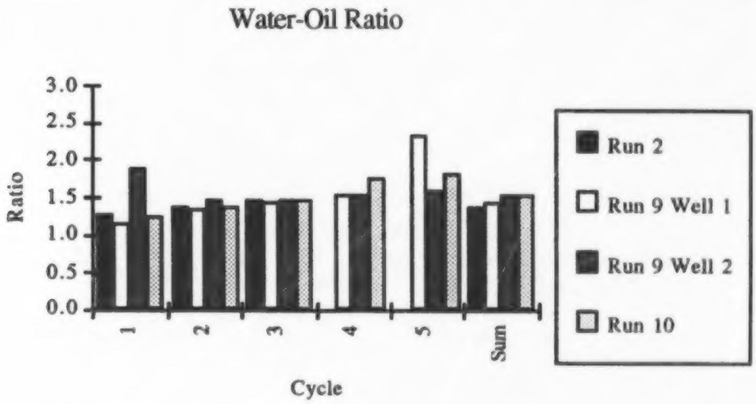

Figure 5.8.1.18 Multiwell cyclic steaming Runs 2, 9 and 10 water-oil ratio.

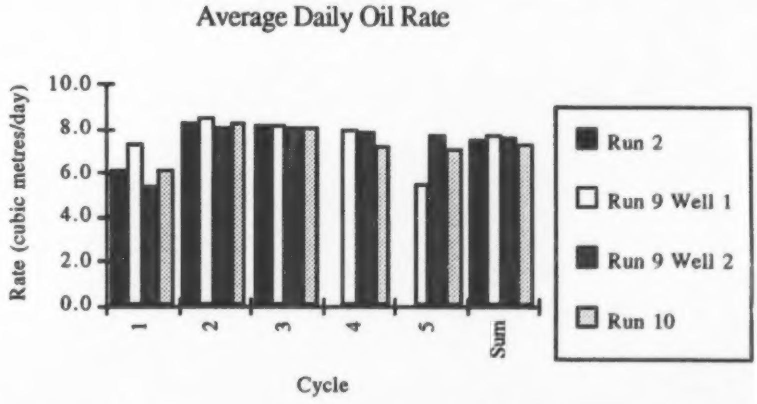

Figure 5.8.1.19 Multiwell cyclic steaming Runs 2, 9 and 10 average daily oil rate.

5.8.2 Four-Well Runs

Two runs with four regions were studied. Both runs were very similar, the major difference being which pair of wells were cycled together. Figure 5.8.2.1 summarizes the data and operating conditions, Tables 5.8.2.1 and 5.8.2.2 summarize the results of Runs 12 and 13, which are illustrated in Figures 5.8.2.2 to 5.8.2.7. Figure 5.8.2.2 illustrates the SOR, Figure 5.8.2.3 illustrates the WOR and Figure 5.8.2.4 illustrates the ADOR for Run 12 while Figure 5.8.2.5 illustrates the SOR, Figure 5.8.2.6 illustrates the WOR and Figure 5.8.2.7 illustrates the ADOR for Run 13.

For both runs, the paired wells behaviour was identical. In addition, the wells which had the longer production period on the first cycle performed better; that is, the SOR was lower (Figures 5.8.2.2 and 5.8.2.5), the WOR was lower (Figures 5.8.2.3 and 5.8.2.6) and the ADOR was higher (Figures 5.8.2.4 and 5.8.2.7) although this advantage diminished in later cycles.

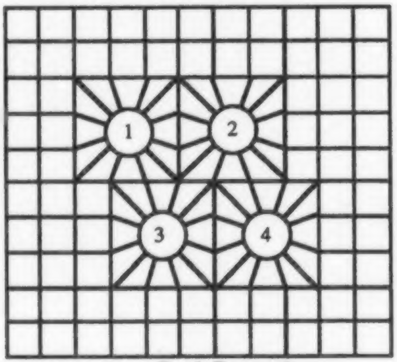
Runs Cyclic 12 and 13

- Grid Dimensions
  All grid blocks are the same size
  $\Delta x =$ 97.5 metres
  $\Delta y =$ 97.5 metres
  $\Delta z =$ 24.4 metres

- Rock Properties
  $k_x = k_y = 2000$ md
  $k_r = k_\theta = 2000$ md
  $k_z = 1000$ md
  $\phi = 0.30$

- Initial Conditions
  $P = 500$ kPa
  $T = 51.7$ °C
  $S_w = 0.20$
  $S_o = 0.80$
  $S_g = 0.00$

	Region 1	Region 2	Region 3	Region 4
Δr_1	25.0	25.0	25.0	25.0
Δr_2	140.0*	140.0*	140.0*	140.0*

* calculated internally

Figure 5.8.2.1 Multiwell cyclic steaming Runs 12 and 13 data summary.
(continued next page)

- Operating Conditions

Fixed parameters		Variable parameters	
BHP_{max} (kPa)	6900	Production time (days)	15, 35 & 70
BHP_{min} (kPa)	120	Mode together and staggered	
q_L (m^3/d)	20	No. of cycles	3 & 4
q_T (m^3/d)	100		
x	0.7		
T_{inj} (°C)	250		

	Run Cyclic 12				Run Cyclic 13			
Time (days)	Regions 2 and 3		Regions 1 and 4		Regions 1 and 3		Regions 2 and 4	
0–20	q_T (m^3/d)	100	q_T (m^3/d)	100	q_T (m^3/d)	100	q_T (m^3/d)	100
20–55	q_L (m^3/d)	20	q_L (m^3/d)	20	q_L (m^3/d)	20	q_L (m^3/d)	20
55–75	q_L (m^3/d)	20	q_T (m^3/d)	100	q_L (m^3/d)	20	q_T (m^3/d)	100
75–90	q_L (m^3/d)	20	q_L (m^3/d)	20	q_L (m^3/d)	20	q_L (m^3/d)	20
90–110	q_T (m^3/d)	100	q_L (m^3/d)	20	q_T (m^3/d)	100	q_L (m^3/d)	20
110–145	q_L (m^3/d)	20	q_L (m^3/d)	20	q_L (m^3/d)	20	q_L (m^3/d)	20
145–165	q_L (m^3/d)	20	q_T (m^3/d)	100	q_L (m^3/d)	20	q_T (m^3/d)	100
165–180	q_L (m^3/d)	20	q_L (m^3/d)	20	q_L (m^3/d)	20	q_L (m^3/d)	20
180–200	q_T (m^3/d)	100	q_L (m^3/d)	20	q_T (m^3/d)	100	q_L (m^3/d)	20
200–235	q_L (m^3/d)	20	q_L (m^3/d)	20	q_L (m^3/d)	20	q_L (m^3/d)	20
235–255	q_L (m^3/d)	20	q_T (m^3/d)	100	q_L (m^3/d)	20	q_T (m^3/d)	100
255–270	q_L (m^3/d)	20	q_L (m^3/d)	20	q_L (m^3/d)	20	q_L (m^3/d)	20

- Well Parameters

	Well/Region 1	Well/Region 2
Index	+1/-1	+1/-1
Productivity	Internally calculated	Internally calculated
J* multiplier	1.0	1.0
f_h	1.0	1.0
f	1.0	1.0
c_g	0.5	0.5
s	0.0	0.0
r_w (metres)	0.09	0.09

Figure 5.8.2.1 Multiwell cyclic steaming Runs 12 and 13 data summary. (continued from previous page)

Well	Cycle	Q_{inj} (m^3)	Q_w (m^3)	Q_o (m^3)	Time Inject (days)	Time Prod (days)	SOR	SOR cum	WOR	WOR cum	ADOR (m^3/d)
1	1	1974.3	440.2	256.4	20.0	35.0	7.7	7.7	1.7	1.7	7.3
	2	2000.0	829.2	570.7	20.0	70.0	3.5	4.8	1.5	1.5	8.2
	3	1752.3	846.7	602.8	17.5	72.5	2.9	4.0	1.4	1.5	8.3
	4	1999.9	192.1	107.9	20.0	15.0	18.5	5.0	1.8	1.5	7.2
	Sum	7726.5	2308.2	1537.8	77.5	192.5	5.0		1.5		8.0
2	1	1974.3	702.2	694.3	20.0	70.0	2.8	2.8	1.0	1.0	9.9
	2	2000.2	793.0	607.1	20.0	70.0	3.3	3.1	1.3	1.1	8.7
	3	1999.7	825.2	575.0	20.0	70.0	3.5	3.2	1.4	1.2	8.2
	4										
	Sum	5974.2	2320.4	1876.4	60.0	210.0	3.2		1.2		8.9
3	1	1974.3	702.2	694.3	20.0	70.0	2.8	2.8	1.0	1.0	9.9
	2	2000.0	792.9	607.2	20.0	70.0	3.3	3.1	1.3	1.1	8.7
	3	1999.9	819.7	574.9	20.0	70.0	3.5	3.2	1.4	1.2	8.2
	4										
	Sum	5974.2	2314.8	1876.4	60.0	210.0	3.2		1.2		8.9
4	1	1974.3	440.3	256.3	20.0	35.0	7.7	7.7	1.7	1.7	7.3
	2	2000.0	829.2	570.7	20.0	70.0	3.5	4.8	1.5	1.5	8.2
	3	1752.3	846.7	602.8	17.5	72.5	2.9	4.0	1.4	1.5	8.3
	4	1999.9	192.1	108.0	20.0	15.0	18.5	5.0	1.8	1.5	7.2
	Sum	7726.5	2308.6	1537.8	77.5	192.5	5.0		1.5		8.0

Table 5.8.2.1 Multiwell cyclic steaming Run 12 results summary.

Well	Cycle	Q_{inj} (m^3)	Q_w (m^3)	Q_o (m^3)	Time Inject (days)	Time Prod (days)	SOR	SOR cum	WOR	WOR cum	ADOR (m^3/d)
1	1	1974.3	702.7	693.9	20.0	70.0	2.8	2.8	1.0	1.0	9.9
	2	2000.0	797.3	602.6	20.0	70.0	3.3	3.1	1.3	1.2	8.6
	3	2000.0	828.0	572.1	20.0	70.0	3.5	3.2	1.4	1.2	8.2
	4										
	Sum	5974.3	2328.0	1868.6	60.0	210.0	3.2		1.2		8.9
2	1	1974.3	440.4	256.4	20.0	35.0	7.7	7.7	1.7	1.7	7.3
	2	2000.2	834.6	565.2	20.0	70.0	3.5	4.8	1.5	1.6	8.1
	3	1774.3	843.1	602.0	17.7	72.3	2.9	4.0	1.4	1.5	8.6
	4	2000.0	192.2	107.8	20.0	15.0	18.6	5.1	1.8	1.5	7.2
	Sum	7748.8	2310.3	1531.4	80.0	190.0	5.1		1.5		8.1
3	1	1974.3	702.6	694.0	20.0	70.0	2.8	2.8	1.0	1.0	9.9
	2	2000.0	797.9	602.1	20.0	70.0	3.3	3.1	1.3	1.2	8.6
	3	2000.0	828.9	571.2	20.0	70.0	3.5	3.2	1.5	1.2	8.2
	4										
	Sum	5974.3	2329.4	1867.3	60.0	210.0	3.2		1.2		8.9
4	1	1974.3	440.3	256.3	20.0	35.0	7.7	7.7	1.7	1.7	7.3
	2	2000.2	833.9	566.0	20.0	70.0	3.5	4.8	1.5	1.5	8.1
	3	1774.3	842.3	602.9	17.7	72.3	2.9	4.0	1.4	1.5	8.6
	4	2000.0	192.1	107.9	20.0	15.0	18.5	5.1	1.8	1.5	7.2
	Sum	7748.8	2308.6	1533.1	80.0	190.0	5.1		1.5		8.1

Table 5.8.2.2 Multiwell cyclic steaming Run 13 results summary.

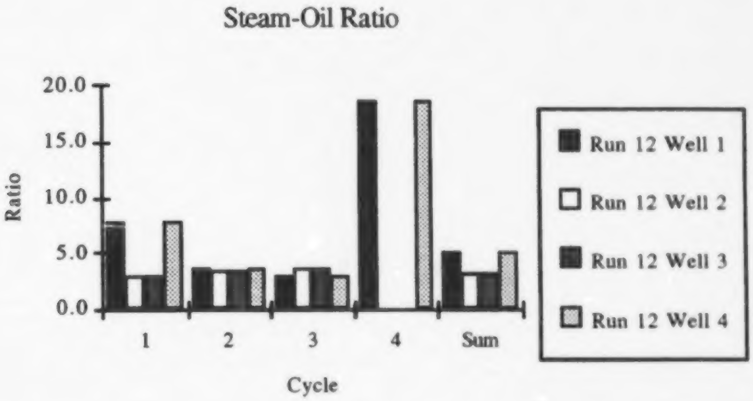

Figure 5.8.2.2 Multiwell cyclic steaming Run 12 steam-oil ratio.

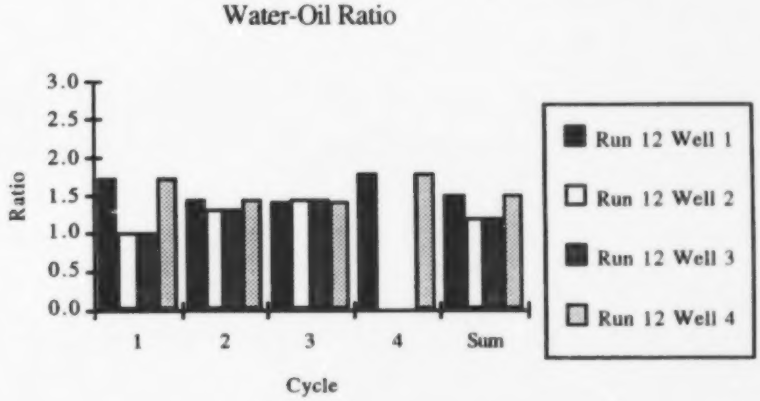

Figure 5.8.2.3 Multiwell cyclic steaming Run 12 water-oil ratio.

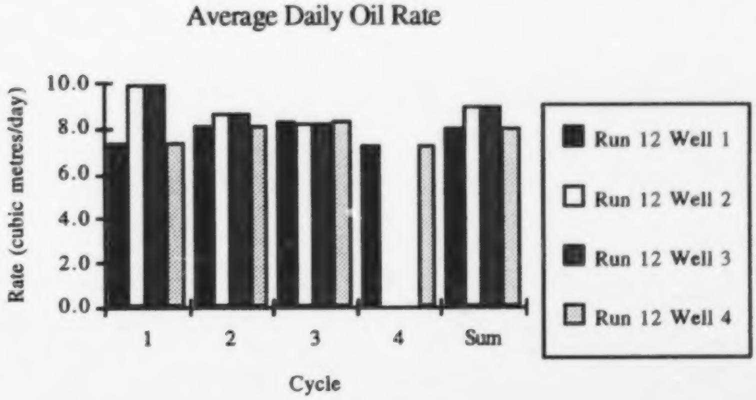

Figure 5.8.2.4 Multiwell cyclic steaming Run 12 average daily oil rate.

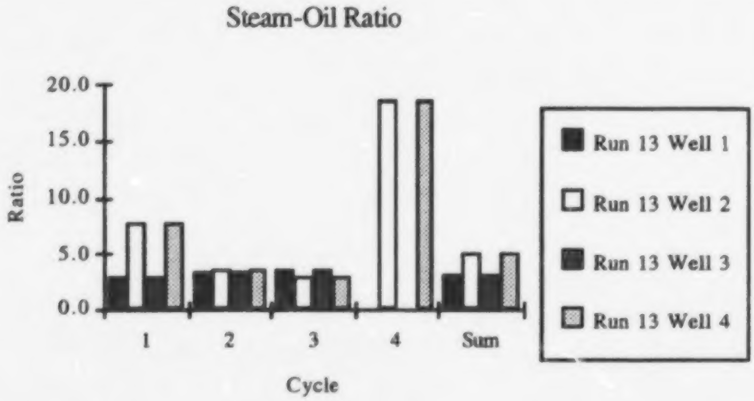
Steam-Oil Ratio

Figure 5.8.2.5 Multiwell cyclic steaming Run 13 steam-oil ratio.

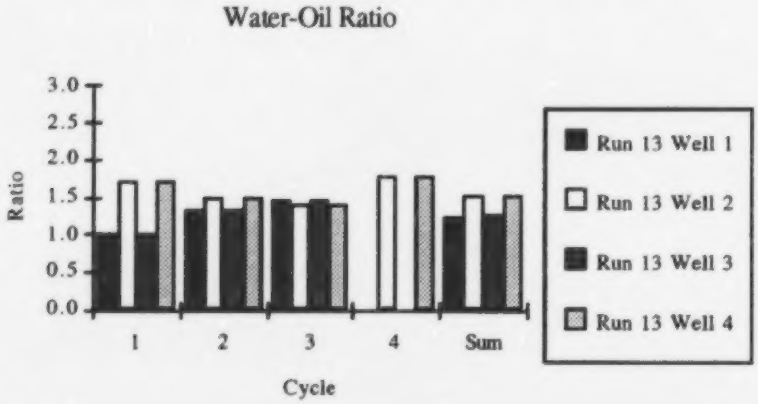
Water-Oil Ratio

Figure 5.8.2.6 Multiwell cyclic steaming Run 13 water-oil ratio.

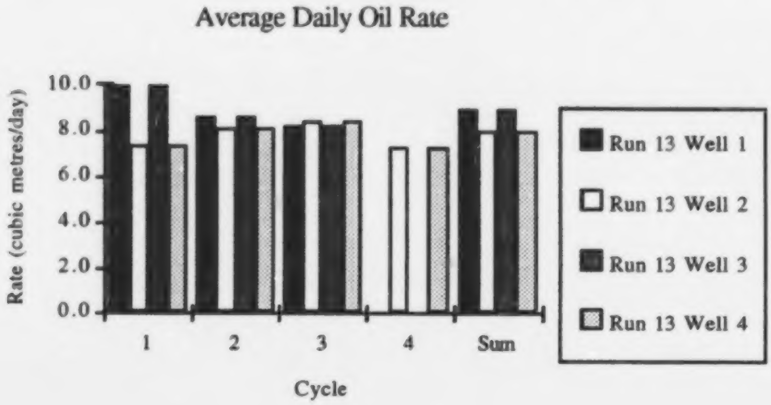
Average Daily Oil Rate

Figure 5.8.2.7 Multiwell cyclic steaming Run 13 average daily oil rate.

5.9 Cyclic to Continuous Steaming

The objective of this section is to show the use of hyperhybrid grids to study the behaviour of a pair of cyclic steaming wells when one is maintained on continuous injection after a number of cycles. The parameters varied were continuous steam injection rate, continuous steam injection time, number of cycles prior to continuous steam injection and non-Newtonian oil behaviour.

The grid design and properties used were the same as in the previous section and they are illustrated in Figure 5.8.1.1 (pages 226–227). The operating conditions for each run are shown in Table 5.9.0.1.

Table 5.9.0.2 summarizes the results of the runs for the continuous injection period. For each run, the injection and production rates, well grid block pressure and temperature and well pressure history versus time as well as pressure, temperature and oil saturation profiles between wells at selected times are presented in Figures 5.9.0.1 to 5.9.0.40. Figures 5.9.0.1 to 5.9.0.8 are for Run 1, Figures 5.9.0.9 to 5.9.0.16 are for Run 2, Figures 5.9.0.17 to 5.9.0.24 are for Run 3, Figures 5.9.0.25 to 5.9.0.32 are for Run 4 and Figures 5.9.0.33 to 5.9.0.40 are for Run 5.

Runs 1 and 2 differed in the rate of continuous steam injection. The result was a lower SOR for Run 2; however, Run 1 had the higher oil rate, producing almost 200 m^3 more. Figure 5.9.0.2 shows that the oil production rate was still increasing at the end of the run whereas the rate in Run 2 (Figure 5.9.0.10) was reaching a plateau. The well pressure for the producing well in both runs was at the specified operating minimum. At the end of the run, the pressure profile between wells was much steeper in Run 1 (Figures 5.9.0.6 and 5.9.0.14). Also, the temperature in the injection well block was higher in Run 1, although the heat had not moved out of the grid block yet as can be seen in the temperature profiles (Figures 5.9.0.7 and 5.9.0.15). Consistent with these results are the oil saturation profiles (Figures 5.9.0.8 and 5.9.0.16).

Although Runs 3 and 4, with the same number of cycles per well prior to continuous steaming, differed in both the rate of continuous steam injection and continuous steam injection time, the total volume of steam injected was somewhat similar (difference of approximately 10%) as can be seen in Figures 5.9.0.17 and 5.9.0.25 for Runs 3 and 4, respectively. Run 4, with the larger time for production, had the better SOR and almost twice the oil production. Note that the produced water was less than doubled in Run 4. Comparing Figures 5.9.0.18 and 5.9.0.26, the production rate of Run 3 was similar to the production rate of the early part of the continuous period in Run 4. Clearly, Run 4 benefitted from a longer continuous injection, hence, production period. It is interesting to note that the pressure profile between wells was higher for Run 3 due to the higher injection rate (Figures 5.9.0.22 and 5.0.0.30) whereas the temperature profiles differed very little as can be seen in Figures 5.9.0.23 and 5.9.0.31 for Runs 3 and 4, respectively. Also the oil saturation profiles differed very little (Figures 5.9.0.24 and 5.9.0.32) although Run 4 had a slightly higher oil saturation at the end of the run.

The major difference between Runs 2 and 4 was the number of steaming cycles prior to continuous steam injection. The SOR for the continuous period was similar for both runs whereas the WOR was much higher for Run 4. This higher WOR was due to the injection water from the previous cyclic steaming period returning to the well. The amount of water in Run 4 was almost 2.5 times greater. This would seem to suggest that fewer cycles prior to continuous steaming is better; however, examination of the well grid block pressure (Figures 5.9.0.11 and 5.9.0.27) showed that Run 4 had the potential for much more production. In addition, the production well pressure in Run 2 was operating at the specified minimum whereas Run 4 was not (Figures 5.9.0.13 and 5.9.0.29). The oil saturation profiles (Figures 5.9.0.16 and 5.9.0.32) and grid block temperature profiles (Figures 5.9.0.15 and 5.9.0.31) showed the effects of multiple cycles prior to continuous steam injection. Run 4 was much hotter and more water was in the well grid block at the end of the run. Lastly, the pressure profile between wells was higher and slightly steeper for Run 4 (Figures 5.9.0.14 and 5.9.0.30). Run 4 would have benefitted from a longer continuous injection period.

The non-Newtonian run (Run 5) can be compared with Run 4. Note that Run 4 was ten days shorter in the continuous period. The non-Newtonian run produced approximately 150 m^3 more oil and only 20 m^3 more water than Run 4. However, taking the difference in the continuous period into account, the runs performed similarly. Hence, the non-Newtonian oil affected only the behaviour locally as discussed in Section 5.6. Note, however, that the production rate at the end of the period was higher in Run 5. The well grid block pressures (Figures 5.9.0.27 and 5.9.0.35) were similar for both runs and as a consequence, the pressure profiles were very similar (Figures 5.9.0.30 and 5.9.0.38). The same is true for the well pressure (Figures 5.9.0.29 and 5.9.0.37). As a result of both runs receiving the same quantity of steam, the temperature profiles were very similar as seen in Figures 5.9.0.31 and 5.9.0.39 for Runs 4 and 5, respectively. Although the oil saturation profiles appear to be very similar (Figures 5.9.0.32 and 5.0.0.40), in Run 5 the oil saturation was slightly lower at the times indicated on the figures which accounts for Run 5 producing more oil than Run 4.

Run	Number of cycles	Cyclic**		Continuous***		
		q_T (m^3/day)	q_L (m^3/day)	Time (days)	q_T (m^3/day)	q_L (m^3/day)
1	1	100	20	100	50	20
2	1	100	20	100	25	20
3	3	100	20	50	50	20
4	3	100	20	100	25	20
5*	3	100	20	100	25	20

BHP$_{max}$ (kPa)	6900
BHP$_{min}$ (kPa)	120
x	0.7
T_{inj} (°C)	250

* non-Newtonian oil behaviour
** Cycle is 20 days injection and 35 days production
*** Continuous injection is in Region 2

Table 5.9.0.1 Cyclic to continuous steaming Runs 1–5 operating conditions.

Run	Time (days)	Steam injected (m^3)	Water produced (m^3)	Oil produced (m^3)	SOR	WOR
1	100.0	5000.0	437.9	1142.6	4.38	0.38
2	100.0	2499.6	396.9	935.7	2.68	0.43
3	49.6	2480.0	576.2	415.9	5.96	1.39
4	89.8	2244.3	974.4	821.2	2.73	1.19
5	100.0	2499.9	993.0	970.9	2.57	1.02

Table 5.9.0.2 Cyclic to continuous steaming Runs 1–5 results summary.

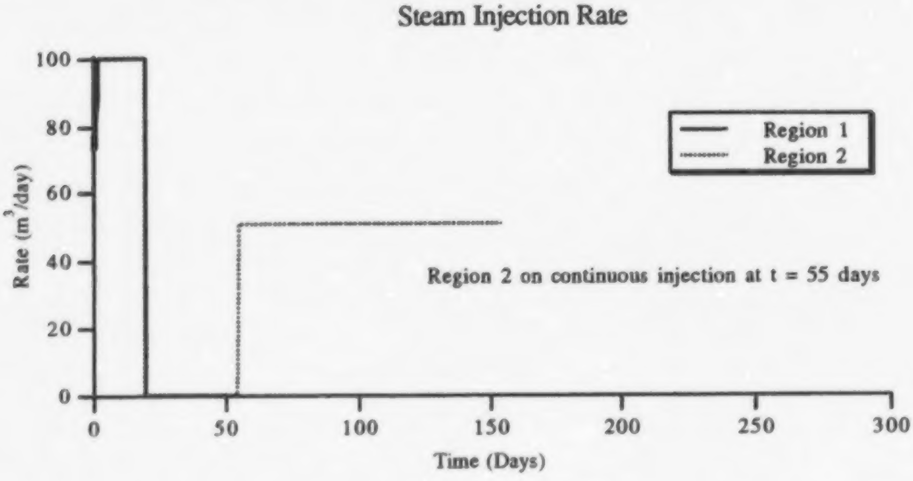

Figure 5.9.0.1 Cyclic to continuous steaming Run 1 Steam injection rate.

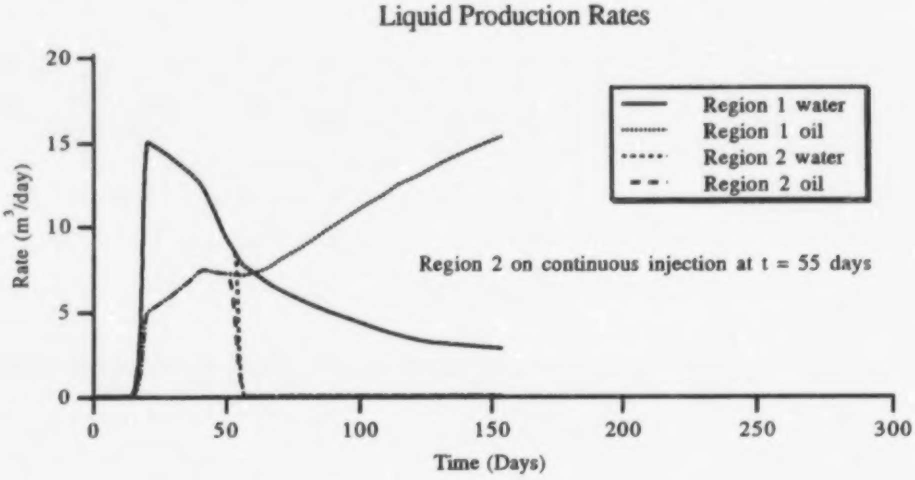

Figure 5.9.0.2 Cyclic to continuous steaming Run 1 Liquid production rates.

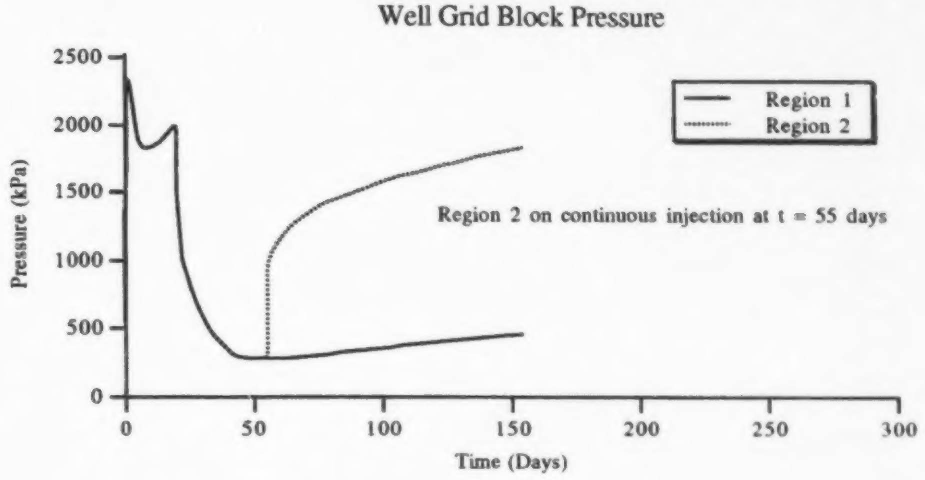

Figure 5.9.0.3 Cyclic to continuous steaming Run 1 Well grid block pressure.

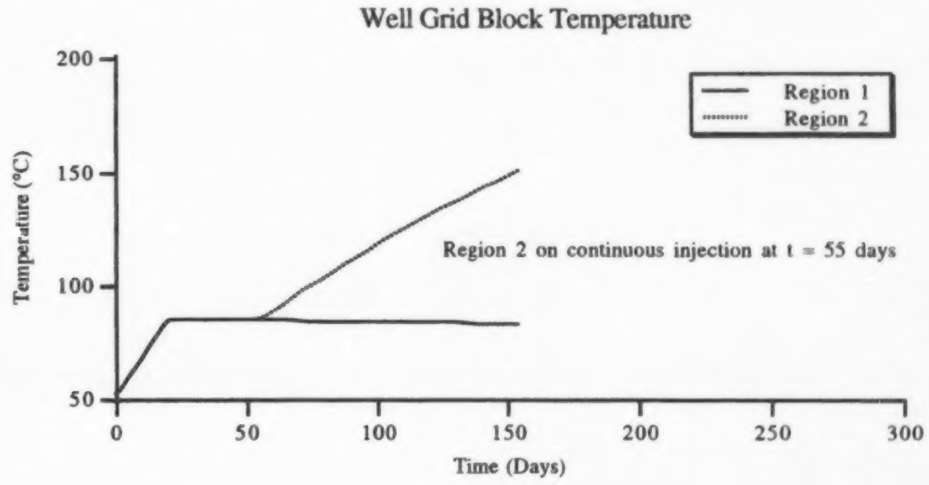

Figure 5.9.0.4 Cyclic to continuous steaming Run 1 Well grid block temperature.

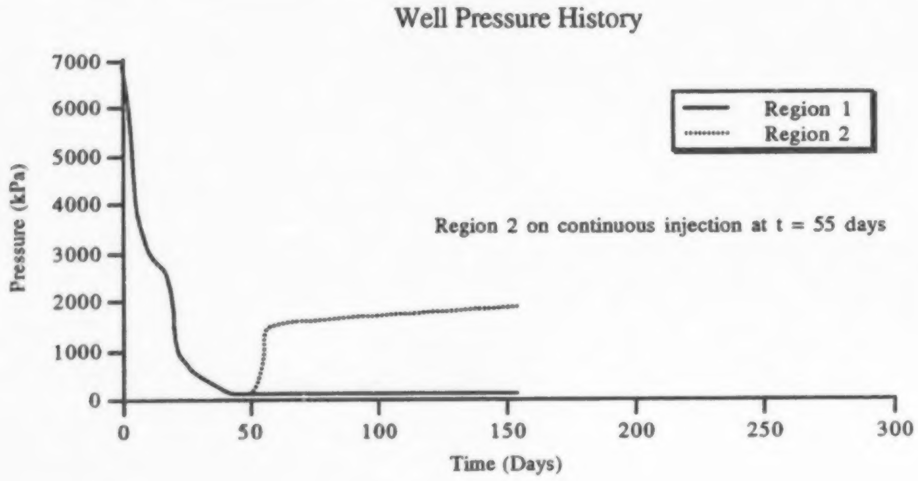

Figure 5.9.0.5 Cyclic to continuous steaming Run 1 Well pressure history.

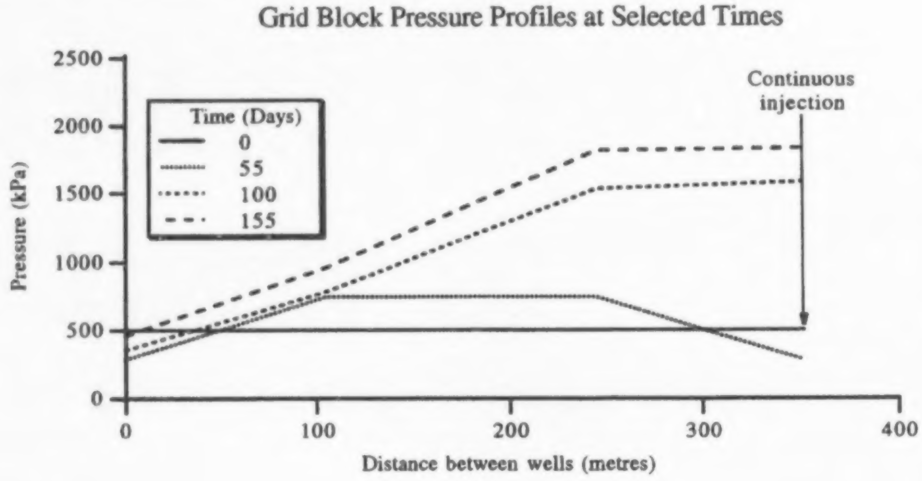

Figure 5.9.0.6

Cyclic to continuous steaming Run 1 Grid block pressure profiles at selected times.

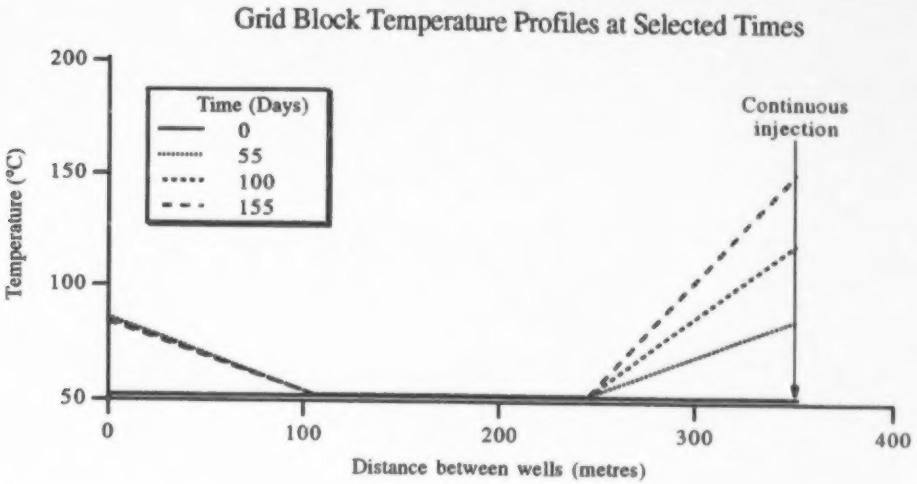

Figure 5.9.0.7

Cyclic to continuous steaming Run 1 Grid block temperature profiles at selected times.

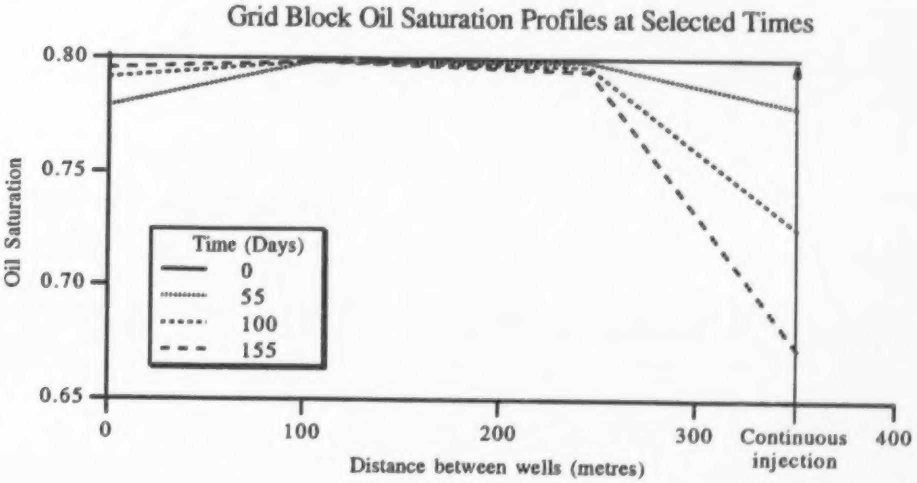

Figure 5.9.0.8

Cyclic to continuous steaming Run 1 Grid block oil saturation profiles at selected times.

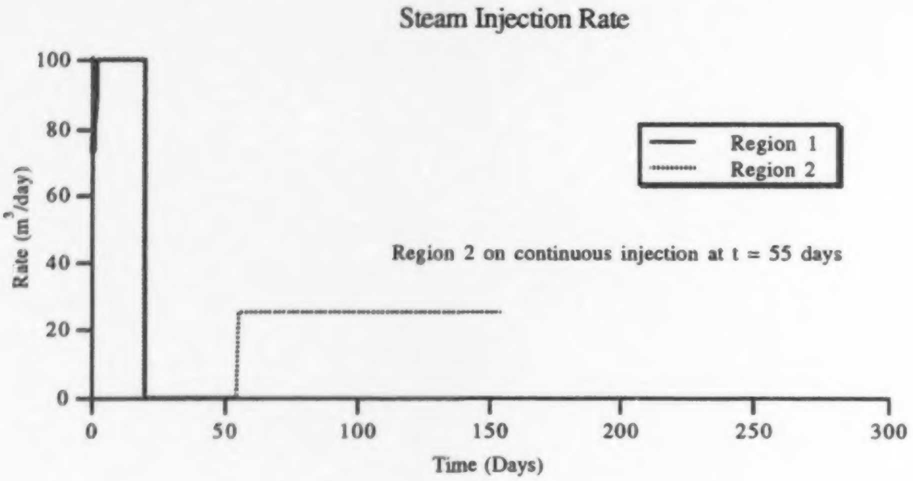

Figure 5.9.0.9 Cyclic to continuous steaming Run 2 Steam injection rate.

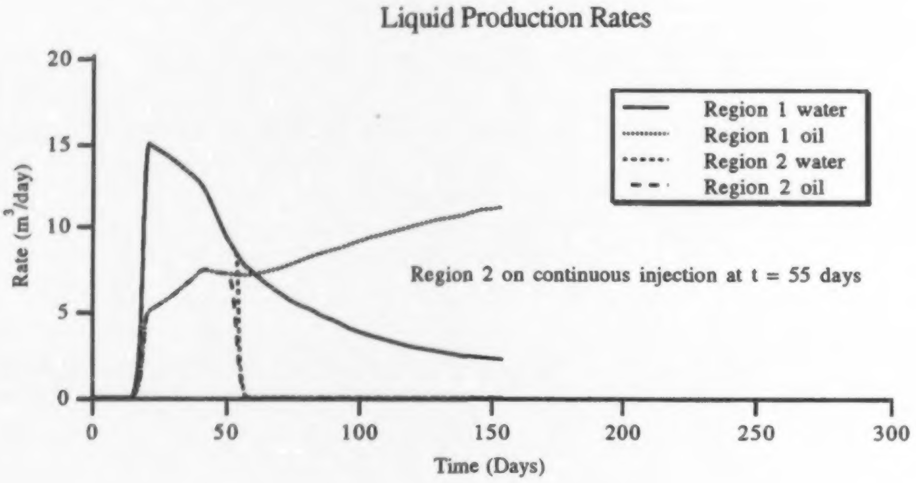

Figure 5.9.0.10 Cyclic to continuous steaming Run 2 Liquid production rates.

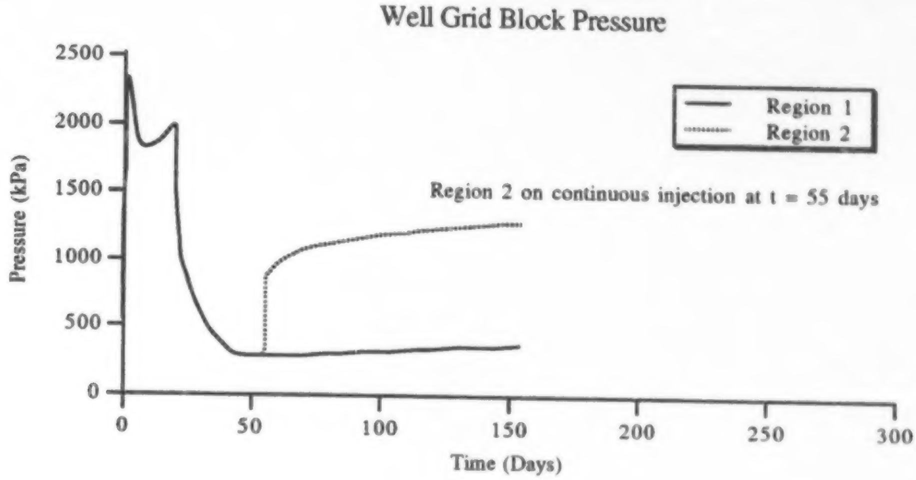

Figure 5.9.0.11 Cyclic to continuous steaming Run 2 Well grid block pressure.

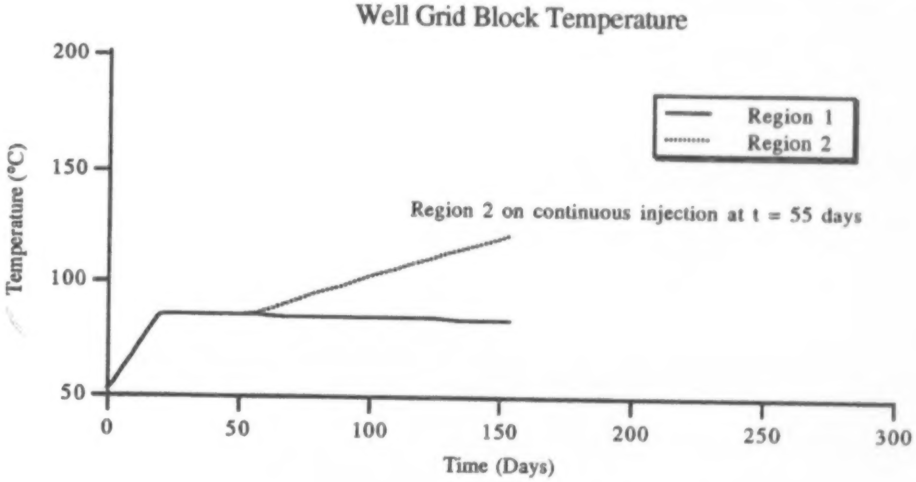

Figure 5.9.0.12 Cyclic to continuous steaming Run 2 Well grid block temperature.

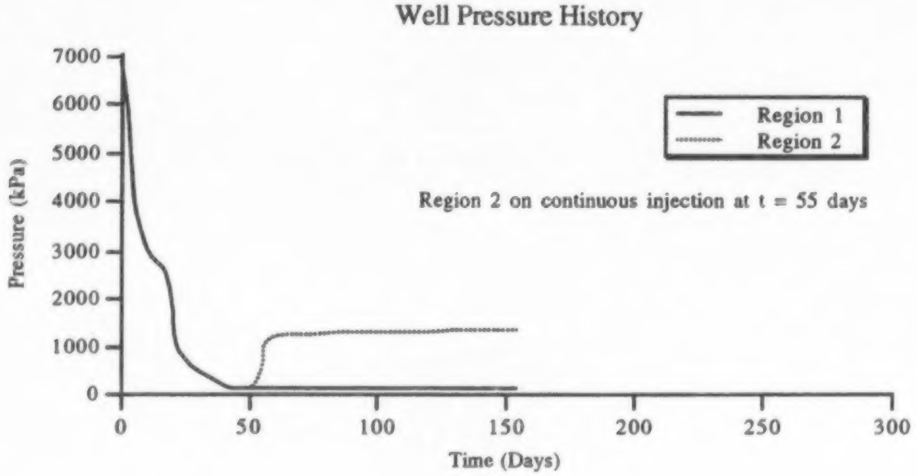

Figure 5.9.0.13 Cyclic to continuous steaming Run 2 Well pressure history.

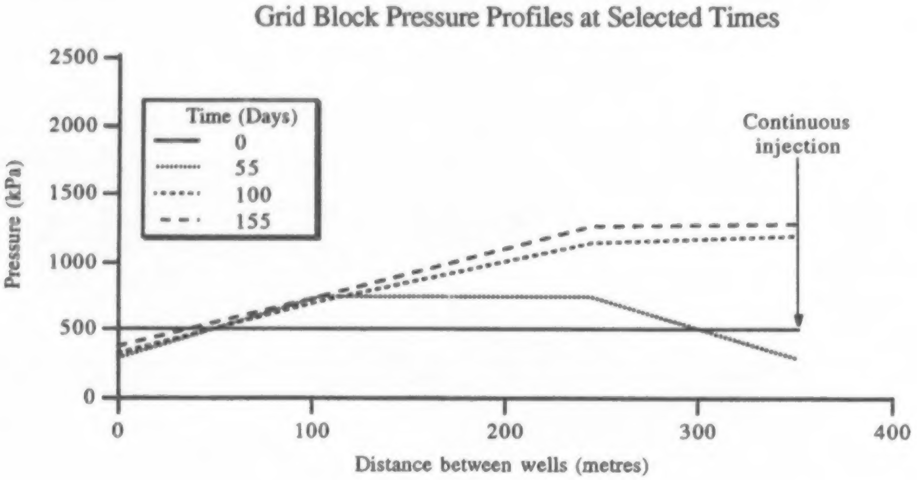

Figure 5.9.0.14

Cyclic to continuous steaming Run 2 Grid block pressure profiles at selected times.

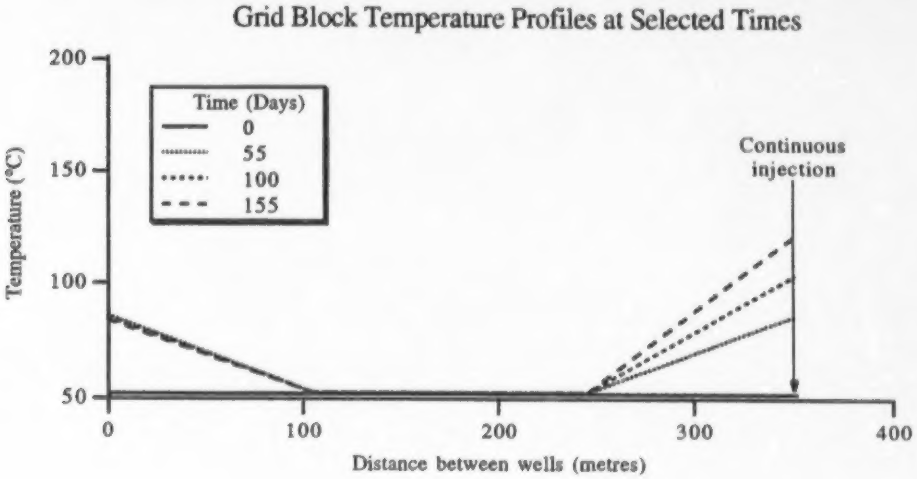

Figure 5.9.0.15

Cyclic to continuous steaming Run 2 Grid block temperature profiles at selected times.

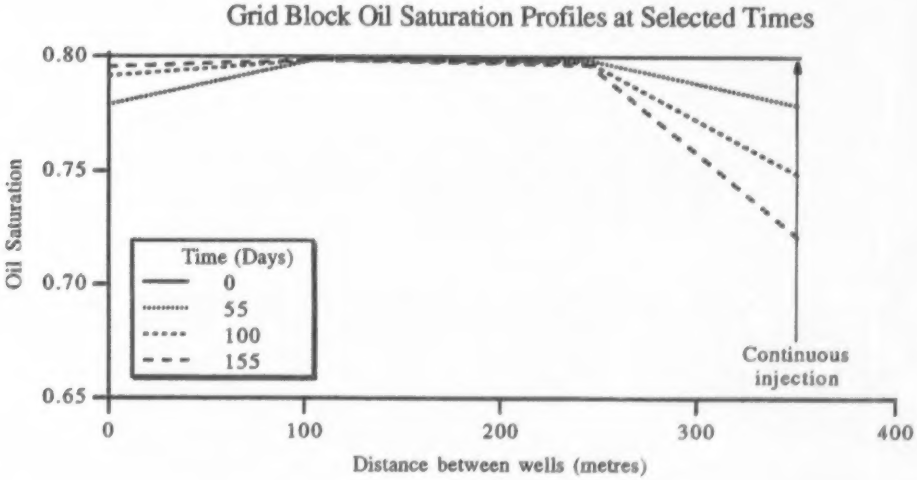

Figure 5.9.0.16

Cyclic to continuous steaming Run 2 Grid block oil saturation profiles at selected times.

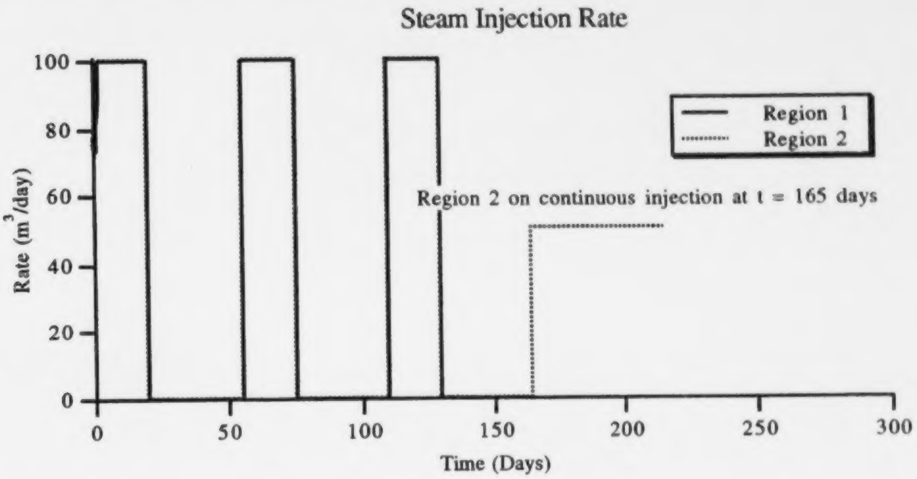

Figure 5.9.0.17 Cyclic to continuous steaming Run 3 Steam injection rate.

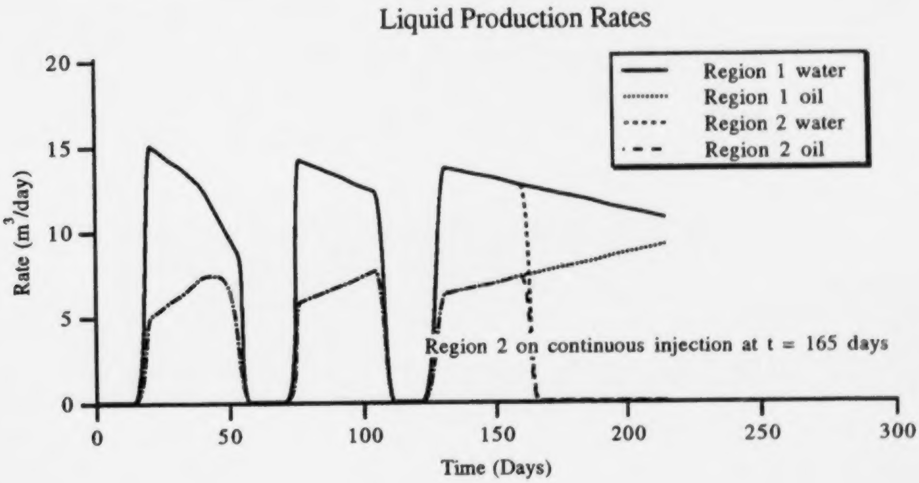

Figure 5.9.0.18 Cyclic to continuous steaming Run 3 Liquid production rates.

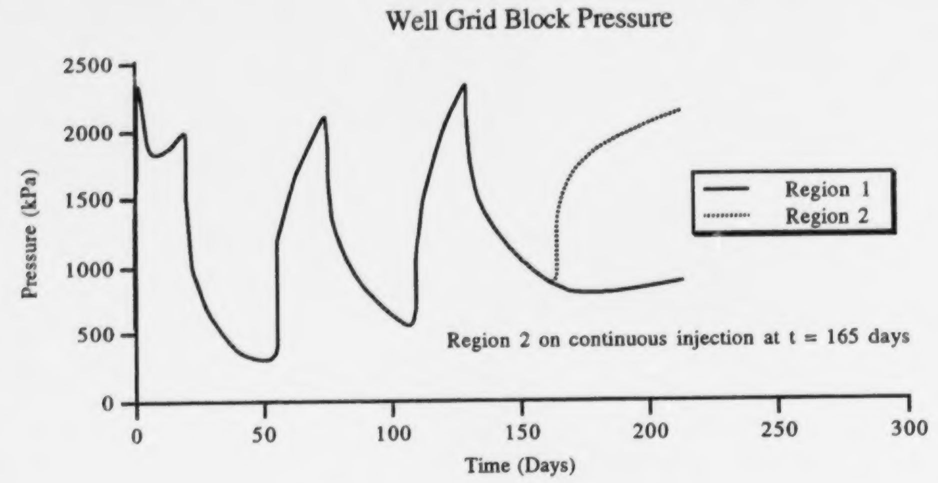

Figure 5.9.0.19 Cyclic to continuous steaming Run 3 Well grid block pressure.

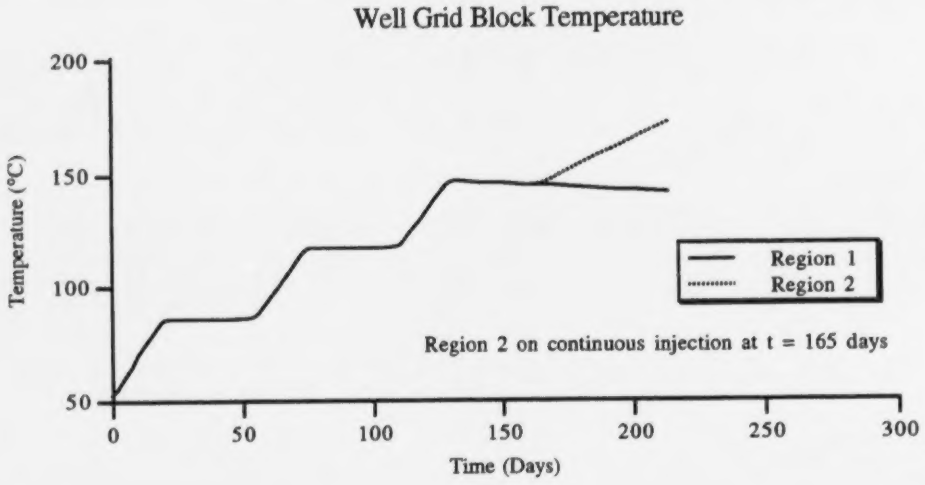

Figure 5.9.0.20 Cyclic to continuous steaming Run 3 Well grid block temperature.

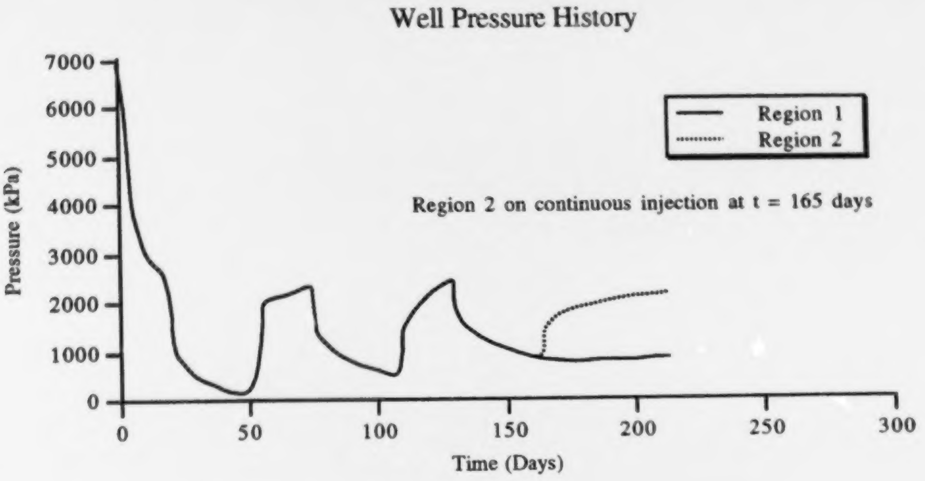

Figure 5.9.0.21 Cyclic to continuous steaming Run 3 Well pressure history.

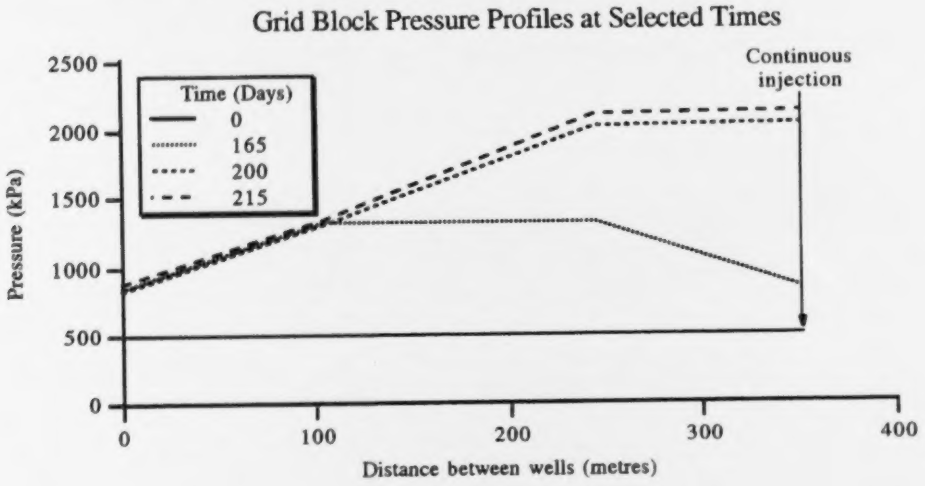

Figure 5.9.0.22

Cyclic to continuous steaming Run 3 Grid block pressure profiles at selected times.

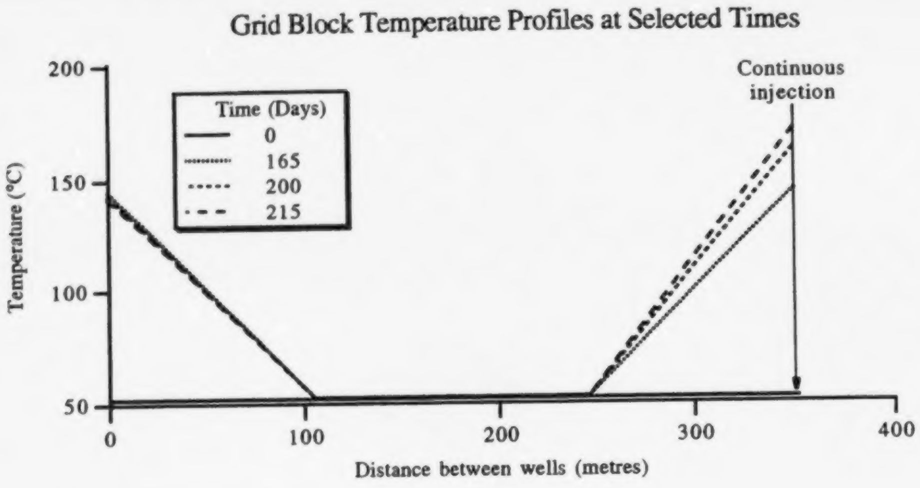

Figure 5.9.0.23

Cyclic to continuous steaming Run 3 Grid block temperature profiles at selected times.

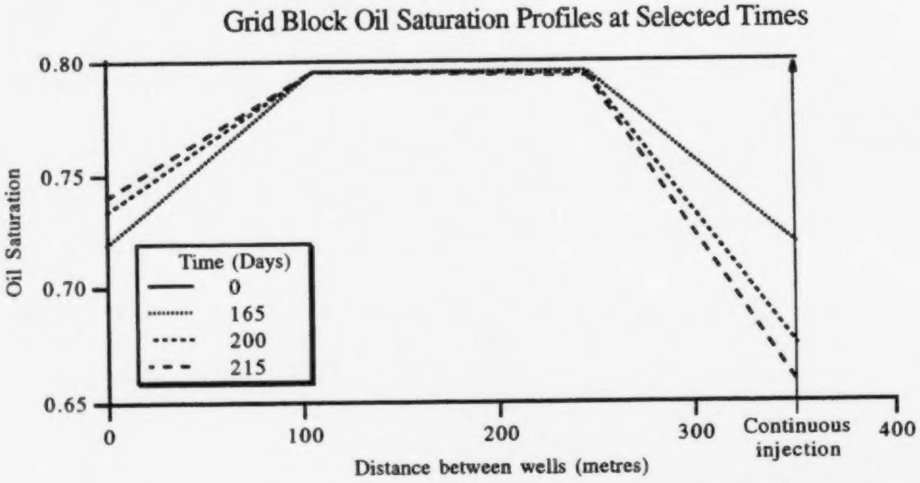

Figure 5.9.0.24

Cyclic to continuous steaming Run 3 Grid block oil saturation profiles at selected times.

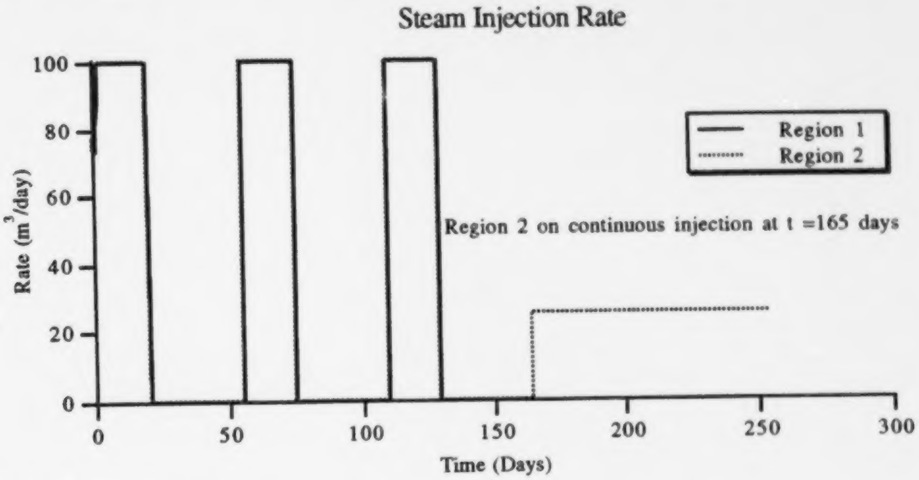

Figure 5.9.0.25 Cyclic to continuous steaming Run 4 Steam injection rate.

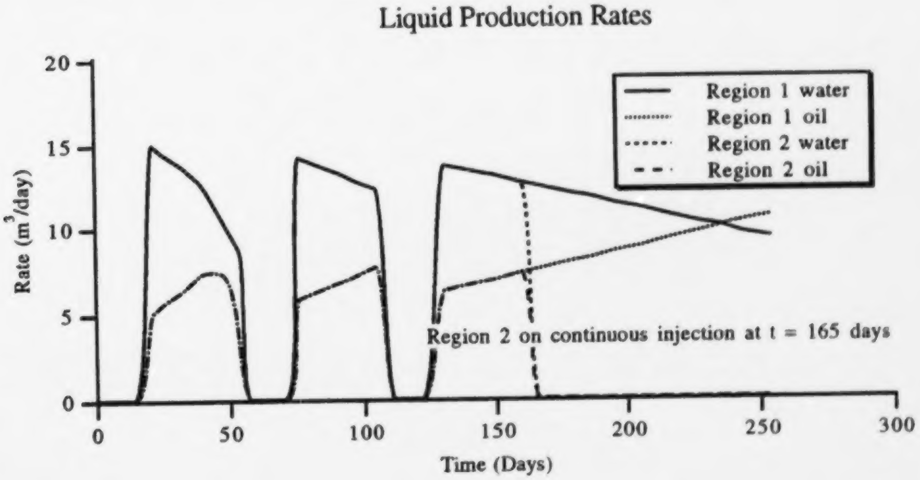

Figure 5.9.0.26 Cyclic to continuous steaming Run 4 Liquid production rates.

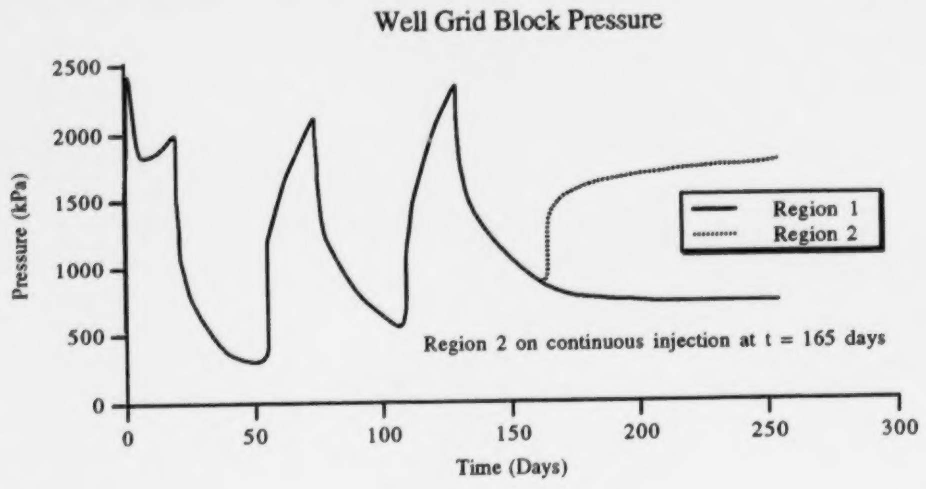

Figure 5.9.0.27 Cyclic to continuous steaming Run 4 Well grid block pressure.

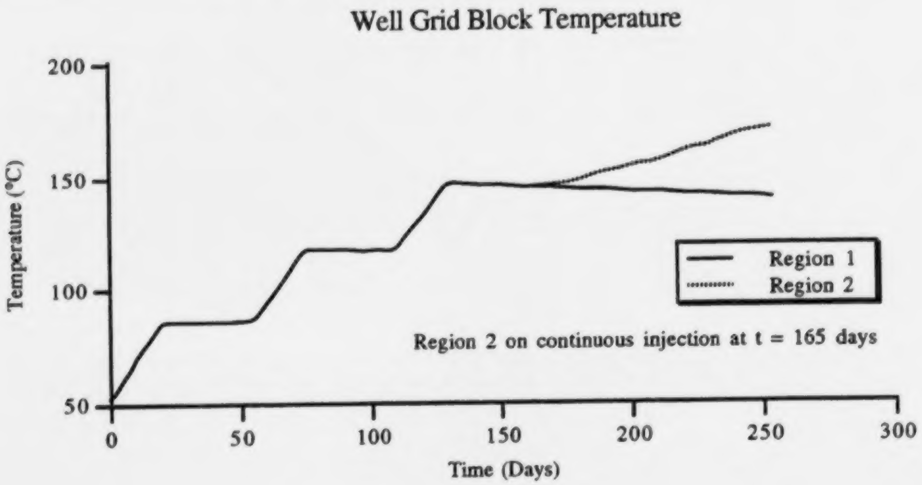

Figure 5.9.0.28 Cyclic to continuous steaming Run 4 Well grid block temperature.

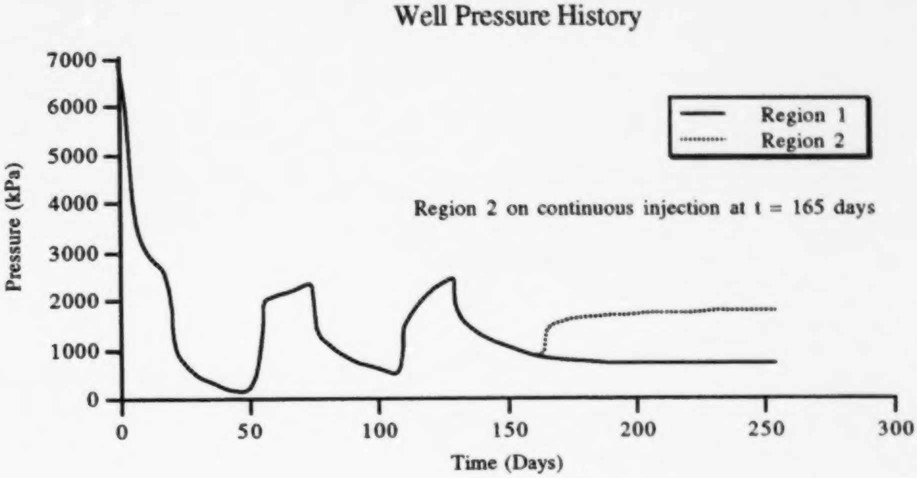

Figure 5.9.0.29 Cyclic to continuous steaming Run 4 Well pressure history.

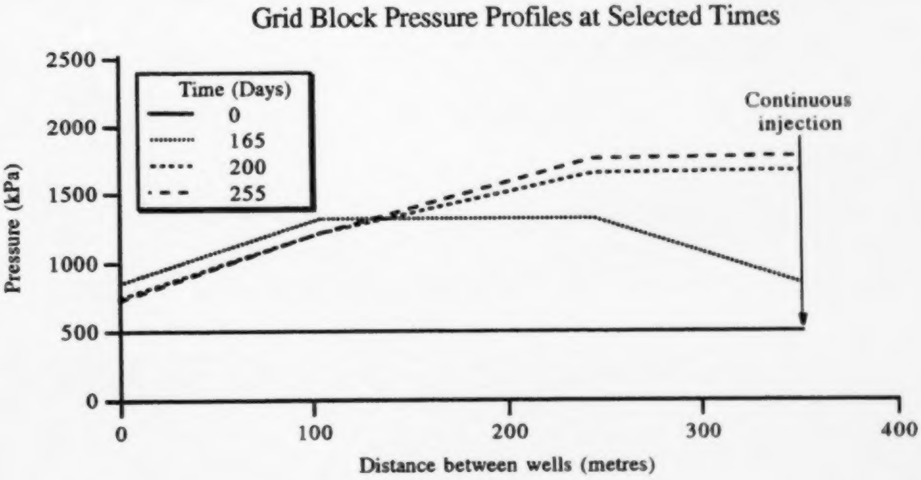

Figure 5.9.0.30

Cyclic to continuous steaming Run 4 Grid block pressure profiles at selected times.

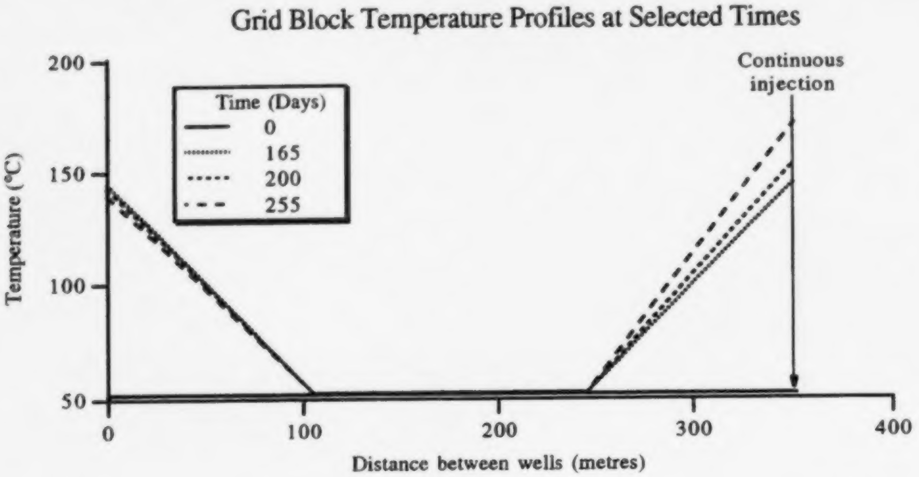

Figure 5.9.0.31

Cyclic to continuous steaming Run 4 Grid block temperature profiles at selected times.

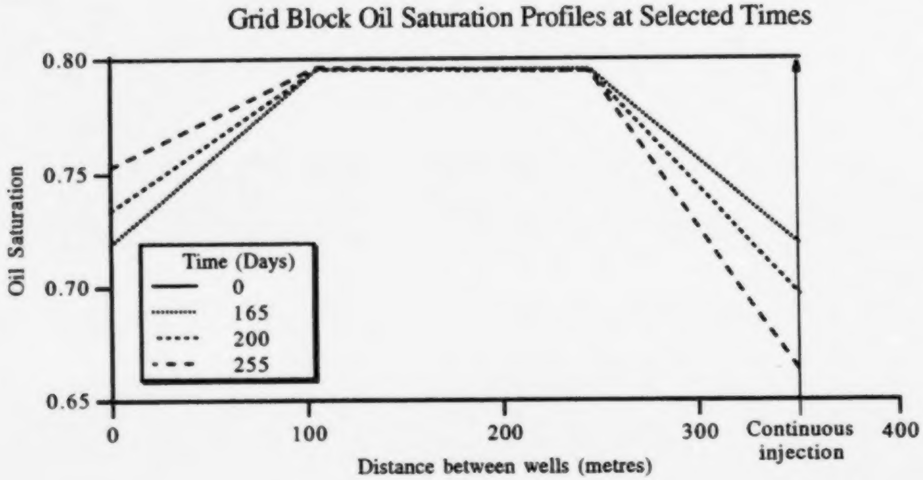

Figure 5.9.0.32

Cyclic to continuous steaming Run 4 Grid block oil saturation profiles at selected times.

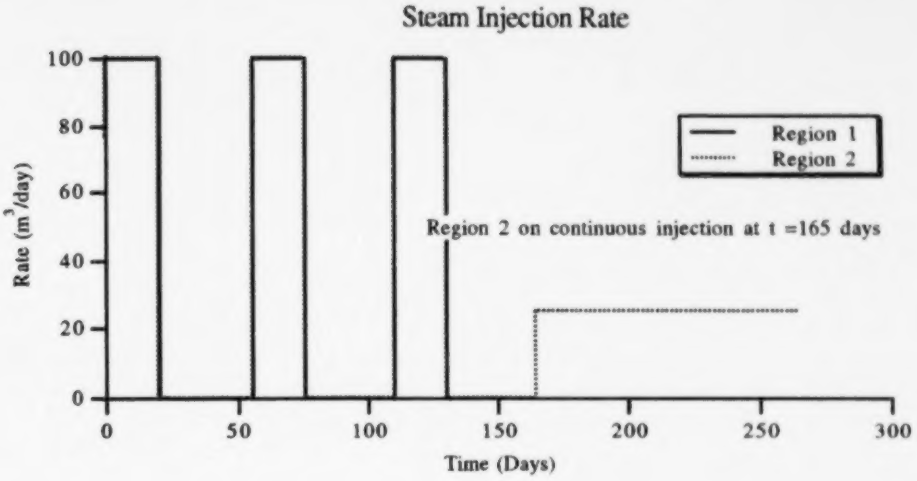

Figure 5.9.0.33 Cyclic to continuous steaming Run 5 Steam injection rate.

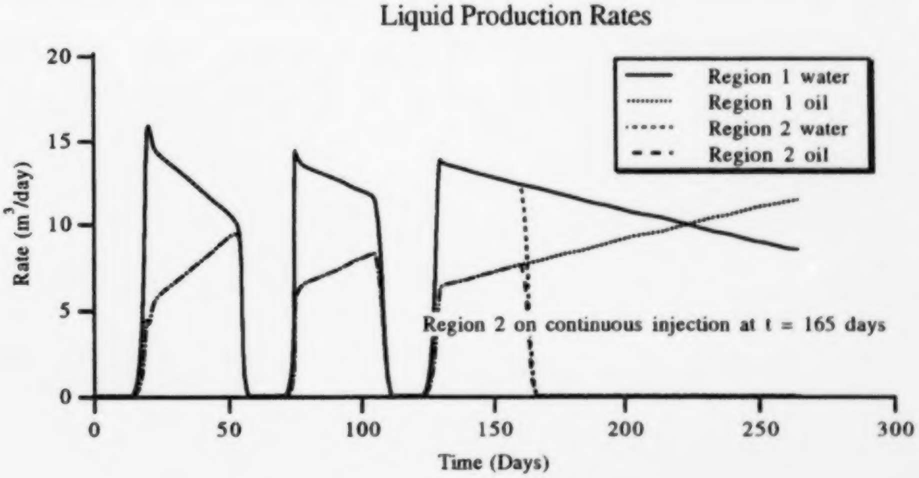

Figure 5.9.0.34 Cyclic to continuous steaming Run 5 Liquid production rates.

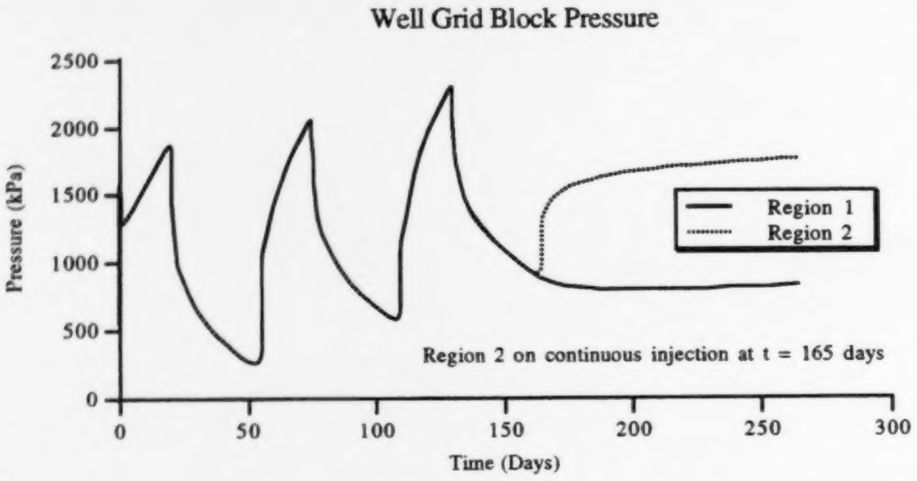

Figure 5.9.0.35 Cyclic to continuous steaming Run 5 Well grid block pressure.

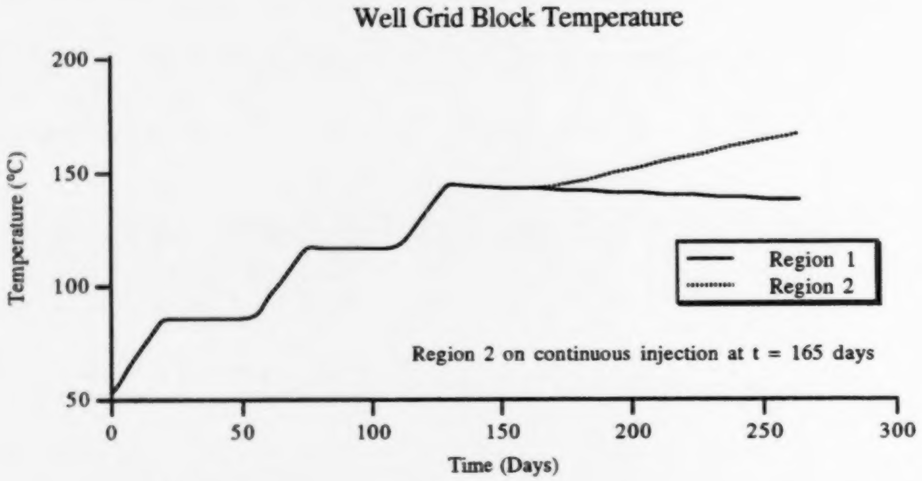

Figure 5.9.0.36 Cyclic to continuous steaming Run 5 Well grid block temperature.

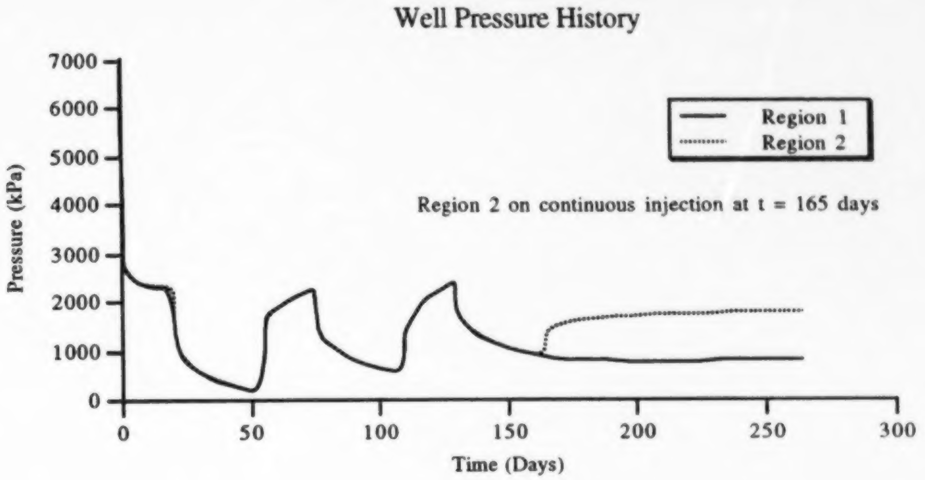

Figure 5.9.0.37 Cyclic to continuous steaming Run 5 Well pressure history.

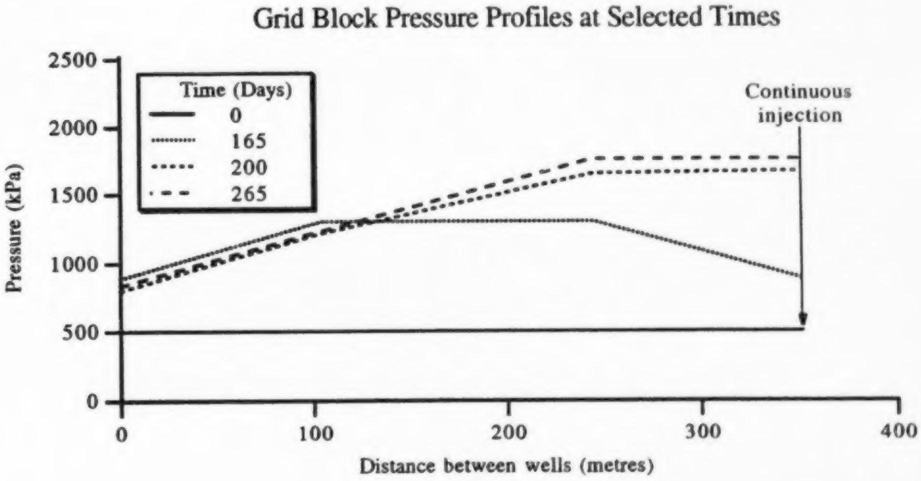

Figure 5.9.0.38

Cyclic to continuous steaming Run 5 Grid block pressure profiles at selected times.

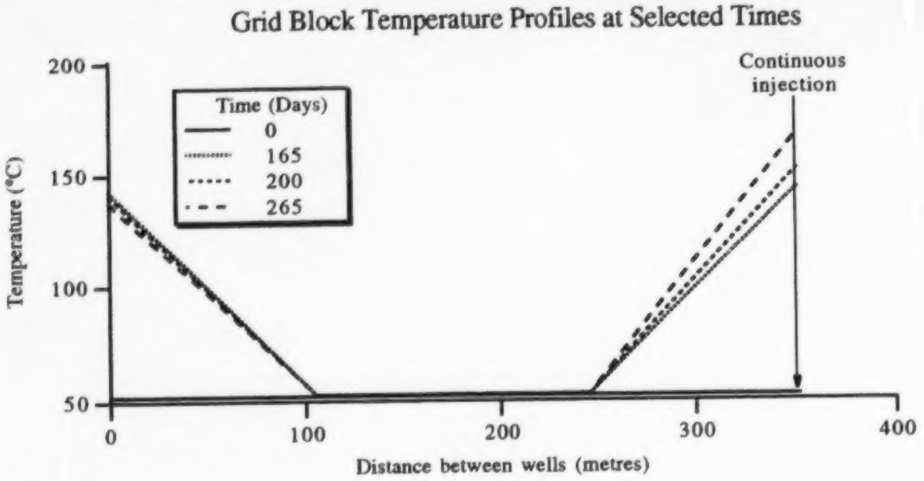

Figure 5.9.0.39

Cyclic to continuous steaming Run 5 Grid block temperature profiles at selected times.

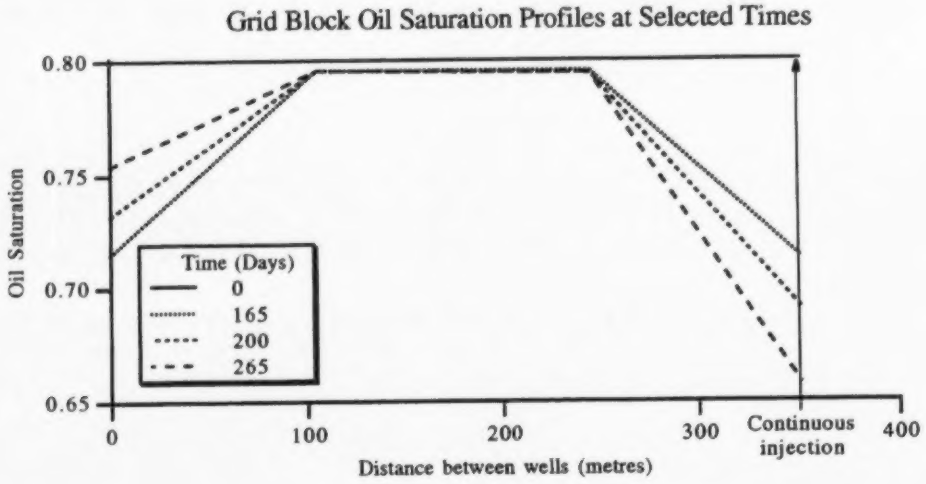

Figure 5.9.0.40

Cyclic to continuous steaming Run 5 Grid block oil saturation profiles at selected times.

CONCLUSIONS

A thermal reservoir simulator was developed with the objective of improving the resolution of the information concerning the flow of fluids and energy around a well and between wells. To accomplish this objective, it was necessary to develop further a grid refinement method. This investigation presents the following contributions to the body of simulation knowledge.

- Hyperhybrid grid refinement was developed and used for the first time for thermal reservoir simulation.
- A method for using contiguous hyperhybrid and hybrid grid refined regions was developed and incorporated for the first time in a simulator.
- The presentation of the results of the first study of the interwell interference problem of multiple cyclic steam stimulations using hyperhybrid grid refinement was given here.
- Using hyperhybrid grid refinement for the first time, several local well effects were studied in the context of cyclic steam stimulation and results presented here.
- Using hyperhybrid grid refinement, the change from cyclic steaming to continuous steaming was examined.
- If a well is not in operation, or deactivated, for an extended period of time, or is not yet drilled until later in the simulation, then the hyperhybrid grid refinement should be removed/inserted when required because the grid affects the simulation results.

With better well region representation, it has been shown that hyperhybrid grid refinement is useful in studying well operating changes and well interactions, particularly when the regions are made contiguous. Although not explicitly demonstrated here, hyperhybrid grid refinement has the potential to reduce the number of grid blocks in a problem through appropriate grid design. This leads to reduced memory requirements and reduced computation requirements.

It is recommended that (contiguous) hyperhybrid grid refinement be used for analyzing problems where the local well region behaviour is important in the context of a field simulation. Of greater significance, it is recommended that this refinement technique be used to study interwell interactions where near-well effects are important and the communication path between the wells requires better representation.

In the process of developing this model, several ideas for further research and development became apparent.

- To overcome the limitation imposed by using circular hyperhybrid grids, a commercial simulator should also incorporate elliptical hyperhybrid grid refinement to represent anisotropic flow with uneven spacing in the fundamental grid system.
- The number of angular subdivisions of a hybrid grid should be increased beyond four. This will require the development of a technique similar to conventional local grid refinement in the calculation of the interblock transmissibilities.
- The hyperhybrid grid refinement process should be developed to be dynamic instead of static. This would be useful for simulating a field over a long period of time where wells are either not operating for extended periods of time or are not yet drilled until later in the life of the field.
- The combination of hyperhybrid grid refinement and conventional local grid refinement as contiguous regions (composite hyperhybrid grid refinement) would be useful to study interwell effects and hence techniques should be developed.

REFERENCES

Abdul-Majeed, G.H., Kattan, R.R. and Salman, N.H. (1990), "New Correlation for Estimating the Viscosity of Undersaturated Crude Oils", *J. Can. Pet. Tech.* (May–June 1990), 80–85.

Abou-Kassem, J.H. and Aziz, K. (1985), "Analytical Well Models for Reservoir Simulation", *Soc. Pet. Eng. J.*, (August 1985), 573–579.

Abou-Kassem, J.H. and Aziz, K. (1985a), "Handling of Phase Change in Thermal Simulators", *J. Pet. Tech.*, (September 1985), 161–163.

Akbar, A.M., Arnold, M.D. and Harvey, A.H. (1974), "Numerical Simulation of Individual Wells in a Field Simulation Model", *Soc. Pet. Eng. J.* (August 1974), 315–320.

Al-Khafaji, A.H., Al-Doury, M.M. and Al-Dulaimy, S.N. (1989), "Enthalpy and Latent Heat Mathematical Correlation", *J. Petroleum Res.* Vol. 8, No. 1, 71–82.

Amyx, J.W., Bass , D.M. Jr. and Whiting, R.L. (1960), *Petroleum Reservoir Engineering Physical Properties*, McGraw-Hill Book Company, New York.

Au, D.K., Behie, A., Rubin, B. and Vinsome, K. (1980), "Techniques for Fully Implicit Simulation", SPE 9302 presented at the SPE-AIME 55th Annual Fall Meeting, Dallas, September 21–24, 1980.

Aziz, K., Ramesh, A.B. and Woo, P.T. (1987), "Fourth SPE Comparative Solution Project: Comparison of Steam Injection Simulators", *J. Pet. Tech.* (December 1987), 1576–1584.

Aziz, K. and Settari, A. (1979), *Petroleum Reservoir Simulation*, Applied Science Publishers, London.

Aziz, K. and Wong, T.W. (1988), "Considerations in the Development of Multipurpose Reservoir Simulation Models", presented at the First International Forum on Reservoir Simulation, Alpbach, Austria, September 12–16, 1988.

Baker, L.E. (1988), "Three-Phase Relative Permeability Correlations", SPE 17369 presented at the SPE/DOE Enhanced Oil Recovery Symposium, Tulsa, April 17–20, 1988.

Bank, R.E. and Sherman, A.H. (1979), "A Multi-level Iterative Method for Solving Finite Element Equations", SPE 7683 presented at the SPE-AIME 5th Annual Symposium on Reservoir Simulation, January 31–February 2, 1979.

Bear, J. (1972), *Dynamics of Fluids in Porous Media*, American Elsevier Publishing Co., New York.

Beggs, H.D. and Robinson, J.R. (1975), "Estimating the Viscosity of Crude Oil Systems", *J. Pet. Tech.* (September 1975), 1140–1141.

Behie, G.A. and Forsyth, P.A. Jr. (1981), "Multi-grid Solution of the Pressure Equation in Reservoir Simulation", Computer Modelling Group technical report CMG.R17.01 (July 1981).

Behie, G.A. and Forsyth, P.A. Jr. (1982), "Multi-grid Solution of Three-Dimensional Problems With Discontinuous Coefficients", Computer Modelling Group technical report CMG.R17.02 (November 1982).

Behie, G.A. and Forsyth, P.A. Jr. (1983), "Multi-grid Solution of the Pressure Equation in Reservoir Simulation", *Soc. Pet. Eng. J.* (August 1983), 623–632.

Behie, A., Forsyth, P.A. Jr. and Sammon, P.H. (1984), "Adaptive Implicit and Local Mesh Refinement Applied to Thermal Simulation", Computer Modelling Group technical report CMG.R6.18 (December 1984).

Biterge, M.B. and Ertekin, T. (1989), "The Development and Testing of a Static/Dynamic Local Grid Refinement Technique", SPE 19803 presented at the 64th Annual Technical Conference, San Antonio, October 8–11, 1989.

Bird, R.B., Stewart, W.E. and Lightfoot, E.N. (1960), *Transport Phenomena*, John Wiley & Sons, New York.

Biterge, M.B. and Ertekin, T. (1992), "Development and Testing of a Static/Dynamic Local Grid Refinement Technique", *J. Pet. Tech.* (April 1992), 487–495.

Blair, P.M. and Weinaug, C.F. (1969), "Solution of Two-Phase Flow Problems Using Implicit Difference Equations", *Soc. Pet. Eng. J.* (December 1969), 417–424.

Boberg, T.C., Rotter, M.B. and Stark, S.D. (1990), "History Match of Multiwell Simulation Models of Cyclic Steam Stimulation Models Process at Cold Lake", SPE 20743 presented at the 65th Annual Technical Conference, New Orleans, September 23–26, 1990.

Boberg, T.C., Rotter, M.B. and Stark, S.D. (1992), "History Match of Multiwell Simulation Models of the Cyclic Steam Stimulation Process at Cold Lake", *SPE Reservoir Eng. J.* (August 1992), 321–328.

Brand, C.W. and Heinemann, Z.E. (1989) "A New Iterative Solution Technique for Reservoir Simulation on Locally Refined Grids", SPE 18410 presented at the SPE-AIME 10th Annual Symposium on Reservoir Simulation, February 6–8, 1989.

Brand, C.W. and Heinemann, Z.E. (1990) "A New Iterative Solution Technique for Reservoir Simulation Equations on Locally Refined Grids", *SPE Reservoir Engineering J.* (November 1990), 555–560.

Calhoun, J.C. Jr. (1976), *Fundamentals of Reservoir Engineering*, University of Oklahoma Press, Norman.

Carey, G.F. and Chow, S.S. (1987), "Well Singularities in Reservoir Simulation", *SPE Reservoir Engineering J.* (November 1987), 713–719.

Chang, M-M., Tomutsa, L. and Tham, M.K. (1989), "Predicting Horizontal/Slanted Well Production by Mathematical Modeling", SPE 18854 presented at the SPE Production Operations Symposium, March 13–14, 1989.

Chappelear, J.E. and Hirasaki, G.J. (1976),"A Model of Oil-Water Coning for Two-Dimensional, Areal Reservoir Simulation", *Soc. Pet. Eng. J.* (April 1976), 65–72.

Chew, J. and Connally, C.A. Jr. (1959), "A Viscosity Correlation for Gas-Saturated Crude Oils", *Petroleum Transactions AIME*, Vol. 216, 23–25.

Christoffersen, K. and Whitson, C.H. (1989), "TABLE—A FORTRAN Subroutine for Generating Tables", *SPE Computer Applications J.*

Ciment, M. and Sweet, R.A. (1973), "Mesh Refinements for Parabolic Equations", *J. Computational Physics*, Vol. 12, 513–525.

Closmann, P.J. and Seba, R.D. (1990), "A Correlation of Viscosity and Molecular Weight", *J. Can. Pet. Tech.* (July–August 1990), 115–116.

Coats, K.H. (1976), "Simulation of Steamflooding With Distillation and Solution Gas", *Soc. Pet. Eng. J.* (October 1976), 235–247.

Coats, K.H. (1978), "A Highly Implicit Steamflood Model", *Soc. Pet. Eng. J.* (October 1978), 369–383.

Coats, K.H. (1980), "In-Situ Combustion Model", *Soc. Pet. Eng. J.* (December 1980), 534–554.

Coats, K.H. (1982), "Reservoir Simulation: State of the Art", Distinguished Author Series, *J. Pet. Tech.* (August 1982), 1633–1642.

Coats K.H., George, W.D., Chu, C. and Marcum, B.E. (1974), "Three-Dimensional Simulation of Steamflooding", *Soc. Pet. Eng. J.* (December 1974), 573–592.

Collins, D. (1989), "Near-Well Local Grid Refinement Using Hybrid Grids", Computer Modelling Group Twenty-third Meeting of the TAC and Member's Annual General Meeting Proceedings, May 24–25, 1989, 111–127.

Collins, D.A. and Mourits, F.M. (1991), "Multigrid Methods Applied to Near-Well Modelling in Reservoir Simulation", SPE 26607, Unsolicited.

Collins, D.A., Nghiem, L.X., Sharma, R. and Agarwal, R.K. (1991), "Field-Scale Simulation of Horizontal Wells with Hybrid Grids", SPE 21218 presented at the SPE 11th Symposium on Reservoir Simulation, Anaheim, February 17–20, 1991.

Crichlow, H.B. (1977), *Modern Reservoir Engineering—A Simulation Approach*, Prentice-Hall, Englewood Cliffs.

Crookston, R.B., Culham, W.E. and Chen, W.H. (1979), "A Numerical Simulation Model for Thermal Recovery Processes", *Soc. Pet. Eng. J.* (February 1979), 37–58.

Dranchuk, P.M. and Abou-Kassem, J.H. (1975), "Calculation of Z Factors for Natural Gases Using Equations of State", *J. Can. Pet. Tech.* (July–September 1975), 34–36.

Earlougher, R.C. Jr. (1977), *Advances in Well Test Analysis*, SPE Monograph Volume 5.

Earlougher, R.C. Jr. and Ramey, H.J. Jr. (1973), "Interference Analysis in Bounded Systems", *J. Can. Pet. Tech.* (October–December 1973), 33–45.

Earlougher, R.C. Jr., Ramey, H.J. Jr., Miller, F.G. and Muller, T.D. (1968), "Pressure Distribution in Rectangular Reservoirs", *Transactions AIME* Vol 243, 199–208.

Egbogah, E.O. and Ng, J.T. (1990), "An Improved Temperature-Viscosity Correlation for Crude Oil Systems", *J. Pet. Science and Engineering*, Vol. 4, 197–200.

Ejiogu, G.C. and Fiori, M. (1987), "High-Pressure Saturated-Steam Correlations", *J. Pet. Tech.* (December 1987), 1585–1590.

El-Khatib, N.A.F. (Unpublished), "A General Mathematical Model for Oil Recovery Processes".

Emanuel, A.S. and Cook, G.W. (1974), "Pseudo-Relative Permeability for Well Modeling", *Soc. Pet. Eng. J.* (February 1974), 7–9.

Ewing, R.E. (1988), "Adaptive Grid-Refinement Techniques for Treating Singularities, Heterogeneities, and Dispersion", *Numerical Simulation in Oil Recovery*, M.F. Wheeler Editor, Springer-Verlag, New York.

Ewing, R. E. and Lazorov, R.D. (1988), "Adaptive Local Grid Refinement", SPE 17806 presented at the SPE Rocky Mountain Regional Meeting, May 11–13, 1988.

Ewing, R.E., Boyett, B.A., Babu, D.K. and Heinemann, R.F. (1989), "Efficient Use of Locally Refined Grids for Multiphase Reservoir Simulation", SPE 18413 presented at the SPE Symposium on Reservoir Simulation, February 6–8, 1989.

Farouq Ali, S.M. and Abou-Kassem, J.H. (1988), "Simulation of Thermal Recovery Processes", Presented at the First International Forum on Reservoir Simulation, Alpbach, Austria, September 12–16, 1988.

Fassihi, M.R., Meyers, K.O. and Weisbrad, K.R. (1990), "Thermal Alteration of Viscous Crude Oils", *SPE Reservoir Engineering J.* (August 1990), 393–401.

Fletcher, C.A.J. (1988), *Computational Techniques for Fluid Dynamics Volumes I and II*, Springer-Verlag, New York.

Forsyth, P.A. Jr. (1984), "Detection and Modelling of Pinch Outs", Computer Modelling Group technical report CMG.R6.15 (April 1984).

Forsyth, P.A. Jr. (1989), "A Control Volume Finite Element Method for Local Mesh Refinement", SPE 18415 presented at the SPE-AIME 10th Annual Symposium on Reservoir Simulation, February 6–8, 1989.

Forsyth, P.A. Jr. (1990), "A Control-Volume Finite-Element Method for Local Mesh Refinement in Thermal Reservoir Simulation", *SPE Reservoir Engineering J.* (November 1990), 561–566.

Forsyth, P.A. Jr. and Sammon, P.H. (1984), "Local Mesh Refinement in Reservoir Simulation", Computer Modelling Group technical report CMG.R6.13 (March 1984).

Forsyth, F.A. Jr. and Sammon, P.H. (1984a), "Dynamic Mesh Refinement in Reservoir Simulation", Computer Modelling Group technical report CMG.R6.17 (August 1984).

Forsyth, P.A. Jr. and Sammon, P.H. (1985), "Local Mesh Refinement and Modelling of Faults and Pinchouts", SPE 13524 presented at the 1985 Reservoir Simulation Symposium, Dallas, February 10–13, 1985.

Forsyth, P.A. Jr. and Sammon, P.H. (1986), "Local Mesh Refinement and Modelling of Faults and Pinchouts", *SPE Formation Evaluation J.* (June 1986), 275–285.

Gogarty, W.B. (1967), "Rheological Properties of Pseudoplastic Fluids in Porous Media", *Soc. Pet. Eng. J.* (June 1967), 149–160.

Gottardi, G. and Vignati, L. (1990), "Hybrid Grid Black Oil Reservoir Simulator", *J. Pet. Science and Engineering*, Vol. 3, 345–360.

Grabowski, J.W., Vinsome, P.K., Lin, R.C., Behie, A. and Rubin, B. (1979), "A Fully Implicit General Purpose Finite-Difference Thermal Model for In Situ Combustion and Steam", SPE 8396 presented at the 54th Annual Technical Conference of the SPE, Las Vegas, September 23–26, 1979.

Han, D.K., Han, D.L., Yan, C.Z. and Peng, L.T. (1987), "A More Flexible Approach of Dynamic Local Grid Refinement for Reservoir Modelling", SPE 16014 presented at the SPE-AIME 9th Symposium on Reservoir Simulation, San Antonio, February 1–4, 1987.

Heinemann, Z.E. and Brand, C.W. (1988), "Gridding Techniques in Reservoir Simulation", presented at the First International Forum on Reservoir Simulation, Alpbach, Austria, September 12–16, 1988.

Heinemann, Z.E. and Brand, C.W. (1989), "Modeling Reservoir Geometry With Irregular Grids", SPE 18412 presented at the SPE-AIME 10th Annual Symposium on Reservoir Simulation, February 6–8, 1989.

Heinemann, Z.E., Brand, C.W., Munka, M. and Chen, Y.M. (1991), "Modeling Reservoir Geometry With Irregular Grids", *SPE Reservoir Engineering J.*, (May 1991), 225-232.

Heinemann, Z.E., Gerken, G. and von Hantelmann, G. (1983), "Using Local Grid Refinement in a Multiple-Application Reservoir Simulator", SPE 12255 presented at SPE-AIME 7th Reservoir Simulation Symposium, San Francisco, November 15–18, 1983.

Henderson, J.H. and Weber, L. (1965), "Physical Upgrading of Heavy Crude Oils by the Application of Heat", *J. Can. Pet. Tech.* (October–December 1965), 206–212.

Hiebert, A.D., Fung, L.S.-K., Oballa, V. and Mourits, F.M. (1991), "Comparison of Discretization Methods for Modelling Near-Well Phenomena in Thermal Processes", Presented at the Fourth Petroleum Conference of the South Saskatchewan Section of the Petroleum Society of CIM, Regina, October 7–9, 1991.

Honarpour, M., Koederitz, L. and Harvey, A.H. (1986), *Relative Permeability of Petroleum Reservoirs*, CRC Press Inc., Boca Raton.

Houpeurt, A.H. and Thelliez, M.B. (1974), "Predicting the Viscosity of Hydrocarbon Liquid Phases from Their Composition", SPE 5057 presented at the 49th Annual Fall Meeting of the SPE-AIME, Houston, October 6–9, 1974.

Kasraie, M. (1987), *Simulation of Modified Steam Injection Processes*, Ph.D. Thesis, University of Alberta.

Kasraie, M. and Farouq Ali, S.M. (1989), "Role of Foam, Non-Newtonian Flow, and Thermal Upgrading in Steam Injection", SPE 18784 presented at the California Regional Meeting, Bakersfield, April 5–7, 1989.

Ko, S.C.M., Aziz, K. and Settari, A. (1980), "Computer Simulation of Water Coning by a Sequential Solution Method", *J. Can. Pet. Tech.* (January–March 1980), 61–73.

Kokal, S.L. and Maini, B.B. (1990), "An improved model for estimating three-phase oil-water-gas relative permeabilities from two-phase oil-water and oil-gas data", *J. Can. Pet. Tech.* (March–April 1990), 105–114.

Kuniansky, J. and Hillestad, J.G. (1980), "Reservoir Simulation Using Bottomhole Pressure Boundary Conditions", *Soc. Pet. Eng. J.* (December 1980), 473–486.

Lake, L.W. (1989), *Enhanced Oil Recovery*, Prentice Hall, Englewood Cliffs.

Lee, S.H. (1987), "Analysis of Productivity of Inclined Wells and Its Implication on Finite Difference Reservoir Simulation", SPE 16002 presented at the SPE-AIME 9th Symposium on Reservoir Simulation, San Antonio, February 1–4, 1987.

Lee, S.H. (1989), "Analysis of Productivity of Inclined Wells and Its Implication on Finite-Difference Reservoir Simulation", *SPE Production Engineering J.*, (May 1989), 173-180.

Letkeman, J.P. and Ridings, R.L. (1970), "A Numerical Coning Model", *Soc. Pet. Eng. J.* (December 1970), 418–424.

Litlehamar, T. and Larsen, L. (1986), "Matching Simulator Wellblock Pressures With Observed Buildup Pressures in Two-Layer Reservoirs", *SPE Reservoir Engineering J.* (March 1986), 183–193.

Little, J.E. and Kennedy, H.T. (1968), "A Correlation of the Viscosity of Hydrocarbon Systems With Pressure, Temperature and Composition", *Soc. Pet. Eng. J.* (June 1968), 157–162.

Lohrenz, J., Bray, B.G. and Clark, C.R. (1964), "Calculating Viscosities of Reservoir Fluids From Their Compositions", *J. Pet. Tech.* (October 1964), 1171–1176.

MacDonald, R.C. and Coats, K.H. (1970), "Methods for Numerical Simulation of Water and Gas Coning", *Soc. Pet. Eng. J.* (December 1970), 425–436.

Markatos, N.C., Tatchell, D.G., Cross, M. and Rhodes, N. (1986), Editors of *Numerical Simulation of Fluid Flow and Heat/Mass Transfer Processes*, Springer-Verlag, New York.

Mattax, C.C. and Dalton, R.L. (1990), "Reservoir Simulation", Distinguished Author Series, *J. Pet. Tech.* (June 1990), 692–695.

Mattax, C.C. and Dalton, R.L. (1990a), *Reservoir Simulation*, SPE Monograph Vol. 13, Society of Petroleum Engineers, Richardson.

Mazza, A.G. and Cormack, D.E. (1988), "Thermal Cracking of the Major Chemical Fractions of Athabasca Bitumen", *AOSTRA J. of Research*, Vol. 4, No. 3, 193–208.

Mazza, A.G. and Cormack, D.E. (1988a), "Thermal Cracking of Athabasca Bitumen", *AOSTRA J. of Research*, Vol. 4, No. 3, 221–230.

McKinley, R.M., Jahns, H.O., Harris, W.W. and Greenkorn, R.A. (1966), "Non-Newtonian Flow in Porous Media", *A.I.Ch.E. J.*, Vol. 12, No. 1 (January 1966), 17–20.

Mehrotra, A.K. (1991), "Modeling Temperature and Composition Dependence for the Viscosity of Diluted Bitumens", *J. of Pet. Science and Engineering*, Vol. 5, 261–272.

Miller, K.A. (1986), "Interim progress report on Husky's Pikes Peak pilot", *J. Can. Pet. Tech.* (March–April 1986), 42–46.

Monin, J.C. and Audlbert, A. (1988), "Thermal Cracking of Heavy-Oil/Mineral Matrix Systems", *SPE Reservoir Engineering J.* (November 1988), 1243–1250.

Mrosovsky, I. and Ridings, R. L. (1974), "Two-Dimensional Radial Treatment of Wells Within a Three-Dimensional Reservoir Model", *Soc. Pet. Eng. J.* (April 1974), 127–131.

Muskat, M. (1937), *The Flow of Homogeneous Fluids Through Porous Media*, McGraw-Hill Book Co. Inc., New York.

Naar, J. and Henderson, J.H. (1961), "An Imbibition Model—Its Application to Flow Behaviour and the Prediction of Oil Recovery", *Soc. Pet. Eng. J.* (June 1961), 61–70.

Naar, J. and Wygal, R.J. (1961), "Three-Phase Imbibition Relative Permeability", *Soc. Pet. Eng. J.* (December 1961), 254–258.

Naar, J., Wygal, R.J. and Henderson, J.H. (1962), "Imbibition Relative Permeability in Unconsolidated Porous Media", *Soc. Pet. Eng. J.* (March 1962), 13–17.

Nacul, E.C. and Aziz, K. (1991), "Use of Irregular Grid in Reservoir Simulation", SPE 22886 presented at the 66th Annual Technical Meeting, Dallas, October 6–9, 1991.

Nghiem, L.X. and Rozon, B. (1988), "A Unified and Flexible Approach for Handling and Solving Large Systems of Equations in Reservoir Simulation", Computer Modelling Group Technical Report CMG 88.07.S (July 1988).

Nolan, J.S. and Berry, D.W. (1972), "Test of the Stability and Time-Step Sensitivity of Semi-Implicit Reservoir Simulation Techniques", *Soc. Pet. Eng. J.* (June 1972), 253–266.

Odeh, A.S. (1983), "The Proper Interpretation of Field-Determined Buildup Pressure and Skin Values for Simulator Use", SPE 11759 presented at the Reservoir Simulation Symposium, San Francisco, November 15–18, 1983.

Odeh, A.S. (1985), "The Proper Interpretation of Field-Determined Buildup Pressure and Skin Values for Simulator Use", *Soc. Pet. Eng. J.* (February 1985), 125–131.

Odeh, A.S. and Al Hussainy, R. (1969), "Generalized Equations Relating Pressure of Individual Wells and Grids in Reservoir Modeling", *Soc. Pet. Eng. J.* (September 1969), 277–278.

Odeh, A.S. and Yang, H.T. (1979), "Flow of Non-Newtonian Power-Law Fluids Through Porous Media", *Soc. Pet. Eng. J.* (June 1979), 155–163.

Palagi, C.L. and Aziz, K. (1991), "Use of Voronoi Grid in Reservoir Simulation", SPE 22889 presented at the 66th Annual Technical Meeting, Dallas, October 6–9, 1991.

Pascal, H. (1990), "Non-isothermal Flow of non-Newtonian Fluids through a Porous Medium", *Int. J. Heat and Mass Transfer*, Vol. 33, No. 9, 1937–1944.

Peaceman, D.W. (1977), *Fundamentals of Numerical Reservoir Simulation*, Elsevier Scientific Publishing Company, Amsterdam.

Peaceman, D.W. (1978), "Interpretation of Well-Block Pressures in Numerical Reservoir Simulation", *Soc. Pet. Eng. J.* (June 1978), 183–194.

Peaceman, D.W. (1982), "Interpretation of Well-Block Pressures in Numerical Reservoir Simulation With Nonsquare Grid Blocks and Anisotropic Permeability", SPE 10528 presented at the 6th Symposium on Reservoir Simulation, New Orleans, January 31–February 3, 1982.

Peaceman, D.W. (1983), "Interpretation of Well-Block Pressures in Numerical Reservoir Simulation With Nonsquare Grid Blocks and Anisotropic Permeability", *Soc. Pet. Eng. J.* (June 1983), 531–543.

Peaceman, D.W. (1987), "Interpretation of Well-Block Pressures in Numerical Reservoir Simulation—Part 3: Some Additional Well Geometries", SPE 16976 presented at the 62nd Annual Technical Conference of the SPE, Dallas, September 27–30, 1987.

Peaceman, D.W. (1988), "Near-singularities of Pressure and Saturation at the Wellbore in Reservoir Modeling", presented at the First International Forum on Reservoir Simulation, Alpbach, Austria, September 12–16, 1988.

Peaceman, D.W. (1990), "Interpretation of Well-Block Pressures in Numerical Reservoir Simulation: Part 3—Off-Center and Multiple Wells Within a Wellblock", *SPE Reservoir Engineering J.* (May 1990), 227–232.

Pedrosa, O.A. Jr. (1984), *Use of Hybrid Grid in Reservoir Simulation*, Ph.D. Thesis, Stanford University, Stanford, CA.

Pedrosa, O.A. Jr. and Aziz, K. (1985), "Use of Hybrid Grid in Reservoir Simulation", SPE 13507 presented at the SPE-AIME 1985 Middle East Oil Technical Conference, Bahrain, March 11–14, 1985.

Pedrosa, O.A. Jr. and Aziz, K. (1986), "Use of a Hybrid Grid in Reservoir Simulation", *Soc. Pet. Eng. Reservoir Eng. J.* (November 1986), 611–621.

Peled, A. (1987), "The Next Computer Revolution", *Scientific American*, (October 1987), 57–64.

Poon, D. and Kisman, K. (1991), "Non-Newtonian Effects on the Primary Production of Heavy Oil Reservoirs", CIM/AOSTRA 91–33 presented at the 1991 Technical Conference, Banff, April 21–24, 1991.

Prats, M. (1982), *Thermal Recovery,* SPE Monograph Volume 7, Soc. Pet. Eng. of AIME, New York.

Press, W.H., Teukolsky, S.A., Vetterling, W.T. and Flannery, B.P. (1992), *Numerical Recipes in FORTRAN, The Art of Scientific Computing*, Second Edition, Cambridge University Press, Cambridge, 1992.

Quandalle, P. and Besset, P. (1983), "The Use of Flexible Gridding for Improved Reservoir Modelling", SPE 12239 presented at the SPE-AIME 7th Annual Symposium on Reservoir Simulation, San Francisco, November 15–18, 1983.

Quandalle, P. and Besset, P. (1985), "Reduction of Grid Effects Due to Local Sub-Gridding in Simulations Using a Composite Grid", SPE 13527 presented at the 1985 Reservoir Simulation Symposium, Dallas, February 10–13, 1985.

Reid, R.C., Prausnitz, J.M. and Poling, B.E. (1987), *The Properties of Gases and Liquids*, Fourth Edition, McGraw-Hill Book Company, New York.

Reid, R.C., Prausnitz, J.M. and Sherwood, T.K. (1977), *The Properties of Gases and Liquids*, Third Edition, McGraw-Hill Book Company, New York.

Rubin, B. and Buchanan, W.L. (1985), "A General Purpose Thermal Model", *Soc. Pet. Eng. J.* (April 1985), 202–214.

Samadi, F.R. and Hill, G.A. (1987), "Thermal Effect on the Permanent Viscosity of a Saskatchewan Heavy Oil", SPE 17079 Unsolicited.

Savin, J.G. (1969), "Non-Newtonian Flow Through Porous Media", *Ind. & Eng. Chem.* (October 1969), Vol. 61, No. 10. 18–47.

Schwabe, K. and Brand, J. (1967), "Prediction of Reservoir Behavior Using Numerical Simulators", SPE 1857 presented at the SPE-AIME 42nd Annual Fall Meeting, Houston, October 1–4, 1967.

Settari, A. and Aziz, K. (1972), "Use of Irregular Grid in Reservoir Simulation", *Soc. Pet. Eng. J.* (April 1972), 103–114.

Settari, A. and Aziz, K. (1974), "A Computer Model for Two-Phase Coning Simulation", *Soc. Pet. Eng. J.* (June 1974), 221–236.

Settari, A. and Aziz, K. (1974a), "Use of Irregular Grid in Cylindrical Coordinates", *Soc. Pet. Eng. J.* (August 1974), 396–405.

Shiralkar, G.S. (1988), "Calculation of Flowing Well Pressures in Reservoir Simulation Using Nine-Point Differencing", CIM 88-39-01 presented at the 39th Annual Technical Meeting of the Petroleum Society of CIM, Calgary, June 12–16, 1988.

Shiralkar, G.S. (1989), "Calculation of Flowing Well Pressures in Reservoir Simulation Using Nine-Point Differencing", *J. Can. Pet. Tech.* (November–December 1989).

Shu, W.R. (1984), "A Viscosity Correlation for Mixtures of Heavy Oil, Bitumen, and Petroleum Fractions", *Soc. Pet. Eng. J.* (June 1984), 277–282.

Shu, W.R. and Hartman, K.J. (1986), "Thermal Visbreaking of Heavy Oil During Steam Recovery Processes", *SPE Reservoir Engineering J.* (September 1986), 474–482.

Siu, A.L. and Nghiem, L.X. (1982), "On The Modelling of Non-radial Flow Around Wells in Reservoir Simulation", Computer Modelling Group technical report CMG.R8.05 (December 1982).

Sonier, F., Besset, P. and Ombret, O. (1973), "A Numerical Model of Multiphase Flow Around a Well", *Soc. Pet. Eng. J.* (December 1973), 311–320.

Sonier, F. and Chaumet, P. (1974), "A Fully Implicit Three-Dimensional Model in Curvilinear Coordinates", *Soc. Pet. Eng. J.* (August 1974).

Spivak, A. and Coats, K.H. (1970), "Numerical Simulation of Coning Using Implicit Production Terms", *Soc. Pet. Eng. J.* (September 1970), 257–267.

Starley, G.P. (1988), "A Material-Balance Method for Deriving Interblock Water/Oil Pseudofunctions for Coarse-Grid Reservoir Simulation", *SPE Reservoir Engineering J.* (August 1988).

Stone, H.L. (1970), "Probability Model for Estimating Three-Phase Relative Permeability", *J. Pet. Tech.* (February 1970), 214–218.

Stone, H.L. (1973), "Estimation of Three-Phase Relative Permeability and Residual Oil Data", *J. Can. Pet. Tech.* (October–December 1973), 53–61.

Tan, T.B. (1987), "Implementation of an Improved Adaptive Implicit Method in a Thermal Compositional Simulator", SPE 16028 presented at the Ninth SPE Symposium on Reservoir Simulation, San Antonio, February 1–4, 1987.

Tan, T.B. (1988), "Implementation of an Improved Adaptive Implicit Method in a Thermal Compositional Simulator", *SPE Reservoir Eng. J.* (November 1988), 1123–1128.

Tan, T.B. (1990), "Representation of hysteresis in capillary pressure for reservoir simulation models", *J. Can. Pet. Tech.* (July–August 1990), 84–88.

Thomas, G.W. (1983), "An Extension of Pseudofunction Concepts", SPE 12274 presented at the Reservoir Simulation Symposium, San Francisco, November 15–18, 1983.

Tortike, W.S. and Farouq Ali, S.M. (1989), "Saturated-Steam-Property Functional Correlations for Fully Implicit Thermal Reservoir Simulation", *SPE Reservoir Eng. J.* (November 1989), 471–474.

van Poollen, H.K., Breitenbach, E.A. and Thurnau, D.H. (1968), "Treatment of Individual Wells and Grids in Reservoir Modeling", *Soc. Pet. Eng. J.* (December 1968), 341–346.

van Poollen, H.K., Bixel, H.C. and Jargon, J.R. (1970)," Individual well pressures in reservoir modeling", *Oil and Gas J.* (October 26, 1970), 78–80.

Venkatesan, V.N. and Shu, W.R. (1986), "Alteration in Heavy Oil Characteristics During Thermal Recovery", *J. Can. Pet. Tech.* (July–August 1986), 66–71.

Vinsome, P.K.W. and Westerveld, J. (1980), "A Simple Method for Predicting Cap and Base Rock Heat Losses in Thermal Reservoir Simulators", *J. Can. Pet. Tech.* (July–September), 87–90.

Vittoratos, E., Scott, G.R. and Beattie, C.I. (1988), "Cold Lake Cyclic Steam Stimulation: A Multi-well Process", SPE 17422.

von Rosenberg, D.U. (1982), "Local Mesh Refinement for Finite Difference Methods", SPE 10974 presented at the SPE-AIME 57th Annual Fall Meeting, New Orleans, September 26–29, 1982.

Wasserman, M.L. (1987), “Local Grid Refinement for Three-Dimensional Simulators”, SPE 16013 presented at the SPE-AIME 9th Symposium on Reservoir Simulation, San Antonio, February 1–4, 1987.

Weinstein, H.G., Chappelear, J.E. and Nolan, J.S. (1986), “Second Comparative Solution Project: A Three-Phase Coning Study”, *J. Pet. Tech.* (March 1986), 345–353.

Williamson, A.S. and Chappelear, J.E. (1981), “Representing Wells in Numerical Reservoir Simulation: Part 1—Theory, Part 2—Implementation”, *Soc. Pet. Eng. J.* (June 1981), 323–344.

Woods, E.G. and Khurana, A.K. (1977), “Pseudofunctions for Water Coning in a Three-Dimensional Reservoir Simulator”, *Soc. Pet. Eng. J.* (August 1977), 251–262.

APPENDIX I—Development of Mathematical and Numerical Models

I.1 Mathematical Model

The following development is based on a number of sources: Aziz and Settari (1979), El-Khatib (unpublished), Farouq Ali and Abou-Kassem (1988), Kasraie (1987), Bird, Stewart and Lightfoot (1960), Lake (1989), Peaceman (1977), Prats (1982) and Aziz and Wong (1988).

In the development of the mathematical model, there are, in general, three balance equations of interest: the mass (or mole) balance of a component, the momentum balance of a phase and the total energy balance of a phase. This section provides the mathematical development of each of these balance equations. At the end of this section is a summary of the assumptions used in the development.

These equations can be derived on a mass, molar or volume basis. The objective here is to derive, on a molar basis, multiphase, multicomponent, non-isothermal flow with reactions taking place amongst the components and matrix and accounting for the diffusion/dispersion of components between phases. The problem will be simplified prior to proceeding to the numerical model.

I.1.1 Equations of Continuity for a Multicomponent Mixture

Consider a control volume element $\Delta x\ \Delta y\ \Delta z$ through which a multicomponent mixture is flowing, as illustrated in Figure I.1.1.1. It is assumed that the control volume is representative of the porous medium. The control volume should be large compared to the size of the pores but small compared to the size of the reservoir (Bear (1972)).

Flow can enter and leave any face of the element. Input of component i across the face at x is given by

$$n_{ix}\big|_x \Delta y \Delta z \qquad \text{(I.1.1.1)}$$

and output of component i across the face at $x + \Delta x$ is given by

$$n_{ix}\big|_{x+\Delta x}\,\Delta y\,\Delta z \ , \qquad \text{(I.1.1.2)}$$

where n_{ix} is the rectangular x component of the mass flux vector

$$\vec{n}_i = \rho_i \vec{v}_i \ . \qquad \text{(I.1.1.3)}$$

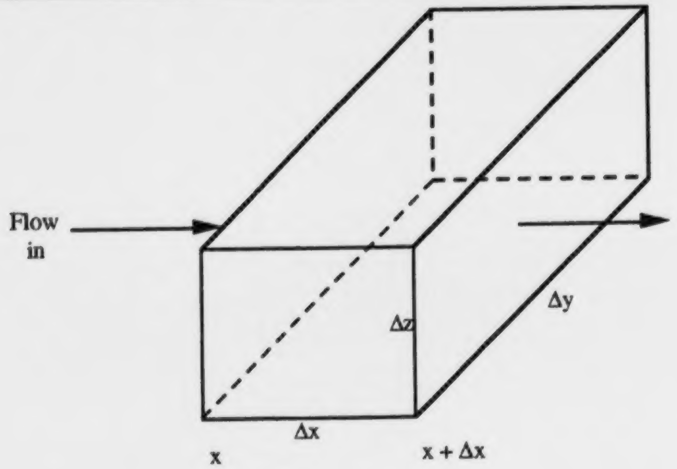

Figure I.1.1.1 Control volume representation of reservoir.

Similar expressions to Equations I.1.1.1 and I.1.1.2 can be written at y, $y + \Delta y$, z and $z + \Delta z$. The time rate of change of mass of component i is given by

$$\frac{\partial}{\partial t}\rho_i \phi\,\Delta x\,\Delta y\,\Delta z \ . \qquad \text{(I.1.1.4)}$$

The rate of generation of component i is given by

$$r_i\,\Delta x\,\Delta y\,\Delta z \ , \qquad \text{(I.1.1.5)}$$

noting that it has been assumed that component i does not react with the matrix material. Finally, the removal of mass of component i, mass depletion (accumulation) due to a sink (source) of strength $\tilde{q}$ is given by

$$\tilde{q}_i\,\Delta x\,\Delta y\,\Delta z \ . \qquad \text{(I.1.1.6)}$$

In words, the balance equation can be written as

$$\begin{array}{c}\text{Time rate of change}\\ \text{of mass of } i \text{ in}\\ \text{volume element}\end{array} = \begin{array}{c}\text{Input of } i\\ \text{across each}\\ \text{face}\end{array} - \begin{array}{c}\text{Output of } i\\ \text{across each}\\ \text{face}\end{array} + \begin{array}{c}\text{Rate of generation}\\ \text{of } i \text{ by chemical}\\ \text{reaction}\end{array} - \begin{array}{c}\text{Removal of mass}\\ i \text{ due to sink}\end{array} , \qquad \text{(I.1.1.7)}$$

or

$$\frac{\partial}{\partial t}(\rho_i\phi\,\Delta x\,\Delta y\,\Delta z)\Delta t = \left(n_{ix}\big|_x - n_{ix}\big|_{x+\Delta x}\right)\Delta y\,\Delta z\,\Delta t + \left(n_{iy}\big|_y - n_{iy}\big|_{y+\Delta y}\right)\Delta x\,\Delta z\,\Delta t$$
$$+\left(n_{iz}\big|_z - n_{iz}\big|_{z+\Delta z}\right)\Delta x\,\Delta y\,\Delta t + r_i\Delta x\,\Delta y\,\Delta z\,\Delta t - \bar{q}_i\Delta x\,\Delta y\,\Delta z\,\Delta t \ . \qquad \text{(I.1.1.8)}$$

If it is assumed that Δx, Δy and Δz are invariant with time, then Equation I.1.1.8 becomes, upon dividing by $\Delta x\ \Delta y\ \Delta z\ \Delta t$,

$$\frac{\partial}{\partial t}(\rho_i\phi\,) = \frac{n_{ix}\big|_x - n_{ix}\big|_{x+\Delta x}}{\Delta x} + \frac{n_{iy}\big|_y - n_{iy}\big|_{y+\Delta y}}{\Delta y} + \frac{n_{iz}\big|_z - n_{iz}\big|_{z+\Delta z}}{\Delta z} + r_i - \bar{q}_i \ . \qquad \text{(I.1.1.9)}$$

Taking the limit as $\Delta x \to 0$, $\Delta y \to 0$ and $\Delta z \to 0$ and noting that a first derivative is defined by a limit as

$$\frac{\partial}{\partial x}f(x) = \lim_{\Delta x\to 0}\frac{f(x+\Delta x)-f(x)}{\Delta x} \ , \qquad \text{(I.1.1.10)}$$

Equation I.1.1.9 becomes

$$\frac{\partial}{\partial t}(\rho_i\phi) = -\frac{\partial}{\partial x}n_{ix} - \frac{\partial}{\partial y}n_{iy} - \frac{\partial}{\partial z}n_{iz} + r_i - \bar{q}_i \ . \qquad \text{(I.1.1.11)}$$

As the mass flux densities for each of the phases are $\rho_o\vec{v}_o$, $\rho_w\vec{v}_w$ and $\rho_g\vec{v}_g$, then the mass flux density for component i is

$$\vec{n}_i = x_{io}\rho_o\vec{v}_o + x_{iw}\rho_w\vec{v}_w + x_{ig}\rho_g\vec{v}_g \ . \qquad \text{(I.1.1.12)}$$

The amount of moles of component i per unit bulk volume of porous medium is

$$\rho_i\phi = \phi\left(x_{io}\rho_o S_o + x_{iw}\rho_w S_w + x_{ig}\rho_g S_g\right) \ . \qquad \text{(I.1.1.13)}$$

Hence, Equation I.1.1.11 becomes

$$-\nabla\bullet\left(x_{io}\rho_o\vec{v}_o + x_{iw}\rho_w\vec{v}_w + x_{ig}\rho_g\vec{v}_g\right)$$

$$= \frac{\partial}{\partial t}\left[\phi\left(x_{io}\rho_o S_o + x_{iw}\rho_w S_w + x_{ig}\rho_g S_g\right)\right] - r_i + \tilde{q}_i \ , \qquad \text{(I.1.1.14)}$$

which can be written more compactly as

$$-\sum_{p=o,w,g} \nabla \bullet \left(x_{ip}\rho_p \vec{v}_p\right) = \frac{\partial}{\partial t}\left[\phi \sum_{p=o,w,g} x_{ip}\rho_p S_p\right] - r_i + \tilde{q}_i \ . \qquad \text{(I.1.1.15)}$$

Note that $\tilde{q}$ is negative for a source (injection) and positive for a sink (production). Equation I.1.1.15 is for *p* phases, but excludes the matrix. Let *f* denote the rock "phase", then the balance equation for the matrix is given by

$$\frac{\partial}{\partial t}(1-\phi)\rho_f x_{if} = (1-\phi) r_{kf} \ . \qquad \text{(I.1.1.16)}$$

Equation I.1.1.15 now becomes

$$-\sum_{p=o,w,g} \nabla \bullet \left(x_{ip}\rho_p \vec{v}_p\right) + (1-\phi) r_{kf} = \frac{\partial}{\partial t}\left[\phi \sum_{p=o,w,g} x_{ip}\rho_p S_p + (1-\phi)\rho_f x_{if}\right] - \phi \sum_{p=o,w,g} S_p r_{ip} + \tilde{q}_i \ , \qquad \text{(I.1.1.17)}$$

where

$$r_i = \phi \sum_{p=o,w,g} S_p r_{ip} \ . \qquad \text{(I.1.1.18)}$$

Consider the molecular diffusion within each phase, assuming phase equilibrium is attained instantaneously. In most cases encountered in oil recovery processes, diffusion can be expressed in terms of binary diffusion by lumping all components except one into one pseudo-component. In terms of the mole fraction, the rate of diffusion of component *i* in phase *p* may be expressed by Fick's law as

$$\vec{J}_{ip} = -D_{ip} \nabla x_{ip} \rho_p \qquad \text{(I.1.1.19)}$$

and the diffusive flux can be written as the expression

$$-\phi \rho_p S_p D_{ip} \nabla x_{ip} \rho_p \ . \qquad \text{(I.1.1.20)}$$

The final mole balance equation is now

$$\frac{\partial}{\partial t}\left[\phi \sum_{p=o,w,g} x_{ip}\rho_p S_p + (1-\phi)\rho_f x_{if}\right] + \sum_{p=o,w,g} \nabla \bullet \left(x_{ip}\rho_p \vec{v}_p - \phi\rho_p S_p D_{ip} \nabla x_{ip}\rho_p\right)$$

$$-\phi \sum_{p=o,w,g} S_p r_{ip} + (1-\phi) r_{if} + \tilde{q}_i = 0 \ . \qquad \text{(I.1.1.21)}$$

I.1.2 Momentum Equation

The momentum equation generally accepted in the petroleum literature is Darcy's law. As noted by Aziz and Wong (1988), Darcy's law works well for a large number of cases typically of interest in the industry. Darcy's law written for each phase is

$$\vec{v}_p = -\frac{kk_{rp}}{\mu_p}\left(\nabla p_p - \rho_p g \nabla D\right) \ , \qquad \text{(I.1.2.1)}$$

where p represents the oleic, aqueous and gaseous phases. The assumptions that must be made for Darcy's law to be valid are:

- the entire pore space of the reservoir material is filled with the fluid flowing (modified for multiphase flow by introducing the concept of relative permeability),
- $\vec{v}_p$ is not an actual, but an apparent, velocity equivalent to $\tilde{q}/A$,
- the fluid is homogeneous,
- there are no chemical reactions occurring between the porous medium and the fluid,
- the permeability is independent of fluid, temperature, pressure and location,
- the flow is laminar and viscous,
- there are no electrokinetic effects[1],
- there are no Klinkenberg effects, and
- the fluid is Newtonian.

I.1.3 Combined Continuity/Momentum Balance Equations

Combining Equation I.1.2.1 with Equation I.1.1.21 yields

$$\sum_{p=o,w,g} \nabla \bullet \left(x_{ip}\rho_p \left[-\frac{kk_{rp}}{\mu_p}\left(\nabla p_p - \rho_p g \nabla D\right)\right] - \phi\rho_p S_p D_{ip} \nabla x_{ip}\rho_p \right)$$

---

[1] Streaming potential—production of a potential difference when a liquid is forced through a porous membrane or capillary; this can be measured and is commonly called the zeta potential.

$$+\frac{\partial}{\partial t}\left[\phi \sum_{p=o,w,g} x_{ip}\rho_p S_p + (1-\phi)\rho_f x_{if}\right] - \phi \sum_{p=o,w,g} S_p r_{ip} + (1-\phi) r_{kf} + \tilde{q}_i = 0 \ . \qquad \text{(I.1.3.1)}$$

Defining capillary pressures as

$$P_{cow} = p_o - p_w \qquad \text{(I.1.3.2)}$$

and

$$P_{cgo} = p_g - p_o \ , \qquad \text{(I.1.3.3)}$$

and noting that

$$\sum_{p=o,w,g} S_p = 1 \ , \qquad \text{(I.1.3.4)}$$

then Equation I.1.3.1 can be expanded as

$$\begin{aligned}
&-\frac{\partial}{\partial t}\left[\phi x_{io}\rho_o\left(1 - S_w - S_g\right) + \phi x_{iw}\rho_w S_w + \phi x_{ig}\rho_g S_g + (1-\phi)\rho_f x_{if}\right] \\
&\quad +\nabla \bullet \left[\left(x_{io}\rho_o \frac{kk_{ro}}{\mu_o} + x_{iw}\rho_w \frac{kk_{rw}}{\mu_w} + x_{ig}\rho_g \frac{kk_{rg}}{\mu_g}\right)\nabla p_o\right] \\
&\quad -\nabla \bullet \left[x_{iw}\rho_w \frac{kk_{rw}}{\mu_w} \nabla P_{cow}\right] + \nabla \bullet \left[x_{ig}\rho_g \frac{kk_{rg}}{\mu_g} \nabla P_{cgo}\right] \\
&\quad -\nabla \bullet \left[\left(x_{io}\rho_o \frac{kk_{ro}}{\mu_o}\rho_o g + x_{iw}\rho_w \frac{kk_{rw}}{\mu_w}\rho_w g + x_{ig}\rho_g \frac{kk_{rg}}{\mu_g}\rho_g g\right)\nabla D\right] \\
&\quad -\nabla \bullet \sum_{p=o,w,g} \phi\rho_p S_p \vec{J}^{*}_{ip} + \phi \sum_{p=o,w,g} S_p r_{ip} - (1-\phi) r_{kf} - \tilde{q}_i = 0 \ , \qquad \text{(I.1.3.5)}
\end{aligned}$$

where $\vec{J}^{*}_{ip}$ is defined by Equation I.1.1.19, but includes dispersion effects also. That is, $\vec{J}^{*}_{ip}$ is a diffusion/dispersion term.

If it is further assumed, for the purposes of this study, that diffusion/dispersion effects are negligible, no chemical reactions occur and there is no rock dissolution, then Equation I.1.3.5 simplifies to

$$-\frac{\partial}{\partial t}\left[\phi x_{io}\rho_o\left(1 - S_w - S_g\right) + \phi x_{iw}\rho_w S_w + \phi x_{ig}\rho_g S_g\right]$$

$$+\nabla\bullet\left[\left(x_{io}\rho_o\frac{kk_{ro}}{\mu_o}+x_{iw}\rho_w\frac{kk_{rw}}{\mu_w}+x_{ig}\rho_g\frac{kk_{rg}}{\mu_g}\right)\nabla p_o\right]$$

$$-\nabla\bullet\left[x_{iw}\rho_w\frac{kk_{rw}}{\mu_w}\nabla P_{cow}\right]+\nabla\bullet\left[x_{ig}\rho_g\frac{kk_{rg}}{\mu_g}\nabla P_{cgo}\right]$$

$$-\nabla\bullet\left[\left(x_{io}\rho_o\frac{kk_{ro}}{\mu_o}\rho_o g+x_{iw}\rho_w\frac{kk_{rw}}{\mu_w}\rho_w g+x_{ig}\rho_g\frac{kk_{rg}}{\mu_g}\rho_g g\right)\nabla D\right]-\tilde{q}_i=0\ . \qquad \text{(I.1.3.6)}$$

Equation I.1.3.6 can be written in a more compact notation as

$$\nabla\bullet\sum_{p=o,w,g}\frac{x_{ip}\rho_p kk_{rp}}{\mu_p}\left(\nabla p_p-\rho_p g\nabla D\right)=\frac{\partial}{\partial t}\left[\phi\sum_{p=o,w,g}x_{ip}\rho_p S_p\right]+\tilde{q}_i\ . \qquad \text{(I.1.3.7)}$$

The master phase concept introduced by Coats (1980) is a practical method of handling the mole fraction variables. The number of mole fraction variables is reduced effectively from one for each component for each phase to one for each component (Tan 1987, 1988). The unknown x_{ip} is calculated from

$$x_{ip}=K_{vip}X_i\ , \qquad \text{(I.1.3.8)}$$

where K_{vip} represents the equilibrium values and X_i represents the mole fraction of component i in that component's master phase. If phase p is the master phase for component i, the K_{vip} is defined as unity. Also, if component i is not present (or insoluble) in phase p, the K_{vip} is defined as zero. Figure I.1.3.1 summarizes the master phase and soluble phases for several components. Note that the master phase for a soluble gas component is the oleic phase. Equation I.1.3.7 now becomes

$$\nabla\bullet\sum_{p=o,w,g}\frac{K_{vip}X_i\rho_p kk_{rp}}{\mu_p}\left(\nabla p_p-\rho_p g\nabla D\right)=\frac{\partial}{\partial t}\left[\phi\sum_{p=o,w,g}K_{vip}X_i\rho_p S_p\right]+\tilde{q}_i\ . \qquad \text{(I.1.3.9)}$$

	Phase		
Component	Aqueous	Oleic	Gaseous
Water	M		x
Heavy Oil		M	
Light Oil		M	
Gas (insoluble)			M
Gas (soluble)		M	x

M–Master phase
x–Soluble/present in phase

Figure I.1.3.1 Phase distribution of a multicomponent system.

I.1.4 Total Energy Balance Equation

The energy balance equation for the reservoir system can be obtained by applying the First Law of Thermodynamics. This energy balance equation can be expressed in the form of internal energy, enthalpy or the total energy.

Neglecting the kinetic energy and mechanical work done by the thermal expansion of the reservoir on its surroundings, the First law of Thermodynamics can be written as

$$\text{Net energy transfer} + \text{Energy input from sources} = \text{Gain in internal energy} \; . \qquad \text{(I.1.4.1)}$$

Assume that at every point in the reservoir, a condition of thermodynamic equilibrium exists. Consider Figure I.1.1.1 with energy transfer through all six faces. Input of energy across face at x is given by

$$u_{e,x}\,\Delta y\,\Delta z\,\Delta t \; , \qquad \text{(I.1.4.2)}$$

where $u_{e,x}$ is the total energy flux in the x direction. The output of total energy across the face at $x + \Delta x$ is given by

$$\left(u_{e,x} + \Delta u_{e,x}\right)\Delta y\,\Delta z\,\Delta t \; , \qquad \text{(I.1.4.3)}$$

where

$$\Delta u_{e,x} = u_e\big|_x - u_e\big|_{x+\Delta x} \; . \qquad \text{(I.1.4.4)}$$

The net energy transferred to the volume element is obtained, as before, by combining Expressions I.1.4.2 and I.1.4.3 with similar expressions in the y and z directions to yield

$$\text{net energy transfer} = -\left(\Delta u_{e,x}\Delta y\,\Delta z + \Delta u_{e,y}\Delta x\,\Delta z + \Delta u_{e,z}\Delta x\,\Delta y\right)\Delta t \; . \qquad \text{(I.1.4.5)}$$

The rate of energy input from sources (or output from sinks) per unit volume is given by

$$\text{energy input from sources} = \tilde{q}\,\Delta x\,\Delta y\,\Delta z\,\Delta t \; . \qquad \text{(I.1.4.6)}$$

The internal energy of the volume element at any time t is given by

$$\text{internal energy at time } t = \rho E\,\Delta x\,\Delta y\,\Delta z \; , \qquad \text{(I.1.4.7)}$$

and the internal energy of the volume element at time $t + \Delta t$ is given by the expression

$$\text{internal energy at time } t + \Delta t = \left[\rho E + \Delta(\rho E)\right] \Delta x \, \Delta y \, \Delta z \ . \tag{I.1.4.8}$$

hence

$$\text{gain in internal energy} = \Delta(\rho E) \, \Delta x \, \Delta y \, \Delta z \ . \tag{I.1.4.9}$$

Substituting Equations I.1.4.5–I.1.4.9 into Equation I.1.4.1 and dividing by $\Delta x \, \Delta y \, \Delta z \, \Delta t$ yields

$$-\left[\frac{u_{e,x}\big|_x - u_{e,x}\big|_{x+\Delta x}}{\Delta x} + \frac{u_{e,y}\big|_y - u_{e,y}\big|_{y+\Delta y}}{\Delta y} + \frac{u_{e,z}\big|_z - u_{e,z}\big|_{z+\Delta z}}{\Delta z}\right] - \tilde{q} = \frac{\Delta(\rho E)}{\Delta t} \ . \tag{I.1.4.10}$$

Using the definition of a derivative, Equation I.1.1.10, Equation I.1.4.10 becomes

$$\frac{\partial}{\partial t}(\rho E) = -\frac{\partial}{\partial x} u_{e,x} - \frac{\partial}{\partial y} u_{e,y} - \frac{\partial}{\partial z} u_{e,z} - \tilde{q} \ . \tag{I.1.4.11}$$

For N_p phases, the internal energy per unit bulk volume is

$$(\rho E) = (1 - \phi) M_f \, \Delta\theta + \phi \sum_{p=o,w,g} S_p \rho_p E_p \ , \tag{I.1.4.12}$$

where M_f is the volumetric heat capacity of the reservoir matrix.

Heat conduction is the process by which heat is transferred through the non-flowing materials by molecular collisions from a region of high temperature to a region of low temperature. Fourier's law expresses this physics as

$$u_{\lambda x} = -\lambda_c \frac{\partial \theta}{\partial x} \ . \tag{I.1.4.13}$$

It is assumed that the medium is homogeneous and isotropic.

Heat convection is the process by which energy is transferred by a flowing fluid. The convective energy flux is given by

$$u_T = u\rho\left(H + \frac{gz}{Jg_c} + \frac{|u|^2}{2\phi^2 Jg_c}\right) , \tag{I.1.4.14}$$

where the terms in parentheses represent the total energy E_t, the second term is the gravitational potential energy and the third term is the kinetic energy. The specific enthalpy, H, can be expressed as

$$H = C_p(\theta - \theta_r) , \tag{I.1.4.15}$$

if the heat capacity of the phase is not a strong function of temperature. When conduction and convection occur simultaneously, dispersion of a flowing fluid as it moves through the porous medium increases the apparent, or effective, thermal conductivity of the medium.

Neglecting radiation energy transfer, and other forms of energy such as nuclear and electromagnetic, we have the total energy flux due to conductive/convective components. In the x direction

$$u_{e,x} = u_{\lambda x} + u_{T,x} = -\lambda_c \frac{\partial \theta}{\partial x} + u_x \rho_f H_f , \tag{I.1.4.16}$$

in the y direction

$$u_{e,y} = -\lambda_c \frac{\partial \theta}{\partial y} + u_y \rho_f H_f , \tag{I.1.4.17}$$

and in the z direction

$$u_{e,z} = -\lambda_c \frac{\partial \theta}{\partial z} + u_z \rho_f \left(H_f + \frac{gz}{Jg_c}\right) , \tag{I.1.4.18}$$

where the kinetic energy term has been dropped because, from a practical point of view, this term is negligible compared to the other terms. The total energy flux components in the x, y, and z directions are the sum of a conductive heat and a convective energy flux for each phase flowing in the porous medium; thus, the above equations now become

$$u_{e,x} = -\lambda_c \frac{\partial \theta}{\partial x} + \sum_{p=o,w,g} u_{p,x} \rho_p H_p , \tag{I.1.4.19}$$

$$u_{e,y} = -\lambda_c \frac{\partial \theta}{\partial y} + \sum_{p=o,w,g} u_{p,y} \rho_p H_p , \tag{I.1.4.20}$$

and

$$u_{e,z} = -\lambda_c \frac{\partial \theta}{\partial z} + \sum_{p=o,w,g} u_{p,z}\rho_p\left(H_p + \frac{gz}{Jg_c}\right) . \qquad \text{(I.1.4.21)}$$

Prats (1982) summarizes "the total rate of heat input from sources per unit volume is made up of contributions such as heat from injection and production wells, heats of combustion and reaction and endothermic heats of mineral decomposition. Heat sources in principle can be functions of space and time, such as a moving combustion front. The strength of any source may be affected by the dependent variables of the system, such as temperature and concentration and may vary with time".

Equation I.1.4.11 may be written, using Equations I.1.4.19 to I.1.4.21, as

$$\frac{\partial}{\partial x}\left[-\lambda_c \frac{\partial \theta}{\partial x} + \sum_{p=o,w,g} u_{p,x}\rho_p H_p\right] + \frac{\partial}{\partial y}\left[-\lambda_c \frac{\partial \theta}{\partial y} + \sum_{p=o,w,g} u_{p,y}\rho_p H_p\right]$$
$$+\frac{\partial}{\partial z}\left[-\lambda_c \frac{\partial \theta}{\partial z} + \sum_{p=o,w,g} u_{p,z}\rho_p\left(H_p + \frac{gz}{Jg_c}\right)\right] = -\frac{\partial}{\partial t}\left[(1-\phi)M_f\Delta\theta + \phi \sum_{p=o,w,g} S_p\rho_p E_p\right] - \tilde{q} \ . \qquad \text{(I.1.4.22)}$$

Substituting Darcy's law, Equation I.1.2.1, into Equation I.1.4.22 yields

$$\frac{\partial}{\partial x}\left[\lambda_c \frac{\partial \theta}{\partial x} + \sum_{p=o,w,g} \frac{kk_{rp}}{\mu_p}\rho_p H_p\left(\nabla p_p - \rho_p g\nabla D\right)\right] + \frac{\partial}{\partial y}\left[\lambda_c \frac{\partial \theta}{\partial y} + \sum_{p=o,w,g} \frac{kk_{rp}}{\mu_p}\rho_p H_p\left(\nabla p_p - \rho_p g\nabla D\right)\right]$$
$$+\frac{\partial}{\partial z}\left[\lambda_c \frac{\partial \theta}{\partial z} + \sum_{p=o,w,g} \frac{kk_{rp}}{\mu_p}\rho_p H_p\left(\nabla p_p - \rho_p g\nabla D\right)\right] = \frac{\partial}{\partial t}\left[(1-\phi)M_f\Delta\theta + \phi \sum_{p=o,w,g} S_p\rho_p E_p\right] + \tilde{q} \ , \qquad \text{(I.1.4.23)}$$

where the gravitational potential energy term has been neglected. Equation I.1.4.23 can be written more generally as

$$\nabla\cdot \sum_{p=o,w,g} \frac{H_p\rho_p kk_{rp}}{\mu_p}\left(\nabla p_p - \rho_p g\nabla D\right) + \nabla\cdot\left(\lambda_c\nabla\theta\right) = \frac{\partial}{\partial t}\left[(1-\phi)M_f\Delta\theta + \phi \sum_{p=o,w,g} S_p\rho_p E_p\right] + \tilde{q} \ , \qquad \text{(I.1.4.24)}$$

where $\tilde{q}$ accounts for injection, production and heat loss to the overburden and underburden.

I.2 Numerical Model

The numerical treatment of the mathematical equations derived in Section I.1 is a finite difference approximation. Note that any approximation method attempts to replace the original partial differential equation problem by another problem that is *easier* to solve and whose solution is close to the solution of the original partial differential equation.

I.2.1 Treatment of Transmissibilities

Consider the definition of transmissibility required in the following section,

$$T_{px\,i+\frac{1}{2},j,k} = \frac{\lambda_{px\,i+\frac{1}{2},j,k}\; A_{x\,i+\frac{1}{2},j,k}}{\Delta x_{i+\frac{1}{2},j,k}} , \qquad \text{(I.2.1.1)}$$

which can be written as

$$T_{px\,i+\frac{1}{2},j,k} = \left[\frac{A_x k_x}{\Delta x}\right]_{i+\frac{1}{2},j,k} \left[\frac{K_{vip} X_i \rho_p k_{rp}}{\mu_p}\right]_{i+\frac{1}{2},j,k} . \qquad \text{(I.2.1.2)}$$

Applying the concept of upstream weighting[1], Equation I.2.1.2 can be written as

$$T_{px\,i+\frac{1}{2},j,k} = \left[\frac{A_x k_x}{\Delta x}\right]_{i+\frac{1}{2},j,k} \left(\omega_{px\,i,j,k} \left[\frac{K_{vip} X_i \rho_p k_{rp}}{\mu_p}\right]_{i,j,k} + \left(1 - \omega_{px\,i,j,k}\right) \left[\frac{K_{vip} X_i \rho_p k_{rp}}{\mu_p}\right]_{i+1,j,k} \right) , \qquad \text{(I.2.1.3)}$$

where

$$\omega_{px\,i,j,k} = 0 \qquad \Phi^{n+1}_{p\,i+1,j,k} \geq \Phi^{n+1}_{p\,i,j,k} , \qquad \text{(I.2.1.4)}$$

$$\omega_{px\,i,j,k} = 1 \qquad \Phi^{n+1}_{p\,i+1,j,k} < \Phi^{n+1}_{p\,i,j,k} , \qquad \text{(I.2.1.5)}$$

and

---

[1] This subject is explained in the literature such as Aziz and Settari (1979) and Farouq Ali and Abou–Kassem (1988).

$$\left[\frac{A_x k_x}{\Delta x}\right]_{i+\frac{1}{2},j,k} = \frac{2 A_{x_{i,j,k}} k_{x_{i,j,k}} A_{x_{i+1,j,k}} k_{x_{i+1,j,k}}}{A_{x_{i,j,k}} k_{x_{i,j,k}} \Delta x_{i+1,j,k} + A_{x_{i+1,j,k}} k_{x_{i+1,j,k}} \Delta x_{i,j,k}} , \qquad \text{(I.2.1.6)}$$

with

$$A_{x_{i,j,k}} = \Delta y_{i,j,k} \Delta z_{i,j,k} . \qquad \text{(I.2.1.7)}$$

Equation I.2.1.3 can be written in a similar form for the transmissibility on the opposite face as

$$T_{px_{i-\frac{1}{2},j,k}} = \left[\frac{A_x k_x}{\Delta x}\right]_{i-\frac{1}{2},j,k} \left(\omega^*_{px_{i,j,k}} \left[\frac{K_{vip} X_i \rho_p k_{rp}}{\mu_p}\right]_{i,j,k} + \left(1 - \omega^*_{px_{i,j,k}}\right) \left[\frac{K_{vip} X_i \rho_p k_{rp}}{\mu_p}\right]_{i-1,j,k} \right) , \qquad \text{(I.2.1.8)}$$

where

$$\omega^*_{px_{i,j,k}} = 1 \qquad \Phi^{n+1}_{p_{i,j,k}} \geq \Phi^{n+1}_{p_{i-1,j,k}} \qquad \text{(I.2.1.9)}$$

and

$$\omega^*_{px_{i,j,k}} = 0 \qquad \Phi^{n+1}_{p_{i,j,k}} < \Phi^{n+1}_{p_{i-1,j,k}} . \qquad \text{(I.2.1.10)}$$

Similar expressions can be written for T_{py} and T_{pz} which represent the mass transfer transmissibilities in the *y* and *z* directions, respectively.

The energy balance equation requires a thermal conductivity transmissibility, the treatment of which is similar to that above except that upstream weighting is not required because it is assumed that the thermal conductivity is not a function of temperature. For example,

$$T_{cx_{i+\frac{1}{2},j,k}} = \left[\frac{A_x \lambda_{cx}}{\Delta x}\right]_{i+\frac{1}{2},j,k} = \frac{2 A_{x_{i,j,k}} \lambda_{cx_{i,j,k}} A_{x_{i+1,j,k}} \lambda_{cx_{i+1,j,k}}}{A_{x_{i,j,k}} \lambda_{cx_{i,j,k}} \Delta x_{i+1,j,k} + A_{x_{i+1,j,k}} \lambda_{cx_{i+1,j,k}} \Delta x_{i,j,k}} . \qquad \text{(I.2.1.11)}$$

Similar expressions can be written for the other faces/directions.

The convective term generates an expression similar to the mass transfer transmissibility,

$$T^{*}_{\substack{px \\ i+\frac{1}{2},j,k}} = \left[\frac{A_x k_x k_{rp} \rho_p h_p}{\mu_p \Delta x}\right]_{i+\frac{1}{2},j,k} = \left[\frac{A_x k_x}{\Delta x}\right]_{i+\frac{1}{2},j,k} \left[\frac{k_{rp} \rho_p h_p}{\mu_p}\right]_{i+\frac{1}{2},j,k}, \tag{I.2.1.12}$$

and in upstream weighting notation,

$$T^{*}_{\substack{px \\ i+\frac{1}{2},j,k}} = \left[\frac{A_x k_x}{\Delta x}\right]_{i+\frac{1}{2},j,k} \left(\omega_{\substack{px \\ i,j,k}} \left[\frac{\rho_p k_{rp} h_p}{\mu_p}\right]_{i,j,k} + \left(1 - \omega_{\substack{px \\ i,j,k}}\right) \left[\frac{\rho_p k_{rp} h_p}{\mu_p}\right]_{i+1,j,k} \right), \tag{I.2.1.13}$$

with similar terms for the remaining faces/directions.

Consider the definition of transmissibility for a cylindrical system,

$$T_{\substack{pr \\ i+\frac{1}{2},j,k}} = \frac{\lambda_{\substack{pr \\ i+\frac{1}{2},j,k}} \; A_{\substack{r \\ i+\frac{1}{2},j,k}}}{\Delta r_{i+\frac{1}{2},j,k}}, \tag{I.2.1.14}$$

which can be written as

$$T_{\substack{pr \\ i+\frac{1}{2},j,k}} = \left[\frac{A_r k_r}{\Delta r}\right]_{i+\frac{1}{2},j,k} \left[\frac{x_{ip} \rho_p k_{rp}}{\mu_p}\right]_{i+\frac{1}{2},j,k}. \tag{I.2.1.15}$$

Applying the concept of upstream weighting, Equation I.2.1.15 can be written as

$$T_{\substack{pr \\ i+\frac{1}{2},j,k}} = \left[\frac{A_r k_r}{\Delta r}\right]_{i+\frac{1}{2},j,k} \left(\omega_{\substack{pr \\ i,j,k}} \left[\frac{x_{ip} \rho_p k_{rp}}{\mu_p}\right]_{i,j,k} + \left(1 - \omega_{\substack{pr \\ i,j,k}}\right) \left[\frac{x_{ip} \rho_p k_{rp}}{\mu_p}\right]_{i+1,j,k} \right), \tag{I.2.1.16}$$

where

$$\omega_{\substack{pr \\ i,j,k}} = 0 \qquad \Phi^{n+1}_{\substack{p \\ i+1,j,k}} \geq \Phi^{n+1}_{\substack{p \\ i,j,k}}, \tag{I.2.1.17}$$

$$\omega_{\substack{pr \\ i,j,k}} = 1 \qquad \Phi^{n+1}_{\substack{p \\ i+1,j,k}} < \Phi^{n+1}_{\substack{p \\ i,j,k}}, \tag{I.2.1.18}$$

and

$$\left[\frac{A_r k_r}{\Delta r}\right]_{i+\frac{1}{2},j,k} = \frac{\alpha_j \Delta z_k k_{r_i} k_{r_{i+1}}}{k_{r_i} \ln\left(\frac{r_{i+1}}{r_{i+\frac{1}{2}}}\right) + k_{r_{i+1}} \ln\left(\frac{r_{i+\frac{1}{2}}}{r_i}\right)} . \qquad \text{(I.2.1.19)}$$

Similarly,

$$T_{p\alpha_{i,j+\frac{1}{2},k}} = \left[\frac{A_\alpha k_\alpha}{\Delta\alpha}\right]_{i,j+\frac{1}{2},k} \left(\omega_{p\alpha_{i,j,k}} \left[\frac{x_{ip}\rho_p k_{rp}}{\mu_p}\right]_{i,j,k} + \left(1-\omega_{p\alpha_{i,j,k}}\right)\left[\frac{x_{ip}\rho_p k_{rp}}{\mu_p}\right]_{i,j+1,k} \right) \qquad \text{(I.2.1.20)}$$

and

$$T_{pz_{i,j,k+\frac{1}{2}}} = \left[\frac{A_z k_z}{\Delta z}\right]_{i,j,k+\frac{1}{2}} \left(\omega_{pz_{i,j,k}} \left[\frac{x_{ip}\rho_p k_{rp}}{\mu_p}\right]_{i,j,k} + \left(1-\omega_{pz_{i,j,k}}\right)\left[\frac{x_{ip}\rho_p k_{rp}}{\mu_p}\right]_{i,j,k+1} \right), \qquad \text{(I.2.1.21)}$$

where

$$\left[\frac{A_\alpha k_\alpha}{\Delta\alpha}\right]_{i,j+\frac{1}{2},k} = \frac{r_{i+\frac{1}{2}} - r_{i-\frac{1}{2}}}{r_i} \Delta z_k \frac{2 k_{\alpha_j} k_{\alpha_{j+1}}}{\alpha_j k_{\alpha_{j+1}} + \alpha_{j+1} k_{\alpha_j}} \qquad \text{(I.2.1.22)}$$

and

$$\left[\frac{A_z k_z}{\Delta z}\right]_{i,j,k+\frac{1}{2}} = \frac{2 A_{z_k} k_{z_k} k_{z_{k+1}}}{\Delta z_k k_{z_{k+1}} + \Delta z_{k+1} k_{z_k}} . \qquad \text{(I.2.1.23)}$$

These above expressions represent the mass transfer transmissibilities.

As above (Equation I.2.1.11), the energy balance equation requires a thermal conductivity transmissibility. For example,

$$\left[\frac{A_r \lambda_{cr}}{\Delta r}\right]_{i+\frac{1}{2},j,k} = \frac{\alpha_j \Delta z_k \lambda_{cr_{i,j,k}} \lambda_{cr_{i+1,j,k}}}{\lambda_{cr_{i,j,k}} \ln\left(\frac{r_{i+1}}{r_{i+\frac{1}{2}}}\right) + \lambda_{cr_{i+1,j,k}} \ln\left(\frac{r_{i+\frac{1}{2}}}{r_i}\right)} , \qquad \text{(I.2.1.24)}$$

$$\left[\frac{A_\alpha \lambda_{c\alpha}}{\Delta\alpha}\right]_{i,j+\frac{1}{2},k} = \frac{r_{i+\frac{1}{2}} - r_{i-\frac{1}{2}}}{r_i} \Delta z_k \frac{2\lambda_{\alpha_j}\lambda_{\alpha_{j+1}}}{\alpha_j \lambda_{\alpha_{j+1}} + \alpha_{j+1}\lambda_{\alpha_j}} , \qquad (I.2.1.25)$$

and

$$\left[\frac{A_z \lambda_{cz}}{\Delta z}\right]_{i,j,k+\frac{1}{2}} = \frac{2A_z \lambda_{z_k} \lambda_{z_{k+1}}}{\Delta z_k \lambda_{z_{k+1}} + \Delta z_{k+1} \lambda_{z_k}} . \qquad (I.2.1.26)$$

Similar expressions can be written for the other faces/directions.

The convective term generates an expression similar to the mass transfer transmissibility

$$T^*_{pr_{i+\frac{1}{2},j,k}} = \left[\frac{A_x k_x k_{rp} \rho_p}{\mu_p \Delta r}\right]_{i+\frac{1}{2},j,k} = \left[\frac{A_r k_r}{\Delta r}\right]_{i+\frac{1}{2},j,k}\left[\frac{k_{rp}\rho_p}{\mu_p}\right]_{i+\frac{1}{2},j,k} , \qquad (I.2.1.27)$$

$$T^*_{p\alpha_{i,j+\frac{1}{2},k}} = \left[\frac{A_\alpha k_\alpha}{\Delta\alpha}\right]_{i,j+\frac{1}{2},k}\left[\frac{k_{rp}\rho_p}{\mu_p}\right]_{i,j+\frac{1}{2},k} , \qquad (I.2.1.28)$$

and

$$T^*_{pz_{i,j,k+\frac{1}{2}}} = \left[\frac{A_z k_z}{\Delta z}\right]_{i,j,k+\frac{1}{2}}\left[\frac{k_{rp}\rho_p}{\mu_p}\right]_{i,j,k+\frac{1}{2}} \qquad (I.2.1.29)$$

with similar terms for the remaining faces/directions.

I.2.2 Combined Continuity/Momentum Balance Equations

Consider Equation I.1.3.8,

$$\nabla \cdot \sum_{p=o,w,g} \frac{K_{vip} X_i \rho_p k k_{rp}}{\mu_p}\left(\nabla p_p - \rho_p g \nabla D\right) = \frac{\partial}{\partial t}\left[\phi \sum_{p=o,w,g} K_{vip} X_i \rho_p S_p\right] + \tilde{q}_i , \qquad (I.2.2.1)$$

in a one dimensional Cartesian coordinate system:

$$\frac{\partial}{\partial x}\left[\frac{K_{vip}X_i\rho_p k_x k_{rp}}{\mu_p}\left(\frac{\partial p_p}{\partial x}-\rho_p g\frac{\partial z}{\partial x}\right)\right]=\frac{\partial}{\partial t}\left[\phi K_{vip}X_i\rho_p S_p\right]+\tilde{q}_{ip} \qquad p=o,w,g\ . \qquad (\text{I.2.2.2})$$

The finite difference approximation of the operator, $\frac{\partial}{\partial x}\left[\lambda\frac{\partial U}{\partial x}\right]$, is

$$\frac{\partial}{\partial x}\left[\lambda\frac{\partial U}{\partial x}\right]=\frac{\lambda_{i+\frac{1}{2}}\frac{u_{i+1}-u_i}{\Delta x_{i+\frac{1}{2}}}-\lambda_{i-\frac{1}{2}}\frac{u_i-u_{i-1}}{\Delta x_{i-\frac{1}{2}}}}{\Delta x_i}\ . \qquad (\text{I.2.2.3})$$

Defining

$$\lambda_{p_{i\pm\frac{1}{2}}}=\frac{1}{2}\left(\lambda_{p_i}+\lambda_{p_{i\pm1}}\right) \qquad (\text{I.2.2.4})$$

and

$$\lambda_{px}=\frac{K_{vip}X_i\rho_p k_x k_{rp}}{\mu_p}\ , \qquad (\text{I.2.2.5})$$

Equation I.2.2.2 can now be written as

$$\frac{1}{\Delta x_i}\lambda_{px_{i+\frac{1}{2}}}\left[\frac{\left(p_{p_{i+1}}-p_{p_i}\right)-\rho_{p_{i+\frac{1}{2}}}g\left(z_{i+1}-z_i\right)}{\Delta x_{i+\frac{1}{2}}}\right]+\frac{1}{\Delta x_i}\lambda_{px_{i-\frac{1}{2}}}\left[\frac{\left(p_{p_{i-1}}-p_{p_i}\right)-\rho_{p_{i-\frac{1}{2}}}g\left(z_{i-1}-z_i\right)}{\Delta x_{i-\frac{1}{2}}}\right]$$
$$=\frac{\partial}{\partial t}\left[\phi K_{vip}X_i\rho_p S_p\right]+\tilde{q}_{ip_i} \qquad p=o,w,g\ . \qquad (\text{I.2.2.6})$$

Multiplying by $\Delta x\,\Delta y\,\Delta z$ and applying a backward difference approximation to the time derivative results in

$$\frac{\lambda_{p_{i+\frac{1}{2}}}A_{i+\frac{1}{2}}}{\Delta x_{i+\frac{1}{2}}}\left[\left(p_{p_{i+1}}-p_{p_i}\right)-\rho_{p_{i+\frac{1}{2}}}g\left(z_{i+1}-z_i\right)\right]+\frac{\lambda_{p_{i-\frac{1}{2}}}A_{i-\frac{1}{2}}}{\Delta x_{i-\frac{1}{2}}}\left[\left(p_{p_{i-1}}-p_{p_i}\right)-\rho_{p_{i-\frac{1}{2}}}g\left(z_{i-1}-z_i\right)\right]$$
$$=\frac{V_{bi}}{\Delta t}\left(\left[\phi K_{vip}X_i\rho_p S_p\right]_i^{n+1}-\left[\phi K_{vip}X_i\rho_p S_p\right]_i^{n}\right)+V_{bi}\tilde{q}_{ip_i} \qquad p=o,w,g\ , \qquad (\text{I.2.2.7})$$

where

$$V_{bi} = \Delta x_i \, \Delta y_i \, \Delta z_i \ . \qquad \text{(I.2.2.8)}$$

Defining

$$T_{px\,i+\frac{1}{2},j,k} = \frac{\lambda_{px\,i+\frac{1}{2},j,k} \; A_{x\,i+\frac{1}{2},j,k}}{\Delta x_{i+\frac{1}{2},j,k}} \ , \qquad \text{(I.2.2.9)}$$

and noting that similar terms can be defined for the remaining *x* direction, *y* and *z* directions. Equation I.2.2.1 can be written in residual form as

$$
\begin{aligned}
F^{n+1}_{i\ i,j,k} = {} & \\
& T^{n+1}_{ox\ i+\frac{1}{2},j,k}\left[\left(p^{n+1}_{o\ i+1,j,k} - p^{n+1}_{o\ i,j,k}\right) - \rho^{n+1}_{o\ i+\frac{1}{2},j,k}\, g\left(z_{i+1,j,k} - z_{i,j,k}\right)\right] \\
& \qquad + T^{n+1}_{ox\ i-\frac{1}{2},j,k}\left[\left(p^{n+1}_{o\ i-1,j,k} - p^{n+1}_{o\ i,j,k}\right) - \rho^{n+1}_{o\ i-\frac{1}{2},j,k}\, g\left(z_{i-1,j,k} - z_{i,j,k}\right)\right] \\
& + T^{n+1}_{oy\ i,j+\frac{1}{2},k}\left[\left(p^{n+1}_{o\ i,j+1,k} - p^{n+1}_{o\ i,j,k}\right) - \rho^{n+1}_{o\ i,j+\frac{1}{2},k}\, g\left(z_{i,j+1,k} - z_{i,j,k}\right)\right] \\
& \qquad + T^{n+1}_{oy\ i,j-\frac{1}{2},k}\left[\left(p^{n+1}_{o\ i,j-1,k} - p^{n+1}_{o\ i,j,k}\right) - \rho^{n+1}_{o\ i,j-\frac{1}{2},k}\, g\left(z_{i,j-1,k} - z_{i,j,k}\right)\right] \\
& + T^{n+1}_{oz\ i,j,k+\frac{1}{2}}\left[\left(p^{n+1}_{o\ i,j,k+1} - p^{n+1}_{o\ i,j,k}\right) - \rho^{n+1}_{o\ i,j,k+\frac{1}{2}}\, g\left(z_{i,j,k+1} - z_{i,j,k}\right)\right] \\
& \qquad + T^{n+1}_{oz\ i,j,k-\frac{1}{2}}\left[\left(p^{n+1}_{o\ i,j,k-1} - p^{n+1}_{o\ i,j,k}\right) - \rho^{n+1}_{o\ i,j,k-\frac{1}{2}}\, g\left(z_{i,j,k-1} - z_{i,j,k}\right)\right] \\
& - \frac{V_{b\ i,j,k}}{\Delta t}\left(\left[\phi K_{vio} X_i \rho_o S_o\right]^{n+1}_{i,j,k} - \left[\phi K_{vio} X_i \rho_o S_o\right]^{n}_{i,j,k}\right) - V_{b\ i,j,k}\ \tilde{q}_{io\ i,j,k} \\
& + T^{n+1}_{wx\ i+\frac{1}{2},j,k}\left[\left(p^{n+1}_{w\ i+1,j,k} - p^{n+1}_{w\ i,j,k}\right) - \rho^{n+1}_{w\ i+\frac{1}{2},j,k}\, g\left(z_{i+1,j,k} - z_{i,j,k}\right)\right]
\end{aligned}
$$

$$+T_{wx}{}^{n+1}_{i-\frac{1}{2},j,k}\left[\left(p_w{}^{n+1}_{i-1,j,k}-p_w{}^{n+1}_{i,j,k}\right)-\rho_w{}^{n+1}_{i-\frac{1}{2},j,k}\,g\left(z_{i-1,j,k}-z_{i,j,k}\right)\right]$$

$$+T_{wy}{}^{n+1}_{i,j+\frac{1}{2},k}\left[\left(p_w{}^{n+1}_{i,j+1,k}-p_w{}^{n+1}_{i,j,k}\right)-\rho_w{}^{n+1}_{i,j+\frac{1}{2},k}\,g\left(z_{i,j+1,k}-z_{i,j,k}\right)\right]$$

$$+T_{wy}{}^{n+1}_{i,j-\frac{1}{2},k}\left[\left(p_w{}^{n+1}_{i,j-1,k}-p_w{}^{n+1}_{i,j,k}\right)-\rho_w{}^{n+1}_{i,j-\frac{1}{2},k}\,g\left(z_{i,j-1,k}-z_{i,j,k}\right)\right]$$

$$+T_{wz}{}^{n+1}_{i,j,k+\frac{1}{2}}\left[\left(p_w{}^{n+1}_{i,j,k+1}-p_w{}^{n+1}_{i,j,k}\right)-\rho_w{}^{n+1}_{i,j,k+\frac{1}{2}}\,g\left(z_{i,j,k+1}-z_{i,j,k}\right)\right]$$

$$+T_{wz}{}^{n+1}_{i,j,k-\frac{1}{2}}\left[\left(p_w{}^{n+1}_{i,j,k-1}-p_w{}^{n+1}_{i,j,k}\right)-\rho_w{}^{n+1}_{i,j,k-\frac{1}{2}}\,g\left(z_{i,j,k-1}-z_{i,j,k}\right)\right]$$

$$-\frac{V_{b_{i,j,k}}}{\Delta t}\left(\left[\phi K_{viw}X_i\rho_w S_w\right]^{n+1}_{i,j,k}-\left[\phi K_{viw}X_i\rho_w S_w\right]^{n}_{i,j,k}\right)-V_{b_{i,j,k}}\,\tilde{q}_{iw_{i,j,k}}$$

$$+T_{gx}{}^{n+1}_{i+\frac{1}{2},j,k}\left[\left(p_g{}^{n+1}_{i+1,j,k}-p_g{}^{n+1}_{i,j,k}\right)-\rho_g{}^{n+1}_{i+\frac{1}{2},j,k}\,g\left(z_{i+1,j,k}-z_{i,j,k}\right)\right]$$

$$+T_{gx}{}^{n+1}_{i-\frac{1}{2},j,k}\left[\left(p_g{}^{n+1}_{i-1,j,k}-p_g{}^{n+1}_{i,j,k}\right)-\rho_g{}^{n+1}_{i-\frac{1}{2},j,k}\,g\left(z_{i-1,j,k}-z_{i,j,k}\right)\right]$$

$$+T_{gy}{}^{n+1}_{i,j+\frac{1}{2},k}\left[\left(p_g{}^{n+1}_{i,j+1,k}-p_g{}^{n+1}_{i,j,k}\right)-\rho_g{}^{n+1}_{i,j+\frac{1}{2},k}\,g\left(z_{i,j+1,k}-z_{i,j,k}\right)\right]$$

$$+T_{gy}{}^{n+1}_{i,j-\frac{1}{2},k}\left[\left(p_g{}^{n+1}_{i,j-1,k}-p_g{}^{n+1}_{i,j,k}\right)-\rho_g{}^{n+1}_{i,j-\frac{1}{2},k}\,g\left(z_{i,j-1,k}-z_{i,j,k}\right)\right]$$

$$+T_{gz}{}^{n+1}_{i,j,k+\frac{1}{2}}\left[\left(p_g{}^{n+1}_{i,j,k+1}-p_g{}^{n+1}_{i,j,k}\right)-\rho_g{}^{n+1}_{i,j,k+\frac{1}{2}}\,g\left(z_{i,j,k+1}-z_{i,j,k}\right)\right]$$

$$+T_{gz}{}^{n+1}_{i,j,k-\frac{1}{2}}\left[\left(p_g{}^{n+1}_{i,j,k-1}-p_g{}^{n+1}_{i,j,k}\right)-\rho_g{}^{n+1}_{i,j,k-\frac{1}{2}}\,g\left(z_{i,j,k-1}-z_{i,j,k}\right)\right]$$

$$-\frac{\underset{i,j,k}{V_b}}{\Delta t}\left(\left[\phi K_{vig}X_i\rho_g S_g\right]_{i,j,k}^{n+1}-\left[\phi K_{vig}X_i\rho_g S_g\right]_{i,j,k}^{n}\right)-\underset{i,j,k}{V_b}\;\underset{i,j,k}{\tilde{q}_{ig}}\;, \tag{I.2.2.10}$$

which can be written in the following, more compact, form

$$\begin{aligned}\underset{i,j,k}{F_i^{n+1}}=\sum_p\Bigg[\sum_m \underset{l}{T_p^{n+1}}\bigg[\bigg(\underset{m}{p_p^{n+1}}-\underset{i,j,k}{p_p^{n+1}}\bigg)-\underset{l}{\rho_p^{n+1}}g\left(z_m-z_{i,j,k}\right)\bigg]\\ -\frac{\underset{i,j,k}{V_b}}{\Delta t}\left(\left[\phi K_{vip}X_i\rho_p S_p\right]_{i,j,k}^{n+1}-\left[\phi K_{vip}X_i\rho_p S_p\right]_{i,j,k}^{n}\right)-\underset{i,j,k}{V_b}\;\underset{i,j,k}{\tilde{q}_{ip}^{n+1}}\Bigg]\;,\end{aligned} \tag{I.2.2.11}$$

where *p* represents the aqueous, oleic and gaseous phase, *m* represents the grid blocks adjacent to block *i, j, k* (*i*+1, *j*, *k*; *i*-1, *j*, *k*; *i*, *j*+1, *k*; *i*, *j*-1, *k*; *i*, *j*, *k*+1; *i*, *j*, *k*-1) and *l* represents the interface between block *i*, *j*, *k* and the six adjacent blocks (*i*+1/2, *j*, *k*; *i*-1/2, *j*, *k*; *i*, *j*+1/2, *k*; *i*, *j*-1/2, *k*; *i*, *j*, *k*+1/2; *i*, *j*, *k*-1/2).

I.2.3 Total Energy Balance Equation

Consider Equation I.1.4.24:

$$\nabla\bullet\sum_{p=o,w,g}\frac{H_p\rho_p kk_{rp}}{\mu_p}\left(\nabla p_p-\rho_p g\nabla D\right)+\nabla\bullet(\lambda\nabla\theta)=\frac{\partial}{\partial t}\left[(1-\phi)M_f\Delta\theta+\phi\sum_{p=o,w,g}S_p\rho_p E_p\right]+\tilde{q}\;. \tag{I.2.3.1}$$

The quantity $\tilde{q}$ in Equation I.2.3.1 is made of the components of heat loss to the overburden/underburden and heat produced/injected along with the fluids:

$$q^{n+1}=q_{loss}+\left[q_o\sum_i K_{vio}X_i e_{io}\right]_{i,j,k}^{n+1}+\left[q_w\sum_i K_{viw}X_i e_{iw}\right]_{i,j,k}^{n+1}+\left[q_g\sum_i K_{vig}X_i e_{ig}\right]_{i,j,k}^{n+1}\;. \tag{I.2.3.2}$$

The finite difference form of Equation I.2.3.1, upon multiplying by

$$V_{bi}=\Delta x_i\,\Delta y_i\,\Delta z_i\;, \tag{I.2.3.3}$$

becomes

$$G_{i,j,k}^{n+1} =$$

$$T^{*\,n+1}_{ox,\,i+\frac{1}{2},j,k}\left[\left(p_{o,\,i+1,j,k}^{n+1} - p_{o,\,i,j,k}^{n+1}\right) - \rho_{o,\,i+\frac{1}{2},j,k}^{n+1}\, g\left(z_{i+1,j,k} - z_{i,j,k}\right)\right]$$

$$+T^{*\,n+1}_{ox,\,i-\frac{1}{2},j,k}\left[\left(p_{o,\,i-1,j,k}^{n+1} - p_{o,\,i,j,k}^{n+1}\right) - \rho_{o,\,i-\frac{1}{2},j,k}^{n+1}\, g\left(z_{i-1,j,k} - z_{i,j,k}\right)\right]$$

$$+T^{*\,n+1}_{oy,\,i,j+\frac{1}{2},k}\left[\left(p_{o,\,i,j+1,k}^{n+1} - p_{o,\,i,j,k}^{n+1}\right) - \rho_{e,\,i,j+\frac{1}{2},k}^{n+1}\, g\left(z_{i,j+1,k} - z_{i,j,k}\right)\right]$$

$$+T^{*\,n+1}_{oy,\,i,j-\frac{1}{2},k}\left[\left(p_{o,\,i,j-1,k}^{n+1} - p_{o,\,i,j,k}^{n+1}\right) - \rho_{o,\,i,j-\frac{1}{2},k}^{n+1}\, g\left(z_{i,j-1,k} - z_{i,j,k}\right)\right]$$

$$+T^{*\,n+1}_{oz,\,i,j,k+\frac{1}{2}}\left[\left(p_{o,\,i,j,k+1}^{n+1} - p_{o,\,i,j,k}^{n+1}\right) - \rho_{o,\,i,j,k+\frac{1}{2}}^{n+1}\, g\left(z_{i,j,k+1} - z_{i,j,k}\right)\right]$$

$$+T^{*\,n+1}_{oz,\,i,j,k-\frac{1}{2}}\left[\left(p_{o,\,i,j,k-1}^{n+1} - p_{o,\,i,j,k}^{n+1}\right) - \rho_{o,\,i,j,k-\frac{1}{2}}^{n+1}\, g\left(z_{i,j,k-1} - z_{i,j,k}\right)\right]$$

$$-\frac{V_{b\,i,j,k}}{\Delta t}\left(\left[\phi E_o \rho_o S_o\right]_{i,j,k}^{n+1} - \left[\phi E_o \rho_o S_o\right]_{i,j,k}^{n}\right)$$

$$+T^{*\,n+1}_{wx,\,i+\frac{1}{2},j,k}\left[\left(p_{w,\,i+1,j,k}^{n+1} - p_{w,\,i,j,k}^{n+1}\right) - \rho_{w,\,i+\frac{1}{2},j,k}^{n+1}\, g\left(z_{i+1,j,k} - z_{i,j,k}\right)\right]$$

$$+T^{*\,n+1}_{wx,\,i-\frac{1}{2},j,k}\left[\left(p_{w,\,i-1,j,k}^{n+1} - p_{w,\,i,j,k}^{n+1}\right) - \rho_{w,\,i-\frac{1}{2},j,k}^{n+1}\, g\left(z_{i-1,j,k} - z_{i,j,k}\right)\right]$$

$$+T^{*\,n+1}_{wy,\,i,j+\frac{1}{2},k}\left[\left(p_{w,\,i,j+1,k}^{n+1} - p_{w,\,i,j,k}^{n+1}\right) - \rho_{w,\,i,j+\frac{1}{2},k}^{n+1}\, g\left(z_{i,j+1,k} - z_{i,j,k}\right)\right]$$

$$+T^{*\,n+1}_{wy,\,i,j-\frac{1}{2},k}\left[\left(p_{w,\,i,j-1,k}^{n+1} - p_{w,\,i,j,k}^{n+1}\right) - \rho_{w,\,i,j-\frac{1}{2},k}^{n+1}\, g\left(z_{i,j-1,k} - z_{i,j,k}\right)\right]$$

$$+\underset{i,j,k+\frac{1}{2}}{\overset{n+1}{T^{*}_{wz}}}\left[\left(\underset{i,j,k+1}{p_w^{n+1}}-\underset{i,j,k}{p_w^{n+1}}\right)-\underset{i,j,k+\frac{1}{2}}{\rho_w^{n+1}}\,g\left(z_{i,j,k+1}-z_{i,j,k}\right)\right]$$

$$+\underset{i,j,k-\frac{1}{2}}{\overset{n+1}{T^{*}_{wz}}}\left[\left(\underset{i,j,k-1}{p_w^{n+1}}-\underset{i,j,k}{p_w^{n+1}}\right)-\underset{i,j,k-\frac{1}{2}}{\rho_w^{n+1}}\,g\left(z_{i,j,k-1}-z_{i,j,k}\right)\right]$$

$$-\frac{\underset{i,j,k}{V_b}}{\Delta t}\left(\left[\phi E_w\rho_w S_w\right]^{n+1}_{i,j,k}-\left[\phi E_w\rho_w S_w\right]^{n}_{i,j,k}\right)$$

$$+\underset{i+\frac{1}{2},j,k}{\overset{n+1}{T^{*}_{gx}}}\left[\left(\underset{i+1,j,k}{p_g^{n+1}}-\underset{i,j,k}{p_g^{n+1}}\right)-\underset{i+\frac{1}{2},j,k}{\rho_g^{n+1}}\,g\left(z_{i+1,j,k}-z_{i,j,k}\right)\right]$$

$$+\underset{i-\frac{1}{2},j,k}{\overset{n+1}{T^{*}_{gx}}}\left[\left(\underset{i-1,j,k}{p_g^{n+1}}-\underset{i,j,k}{p_g^{n+1}}\right)-\underset{i-\frac{1}{2},j,k}{\rho_g^{n+1}}\,g\left(z_{i-1,j,k}-z_{i,j,k}\right)\right]$$

$$+\underset{i,j+\frac{1}{2},k}{\overset{n+1}{T^{*}_{gy}}}\left[\left(\underset{i,j+1,k}{p_g^{n+1}}-\underset{i,j,k}{p_g^{n+1}}\right)-\underset{i,j+\frac{1}{2},k}{\rho_g^{n+1}}\,g\left(z_{i,j+1,k}-z_{i,j,k}\right)\right]$$

$$+\underset{i,j-\frac{1}{2},k}{\overset{n+1}{T^{*}_{gy}}}\left[\left(\underset{i,j-1,k}{p_g^{n+1}}-\underset{i,j,k}{p_g^{n+1}}\right)-\underset{i,j-\frac{1}{2},k}{\rho_g^{n+1}}\,g\left(z_{i,j-1,k}-z_{i,j,k}\right)\right]$$

$$+\underset{i,j,k+\frac{1}{2}}{\overset{n+1}{T^{*}_{gz}}}\left[\left(\underset{i,j,k+1}{p_g^{n+1}}-\underset{i,j,k}{p_g^{n+1}}\right)-\underset{i,j,k+\frac{1}{2}}{\rho_g^{n+1}}\,g\left(z_{i,j,k+1}-z_{i,j,k}\right)\right]$$

$$+\underset{i,j,k-\frac{1}{2}}{\overset{n+1}{T^{*}_{gz}}}\left[\left(\underset{i,j,k-1}{p_g^{n+1}}-\underset{i,j,k}{p_g^{n+1}}\right)-\underset{i,j,k-\frac{1}{2}}{\rho_g^{n+1}}\,g\left(z_{i,j,k-1}-z_{i,j,k}\right)\right]$$

$$-\frac{\underset{i,j,k}{V_b}}{\Delta t}\left(\left[\phi E_g\rho_g S_g\right]^{n+1}_{i,j,k}-\left[\phi E_g\rho_g S_g\right]^{n}_{i,j,k}\right)$$

$$+\underset{i+\frac{1}{2},j,k}{T_{cx}^{n+1}}\left[\theta^{n+1}_{i+1,j,k}-\theta^{n+1}_{i,j,k}\right]+\underset{i-\frac{1}{2},j,k}{T_{cx}^{n+1}}\left[\theta^{n+1}_{i-1,j,k}-\theta^{n+1}_{i,j,k}\right]$$

$$+\underset{i,j+\frac{1}{2},k}{T_{cy}^{n+1}}\left[\theta^{n+1}_{i,j+1,k}-\theta^{n+1}_{i,j,k}\right]+\underset{i,j-\frac{1}{2},k}{T_{cy}^{n+1}}\left[\theta^{n+1}_{i,j-1,k}-\theta^{n+1}_{i,j,k}\right]$$

$$+\underset{i,j,k+\frac{1}{2}}{T_{cz}^{n+1}}\left[\theta^{n+1}_{i,j,k+1}-\theta^{n+1}_{i,j,k}\right]-\underset{i,j,k-\frac{1}{2}}{T_{cz}^{n+1}}\left[\theta^{n+1}_{i,j,k-1}-\theta^{n+1}_{i,j,k}\right]$$

$$-\frac{{V_b}_{i,j,k}}{\Delta t}\left(\left[(1-\phi)M_f\Delta\theta\right]^{n+1}_{i,j,k}-\left[(1-\phi)M_f\Delta\theta\right]^{n}_{i,j,k}\right)-{V_b}_{i,j,k}\,\tilde{q}_{i,j,k}\ , \tag{I.2.3.4}$$

which can be written in the following, more compact, form:

$$G^{n+1}_{i,j,k}=\sum_{p=o,w,g}\left[\sum_{m}{T^{*}_{p}}^{n+1}_{l}\left[\left({p_p^{n+1}}_{m}-{p_p^{n+1}}_{i,j,k}\right)-{\rho_p^{n+1}}_{l}\,g\left(z_m-z_{i,j,k}\right)\right]-\frac{{V_b}_{i,j,k}}{\Delta t}\left(\left[\phi E_p\rho_pS_p\right]^{n+1}_{i,j,k}-\left[\phi E_p\rho_pS_p\right]^{n}_{i,j,k}\right)\right]$$

$$+\sum_{m}{T_c^{n+1}}_{l}\left[\theta_m^{n+1}-\theta^{n+1}_{i,j,k}\right]-\frac{{V_b}_{i,j,k}}{\Delta t}\left(\left[(1-\phi)\rho_fH_f\right]^{n+1}_{i,j,k}-\left[(1-\phi)\rho_fH_f\right]^{n}_{i,j,k}\right)-{V_b}_{i,j,k}\,\tilde{q}_{i,j,k}\ . \tag{I.2.3.5}$$

I.2.4 Cylindrical Form of Equations

Beginning with Equations I.2.2.1, the combined continuity/momentum balance equation, and I.2.3.1, the total energy balance equation, it is a straightforward matter to derive the finite difference equations similar to Equations I.2.2.11 and I.2.3.5. However, it is much simpler to write the finite difference equations in cylindrical form directly by noting that the only differences lie in the geometric portion of the definitions of transmissibilities and block bulk volume. Thus, in finite difference form,

$${F_i^{n+1}}_{i,j,k}=$$

$${T_{or}^{n+1}}_{i+\frac{1}{2},j,k}\left[\left({p_o^{n+1}}_{i+1,j,k}-{p_o^{n+1}}_{i,j,k}\right)-{\rho_o^{n+1}}_{i+\frac{1}{2},j,k}\,g\left(z_{i+1,j,k}-z_{i,j,k}\right)\right]$$

$$+{T_{or}^{n+1}}_{i-\frac{1}{2},j,k}\left[\left({p_o^{n+1}}_{i-1,j,k}-{p_o^{n+1}}_{i,j,k}\right)-{\rho_o^{n+1}}_{i-\frac{1}{2},j,k}\,g\left(z_{i-1,j,k}-z_{i,j,k}\right)\right]$$

$$+{T_{o\alpha}^{n+1}}_{i,j+\frac{1}{2},k}\left[\left({p_o^{n+1}}_{i,j+1,k}-{p_o^{n+1}}_{i,j,k}\right)-{\rho_o^{n+1}}_{i,j+\frac{1}{2},k}\,g\left(z_{i,j+1,k}-z_{i,j,k}\right)\right]$$

$$+{T_{o\alpha}^{n+1}}_{i,j-\frac{1}{2},k}\left[\left({p_o^{n+1}}_{i,j-1,k}-{p_o^{n+1}}_{i,j,k}\right)-{\rho_o^{n+1}}_{i,j-\frac{1}{2},k}\,g\left(z_{i,j-1,k}-z_{i,j,k}\right)\right]$$

$$+{T_{oz}^{n+1}}_{i,j,k+\frac{1}{2}}\left[\left({p_o^{n+1}}_{i,j,k+1}-{p_o^{n+1}}_{i,j,k}\right)-{\rho_o^{n+1}}_{i,j,k+\frac{1}{2}}\,g\left(z_{i,j,k+1}-z_{i,j,k}\right)\right]$$

$$+T_{oz\,i,j,k-\frac{1}{2}}^{n+1}\left[\left(p_{o\,i,j,k-1}^{n+1}-p_{o\,i,j,k}^{n+1}\right)-\rho_{o\,i,j,k-\frac{1}{2}}^{n+1}\,g\left(z_{i,j,k-1}-z_{i,j,k}\right)\right]$$

$$-\frac{V_{b\,i,j,k}}{\Delta t}\left(\left[\phi K_{vio}X_i\rho_oS_o\right]_{i,j,k}^{n+1}-\left[\phi K_{vio}X_i\rho_oS_o\right]_{i,j,k}^{n}\right)-V_{b\,i,j,k}\,\tilde{q}_{io\,i,j,k}$$

$$+T_{wr\,i+\frac{1}{2},j,k}^{n+1}\left[\left(p_{w\,i+1,j,k}^{n+1}-p_{w\,i,j,k}^{n+1}\right)-\rho_{w\,i+\frac{1}{2},j,k}^{n+1}\,g\left(z_{i+1,j,k}-z_{i,j,k}\right)\right]$$

$$+T_{wr\,i-\frac{1}{2},j,k}^{n+1}\left[\left(p_{w\,i-1,j,k}^{n+1}-p_{w\,i,j,k}^{n+1}\right)-\rho_{w\,i-\frac{1}{2},j,k}^{n+1}\,g\left(z_{i-1,j,k}-z_{i,j,k}\right)\right]$$

$$+T_{w\alpha\,i,j+\frac{1}{2},k}^{n+1}\left[\left(p_{w\,i,j+1,k}^{n+1}-p_{w\,i,j,k}^{n+1}\right)-\rho_{w\,i,j+\frac{1}{2},k}^{n+1}\,g\left(z_{i,j+1,k}-z_{i,j,k}\right)\right]$$

$$+T_{w\alpha\,i,j-\frac{1}{2},k}^{n+1}\left[\left(p_{w\,i,j-1,k}^{n+1}-p_{w\,i,j,k}^{n+1}\right)-\rho_{w\,i,j-\frac{1}{2},k}^{n+1}\,g\left(z_{i,j-1,k}-z_{i,j,k}\right)\right]$$

$$+T_{wz\,i,j,k+\frac{1}{2}}^{n+1}\left[\left(p_{w\,i,j,k+1}^{n+1}-p_{w\,i,j,k}^{n+1}\right)-\rho_{w\,i,j,k+\frac{1}{2}}^{n+1}\,g\left(z_{i,j,k+1}-z_{i,j,k}\right)\right]$$

$$+T_{wz\,i,j,k-\frac{1}{2}}^{n+1}\left[\left(p_{w\,i,j,k-1}^{n+1}-p_{w\,i,j,k}^{n+1}\right)-\rho_{w\,i,j,k-\frac{1}{2}}^{n+1}\,g\left(z_{i,j,k-1}-z_{i,j,k}\right)\right]$$

$$-\frac{V_{b\,i,j,k}}{\Delta t}\left(\left[\phi K_{viw}X_i\rho_wS_w\right]_{i,j,k}^{n+1}-\left[\phi K_{viw}X_i\rho_wS_w\right]_{i,j,k}^{n}\right)-V_{b\,i,j,k}\,\tilde{q}_{iw\,i,j,k}$$

$$+T_{gr\,i+\frac{1}{2},j,k}^{n+1}\left[\left(p_{g\,i+1,j,k}^{n+1}-p_{g\,i,j,k}^{n+1}\right)-\rho_{g\,i+\frac{1}{2},j,k}^{n+1}\,g\left(z_{i+1,j,k}-z_{i,j,k}\right)\right]$$

$$+T_{gr\,i-\frac{1}{2},j,k}^{n+1}\left[\left(p_{g\,i-1,j,k}^{n+1}-p_{g\,i,j,k}^{n+1}\right)-\rho_{g\,i-\frac{1}{2},j,k}^{n+1}\,g\left(z_{i-1,j,k}-z_{i,j,k}\right)\right]$$

$$+T_{g\alpha\,i,j+\frac{1}{2},k}^{n+1}\left[\left(p_{g\,i,j+1,k}^{n+1}-p_{g\,i,j,k}^{n+1}\right)-\rho_{g\,i,j+\frac{1}{2},k}^{n+1}\,g\left(z_{i,j+1,k}-z_{i,j,k}\right)\right]$$

$$+T^{n+1}_{g\alpha\, i,j-\frac{1}{2},k}\left[\left(p^{n+1}_{g\, i,j-1,k} - p^{n+1}_{g\, i,j,k}\right) - \rho^{n+1}_{g\, i,j-\frac{1}{2},k}\, g\left(z_{i,j-1,k} - z_{i,j,k}\right)\right]$$

$$+T^{n+1}_{gz\, i,j,k+\frac{1}{2}}\left[\left(p^{n+1}_{g\, i,j,k+1} - p^{n+1}_{g\, i,j,k}\right) - \rho^{n+1}_{g\, i,j,k+\frac{1}{2}}\, g\left(z_{i,j,k+1} - z_{i,j,k}\right)\right]$$

$$+T^{n+1}_{gz\, i,j,k-\frac{1}{2}}\left[\left(p^{n+1}_{g\, i,j,k-1} - p^{n+1}_{g\, i,j,k}\right) - \rho^{n+1}_{g\, i,j,k-\frac{1}{2}}\, g\left(z_{i,j,k-1} - z_{i,j,k}\right)\right]$$

$$-\frac{V_{b\, i,j,k}}{\Delta t}\left(\left[\phi K_{vig} X_i \rho_g S_g\right]^{n+1}_{i,j,k} - \left[\phi K_{vig} X_i \rho_g S_g\right]^{n}_{i,j,k}\right) - V_{b\, i,j,k}\, \tilde{q}_{ig\, i,j,k} \tag{I.2.4.1}$$

and

$$G^{n+1}_{i,j,k} =$$

$$\overset{*}{T}{}^{n+1}_{or\, i+\frac{1}{2},j,k}\left[\left(p^{n+1}_{o\, i+1,j,k} - p^{n+1}_{o\, i,j,k}\right) - \rho^{n+1}_{o\, i+\frac{1}{2},j,k}\, g\left(z_{i+1,j,k} - z_{i,j,k}\right)\right]$$

$$+\overset{*}{T}{}^{n+1}_{or\, i-\frac{1}{2},j,k}\left[\left(p^{n+1}_{o\, i-1,j,k} - p^{n+1}_{o\, i,j,k}\right) - \rho^{n+1}_{o\, i-\frac{1}{2},j,k}\, g\left(z_{i-1,j,k} - z_{i,j,k}\right)\right]$$

$$+\overset{*}{T}{}^{n+1}_{o\alpha\, i,j+\frac{1}{2},k}\left[\left(p^{n+1}_{o\, i,j+1,k} - p^{n+1}_{o\, i,j,k}\right) - \rho^{n+1}_{o\, i,j+\frac{1}{2},k}\, g\left(z_{i,j+1,k} - z_{i,j,k}\right)\right]$$

$$+\overset{*}{T}{}^{n+1}_{o\alpha\, i,j-\frac{1}{2},k}\left[\left(p^{n+1}_{o\, i,j-1,k} - p^{n+1}_{o\, i,j,k}\right) - \rho^{n+1}_{o\, i,j-\frac{1}{2},k}\, g\left(z_{i,j-1,k} - z_{i,j,k}\right)\right]$$

$$+\overset{*}{T}{}^{n+1}_{oz\, i,j,k+\frac{1}{2}}\left[\left(p^{n+1}_{o\, i,j,k+1} - p^{n+1}_{o\, i,j,k}\right) - \rho^{n+1}_{o\, i,j,k+\frac{1}{2}}\, g\left(z_{i,j,k+1} - z_{i,j,k}\right)\right]$$

$$+\overset{*}{T}{}^{n+1}_{oz\, i,j,k-\frac{1}{2}}\left[\left(p^{n+1}_{o\, i,j,k-1} - p^{n+1}_{o\, i,j,k}\right) - \rho^{n+1}_{o\, i,j,k-\frac{1}{2}}\, g\left(z_{i,j,k-1} - z_{i,j,k}\right)\right]$$

$$-\frac{V_{b\, i,j,k}}{\Delta t}\left(\left[\phi E_o \rho_o S_o\right]^{n+1}_{i,j,k} - \left[\phi E_o \rho_o S_o\right]^{n}_{i,j,k}\right)$$

$$+T^{*\,n+1}_{wr\;i+\frac{1}{2},j,k}\left[\left(p^{n+1}_{w\;i+1,j,k}-p^{n+1}_{w\;i,j,k}\right)-\rho^{n+1}_{w\;i+\frac{1}{2},j,k}\,g\left(z_{i+1,j,k}-z_{i,j,k}\right)\right]$$

$$+T^{*\,n+1}_{wr\;i-\frac{1}{2},j,k}\left[\left(p^{n+1}_{w\;i-1,j,k}-p^{n+1}_{w\;i,j,k}\right)-\rho^{n+1}_{w\;i-\frac{1}{2},j,k}\,g\left(z_{i-1,j,k}-z_{i,j,k}\right)\right]$$

$$+T^{*\,n+1}_{w\alpha\;i,j+\frac{1}{2},k}\left[\left(p^{n+1}_{w\;i,j+1,k}-p^{n+1}_{w\;i,j,k}\right)-\rho^{n+1}_{w\;i,j+\frac{1}{2},k}\,g\left(z_{i,j+1,k}-z_{i,j,k}\right)\right]$$

$$+T^{*\,n+1}_{w\alpha\;i,j-\frac{1}{2},k}\left[\left(p^{n+1}_{w\;i,j-1,k}-p^{n+1}_{w\;i,j,k}\right)-\rho^{n+1}_{w\;i,j-\frac{1}{2},k}\,g\left(z_{i,j-1,k}-z_{i,j,k}\right)\right]$$

$$+T^{*\,n+1}_{wz\;i,j,k+\frac{1}{2}}\left[\left(p^{n+1}_{w\;i,j,k+1}-p^{n+1}_{w\;i,j,k}\right)-\rho^{n+1}_{w\;i,j,k+\frac{1}{2}}\,g\left(z_{i,j,k+1}-z_{i,j,k}\right)\right]$$

$$+T^{*\,n+1}_{wz\;i,j,k-\frac{1}{2}}\left[\left(p^{n+1}_{w\;i,j,k-1}-p^{n+1}_{w\;i,j,k}\right)-\rho^{n+1}_{w\;i,j,k-\frac{1}{2}}\,g\left(z_{i,j,k-1}-z_{i,j,k}\right)\right]$$

$$-\frac{V_{b\;i,j,k}}{\Delta t}\left(\left[\phi E_w\rho_w S_w\right]^{n+1}_{i,j,k}-\left[\phi E_w\rho_w S_w\right]^{n}_{i,j,k}\right)$$

$$+T^{*\,n+1}_{gr\;i+\frac{1}{2},j,k}\left[\left(p^{n+1}_{g\;i+1,j,k}-p^{n+1}_{g\;i,j,k}\right)-\rho^{n+1}_{g\;i+\frac{1}{2},j,k}\,g\left(z_{i+1,j,k}-z_{i,j,k}\right)\right]$$

$$+T^{*\,n+1}_{gr\;i-\frac{1}{2},j,k}\left[\left(p^{n+1}_{g\;i-1,j,k}-p^{n+1}_{g\;i,j,k}\right)-\rho^{n+1}_{g\;i-\frac{1}{2},j,k}\,g\left(z_{i-1,j,k}-z_{i,j,k}\right)\right]$$

$$+T^{*\,n+1}_{g\alpha\;i,j+\frac{1}{2},k}\left[\left(p^{n+1}_{g\;i,j+1,k}-p^{n+1}_{g\;i,j,k}\right)-\rho^{n+1}_{g\;i,j+\frac{1}{2},k}\,g\left(z_{i,j+1,k}-z_{i,j,k}\right)\right]$$

$$+T^{*\,n+1}_{g\alpha\;i,j-\frac{1}{2},k}\left[\left(p^{n+1}_{g\;i,j-1,k}-p^{n+1}_{g\;i,j,k}\right)-\rho^{n+1}_{g\;i,j-\frac{1}{2},k}\,g\left(z_{i,j-1,k}-z_{i,j,k}\right)\right]$$

$$
\begin{aligned}
&+T^{*\,n+1}_{gz\;i,j,k+\frac{1}{2}}\left[\left(p^{n+1}_{g\;i,j,k+1}-p^{n+1}_{g\;i,j,k}\right)-\rho^{n+1}_{g\;i,j,k+\frac{1}{2}}\,g\left(z_{i,j,k+1}-z_{i,j,k}\right)\right]\\
&\qquad\qquad+T^{*\,n+1}_{gz\;i,j,k-\frac{1}{2}}\left[\left(p^{n+1}_{g\;i,j,k-1}-p^{n+1}_{g\;i,j,k}\right)-\rho^{n+1}_{g\;i,j,k-\frac{1}{2}}\,g\left(z_{i,j,k-1}-z_{i,j,k}\right)\right]\\
&-\frac{V_{b\;i,j,k}}{\Delta t}\left(\left[\phi E_g\rho_g S_g\right]^{n+1}_{i,j,k}-\left[\phi E_g\rho_g S_g\right]^{n}_{i,j,k}\right)\\
&+T^{n+1}_{cr\;i+\frac{1}{2},j,k}\left[\theta^{n+1}_{i+1,j,k}-\theta^{n+1}_{i,j,k}\right]+T^{n+1}_{cr\;i-\frac{1}{2},j,k}\left[\theta^{n+1}_{i-1,j,k}-\theta^{n+1}_{i,j,k}\right]\\
&+T^{n+1}_{c\alpha\;i,j+\frac{1}{2},k}\left[\theta^{n+1}_{i,j+1,k}-\theta^{n+1}_{i,j,k}\right]+T^{n+1}_{c\alpha\;i,j-\frac{1}{2},k}\left[\theta^{n+1}_{i,j-1,k}-\theta^{n+1}_{i,j,k}\right]\\
&+T^{n+1}_{cz\;i,j,k+\frac{1}{2}}\left[\theta^{n+1}_{i,j,k+1}-\theta^{n+1}_{i,j,k}\right]-T^{n+1}_{cz\;i,j,k-\frac{1}{2}}\left[\theta^{n+1}_{i,j,k-1}-\theta^{n+1}_{i,j,k}\right]\\
&-\frac{V_{b\;i,j,k}}{\Delta t}\left(\left[(1-\phi)\rho_f H_f\right]^{n+1}_{i,j,k}-\left[(1-\phi)\rho_f H_f\right]^{n}_{i,j,k}\right)-V_{b\;i,j,k}\,\tilde{q}_{i,j,k}\;.
\end{aligned}
\tag{I.2.4.2}
$$

Note that the compact forms expressed by Equations I.2.2.11 and I.2.3.5 are the compact forms of Equations I.2.4.1 and I.2.4.2, respectively.

I.3 Fundamental Grid Construction

Figure I.3.0.1 illustrates a one-dimensional block-centred grid. In the block-centred grid, the block boundaries are selected first and then the nodes are placed in the centre of the blocks thus

$$\delta_{i^-}=\delta_{i^+}=\frac{\Delta x_i}{2}\ , \tag{I.3.0.1}$$

and

$$\Delta x_{i\pm\frac{1}{2}}=\frac{1}{2}\left(\Delta x_i+\Delta x_{i\pm1}\right)\ . \tag{I.3.0.2}$$

For the point-distributed grid, shown in Figure I.3.0.2, the nodes are selected first and then the block boundaries are placed mid-way between the nodes. Notice the subtle difference in size of the blocks (that is, the nodes are no longer automatically in the centre of the grid blocks) in Figures I.3.0.1 and I.3.0.2. The equations similar to Equations I.3.0.1 and I.3.0.2 are

$$\delta_{i\pm} = \delta_{i\pm 1} = \frac{\Delta x_{i\pm 1/2}}{2} , \tag{I.3.0.3}$$

and

$$\Delta x_i = \frac{1}{2}\left(\Delta x_{i+1/2} + \Delta x_{i-1/2}\right) = \delta_{i+} + \delta_{i-} . \tag{I.3.0.4}$$

Analogous expressions can be written for the *y* and *z* directions.

The bulk volume can now be determined from the elementary expression

$$V_{b_{i,j,k}} = \Delta x_{i,j,k} \Delta y_{i,j,k} \Delta z_{i,j,k} , \tag{I.3.0.5}$$

where the notation has been expanded to express a three-dimensional system. The block node is located in the centre of the block.

Expressions analogous to the above equations for a point-distributed grid in cylindrical coordinates (block-centred grid expressions are not included here) are given by

$$r^L_{i\pm 1/2} = \frac{r_{i\pm 1} - r_i}{\ln\left(r_{i\pm 1}/r_i\right)} , \tag{I.3.0.6}$$

$$\alpha_{j\pm 1/2} = \frac{1}{2}\left(\alpha_j + \alpha_{j\pm 1}\right) , \tag{I.3.0.7}$$

and

$$\Delta z_k = \frac{1}{2}\left(\Delta z_{k+1/2} + \Delta z_{k-1/2}\right) , \tag{I.3.0.8}$$

noting that the boundary for calculating the interblock transmissibility is logarithmic in *r* but the boundary for calculating the block volume is logarithmic in r^2. Details can be found in Settari and Aziz (1972, 1974) and Aziz and Settari (1979). The block bulk volume is given by

$$V_{b_{i,j,k}} = \frac{\alpha_j}{2}\left(r^2_{i+1/2} - r^2_{i-1/2}\right)\Delta z_k \ . \tag{I.3.0.9}$$

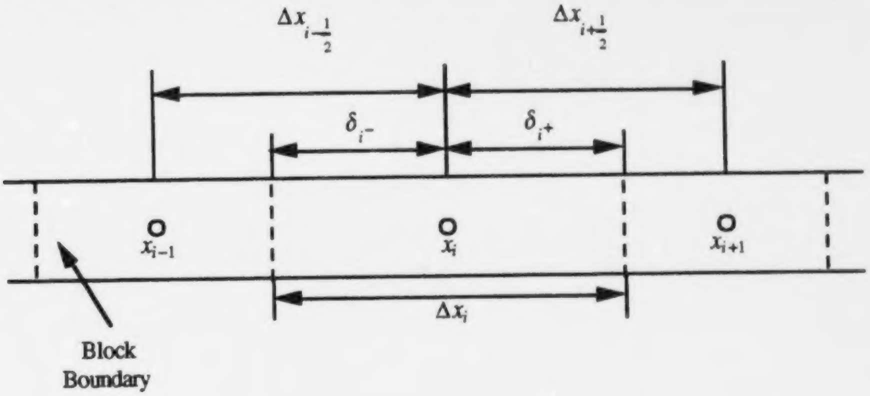
$\Delta x_{i-\frac{1}{2}}$
$\Delta x_{i+\frac{1}{2}}$
δ_{i^-}
δ_{i^+}
x_{i-1}
x_i
x_{i+1}
Δx_i
Block Boundary

Figure I.3.0.1 Block-centred grid.

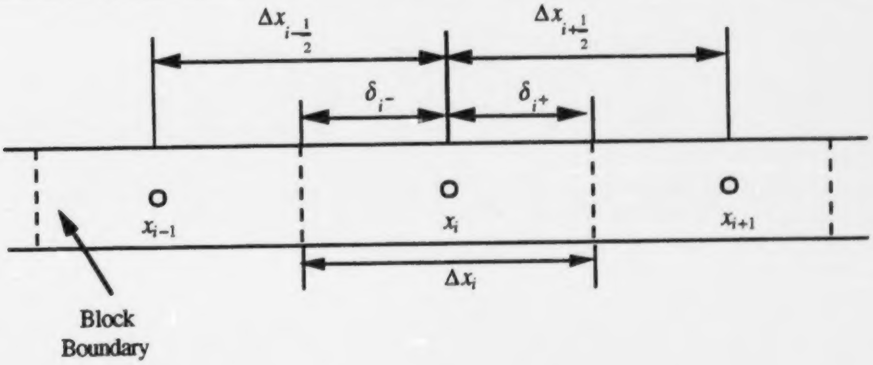
$\Delta x_{i-\frac{1}{2}}$
$\Delta x_{i+\frac{1}{2}}$
δ_{i^-}
δ_{i^+}
x_{i-1}
x_i
x_{i+1}
Δx_i
Block Boundary

Figure I.3.0.2 Point-distributed grid

APPENDIX II—Derivatives of Equations at Nodes other than *i, j, k*

II.1 Derivatives of the *F* Equations at Nodes *i*+1, *j*, *k* and *i*-1, *j*, *k* and other nodes

The partial derivatives required for the *F* equation are given below. For the pressure derivatives at nodes *i*+1, *j*, *k* and *i*-1, *j*, *k*,

$$\frac{\partial F_{i\;i,j,k}^{n+1}}{\partial p_{o\;i+1,j,k}^{n+1}} = \sum_{p=1}^{N_p} \frac{\partial T_{p\;i+\frac{1}{2},j,k}^{n+1}}{\partial p_{o\;i+1,j,k}^{n+1}} \left[\left(p_{p\;i+1,j,k}^{n+1} - p_{p\;i,j,k}^{n+1} \right) - \rho_{p\;i+\frac{1}{2},j,k}^{n+1}\, g\left(z_{i+1,j,k} - z_{i,j,k} \right) \right]$$
$$+ T_{p\;i+\frac{1}{2},j,k}^{n+1} \left(\left[\frac{\partial p_p}{\partial p_o} \right]_{i+1,j,k}^{n+1} - \frac{\partial \rho_{p\;i+\frac{1}{2},j,k}^{n+1}}{\partial p_{o\;i+1,j,k}^{n+1}}\, g\left(z_{i+1,j,k} - z_{i,j,k} \right) \right), \qquad \text{(II.1.0.1)}$$

$$\frac{\partial F_{i\;i,j,k}^{n+1}}{\partial p_{o\;i-1,j,k}^{n+1}} = \sum_{p=1}^{N_p} \frac{\partial T_{p\;i-\frac{1}{2},j,k}^{n+1}}{\partial p_{o\;i-1,j,k}^{n+1}} \left[\left(p_{p\;i-1,j,k}^{n+1} - p_{p\;i,j,k}^{n+1} \right) - \rho_{p\;i-\frac{1}{2},j,k}^{n+1}\, g\left(z_{i-1,j,k} - z_{i,j,k} \right) \right]$$
$$+ T_{p\;i-\frac{1}{2},j,k}^{n+1} \left(\left[\frac{\partial p_p}{\partial p_o} \right]_{i-1,j,k}^{n+1} - \frac{\partial \rho_{p\;i-\frac{1}{2},j,k}^{n+1}}{\partial p_{o\;i-1,j,k}^{n+1}}\, g\left(z_{i-1,j,k} - z_{i,j,k} \right) \right), \qquad \text{(II.1.0.2)}$$

$$\frac{\partial T_{px\;i+\frac{1}{2},j,k}^{n+1}}{\partial p_{o\;i+1,j,k}^{n+1}} = \left[\frac{A_x k_x}{\Delta x} \right]_{i+\frac{1}{2},j,k} \left(1 - \omega_{px\;i,j,k} \right) \left[\frac{X_i k_{rp}}{\mu_p} \left(K_{vip} \frac{\partial \rho_p}{\partial p_o} + \rho_p \frac{\partial K_{vip}}{\partial p_o} - \frac{K_{vip} \rho_p}{\mu_p} \frac{\partial \mu_p}{\partial p_o} \right) \right]_{i+1,j,k}^{n+1}, \qquad \text{(II.1.0.3)}$$

and

$$\frac{\partial T_{px\;i-\frac{1}{2},j,k}^{n+1}}{\partial p_{o\;i-1,j,k}^{n+1}} = \left[\frac{A_x k_x}{\Delta x} \right]_{i-\frac{1}{2},j,k} \left(1 - \omega_{px\;i,j,k}^{*} \right) \left[\frac{X_i k_{rp}}{\mu_p} \left(K_{vip} \frac{\partial \rho_p}{\partial p_o} + \rho_p \frac{\partial K_{vip}}{\partial p_o} - \frac{K_{vip} \rho_p}{\mu_p} \frac{\partial \mu_p}{\partial p_o} \right) \right]_{i-1,j,k}^{n+1}. \qquad \text{(II.1.0.4)}$$

For the aqueous saturation derivatives at nodes *i*+1, *j*, *k* and *i*-1, *j*, *k*,

$$\frac{\partial F^{n+1}_{i\;\,i,j,k}}{\partial S^{n+1}_{w\;\,i+1,j,k}} = \sum_{p=1}^{N_p} \frac{\partial T^{n+1}_{p\;\,i+\frac{1}{2},j,k}}{\partial S^{n+1}_{w\;\,i+1,j,k}} \left[\left(p^{n+1}_{p\;\,i+1,j,k} - p^{n+1}_{p\;\,i,j,k}\right) - \rho^{n+1}_{p\;\,i+\frac{1}{2},j,k}\, g\left(z_{i+1,j,k} - z_{i,j,k}\right)\right] + T^{n+1}_{p\;\,i+\frac{1}{2},j,k}\left[\frac{\partial p_p}{\partial S_w}\right]^{n+1}_{i+1,j,k}, \qquad \text{(II.1.0.5)}$$

$$\frac{\partial F^{n+1}_{i\;\,i,j,k}}{\partial S^{n+1}_{w\;\,i-1,j,k}} = \sum_{p=1}^{N_p} \frac{\partial T^{n+1}_{p\;\,i-\frac{1}{2},j,k}}{\partial S^{n+1}_{w\;\,i-1,j,k}} \left[\left(p^{n+1}_{p\;\,i-1,j,k} - p^{n+1}_{p\;\,i,j,k}\right) - \rho^{n+1}_{p\;\,i-\frac{1}{2},j,k}\, g\left(z_{i-1,j,k} - z_{i,j,k}\right)\right] + T^{n+1}_{p\;\,i-\frac{1}{2},j,k}\left[\frac{\partial p_p}{\partial S_w}\right]^{n+1}_{i-1,j,k}, \qquad \text{(II.1.0.6)}$$

$$\frac{\partial T^{n+1}_{px\;\,i+\frac{1}{2},j,k}}{\partial S^{n+1}_{w\;\,i+1,j,k}} = \left[\frac{A_x k_x}{\Delta x}\right]_{i+\frac{1}{2},j,k}\left(1 - \omega_{px\;\,i,j,k}\right)\left[\frac{K_{vip} X_i \rho_p}{\mu_p}\frac{\partial k_{rp}}{\partial S_w}\right]^{n+1}_{i+1,j,k}, \qquad \text{(II.1.0.7)}$$

and

$$\frac{\partial T^{n+1}_{px\;\,i-\frac{1}{2},j,k}}{\partial S^{n+1}_{w\;\,i-1,j,k}} = \left[\frac{A_x k_x}{\Delta x}\right]_{i-\frac{1}{2},j,k}\left(1 - \omega^{*}_{px\;\,i,j,k}\right)\left[\frac{K_{vip} X_i \rho_p}{\mu_p}\frac{\partial k_{rp}}{\partial S_w}\right]^{n+1}_{i-1,j,k}. \qquad \text{(II.1.0.8)}$$

For the oleic saturation derivatives at nodes i+1, j, k and i-1, j, k,

$$\frac{\partial F^{n+1}_{i\;\,i,j,k}}{\partial S^{n+1}_{o\;\,i+1,j,k}} = \sum_{p=1}^{N_p} \frac{\partial T^{n+1}_{p\;\,i+\frac{1}{2},j,k}}{\partial S^{n+1}_{o\;\,i+1,j,k}} \left[\left(p^{n+1}_{p\;\,i+1,j,k} - p^{n+1}_{p\;\,i,j,k}\right) - \rho^{n+1}_{p\;\,i+\frac{1}{2},j,k}\, g\left(z_{i+1,j,k} - z_{i,j,k}\right)\right] + T^{n+1}_{p\;\,i+\frac{1}{2},j,k}\left[\frac{\partial p_p}{\partial S_o}\right]^{n+1}_{i+1,j,k}, \qquad \text{(II.1.0.9)}$$

$$\frac{\partial F^{n+1}_{i\;\,i,j,k}}{\partial S^{n+1}_{o\;\,i-1,j,k}} = \sum_{p=1}^{N_p} \frac{\partial T^{n+1}_{p\;\,i-\frac{1}{2},j,k}}{\partial S^{n+1}_{o\;\,i-1,j,k}} \left[\left(p^{n+1}_{p\;\,i-1,j,k} - p^{n+1}_{p\;\,i,j,k}\right) - \rho^{n+1}_{p\;\,i-\frac{1}{2},j,k}\, g\left(z_{i-1,j,k} - z_{i,j,k}\right)\right] + T^{n+1}_{p\;\,i-\frac{1}{2},j,k}\left[\frac{\partial p_p}{\partial S_o}\right]^{n+1}_{i-1,j,k}, \qquad \text{(II.1.0.10)}$$

$$\frac{\partial T^{n+1}_{px\;\,i+\frac{1}{2},j,k}}{\partial S^{n+1}_{o\;\,i+1,j,k}} = \left[\frac{A_x k_x}{\Delta x}\right]_{i+\frac{1}{2},j,k}\left(1 - \omega_{px\;\,i,j,k}\right)\left[\frac{K_{vip} X_i \rho_p}{\mu_p}\frac{\partial k_{rp}}{\partial S_o}\right]^{n+1}_{i+1,j,k}, \qquad \text{(II.1.0.11)}$$

and

$$\frac{\partial T^{n+1}_{px\;\,i-\frac{1}{2},j,k}}{\partial S^{n+1}_{o\;\,i-1,j,k}} = \left[\frac{A_x k_x}{\Delta x}\right]_{i-\frac{1}{2},j,k}\left(1 - \omega^{*}_{px\;\,i,j,k}\right)\left[\frac{K_{vip} X_i \rho_p}{\mu_p}\frac{\partial k_{rp}}{\partial S_o}\right]^{n+1}_{i-1,j,k}. \qquad \text{(II.1.0.12)}$$

For the gaseous saturation derivatives at nodes *i*+1, *j*, *k* and *i*-1, *j*, *k*,

$$\frac{\partial F_{i_{i,j,k}}^{n+1}}{\partial S_{g_{i+1,j,k}}^{n+1}}=\sum_{p=1}^{N_p}\frac{\partial T_{p_{i+\frac{1}{2},j,k}}^{n+1}}{\partial S_{g_{i+1,j,k}}^{n+1}}\left[\left(p_{p_{i+1,j,k}}^{n+1}-p_{p_{i,j,k}}^{n+1}\right)-\rho_{p_{i+\frac{1}{2},j,k}}^{n+1}\,g\left(z_{i+1,j,k}-z_{i,j,k}\right)\right]+T_{p_{i+\frac{1}{2},j,k}}^{n+1}\left[\frac{\partial p_p}{\partial S_g}\right]_{i+1,j,k}^{n+1}, \tag{II.1.0.13}$$

$$\frac{\partial F_{i_{i,j,k}}^{n+1}}{\partial S_{g_{i-1,j,k}}^{n+1}}=\sum_{p=1}^{N_p}\frac{\partial T_{p_{i-\frac{1}{2},j,k}}^{n+1}}{\partial S_{g_{i-1,j,k}}^{n+1}}\left[\left(p_{p_{i-1,j,k}}^{n+1}-p_{p_{i,j,k}}^{n+1}\right)-\rho_{p_{i-\frac{1}{2},j,k}}^{n+1}\,g\left(z_{i-1,j,k}-z_{i,j,k}\right)\right]+T_{p_{i-\frac{1}{2},j,k}}^{n+1}\left[\frac{\partial p_p}{\partial S_g}\right]_{i-1,j,k}^{n+1}, \tag{II.1.0.14}$$

$$\frac{\partial T_{px_{i+\frac{1}{2},j,k}}^{n+1}}{\partial S_{g_{i+1,j,k}}^{n+1}}=\left[\frac{A_x k_x}{\Delta x}\right]_{i+\frac{1}{2},j,k}\left(1-\omega_{px_{i,j,k}}\right)\left[\frac{K_{vip}X_i\rho_p}{\mu_p}\frac{\partial k_{rp}}{\partial S_g}\right]_{i+1,j,k}^{n+1}, \tag{II.1.0.15}$$

and

$$\frac{\partial T_{px_{i-\frac{1}{2},j,k}}^{n+1}}{\partial S_{g_{i-1,j,k}}^{n+1}}=\left[\frac{A_x k_x}{\Delta x}\right]_{i-\frac{1}{2},j,k}\left(1-\omega^{*}_{px_{i,j,k}}\right)\left[\frac{K_{vip}X_i\rho_p}{\mu_p}\frac{\partial k_{rp}}{\partial S_g}\right]_{i-1,j,k}^{n+1}. \tag{II.1.0.16}$$

For the temperature derivatives at nodes *i*+1, *j*, *k* and *i*-1, *j*, *k*,

$$\begin{aligned}\frac{\partial F_{i_{i,j,k}}^{n+1}}{\partial \theta_{i+1,j,k}^{n+1}}=&\sum_{p=1}^{N_p}\frac{\partial T_{p_{i+\frac{1}{2},j,k}}^{n+1}}{\partial \theta_{i+1,j,k}^{n+1}}\left[\left(p_{p_{i+1,j,k}}^{n+1}-p_{p_{i,j,k}}^{n+1}\right)-\rho_{p_{i+\frac{1}{2},j,k}}^{n+1}\,g\left(z_{i+1,j,k}-z_{i,j,k}\right)\right]\\&+T_{p_{i+\frac{1}{2},j,k}}^{n+1}\left(\left[\frac{\partial p_p}{\partial \theta}\right]_{i+1,j,k}^{n+1}-\frac{\partial \rho_{p_{i+\frac{1}{2},j,k}}^{n+1}}{\partial \theta_{i+1,j,k}^{n+1}}g\left(z_{i+1,j,k}-z_{i,j,k}\right)\right),\end{aligned} \tag{II.1.0.17}$$

$$\begin{aligned}\frac{\partial F_{i_{i,j,k}}^{n+1}}{\partial \theta_{i-1,j,k}^{n+1}}=&\sum_{p=1}^{N_p}\frac{\partial T_{p_{i-\frac{1}{2},j,k}}^{n+1}}{\partial \theta_{i-1,j,k}^{n+1}}\left[\left(p_{p_{i-1,j,k}}^{n+1}-p_{p_{i,j,k}}^{n+1}\right)-\rho_{p_{i-\frac{1}{2},j,k}}^{n+1}\,g\left(z_{i-1,j,k}-z_{i,j,k}\right)\right]\\&+T_{p_{i-\frac{1}{2},j,k}}^{n+1}\left(\left[\frac{\partial p_p}{\partial \theta}\right]_{i-1,j,k}^{n+1}-\frac{\partial \rho_{p_{i-\frac{1}{2},j,k}}^{n+1}}{\partial \theta_{i-1,j,k}^{n+1}}g\left(z_{i-1,j,k}-z_{i,j,k}\right)\right),\end{aligned} \tag{II.1.0.18}$$

$$\frac{\partial T^{n+1}_{px_{i+\frac{1}{2},j,k}}}{\partial \theta^{n+1}_{i+1,j,k}} = \left[\frac{A_x k_x}{\Delta x}\right]_{i+\frac{1}{2},j,k} \left(1 - \omega_{px_{i,j,k}}\right)$$

$$\left[\frac{X_i}{\mu_p}\left(K_{vip}\rho_p \frac{\partial k_{rp}}{\partial \theta} + K_{vip}k_{rp}\frac{\partial \rho_p}{\partial \theta} + \rho_p k_{rp}\frac{\partial K_{vip}}{\partial \theta} - \frac{K_{vip}\rho_p k_{rp}}{\mu_p}\frac{\partial \mu_p}{\partial \theta}\right)\right]^{n+1}_{i+1,j,k}, \qquad \text{(II.1.0.19)}$$

and

$$\frac{\partial T^{n+1}_{px_{i-\frac{1}{2},j,k}}}{\partial \theta^{n+1}_{i-1,j,k}} = \left[\frac{A_x k_x}{\Delta x}\right]_{i-\frac{1}{2},j,k} \left(1 - \omega^{*}_{px_{i,j,k}}\right)$$

$$\left[\frac{X_i}{\mu_p}\left(K_{vip}\rho_p \frac{\partial k_{rp}}{\partial \theta} + K_{vip}k_{rp}\frac{\partial \rho_p}{\partial \theta} + \rho_p k_{rp}\frac{\partial K_{vip}}{\partial \theta} - \frac{K_{vip}\rho_p k_{rp}}{\mu_p}\frac{\partial \mu_p}{\partial \theta}\right)\right]^{n+1}_{i-1,j,k}. \qquad \text{(II.1.0.20)}$$

For the composition derivatives at nodes $i+1, j, k$ and $i-1, j, k$,

$$\frac{\partial F^{n+1}_{i_{i,j,k}}}{\partial X^{n+1}_{j_{i+1,j,k}}} = \sum_{p=1}^{N_p} \frac{\partial T^{n+1}_{p_{i+\frac{1}{2},j,k}}}{\partial X^{n+1}_{j_{i+1,j,k}}} \left[\left(p^{n+1}_{p_{i+1,j,k}} - p^{n+1}_{p_{i,j,k}}\right) - \rho^{n+1}_{p_{i+\frac{1}{2},j,k}}\, g\left(z_{i+1,j,k} - z_{i,j,k}\right)\right]$$

$$+T^{n+1}_{p_l}\left(\left[\frac{\partial p_p}{\partial X_j}\right]^{n+1}_{i+1,j,k} - \frac{\partial \rho^{n+1}_{p_{i+\frac{1}{2},j,k}}}{\partial X^{n+1}_{j_{i+1,j,k}}}\, g\left(z_{i+1,j,k} - z_{i,j,k}\right)\right), \qquad \text{(II.1.0.21)}$$

$$\frac{\partial F^{n+1}_{i_{i,j,k}}}{\partial X^{n+1}_{j_{i-1,j,k}}} = \sum_{p=1}^{N_p} \frac{\partial T^{n+1}_{p_{i-\frac{1}{2},j,k}}}{\partial X^{n+1}_{j_{i-1,j,k}}} \left[\left(p^{n+1}_{p_{i-1,j,k}} - p^{n+1}_{p_{i,j,k}}\right) - \rho^{n+1}_{p_{i-\frac{1}{2},j,k}}\, g\left(z_{i-1,j,k} - z_{i,j,k}\right)\right]$$

$$+T^{n+1}_{p_l}\left(\left[\frac{\partial p_p}{\partial X_j}\right]^{n+1}_{i-1,j,k} - \frac{\partial \rho^{n+1}_{p_{i-\frac{1}{2},j,k}}}{\partial X^{n+1}_{j_{i-1,j,k}}}\, g\left(z_{i-1,j,k} - z_{i,j,k}\right)\right), \qquad \text{(II.1.0.22)}$$

$$\frac{\partial T^{n+1}_{px_{i+\frac{1}{2},j,k}}}{\partial X^{n+1}_{j_{i+1,j,k}}} = \left[\frac{A_x k_x}{\Delta x}\right]_{i+\frac{1}{2},j,k} \left(1 - \omega_{px_{i,j,k}}\right)\left[\frac{K_{vip}k_{rp}}{\mu_p}\left(X_i\frac{\partial \rho_p}{\partial X_j} + \rho_p\frac{\partial X_i}{\partial X_j} - \frac{X_i\rho_p}{\mu_p}\frac{\partial \mu_p}{\partial X_j}\right)\right]^{n+1}_{i+1,j,k}, \qquad \text{(II.1.0.23)}$$

and

$$\frac{\partial T^{n+1}_{px\,i-\frac{1}{2},j,k}}{\partial X^{n+1}_{j\,i-1,j,k}} = \left[\frac{A_x k_x}{\Delta x}\right]_{i-\frac{1}{2},j,k}\left(1-\omega^{*}_{px\,i,j,k}\right)\left[\frac{K_{vip}k_{rp}}{\mu_p}\left(X_i\frac{\partial \rho_p}{\partial X_j}+\rho_p\frac{\partial X_i}{\partial X_j}-\frac{X_i\rho_p}{\mu_p}\frac{\partial \mu_p}{\partial X_j}\right)\right]^{n+1}_{i-1,j,k}, \tag{II.1.0.24}$$

where

$$\frac{\partial X_i}{\partial X_j}=\begin{cases}1 & i=j\\ 0 & i\neq j\end{cases}. \tag{II.1.0.25}$$

Similar expressions exist for the other nodes surrounding Node *i*, *j*, *k*.

II.2 Derivatives of the *G* Equation at Nodes *i*+1, *j*, *k* and *i*-1, *j*, *k* and other nodes

The partial derivatives required for the *G* equation are given below. For the pressure derivatives at nodes *i*+1, *j*, *k* and *i*-1, *j*, *k*,

$$\begin{aligned}\frac{\partial G^{n+1}_{i,j,k}}{\partial p^{n+1}_{o\,i+1,j,k}} &= \sum_{p=1}^{N_p}\frac{\partial \overset{n+1}{T^{*}_{p\,i+\frac{1}{2},j,k}}}{\partial p^{n+1}_{o\,i+1,j,k}}\left[\left(p^{n+1}_{p\,i+1,j,k}-p^{n+1}_{p\,i,j,k}\right)-\rho^{n+1}_{p\,i+\frac{1}{2},j,k}\,g\left(z_{i+1,j,k}-z_{i,j,k}\right)\right]\\ &+\overset{n+1}{T^{*}_{p\,i+\frac{1}{2},j,k}}\left(\left[\frac{\partial p_p}{\partial p_o}\right]^{n+1}_{i+1,j,k}-\frac{\partial \rho^{n+1}_{p\,i+\frac{1}{2},j,k}}{\partial p^{n+1}_{o\,i+1,j,k}}g\left(z_{i+1,j,k}-z_{i,j,k}\right)\right),\end{aligned} \tag{II.2.0.1}$$

$$\begin{aligned}\frac{\partial G^{n+1}_{i,j,k}}{\partial p^{n+1}_{o\,i-1,j,k}} &= \sum_{p=1}^{N_p}\frac{\partial \overset{n+1}{T^{*}_{p\,i-\frac{1}{2},j,k}}}{\partial p^{n+1}_{o\,i-1,j,k}}\left[\left(p^{n+1}_{p\,i-1,j,k}-p^{n+1}_{p\,i,j,k}\right)-\rho^{n+1}_{p\,i-\frac{1}{2},j,k}\,g\left(z_{i-1,j,k}-z_{i,j,k}\right)\right]\\ &+\overset{n+1}{T^{*}_{p\,i-\frac{1}{2},j,k}}\left(\left[\frac{\partial p_p}{\partial p_o}\right]^{n+1}_{i-1,j,k}-\frac{\partial \rho^{n+1}_{p\,i-\frac{1}{2},j,k}}{\partial p^{n+1}_{o\,i-1,j,k}}g\left(z_{i-1,j,k}-z_{i,j,k}\right)\right),\end{aligned} \tag{II.2.0.2}$$

$$\frac{\partial T^{*\,n+1}_{px\;i+\frac{1}{2},j,k}}{\partial p^{n+1}_{o\;i+1,j,k}} = \left[\frac{A_x k_x}{\Delta x}\right]_{i+\frac{1}{2},j,k}\left(1-\omega_{px\;i,j,k}\right)\left[\frac{k_{rp}}{\mu_p}\left(H_p\frac{\partial\rho_p}{\partial p_o}+\rho_p\frac{\partial H_p}{\partial p_o}-\frac{H_p\rho_p}{\mu_p}\frac{\partial\mu_p}{\partial p_o}\right)\right]^{n+1}_{i+1,j,k},\text{(II.2.0.3)}$$

and

$$\frac{\partial T^{*\,n+1}_{px\;i-\frac{1}{2},j,k}}{\partial p^{n+1}_{o\;i-1,j,k}} = \left[\frac{A_x k_x}{\Delta x}\right]_{i-\frac{1}{2},j,k}\left(1-\omega^{*}_{px\;i,j,k}\right)\left[\frac{k_{rp}}{\mu_p}\left(H_p\frac{\partial\rho_p}{\partial p_o}+\rho_p\frac{\partial H_p}{\partial p_o}-\frac{H_p\rho_p}{\mu_p}\frac{\partial\mu_p}{\partial p_o}\right)\right]^{n+1}_{i-1,j,k}.\text{(II.2.0.4)}$$

For the aqueous saturation derivatives at nodes *i*+1, *j*, *k* and *i*-1, *j*, *k*,

$$\frac{\partial G^{n+1}_{i,j,k}}{\partial S^{n+1}_{w\;i+1,j,k}} = \sum_{p=1}^{N_p}\frac{\partial T^{*\,n+1}_{p\;i+\frac{1}{2},j,k}}{\partial S^{n+1}_{w\;i+1,j,k}}\left[\left(p^{n+1}_{p\;i+1,j,k}-p^{n+1}_{p\;i,j,k}\right)-\rho^{n+1}_{p\;i+\frac{1}{2},j,k}\,g\left(z_{i+1,j,k}-z_{i,j,k}\right)\right]+T^{*\,n+1}_{p\;i+\frac{1}{2},j,k}\left[\frac{\partial p_p}{\partial S_w}\right]^{n+1}_{i+1,j,k},\quad\text{(II.2.0.5)}$$

$$\frac{\partial G^{n+1}_{i,j,k}}{\partial S^{n+1}_{w\;i-1,j,k}} = \sum_{p=1}^{N_p}\frac{\partial T^{*\,n+1}_{p\;i-\frac{1}{2},j,k}}{\partial S^{n+1}_{w\;i-1,j,k}}\left[\left(p^{n+1}_{p\;i-1,j,k}-p^{n+1}_{p\;i,j,k}\right)-\rho^{n+1}_{p\;i-\frac{1}{2},j,k}\,g\left(z_{i-1,j,k}-z_{i,j,k}\right)\right]+T^{*\,n+1}_{p\;i-\frac{1}{2},j,k}\left[\frac{\partial p_p}{\partial S_w}\right]^{n+1}_{i-1,j,k},\quad\text{(II.2.0.6)}$$

$$\frac{\partial T^{*\,n+1}_{px\;i+\frac{1}{2},j,k}}{\partial S^{n+1}_{w\;i+1,j,k}} = \left[\frac{A_x k_x}{\Delta x}\right]_{i+\frac{1}{2},j,k}\left(1-\omega_{px\;i,j,k}\right)\left[\frac{H_p\rho_p}{\mu_p}\frac{\partial k_{rp}}{\partial S_w}\right]^{n+1}_{i+1,j,k},\qquad\text{(II.2.0.7)}$$

and

$$\frac{\partial T^{*\,n+1}_{px\;i-\frac{1}{2},j,k}}{\partial S^{n+1}_{w\;i-1,j,k}} = \left[\frac{A_x k_x}{\Delta x}\right]_{i-\frac{1}{2},j,k}\left(1-\omega^{*}_{px\;i,j,k}\right)\left[\frac{H_p\rho_p}{\mu_p}\frac{\partial k_{rp}}{\partial S_w}\right]^{n+1}_{i-1,j,k}.\qquad\text{(II.2.0.8)}$$

For the oleic saturation derivatives at nodes *i*+1, *j*, *k* and *i*-1, *j*, *k*,

$$\frac{\partial G^{n+1}_{i,j,k}}{\partial S^{n+1}_{o\,i+1,j,k}} = \sum_{p=1}^{N_p} \frac{\partial T^{*\,n+1}_{p\,i+\frac{1}{2},j,k}}{\partial S^{n+1}_{o\,i+1,j,k}} \left[\left(p^{n+1}_{p\,i+1,j,k} - p^{n+1}_{p\,i,j,k} \right) - \rho^{n+1}_{p\,i+\frac{1}{2},j,k}\, g\left(z_{i+1,j,k} - z_{i,j,k} \right) \right] + T^{*\,n+1}_{p\,i+\frac{1}{2},j,k} \left[\frac{\partial p_p}{\partial S_o} \right]^{n+1}_{i+1,j,k}, \qquad \text{(II.2.0.9)}$$

$$\frac{\partial G^{n+1}_{i,j,k}}{\partial S^{n+1}_{o\,i-1,j,k}} = \sum_{p=1}^{N_p} \frac{\partial T^{*\,n+1}_{p\,i-\frac{1}{2},j,k}}{\partial S^{n+1}_{o\,i-1,j,k}} \left[\left(p^{n+1}_{p\,i-1,j,k} - p^{n+1}_{p\,i,j,k} \right) - \rho^{n+1}_{p\,i-\frac{1}{2},j,k}\, g\left(z_{i-1,j,k} - z_{i,j,k} \right) \right] + T^{*\,n+1}_{p\,i-\frac{1}{2},j,k} \left[\frac{\partial p_p}{\partial S_o} \right]^{n+1}_{i-1,j,k}, \qquad \text{(II.2.0.10)}$$

$$\frac{\partial T^{*\,n+1}_{px\,i+\frac{1}{2},j,k}}{\partial S^{n+1}_{o\,i+1,j,k}} = \left[\frac{A_x k_x}{\Delta x} \right]_{i+\frac{1}{2},j,k} \left(1 - \omega_{px\,i,j,k} \right) \left[\frac{H_p \rho_p}{\mu_p} \frac{\partial k_{rp}}{\partial S_o} \right]^{n+1}_{i+1,j,k}, \qquad \text{(II.2.0.11)}$$

and

$$\frac{\partial T^{*\,n+1}_{px\,i-\frac{1}{2},j,k}}{\partial S^{n+1}_{o\,i-1,j,k}} = \left[\frac{A_x k_x}{\Delta x} \right]_{i-\frac{1}{2},j,k} \left(1 - \omega^{*}_{px\,i,j,k} \right) \left[\frac{H_p \rho_p}{\mu_p} \frac{\partial k_{rp}}{\partial S_o} \right]^{n+1}_{i-1,j,k}. \qquad \text{(II.2.0.12)}$$

For the gaseous saturation derivatives at nodes $i+1, j, k$ and $i-1, j, k$,

$$\frac{\partial G^{n+1}_{i,j,k}}{\partial S^{n+1}_{g\,i+1,j,k}} = \sum_{p=1}^{N_p} \frac{\partial T^{*\,n+1}_{p\,i+\frac{1}{2},j,k}}{\partial S^{n+1}_{g\,i+1,j,k}} \left[\left(p^{n+1}_{p\,i+1,j,k} - p^{n+1}_{p\,i,j,k} \right) - \rho^{n+1}_{p\,i+\frac{1}{2},j,k}\, g\left(z_{i+1,j,k} - z_{i,j,k} \right) \right] + T^{*\,n+1}_{p\,i+\frac{1}{2},j,k} \left[\frac{\partial p_p}{\partial S_g} \right]^{n+1}_{i+1,j,k}, \qquad \text{(II.2.0.13)}$$

$$\frac{\partial G^{n+1}_{i,j,k}}{\partial S^{n+1}_{g\,i-1,j,k}} = \sum_{p=1}^{N_p} \frac{\partial T^{*\,n+1}_{p\,i-\frac{1}{2},j,k}}{\partial S^{n+1}_{g\,i-1,j,k}} \left[\left(p^{n+1}_{p\,i-1,j,k} - p^{n+1}_{p\,i,j,k} \right) - \rho^{n+1}_{p\,i-\frac{1}{2},j,k}\, g\left(z_{i-1,j,k} - z_{i,j,k} \right) \right] + T^{*\,n+1}_{p\,i-\frac{1}{2},j,k} \left[\frac{\partial p_p}{\partial S_g} \right]^{n+1}_{i-1,j,k}, \qquad \text{(II.2.0.14)}$$

$$\frac{\partial T^{*\,n+1}_{px\,i+\frac{1}{2},j,k}}{\partial S^{n+1}_{g\,i+1,j,k}} = \left[\frac{A_x k_x}{\Delta x} \right]_{i+\frac{1}{2},j,k} \left(1 - \omega_{px\,i,j,k} \right) \left[\frac{H_p \rho_p}{\mu_p} \frac{\partial k_{rp}}{\partial S_g} \right]^{n+1}_{i+1,j,k}, \qquad \text{(II.2.0.15)}$$

and

$$\frac{\partial T^{*\,n+1}_{px\;i-\frac{1}{2},j,k}}{\partial S^{n+1}_{g\;i-1,j,k}}=\left[\frac{A_x k_x}{\Delta x}\right]_{i-\frac{1}{2},j,k}\left(1-\omega^{*}_{px\;i,j,k}\right)\left[\frac{H_p\rho_p}{\mu_p}\frac{\partial k_{rp}}{\partial S_g}\right]^{n+1}_{i-1,j,k}. \tag{II.2.0.16}$$

For the temperature derivatives at nodes i+1, j, k and i-1, j, k,

$$\frac{\partial G^{n+1}_{i,j,k}}{\partial \theta^{n+1}_{i+1,j,k}}=\sum_{p=1}^{N_p}\frac{\partial T^{*\,n+1}_{p\;i+\frac{1}{2},j,k}}{\partial \theta^{n+1}_{i+1,j,k}}\left[\left(p^{n+1}_{p\;i+1,j,k}-p^{n+1}_{p\;i,j,k}\right)-\rho^{n+1}_{p\;i+\frac{1}{2},j,k}\,g\left(z_{i+1,j,k}-z_{i,j,k}\right)\right]$$
$$+T^{*\,n+1}_{p\;i+\frac{1}{2},j,k}\left(\left[\frac{\partial p_p}{\partial \theta}\right]^{n+1}_{i+1,j,k}-\frac{\partial \rho^{n+1}_{p\;i+\frac{1}{2},j,k}}{\partial \theta^{n+1}_{i+1,j,k}}\,g\left(z_{i+1,j,k}-z_{i,j,k}\right)\right)+T^{n+1}_{cx\;i+\frac{1}{2},j,k}\;, \tag{II.2.0.17}$$

$$\frac{\partial G^{n+1}_{i,j,k}}{\partial \theta^{n+1}_{i-1,j,k}}=\sum_{p=1}^{N_p}\frac{\partial T^{*\,n+1}_{p\;i-\frac{1}{2},j,k}}{\partial \theta^{n+1}_{i-1,j,k}}\left[\left(p^{n+1}_{p\;i-1,j,k}-p^{n+1}_{p\;i,j,k}\right)-\rho^{n+1}_{p\;i-\frac{1}{2},j,k}\,g\left(z_{i-1,j,k}-z_{i,j,k}\right)\right]$$
$$+T^{*\,n+1}_{p\;i-\frac{1}{2},j,k}\left(\left[\frac{\partial p_p}{\partial \theta}\right]^{n+1}_{i-1,j,k}-\frac{\partial \rho^{n+1}_{p\;i-\frac{1}{2},j,k}}{\partial \theta^{n+1}_{i-1,j,k}}\,g\left(z_{i-1,j,k}-z_{i,j,k}\right)\right)+T^{n+1}_{cx\;i-\frac{1}{2},j,k}\;, \tag{II.2.0.18}$$

$$\frac{\partial T^{*\,n+1}_{px\;i+\frac{1}{2},j,k}}{\partial \theta^{n+1}_{i+1,j,k}}=\left[\frac{A_x k_x}{\Delta x}\right]_{i+\frac{1}{2},j,k}\left(1-\omega_{px\;i,j,k}\right)$$
$$\left[\frac{1}{\mu_p}\left(H_p\rho_p\frac{\partial k_{rp}}{\partial \theta}+H_p k_{rp}\frac{\partial \rho_p}{\partial \theta}+\rho_p k_{rp}\frac{\partial H_p}{\partial \theta}-\frac{H_p\rho_p k_{rp}}{\mu_p}\frac{\partial \mu_p}{\partial \theta}\right)\right]^{n+1}_{i+1,j,k}, \tag{II.2.0.19}$$

and

$$\frac{\partial T^{*\,n+1}_{px\;i-\frac{1}{2},j,k}}{\partial \theta^{n+1}_{i-1,j,k}}=\left[\frac{A_x k_x}{\Delta x}\right]_{i-\frac{1}{2},j,k}\left(1-\omega^{*}_{px\;i,j,k}\right)$$

$$\left[\frac{1}{\mu_p}\left(H_p\rho_p\frac{\partial k_{rp}}{\partial\theta}+H_pk_{rp}\frac{\partial\rho_p}{\partial\theta}+\rho_pk_{rp}\frac{\partial H_p}{\partial\theta}-\frac{H_p\rho_pk_{rp}}{\mu_p}\frac{\partial\mu_p}{\partial\theta}\right)\right]_{i-1,j,k}^{n+1} . \tag{II.2.0.20}$$

For the composition derivatives at nodes *i*+1, *j*, *k* and *i*-1, *j*, *k*,

$$\frac{\partial G_{i,j,k}^{n+1}}{\underset{i+1,j,k}{\partial X_j^{n+1}}}=\sum_{p=1}^{N_p}\frac{\partial \underset{i+\frac{1}{2},j,k}{T_p^{*\,n+1}}}{\underset{i+1,j,k}{\partial X_j^{n+1}}}\left[\left(\underset{i+1,j,k}{p_p^{n+1}}-\underset{i,j,k}{p_p^{n+1}}\right)-\underset{i+\frac{1}{2},j,k}{\rho_p^{n+1}}\;g\left(z_{i+1,j,k}-z_{i,j,k}\right)\right]$$
$$+\underset{l}{T_p^{*\,n+1}}\left(\left[\frac{\partial p_p}{\partial X_j}\right]_{i+1,j,k}^{n+1}-\frac{\partial \underset{i+\frac{1}{2},j,k}{\rho_p^{n+1}}}{\underset{i+1,j,k}{\partial X_j^{n+1}}}g\left(z_{i+1,j,k}-z_{i,j,k}\right)\right) , \tag{II.2.0.21}$$

$$\frac{\partial G_{i,j,k}^{n+1}}{\underset{i-1,j,k}{\partial X_j^{n+1}}}=\sum_{p=1}^{N_p}\frac{\partial \underset{i-\frac{1}{2},j,k}{T_p^{*\,n+1}}}{\underset{i-1,j,k}{\partial X_j^{n+1}}}\left[\left(\underset{i-1,j,k}{p_p^{n+1}}-\underset{i,j,k}{p_p^{n+1}}\right)-\underset{i-\frac{1}{2},j,k}{\rho_p^{n+1}}\;g\left(z_{i-1,j,k}-z_{i,j,k}\right)\right]$$
$$+\underset{l}{T_p^{*\,n+1}}\left(\left[\frac{\partial p_p}{\partial X_j}\right]_{i-1,j,k}^{n+1}-\frac{\partial \underset{i-\frac{1}{2},j,k}{\rho_p^{n+1}}}{\underset{i-1,j,k}{\partial X_j^{n+1}}}g\left(z_{i-1,j,k}-z_{i,j,k}\right)\right) , \tag{II.2.0.22}$$

$$\frac{\partial \underset{i+\frac{1}{2},j,k}{T_{px}^{*\,n+1}}}{\underset{i+1,j,k}{\partial X_j^{n+1}}}=\left[\frac{A_xk_x}{\Delta x}\right]_{i+\frac{1}{2},j,k}\left(1-\underset{i,j,k}{\omega_{px}}\right)\left[\frac{k_{rp}}{\mu_p}\left(H_p\frac{\partial\rho_p}{\partial X_j}+\rho_p\frac{\partial H_p}{\partial X_j}-\frac{H_p\rho_p}{\mu_p}\frac{\partial\mu_p}{\partial X_j}\right)\right]_{i+1,j,k}^{n+1} , \tag{II.2.0.23}$$

and

$$\frac{\partial \underset{i-\frac{1}{2},j,k}{T_{px}^{*\,n+1}}}{\underset{i-1,j,k}{\partial X_j^{n+1}}}=\left[\frac{A_xk_x}{\Delta x}\right]_{i-\frac{1}{2},j,k}\left(1-\underset{i,j,k}{\omega_{px}}\right)\left[\frac{k_{rp}}{\mu_p}\left(H_p\frac{\partial\rho_p}{\partial X_j}+\rho_p\frac{\partial H_p}{\partial X_j}-\frac{H_p\rho_p}{\mu_p}\frac{\partial\mu_p}{\partial X_j}\right)\right]_{i-1,j,k}^{n+1} . \tag{II.2.0.24}$$

Similar expressions exist for the other nodes surrounding Node *i*, *j*, *k*.

APPENDIX III—Derivatives of Well Equation

III.1 Shut-in Well

The shut-in well constraint is given by

$$\underset{i,j}{W_1^{n+1}} = -\sum_{k}\sum_{p=1}^{N_p}\sum_{i=1}^{N_c} J'_{i,j,k}\left[K_{vip}X_i\frac{k_{rp}}{\mu_p}\frac{\rho_p}{\rho_{p,STC}}\right]_{i,j,k}^{n+1}\left[p_o - p_{wf}\right]_{i,j,k}^{n+1} = 0\ . \qquad \text{(III.1.0.1)}$$

For the pressure derivative at node *i*, *j*, *k*,

$$\frac{\partial \underset{i,j}{W_1^{n+1}}}{\partial \underset{i,j,k}{p_o^{n+1}}} = -J'_{i,j,k}\sum_{p=1}^{N_p}\left[\frac{k_{rp}}{\mu_p}\frac{\rho_p}{\rho_{p,STC}}\sum_{i=1}^{N_c}\frac{\partial K_{vip}}{\partial p_o}X_i + \frac{k_{rp}}{\mu_p}\frac{1}{\rho_{p,STC}}\left(\frac{\partial \rho_p}{\partial p_o} - \frac{\rho_p}{\mu_p}\frac{\partial \mu_p}{\partial p_o}\right)\right]_{i,j,k}^{n+1}\left[p_o - p_{wf}\right]_{i,j,k}^{n+1}$$

$$+\left[\frac{k_{rp}}{\mu_p}\frac{\rho_p}{\rho_{p,STC}}\right]_{i,j,k}^{n+1}. \qquad \text{(III.1.0.2)}$$

For the aqueous, oleic and gaseous phase saturation derivatives,

$$\frac{\partial \underset{i,j}{W_1^{n+1}}}{\partial \underset{i,j,k}{S_w^{n+1}}} = -J'_{i,j,k}\sum_{p=1}^{N_p}\left[\frac{1}{\mu_p}\frac{\rho_p}{\rho_{p,STC}}\frac{\partial k_{rp}}{\partial S_w}\right]_{i,j,k}^{n+1}\left[p_o - p_{wf}\right]_{i,j,k}^{n+1}\ , \qquad \text{(III.1.0.3)}$$

$$\frac{\partial \underset{i,j}{W_1^{n+1}}}{\partial \underset{i,j,k}{S_o^{n+1}}} = -J'_{i,j,k}\sum_{p=1}^{N_p}\left[\frac{1}{\mu_p}\frac{\rho_p}{\rho_{p,STC}}\frac{\partial k_{rp}}{\partial S_o}\right]_{i,j,k}^{n+1}\left[p_o - p_{wf}\right]_{i,j,k}^{n+1}\ , \qquad \text{(III.1.0.4)}$$

and

$$\frac{\partial \underset{i,j}{W_1^{n+1}}}{\partial \underset{i,j,k}{S_g^{n+1}}} = -J'_{i,j,k}\sum_{p=1}^{N_p}\left[\frac{1}{\mu_p}\frac{\rho_p}{\rho_{p,STC}}\frac{\partial k_{rp}}{\partial S_g}\right]_{i,j,k}^{n+1}\left[p_o - p_{wf}\right]_{i,j,k}^{n+1}\ , \qquad \text{(III.1.0.5)}$$

respectively. For the temperature derivative at node *i*, *j*, *k*,

$$\frac{\partial \underset{i,j}{W_1^{n+1}}}{\partial \theta_{i,j,k}^{n+1}} = -J'_{i,j,k}\sum_{p=1}^{N_p}\left[\frac{k_{rp}}{\mu_p}\frac{\rho_p}{\rho_{p,STC}}\sum_{i=1}^{N_c}\frac{\partial K_{vip}}{\partial \theta}X_i + \frac{1}{\mu_p}\frac{\rho_p}{\rho_{p,STC}}\frac{\partial k_{rp}}{\partial \theta}\right.$$

$$+\frac{k_{rp}}{\mu_p}\frac{1}{\rho_{p,STC}}\left(\frac{\partial \rho_p}{\partial \theta}-\frac{\rho_p}{\mu_p}\frac{\partial \mu_p}{\partial \theta}\right)\Bigg]_{i,j,k}^{n+1}\left[p_o-p_{wf}\right]_{i,j,k}^{n+1} . \tag{III.1.0.6}$$

For each composition derivative at node *i*, *j*, *k*,

$$\frac{\partial W_{1\,i,j}^{n+1}}{\partial X_{j\,i,j,k}^{n+1}}=$$

$$-J'_{i,j,k}\sum_{p=1}^{N_p}\left[\frac{k_{rp}}{\mu_p}\frac{\rho_p}{\rho_{p,STC}}\sum_{i=1}^{N_c}K_{vip}\frac{\partial X_i}{\partial X_j}+\frac{k_{rp}}{\mu_p}\frac{1}{\rho_{p,STC}}\left(\frac{\partial \rho_p}{\partial X_j}-\frac{\rho_p}{\mu_p}\frac{\partial \mu_p}{\partial X_j}\right)\right]_{i,j,k}^{n+1}\left[p_o-p_{wf}\right]_{i,j,k}^{n+1} . \tag{III.1.0.7}$$

For the well pressure derivative at node *i*, *j*,

$$\frac{\partial W_{1\,i,j}^{n+1}}{\partial p_{wf\,i,j}}=\sum_{k}J'_{i,j,k}\sum_{p=1}^{N_p}\left[\frac{k_{rp}}{\mu_p}\frac{\rho_p}{\rho_{p,STC}}\right]_{i,j,k}^{n+1} . \tag{III.1.0.8}$$

At nodes *i*±1, *j*, *k* and *i*, *j*±1, *k*, all derivatives are zero. At nodes *i*, *j*, *k*±1, the pressure derivative is given by

$$\frac{\partial W_{1\,i,j}^{n+1}}{\partial p_{o\,i,j,k\pm1}^{n+1}}=-J'_{i,j,k\pm1}\sum_{p=1}^{N_p}\left[\frac{k_{rp}}{\mu_p}\frac{\rho_p}{\rho_{p,STC}}\sum_{i=1}^{N_c}\frac{\partial K_{vip}}{\partial p_o}X_i+\frac{k_{rp}}{\mu_p}\frac{1}{\rho_{p,STC}}\left(\frac{\partial \rho_p}{\partial p_o}-\frac{\rho_p}{\mu_p}\frac{\partial \mu_p}{\partial p_o}\right)\right]_{i,j,k\pm1}^{n+1}\left[p_o-p_{wf}\right]_{i,j,k\pm1}^{n+1}$$

$$+\left[\frac{k_{rp}}{\mu_p}\frac{\rho_p}{\rho_{p,STC}}\right]_{i,j,k\pm1}^{n+1} . \tag{III.1.0.9}$$

This equation is identical to Equation III.1.0.2 except for the change in the subscript *i*, *j*, *k* to *i*, *j*, *k*±1; the same is true for Equations III.1.0.3 to III.1.0.7.

III.2 Constant Total Volume Injection Well

The constant total volume injection well constraint is given by

$$W_{2\,i,j}^{n+1}=q_{i,j}^{T}-\sum_{k}\sum_{p=1}^{N_p}\sum_{i=1}^{N_c}J'_{i,j,k}\left(\sum_{m=1}^{N_p}\frac{k_{rm}}{\mu_{rm}}\right)_{i,j,k}^{n+1}\left[K_{vip}X_i\frac{\rho_{p\,wb}}{\rho_{p,STC}}\right]_{i,j,k}^{n+1}\left[p_o-p_{wf}\right]_{i,j,k}^{n+1}=0 , \tag{III.2.0.1}$$

where

$$\left(K_{v11}X_1\right)_k = 1 - x \ , \tag{III.2.0.2}$$

$$\left(K_{v13}X_1\right)_k = x \ , \tag{III.2.0.3}$$

and

$$\left(K_{vip}X_i\right)_k = 0 \qquad\qquad i \neq 1 \ . \tag{III.2.0.4}$$

The required derivatives are given by

$$\frac{\partial W^{n+1}_{2_{i,j}}}{\partial p^{n+1}_{o_{i,j,k}}} = -J'_{i,j,k} \sum_{p=1}^{N_p} \sum_{i=1}^{N_c} \left(K_{vip} X_i \frac{\rho_{p_{wb}}}{\rho_{p,STC}} \right)^{n+1}_{i,j,k} \left[\left(\sum_{m=1}^{N_p} - \frac{k_{rm}}{\mu_m^2} \frac{\partial \mu_m}{\partial p_o} \right)^{n+1}_{i,j,k} \left(p_o - p_{wf} \right)^{n+1}_{i,j,k} + \left(\sum_{m=1}^{N_p} \frac{k_{rm}}{\mu_m} \right)^{n+1}_{i,j,k} \right] , \tag{III.2.0.5}$$

$$\frac{\partial W^{n+1}_{2_{i,j}}}{\partial S^{n+1}_{w_{i,j,k}}} = -J'_{i,j,k} \sum_{p=1}^{N_p} \sum_{i=1}^{N_c} \left(K_{vip} X_i \frac{\rho_{p_{wb}}}{\rho_{p,STC}} \right)^{n+1}_{i,j,k} \left[\left(\sum_{m=1}^{N_p} \frac{1}{\mu_m} \frac{\partial \mu_m}{\partial S_w} \right)^{n+1}_{i,j,k} \left(p_o - p_{wf} \right)^{n+1}_{i,j,k} \right] , \tag{III.2.0.6}$$

$$\frac{\partial W^{n+1}_{2_{i,j}}}{\partial S^{n+1}_{o_{i,j,k}}} = -J'_{i,j,k} \sum_{p=1}^{N_p} \sum_{i=1}^{N_c} \left(K_{vip} X_i \frac{\rho_{p_{wb}}}{\rho_{p,STC}} \right)^{n+1}_{i,j,k} \left[\left(\sum_{m=1}^{N_p} \frac{1}{\mu_m} \frac{\partial \mu_m}{\partial S_o} \right)^{n+1}_{i,j,k} \left(p_o - p_{wf} \right)^{n+1}_{i,j,k} \right] , \tag{III.2.0.7}$$

$$\frac{\partial W^{n+1}_{2_{i,j}}}{\partial S^{n+1}_{g_{i,j,k}}} = -J'_{i,j,k} \sum_{p=1}^{N_p} \sum_{i=1}^{N_c} \left(K_{vip} X_i \frac{\rho_{p_{wb}}}{\rho_{p,STC}} \right)^{n+1}_{i,j,k} \left[\left(\sum_{m=1}^{N_p} \frac{1}{\mu_m} \frac{\partial \mu_m}{\partial S_g} \right)^{n+1}_{i,j,k} \left(p_o - p_{wf} \right)^{n+1}_{i,j,k} \right] , \tag{III.2.0.8}$$

$$\frac{\partial W^{n+1}_{2_{i,j}}}{\partial \Theta^{n+1}_{i,j,k}} = -J'_{i,j,k} \sum_{p=1}^{N_p} \sum_{i=1}^{N_c} \left(K_{vip} X_i \frac{\rho_{p_{wb}}}{\rho_{p,STC}} \right)^{n+1}_{i,j,k} \left[\left(\sum_{m=1}^{N_p} \frac{1}{\mu_m} \left(\frac{\partial k_{rm}}{\partial \Theta} - \frac{k_{rm}}{\mu_m} \frac{\partial \mu_m}{\partial \Theta} \right) \right)^{n+1}_{i,j,k} \left(p_o - p_{wf} \right)^{n+1}_{i,j,k} \right] , \tag{III.2.0.9}$$

$$\frac{\partial W^{n+1}_{2_{i,j}}}{\partial X^{n+1}_{j_{i,j,k}}} = -J'_{i,j,k} \sum_{p=1}^{N_p} \sum_{i=1}^{N_c} \left(K_{vip} X_i \frac{\rho_{p_{wb}}}{\rho_{p,STC}} \right)^{n+1}_{i,j,k} \left[\left(\sum_{m=1}^{N_p} - \frac{k_{rm}}{\mu_m^2} \frac{\partial \mu_m}{\partial X_j} \right)^{n+1}_{i,j,k} \left(p_o - p_{wf} \right)^{n+1}_{i,j,k} \right] , \tag{III.2.0.10}$$

and

$$\frac{\partial W^{n+1}_{2_{i,j}}}{\partial p^{n+1}_{wf_{i,j}}} = -J'_{i,j,k} \sum_{p=1}^{N_p} \sum_{i=1}^{N_c} \left(K_{vip} X_i \frac{1}{\rho_{p,STC}} \right)^{n+1}_{i,j,k}$$

$$\left[\left(\frac{\partial \rho_{p_{wb}}}{\partial p_{wf}} \sum_{m=1}^{N_p} \frac{k_{rm}}{\mu_m}\right)_{i,j,k}^{n+1} \left(p_o - p_{wf}\right)_{i,j,k}^{n+1} - \left(\rho_{p_{wb}} \sum_{m=1}^{N_p} \frac{k_{rm}}{\mu_m}\right)_{i,j,k}^{n+1}\right] . \qquad \text{(III.2.0.11)}$$

III.3 Constant Pressure Production/Injection Well

The constant pressure well constraint is given by

$$\underset{i,j}{W_3^{n+1}} = \underset{i,j}{p_{wfs}} - \underset{i,j}{p_{wf}^{n+1}} = 0 \ . \qquad \text{(III.3.0.1)}$$

All derivatives are equal to zero except for

$$\frac{\partial \underset{i,j}{W_3^{n+1}}}{\partial \underset{i,j}{p_{wf}^{n+1}}} = -1 \ . \qquad \text{(III.3.0.2)}$$

Thus, if the bottom hole pressure is specified, p_{wfs}, then p_{wf} is not an unknown and does not contribute to the Jacobian.

III.4 Constant Liquid Rate Production Well

The constant liquid rate production well constraint is given by

$$\underset{i,j}{W_4^{n+1}} = \underset{i,j}{q_L} - \sum_{k} \sum_{p=w,o} \sum_{i=1}^{N_c} J'_{i,j,k} \left[K_{vip} X_i \frac{k_{rp}}{\mu_p} \frac{\rho_p}{\rho_{p,STC}}\right]_{i,j,k}^{n+1} \left[p_o - p_{wf}\right]_{i,j,k}^{n+1} = 0 \ . \qquad \text{(III.4.0.1)}$$

All derivatives are similar to those is Section III.1 above.

III.5 Constant Oil Rate Production Well

The constant oil rate production well constraint is given by

$$\underset{i,j}{W_5^{n+1}} = \underset{i,j}{q_o} - \sum_{k} \sum_{i=1}^{N_c} J'_{i,j,k} \left[K_{vio} X_i \frac{k_{ro}}{\mu_o} \frac{\rho_o}{\rho_{o,STC}}\right]_{i,j,k}^{n+1} \left[p_o - p_{wf}\right]_{i,j,k}^{n+1} = 0 \ . \qquad \text{(III.5.0.1)}$$

All derivatives are similar to those is Section III.1 above.

APPENDIX IV—Extracts from a Typical Set of Input and Output Files

IV.1 Data Input File

```
$GRIDDATA
     NX = 11, NY = 10, NZ = 1
     XGRID =  11*97.5
     YGRID =  10*97.5
     ZGRID =  24.4

 IHYBRID(6,3,1) = 1 IHYBRID(6,3,2) = 3 IHYBRID(6,3,3) = 1 IHYBRID(6,3,4) = 1
 IHYBRID(7,3,1) = 1 IHYBRID(7,3,2) = 3 IHYBRID(7,3,3) = 0 IHYBRID(7,3,4) = 1
 IHYBRID(8,3,1) = 1 IHYBRID(8,3,2) = 3 IHYBRID(8,3,3) = 0 IHYBRID(8,3,4) = 1
 IHYBRID(6,4,1) = 1 IHYBRID(6,4,2) = 3 IHYBRID(6,4,3) = 0 IHYBRID(6,4,4) = 1
 IHYBRID(7,4,1) = 1 IHYBRID(7,4,2) = 3 IHYBRID(7,4,3) = 0 IHYBRID(7,4,4) = 1
 IHYBRID(8,4,1) = 1 IHYBRID(8,4,2) = 3 IHYBRID(8,4,3) = 0 IHYBRID(8,4,4) = 1
 IHYBRID(6,5,1) = 1 IHYBRID(6,5,2) = 3 IHYBRID(6,5,3) = 0 IHYBRID(6,5,4) = 1
 IHYBRID(7,5,1) = 1 IHYBRID(7,5,2) = 3 IHYBRID(7,5,3) = 0 IHYBRID(7,5,4) = 1
 IHYBRID(8,5,1) = 1 IHYBRID(8,5,2) = 3 IHYBRID(8,5,3) = 0 IHYBRID(8,5,4) = 1
 IHYBRID(6,3,5) = 6 IHYBRID(6,3,6) = 3
 IHYBRID(7,3,5) = 6 IHYBRID(7,3,6) = 3
 IHYBRID(8,3,5) = 6 IHYBRID(8,3,6) = 3
 IHYBRID(6,4,5) = 6 IHYBRID(6,4,6) = 3
 IHYBRID(7,4,5) = 6 IHYBRID(7,4,6) = 3
 IHYBRID(8,4,5) = 6 IHYBRID(8,4,6) = 3
 IHYBRID(6,5,5) = 6 IHYBRID(6,5,6) = 3
 IHYBRID(7,5,5) = 6 IHYBRID(7,5,6) = 3
 IHYBRID(8,5,5) = 6 IHYBRID(8,5,6) = 3
 NR$(1) =  2
 NT$(1) =  12
 DR$(1,1) = 25.
 DR$(1,2) = 25.

 IHYBRID(4,6,1) = 1 IHYBRID(4,6,2) = 3 IHYBRID(4,6,3) = 1 IHYBRID(4,6,4) = 2
 IHYBRID(5,6,1) = 1 IHYBRID(5,6,2) = 3 IHYBRID(5,6,3) = 0 IHYBRID(5,6,4) = 2
 IHYBRID(6,6,1) = 1 IHYBRID(6,6,2) = 3 IHYBRID(6,6,3) = 0 IHYBRID(6,6,4) = 2
 IHYBRID(4,7,1) = 1 IHYBRID(4,7,2) = 3 IHYBRID(4,7,3) = 0 IHYBRID(4,7,4) = 2
 IHYBRID(5,7,1) = 1 IHYBRID(5,7,2) = 3 IHYBRID(5,7,3) = 0 IHYBRID(5,7,4) = 2
 IHYBRID(6,7,1) = 1 IHYBRID(6,7,2) = 3 IHYBRID(6,7,3) = 0 IHYBRID(6,7,4) = 2
 IHYBRID(4,8,1) = 1 IHYBRID(4,8,2) = 3 IHYBRID(4,8,3) = 0 IHYBRID(4,8,4) = 2
 IHYBRID(5,8,1) = 1 IHYBRID(5,8,2) = 3 IHYBRID(5,8,3) = 0 IHYBRID(5,8,4) = 2
 IHYBRID(6,8,1) = 1 IHYBRID(6,8,2) = 3 IHYBRID(6,8,3) = 0 IHYBRID(6,8,4) = 2
 IHYBRID(4,6,5) = 4 IHYBRID(4,6,6) = 6
 IHYBRID(5,6,5) = 4 IHYBRID(5,6,6) = 6
 IHYBRID(6,6,5) = 4 IHYBRID(6,6,6) = 6
 IHYBRID(4,7,5) = 4 IHYBRID(4,7,6) = 6
 IHYBRID(5,7,5) = 4 IHYBRID(5,7,6) = 6
 IHYBRID(6,7,5) = 4 IHYBRID(6,7,6) = 6
 IHYBRID(4,8,5) = 4 IHYBRID(4,8,6) = 6
 IHYBRID(5,8,5) = 4 IHYBRID(5,8,6) = 6
 IHYBRID(6,8,5) = 4 IHYBRID(6,8,6) = 6
 NR$(2) =  2
 NT$(2) =  12
 DR$(2,1) = 25.
 DR$(2,2) = 25.
$END
$ROCKDATAq
     PERMXq =  2000.
     PERMYq =  2000.
     PERMZq =  1000.
     CONDXq =     3.5
     CONDYq =     3.5
     CONDZq =     3.5
     PORREFq =      0.30
     CPRq      = 2347.0D+03       CPRTq      = 0.0
     ROCKDENSITYq          = 2100.
     KAPPAq      = 3.528D-06      LAMDAq      = 0.0

     PERMXq$(1) =  2000.
     PERMYq$(1) =  2000.
     PERMZq$(1) =  1000.
     CONDXq$(1) =     3.5
     CONDYq$(1) =     3.5
     CONDZq$(1) =     3.5
     PORREFq$(1) = 0.30
     CPRq$(1) = 2347.0D+03        CPRTq$(1) = 0.0
     ROCKDENSITYq$(1) =   2100.
     KAPPAq$(1) = 3.528D-06       LAMDAq$(1) = 0.0

     PERMXq$(2) =  2000.
     PERMYq$(2) =  2000.
     PERMZq$(2) =  1000.
     CONDXq$(2) =     3.5
     CONDYq$(2) =     3.5
     CONDZq$(2) =     3.5
     PORREFq$(2) = 0.30
     CPRq$(2) = 2347.0D+03        CPRTq$(2) = 0.0
     ROCKDENSITYq$(2) =   2100.
     KAPPAq$(2) = 3.528D-06       LAMDAq$(2) = 0.0
 $END
 $ROCKDATA
     PORPRESREF = 500.D+03
     ROCKCOMP = 5.0D-10
     PC         = 0.,0.,0.,0.,0.,0.,0.,0.
     TEMPRES   = 324.85
 $END
```

```
$MISCDATA
      TempRefEnergy = 300.0
      ZWARN = 0, EZ = 1D-06
      ITEST = 20*0              ITEST(16) = 1
      IOdetail = 11, IOrun = 12
      IPRINT = 30*0
      IPRINT(27) = 1
      IPRINT(28) = 1
      IPRINT(29) = 1
      MaxTimeStep = 999
      Cut = 2.0
      MaxCuts = 2
      TolPressure = 7.0         TolPressure = 5.0D+03
      TolTemperature = 0.1      TolTemperature = 1.0
      TolComp = 0.003           TolComp = 0.1
      TolSaturation = 0.015     TolSaturation = 0.1
      RunName = ' RUN CYCLIC 1'
$END
$FLUIDDATA
      THRMLEXP = 0.0       -1.9095D-06 -1.9095D-06  0.0
      COMPRES  = 7.30D-10, 7.30D-10, 7.30D-10, 0.0
      PRESREF  = 500.D+03, 500.D+03, 500.D+03, 500.D+03
      TEMPREF  = 324.85,   324.85,   324.85,   324.85
      TCRIT    = 647.286,  617.4,    617.4,    190.55
      PCRIT    = 22118.0D+03, 2099.0D+03, 2099.0D+03, 4604.0D+03
      MOLWT    = 18.015, 600.0, 600.0, 16.043
      PTLVOL(1,1) = 0.0000
      PTLVOL(2,1) = 0.0000
      PTLVOL(3,1) = 0.0000
      PTLVOL(4,1) = 0.0000
      PTLVOL(1,2) = 0.0000
      PTLVOL(2,2) = 0.6173
      PTLVOL(3,2) = 0.6173
      PTLVOL(4,2) = 0.0000
      PTLVOL(1,3) = 0.0000
      PTLVOL(2,3) = 0.0000
      PTLVOL(3,3) = 0.0000
      PTLVOL(4,3) = 24.658

      B = 1., Y = 0.609, MN = 0.000425, P = 0.00243, KR = 100.
      APOWER(1) = 0.00219, APOWER(2) = 0.00219
      BPOWER(1) = 684.,    BPOWER(2) = 684.
      KPOWER(1) = 289.,    KPOWER(2) = 289.
      NPOWER(1) = -0.506,  NPOWER(2) = -0.506
      SPOWER(1) = 3.44,    SPOWER(2) = 3.44

      AOIL = 0.0, 1.0D-07, 0.000639, 1.0
      BOIL = 0.0,    4900.,    2303., 0.0
      NEWT = 0

      AGAS = 0.0,    0.0,      0.0,      6.647D-10
      BGAS = 0.0,    0.0,      0.0,      1.709

      Cp1 = 0.0,  0.0,  0.0,  0.0,
            0.0,  2090., 2090., 0,
            0.0,  0.0, 0.0, 1050.
      Cp2 = 0.0,  0.0, 0.0, 0.0,
            0.0   0.0, 0.0, 0.0,
            0.0,  0.0, 0.0, 0.0
      Cp3 = 0.0,  0.0, 0.0, 0.0,
            0.0   0.0, 0.0, 0.0,
            0.0,  0.0, 0.0, 0.0
      Cp4 = 0.0,  0.0, 0.0, 0.0,
            0.0   0.0, 0.0, 0.0,
            0.0,  0.0, 0.0, 0.0

      ARRHENIUS = 2.952D11, ACTIVATION = 31800., MODELTEMP = 0
      ICRACK = 0

      Pbubble = 10000.D+03
$END
$EQUILDATA
      Kv1 = 1.0,0.0,0.0,0.0, 0.0,1.0,1.0,0.0, 0.0,0.0,0.0,1.0
      Kv2 = 0.0,0.0,0.0,0.0, 0.0,0.0,0.0,0.0, 0.0,0.0,0.0,0.0
      Kv3 = 0.0,0.0,0.0,0.0, 0.0,0.0,0.0,0.0, 0.0,0.0,0.0,0.0
      Kv4 = 0.0,0.0,0.0,0.0, 0.0,0.0,0.0,0.0, 0.0,0.0,0.0,0.0
      Kv5 = 0.0,0.0,0.0,0.0, 0.0,0.0,0.0,0.0, 0.0,0.0,0.0,0.0
$END
$INPUTRELPERM
      MODEL = 2
      TREF1 = 324.85
      TREF2 = 400.
      NW = 1.2
      NOW = 2.0
      NOG = 2.0
      NG = 1.5
      SWCTREF1 = 0.20,     KRWROTREF1 = 0.20
      SWCTREF2 = 0.20,     KRWROTREF2 = 0.20
      SORWTREF1 = 0.15,    KROIWTREF1 = 0.80
      SORWTREF2 = 0.15,    KROIWTREF2 = 0.80
      SORGTREF1 = 0.10,    KRGROTREF1 = 0.20
      SORGTREF2 = 0.10,    KRGROTREF2 = 0.20
      SGCTREF1 = 0.06
      SGCTREF2 = 0.06
      RELWARN = 0
$END
$INITIALDATAq
      PRESSUREq = 500.D+03
      TEMPERATUREq = 324.85
      PWFq = 500.D+03
      COMPWATERq = 1.0
      COMPHEAVYq = 1.0
      COMPLIGHTq = 0.0
      COMPMETHANEq = 1.0
      SATAQUEOUSq = 0.20
      SATOLEICq =    0.80
      SATGASEOUSq = 0.00
$END
```

```
$INITIALDATA
     IBypass = 1
     IPcow = 0, IPcgo = 0
     INITCount = 50
     TolINIT = 1.0
     ITABLE = 1,1
     PcgoRef =     0.0,       KcgoRef = 1
     PoRef   =   500.0D03,    KRef    = 2
     PcowRef =     0.0,       KcowRef = 3
                              Kwm     = 3
$END
$RECURRENT
     TimeStop = 165.
     CumTime =     0.0
     ITIMESTEP = 0

     DTMAX =     5.0            DTMIN = 0.0001     DSMAX = 0.2
     DPMAX =   300.0D03         DTPMAX = 80.0      DXMAX = 0.2
     MINITN = 2,                MAXITN = 15
     OMEGAconstant = 1.0        RatioMax = 1.5     RatioMin = 0.5
     Accel = 0.0                MinAccel = 2       MaxAccel = 10

     dTime =      0.01
     TimeEnd =  20.0

     Iplot1(5,4,1) = 1
     Iplot1(5,5,1) = 1
     Iplot1(7,6,1) = 1
     Iplot1(8,6,1) = 1

     IPlot2(6,3) = 1
     IPlot2(4,6) = 1

     IPlot1$(1,1,1,1) = 1
     IPlot1$(1,2,9,1) = 1
     IPlot1$(2,1,1,1) = 1
     IPlot1$(2,2,3,1) = 1

     BHPmax(1,6,3)           = 6900.0D+03  BHPmax(1,4,6)            = 6900.0D+03
     BHPmin(1,6,3)           =  120.0D+03  BHPmin(1,4,6)            =  120.0D+03
     QTmax(1,6,3)            =  100.0      QTmax(1,4,6)             =  100.0
     QUALITY(1,6,3)          =    0.7      QUALITY(1,4,6)           =    0.7
     TempInj(1,6,3)          =  523.15     TempInj(1,4,6)           =  523.15
     INDEX(1,6,3,1)          =   -1        INDEX(1,4,6,1)           =   -1
     PRODINDEX(1,6,3,1)      =    0        PRODINDEX(1,4,6,1)       =    0
     ProdMultiply(1,6,3,1)   =    1.0      ProdMultiply(1,4,6,1)    =    1.0
     FracThick(1,6,3,1)      =    1.       FracThick(1,4,6,1)       =    1.
     WellFactor(1,6,3,1)     =    1.       WellFactor(1,4,6,1)      =    1.
     Cg(1,6,3,1)             =    0.5      Cg(1,4,6,1)              =    0.5
     SKIN(1,6,3,1)           =    0.0      SKIN(1,4,6,1)            =    0.0
     Rw(1,6,3,1)             =    0.09     Rw(1,4,6,1)              =    0.09
     IPRODINDEX(1,6,3,1)     =    1        IPRODINDEX(1,4,6,1)      =    1
$END
```

IV.2 Abbreviated Plot Files

```
PLOT FILE 1

 I  J  K     Time      Po       T    Sw    So    Sg    X1    X2    X3    X4    Pwf1    Pwf2
-- -- -- --------- ------ ----- ----- ----- ----- ----- ----- ----- ----- ------  ------
 5  4  1    0.0000  500.0  51.7 0.200 0.800 0.000 1.000 1.000 0.000 0.973   500.0   500.0
 5  5  1    0.0000  500.0  51.7 0.200 0.800 0.000 1.000 1.000 0.000 0.973   500.0   500.0
 7  6  1    0.0000  500.0  51.7 0.200 0.800 0.000 1.000 1.000 0.000 0.973   500.0   500.0
 8  6  1    0.0000  500.0  51.7 0.200 0.800 0.000 1.000 1.000 0.000 0.973   500.0   500.0
 5  4  1   20.0000 1273.2  51.7 0.200 0.800 0.000 1.000 1.000 0.000 0.989   500.0   500.0
 5  5  1   20.0000 1473.4  51.7 0.200 0.800 0.000 1.000 1.000 0.000 0.990   500.0   500.0
 7  6  1   20.0000 1473.4  51.7 0.200 0.800 0.000 1.000 1.000 0.000 0.990   500.0   500.0
 8  6  1   20.0000 1209.5  51.7 0.200 0.800 0.000 1.000 1.000 0.000 0.988   500.0   500.0
 5  4  1   55.0000  824.2  51.7 0.200 0.800 0.000 1.000 1.000 0.000 0.984   500.0   500.0
 5  5  1   55.0000  802.7  51.7 0.200 0.800 0.000 1.000 1.000 0.000 0.984   500.0   500.0
 7  6  1   55.0000  802.7  51.7 0.200 0.800 0.000 1.000 1.000 0.000 0.984   500.0   500.0
 8  6  1   55.0000  820.2  51.7 0.200 0.800 0.000 1.000 1.000 0.000 0.984   500.0   500.0
 5  4  1   75.0000 1586.2  51.7 0.200 0.800 0.000 1.000 1.000 0.000 0.991   500.0   500.0
 5  5  1   75.0000 1764.0  51.7 0.200 0.800 0.000 1.000 1.000 0.000 0.992   500.0   500.0
 7  6  1   75.0000 1764.0  51.7 0.200 0.800 0.000 1.000 1.000 0.000 0.992   500.0   500.0
 8  6  1   75.0000 1524.2  51.7 0.200 0.800 0.000 1.000 1.000 0.000 0.991   500.0   500.0
 5  4  1  110.0000 1115.8  51.7 0.200 0.800 0.000 1.000 1.000 0.000 0.989   500.0   500.0
 5  5  1  110.0000 1092.7  51.7 0.200 0.800 0.000 1.000 1.000 0.000 0.989   500.0   500.0
 7  6  1  110.0000 1092.7  51.7 0.200 0.800 0.000 1.000 1.000 0.000 0.989   500.0   500.0
 8  6  1  110.0000 1112.1  51.7 0.200 0.800 0.000 1.000 1.000 0.000 0.989   500.0   500.0
 5  4  1  130.0000 1897.4  51.7 0.200 0.800 0.000 1.000 1.000 0.000 0.992   500.0   500.0
 5  5  1  130.0000 2061.9  51.7 0.201 0.799 0.000 1.000 1.000 0.000 0.993   500.0   500.0
 7  6  1  130.0000 2061.9  51.7 0.201 0.799 0.000 1.000 1.000 0.000 0.993   500.0   500.0
 8  6  1  130.0000 1838.4  51.7 0.201 0.799 0.000 1.000 1.000 0.000 0.992   500.0   500.0
 5  4  1  165.0000 1412.4  51.7 0.201 0.799 0.000 1.000 1.000 0.000 0.991   500.0   500.0
 5  5  1  165.0000 1388.8  51.7 0.201 0.799 0.000 1.000 1.000 0.000 0.991   500.0   500.0
 7  6  1  165.0000 1388.8  51.7 0.201 0.799 0.000 1.000 1.000 0.000 0.991   500.0   500.0
 8  6  1  165.0000 1409.6  51.7 0.201 0.799 0.000 1.000 1.000 0.000 0.991   500.0   500.0
```

```
PLOT FILE 2

                     Well 1 Well 1  Well 1   Well 1  Well 1    Well 1 Well 2 Well 2   Well 2    Well 2  Well 2    Well 2
 I  J       Time       Wat    Oil     Gas   CumWat  CumOil    CumGas    Wat    Oil      Gas    CumWat  CumOil    CumGas
-- -- ---------- ------ ------ ------- -------- ------- --------- ------ ------ -------- --------- ------- ---------
 4  6     0.0100  -77.1    0.0     0.0     -0.8     0.0       0.0    0.0    0.0      0.0       0.0     0.0       0.0
 6  3     0.0100  -77.1    0.0     0.0     -0.8     0.0       0.0    0.0    0.0      0.0       0.0     0.0       0.0
 4  6    20.0000 -100.0    0.0     0.0  -1974.3     0.0       0.0    0.0    0.0      0.0       0.0     0.0       0.0
 6  3    20.0000 -100.0    0.0     0.0  -1974.3     0.0       0.0    0.0    0.0      0.0       0.0     0.0       0.0
 4  6    20.0100    0.0    0.0     0.0  -1974.3     0.0       0.0   15.1    4.9      0.0       0.2     0.0       0.0
 6  3    20.0100    0.0    0.0     0.0  -1974.3     0.0       0.0   15.1    4.9      0.0       0.2     0.0       0.0
 4  6    55.0000    0.0    0.0     0.0  -1974.3     0.0       0.0    8.1    7.1      0.0     356.2   188.4       0.0
 6  3    55.0000    0.0    0.0     0.0  -1974.3     0.0       0.0    8.1    7.1      0.0     356.3   188.5       0.0
 4  6    55.0100 -100.0    0.0     0.0  -1975.3     0.0       0.0    0.0    0.0      0.0     356.2   188.4       0.0
 6  3    55.0100 -100.0    0.0     0.0  -1975.3     0.0       0.0    0.0    0.0      0.0     356.3   188.5       0.0
 4  6    75.0000 -100.0    0.0     0.0  -3974.5     0.0       0.0    0.0    0.0      0.0     356.2   188.4       0.0
 6  3    75.0000 -100.0    0.0     0.0  -3974.5     0.0       0.0    0.0    0.0      0.0     356.3   188.5       0.0
 4  6    75.0100    0.0    0.0     0.0  -3974.5     0.0       0.0   14.3    5.7      0.0     356.3   188.5       0.0
 6  3    75.0100    0.0    0.0     0.0  -3974.5     0.0       0.0   14.3    5.7      0.0     356.5   188.6       0.0
 4  6   110.0000    0.0    0.0     0.0  -3974.5     0.0       0.0   12.1    7.9      0.0     813.0   431.6       0.0
 6  3   110.0000    0.0    0.0     0.0  -3974.5     0.0       0.0   12.1    7.9      0.0     813.2   431.7       0.0
 4  6   110.0100 -100.0    0.0     0.0  -3975.5     0.0       0.0    0.0    0.0      0.0     813.0   431.6       0.0
 6  3   110.0100 -100.0    0.0     0.0  -3975.5     0.0       0.0    0.0    0.0      0.0     813.2   431.7       0.0
 4  6   130.0000 -100.0    0.0     0.0  -5974.5     0.0       0.0    0.0    0.0      0.0     813.0   431.6       0.0
 6  3   130.0000 -100.0    0.0     0.0  -5974.5     0.0       0.0    0.0    0.0      0.0     813.2   431.7       0.0
 4  6   130.0100    0.0    0.0     0.0  -5974.5     0.0       0.0   13.7    6.1      0.0     813.1   431.6       0.0
 6  3   130.0100    0.0    0.0     0.0  -5974.5     0.0       0.0   13.7    6.1      0.0     813.3   431.7       0.0
 4  6   165.0000    0.0    0.0     0.0  -5974.5     0.0       0.0   12.6    7.4      0.0    1272.6   671.9       0.0
 6  3   165.0000    0.0    0.0     0.0  -5974.5     0.0       0.0   12.6    7.4      0.0    1272.8   672.0       0.0
```

```
PLOT FILE 3

 I  J  L  M  K       Time       Po     T    Sw    So    Sg    X1    X2    X3     X4      Pwf1      Pwf2
-- -- -- -- -- ---------- -------- ----- ----- ----- ----- ----- ----- ----- ------ --------- ---------
 4  6  1  1  1     0.0000    500.0  51.7 0.200 0.800 0.000 1.000 1.000 0.000  0.973     500.0     500.0
 4  6  2  3  1     0.0000    500.0  51.7 0.200 0.800 0.000 1.000 1.000 0.000  0.973     500.0     500.0
 6  3  1  1  1     0.0000    500.0  51.7 0.200 0.800 0.000 1.000 1.000 0.000  0.973     500.0     500.0
 6  3  2  9  1     0.0000    500.0  51.7 0.200 0.800 0.000 1.000 1.000 0.000  0.973     500.0     500.0
 4  6  1  1  1    20.0000   1990.2  85.6 0.246 0.754 0.000 1.000 1.000 0.000  0.974    2546.9     500.0
 4  6  2  3  1    20.0000   1713.5  51.7 0.202 0.798 0.000 1.000 1.000 0.000  0.992    2546.9     500.0
 6  3  1  1  1    20.0000   1990.2  85.6 0.246 0.754 0.000 1.000 1.000 0.000  0.974    2546.9     500.0
 6  3  2  9  1    20.0000   1713.5  51.7 0.202 0.798 0.000 1.000 1.000 0.000  0.992    2546.9     500.0
 4  6  1  1  1    55.0000    268.6  86.0 0.222 0.778 0.000 1.000 1.000 0.000  0.662    2546.9     120.0
 4  6  2  3  1    55.0000    736.8  51.7 0.202 0.798 0.000 1.000 1.000 0.000  0.982    2546.9     120.0
 6  3  1  1  1    55.0000    268.7  86.0 0.222 0.778 0.000 1.000 1.000 0.000  0.662    2546.9     120.0
 6  3  2  9  1    55.0000    736.8  51.7 0.202 0.798 0.000 1.000 1.000 0.000  0.982    2546.9     120.0
 4  6  1  1  1    75.0000   2113.3 116.9 0.271 0.729 0.000 1.000 1.000 0.000  0.918    2343.8     120.0
 4  6  2  3  1    75.0000   1987.6  51.8 0.204 0.796 0.000 1.000 1.000 0.000  0.993    2343.8     120.0
 6  3  1  1  1    75.0000   2113.3 116.9 0.271 0.729 0.000 1.000 1.000 0.000  0.918    2343.9     120.0
 6  3  2  9  1    75.0000   1987.6  51.8 0.204 0.796 0.000 1.000 1.000 0.000  0.993    2343.9     120.0
 4  6  1  1  1   110.0000    495.5 115.8 0.249 0.751 0.000 1.000 1.000 0.000  0.719    2343.8     432.4
 4  6  2  3  1   110.0000   1023.7  51.8 0.204 0.796 0.000 1.000 1.000 0.000  0.988    2343.8     432.4
 6  3  1  1  1   110.0000    495.5 115.8 0.249 0.751 0.000 1.000 1.000 0.000  0.719    2343.9     432.4
 6  3  2  9  1   110.0000   1023.8  51.8 0.204 0.796 0.000 1.000 1.000 0.000  0.988    2343.9     432.4
 4  6  1  1  1   130.0000   2343.8 144.4 0.300 0.700 0.000 1.000 1.000 0.000  0.838    2461.4     432.4
 4  6  2  3  1   130.0000   2274.2  52.0 0.205 0.795 0.000 1.000 1.000 0.000  0.994    2461.4     432.4
 6  3  1  1  1   130.0000   2343.8 144.4 0.300 0.700 0.000 1.000 1.000 0.000  0.838    2461.5     432.4
 6  3  2  9  1   130.0000   2274.2  52.0 0.205 0.795 0.000 1.000 1.000 0.000  0.994    2461.5     432.4
 4  6  1  1  1   165.0000    841.7 142.8 0.281 0.719 0.000 1.000 1.000 0.000  0.583    2461.4     812.6
 4  6  2  3  1   165.0000   1323.9  52.0 0.205 0.795 0.000 1.000 1.000 0.000  0.990    2461.4     812.6
 6  3  1  1  1   165.0000    841.7 142.8 0.281 0.719 0.000 1.000 1.000 0.000  0.583    2461.5     812.5
 6  3  2  9  1   165.0000   1323.9  52.0 0.205 0.795 0.000 1.000 1.000 0.000  0.990    2461.5     812.5
```

IV.3 Abbreviated Run File

```
RUN CYCLIC 1

COMPONENT PROPERTY DATA

  ICOMP     MOLWT     PCRIT     TCRIT    THRMLEXP     COMPRES     PRESREF  TEMPREF
          Kg/Kmole     kPa        K     Vol/Vol/K  Vol/Vol/Pa     kPa        K
  -----   --------   -------   -------  ---------  ----------   -------  -------
      1     18.015   22118.0   647.286  0.000D+00   .730D-09      500.0    324.9
      2    600.000    2099.0   617.400  -.191D-05   .730D-09      500.0    324.9
      3    600.000    2099.0   617.400  -.191D-05   .730D-09      500.0    324.9
      4     16.043    4604.0   190.550  0.000D+00   .000D+00      500.0    324.9

  ICOMP     AOIL       BOIL      AGAS       BGAS
            Pa.s        K       Pa.s/K
  -----  ---------   ------  ----------   -----
      1  0.0000000      0.0  0.0000D+00   0.000
      2  0.0000001   4900.0  0.0000D+00   0.000
      3  0.0006390   2303.0  0.0000D+00   0.000
      4  1.0000000      0.0  0.6647D-09   1.709


PARTIAL VOLUME COMPONENT DATA

 COMPONENT    AQUEOUS      OLEIC      GASEOUS
             M3/Kmole    M3/Kmole    M3/Kmole
 ---------  ----------  ----------  ----------
  WATER     0.1811D-01  0.0000D+00  0.6990D+03
  HEAVY     0.0000D+00  0.6173D+00  0.0000D+00
  LIGHT     0.0000D+00  0.6173D+00  0.0000D+00
  METHANE   0.0000D+00  0.0000D+00  0.2466D+02
```

```
HEAT CAPACITY COMPONENT DATA

                          Cp1          Cp2          Cp3          Cp4
 COMPONENT  PHASE      J/Kg-K      J/Kg-K2      J/Kg-K3      J/Kg-K4
 ---------  -----   ----------   ----------   ----------   ----------
     1        1     0.0000D+00   0.0000D+00   0.0000D+00   0.0000D+00
     2        1     0.0000D+00   0.0000D+00   0.0000D+00   0.0000D+00
     3        1     0.0000D+00   0.0000D+00   0.0000D+00   0.0000D+00
     4        1     0.0000D+00   0.0000D+00   0.0000D+00   0.0000D+00
     1        2     0.0000D+00   0.0000D+00   0.0000D+00   0.0000D+00
     2        2     0.2090D+04   0.0000D+00   0.0000D+00   0.0000D+00
     3        2     0.2090D+04   0.0000D+00   0.0000D+00   0.0000D+00
     4        2     0.0000D+00   0.0000D+00   0.0000D+00   0.0000D+00
     1        3     0.0000D+00   0.0000D+00   0.0000D+00   0.0000D+00
     2        3     0.0000D+00   0.0000D+00   0.0000D+00   0.0000D+00
     3        3     0.0000D+00   0.0000D+00   0.0000D+00   0.0000D+00
     4        3     0.1050D+04   0.0000D+00   0.0000D+00   0.0000D+00

  TempRefEnergy (K) =   300.000

NON-NEWTONIAN OIL PARAMETERS

 COMPONENT   Apower  Bpower  Kpower  Npower  Spower
 ---------  -------  ------  ------  ------  ------
   HEAVY    0.00219    20.0   150.0  -0.506    2.00
   LIGHT    0.00219    20.0   150.0  -0.506    2.00

NON-NEWTONIAN OIL SHEAR PARAMETERS

  B     Y        MN         P       KR   FLAG
 ---  -----  --------  -------  -----  ----
 1.0  0.609  0.000425  0.00243  100.0    0

EQUILIBRIUM DATA

                          Kv1          Kv2          Kv3          Kv4          Kv5
 COMPONENT  PHASE                       Pa         1/Pa            K            K
 ---------  -----   ----------   ----------   ----------   ----------   ----------
     1        1     0.1000D+01   0.0000D+00   0.0000D+00   0.0000D+00   0.0000D+00
     2        1     0.0000D+00   0.0000D+00   0.0000D+00   0.0000D+00   0.0000D+00
     3        1     0.0000D+00   0.0000D+00   0.0000D+00   0.0000D+00   0.0000D+00
     4        1     0.0000D+00   0.0000D+00   0.0000D+00   0.0000D+00   0.0000D+00
     1        2     0.0000D+00   0.0000D+00   0.0000D+00   0.0000D+00   0.0000D+00
     2        2     0.1000D+01   0.0000D+00   0.0000D+00   0.0000D+00   0.0000D+00
     3        2     0.1000D+01   0.0000D+00   0.0000D+00   0.0000D+00   0.0000D+00
     4        2     0.0000D+00   0.0000D+00   0.0000D+00   0.0000D+00   0.0000D+00
     1        3     0.0000D+00   0.0000D+00   0.0000D+00   0.0000D+00   0.0000D+00
     2        3     0.0000D+00   0.0000D+00   0.0000D+00   0.0000D+00   0.0000D+00
     3        3     0.0000D+00   0.0000D+00   0.0000D+00   0.0000D+00   0.0000D+00
     4        3     0.1000D+01   0.0000D+00   0.0000D+00   0.0000D+00   0.0000D+00

RELATIVE PERMEABILITY PARAMETERS

 PARAMETER  REFERENCE 1  REFERENCE 2
 ---------  -----------  -----------
  TEMP (K)     324.850      400.000
  Swc            0.200        0.200
  Sorw           0.150        0.150
  Sorg           0.100        0.100
  Sgc            0.060        0.060
  Krwro          0.200        0.200
  Kroiw          0.800        0.800
  Krgro          0.200        0.200

  MODEL =     2
  NW =        1.20
  NOW =       2.00
  NOG =       2.00
  NG =        1.50
  RELWARN =   0

MISCELLANEOUS DATA

  Bubble Point Pressure (kPa)    =   10000.00
  Energy Reference Temperature (C) =     26.85

MISCELLANEOUS ROCK PROPERTIES

 Porosity Ref P (kPa) .5000D+03
 Rock Comp (1/kPa)    .5000D-06

CAPILLARY PRESSURE PARAMETERS

        PC 1/5  PC 2/6  PC 3/7  PC 4/8
          kPa     kPa     kPa     1/K
 ----   ------  ------  ------  ------
 Pcow      0.0     0.0     0.0     0.0
 Pcgo      0.0     0.0     0.0     0.0
```

```
WATER PHASE PRESSURE (kPa)

 K = 1  I = 1  I = 2  I = 3  I = 4  I = 5  I = 6  I = 7  I = 8  I = 9 I = 10 I = 11
------ ------ ------ ------ ------ ------ ------ ------ ------ ------ ------ ------
J = 1   500.0  500.0  500.0  500.0  500.0  500.0  500.0  500.0  500.0  500.0  500.0
J = 2   500.0  500.0  500.0  500.0  500.0  500.0  500.0  500.0  500.0  500.0  500.0
J = 3   500.0  500.0  500.0  500.0  500.0    0.0    0.0    0.0  500.0  500.0  500.0
J = 4   500.0  500.0  500.0  500.0  500.0    0.0    0.0    0.0  500.0  500.0  500.0
J = 5   500.0  500.0  500.0  500.0  500.0    0.0    0.0    0.0  500.0  500.0  500.0
J = 6   500.0  500.0  500.0    0.0    0.0    0.0  500.0  500.0  500.0  500.0  500.0
J = 7   500.0  500.0  500.0    0.0    0.0    0.0  500.0  500.0  500.0  500.0  500.0
J = 8   500.0  500.0  500.0    0.0    0.0    0.0  500.0  500.0  500.0  500.0  500.0
J = 9   500.0  500.0  500.0  500.0  500.0  500.0  500.0  500.0  500.0  500.0  500.0
J = 10  500.0  500.0  500.0  500.0  500.0  500.0  500.0  500.0  500.0  500.0  500.0
```

```
OIL PHASE PRESSURE (kPa)

 K = 1  I = 1  I = 2  I = 3  I = 4  I = 5  I = 6  I = 7  I = 8  I = 9 I = 10 I = 11
------ ------ ------ ------ ------ ------ ------ ------ ------ ------ ------ ------
J = 1   500.0  500.0  500.0  500.0  500.0  500.0  500.0  500.0  500.0  500.0  500.0
J = 2   500.0  500.0  500.0  500.0  500.0  500.0  500.0  500.0  500.0  500.0  500.0
J = 3   500.0  500.0  500.0  500.0  500.0    0.0    0.0    0.0  500.0  500.0  500.0
J = 4   500.0  500.0  500.0  500.0  500.0    0.0    0.0    0.0  500.0  500.0  500.0
J = 5   500.0  500.0  500.0  500.0  500.0    0.0    0.0    0.0  500.0  500.0  500.0
J = 6   500.0  500.0  500.0    0.0    0.0    0.0  500.0  500.0  500.0  500.0  500.0
J = 7   500.0  500.0  500.0    0.0    0.0    0.0  500.0  500.0  500.0  500.0  500.0
J = 8   500.0  500.0  500.0    0.0    0.0    0.0  500.0  500.0  500.0  500.0  500.0
J = 9   500.0  500.0  500.0  500.0  500.0  500.0  500.0  500.0  500.0  500.0  500.0
J = 10  500.0  500.0  500.0  500.0  500.0  500.0  500.0  500.0  500.0  500.0  500.0
```

```
GAS PHASE PRESSURE (kPa)

 K = 1  I = 1  I = 2  I = 3  I = 4  I = 5  I = 6  I = 7  I = 8  I = 9 I = 10 I = 11
------ ------ ------ ------ ------ ------ ------ ------ ------ ------ ------ ------
J = 1   500.0  500.0  500.0  500.0  500.0  500.0  500.0  500.0  500.0  500.0  500.0
J = 2   500.0  500.0  500.0  500.0  500.0  500.0  500.0  500.0  500.0  500.0  500.0
J = 3   500.0  500.0  500.0  500.0  500.0    0.0    0.0    0.0  500.0  500.0  500.0
J = 4   500.0  500.0  500.0  500.0  500.0    0.0    0.0    0.0  500.0  500.0  500.0
J = 5   500.0  500.0  500.0  500.0  500.0    0.0    0.0    0.0  500.0  500.0  500.0
J = 6   500.0  500.0  500.0    0.0    0.0    0.0  500.0  500.0  500.0  500.0  500.0
J = 7   500.0  500.0  500.0    0.0    0.0    0.0  500.0  500.0  500.0  500.0  500.0
J = 8   500.0  500.0  500.0    0.0    0.0    0.0  500.0  500.0  500.0  500.0  500.0
J = 9   500.0  500.0  500.0  500.0  500.0  500.0  500.0  500.0  500.0  500.0  500.0
J = 10  500.0  500.0  500.0  500.0  500.0  500.0  500.0  500.0  500.0  500.0  500.0
```

```
TEMPERATURE (C)

 K = 1  I = 1  I = 2  I = 3  I = 4  I = 5  I = 6  I = 7  I = 8  I = 9 I = 10 I = 11
------ ------ ------ ------ ------ ------ ------ ------ ------ ------ ------ ------
J = 1    51.7   51.7   51.7   51.7   51.7   51.7   51.7   51.7   51.7   51.7   51.7
J = 2    51.7   51.7   51.7   51.7   51.7   51.7   51.7   51.7   51.7   51.7   51.7
J = 3    51.7   51.7   51.7   51.7   51.7    0.0    0.0    0.0   51.7   51.7   51.7
J = 4    51.7   51.7   51.7   51.7   51.7    0.0    0.0    0.0   51.7   51.7   51.7
J = 5    51.7   51.7   51.7   51.7   51.7    0.0    0.0    0.0   51.7   51.7   51.7
J = 6    51.7   51.7   51.7    0.0    0.0    0.0   51.7   51.7   51.7   51.7   51.7
J = 7    51.7   51.7   51.7    0.0    0.0    0.0   51.7   51.7   51.7   51.7   51.7
J = 8    51.7   51.7   51.7    0.0    0.0    0.0   51.7   51.7   51.7   51.7   51.7
J = 9    51.7   51.7   51.7   51.7   51.7   51.7   51.7   51.7   51.7   51.7   51.7
J = 10   51.7   51.7   51.7   51.7   51.7   51.7   51.7   51.7   51.7   51.7   51.7
```

```
COMPOSITION - WATER COMPONENT

 K = 1   I = 1    I = 2    I = 3    I = 4    I = 5    I = 6    I = 7    I = 8    I = 9    I = 10  I = 11
------ -------- -------- -------- -------- -------- -------- -------- -------- -------- -------- ------
J = 1   1.00000  1.00000  1.00000  1.00000  1.00000  1.00000  1.00000  1.00000  1.00000  1.00000    1.0
J = 2   1.00000  1.00000  1.00000  1.00000  1.00000  1.00000  1.00000  1.00000  1.00000  1.00000    1.0
J = 3   1.00000  1.00000  1.00000  1.00000  1.00000  1.00000  1.00000  1.00000  1.00000  1.00000    1.0
J = 4   1.00000  1.00000  1.00000  1.00000  1.00000  1.00000  1.00000  1.00000  1.00000  1.00000    1.0
J = 5   1.00000  1.00000  1.00000  1.00000  1.00000  1.00000  1.00000  1.00000  1.00000  1.00000    1.0
J = 6   1.00000  1.00000  1.00000  1.00000  1.00000  1.00000  1.00000  1.00000  1.00000  1.00000    1.0
J = 7   1.00000  1.00000  1.00000  1.00000  1.00000  1.00000  1.00000  1.00000  1.00000  1.00000    1.0
J = 8   1.00000  1.00000  1.00000  1.00000  1.00000  1.00000  1.00000  1.00000  1.00000  1.00000    1.0
J = 9   1.00000  1.00000  1.00000  1.00000  1.00000  1.00000  1.00000  1.00000  1.00000  1.00000    1.0
J = 10  1.00000  1.00000  1.00000  1.00000  1.00000  1.00000  1.00000  1.00000  1.00000  1.00000    1.0
```

```
COMPOSITION - HEAVY COMPONENT

 K = 1   I = 1    I = 2    I = 3    I = 4    I = 5    I = 6    I = 7    I = 8    I = 9    I = 10  I = 11
------ -------- -------- -------- -------- -------- -------- -------- -------- -------- -------- ------
J = 1   1.00000  1.00000  1.00000  1.00000  1.00000  1.00000  1.00000  1.00000  1.00000  1.00000    1.0
J = 2   1.00000  1.00000  1.00000  1.00000  1.00000  1.00000  1.00000  1.00000  1.00000  1.00000    1.0
J = 3   1.00000  1.00000  1.00000  1.00000  1.00000  0.00000  0.00000  0.00000  1.00000  1.00000    1.0
J = 4   1.00000  1.00000  1.00000  1.00000  1.00000  0.00000  0.00000  0.00000  1.00000  1.00000    1.0
J = 5   1.00000  1.00000  1.00000  1.00000  1.00000  0.00000  0.00000  0.00000  1.00000  1.00000    1.0
J = 6   1.00000  1.00000  1.00000  0.00000  0.00000  0.00000  1.00000  1.00000  1.00000  1.00000    1.0
J = 7   1.00000  1.00000  1.00000  0.00000  0.00000  0.00000  1.00000  1.00000  1.00000  1.00000    1.0
J = 8   1.00000  1.00000  1.00000  0.00000  0.00000  0.00000  1.00000  1.00000  1.00000  1.00000    1.0
J = 9   1.00000  1.00000  1.00000  1.00000  1.00000  1.00000  1.00000  1.00000  1.00000  1.00000    1.0
J = 10  1.00000  1.00000  1.00000  1.00000  1.00000  1.00000  1.00000  1.00000  1.00000  1.00000    1.0
```

```
COMPOSITION - LIGHT COMPONENT

 K = 1   I = 1    I = 2    I = 3    I = 4    I = 5    I = 6    I = 7    I = 8    I = 9    I = 10  I = 11
------ -------- -------- -------- -------- -------- -------- -------- -------- -------- -------- ------
J = 1   0.00000  0.00000  0.00000  0.00000  0.00000  0.00000  0.00000  0.00000  0.00000  0.00000    0.0
J = 2   0.00000  0.00000  0.00000  0.00000  0.00000  0.00000  0.00000  0.00000  0.00000  0.00000    0.0
J = 3   0.00000  0.00000  0.00000  0.00000  0.00000  0.00000  0.00000  0.00000  0.00000  0.00000    0.0
J = 4   0.00000  0.00000  0.00000  0.00000  0.00000  0.00000  0.00000  0.00000  0.00000  0.00000    0.0
J = 5   0.00000  0.00000  0.00000  0.00000  0.00000  0.00000  0.00000  0.00000  0.00000  0.00000    0.0
J = 6   0.00000  0.00000  0.00000  0.00000  0.00000  0.00000  0.00000  0.00000  0.00000  0.00000    0.0
J = 7   0.00000  0.00000  0.00000  0.00000  0.00000  0.00000  0.00000  0.00000  0.00000  0.00000    0.0
J = 8   0.00000  0.00000  0.00000  0.00000  0.00000  0.00000  0.00000  0.00000  0.00000  0.00000    0.0
J = 9   0.00000  0.00000  0.00000  0.00000  0.00000  0.00000  0.00000  0.00000  0.00000  0.00000    0.0
J = 10  0.00000  0.00000  0.00000  0.00000  0.00000  0.00000  0.00000  0.00000  0.00000  0.00000    0.0

COMPOSITION - METHANE COMPONENT

 K = 1   I = 1    I = 2    I = 3    I = 4    I = 5    I = 6    I = 7    I = 8    I = 9    I = 10  I = 11
------ -------- -------- -------- -------- -------- -------- -------- -------- -------- -------- ------
J = 1   0.97302  0.97302  0.97302  0.97302  0.97302  0.97302  0.97302  0.97302  0.97302  0.97302    1.0
J = 2   0.97302  0.97302  0.97302  0.97302  0.97302  0.97302  0.97302  0.97302  0.97302  0.97302    1.0
J = 3   0.97302  0.97302  0.97302  0.97302  0.97302  0.00000  0.00000  0.00000  0.97302  0.97302    1.0
J = 4   0.97302  0.97302  0.97302  0.97302  0.97302  0.00000  0.00000  0.00000  0.97302  0.97302    1.0
J = 5   0.97302  0.97302  0.97302  0.97302  0.97302  0.00000  0.00000  0.00000  0.97302  0.97302    1.0
J = 6   0.97302  0.97302  0.97302  0.00000  0.00000  0.00000  0.97302  0.97302  0.97302  0.97302    1.0
J = 7   0.97302  0.97302  0.97302  0.00000  0.00000  0.00000  0.97302  0.97302  0.97302  0.97302    1.0
J = 8   0.97302  0.97302  0.97302  0.00000  0.00000  0.00000  0.97302  0.97302  0.97302  0.97302    1.0
J = 9   0.97302  0.97302  0.97302  0.97302  0.97302  0.97302  0.97302  0.97302  0.97302  0.97302    1.0
J = 10  0.97302  0.97302  0.97302  0.97302  0.97302  0.97302  0.97302  0.97302  0.97302  0.97302    1.0

WATER PHASE SATURATION

 K = 1   I = 1    I = 2    I = 3    I = 4    I = 5    I = 6    I = 7    I = 8    I = 9    I = 10  I = 11
------ -------- -------- -------- -------- -------- -------- -------- -------- -------- -------- ------
J = 1    0.2000   0.2000   0.2000   0.2000   0.2000   0.2000   0.2000   0.2000   0.2000   0.2000    0.2
J = 2    0.2000   0.2000   0.2000   0.2000   0.2000   0.2000   0.2000   0.2000   0.2000   0.2000    0.2
J = 3    0.2000   0.2000   0.2000   0.2000   0.2000   0.0000   0.0000   0.0000   0.2000   0.2000    0.2
J = 4    0.2000   0.2000   0.2000   0.2000   0.2000   0.0000   0.0000   0.0000   0.2000   0.2000    0.2
J = 5    0.2000   0.2000   0.2000   0.2000   0.2000   0.0000   0.0000   0.0000   0.2000   0.2000    0.2
J = 6    0.2000   0.2000   0.2000   0.0000   0.0000   0.0000   0.2000   0.2000   0.2000   0.2000    0.2
J = 7    0.2000   0.2000   0.2000   0.0000   0.0000   0.0000   0.2000   0.2000   0.2000   0.2000    0.2
J = 8    0.2000   0.2000   0.2000   0.0000   0.0000   0.0000   0.2000   0.2000   0.2000   0.2000    0.2
J = 9    0.2000   0.2000   0.2000   0.2000   0.2000   0.2000   0.2000   0.2000   0.2000   0.2000    0.2
J = 10   0.2000   0.2000   0.2000   0.2000   0.2000   0.2000   0.2000   0.2000   0.2000   0.2000    0.2

OIL PHASE SATURATION

 K = 1   I = 1    I = 2    I = 3    I = 4    I = 5    I = 6    I = 7    I = 8    I = 9    I = 10  I = 11
------ -------- -------- -------- -------- -------- -------- -------- -------- -------- -------- ------
J = 1    0.8000   0.8000   0.8000   0.8000   0.8000   0.8000   0.8000   0.8000   0.8000   0.8000    0.8
J = 2    0.8000   0.8000   0.8000   0.8000   0.8000   0.8000   0.8000   0.8000   0.8000   0.8000    0.8
J = 3    0.8000   0.8000   0.8000   0.8000   0.8000   0.0000   0.0000   0.0000   0.8000   0.8000    0.8
J = 4    0.8000   0.8000   0.8000   0.8000   0.8000   0.0000   0.0000   0.0000   0.8000   0.8000    0.8
J = 5    0.8000   0.8000   0.8000   0.8000   0.8000   0.0000   0.0000   0.0000   0.8000   0.8000    0.8
J = 6    0.8000   0.8000   0.8000   0.0000   0.0000   0.0000   0.8000   0.8000   0.8000   0.8000    0.8
J = 7    0.8000   0.8000   0.8000   0.0000   0.0000   0.0000   0.8000   0.8000   0.8000   0.8000    0.8
J = 8    0.8000   0.8000   0.8000   0.0000   0.0000   0.0000   0.8000   0.8000   0.8000   0.8000    0.8
J = 9    0.8000   0.8000   0.8000   0.8000   0.8000   0.8000   0.8000   0.8000   0.8000   0.8000    0.8
J = 10   0.8000   0.8000   0.8000   0.8000   0.8000   0.8000   0.8000   0.8000   0.8000   0.8000    0.8

GAS PHASE SATURATION

 K = 1   I = 1    I = 2    I = 3    I = 4    I = 5    I = 6    I = 7    I = 8    I = 9    I = 10  I = 11
------ -------- -------- -------- -------- -------- -------- -------- -------- -------- -------- ------
J = 1    0.0000   0.0000   0.0000   0.0000   0.0000   0.0000   0.0000   0.0000   0.0000   0.0000    0.0
J = 2    0.0000   0.0000   0.0000   0.0000   0.0000   0.0000   0.0000   0.0000   0.0000   0.0000    0.0
J = 3    0.0000   0.0000   0.0000   0.0000   0.0000   0.0000   0.0000   0.0000   0.0000   0.0000    0.0
J = 4    0.0000   0.0000   0.0000   0.0000   0.0000   0.0000   0.0000   0.0000   0.0000   0.0000    0.0
J = 5    0.0000   0.0000   0.0000   0.0000   0.0000   0.0000   0.0000   0.0000   0.0000   0.0000    0.0
J = 6    0.0000   0.0000   0.0000   0.0000   0.0000   0.0000   0.0000   0.0000   0.0000   0.0000    0.0
J = 7    0.0000   0.0000   0.0000   0.0000   0.0000   0.0000   0.0000   0.0000   0.0000   0.0000    0.0
J = 8    0.0000   0.0000   0.0000   0.0000   0.0000   0.0000   0.0000   0.0000   0.0000   0.0000    0.0
J = 9    0.0000   0.0000   0.0000   0.0000   0.0000   0.0000   0.0000   0.0000   0.0000   0.0000    0.0
J = 10   0.0000   0.0000   0.0000   0.0000   0.0000   0.0000   0.0000   0.0000   0.0000   0.0000    0.0

IWELL = 1, Pwf (kPa)

 K = 1   I = 1    I = 2    I = 3    I = 4    I = 5    I = 6    I = 7    I = 8    I = 9    I = 10  I = 11
------ -------- -------- -------- -------- -------- -------- -------- -------- -------- -------- ------
J = 1     500.0    500.0    500.0    500.0    500.0    500.0    500.0    500.0    500.0    500.0  500.0
J = 2     500.0    500.0    500.0    500.0    500.0    500.0    500.0    500.0    500.0    500.0  500.0
J = 3     500.0    500.0    500.0    500.0    500.0    500.0      0.0      0.0    500.0    500.0  500.0
J = 4     500.0    500.0    500.0    500.0    500.0      0.0      0.0      0.0    500.0    500.0  500.0
J = 5     500.0    500.0    500.0    500.0    500.0      0.0      0.0      0.0    500.0    500.0  500.0
J = 6     500.0    500.0    500.0    500.0      0.0      0.0    500.0    500.0    500.0    500.0  500.0
J = 7     500.0    500.0    500.0      0.0      0.0      0.0    500.0    500.0    500.0    500.0  500.0
J = 8     500.0    500.0    500.0      0.0      0.0      0.0    500.0    500.0    500.0    500.0  500.0
J = 9     500.0    500.0    500.0    500.0    500.0    500.0    500.0    500.0    500.0    500.0  500.0
J = 10    500.0    500.0    500.0    500.0    500.0    500.0    500.0    500.0    500.0    500.0  500.0
```

```
IWELL = 2, Pwf (kPa)

 K = 1    I = 1    I = 2    I = 3    I = 4    I = 5    I = 6    I = 7    I = 8    I = 9   I = 10 I = 11
------ -------- -------- -------- -------- -------- -------- -------- -------- -------- -------- ------
J = 1     500.0    500.0    500.0    500.0    500.0    500.0    500.0    500.0    500.0    500.0  500.0
J = 2     500.0    500.0    500.0    500.0    500.0    500.0    500.0    500.0    500.0    500.0  500.0
J = 3     500.0    500.0    500.0    500.0    500.0    500.0      0.0      0.0    500.0    500.0  500.0
J = 4     500.0    500.0    500.0    500.0    500.0      0.0      0.0      0.0    500.0    500.0  500.0
J = 5     500.0    500.0    500.0    500.0    500.0      0.0      0.0      0.0    500.0    500.0  500.0
J = 6     500.0    500.0    500.0    500.0      0.0      0.0    500.0    500.0    500.0    500.0  500.0
J = 7     500.0    500.0    500.0      0.0      0.0      0.0    500.0    500.0    500.0    500.0  500.0
J = 8     500.0    500.0    500.0      0.0      0.0      0.0    500.0    500.0    500.0    500.0  500.0
J = 9     500.0    500.0    500.0    500.0    500.0    500.0    500.0    500.0    500.0    500.0  500.0
J = 10    500.0    500.0    500.0    500.0    500.0    500.0    500.0    500.0    500.0    500.0  500.0

HYBRID LOCATION, I =   4 AND J =   6   HYPERHYBRID REGION =   2
WATER PHASE PRESSURE (kPa)

 K = 1    L = 1    L = 2
------ -------- --------
M = 1     500.0    500.0
M = 2     500.0    500.0
M = 3     500.0    500.0
M = 4     500.0    500.0
M = 5     500.0    500.0
M = 6     500.0    500.0
M = 7     500.0    500.0
M = 8     500.0    500.0
M = 9     500.0    500.0
M = 10    500.0    500.0
M = 11    500.0    500.0
M = 12    500.0    500.0

HYBRID LOCATION, I =   4 AND J =   6   HYPERHYBRID REGION =   2
OIL PHASE PRESSURE (kPa)

 K = 1    L = 1    L = 2
------ -------- --------
M = 1     500.0    500.0
M = 2     500.0    500.0
M = 3     500.0    500.0
M = 4     500.0    500.0
M = 5     500.0    500.0
M = 6     500.0    500.0
M = 7     500.0    500.0
M = 8     500.0    500.0
M = 9     500.0    500.0
M = 10    500.0    500.0
M = 11    500.0    500.0
M = 12    500.0    500.0

HYBRID LOCATION, I =   4 AND J =   6   HYPERHYBRID REGION =   2
GAS PHASE PRESSURE (kPa)

 K = 1    L = 1    L = 2
------ -------- --------
M = 1     500.0    500.0
M = 2     500.0    500.0
M = 3     500.0    500.0
M = 4     500.0    500.0
M = 5     500.0    500.0
M = 6     500.0    500.0
M = 7     500.0    500.0
M = 8     500.0    500.0
M = 9     500.0    500.0
M = 10    500.0    500.0
M = 11    500.0    500.0
M = 12    500.0    500.0

HYBRID LOCATION, I =   4 AND J =   6   HYPERHYBRID REGION =   2
TEMPERATURE (C)

 K = 1 L = 1 L = 2
------ ----- -----
M = 1   51.7  51.7
M = 2   51.7  51.7
M = 3   51.7  51.7
M = 4   51.7  51.7
M = 5   51.7  51.7
M = 6   51.7  51.7
M = 7   51.7  51.7
M = 8   51.7  51.7
M = 9   51.7  51.7
M = 10  51.7  51.7
M = 11  51.7  51.7
M = 12  51.7  51.7


HYBRID LOCATION, I =   4 AND J =   6   HYPERHYBRID REGION =   2
COMPOSITION - WATER COMPONENT

 K = 1    L = 1    L = 2
------ -------- --------
M = 1   1.00000  1.00000
M = 2   1.00000  1.00000
M = 3   1.00000  1.00000
M = 4   1.00000  1.00000
M = 5   1.00000  1.00000
M = 6   1.00000  1.00000
M = 7   1.00000  1.00000
M = 8   1.00000  1.00000
M = 9   1.00000  1.00000
M = 10  1.00000  1.00000
M = 11  1.00000  1.00000
M = 12  1.00000  1.00000
```

```
HYBRID LOCATION, I =   4 AND J =   6   HYPERHYBRID REGION =   2
COMPOSITION - HEAVY COMPONENT

 K = 1    L = 1     L = 2
------  --------  --------
M = 1    1.00000   1.00000
M = 2    1.00000   1.00000
M = 3    1.00000   1.00000
M = 4    1.00000   1.00000
M = 5    1.00000   1.00000
M = 6    1.00000   1.00000
M = 7    1.00000   1.00000
M = 8    1.00000   1.00000
M = 9    1.00000   1.00000
M = 10   1.00000   1.00000
M = 11   1.00000   1.00000
M = 12   1.00000   1.00000

HYBRID LOCATION, I =   4 AND J =   6   HYPERHYBRID REGION =   2
COMPOSITION - LIGHT COMPONENT

 K = 1    L = 1     L = 2
------  --------  --------
M = 1    0.00000   0.00000
M = 2    0.00000   0.00000
M = 3    0.00000   0.00000
M = 4    0.00000   0.00000
M = 5    0.00000   0.00000
M = 6    0.00000   0.00000
M = 7    0.00000   0.00000
M = 8    0.00000   0.00000
M = 9    0.00000   0.00000
M = 10   0.00000   0.00000
M = 11   0.00000   0.00000
M = 12   0.00000   0.00000

HYBRID LOCATION, I =   4 AND J =   6   HYPERHYBRID REGION =   2
COMPOSITION - METHANE COMPONENT

 K = 1    L = 1     L = 2
------  --------  --------
M = 1    0.97302   0.97302
M = 2    0.97302   0.97302
M = 3    0.97302   0.97302
M = 4    0.97302   0.97302
M = 5    0.97302   0.97302
M = 6    0.97302   0.97302
M = 7    0.97302   0.97302
M = 8    0.97302   0.97302
M = 9    0.97302   0.97302
M = 10   0.97302   0.97302
M = 11   0.97302   0.97302
M = 12   0.97302   0.97302

HYBRID LOCATION, I =   4 AND J =   6   HYPERHYBRID REGION =   2
WATER PHASE SATURATION

 K = 1   L = 1    L = 2
------  -------  -------
M = 1    0.2000   0.2000
M = 2    0.2000   0.2000
M = 3    0.2000   0.2000
M = 4    0.2000   0.2000
M = 5    0.2000   0.2000
M = 6    0.2000   0.2000
M = 7    0.2000   0.2000
M = 8    0.2000   0.2000
M = 9    0.2000   0.2000
M = 10   0.2000   0.2000
M = 11   0.2000   0.2000
M = 12   0.2000   0.2000

HYBRID LOCATION, I =   4 AND J =   6   HYPERHYBRID REGION =   2
OIL PHASE SATURATION

 K = 1   L = 1    L = 2
------  -------  -------
M = 1    0.8000   0.8000
M = 2    0.8000   0.8000
M = 3    0.8000   0.8000
M = 4    0.8000   0.8000
M = 5    0.8000   0.8000
M = 6    0.8000   0.8000
M = 7    0.8000   0.8000
M = 8    0.8000   0.8000
M = 9    0.8000   0.8000
M = 10   0.8000   0.8000
M = 11   0.8000   0.8000
M = 12   0.8000   0.8000
```

```
HYBRID LOCATION, I =   4 AND J =   6   HYPERHYBRID REGION =   2
GAS PHASE SATURATION

  K = 1  L = 1   L = 2
 ------ ------- -------
 M = 1   0.0000  0.0000
 M = 2   0.0000  0.0000
 M = 3   0.0000  0.0000
 M = 4   0.0000  0.0000
 M = 5   0.0000  0.0000
 M = 6   0.0000  0.0000
 M = 7   0.0000  0.0000
 M = 8   0.0000  0.0000
 M = 9   0.0000  0.0000
 M = 10  0.0000  0.0000
 M = 11  0.0000  0.0000
 M = 12  0.0000  0.0000

HYBRID LOCATION, I =   6 AND J =   3   HYPERHYBRID REGION =   1
WATER PHASE PRESSURE (kPa)

  K = 1   L = 1    L = 2
 ------ -------- --------
 M = 1     500.0    500.0
 M = 2     500.0    500.0
 M = 3     500.0    500.0
 M = 4     500.0    500.0
 M = 5     500.0    500.0
 M = 6     500.0    500.0
 M = 7     500.0    500.0
 M = 8     500.0    500.0
 M = 9     500.0    500.0
 M = 10    500.0    500.0
 M = 11    500.0    500.0
 M = 12    500.0    500.0
HYBRID LOCATION, I =   6 AND J =   3   HYPERHYBRID REGION =   1
OIL PHASE PRESSURE (kPa)

  K = 1   L = 1    L = 2
 ------ -------- --------
 M = 1     500.0    500.0
 M = 2     500.0    500.0
 M = 3     500.0    500.0
 M = 4     500.0    500.0
 M = 5     500.0    500.0
 M = 6     500.0    500.0
 M = 7     500.0    500.0
 M = 8     500.0    500.0
 M = 9     500.0    500.0
 M = 10    500.0    500.0
 M = 11    500.0    500.0
 M = 12    500.0    500.0
HYBRID LOCATION, I =   6 AND J =   3   HYPERHYBRID REGION =   1
GAS PHASE PRESSURE (kPa)

  K = 1   L = 1    L = 2
 ------ -------- --------
 M = 1     500.0    500.0
 M = 2     500.0    500.0
 M = 3     500.0    500.0
 M = 4     500.0    500.0
 M = 5     500.0    500.0
 M = 6     500.0    500.0
 M = 7     500.0    500.0
 M = 8     500.0    500.0
 M = 9     500.0    500.0
 M = 10    500.0    500.0
 M = 11    500.0    500.0
 M = 12    500.0    500.0
HYBRID LOCATION, I =   6 AND J =   3   HYPERHYBRID REGION =   1
TEMPERATURE (C)

  K = 1 L = 1 L = 2
 ------ ----- -----
 M = 1   51.7  51.7
 M = 2   51.7  51.7
 M = 3   51.7  51.7
 M = 4   51.7  51.7
 M = 5   51.7  51.7
 M = 6   51.7  51.7
 M = 7   51.7  51.7
 M = 8   51.7  51.7
 M = 9   51.7  51.7
 M = 10  51.7  51.7
 M = 11  51.7  51.7
 M = 12  51.7  51.7
HYBRID LOCATION, I =   6 AND J =   3   HYPERHYBRID REGION =   1
COMPOSITION - WATER COMPONENT

  K = 1   L = 1    L = 2
 ------ -------- --------
 M = 1   1.00000  1.00000
 M = 2   1.00000  1.00000
 M = 3   1.00000  1.00000
 M = 4   1.00000  1.00000
 M = 5   1.00000  1.00000
 M = 6   1.00000  1.00000
 M = 7   1.00000  1.00000
 M = 8   1.00000  1.00000
 M = 9   1.00000  1.00000
 M = 10  1.00000  1.00000
 M = 11  1.00000  1.00000
 M = 12  1.00000  1.00000
```

```
HYBRID LOCATION, I =   6 AND J =   3   HYPERHYBRID REGION =   1
COMPOSITION - HEAVY COMPONENT

  K = 1    L = 1     L = 2
 ------  --------  --------
 M = 1   1.00000  1.00000
 M = 2   1.00000  1.00000
 M = 3   1.00000  1.00000
 M = 4   1.00000  1.00000
 M = 5   1.00000  1.00000
 M = 6   1.00000  1.00000
 M = 7   1.00000  1.00000
 M = 8   1.00000  1.00000
 M = 9   1.00000  1.00000
 M = 10  1.00000  1.00000
 M = 11  1.00000  1.00000
 M = 12  1.00000  1.00000

HYBRID LOCATION, I =   6 AND J =   3   HYPERHYBRID REGION =   1
COMPOSITION - LIGHT COMPONENT

  K = 1    L = 1     L = 2
 ------  --------  --------
 M = 1   0.00000  0.00000
 M = 2   0.00000  0.00000
 M = 3   0.00000  0.00000
 M = 4   0.00000  0.00000
 M = 5   0.00000  0.00000
 M = 6   0.00000  0.00000
 M = 7   0.00000  0.00000
 M = 8   0.00000  0.00000
 M = 9   0.00000  0.00000
 M = 10  0.00000  0.00000
 M = 11  0.00000  0.00000
 M = 12  0.00000  0.00000

HYBRID LOCATION, I =   6 AND J =   3   HYPERHYBRID REGION =   1
COMPOSITION - METHANE COMPONENT

  K = 1    L = 1     L = 2
 ------  --------  --------
 M = 1   0.97302  0.97302
 M = 2   0.97302  0.97302
 M = 3   0.97302  0.97302
 M = 4   0.97302  0.97302
 M = 5   0.97302  0.97302
 M = 6   0.97302  0.97302
 M = 7   0.97302  0.97302
 M = 8   0.97302  0.97302
 M = 9   0.97302  0.97302
 M = 10  0.97302  0.97302
 M = 11  0.97302  0.97302
 M = 12  0.97302  0.97302

HYBRID LOCATION, I =   6 AND J =   3   HYPERHYBRID REGION =   1
WATER PHASE SATURATION

  K = 1   L = 1    L = 2
 ------  -------  -------
 M = 1    0.2000   0.2000
 M = 2    0.2000   0.2000
 M = 3    0.2000   0.2000
 M = 4    0.2000   0.2000
 M = 5    0.2000   0.2000
 M = 6    0.2000   0.2000
 M = 7    0.2000   0.2000
 M = 8    0.2000   0.2000
 M = 9    0.2000   0.2000
 M = 10   0.2000   0.2000
 M = 11   0.2000   0.2000
 M = 12   0.2000   0.2000

HYBRID LOCATION, I =   6 AND J =   3   HYPERHYBRID REGION =   1
OIL PHASE SATURATION

  K = 1   L = 1    L = 2
 ------  -------  -------
 M = 1    0.8000   0.8000
 M = 2    0.8000   0.8000
 M = 3    0.8000   0.8000
 M = 4    0.8000   0.8000
 M = 5    0.8000   0.8000
 M = 6    0.8000   0.8000
 M = 7    0.8000   0.8000
 M = 8    0.8000   0.8000
 M = 9    0.8000   0.8000
 M = 10   0.8000   0.8000
 M = 11   0.8000   0.8000
 M = 12   0.8000   0.8000

HYBRID LOCATION, I =   6 AND J =   3   HYPERHYBRID REGION =   1
GAS PHASE SATURATION

  K = 1   L = 1    L = 2
 ------  -------  -------
 M = 1    0.0000   0.0000
 M = 2    0.0000   0.0000
 M = 3    0.0000   0.0000
 M = 4    0.0000   0.0000
 M = 5    0.0000   0.0000
 M = 6    0.0000   0.0000
 M = 7    0.0000   0.0000
 M = 8    0.0000   0.0000
 M = 9    0.0000   0.0000
 M = 10   0.0000   0.0000
 M = 11   0.0000   0.0000
 M = 12   0.0000   0.0000
```

```
INITIAL FLUIDS AND ENERGY

  Water (Kmole)          0.838279D+08
  Heavy (Kmole)          0.991989D+07
  Light (Kmole)          0.000000D+00
  Methane (Kmole)        0.000000D+00
  Aqueous Phase (m3)     0.151775D+07
  Oleic Phase (m3)       0.513301D+07
  Gaseous Phase (m3)     0.000000D+00
  Energy (J)             0.151172D+16

CONVERGENCE TOLERANCES

       Parameter         Tolerance  Parameter  Tolerance
  ------------------    ----------  ---------  ---------
  TolPressure (kPa)       5.000000             0.000D+00
  TolTemperature (K)      1.000000
  TolComp                 0.100000
  TolSaturation           0.100000


TIMESTEP SUMMARY

   LoopTime =    0
   Cumulative Time (days)        =       0.0000
   Time Step (days)              =       0.0000
   Minimum Newton iterations     =    2
   Maximum Newton iterations     =   15
   Number of Newton iterations   =    0
   Number of Newton cuts         =    0
   Number of time cuts           =    0
   Acceleration flag             =    0
   Acceleration factor           =  0.00
   Minimum acceleration          =    2
   Maximum acceleration          =   10
   Maximum SPARSE restarts       =    3
   Number of SPARSE restarts     =    0
   Maximum inner iterations      =   10
   Number of inner iterations    =    0
    ITMAX convergence value      =  0.000D+00


Timestep parameters

    PARAMETER                      PARAMETER
 --------------- ---------- ------------- ----------
 TimeStop (days)   165.0000 DSMAX             0.2000
 dTime (days)        0.0100 DPMAX (kPa)     300.0000
 TimeEnd (days)     20.0000 DTPMAX (K)       80.0000
 DTMAX (days)        5.0000 DXMAX             0.2000
 DTMIN (days)        0.0001 OMEGAconstant     1.0000
                            RatioMin          1.5000
                            RatioMax          0.5000

Material and Energy Balances and Residuals

                    INCREMENTAL CUMULATIVE  Residuals  I  J  K  L  M
                         %
 ------------------ ----------- ---------- ---------- -- -- -- -- --
 Water Component     0.0000D+00 0.0000D+00 0.0000D+00  0  0  0  0  0
 Heavy Component     0.0000D+00 0.0000D+00 0.0000D+00  0  0  0  0  0
 Light Component     0.0000D+00 0.0000D+00 0.0000D+00  0  0  0  0  0
 Methane Component   0.0000D+00 0.0000D+00 0.0000D+00  0  0  0  0  0
 Energy              0.0000D+00 0.0000D+00 0.0000D+00  0  0  0  0  0
 Aqueous Phase X                           0.0000D+00  0  0  0  0  0
 Oleic Phase X                             0.0000D+00  0  0  0  0  0
 Gaseous Phase X                           0.0000D+00  0  0  0  0  0
 Saturation                                0.0000D+00  0  0  0  0  0
 Well 1                                    0.0000D+00  0  0  0  0  0
 Well 2                                    0.0000D+00  0  0  0  0  0
----------------------------------------------------------------------------------------


 CHANGE OF WELL STATUS AT TIME (days)     0.0
    These setting in force until time (days)   20.0

    WELL EXISTS AT LOCATION I =  4 J =  6 , WELL NUMBER  1

                                      K   =   1
                          ---------- ---------
                          INDEX            -1
                          IPRODINDEX        1
                                      K   =   1
  -------------- ------ ----------- ----------
  BHPmin (kPa)    120.0 PRODINDEX    0.6223E-10
  BHPmax (kPa)   6900.0 ProdMultiply 1
  QLmax (m3/day)    0.0 FracThick    1
  QOmax (m3/day)    0.0 WellFactor   1
  QTmax (m3/day)  100.0 Cg           0.5
  Quality           0.7 Skin         0.0000E+00
  Inj. Temp (C)   250.0 Rw           0.09
```

```
   WELL EXISTS AT LOCATION I =  6 J =  3 , WELL NUMBER  1
                                   K   =   1
                         ---------- ---------
                         INDEX            -1
                         IPRODINDEX        1
                                   K   =   1
-------------- ------ ------------ ----------
BHPmin (kPa)    120.0 PRODINDEX    0.6223E-10
BHPmax (kPa)   6900.0 ProdMultiply 1
QLmax (m3/day)    0.0 FracThick    1
QOmax (m3/day)    0.0 WellFactor   1
QTmax (m3/day)  100.0 Cg           0.5
Quality           0.7 Skin         0.0000E+00
Inj. Temp (C)   250.0 Rw           0.09
```

IV.4 Abbreviated Log File

```
Opening files and reading data

        Model is dimensioned for      12       10        2
        Problem is dimensioned for    11       10        1

        Hyperhybrid regions are dimensioned for    4 regions.
        Maximum size of each region is NRm =    4      NTm =  12

RUN CYCLIC 1

Beginning initialization

Finished initialization

   Maximum number of unknowns          =   1600
   Maximum number of Jacobian entries =  75000

PLOT FILE 1

  I  J  K     Time      Po     T     Sw    So    Sg    X1    X2    X3    X4    Pwf1   Pwf2
 -- -- -- --------- ------ ----- ----- ----- ----- ----- ----- ----- ----- ------ ------
  5  4  1    0.0000  500.0  51.7 0.200 0.800 0.000 1.000 1.000 0.000 0.973  500.0  500.0
  5  5  1    0.0000  500.0  51.7 0.200 0.800 0.000 1.000 1.000 0.000 0.973  500.0  500.0
  7  6  1    0.0000  500.0  51.7 0.200 0.800 0.000 1.000 1.000 0.000 0.973  500.0  500.0
  8  6  1    0.0000  500.0  51.7 0.200 0.800 0.000 1.000 1.000 0.000 0.973  500.0  500.0

PLOT FILE 3

  I  J  L  M  K    Time        Po       T     Sw    So    Sg    X1    X2    X3     X4      Pwf1      Pwf2
 -- -- -- -- -- --------- -------- ----- ----- ----- ----- ----- ----- ----- ------ -------- --------
  4  6  1  1  1    0.0000     500.0  51.7 0.200 0.800 0.000 1.000 1.000 0.000  0.973     500.0     500.0
  4  6  2  3  1    0.0000     500.0  51.7 0.200 0.800 0.000 1.000 1.000 0.000  0.973     500.0     500.0
  6  3  1  1  1    0.0000     500.0  51.7 0.200 0.800 0.000 1.000 1.000 0.000  0.973     500.0     500.0
  6  3  2  9  1    0.0000     500.0  51.7 0.200 0.800 0.000 1.000 1.000 0.000  0.973     500.0     500.0

LoopTime =              1
ITime    =              1
   Cumulative Time (days) =    0.0100
   dTime (days)           =    0.0100
ITER           1
   Maximum number of unknowns =    1600
   Number of current unknowns =     710

   Maximum number of Jacobian entries =  75000
   Number of current Jacobian entries =  19824
   NSP = 600000

   Actual number of Jacobian entries =  20330
ITER           2
ITER           3

PLOT FILE 2

                     Well 1 Well 1  Well 1  Well 1   Well 1  Well 1  Well 2 Well 2  Well 2  Well 2   Well 2  Well 2
  I  J     Time        Wat    Oil     Gas   CumWat   CumOil  CumGas    Wat    Oil     Gas   CumWat   CumOil  CumGas
 -- -- --------- ------ ------ ------- -------- ------- -------- ------ ------ ------- -------- ------- --------
  4  6    0.0100  -77.1    0.0     0.0     -0.8     0.0      0.0    0.0    0.0     0.0      0.0     0.0      0.0
  6  3    0.0100  -77.1    0.0     0.0     -0.8     0.0      0.0    0.0    0.0     0.0      0.0     0.0      0.0
  5  4  1    0.0100  500.0  51.7 0.200 0.800 0.000 1.000 1.000 0.000 0.973  500.0  500.0
  5  5  1    0.0100  500.0  51.7 0.200 0.800 0.000 1.000 1.000 0.000 0.973  500.0  500.0
  7  6  1    0.0100  500.0  51.7 0.200 0.800 0.000 1.000 1.000 0.000 0.973  500.0  500.0
  8  6  1    0.0100  500.0  51.7 0.200 0.800 0.000 1.000 1.000 0.000 0.973  500.0  500.0
  4  6  1  1  1    0.0100     544.2  51.7 0.200 0.800 0.000 1.000 1.000 0.000  0.973    6900.0     500.0
  4  6  2  3  1    0.0100     500.0  51.7 0.200 0.800 0.000 1.000 1.000 0.000  0.973    6900.0     500.0
  6  3  1  1  1    0.0100     544.2  51.7 0.200 0.800 0.000 1.000 1.000 0.000  0.973    6900.0     500.0
  6  3  2  9  1    0.0100     500.0  51.7 0.200 0.800 0.000 1.000 1.000 0.000  0.973    6900.0     500.0
```

```
LoopTime =          120
ITime    =          120
   Cumulative Time (days) =  165.0000
   dTime (days)           =    8.8495
ITER          1
ITER          2
ITER          3
ITER          4
ITER          5
ITER          6
ITER          7
ITER          8
  4  6  165.0000    0.0    0.0     0.0  -5974.5     0.0      0.0   12.6    7.4     0.0   1272.6   671.9      0.0
  6  3  165.0000    0.0    0.0     0.0  -5974.5     0.0      0.0   12.6    7.4     0.0   1272.8   672.0      0.0
  5  4  1  165.0000 1412.4  51.7 0.201 0.799 0.000 1.000 1.000 0.000 0.991  500.0  500.0
  5  5  1  165.0000 1388.8  51.7 0.201 0.799 0.000 1.000 1.000 0.000 0.991  500.0  500.0
  7  6  1  165.0000 1386.8  51.7 0.201 0.799 0.000 1.000 1.000 0.000 0.991  500.0  500.0
  8  6  1  165.0000 1409.6  51.7 0.201 0.799 0.000 1.000 1.000 0.000 0.991  500.0  500.0
  4  6  1  1  1  165.0000    841.7 142.8 0.281 0.719 0.000 1.000 1.000 0.000  0.583   2461.4    812.6
  4  6  2  3  1  165.0000   1323.9  52.0 0.205 0.795 0.000 1.000 1.000 0.000  0.990   2461.4    812.6
  6  3  1  1  1  165.0000    841.7 142.8 0.281 0.719 0.000 1.000 1.000 0.000  0.583   2461.5    812.5
  6  3  2  9  1  165.0000   1323.9  52.0 0.205 0.795 0.000 1.000 1.000 0.000  0.990   2461.5    812.5

FORTRAN STOP
```

COLOPHON

"Better is the end of a thing than the beginning thereof..."

—Ecclesiastes

This manuscript was produced using Apple Computer, Inc. hardware and the following software: Microsoft Word, Microsoft Excel, WaveMetrics Igor, Claris MacDraw II, Silicon Beach SuperPaint and Design Science MathType. The FORTRAN code was developed initially using Language Systems FORTRAN under the MPW shell. The code was completed, debugged and executed on a VAX 6320.